

UC Davis

UC Davis Electronic Theses and Dissertations

Title

Stereoselective Synthesis of Tri-Substituted Benzodihydrofurans and Dihydrobenzoxanthone Natural Products By C–H Insertion of Donor/Donor Carbenes into Stereogenic Centers

Permalink

<https://escholarship.org/uc/item/1w81n5ss>

Author

Dishman, Sarah N

Publication Date

2023

Peer reviewed|Thesis/dissertation

Stereoselective Synthesis of Tri-Substituted Benzodihydrofurans and Dihydrobenzoxanthone
Natural Products By C–H Insertion of Donor/Donor Carbenes into Stereogenic Centers

By

SARAH NICOLE DISHMAN
DISSERTATION

Submitted in partial satisfaction of the requirements for the degree of

DOCTOR OF PHILOSOPHY

in

Chemistry

in the

OFFICE OF GRADUATE STUDIES

of the

UNIVERSITY OF CALIFORNIA

DAVIS

Approved:

Jared T. Shaw

Annaliese K. Franz

Dean J. Tantillo

Committee in Charge

2023

DEDICATION

“in a world full of temporary things you are a perpetual feeling”
To my best friend of 27 years, this one is for you. To whatever end,
Twin.

To the mother who taught me what true sacrifice was,
in the hope, I’d always have better.

*“I may not have gone where I intended to go, but I think I have ended up where I
needed to be” – Douglas Adams*

Copyright © 2023 Sarah Nicole Dishman
All rights reserved

TABLE OF CONTENTS

Abstract	vii
Acknowledgements	viii
Chapter 1: Divergent Stereochemical Outcomes in the Insertion of Donor/Donor Carbenes into the C–H Bonds of Stereogenic Centers	1
1.1 Introduction	1
1.1.1 Overview of donor/donor carbenes	1
1.1.2 History of C–H insertions into stereogenic centers	6
1.1.2.1 Substrate control: proposed stereoselectivity models	10
1.1.2.2 Catalytic control: proposed stereoselectivity models	13
1.1.2.3 Mechanism proposals	18
1.1.3 Tri-substituted 2,2,3-benzodihydrofurans	26
1.2 Results and Discussion	30
1.2.1 Project Overview	30
1.2.2 Synthesis of donor/donor carbene precursors with stereogenic centers	32
1.2.3 Sterically bulky, highly activated substrates	36
1.2.4 Less bulky, less activated substrates	38
1.2.5 Reaction optimization: conditions screening	40
1.2.5.1 Catalyst screening	40
1.2.5.2 Solvent and temperature screening	42
1.2.5.3 Lewis bases screening	44
1.2.6 Chiral HPLC optimization	45
1.2.7 Synthesis of crystal derivatives for crystallography	48
1.2.8 Substrate scope	52
1.2.9 Mechanistic DFT calculation collaboration with Tantillo Lab	55
1.3 Conclusion	61
1.4 Experimental section	62
1.4.1 General procedures	62
1.4.2 Alcohol substrates	65
1.4.3 Bromo-ether substrates	66
1.4.4 Ketone substrates	69

1.4.5	Hydrazone substrates	74
1.4.6	Insertion substrates	79
1.4.7	Crystal structure substrates	88
1.5	References	91

Chapter 2: Targeted Synthesis of Dihydrobenzoxanthenes: *cycloartobiloxanthone* and

	<i>artoindonesian Z-1</i>	107
2.1	Introduction	107
2.1.1	Isolation of furanodihydrobenzoxanthenes	108
2.1.2	Biosynthetic route	111
2.1.3	Biological testing of furanodihydrobenzoxanthenes	117
2.1.4	Previous synthetic methods to make 6/6/5 framework	121
2.1.4.1	Cascade reactions	122
2.1.4.2	Benzodihydrofuran bicyclic to fused tricyclic core	127
2.1.4.3	Benzylic ketone bicyclic to fused tricyclic core	130
2.2	Results and Discussion: first-generation route	134
2.2.1	Retrosynthesis	134
2.2.2	Right hemisphere: forward synthesis to insertion core	135
2.2.2.1	Isopropyl protecting groups strategy	135
2.2.2.2	Methoxy protecting groups strategy	136
2.2.3	Right hemisphere: benzylic oxidation attempts	141
2.2.4	Right hemisphere: Vilsmeier-Haack reaction	147
2.2.5	Left hemisphere	148
2.2.5.1	Initial route: ester functionality	148
2.2.5.2	Re-route: phenol functionality	149
2.3	Results and Discussion: route scouting	150
2.3.1	Protection of the benzylic ketone: acetal and thioacetal attempts	151
2.3.2	Tempering the ring system electronics: synthesis of ortho-bromine and ortho-fluorine derivatives	152
2.3.2.1	Benzylic oxidation attempts	154
2.3.3	Tosyl protection of phenols	155

2.3.4	Unsubstituted ortho position.....	157
2.3.5	Thioacetal route	161
2.3.6	Cyclopropane route	165
2.3.7	7-methoxytetralone route.....	169
2.3.7.1	Fluorination of the 7-methoxytetralone	171
2.3.7.2	Bromination and chlorination of the 7-methoxytetralone	173
2.3.7.3	Accidental discovery of direct hydroxylation of 7-methoxytetralone	177
2.4	Results and Discussion: second-generation route.....	179
2.4.1	Directed hydroxylation attempts and screening	180
2.4.1.1	Product inhibition theory	184
2.4.2	Directed acetoxylation solution to product inhibition	186
2.4.3	Right hemisphere: forward synthesis to insertion core	190
2.4.3.1	C–H insertion stereoselectivity optimization	191
2.4.4	Right hemisphere: benzylic oxidation attempts and screening	192
2.4.5	Right hemisphere: late-stage sp ² methoxylation	199
2.5	Results and Discussion: final steps to join two hemispheres.....	201
2.5.1	Claisen strategy	201
2.5.2	1,4-addition strategy	202
2.6	Results and Discussion: synthesis of artoindonesianin Z-2.....	204
2.6.1	Synthesis of enantiopure ether.....	205
2.6.2	C–H insertion stereoselectivity data from first-generation route	210
2.7	Conclusion	211
2.8	Experimental section.....	212
2.8.1	Right hemisphere: first-generation route.....	212
2.8.2	Right hemisphere: second-generation route	220
2.8.3	Left hemisphere: phenol functionality.....	232
2.8.4	Left hemisphere: ester functionality	237
2.8.5	Final steps: joining the two hemispheres.....	239
2.9	References.....	241

Appendices

A.1	Quantitative structure-selectivity reaction model	274
A.1.1	Introduction	274
A.1.2	Results and Discussion	274
A.1.3	Experimental Section.....	278
A.1.4	References	286
A.2	Progress Towards the Total Synthesis of pseudorigidol A and pseudorigidol B.....	289
A.2.1	Introduction	289
A.2.2	Results and Discussion	290
A.2.3	Conclusion and Future Work.....	292
A.2.4	Experimental Section.....	293
A.2.5	References	295

ABSTRACT OF DISSERTATION

This dissertation describes two projects in the organic chemistry field centering around the stereoselective synthesis of trisubstituted benzodihydrofurans and related natural products through C–H insertion of donor/donor carbenes into stereogenic centers. The first chapter reports the development of a stereoselective methodology to make 2,2,3-trisubstituted benzodihydrofurans. The method expands intramolecular C–H insertion reactions with donor/donor carbenes to stereogenic insertion centers, thereby enabling benzodihydrofuran formation in high diastereoselectivity and enantioselectivity. Computational studies on the system illuminate the origins of divergent stereochemical outcomes for different substrate classes. The second chapter applies this methodology to the asymmetric synthesis of two dihydrobenzoxanthone natural products, *cycloartobiloxanthone* and *artoindonesianin Z-2*. First, an introduction to the natural product subclass outlines structural variations and biosynthetic pathways for the isolated natural products found in the family and their reported biological activities. Progress towards the synthesis of these two natural products is split into three main stages. The first stage reports a first-generation route and its related benzylic oxidation roadblock. The second stage details numerous route-scouting endeavors. The third stage outlines a second-generation route and future work toward completing the asymmetric synthesis of *cycloartobiloxanthone* and *artoindonesianin Z-2*.

ACKNOWLEDGEMENTS

There have been numerous people who have helped me throughout my graduate career these past five years, and I won't possibly be able to mention every single one. So, to all of those who have made an impact on my journey, no matter how small, I thank you and hope you know I will forever be grateful. First and foremost, my family means the world to me, and they have been an infallible support system to get me to this point in my career.

Lauren – Words will never be able to describe how thankful I am to have you in my life. You've been there to celebrate every high and pick me up after every single low of graduate school. People always ask us what it is like to be a twin, and it's the knowledge that I've never felt alone for a single second in my life. You're my best friend and the other half of me, and I can confidently say I wouldn't be where I'm at without your never-ending support and love.

Mom – You have been selfless and unabated in your support of me over the years. The depth of your love kept me going through even the hardest of times. Thank you for every phone call, for always asking if I needed anything, for the reminder to live my life to the fullest regardless of work and loving me unconditionally no matter what I decided to do with my life. Every day I strive to embody the strength, grit, perseverance, and compassion you have exemplified my entire life.

Billy – Thanks for always being the voice of reason when I was panicking, and picking up every phone call no matter what time zone you happened to be in. You always pushed me to dream bigger, question everything, and know my worth. Your honesty and tough love helped me through more situations than you know.

Dad – I'll be forever grateful that you always started or ended every conversation by asking if I was happy. You were always a reminder to enjoy the small things in life, and not to get caught up

in negativity. Thanks for never judging my choices, and always providing calmness and peace whenever I called.

Second, thanks to all the people I have worked with in the Shaw lab over the years. It's been a wonderful group of talented chemists that pushed me to develop into the chemist I am currently. I can't possibly elaborate on every lab mate, but I want to highlight the following people.

Ben – You're an incredible chemist, an even better mentor, and a genuine friend. Thank you for your everlasting patience with me, and always answering every question I came up with in my stream of consciousness. Your truly humbling work ethic, scientific engagement, light-hearted and carefree attitude, and impeccable aux cord DJ skills were unparalleled. I'll be forever grateful to have the opportunity to develop as a chemist in the workplace environment you so heavily influenced. **Nina** – Your energy is unmatched, your ability to juggle all that life could throw at you was unrivaled, and your compassion and grit was the glue that held the lab together for many years. Thanks for brightening every room you entered, and always being there to support and listen to me. You were and will continue to be one of the main role models I look up to, and I can't wait to see what you will achieve in life. **Garrett** – Thanks for always being willing to talk science and solve a chemistry problem at any hour of the day. Thanks for always lending an ear and supporting all of those around you even to the detriment of yourself. You're one of the most genuine people I know and a true friend. I'll miss your ability to find the humor in every situation, and I look forward to seeing where you end up in your career. **Christine** – You are one of the kindest and most selfless people I encountered in graduate school. Thank you for all your mentorship and support, and for being a damn good teammate on a natural product project. **Linda** – You are a vastly more talented chemist than you will allow yourself to believe, and I'm honored to have been

able to mentor you in my last year of graduate school. I can't wait to continue to see you grow and develop as a chemist, and to hear about all the great things you will achieve.

Next, thanks to all my friends for the support and community you provided me throughout graduate school. **Amanda** and **Andy** – You two are some of the kindest, most easygoing, and biggest hearted friends I have in my life. Amanda, your positivity and relentlessness to see the best in everyone is something to be cherished. Andy, your humor and candor is always refreshing, and your work ethic is incredibly admirable. Here's to every drink we've grabbed over the years, every floating trip, every Tahoe adventure we've gone on, and for all the future memories we'll all have together in our lifetimes. **Jesse** – From almost dying from heat exhaustion on the half dome hike to every post card from London, thanks for being an amazing friend. You are so authentically yourself, and it always helped bring out the best in me. **Winston** – From an awkward admissions dinner to becoming best friends, thank you for your endless support and ability to always bring a smile to my face. Thank you for always building me up and being the light and safety in the seemingly endless waves of abuse throughout grad school. You're truly an authentic and giving soul, and I'll always cherish the friendship we built throughout our time in Davis.

Finally, thank you to my dissertation committee. Thank you to Prof. Dean Tantillo for always being available to help a graduate student and for our scientific discussions and collaborations. Thank you to Prof. Annaliese Franz for all your feedback over the years, for being an excellent role model, and for being an active supporter for all women in organic chemistry. Lastly, thank you to Prof. Jared Shaw for allowing me the opportunity to join your lab and all your guidance over the years. I'm very grateful for the intellectual freedom and independence you enabled me to have throughout all my projects in lab, and the lab environment you helped foster that shaped me into the chemist I am nowadays.

CHAPTER 1

Divergent Stereochemical Outcomes in the Insertion of Donor/Donor Carbenes into the C–H Bonds of Stereogenic Centers¹

1.1. Introduction

The insertion of metal carbenes into C–H bonds enables the efficient and stereoselective synthesis of a wide array of complex organic molecules.^{2,3} Over the past few decades, research surrounding functionalizing C–H bonds, rather than activating C–H bonds, has exploded in popularity.^{4–9} Viewing C–H bonds as functional group handles, rather than inert bonds, has vast applications across many areas such as natural product synthesis³, targeted synthesis³, materials functionalization^{10,11}, biological imaging and conjugation¹², and many more. Although the literature on metal carbenes in C–H functionalization methods is quite expansive, our group has focused on dirhodium donor/donor carbenes for C–H insertions.¹³

1.1.1 Overview of donor/donor carbenes

Metal carbenes are classified by the electronic character of the groups adjacent to the carbene center.¹⁴ Electron-withdrawing groups are called “acceptor groups”, and electron-donating groups are called “donor groups”. This results in five main categories of metal carbenes: acceptor/acceptor, acceptor, donor/acceptor, donor, and donor/donor (Figure 1.1). The reactivity and selectivity of carbenes can be tuned by changing the electronics of the groups adjacent to the carbene. For instance, historically, metal carbenes derived their high reactivity from having one or more electron-withdrawing groups to confer high electrophilicity.¹⁵ The increased reactivity of these acceptor-containing carbenes enabled a wide breadth of reactions they could be used in.

Metal carbene general classification

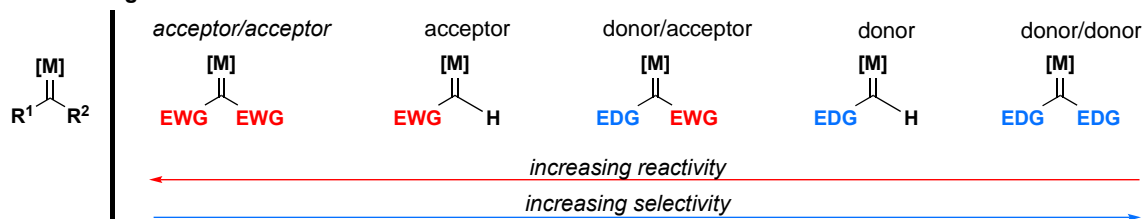
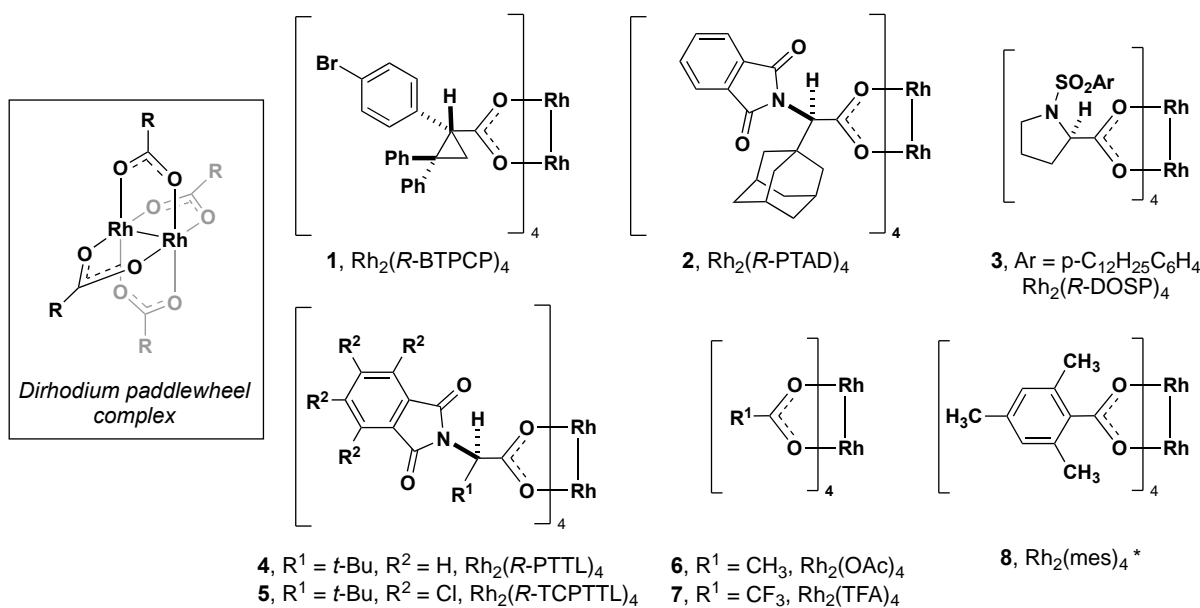


Figure 1.1 Metal carbene spectrum.

Some of the first C–H insertion reactions used acceptor/acceptor carbenes, but these carbenes often produced low chemo-, regio-, and stereoselectivity in reactions.^{16,17} As the field advanced, commercially available dirhodium catalysts possessing tetracarboxylate ligands became the privileged scaffold for stabilizing these carbenes and increased the selectivity of the C–H insertion reactions (Figure 1.2).^{8,18,19}

Commercially available dirhodium catalysts commonly used with donor/donor carbenes



*not commercially available, derived from ligand exchange with $Rh_2(OAc)_4$ and 2,4,6-trimethylbenzoic acid

Figure 1.2 Commercially available dirhodium catalysts commonly used for C–H insertion reactions.

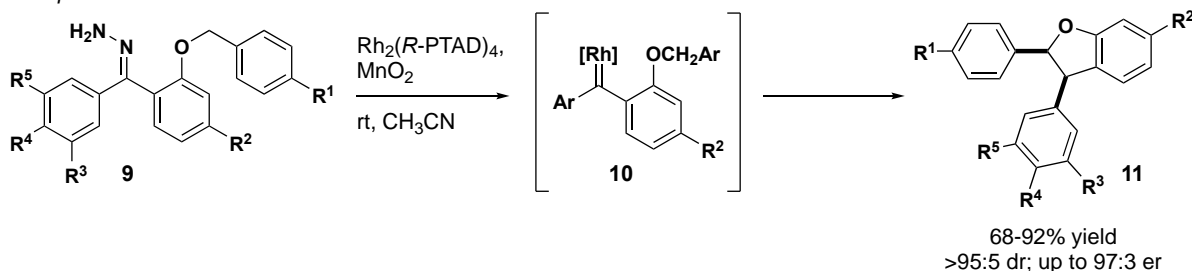
In addition, it was discovered that exchanging one of the groups for an electron-donating group, creating a donor/acceptor carbene, combined with dirhodium catalysts, enabled chemo-, regio-, and stereoselective intra- and intermolecular C–H insertions reactions. Huw Davies' group

has pioneered much of the work with these donor/acceptor carbenes over the past three decades.^{5,8,20–23}

Initially, it was believed that the less electrophilic donor and donor/donor carbenes were not reactive enough to undergo the analogous C–H insertion reactions. However, in 2014 the Shaw Lab reported one of the first examples of an intramolecular C–H insertion with a donor/donor carbene and has been investigating this area for the past decade since the initial report (Figure 1.3).²⁴ Notably, the Che and Zhu groups have been very active in the donor/donor carbene research area.^{25–31} In the Shaw Lab’s initial report, our group developed a one-pot oxidation and insertion method starting from a hydrazone precursor (**9**). This precursor (**9**) is oxidized up to diazo (**12**) using the mild oxidant, MnO₂, then dirhodium catalyst (**2**) is added to form metal carbene (**10**) and undergo the intramolecular C–H insertion (**11**).

Shaw, 2014

One-pot: oxidation & insertion



Two pot: oxidation to diazo then diazo to insertion

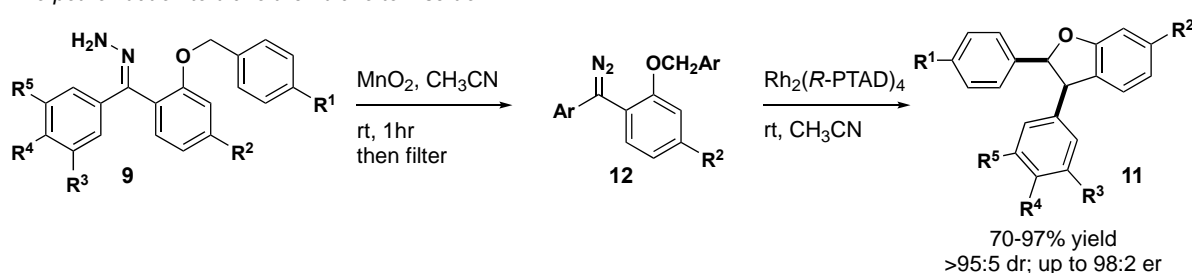


Figure 1.3 Shaw lab initial report of donor/donor carbene C–H insertion.

Our group’s research extended the utility of dirhodium donor/donor carbenes to the synthesis of a wide variety of disubstituted five- and six-membered ring heterocycles (Figure 1.4A).^{32,33} The reduced electrophilicity of these donor/donor carbenes enables the high stereoselectivity of these intramolecular reactions and the high functional group tolerance

exhibited. Albeit less reactive, donor/donor carbenes in C–H insertion reactions still have common by-products that may form through the reaction, especially when using our lab's developed one-pot oxidation to C–H insertion procedure.³⁴ Depending on the rate of diazo formation, carbene formation, and C–H insertion, three main by-products can result (Figure 1.4B). If hydrazone **17** is still left over when the dirhodium catalyst is added to the reaction, then hydrazone **17** can react with carbene **19** to form imine **21**, which can be hydrolyzed to the ketone **22** upon reaction workup. Diazo **18** can also react with metal carbene **19** to form azine **23** in instances where the insertion step is slow, or the concentration of the reaction is high. Finally, the metal carbene **19** can dimerize with itself to form alkene **24**. Surprisingly, O–H insertion with H₂O to form the alcohol **25** is rarely observed with our methodology, so much so that these reactions have been run in wet solvents with minor decreases in yield.

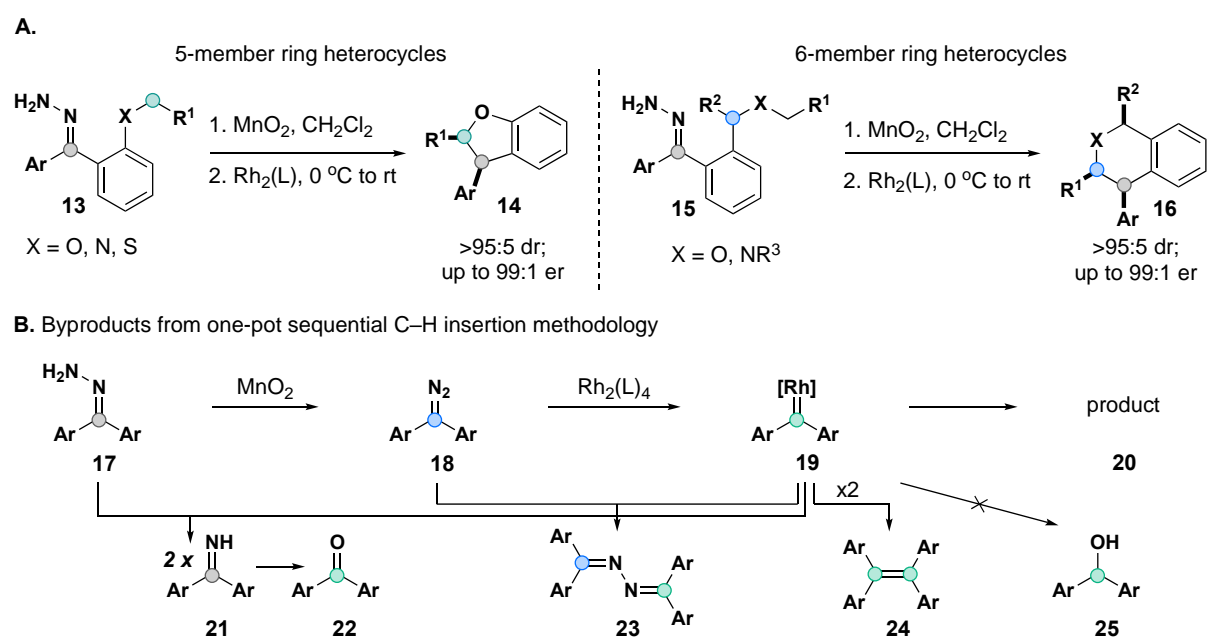


Figure 1.4 A. 5-member and 6-member ring heterocycles **B.** Common by-products observed in the one-pot sequential reactions.

Our group hypothesized that the less reactive donor/donor carbenes proceed through a stepwise mechanism similar to the Fox group's mechanistic proposal^{34,35} (Figure 1.5B). This mechanistic hypothesis is in contrast to donor/acceptor, acceptor/acceptor, and acceptor

carbenes, which proceed through a three-member concerted, asynchronous mechanism³⁶ (Figure 1.5A).

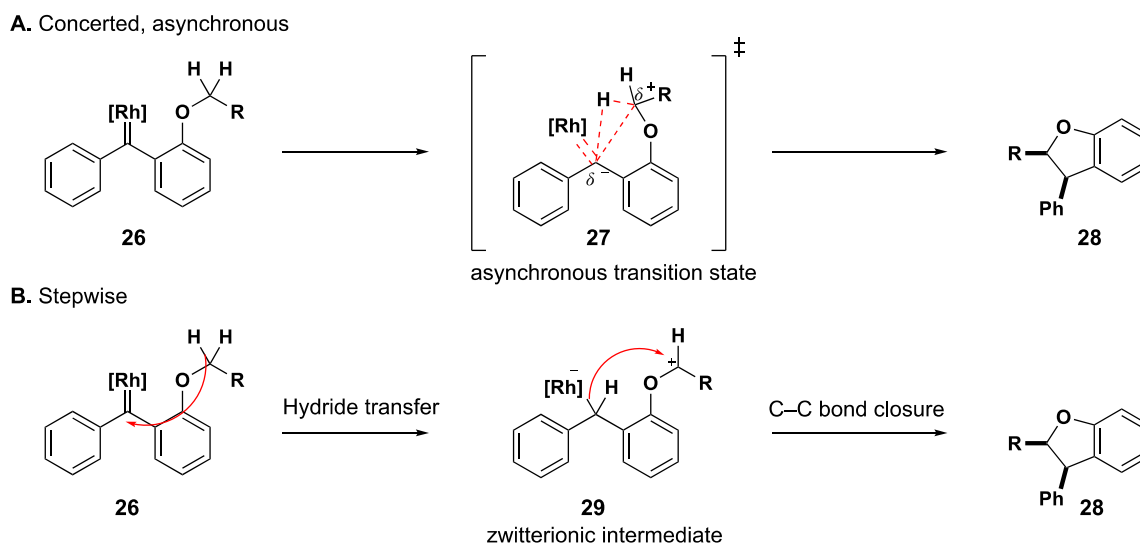


Figure 1.5 A. Concerted, asynchronous C–H insertion mechanism **B.** Stepwise C–H insertion mechanism.

Initially, computational studies in collaboration with the Tantillo group at UC Davis showed that two main steps occur in the stepwise mechanism once the dirhodium carbene (**26**) has been formed. First is the rate-limiting step, where a hydride species transfers from the C–H insertion center to the electrophilic metal-carbene. This step forms a ylide intermediate (**29**) with a carbocation on the former C–H insertion carbon. Second, the now nucleophilic metal center can attack the carbocation to form the new C–C bond. The factors governing the stereoselectivity at each reaction step remained largely unknown. Therefore, we sought to investigate the mechanism further by extending our intramolecular C–H insertion of donor/donor dirhodium carbenes methodology to stereogenic centers resulting in the synthesis of trisubstituted benzodihydrofurans (see section 1.1.2.4 for further discussion of this scaffold)

1.1.2 History of C–H insertions into stereogenic centers

Although few reports of C–H insertion reactions into stereogenic centers are found in the literature, they are mainly seen in some of the earlier work on C–H insertion reactions as useful experimental tools to build stereochemical and mechanistic reaction models. These model studies, beginning in 1973, laid the foundation for Nakamura's proposal in 2002 of a concerted, asynchronous mechanism for C–H insertion reactions (Figure 1.6). However, all the experimental studies with chiral insertion centers that supported this mechanistic proposal only used acceptor containing carbenes. Thereby not covering donor/donor carbene reactivity and the potential change in mechanism that our group had initially proposed. However, discussing these studies is an important point of comparison before launching into the design of the chiral ether stereochemical model system built by our group.

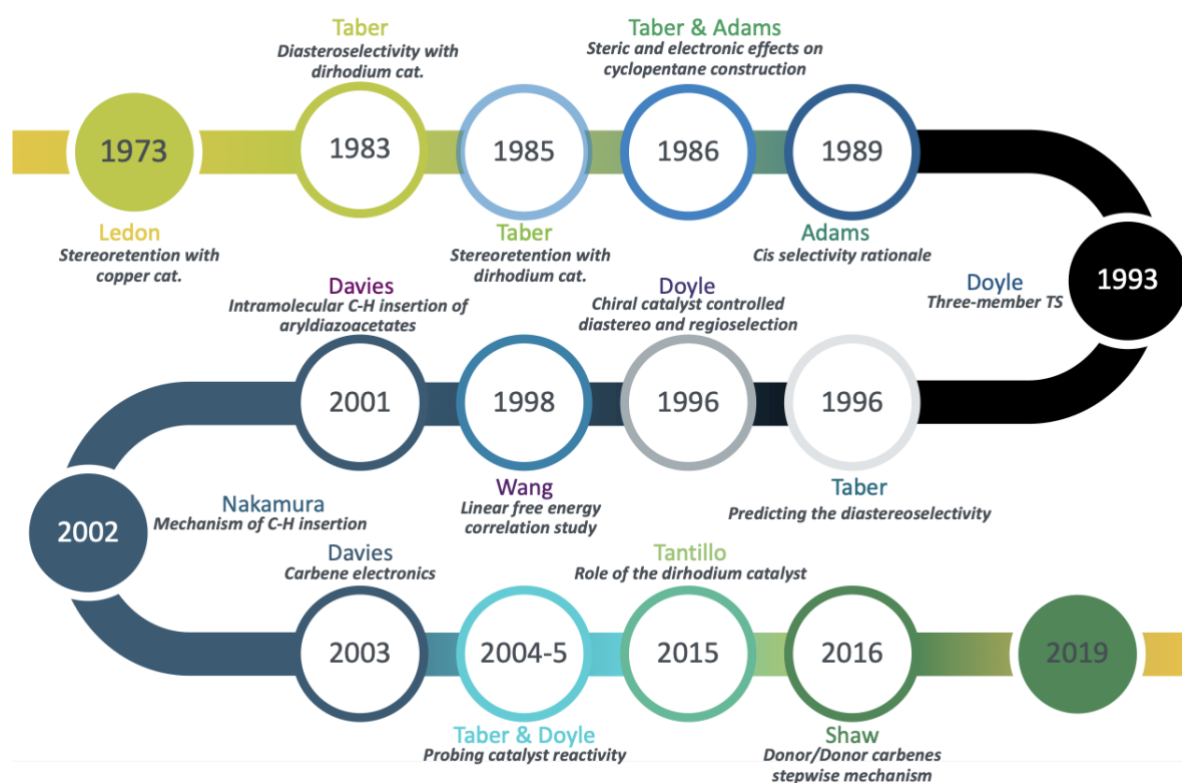


Figure 1.6 Timeline for stereochemical and mechanistic investigations into C–H insertions using tertiary and chiral insertion centers.

Ledon, in 1973, sought to study if an intramolecular C–H insertion with an acceptor/acceptor diazo precursor was a stereoretentive or stereoinvertive process (Figure 1.7 panel A).³⁷ The single *S*-enantiomer of the diazo precursor (**30**) was made and then heated with Cu in chlorobenzene to yield the C–H insertion product **31**. Subsequent ester hydrolysis, decarboxylation, and oxidative opening of the lactone resulted in (*S*)-2-ethyl-2-methylsuccinic acid (**33**), whose optical rotation could be matched to a known standard. This was necessary to confirm that the insertion stereocenter was the *S* configuration. Ledon and colleagues thus referred to the C–H insertion as stereoretentive since the starting material's chiral insertion center was the (*S*) configuration (**30**), and the resulting product was also the (*S*) configuration (**33**). This became the first published result on the stereorention of the insertion center for copper-catalyzed intramolecular C–H insertion systems. Notably, at the time, since this field was still in its infancy, Ledon never used the term carbenoid or metal carbene to describe the active intermediate. Rather, it was hypothesized that the insertion occurred through a free carbene intermediate, with copper acting as a catalyst to promote diazo decomposition.

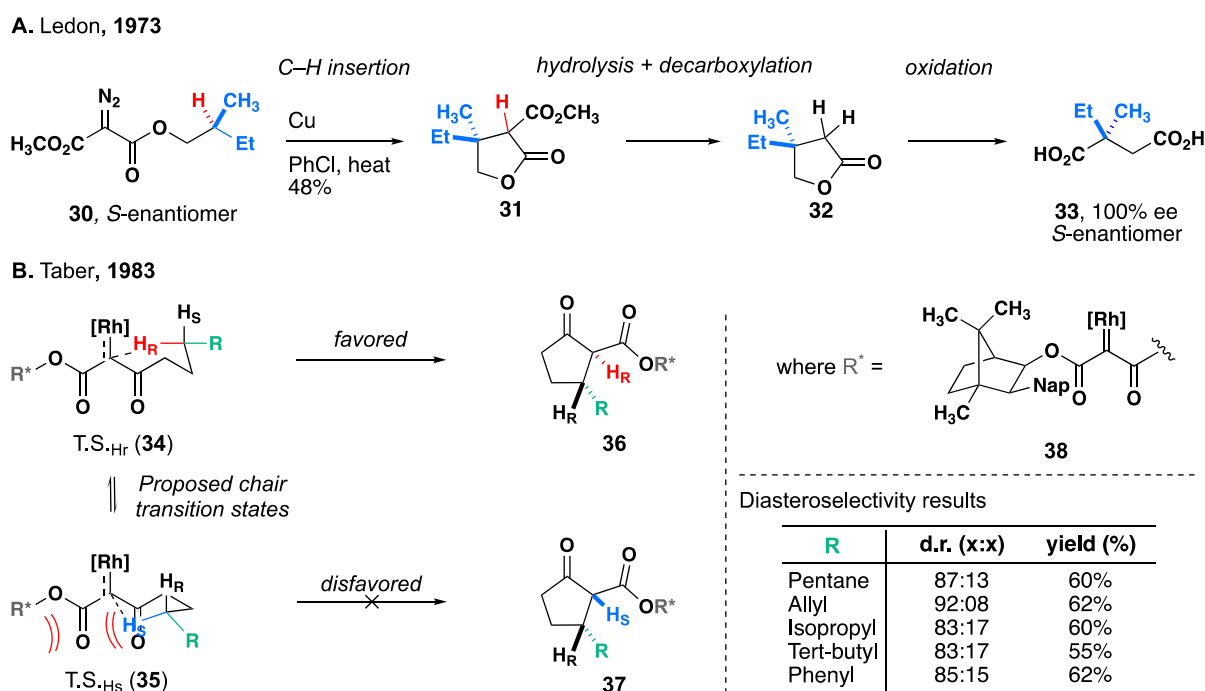


Figure 1.7 A. Ledon's early observations on stereoretention B. Taber's diastereoselective methodology via chiral induction.

A decade later, dirhodium catalysts emerged as the preferred catalyst for forming the hypothesized metal carbenoid intermediate. Using the achiral dirhodium catalyst, $\text{Rh}_2(\text{OAc})_4$ (**6**), Taber in 1983 investigated how a stereogenic center elsewhere on the molecule would affect the intramolecular C–H insertion of an acceptor/acceptor carbene (Figure 1.7B).¹⁷ They hypothesized that the intramolecular C–H insertion underwent a highly ordered transition state due to its substantial preference for 5-membered ring formation (i.e., a chair transition state), and therefore a stereogenic center elsewhere on the molecule could influence the diastereo- and enantioselectivity of the reaction by preferencing either H_R (**34**) or H_S (**35**). They found that a bulky chiral ether containing a naphthalene group (**38**) destabilized the H_S transition state through nonbonding interactions where the naphthalene group covers the front face of the β -keto ester. Therefore, diastereomer **36** was the major product over **37**, even after varying the insertion center's R group.

Based on these initial stereochemical results, C–H insertions began to be applied to the synthesis of chiral natural products. Cane and coworkers were able to use an acceptor carbene (**40**) to insert into the tertiary bridged carbon center on a fused gamma lactone ring system (**41**) to build the third and final ring en route to racemic pentalenolactone E (**42**) (Figure 1.8A).³⁸ They even tried building the 5-5 fused ring system (**39**) via another acceptor/acceptor carbene-based C–H insertion reaction (**43**). However, they quickly discovered that insertions into tertiary C–H bonds were kinetically favored over insertion into secondary C–H bonds resulting in a mixed ratio of spirocycle **45** and pentalenolactone **44**. Attempts were made to increase the yield of the fused gamma lactone ring system (**44**) from C–H insertion by using a more complex substrate (**46**) containing a remote stereogenic center in a similar manner as Taber's chiral induction methodology. However, these attempts failed where the chiral induction increased the ratio of spirocycle **48** to the desired product **47** and decreased the overall yield due to the emergence of an unknown byproduct.

Shortly after, in 1985, Taber and coworkers reported the enantioselective synthesis of (+)- α -cuparenone (**51**) using a dirhodium-catalyzed intramolecular C–H insertion into an enantiopure tertiary center (Figure 1.8B).¹⁶ They observed full stereoretention of the insertion stereogenic center from diazo precursor **49** to cyclopentanone **50**. Absolute stereochemistry was proven by converting **50** to the homologated ester, a known compound, and comparing optical rotations. Therefore, this natural product synthesis confirmed that dirhodium-catalyzed intramolecular C–H insertion does indeed proceed with retention of absolute configuration.

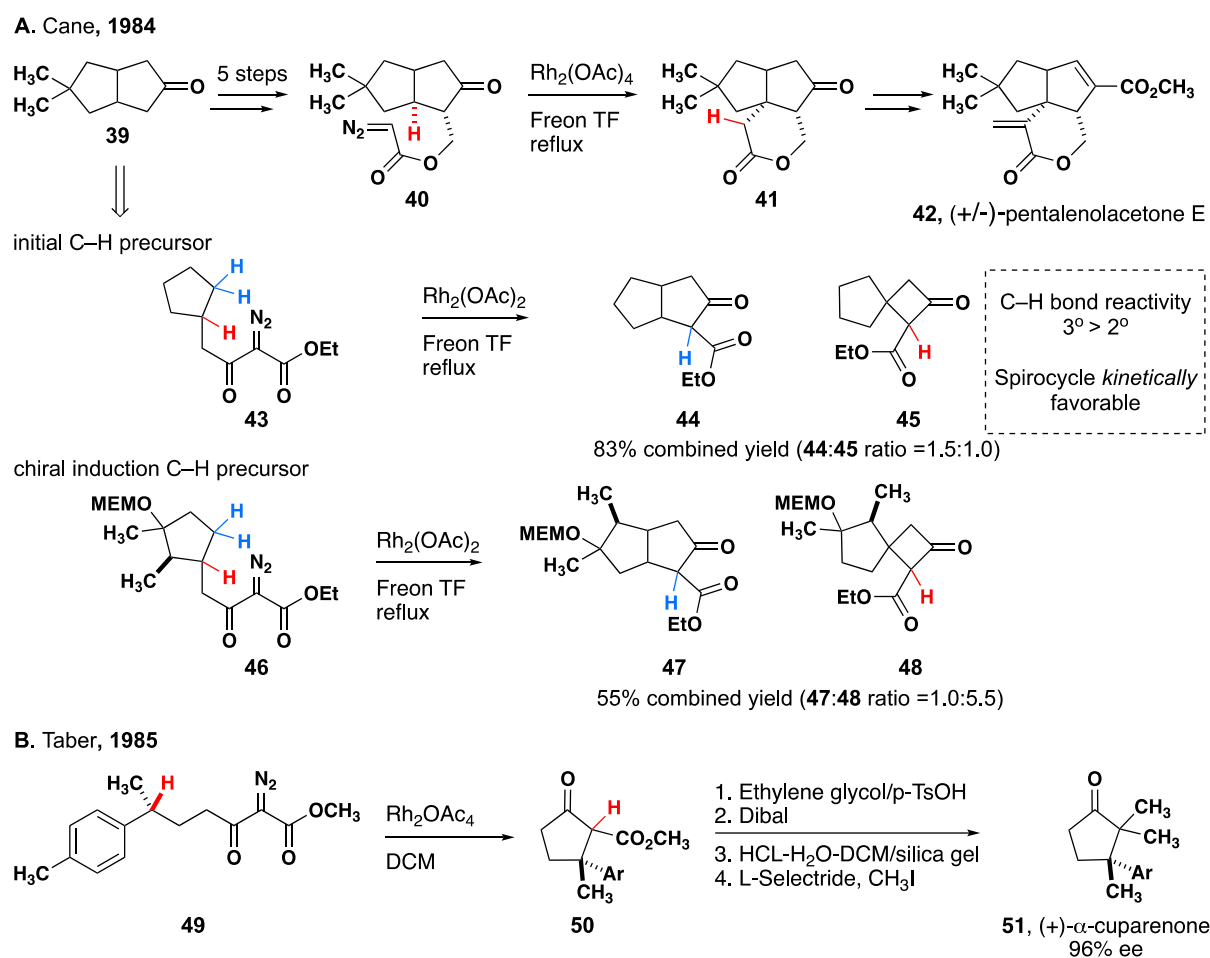


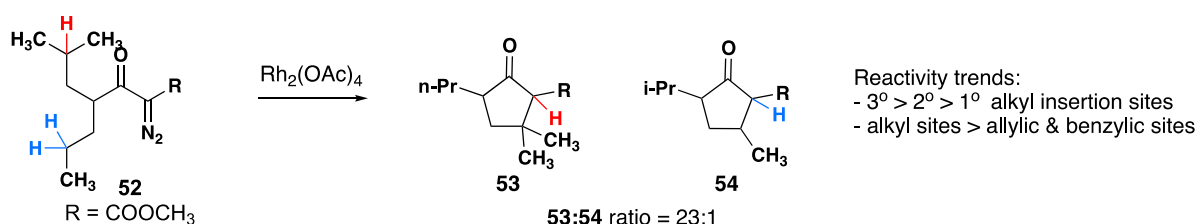
Figure 1.8 Early applications to natural product synthesis: **A.** Cane's synthesis of (+/-)-pentalenolactone E. **B.** Taber's enantioselective synthesis of (+)- α -cuparenone.

In summary, these two reports show how intramolecular C–H insertion became a popular method in the 1980s into the 1990s in natural product synthesis to help set the stereochemistry of the carbon adjacent to the acceptor group.

1.1.2.1 Substrate control: proposed stereoselectivity models

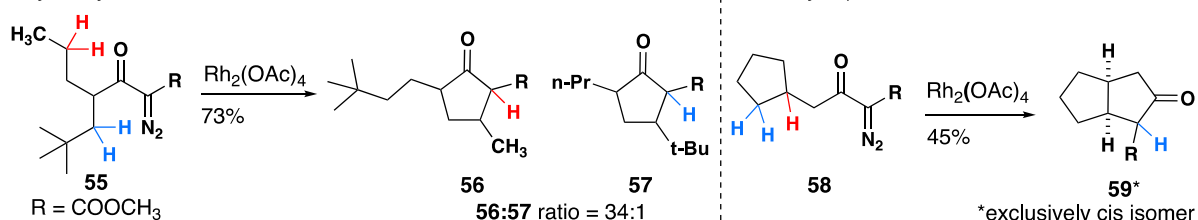
Whether chiral or not, tertiary insertion centers have been commonly used to build stereochemical models to study the electronic and steric effects on C–H insertion reactions. For example, Taber created a detailed study of the factors affecting the regioselectivity of the intramolecular, 5-member ring forming C–H insertion reactions (Figure 1.9).³⁹ By creating substrates like **52**, where two insertion sites could compete with each other for intramolecular cyclopentane formation, the reactivity of different electronically activated C–H bonds was accessed. It was shown that tertiary C–H bonds are more reactive (**53**) than secondary C–H bonds (**54**) which are more reactive than primary C–H bonds. Also, inactivated alkyl C–H insertion centers were always more reactive than allylic or benzylic sites.

Electronic effects



Steric effects

Acyclic systems



Fused cyclohexanes

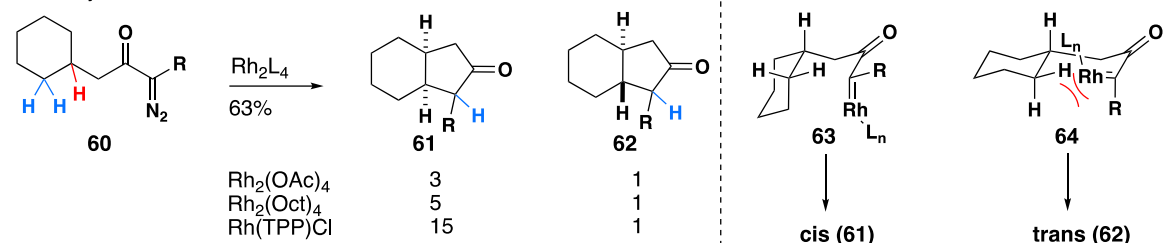


Figure 1.9 Cyclopentane construction by intramolecular C–H insertion: steric and electronic effects.

A similar dual insertion site substrate (**55**) was used to probe the steric influence on the C–H insertion regiochemistry. Insertion into the secondary site adjacent to a methyl group to produce **56** was almost exclusively favored over insertion into the secondary site adjacent to a tert-butyl group (**57**) in a 34 to 1 ratio of **56:57**. Multiple fused ring systems were then examined, where cyclopentane **82** formed exclusively the cis-fused bicyclooctanone **59** most likely due to the cis diastereomer being the largely thermodynamically preferred conformation. Meanwhile, C–H insertion into cyclohexane (**60**) produced a mix of both the cis (**61**) and trans (**62**) fused 6-5 bicyclic ring systems. This product ratio varied based on the dirhodium catalyst used, which was interpreted as evidence for a bound dirhodium carbene in the transition state. As the steric bulk on the catalyst increased, the cis diastereomer was increasingly favored, which was rationalized by the decreased steric interactions in the cis-chair-like transition state (**63**) over the trans-chair-like transition state (**64**). Therefore, the diastereoselectivity of these model systems appears largely controlled by steric interactions around the reacting C–H bond over the electronic activation of that bond.

Adams and coworkers in 1987 and 1989 also observed this preference for the cis-diastereomer in C–H insertion reactions to form 2,5-disubstituted furanones (Figure 1.10).^{40,41} They came to a similar conclusion that the diastereoselectivity of the reaction comes down to steric requirements in the transition state, specifically, how the insertion substrate docks into the catalyst pocket. In the case of the furanone precursors, the ether oxygen was proposed to coordinate with the dirhodium center in the transition state, thereby orienting the preferred conformation of the C–H insertion. In the proposed transition state, the C2 alpha hydrogen is either in a pseudo-axial (**65a**) or a pseudo-equatorial (**65b**) position leading to the cis **66a** and trans **66b** diastereomers, respectively (Figure 1.10A). Therefore, as the size of the C2 substituent increases, the trans diastereomer is disfavored, as seen in the product ratios for **70** vs. **71**. The substituent on C3 can also bump into the catalyst in the proposed trans-transition

state **65b**, resulting in higher diastereoselectivity observed for **72** and **66** versus **71** (Figure 1.10B).

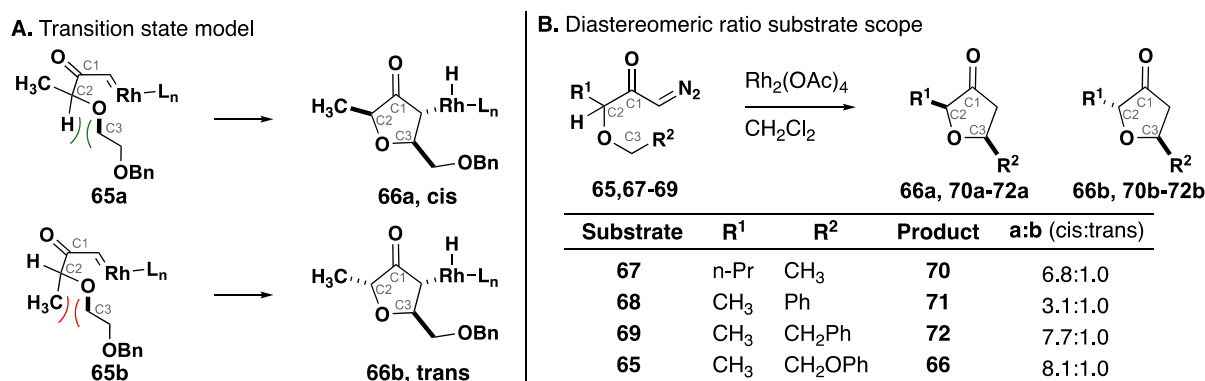


Figure 1.10 A. Stereochemical transition state models for furanone formation by C–H insertion. **B.** Diastereomeric ratio substrate scope.

One of the final big discoveries on how the C–H insertion precursor can affect the stereoselectivity of the reaction focused on the electronic activation of the C–H bond. In 1996, Taber hypothesized that in their synthesis of trisubstituted tetrahydrofurans, the C–H bond adjacent to the oxygen was more reactive than a normal alkyl C–H bond due to the increased electron density from the oxygen (Figure 1.11).³⁹ It was hypothesized that increased electron density/activation of the C–H bond would lead to an earlier 4-membered transition state (See section 1.1.2.3 Figure 1.16) where the chair-like preference isn't as pronounced. Therefore, the reaction is overall less selective. To test this theory, multiple diazo precursors (**73-77**) with varying R groups adjacent to the reacting C–H bond were synthesized, and the ratios of trans (**78-82a**) to cis (**78-82b**) products were measured. When electron-donating R groups like phenyl **73**, alkene **74**, and methyl **75** were present, there was only moderate selectivity for the trans diastereomer over the cis diastereomer. However, when the R groups were switched to more electron-withdrawing groups, like beta-methoxy **76** or beta-phenoxy **77**, the diastereoselectivity increased significantly, favoring the trans diastereomer. These experimental results supported Taber's theory that the electronic activation of the C–H bond

could affect the stereoselectivity of the reaction, where attenuating the electronic activation of the C–H bond delayed the point of commitment to bond formation in the 4-membered transition state thereby increasing the selectivity of the overall reaction.

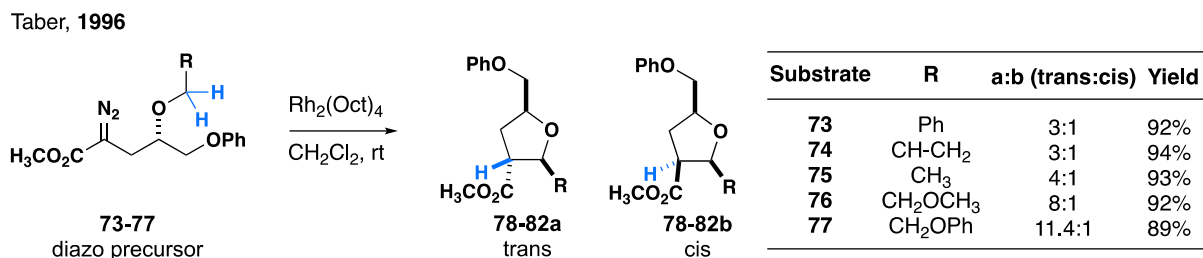


Figure 1.11 Diastereoselectivity as a function of the C–H bond electronic activation.

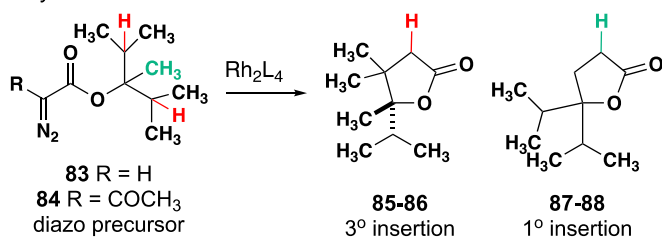
1.1.2.2 Catalytic control: proposed stereoselectivity models

The stereochemical models discussed in the previous section mainly focused on how the substrate imparts stereochemical control over product selectivity through electronic and/or steric factors. However, as C–H insertion research progressed into the 1990s, new dirhodium catalysts were synthesized and began to be used with the methodology resulting in contrasting stereochemical outcomes and models. One of the first such studies was conducted by Doyle and coworkers in 1989⁴², where they claimed that Taber's work in 1986⁴³ (Figure 1.9) generalized reactivity of C–H bonds based on the substitution of the carbon was not practical. Doyle claimed that the stereo-electronic factors governing product formation could not be reduced to a generalization in more complex systems. The steric interactions with the catalyst played a much larger role in product selectivity (Figure 1.12). Doyle demonstrated how the choice of dirhodium catalyst could drastically change the regioselectivity of the reaction for both acceptor (**83**) and acceptor/acceptor carbenes (**84**). For example, the use of Rh₂(acam)₄ greatly favored insertion into the tertiary C–H bond (Figure 1.12 entries 5-6) versus Rh₂(pfb)₄ showed little to no preference for the primary over the tertiary C–H bond (Figure 1.12 entries

1-2). The traditional $\text{Rh}_2(\text{OAc})_4$ catalyst resulted in very different regioselectivity based on the type of carbene used (Figure 1.12 entries 3-4).

Doyle, 1989

Acyclic substrates



Entry	R	Catalyst	3°:1°	Yield
1	H	$\text{Rh}_2(\text{pfb})_4$	32:68	56%
2	COCH ₃	$\text{Rh}_2(\text{pfb})_4$	45:55	45%
3	H	$\text{Rh}_2(\text{OAc})_4$	53:47	81%
4	COCH ₃	$\text{Rh}_2(\text{OAc})_4$	90:10	90%
5	H	$\text{Rh}_2(\text{acam})_4$	99:1	96%
6	COCH ₃	$\text{Rh}_2(\text{acam})_4$	99:1	99%

Catalyst Structures

Cyclic substrates

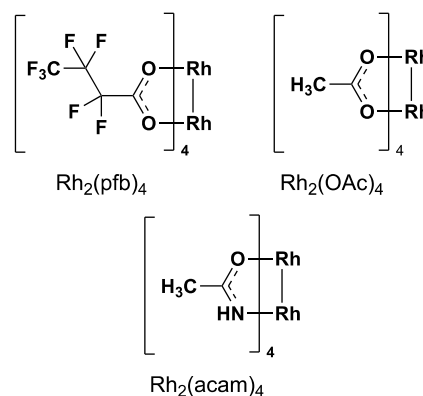
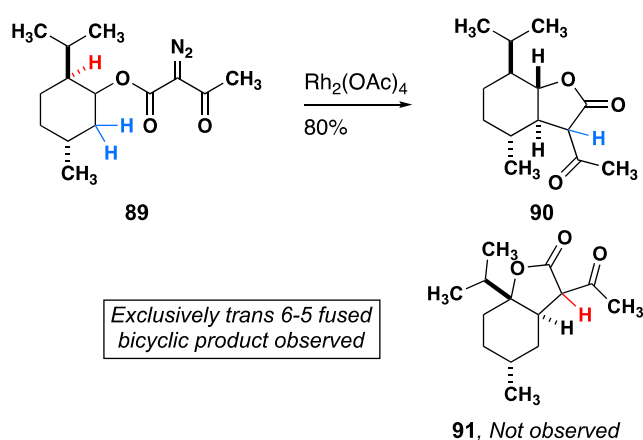


Figure 1.12 Doyle's observations refute Taber's simplified C–H bond reactivity model.

The final nail in the coffin to refute Taber's reactivity scale was a C–H insertion into a highly substituted cyclohexane **89** with both a tertiary and secondary center readily available to form the fused 6-5 bicyclic product. When $\text{Rh}_2(\text{OAc})_4$ was utilized, the trans ring fusion product **90** resulting from insertion into the secondary center was exclusively formed, where no product resulting from the tertiary C–H bond was observed (**91**) even though this should've been the more kinetically reactive bond according to Taber.

Two years later, Taber countered Doyle's claims of the significance of the catalyst pocket over reaction selectivity by showing how a C–H insertion into chiral tertiary center **92** always resulted in the exclusive formation of the cis diastereomer **93** (Figure 1.13).⁴⁴ Rather, variations in the catalyst pocket affected the chemoselectivity of the reaction resulting in

differing ratios of the single diastereomeric insertion product (**93**) and the β -hydride elimination product (**94**). Taber stated that these experimental results suggest a highly ordered transition state that reflects the stereoelectronic effects observed by his group in 1986 as opposed to Doyle's model system published in 1989.

Taber, 1991

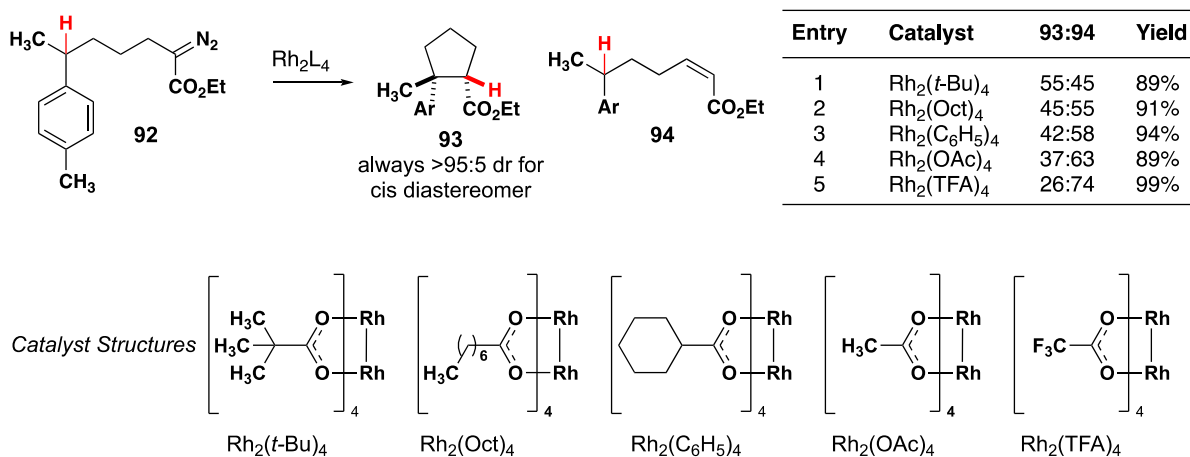


Figure 1.13 Taber 1991 highly diastereoselective C–H insertion into a stereogenic center.

This report was shortly countered again by a paper from Doyle in 1994 that showcased both enantio- and diastereocontrol using their recently published chiral carboxamide catalysts, MEPY (**99**), MEOX (**100**), and MACIM (**101**) (Figure 1.14).⁴⁵

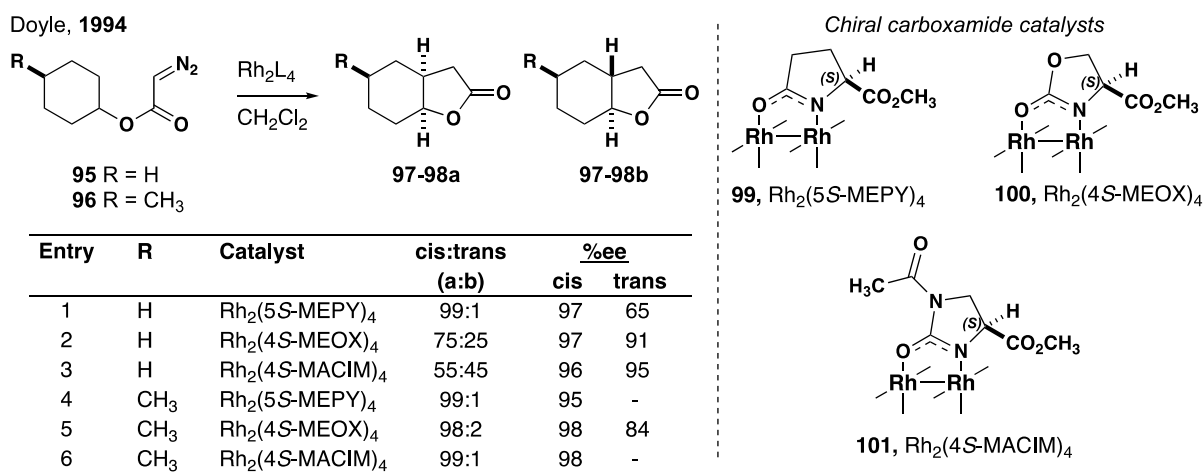


Figure 1.14 Enantio- and diastereocontrol using chiral carboxamide catalysts.

Insertion into different cyclohexanes with an acceptor carbene resulted in fused cyclohexane bicycles with varying levels of diastereoselectivity (dr) and enantioselectivity (er) based on the

catalyst used. For the unsubstituted cyclohexane substrate **95**, Rh₂(5*S*-MEPY)₄ gave the highest dr with a 99:1 ratio of cis:trans (**97a:97b**) with the major diastereomer in 97 % ee. However, using the other two chiral carboxamide catalysts resulted in a drop in diastereoselectivity but not enantioselectivity. Extending the system to a C–H insertion into a substituted cyclohexane **96** drastically increased diastereoselectivity towards the cis diastereomer (**98a**) while maintaining a high enantioselectivity (% ee). This is most likely due to chiral induction effects from the methyl substituent, analogous to what Cane reported in 1984³⁸ (see Section 1.1.2 Figure 1.8)

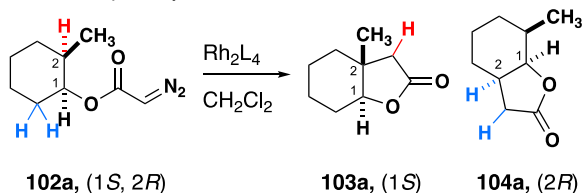
Doyle's studies with the chiral carboxamide catalysts showcased the effect of the chiral catalyst environment on selectivity when interacting with starting material with a remote stereogenic center. However, the question arose, what would occur if the C–H insertion sites were stereogenic centers? Doyle's group answered this in 1996 when they reported an exhaustive investigation into enantiomeric differentiation, also known as when a chiral catalyst prefers one enantiomer of starting material over the other (Figure 1.15).⁴⁶ This study was done by creating match/mismatched pairings of single enantiomers of starting material with each enantiomer of the catalyst and assessing how it affected the selectivity of the reaction.

For both enantiopure (1*S*, 2*R*) cyclohexane **102a** and (1*R*, 2*S*) cyclohexane **102b**, the matched pairings (Figure 1.14A) resulted in high regioselectivity for the 3° insertion site (**103a/b**). Interestingly, the mismatch pairings completely changed the regioselectivity resulting in C–H insertion into the 2° insertion site (**104a/b**). Notably, all the diastereomers were single enantiomers, supporting Ledon's³⁷ and Taber's¹⁶ findings on stereoretention of the insertion center for enantiopure starting material. Match/mismatch pairings completely changing the selectivity of C–H functionalization reactions have been observed before in the cyclopropanation of secondary allylic diazoacetates. In the cyclopropanation methodology,

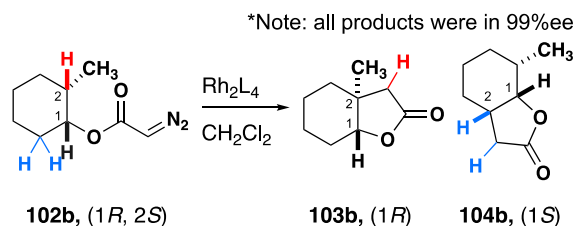
individual enantiomers of starting material produce different diastereomers based on the enantiomer of dirhodium catalyst used.

Doyle, 1996

A. Enantiopure cyclohexane substrates*



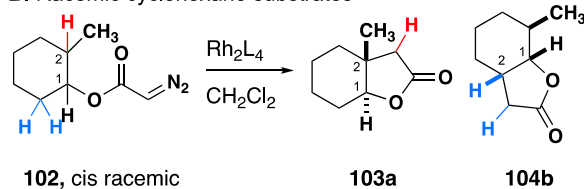
Catalyst	yield	103a : 104a	
$\text{Rh}_2(5S\text{-MEPY})_4$	95%	94 : 1	match
$\text{Rh}_2(5R\text{-MEPY})_4$	79%	4 : 91	mismatch



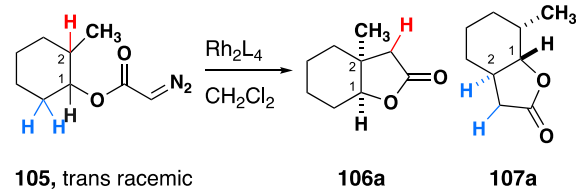
Catalyst	yield	103b : 104b	
$\text{Rh}_2(5S\text{-MEPY})_4$	86%	5 : 90	mismatch
$\text{Rh}_2(5R\text{-MEPY})_4$	74%	92 : 3	match

*Note: all products were in 99% ee

B. Racemic cyclohexane substrates



Catalyst	yield	103a	104b
$\text{Rh}_2(5S\text{-MEPY})_4$	75%	45	49
		(91% ee)	(98% ee)



Catalyst	yield	106a	107a
$\text{Rh}_2(5S\text{-MEPY})_4$	85%	49	40
		(80% ee)	(93% ee)

C. Selectivity rationale using transition state models

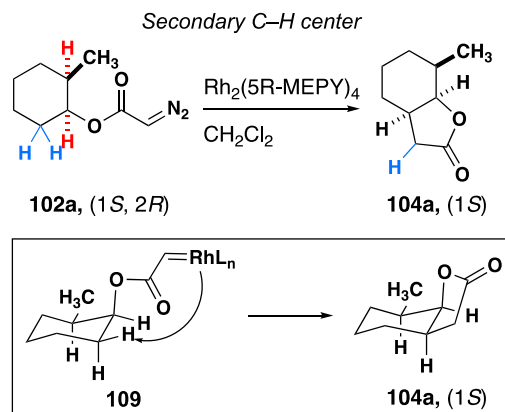
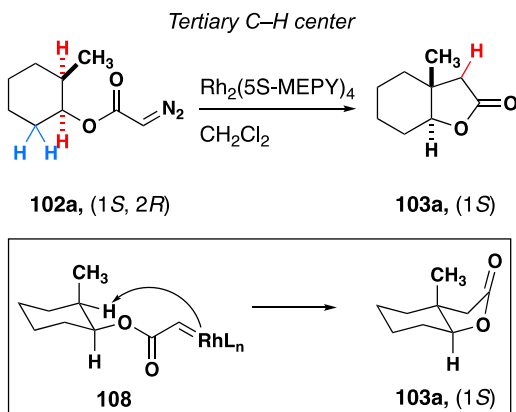


Figure 1.15 Match-mismatch experiments: **A.** Enantiopure starting material **B.** Racemic starting material **C.** Rationalization in the transition state.

These observations are backed up by both cis racemic (**102**) and trans racemic (**105**) starting cyclohexanes, giving about a 1:1 ratio of both regioisomers regardless of the enantiomer of catalyst used. The match/mismatch pairing that changes the regiochemistry is based on the

chair transition state for these C–H insertion substrates. In the matched pairings' transition state (**108**), there is almost exclusive insertion into the equatorial C–H bond at the more reactive 3° insertion center. However, in the mismatch pairings' transition state (**109**), insertion into the 3° center utilizes an axial C–H bond; therefore, the 2° equatorial C–H bond is significantly more favorable, resulting in the changing of the regiochemical preference of the reaction. Access to axial C–H bonds is highly disfavored due to crowding of the cyclohexane ring into the chiral catalyst ligands, once again demonstrating the dirhodium catalyst's power over the selectivity of C–H insertions reactions with chiral insertion centers.

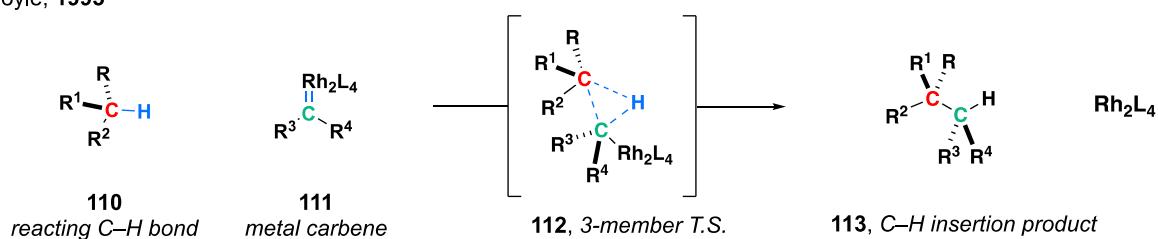
1.1.2.3 Mechanism proposals

Mechanistic models were proposed in the early 1990s due to the mounting experimental stereochemical data for C–H insertion reactions. The first proposal was by Doyle in 1993, who hypothesized that the reaction was undergoing a concerted three-member transition state (**112**) (Figure 1.16A).⁴⁷ Where overlap of the metal carbene's p-orbital with the sigma orbital of the reacting C–H bond initiates the reaction in which C–C and C–H bond formation with the carbene carbon proceeds at the same time as the dirhodium catalyst dissociates. The mechanism accounted for Doyle's previous experimental work⁴², where lower selectivity is observed when catalysts with electron-withdrawing groups are used. Increased electron withdrawal by the ligands increases the electrophilicity of the dirhodium carbene. It causes bond formation to occur at a greater distance from the reacting C–H bond, also known as an earlier transition state, resulting in lower selectivity. Calculated energy differences of intermediates and transition states in the proposed three-member mechanism enabled Doyle to make four main conclusions: 1. The stereoelectronic factors governing the C–H insertion for a class of substrates is always catalyst dependent 2. In systems where each of the possible sites for insertion has equal probability (equal number of C–H bonds), the electronic influences from

substituents will determine the regiochemistry 3. Decreases in the electrophilicity of the carbene via the catalyst ligands will increase the selectivity by preferring a later transition state 4. In systems where each of the possible sites for insertion don't have equal probability, then steric and conformational interactions will determine the regioselectivity. Notably, changing the catalyst electrophilicity will have little effect on the selectivity.

A. Concerted three-membered T.S. mechanism

Doyle, 1993



B. Four-membered T.S. mechanism

Taber, 1996

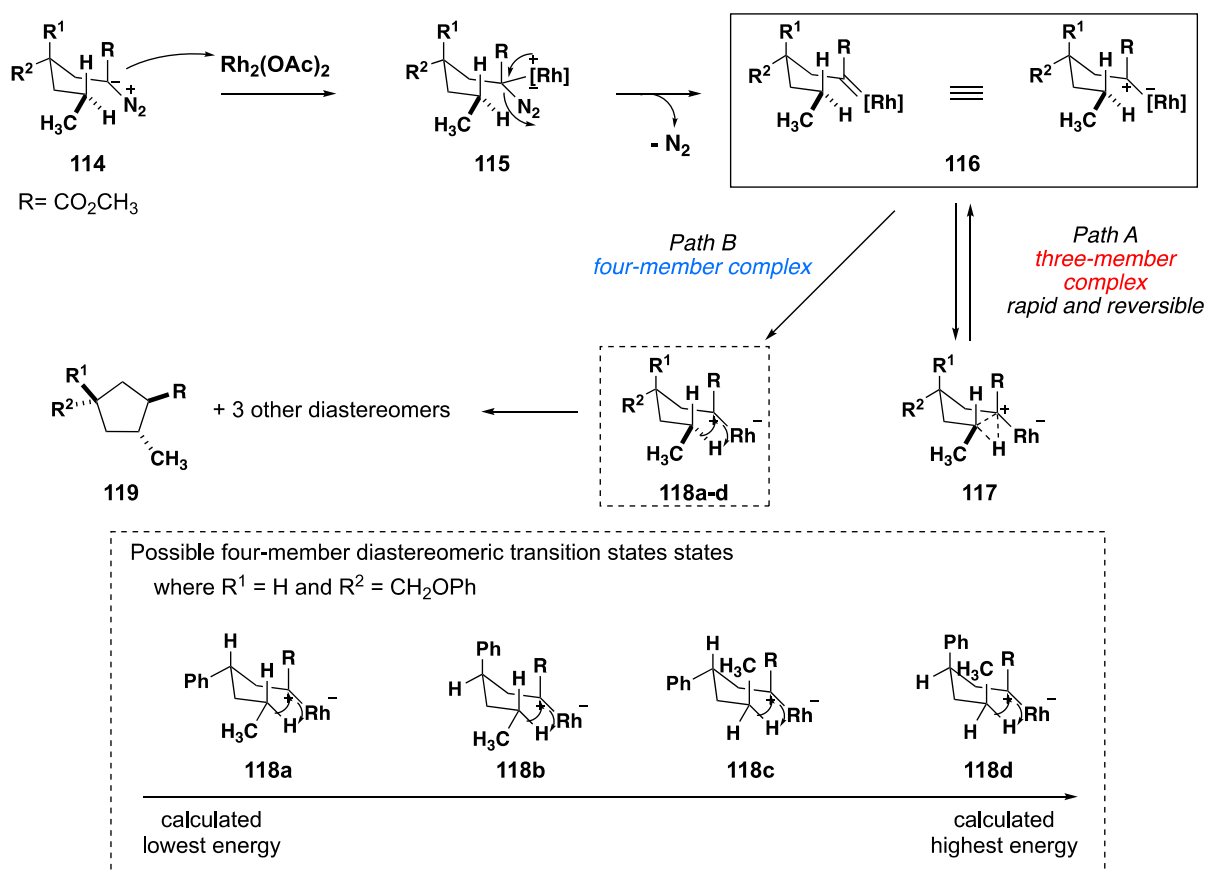


Figure 1.16 A. Doyle's concerted three-member C–H insertion mechanism B. Taber's four-member C–H insertion mechanism.

The second mechanistic proposal was from Taber in 1996, where a four-member transition state mechanism was proposed for the synthesis of trisubstituted tetrahydrofurans via C–H insertion (Figure 1.16B).^{39,48} It was proposed that the starting diazo ester (**114**) will bind to the dirhodium catalyst (**115**) and extrude nitrogen gas to form metal carbene (**116**). From the metal carbene intermediate **116**, the three-member complex (**117**) originally proposed by Doyle can form. However, it is in rapid, reversible equilibrium with the metal carbene **116**. Meanwhile, **116** can form a four-membered chair-like transition state (**118a-d**) with the more activated C–H bond sigma orbital adjacent to the ether oxygen and the metal carbene p orbital. There are four possible diastereomeric chair-like transition states (**118a-d**) that each lead to one of the four possible diastereomers. Using computation, Taber and his co-workers showed that transition state **118a** was the lowest in energy by 3.5 kcal/mol due to both substituents being in the equatorial position in the pseudo-chair. Transition state **118a** led to the predicted major diastereomer **119**, verified by experimental data as the major diastereomer.

A Hammett plot analysis was published shortly after these mechanistic proposals by Wang and co-workers in 1998 (Figure 1.17).⁴⁹ This study aimed to access electronic effects on intramolecular C–H insertion reactions with Rh(II) carbenoids while minimizing possible steric effects that could influence the mechanism. To do so, acyclic benzylic C–H insertion substrates (**120a-g**) were synthesized, originally designed by Taber in 1986 (see section 1.1.2.1 Figure 1.9), where the system's electronics could easily be varied by changing the X-group in the para position. Then the relative reactivities of each substrate were quantified by expressing the relative reaction rate in terms of the final product ratio of benzylic C–H insertion **122a-g** to 2° alkyl C–H insertion **121a-g** using equation 1.1.

$$\text{Equation 1.1. } \frac{k_X}{k_H} = \frac{k_X/k_A}{k_H/k_A} = \frac{[\frac{\mathbf{122a-f}}{\mathbf{121a-f}}]_X}{[\frac{\mathbf{122g}}{\mathbf{121g}}]_H} = \frac{[\text{product ratio}]_{\text{para substituted substrate}}}{[\text{product ratio}]_{\text{unsubstituted substrate}}}$$

Where k_A (rate of alkyl C–H insertion) is assumed to be constant across each different substrate reaction, k_X (rate of benzylic C–H insertion with para substituents) is variable based on the electronics of each substrate, and k_H is the rate of benzylic C–H insertion with no para substituent present. Using this equation, six different substituted substrates (**120a-f**) were tested across three different catalysts. The corresponding relative rates were plotted to obtain a Hammett plot and constant for each catalyst (Figure 1.17B).

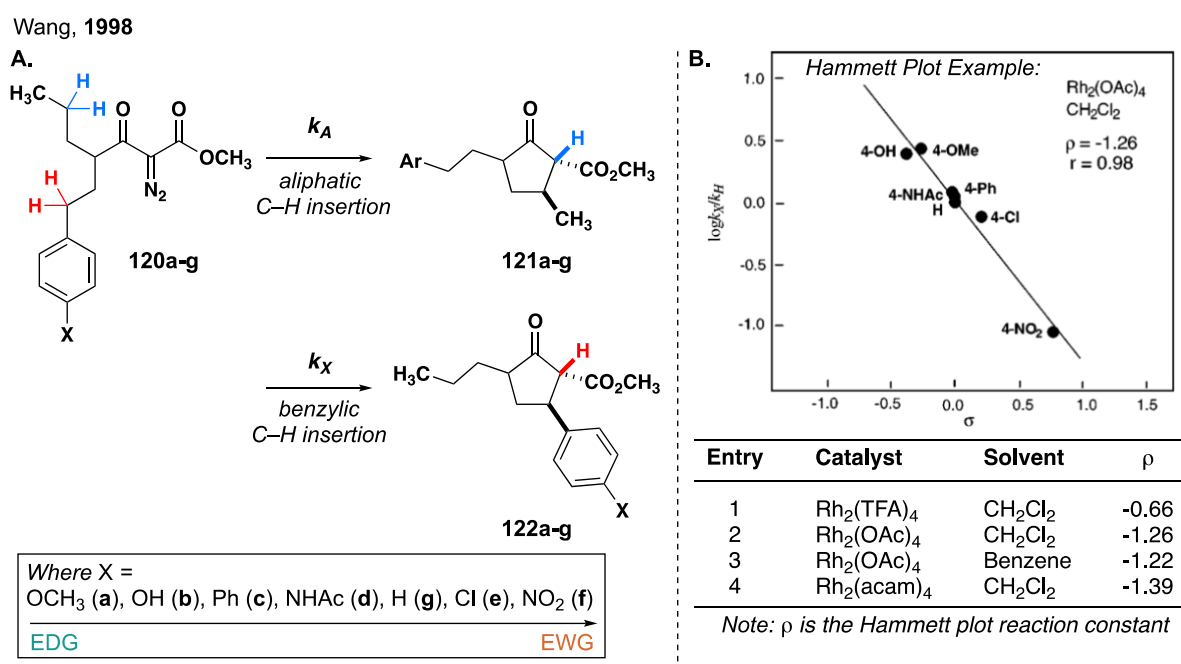


Figure 1.17 Hammett plot analysis of intramolecular C–H insertion reactions with dirhodium carbenes. **A.** Reaction scheme **B.** Hammett plot and calculated constants.

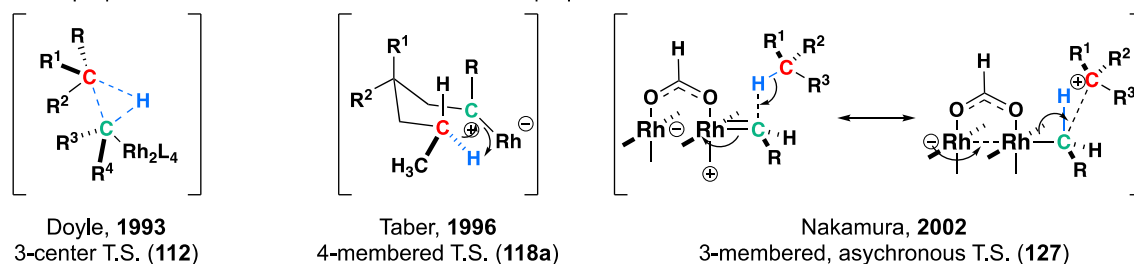
From the Hammett plot analysis, there are three main conclusions: 1. The electronic property of the diazo precursor system significantly affects the reaction 2. There is no significant solvent effect for intramolecular C–H insertions 3. The data supports Doyle’s proposed three-center complex⁴⁷ as the transition state and illustrates the catalyst ligand effect on reaction selectivity (Figure 1.17B). First, the high correlation coefficients on the Hammett plots demonstrate the strong linear free energy relationship between the electronic character of the diazo precursor and the rate of C–H insertion. Second, almost identical Hammett plot reaction constants for

$\text{Rh}_2(\text{OAc})_4$ in CH_2Cl_2 and benzene (Figure 1.17 entries 2-3) show that solvent has little to no effect on the rate of the reaction. Third, these findings correlate to Doyle's proposed mechanistic model since small, negative Hammett constants support a concerted mechanism with a small partial positive development at the C–H carbon atom. Also, Doyle's model proposes that the increased electron-withdrawing ability of the dirhodium ligands leads to earlier transition states and, therefore, a more reactive catalyst and faster C–H insertion result, albeit potentially less selective reaction. This is supported by the Hammett plots where the more electron-withdrawing $\text{Rh}_2(\text{TFA})_4$ catalyst has a much smaller reaction constant (Figure 1.17 entry 1) versus the classical $\text{Rh}_2(\text{OAc})_4$ (Figure 1.17 entries 2-3) or the most electron-rich catalyst $\text{Rh}_2(\text{acam})_4$ (Figure 1.17 entry 4).

The culmination of all these mechanistic experiments and proposals arrived in 2002 when Nakamura and colleagues used DFT studies to propose the mechanism for a concerted, asynchronous C–H insertion reaction catalyzed by $\text{Rh}_2(\text{OAc})_4$ (Figure 1.18A).³⁶ Using B3LYP level theory, key intermediates with their corresponding energies and geometries were calculated. All the calculations reproduced already published experimental data on C–H insertions, such as the activation enthalpy of the nitrogen extrusion step, the kinetic isotope effect observed, and the reactivity order of C–H bonds. The Nakamura mechanism has become the widely accepted mechanism for C–H insertions using acceptor, acceptor/acceptor, and donor/acceptor carbenes precursors, and the full proposed mechanism is as follows. First, the dirhodium catalyst **6** attacks the diazo carbon **123** to form **124**. Then, back donation from the Rh $4d_{xz}$ orbital into the C–N σ^* orbital causes nitrogen extrusion to yield metal carbene complex **125**. This carbene now has a vacant 2p orbital (**129**), making it a highly electrophilic center stabilized by Rh $4d_{xz}$ back-bonding (**131**). From the metal carbene, C–H activation/hydride transfer and C–C formation happen in a quick (low activation barrier calculated), single asynchronous step (**127**) to form the C–H insertion product **128** and

regenerate the dirhodium catalyst **6**. Interestingly, these computations showed that only one rhodium interacts with the carbene, while the other acts as a mobile ligand for the first one to help enhance the metal carbene's electrophilicity and facilitate the cleavage of the rhodium-carbon bond.

A. Previous proposed transition states versus Nakamura's proposal



B. Calculated reaction intermediates with $\text{Rh}_2(\text{OAc})_4$ and B3LYP level of theory

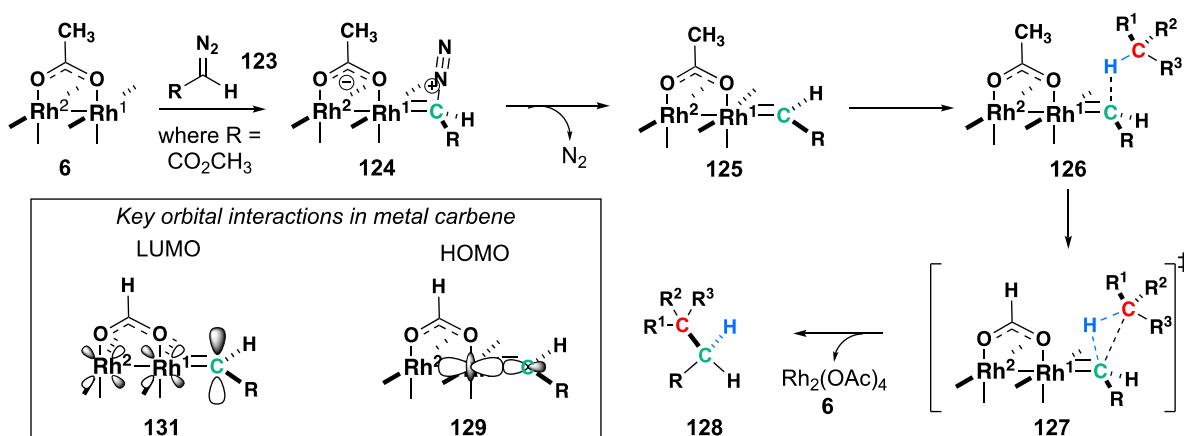


Figure 1.18 **A.** Comparison of Taber's, Doyle's, and Nakamura's transition states **B.** Calculated reaction intermediates for the C–H insertion of acceptor carbenes with $\text{Rh}_2(\text{OAc})_4$.

This work, along with the experimental evidence, culminates in a concerted, asynchronous mechanism for acceptor-based carbene C–H insertions with five key findings about C–H insertion reactivity and selectivity:

1. Activation enthalpy of $\text{Rh}_2(\text{OAc})_4$ catalyzed nitrogen extrusion is the rate-limiting step of the catalytic cycle for secondary C–H insertions.⁵⁰
2. Kinetic isotope effects of C–H bond activation depend on the nature of the carboxylate ligands in the dirhodium catalysts.⁵¹

3. Qualitative structure/reactivity correlation indicates $1^\circ < 2^\circ < 3^\circ$ from least to more reactive C–H bonds and are further enhanced when next to a heteroatom.^{41,43,47}
4. Carboxylate ligands affect the regio- and stereoselectivity.^{49,52,53}
5. Retention of the carbon center configuration at which the C–H insertion occurs.¹⁶

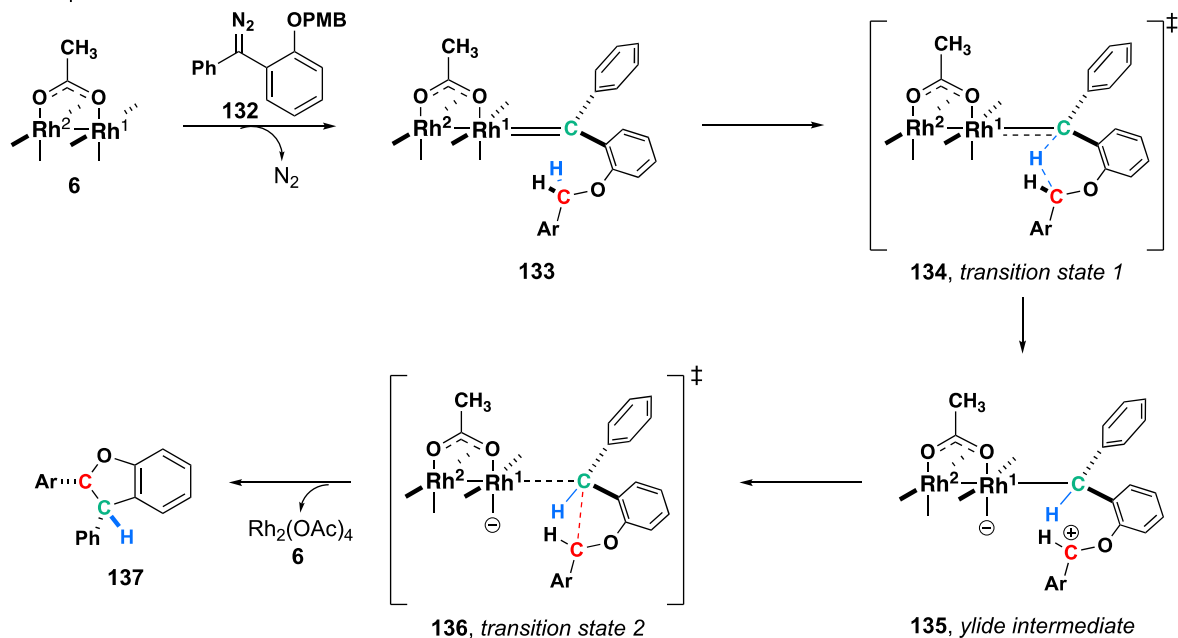
Since 2002, these key findings have held throughout two decades of further experimental and theoretical research with acceptor-containing dirhodium carbene C–H insertions. However, none of these studies examined carbenes with a sole donor group or two pendant donor groups.

When our group published our initial results²⁴ on the intramolecular C–H insertion of donor/donor carbenes with dirhodium catalysts, we hypothesized that these donor/donor carbenes could be undergoing a stepwise mechanism rather than a concerted, asynchronous mechanism. The stepwise hypothesis originated from differences in stereoselectivity we had observed from reported literature and experimental studies published by Joe Fox's group at the University of Delaware on intramolecular cyclopropanation reactions to form cyclobutanes.³⁵ Therefore, the possibility of a stepwise mechanism was explored by our lab via DFT calculations in collaboration with the Fox Lab at UD (Figure 1.19).³⁴ $\text{Rh}_2(\text{OAc})_4$ (**6**) was modeled with an aryl/aryl diazo (**132**) to form a donor/donor carbene (**133**). Two transition states were located, one for hydride transfer (**134**) and one for C–C bond closure (**136**). The barrier between the ylide intermediate **135** and the second transition state (**136**) was very low but high enough to be a separate step. The low activation barrier for C–C bond closure made it a kinetically fast step which was hypothesized to account for the high stereoselectivity of the reactions (Figure 1.19B). These initial computations lent evidence for a stepwise mechanism and a vague rationale for the experimentally observed high enantioselectivity and cis selectivity. However, there were still a lot of unanswered questions surrounding what parts of the mechanism dictated the stereoselectivity, and more concrete experimental evidence of a

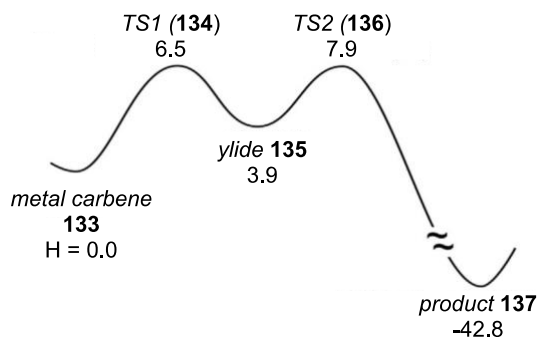
stepwise mechanism was needed since the high stereoselectivity could not be ruled out as coming from a concerted, asynchronous mechanism

Shaw, 2017

A. Stepwise reaction intermediates and transition states



B. Enthalpy ($kcal\ mol^{-1}$) vs reaction coordinate diagram



C. Computed transition state for syn versus anti selectivity

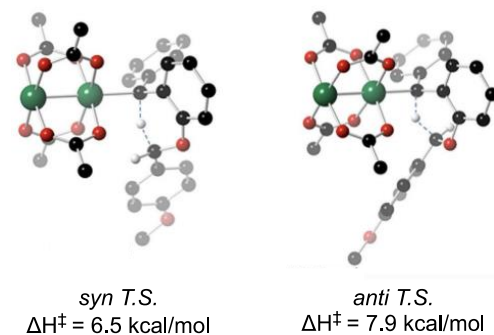


Figure 1.19 Shaw and Tantillo labs' initial stepwise mechanism proposal.

From these gaps in knowledge, the idea was born to build a chiral ether tertiary C–H insertion donor/donor carbene system to help elucidate key points of the mechanism while also creating a powerful methodology for forming trisubstituted benzodihydrofurans.

1.1.3 Tri-substituted 2,2,3-benzodihydrofurans

Benzodihydrofurans are plentiful throughout the natural product literature and the pharmaceutical realm. Trisubstituted benzodihydrofurans have been found in many natural products and patented small molecules, all possessing notable biological activity (Figure 1.20).^{54–63} However, the number of reported synthetic methods to access benzodihydrofurans decreases as the substitution on the core increases. None of the reported methods offer a generalizable method to form the trisubstituted benzodihydrofuran in an enantio- and/or diastereoselective fashion.

Highly substituted benzodihydrofuran cores in biological molecules

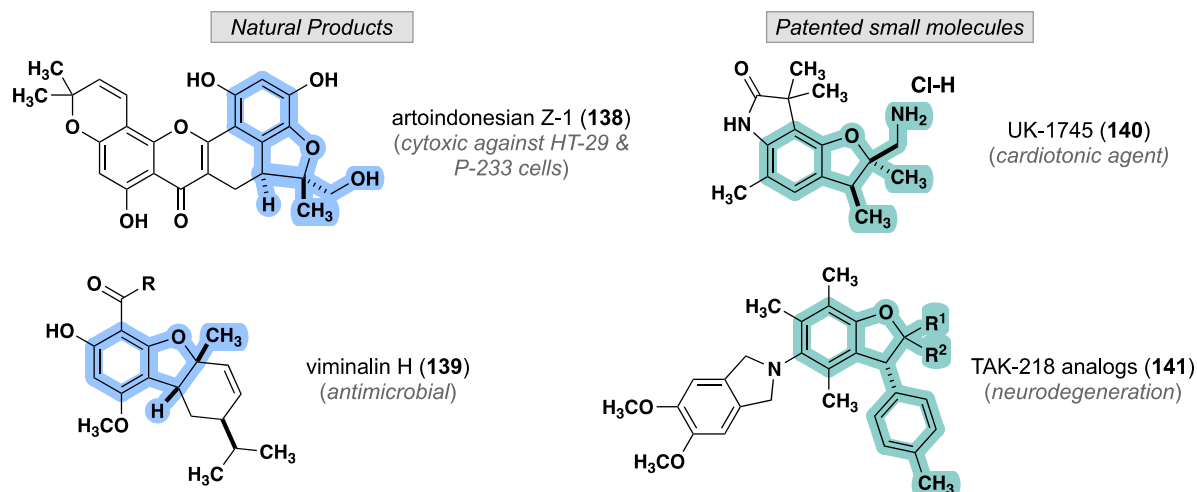


Figure 1.20 Utility of trisubstituted benzodihydrofurans.

The strategies that have enabled access to trisubstituted benzodihydrofuran compounds can be categorized into two main groups: non-stereoselective^{64–67} and stereoselective methods^{22,27,34,68–70}. To start, some standard non-stereoselective methods exist to access the trisubstituted core (Figure 1.21). Traditionally, the general benzofurans scaffold was made in two steps from a Claisen rearrangement with allyl ethers followed by cyclization of the resultant allyl phenol with an acid.^{71–73} Other methods used phenols and alkenes to generate the allyl phenol intermediate that would cyclize to the desired benzodihydrofuran. For example, Tada⁶⁴ was able to electrochemically catalyze the [3+2] cycloaddition of phenol **142** with

trisubstituted alkene **143** to form trisubstituted benzodihydrofuran **143** (Figure 1.21A). This methodology was improved about a decade later to generate the same product **144** through the same mechanism but using a more modern-day microflow electrochemical reactor.⁷⁴

Pd-catalyzed C–H activation methods are also a robust way for C–O bond formation resulting in benzodihydrofurans. Jin-Quan Yu’s group developed a Pd(II) catalyzed method⁶⁵ that uses base, Li₂CO₃ or Na₂HPO₄, and alcohol **145a-b** to generate the hydroxyl anion, which in turn directs C–H bond activation to form benzodihydrofurans **146a-b** in high yield (Figure 1.21B). This method was complementary to the Pd(0) C–O bond formation⁷⁵ reported by Buchwald in 1999, which required an alcohol and an aryl bromide for ring formation.

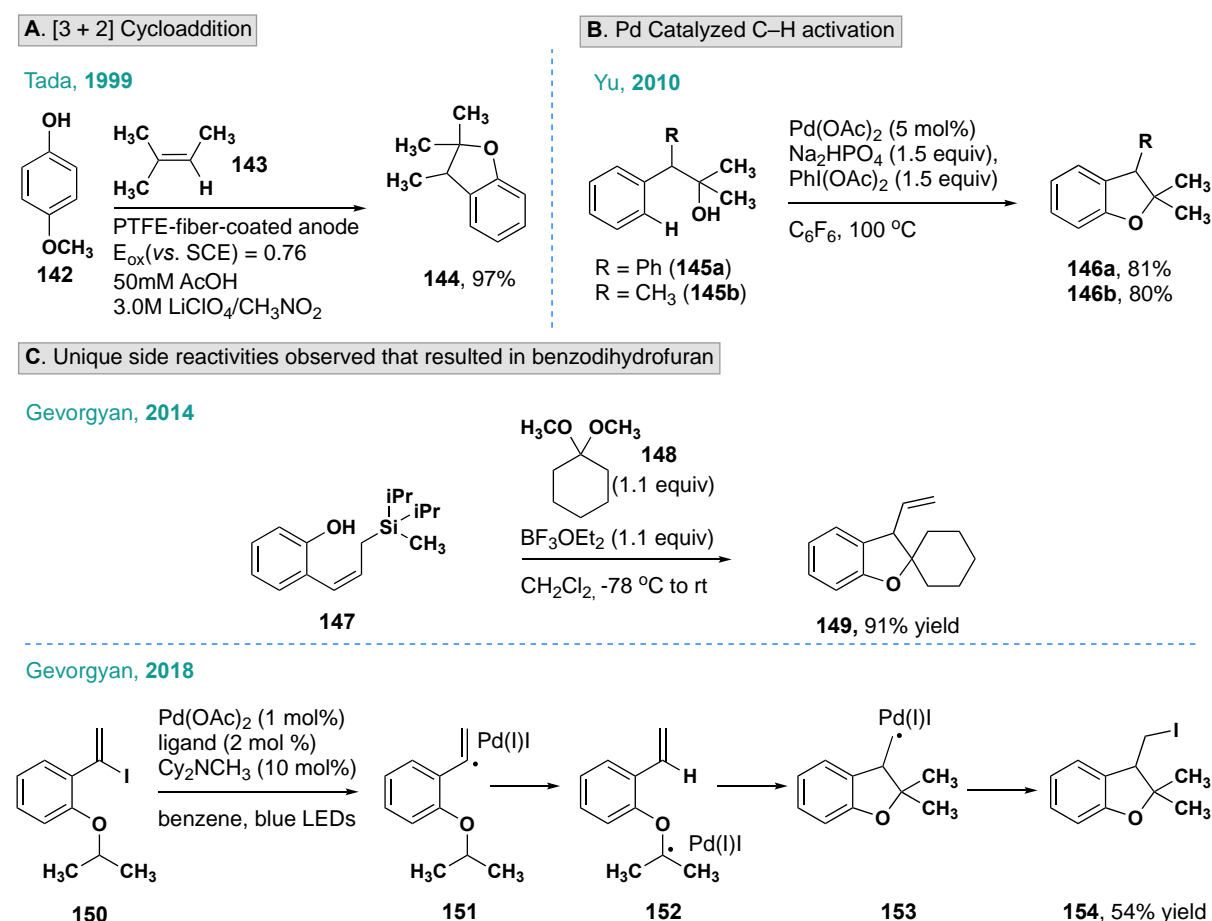


Figure 1.21 Ways to access trisubstituted benzodihydrofurans: non-stereoselective methods.

In 2014, Gevorgyan created a new endo-selective Pd-catalyzed silyl methyl Heck reaction⁶⁶ and wanted to show the utility of the allylic silyloxycycles created (Figure 1.21C). One such

reaction involved ring opening of silyloxycycle to product allylic silyl **147**, which then could undergo an intramolecular Hosomi-Sakurai reaction with 1,1-dimethoxycyclohexane **148** to make the spiro benzodihydrofuran **149** in high yield. Four years later, the same group tried making benzodihydrofurans using new radical Heck conditions with a Pd catalyst and blue LEDs and stumbled upon an unprecedented hydrogen atom translocation/atom-transfer radical cyclization (HAT/ATRC) cascade reaction.⁶⁷ In this reaction, ether **150** undergoes single-electron transfer (SET) to homolyze the C–I bond and form a hybrid vinyl palladium intermediate **151**. This is followed by 1,5 HAT to generate the tertiary radical **152**, which then undergoes a 5-*exo*-trig cyclization to form a primary alkyl radical species **153**. Iodine transfer from the Pd^I species generated earlier in the mechanism yields **154**.

Stereoselective methods to access trisubstituted benzodihydrofurans started appearing in the literature around the early 2000s. For instance, Davies reported the stereoselective intramolecular C–H insertion of donor/acceptor carbenes to make benzodihydrofurans in 2001 (Figure 1.22A).²² In this paper, they inserted into achiral tertiary ethers (**155a-c**) to give trisubstituted benzodihydrofurans (**156a-c**) in moderate to good ee (80-94% ee). Similarly, in Hashimoto's paper on using Rh(II)-catalyzed intramolecular C–H insertion of donor/acceptor carbenes to make dihydrobenzofurans⁶⁸, they reported a single example of a trisubstituted benzodihydrofuran (**156a**) with a single stereocenter. However, since Hashimoto used Rh₂(*S*-PTTL)₄ rather than Rh₂(*S*-DOSP)₄, the trisubstituted core was only obtained in 22% ee even after dropping the reaction temperature to –78 °C. In 2017³⁴, our group showed we could make a similar trisubstituted benzodihydrofuran **158** with a single stereocenter in moderate er from the donor/donor carbene hydrazone precursor **157**. Other C–H insertion methods with ruthenium porphyrin catalysts have also attempted to make a trisubstituted benzodihydrofuran **160**, albeit not stereoselectively.²⁷

Other stereoselective methods exploit Claisen rearrangement and related chemistry with dienes and alkenes (Figure 1.22B). Taguchi and coworkers in 1997 reported a chiral boron catalyst **162** that enabled asymmetric Claisen rearrangements, where a single substrate possessing a highly substituted allyl ether **161** could rearrange to form benzodihydrofuran product **163** in 86% ee.⁶⁹ In 2006, Eom and coworkers⁷⁰ wanted to build a one-pot method for making benzodihydrofurans based on the earlier traditional methods. They set out to do this by using catalytic AgOTf, phenol (**164**), and a diene (**165**) as the starting material.

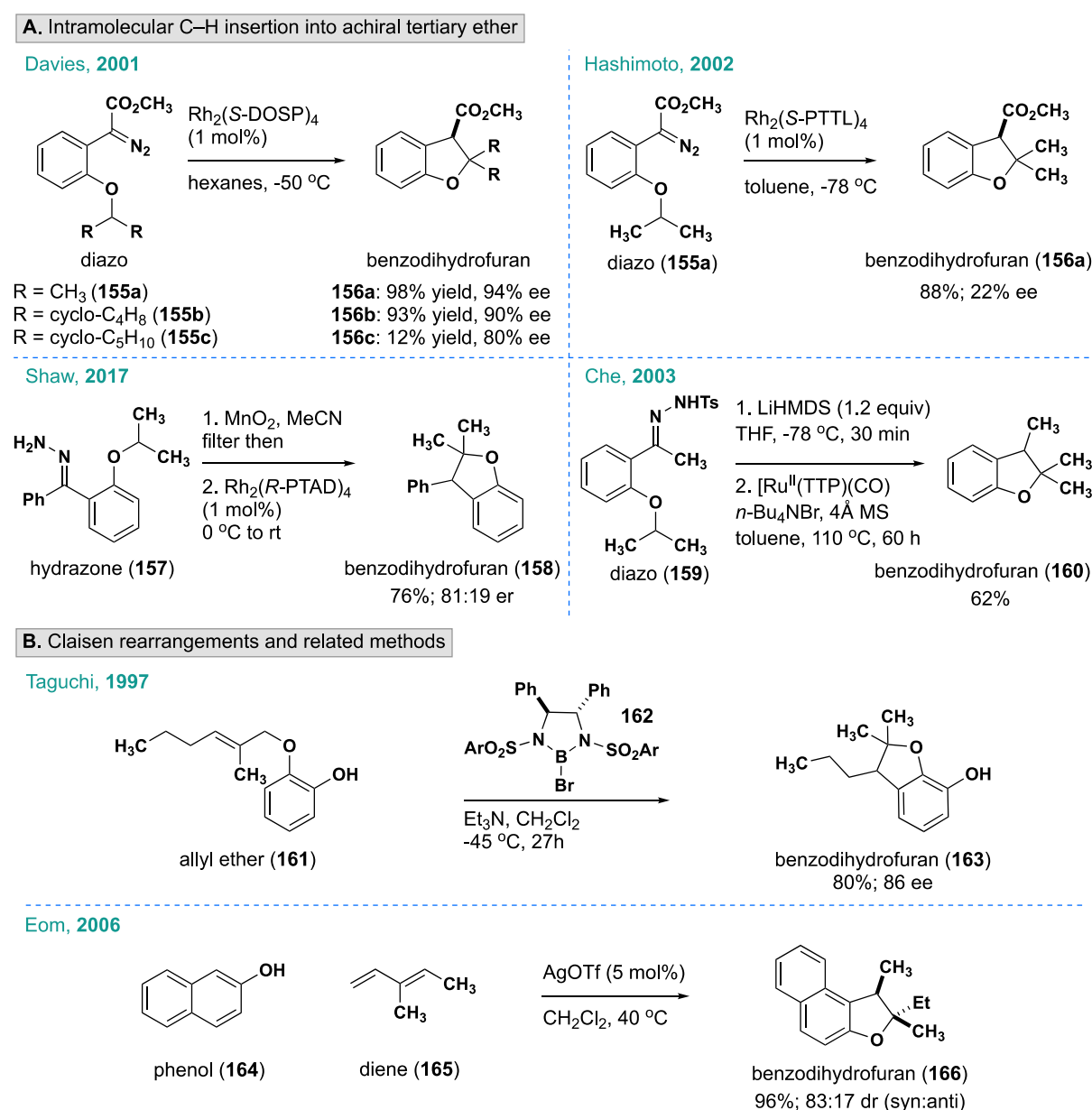


Figure 1.22 Ways to access trisubstituted benzodihydrofurans: stereoselective methods.

First, activation of the diene by Ag(I) coordination initiates the C–C bond formation between the diene and the aryl ring. Then intramolecular C–O bond formation occurs between the phenol and alkene, which is activated by Ag(I) again. Substituted dienes mainly give benzodihydrofuran as the sole product, and in the case of **165**, the trisubstituted benzodihydrofuran **166** is obtained in a moderate 83:17 dr.

As a side note, many more stereoselective methodologies are available for disubstituted benzodihydrofurans. For instance, Xu and co-workers reported in 2021 a powerful stereodivergent synthesis of 2,3-disubstituted benzodihydrofurans via a one-pot C–H functionalization/Oxa-Michael addition cascade where all four stereoisomers were accessible.⁷⁶ However, they did not show any cases where the trisubstituted benzodihydrofuran could result if they started from a more substituted diazo species.

From all the past literature presented above, there was not a generalized method to rapidly stereoselectively access trisubstituted 2,2,3-benzodihydrofurans with varying groups off the furan centers even though it is a highly sought-after core structure. This need for facile stereoselective access to trisubstituted benzodihydrofuran cores, coupled with the desire to probe the origins of stereoselectivity for our groups C–H insertions of donor/donor carbenes methodology, became the driving forces for the development of the C–H insertion of donor/donor carbenes into chiral ethers work discussed below.

1.2 Results and Discussion

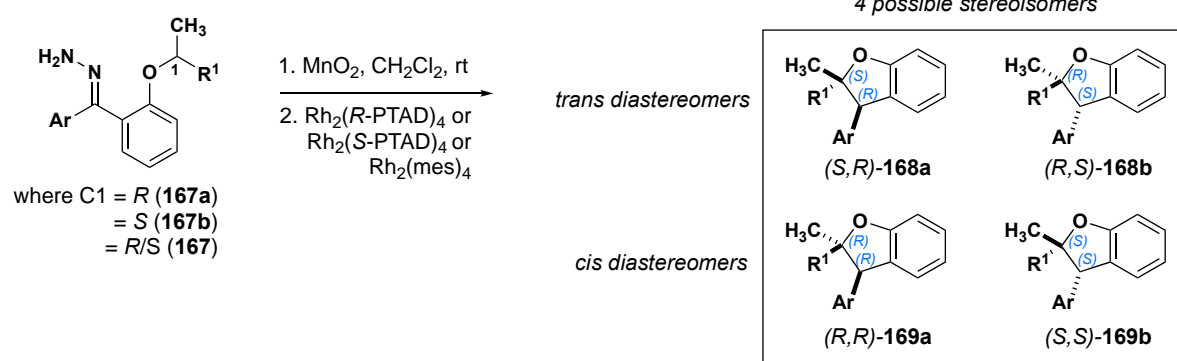
1.2.1 Project Overview

We set off to develop a stereoselective methodology for synthesizing trisubstituted benzodihydrofurans through the C–H insertion of donor/donor carbenes into stereogenic centers in a single step.¹ Experimental data coupled with DFT calculations would give us key insights into whether the C–H insertion mechanism was stepwise or concerted. Finally, this

study would illuminate the stereochemical impact on the carbene center for the first time and delineate the structural factors that enable control over both stereogenic centers.

We had to consider a few key points when designing the methodology and the starting material synthesis. First, insertion into a stereogenic center using a chiral catalyst would create match/mismatched pairings and could lead to possibly four different stereoisomers of the product (**168a-b** and **169a-b**) (Figure 1.23A). Each substrate would need to be easily tested with enantiopure *R*-hydrazone (**167a**) and *S*-hydrazone (**167b**), as well as the racemic hydrazone (**167**), to rule out any kinetic resolution or dynamic kinetic resolution that could be occurring.

A. Reaction design and match/mismatch pairings



B. Hydrazone precursor retrosynthesis

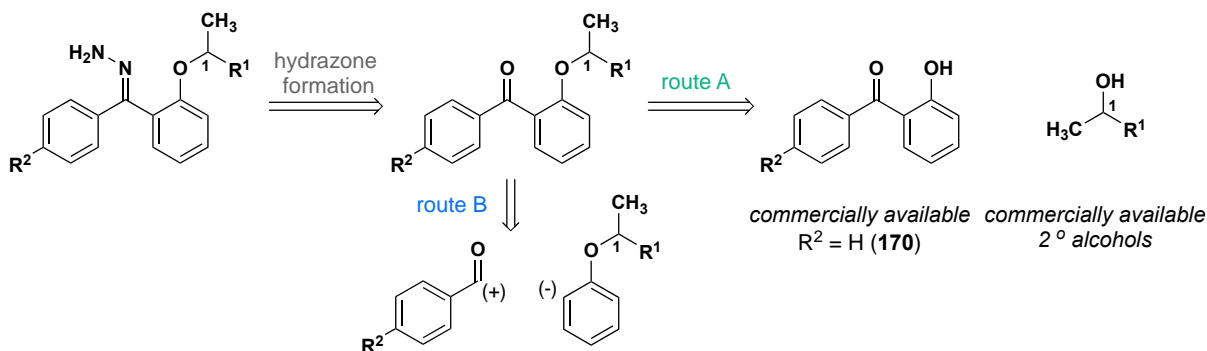


Figure 1.23 A. Reaction design and possible outcomes of match/mismatch pairings B. Retrosynthesis for hydrazone precursors.

All three of these substrates would also have to be tested in the C–H insertion methodology using three different catalysts: a racemic catalyst, the *R* enantiomer of a chiral catalyst, and the *S* enantiomer of the same chiral catalyst. From there, we also wanted to be able to functionalize

the aryl rings to test electronic effects on the carbene. We envisioned all of this could be done by accessing the 2-hydroxybenzophenone core (**170**), which was commercially available, and its substituted derivatives, which had a wide array of methods that could be used to access them in 1-2 steps and had been validated before in the group (see BDB dissertation Section 1.2.2. Table 4).

1.2.2 Synthesis of donor/donor carbene precursors with stereogenic centers

Two main routes were used to access the needed hydrazone precursors. The first, route A, started from 2-hydroxybenzophenone (**170**) and commercially available secondary alcohols (**171a-g**) in a Mitsunobu reaction to form ethers **172a-g** (Figure 1.24A). Installing the chiral ether C–H insertion center via a Mitsunobu reaction was paramount to be able to go in with a single enantiomer of a secondary alcohol and get out a single enantiomer of product.

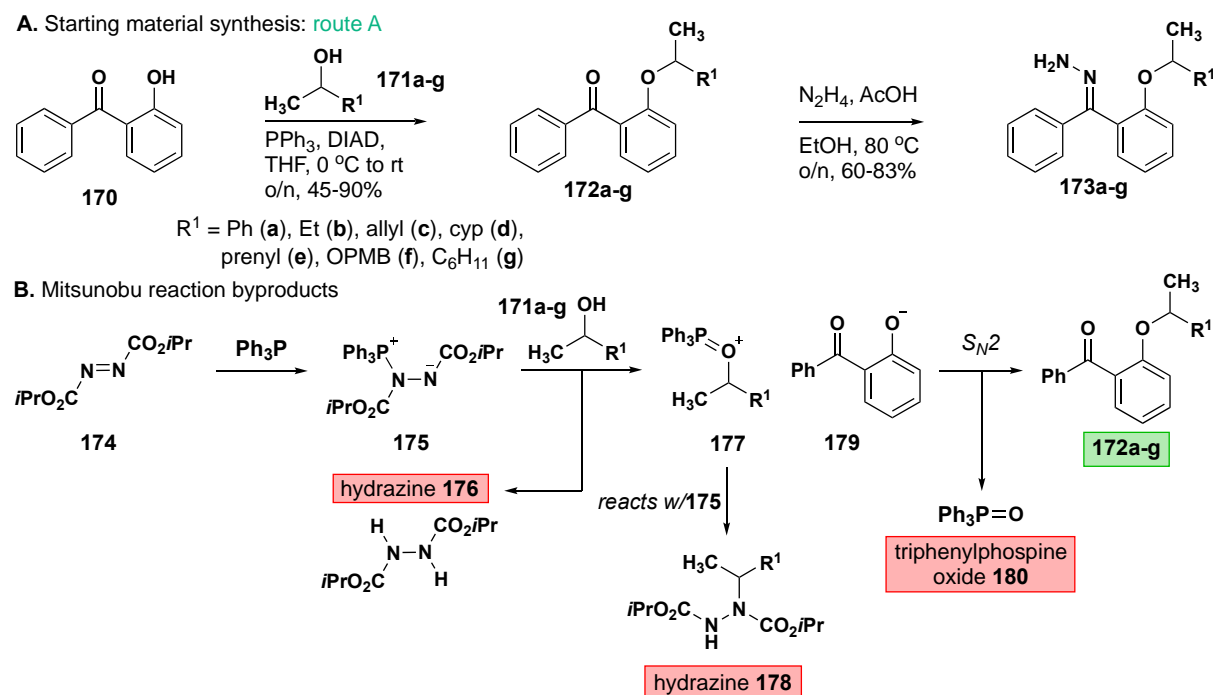


Figure 1.24 A. Synthesis of hydrazone intermediates from 2-hydroxybenzophenone. **B.** Mitsunobu byproducts.

Other possible stereospecific reactions could have also worked, such as an S_N2 alkylation reaction; however, going directly from the alcohol gave the cheapest and widest array of commercially available options.

While the Mitsunobu gave the desired stereochemistry of ether, the product suffered from moderate yields and difficult purifications due to the high volume of byproducts generated throughout the reaction (Figure 1.24B).⁷⁷ Some major byproducts include triphenylphosphine oxide (**180**) and triphenylphosphine (PPh₃), which are water-insoluble and therefore require column chromatography to get rid of. The reduced DIAD-hydrazine **176** is very nonpolar and streaks through the column, proving to be difficult to separate from the desired product. Workarounds to these purification problems have been published and include polymer-supported PPh₃⁷⁸ that can be filtered off and catalytic reactions⁷⁹ to reduce the amount of DIAD needed. Therefore, initial attempts to optimize the reaction revolved around finding the proper purification technique to isolate the desired non-polar ether product **172a-g** from the very non-polar hydrazine **176** and triphenylphosphine oxide **180** that tends to streak through the column (Table 1). Increasing the amount of benzylic secondary alcohol used and solid loading the crude mixture onto celite without any aqueous workup helped increase the isolated yield for benzylic secondary alcohols from 60% to 83% (Table 1 entry 2). However, when secondary alkyl alcohols were used with the same solid loading conditions, the isolated yields dropped significantly from 83% to 23% (Table 1 entry 3). Part of this was due to the alkyl ether products being more non-polar and, therefore, more difficult to separate from the hydrazine (**176**) byproduct. Different column solvent systems were screened, and a gradient of 40% to 100% CH₂Cl₂ in Hexanes was found to be the most effective, albeit a rather slow column to run (Table 1 entries 4-5).

Most of the mass recovery in these reactions correlates to unreacted 2-hydroxybenzophenone **170**, which can be due to the phenol nucleophile being at the end of the

pKa range (pKa < 11) that can be used in a Mitsunobu with the PPh₃/DIAD system. When weaker nucleophiles like a phenol are used, often the nucleophilic attack of **177** by deprotonated hydrazine **175** to form **178** can become a dominant byproduct pathway as hydrazine **175** is a competitive nucleophile to the phenol **179**. There are more reactive coupling reagent pairings that could be used to solve this problem, yet they weren't explored due to cost and time restraints.^{80–82}

Table 1. Mitsunobu reaction optimization

Reaction scheme: 170 (1 equiv) + 171a-g (H₃C-CH(OH)-R¹) → 172a-g (ether product) using PPh₃, DIAD, solvent, and temperature.

Entry	Alcohol Class	Alcohol (equiv)	PPh ₃ (equiv)	DIAD (equiv)	Order of addition	Purification	Temperature (°C)	Yield* (%)
1	benzylic	1.0	1.2	1.2	170 + 171 then PPh ₃ then DIAD	aqueous wkup + liquid load	0 to rt	60%
2	benzylic	1.2	1.2	1.2	170 + 171 then PPh ₃ then DIAD	solid load + EtOAc:Hex	0 to rt	83%
3	alkyl	1.2	1.2	1.2	170 + 171 then PPh ₃ then DIAD	solid load + EtOAc:Hex	0 to rt	23%
4	alkyl	1.2	1.2	1.2	170 + 171 then PPh ₃ then DIAD	solid load + Et ₂ O:Hex	0 to rt	22%
5	alkyl	1.2	1.2	1.2	170 + 171 then PPh ₃ then DIAD	solid load + CH ₂ Cl ₂ :Hex	0 to rt	45%
6	alkyl	1.0	1.3	1.3	170 + 171 then PPh ₃ then DIAD	solid load + CH ₂ Cl ₂ :Hex	0 to rt	90%
7	alkyl	1.2	1.3	1.3	PPh ₃ and DIAD then 170 + 171	solid load + CH ₂ Cl ₂ :Hex	0 to rt	72%
8	alkyl	1.2	1.1	1.1	170 + 171 then PPh ₃ then DIAD	solid load + CH ₂ Cl ₂ :Hex	40 °C	14%

*isolated yield after column chromatography

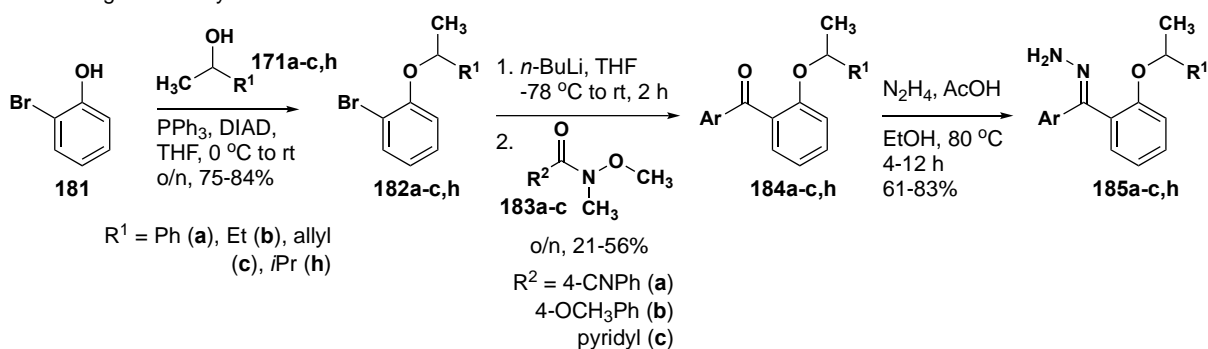
Another workaround to this issue of competitive nucleophilic pathways that was employed instead was switching the secondary alcohol to being the limiting reagent and the phenol being in excess while also slightly increasing the equivalents of PPh₃ and DIAD (Table 1 entry 6), resulting in a 90% yield for the alkyl alcohol substrates. Any changes in the order of addition of all the reagents or increased temperature to aid reactivity only decreased the yield (Table 1 entries 7-8).

From ethers **172a-g**, hydrazone formation using previously optimized and reported conditions from the group was used to give the desired hydrazone precursor **173a-g** in consistently high to near quantitative yields. Although only one hydrazone isomer is drawn, the reaction always gives a mixture of isomers. At room temperature, the mixture was rotameric

on the NMR time scale, significantly broadening the ^1H NMR peaks. For certain substrates, such as **172a** (phenyl ether substrate), the isomers of hydrazone could be separated and isolated by column chromatography. However, this was not necessary since both isomers led to the same desired product upon oxidation to the diazo.

The second, route B, was used to make aryl ring derivatives. Starting from 2-bromophenol **181**, secondary alcohols **171a-c,h** was installed to make ethers **182a-c,h** using the optimized Mitsunobu conditions discussed previously in similar yields (Figure 1.25A).

A. Starting material synthesis: [route B](#)



B. Li-X exchange byproducts

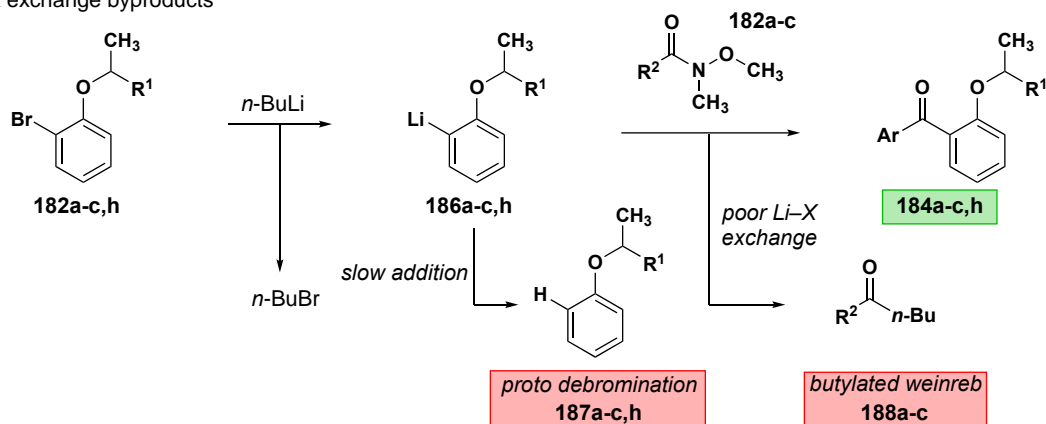


Figure 1.25 A. Synthesis of hydrazone intermediates from 2-bromophenol **B.** Li-X exchange byproducts.

Ethers **182a-c,h** underwent Li-X exchange followed by nucleophilic addition to Weinreb amide derivatives (**183a-c**) yielding ketones (**184a-c,h**). Ortho-substituted lithiates can suffer from slow reactivity in two key areas of the mechanism (Figure 1.25B). First, if Li-X exchange is poor, then excess *n*-BuLi will be in the solution that can add to the electrophile to yield *n*-

butyl ketones **188a-c**. Second, if the ortho-lithiate (**186a-c,h**) slowly adds to the electrophile due to steric hindrance, it will funnel to the proto-debrominated starting material (**187a-c,h**) upon proton exchange with water in the solution and/or upon reaction workup. One solution to decrease byproduct formation is to use *tert*-butyl lithium (*t*-BuLi) rather than *n*-butyl lithium (*n*-BuLi). However, due to safety concerns when using *t*-BuLi on large scale our group avoids using it whenever possible. A second solution to increase the yield of the desired ketones **184a-c,h** is to explore alternative routes to C–C bond formation. However, as discussed earlier, Li–X exchange has proven to be our group's most successful and reliable benzophenone route. Therefore, the final starting material synthesis used the Li–X exchange and nucleophilic addition step to robustly make benzophenone ethers **184a-c,h**, albeit in moderate yields. The hydrazone formation proceeded without any issues in high yields for all the aryl derivative substrates **185a-c,h**.

1.2.3 Sterically bulky, highly activated substrates

Now that the starting hydrazone precursors could be readily accessed, the first question we wanted to ask about this methodology was what level of stereocontrol the substrate and catalyst impart on the C–H insertion reaction. We designed two ether substrate classes that possessed varying levels of reactivity based on the different stabilities of the proposed oxocarbenium intermediate resulting from hydride transfer.

The first substrate class tested was chiral ethers that contained a sterically bulky and highly electronically activated tertiary C–H insertion center (Table 2). This resulted in ether **189** with the adjacent tertiary insertion center containing a methyl and phenyl substituent. The phenyl group created a highly reactive benzylic C–H insertion site as well as significant steric bulk crowding the insertion site, compared to a linear alkyl chain. One of the phenyl rings on the donor/donor carbene core possessed a *p*-cyano group to enable subsequent derivatization for

crystallography and separation by CSP-HPLC (see section 1.2.7) Both the racemic and enantiopure versions of hydrazone **189** were synthesized using route B (Figure 1.25A) and screened across all three dirhodium catalysts to create all possible match-mismatch pairings (Figure 1.23A).

Both racemic **189** and enantiopure **189** yielded the benzodihydrofuran product as a single cis diastereomer (**190**) (Table 2 entries 1-6), irrespective of which catalyst was used. The enantioselectivity followed a similar trend where racemic **189** provided racemic **190** (Table 2 entries 1-3), and enantiopure **189** gave a single enantiomer of **190a** in 97:03 er (Table 2 entries 4-6) regardless of the catalyst employed in the reaction.

Table 2. Alkyl/Aryl stereogenic insertion Center

Entry	Starting Material	Catalyst	dr ^a		er ^b		Yield (%) [*]
			190:191 (cis:trans)	190a, cis-(S,S)	190a, cis-(R,R)	190b, cis-(R,R)	
1	Racemic	Rh ₂ (<i>R</i> -PTAD) ₄	>95:5	49	51	68	
2		Rh ₂ (<i>S</i> -PTAD) ₄	>95:5	49	51	65	
3		Rh ₂ (mes) ₄	>95:5	49	51	65	
4 ^c	Enantiopure (<i>S</i>)	Rh ₂ (<i>R</i> -PTAD) ₄	>95:5	97	03	82	
5		Rh ₂ (<i>S</i> -PTAD) ₄	>95:5	97	03	71	
6		Rh ₂ (mes) ₄	>95:5	97	03	76	

^a dr determined by ¹H NMR analysis of unpurified reaction mixtures

^b er determined by CSP-HPLC on AD column

^c Indicates absolute stereochemistry confirmed by X-ray crystallography

^{*}isolated yield after column chromatography

Therefore, these sterically bulky, highly activated stereogenic C–H insertion centers elicit highly stereoselective substrate-controlled C–H insertion reactions. The structure of the catalyst does not influence the diastereoselectivity of the reaction with **189**, whereas the enantioselectivity is dictated by the configuration of the carbon undergoing insertion. These results are consistent with those of Taber¹⁶ and Doyle⁴⁶ in that the configuration of the insertion

site of (*S*)-**189** is retained in product **190a**, i.e., consistent with a concerted C–H insertion mechanism. The differential results from (*R/S*)-**189** and (*S*)-**189** suggest that the configuration at the insertion site (C1) dictates the configuration at C2 during the insertion reaction. Therefore, these data do not distinguish between a highly stereoselective stepwise mechanism or a highly stereoselective concerted mechanism.

1.2.4 Less bulky, less activated substrates

The second substrate class tested was chiral ethers that contained a less bulky and less electronically activated stereogenic C–H insertion center (**Table 3**). This resulted in ether **192** with the adjacent tertiary insertion center containing a methyl and homoallylic substituent. The homoallylic substituent was used over a fully saturated alkyl chain to enable separation on the CSP-HPLC and crystallography (see sections 1.2.6-7).

Match-mismatch experiments between this new substrate class and chiral catalysts were conducted, and interestingly the C–H insertion reactions showed drastically different stereoselectivity trends compared to the alkyl/aryl substrates. Racemic **192** yielded a 47:53 and 48:52 dr of **193:194** with $\text{Rh}_2(\text{R-PTAD})_4$ and $\text{Rh}_2(\text{S-PTAD})_4$, respectively (Table 3 entries 1-2). There was a slight enrichment towards the *trans* diastereomer (**193**) with achiral $\text{Rh}_2(\text{mes})_4$ yielding a 57:43 dr (Table 3 entry 3). Strikingly, when the er was measured for these entries, the chiral catalysts generated each diastereomer in high er (Table 3 entries 1-2), while the achiral catalyst yielded racemic mixtures of each diastereomer. This starkly contrasts the first class of substrates, where (*R/S*)-**189** led only to racemic products. Conversely, this class of substrates (*R/S*)-**192** can be steered toward enantio-enriched products with the choice of chiral catalysts.

The results with enantiopure (*S*)-**192** were even more striking. Treatment of this substrate with $\text{Rh}_2(\text{R-PTAD})_4$ (**6**) resulted in preferential formation of *trans*-benzodihydrofuran **193**

(Table 3 entry 4) with high enantioselectivity. Use of the same substrate with $\text{Rh}_2(\text{S-PTAD})_4$ resulted in inverted diastereoselectivity with the same enantiomeric preference as the reaction with $\text{Rh}_2(\text{R-PTAD})_4$ (Table 3 entry 5). The eroded enantioselectivity for the formation of **193** with $\text{Rh}_2(\text{S-PTAD})_4$ highlights the mismatch in stereochemical preference between the substrate and the catalyst. Finally, the insertion of (*S*)-**192** with achiral $\text{Rh}_2(\text{mes})_4$ (**8**) showed little diastereoselectivity while retaining the high substrate-induced enantioselectivity (Table 3 entry 6).

Table 3. Alkyl/Alkyl stereogenic insertion centers

Entry	Starting Material	Catalyst	dr ^a 193:194 (<i>trans</i> : <i>cis</i>)	er ^b 193a <i>trans</i> -(<i>S,R</i>)	er ^b 193b <i>trans</i> -(<i>R,S</i>)	er ^b 194a <i>cis</i> -(<i>S,S</i>)	er ^b 194b <i>cis</i> -(<i>R,R</i>)	Yield (%) [*]
1	Racemic	$\text{Rh}_2(\text{R-PTAD})_4$	47:53	91	09	86	14	70
2		$\text{Rh}_2(\text{S-PTAD})_4$	48:52	11	89	16	84	68
3		$\text{Rh}_2(\text{Mes})_4$	57:43	49	51	50	50	91
4 ^c	Enantiopure	$\text{Rh}_2(\text{R-PTAD})_4$	86:14	99	01	01	99	77
5	(<i>S</i>)	$\text{Rh}_2(\text{S-PTAD})_4$	10:90	74	26	01	99	75
6		$\text{Rh}_2(\text{mes})_4$	53:47	98	02	01	99	58

^a dr determined by ¹H NMR analysis of unpurified reaction mixtures

^b er determined by CSP-HPLC on OD column

^c Indicates absolute stereochemistry confirmed by X-ray crystallography

*isolated yield after column chromatography

On the one hand, these results with less bulky, less activated substrates demonstrate that the stereogenic center undergoing insertion controls the magnitude and orientation of enantioselectivity for both newly formed stereogenic centers in the product. The catalyst, conversely, can strongly influence diastereoselectivity, and $\text{Rh}_2(\text{R/S-PTAD})_4$ is a privileged catalyst scaffold for this system. These results are consistent with a highly stereoselective hydride transfer step that is followed by a diastereoselective ring closure that can be controlled by the configuration of the catalyst.

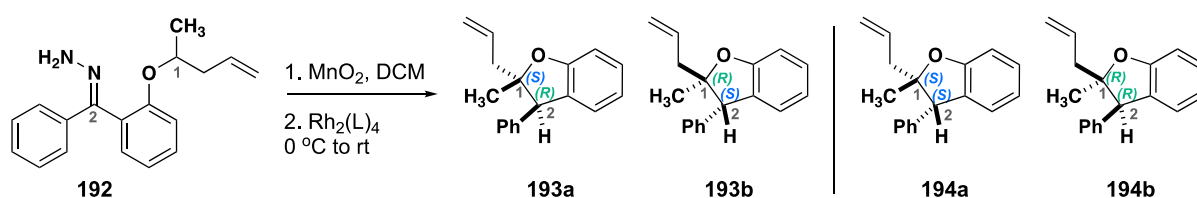
1.2.5 Reaction optimization: conditions screening

1.2.5.1 Catalyst screening

When the initial stereoselectivity data described above was collected, a screen on the reaction conditions was done for the homoallylic substrate **192** since it showed selectivity that is under catalyst control. Therefore, different dirhodium catalysts were screened to see if differences in catalyst reactivity and catalytic pocket shapes would significantly affect the stereoselectivity (Table 4).⁸³ Racemic **192** was used for screening, where a 1:1 dr indicates full catalyst control over the dr due to strong match/mismatching pairings. However, each diastereomer should favor a single enantiomer when using a chiral catalyst and be racemic for achiral catalysts. The more closed catalyst pocket from the chiral crown conformation in $\text{Rh}_2(\text{R-TCPTTL})_4$ ⁸⁴ led to an erosion in enantioselectivity (er) and a shift in diastereomer ratio (dr) (Table 4 entry 2). The much wider open pocket of $\text{Rh}_2(\text{R-DOSP})_4$ ²¹ had similar results to shifting the dr ratio towards the more thermodynamically favored trans diastereomer while also significantly eroding the er favoring the opposite enantiomer compared to $\text{Rh}_2(\text{R-PTAD})_4$ ¹⁸ (Table 4 entry 3 vs. entry 1). Surprisingly, the even bulkier catalyst, $\text{Rh}_2(\text{PhenNTTL})_4$, gave the highest enantiomeric ratio (er) reported to date for this system at 98:02 (Table 4 entry 4). However, this catalyst is underexplored since it hasn't been published in the literature before. Rather it was obtained in small quantities from catalysts shipped from the Fox lab at the University of Delaware for Kellan Lamb's project (see KNL dissertation Chapter 1). If this catalyst were to be explored further, a potential ligand synthesis route could be designed from the cited literature.^{85,86} Mixed ligand catalysts shipped from the Fox group were also tested since they have found luck in their use for enantioselective C–H functionalization reactions with α -alkyl- α -diaoesters.³⁵ Only one of these catalysts, $\text{Rh}_2(\text{TPA})(\text{BPTTL})_3$ ⁸⁷, showed any reactivity,

and isolation of the desired product from byproducts was too little to get enantioselectivity data (Table 4 entry 9). The mixed ligand catalyst $\text{Rh}_2(\text{s-Bu})(\text{S-PTTL})_3$ and Doyle's $\text{Rh}_2(4\text{S-MPPIM})_4$ ¹⁹ showed no reactivity in this donor/donor carbene C–H insertion systems (Table 4 entries 10–11). Since this system would also be used for natural product applications and molecules that may not need to be diastereo- and enantioselective, a range of achiral dirhodium catalysts were also screened for reactivity and yield. $\text{Rh}_2(\text{esp})_4$ gave the lowest yield, followed by $\text{Rh}_2(\text{TPA})_4$ (Table 4 entries 5–6).

Table 4. Catalyst screen



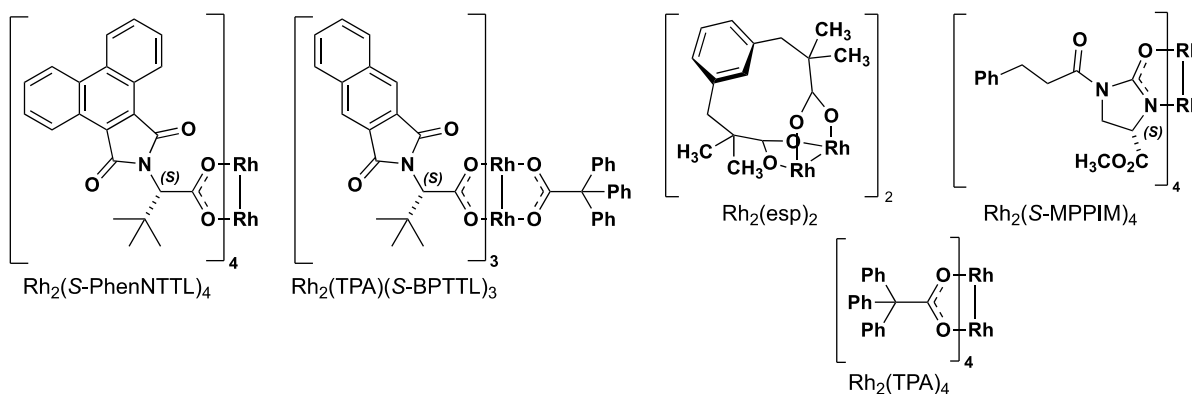
Entry	Catalyst	Yield (%) [*]	dr ^a (193:194) trans:cis	er ^b (193a) trans-(<i>S,R</i>)	er ^b (193b) trans-(<i>R,S</i>)	er ^b (194a) cis-(<i>S,S</i>)	er ^b (194) cis-(<i>R,R</i>)
1	$\text{Rh}_2(\text{R-PTAD})_4$	70	47:53	91	09	86	14
2	$\text{Rh}_2(\text{R-TCP TTL})_4$	31	57:43	76	24	85	15
3	$\text{Rh}_2(\text{R-DOSP})_4$	15	60:40	39	61	37	63
4 ^c	$\text{Rh}_2(\text{S-PhenNTTL})_4$	77	43:57	02	98	13	87
5 ^c	$\text{Rh}_2(\text{esp})_4$	70	49:51	49	51	48	52
6 ^c	$\text{Rh}_2(\text{TPA})_4$	78	52:48	48	52	47	53
7	$\text{Rh}_2(\text{PTCC})_4$	85	48:55	50	50	50	50
8	$\text{Rh}_2(\text{mes})_4$	91	57:43	49	51	50	50
9 ^c	$\text{Rh}_2(\text{TPA})(\text{S-BPTTL})_3$	12	57:43	-	-	-	-
10	$\text{Rh}_2(\text{sBu})(\text{S-PTTL})_3$	NR	-	-	-	-	-
11 ^c	$\text{Rh}_2(4\text{S-MPPIM})_4$	NR	-	-	-	-	-

^a dr determined by ¹H NMR analysis of unpurified reaction mixtures

^b er determined by CSP-HPLC on OD column

^{*}isolated yield after column chromatography

^c Catalyst structures

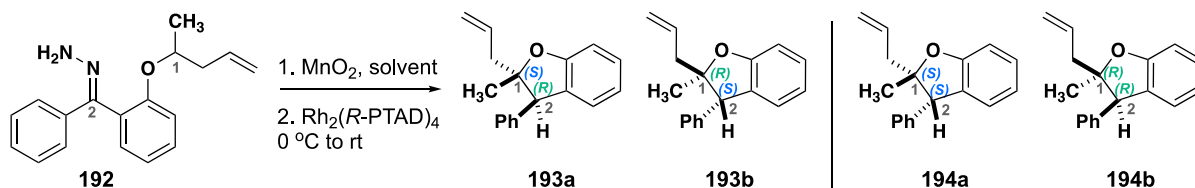


$\text{Rh}_2(\text{PTCC})_4$, which is thought of as the “achiral version” of $\text{Rh}_2(R/S\text{-PTAD})_4$ with a cyclohexane substituent instead of adamantyl, resulted in a jump in yield to 85% (Table 4 entry 7). $\text{Rh}_2(\text{mes})_4$ gave a comparable 91% (Table 4 entry 8), and since this was done on a large scale compared to $\text{Rh}_2(\text{PTCC})_4$, it can be assumed differences in yield are almost negligible when done on the same scale and free of human error.

Therefore, after this screening was complete, it was confirmed that $\text{Rh}_2(\text{mes})_4$ would be the best achiral catalyst to use over $\text{Rh}_2(\text{PTCC})_4$ due to ease of synthesis/access as well as $\text{Rh}_2(\text{PTAD})_4$ was selected as the best chiral catalyst over $\text{Rh}_2(\text{PhenNTTL})_4$ due to limitations in the synthesis of the later.

1.2.5.2 Solvent and temperature screening

Other reaction conditions that were important to explore were the effect of solvent and temperature on the reaction stereoselectivity. Dirhodium catalysts are known to change conformations depending on the solvent they are in due to a multitude of factors such as the polarity of the solvent, H-bonding interactions, Lewis basic sites, etc.^{88–90} These conformations could significantly affect the stereoselective outcome of the reaction. Dichloromethane and acetonitrile were the solvent precedents from past methodologies from our group.^{24,32–34} We found that DCM was the best solvent for yield and stereoselectivity (Table 5 entry 1 vs. entry 2), while MeCN resulted in drops in enantioselectivity. Dichloroethane and benzene gave comparable selectivity to DCM but with significant drops in yield (Table 5 entries 3-4), most likely due to the solubility of the catalyst and substrate. More non-polar solvents like pentanes and cyclohexanes gave poor yields and decreased enantioselectivities, whereas more polar solvents like DMF gave similar yields (Table 5 entries 5-7). Shockingly, the protic solvent isopropyl alcohol gave equal stereoselectivity compared to DCM, albeit with a low yield (Table 5 entry 8).

Table 5. Solvent screen

Entry	Solvent	Yield (%) [*]	dr ^a (193:194) trans:cis	er ^b (193a) trans-(S,R)	er ^b (193b) trans-(R,S)	er ^b (194a) cis-(S,S)	er ^b (194b) cis-(R,R)
1	CH_2Cl_2	70	47:53	91	09	86	14
2	MeCN	23	54:46	82	18	85	15
3	DCE	21	52:48	91	09	90	10
4	Benzene	42	42:58	92	08	88	12
5	Pentane	29	50:50	86	14	83	17
6	Cyclohexanes	9	51:49	83	17	89	11
7	DMF	24	51:49	84	16	83	17
8	IPA	32	48:52	91	09	87	13

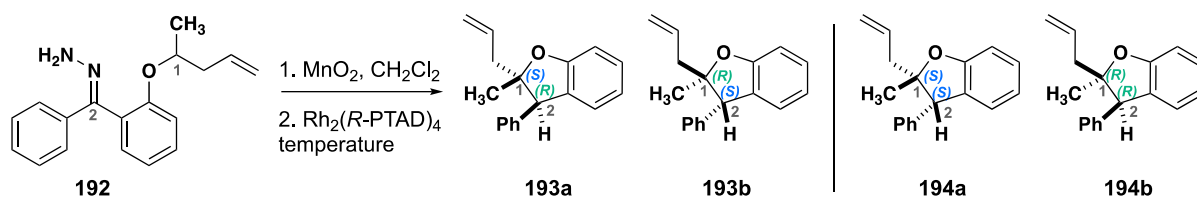
^a dr determined by ^1H NMR analysis of unpurified reaction mixtures

^b er determined by CSP-HPLC on OD column

*isolated yield after column chromatography

The low yield was only due to unreacted hydrazone starting material, which is believed to be due to the slow oxidation of hydrazone to diazo precursor observed in IPA rather than the commonly observed O–H insertion for many other C–H insertion methods.

Next, the temperature was screened to see if it could improve enantioselectivity. The enantioselectivity is determined by the relative rate of each pathway in the enantiodifferentiating step, which is a temperature-dependent calculation. The step is hypothesized to be the hydride transfer step, i.e. the rate-limiting step of the mechanism. Therefore, the hope was that decreasing in temperature would help break past the 91:09 er observed initially. However, temperatures below $-40\text{ }^\circ\text{C}$ had no reactivity (Table 6 entries 1-2), and temperatures between $-27\text{ }^\circ\text{C}$ and $25\text{ }^\circ\text{C}$ (Table 6 entries 3-6) all possessed the same enantioselectivity. It was not until the reaction was heated to $60\text{ }^\circ\text{C}$ that erosion in enantioselectivity was observed (Table 6 entry 7).

Table 6. Temperature screen

Entry	Temperature (°C)	Yield (%) [*]	dr ^a (193:194) trans:cis	er ^b (193a) trans-(<i>S,R</i>)	er ^b (193b) trans-(<i>R,S</i>)	er ^b (194a) cis-(<i>S,S</i>)	er ^b (194b) cis-(<i>R,R</i>)
1	-78	NR	-	-	-	-	-
2	-40	NR	-	-	-	-	-
3	-27	45	46:54	91	09	84	16
4	-10	38	46:54	92	08	87	13
5	0 to 25	70	47:53	91	09	86	14
6	25	42	46:54	90	10	83	17
7	60	16	57:43	80	20	81	19

^a dr determined by ¹H NMR analysis of unpurified reaction mixtures

^b er determined by CSP-HPLC on OD column

*isolated yield after column chromatography

1.2.5.3 Lewis bases screening

Based on the proposed mechanism, a small amount of Lewis bases were screened with the idea that they could influence the diastereoselective outcome (Table 7). Lewis bases are known to axially coordinate to the dirhodium catalyst, plugging up the catalyst and preventing catalytic turnover or potentially binding the distal rhodium site and influencing catalyst conformation.^{91–93} With both effects combined, the thought was that the second C–C bond formation step could be slowed down, and the diastereoselectivity could be influenced. Both pyridine and HMPA were screened by adding 20 mol% of the additive to a solution of the catalyst first, which was then added directly into the diazo solution via a 2-pot C–H insertion method. However, each Lewis base additive only slowed down the reaction and dropped the overall yield rather than influencing the diastereoselectivity (Table 7 entries 1-2).

Table 7. Lewis base screening

Entry	Additive	Yield (%) [*]	dr ^a 193:194 (trans:cis)
1	HMPA	35	47:53
2	pyridine	31	53:47
3	none	70	47:53

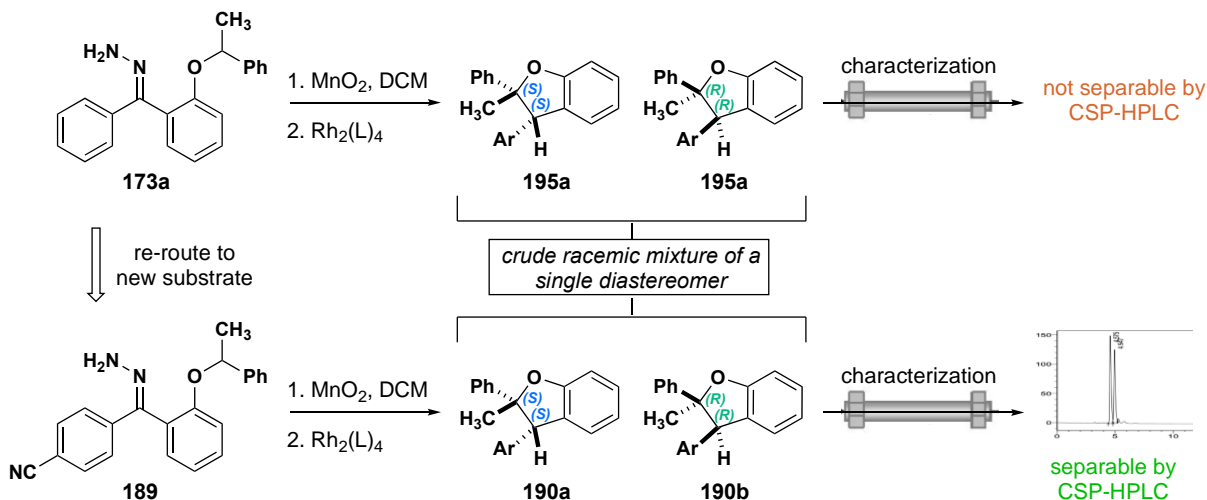
^a dr determined by ¹H NMR analysis of unpurified reaction mixtures

^{*}isolated yield after column chromatography

1.2.6 CSP-HPLC optimization

One of the biggest issues experimentally for this project was the inability to separate diastereomers by column chromatography and enantiomers by CSP-HPLC. The initial compounds designed for each substrate class were too non-polar, and even after extensive screening across different stationary phases (OD, AD, and AS chiral columns), flow rates (0.1 to 2.0 mL/min), solvent polarities (50:50 to 100:00 Hex:IPA), and solvent mixtures (Hex:IPA, Heptane:IPA) neither **173a** nor **173b** could have the enantiomers separated on CSP-HPLC. The first attempt at troubleshooting was to add a polar group to the molecule that would be synthetically easy to make and would not affect the reaction stereoselectivity. Therefore, a *para*-cyano group was added to the carbene aryl ring to increase polarity and, ideally, increase chiral column interaction and retention time to allow the enantiomers to separate (Figure 1.26). Previous results published by the group showed that substitution around the carbene core aryl rings did not affect the stereoselectivity of the reaction, only the rate of reactivity.³⁴ This strategy worked for **189**, and its product enantiomers **190a-b** were separated by CSP-HPLC (AD column, 90:10 Hex:IPA, 1 mL/min, 20 min run, 6 μ L injection of 1mg/mL solution).

Sterically bulky, activated substrate class



Less bulky, less activated substrate class

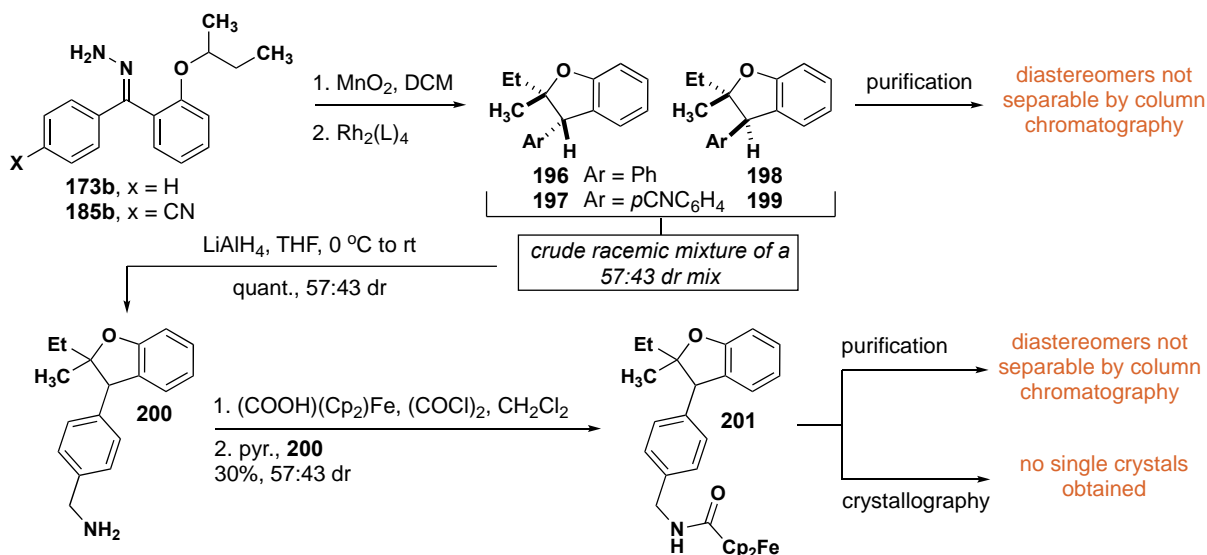


Figure 1.26 Initial substrates and derivatization attempts to separate stereoisomers.

Separating diastereomers from the C–H insertion of **189** was never an issue since only one diastereomer was ever observed (**190**), except in the case of when $\text{Rh}_2(\text{OAc})_4$ where erosion of the dr gave a 90:10 ratio, thereby helping confirm we were only ever observing a single diastereomer in all other cases.

However, the *sec*-butyl ethers **173b** and **185b** gave many more issues since the C–H insertion reaction yielding these always gave a mixture of diastereomers. These diastereomers for both the unsubstituted (**196-197**) and *p*-cyano (**198-199**) derivatives could not be separated

by column chromatography even after extensive solvent system screening. Some attempts were made to derivatize the substituted insertion products (**197**, **199**) by reducing the nitrile to primary amine **200** and then coupling to ferrocene to give **201**. Still, neither of these derivatives had separable diastereomers (Figure 1.26).

We abandoned the *sec*-butyl ether **173b** as the main model substrate and switched to the methyl, homoallylic ether **192** discussed extensively earlier (see section 1.24). The idea was that the slightly longer linear chain would enable better separation between diastereomers and enantiomers. At the same time, the alkene could serve as a functional handle for further derivatization needed to grow a crystal to prove absolute stereochemistry (see section 1.27). However, it was vastly important that it was the homoallylic ether so that the electronic activation of the C–H insertion center would not be changed. We could hopefully replicate the interesting diastereoselectivity trends observed with the *sec*-butyl ether **173a**. Gratifyingly, this substrate **192** gave the same novel diastereoselectivity trends observed with **173a**. Yet, the same roadblock was hit when the diastereomers (**193** and **194**) were attempted to be separated by hand-column chromatography. No solvent system screen attempts nor attempts to get the chiral prep columns working on the group prep HPLC were successful in separating the product diastereomers. Luckily, when the purified mixture of product diastereomers (**193** and **194**) derived from racemic starting material (**192**) and achiral catalyst (**8**) was placed on the CSP-HPLC, four separate peaks were observed! Optimization of the conditions enabled the clean separation of all four peaks on the CSP-HPLC (OD column, 100:0 Hex:IPA, 1.0 mL/min, 20 min, 6 μ L injection of 1mg/mL solution, 283 nm wavelength measurement) (Figure 1.27).

The next challenge was determining which peak coordinated to each diastereomer and enantiomer. As seen in the chromatogram in Figure 127, peaks 1 and 2 are close together, followed by 3 and 4 over three minutes later. Initially, it was assumed that peaks 1 and 2 were the same diastereomers and 3 and 4 were the other diastereomer since diastereomers, in theory,

should separate more easily than enantiomers. Therefore, ten runs on the CSP-HPLC were conducted where 1 mg of compound was loaded onto the column at a time and manually “prepped” to collect peaks 1+2 in one fraction and 3+4 in a separate fraction. If the initial peak assignment theory was correct, these fractions could be concentrated and put on the NMR to get spectra of a single diastereomer for each fraction. Stunningly, when the NMR was taken, both fractions were a 57:43 mix of diastereomers, which matched the dr perfectly from the original crude ^1H NMR after workup.

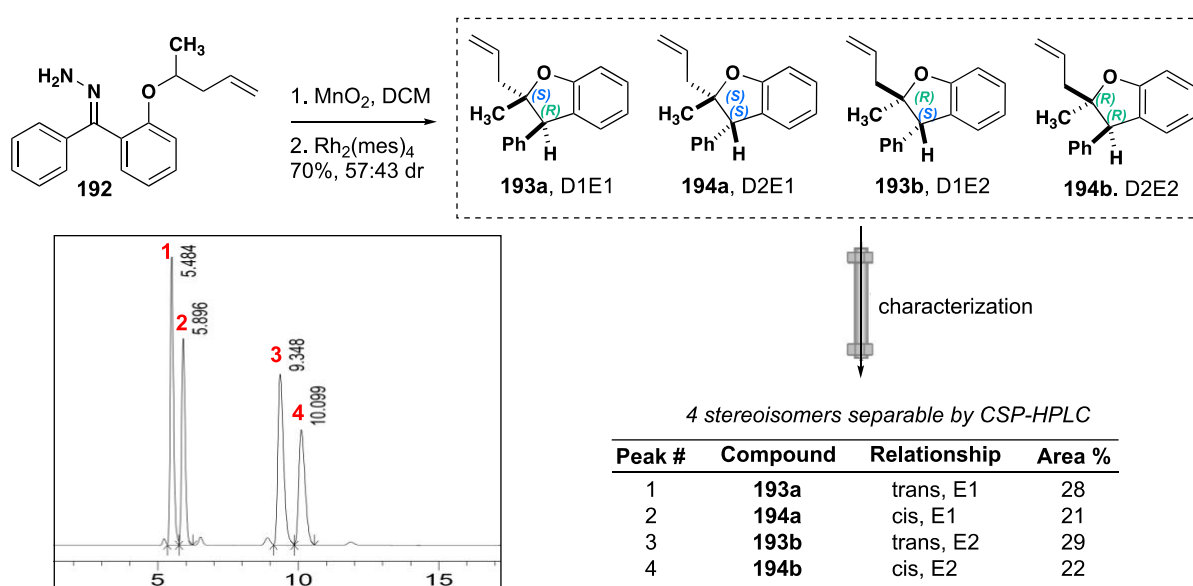


Figure 1.27 Labeled CSP-HPLC traces for methyl, homoallylic C–H insertion products.

This meant that the enantiomers of the product separated easier on the chiral column than the diastereomers did, where peak 1 + 3 were the enantiomers of one diastereomer, and 2 + 4 were the enantiomers of the second diastereomer (Figure 1.27). This was confirmed across all the other CSP-HPLC traces because the dr ratio observed by CSP-HPLC matched the dr ratio observed in the crude ^1H NMR perfectly.

1.2.7 Synthesis of crystal derivatives for crystallography

To prove absolute stereochemistry for the insertion products, single crystals of diastereo- and enantiopure products needed to be grown for x-ray crystallography. All products resulting

directly from C–H insertion were oils, though, and all initial attempts to grow crystals from them failed. Therefore, insertion cores **190** and **193-194** were derivatized until a crystal could be obtained. First, the nitrile group on **190** was reduced to the primary amine **202** with LiAlH₄ in 85% yield (Figure 1.28).⁹⁴ Amine **202** was not crystalline, and attempts to nosyl- (**203**) and tosyl- (**204**) protect the amine either did not work or did not produce a crystalline product, respectively. Next, attempts to form a urea group from isocyanate⁹⁵ (**205**) or CDI and aniline⁹⁶ (**206**) did not work. Coupling reactions to form amides were tried next. The initial couplings with either carboxylic acid substituted ferrocene⁹⁷ or 3-iodobenzoic acid to yield **207** and **208**, respectively, worked no crystals were successfully grown from the purified products.

Therefore, it was hypothesized that rotational freedom from reduction to primary amine **202** contributed to the derivatives' non-crystalline morphology. So, arylbenzothiazole **210** was tried to be synthesized from nitrile **190** and **209** with no luck.⁹⁸ However, adding phenyl lithium to nitrile **190** followed by condensation with 2,4-DNP yielded crystalline solid **211**.^{99,100} Simultaneously, one more coupling reaction with amine **202** was attempted with 1-hydroxy-2-naphthoic acid to yield another crystalline product **212**. Single crystals suited for X-ray crystallography were attempted to be grown from products **211** and **212**. Eventually, **212** gave a suitable single crystal, and an X-ray structure was obtained with the help of Jim Fetting. Note that this carboxylic acid was believed to be the best at crystallization due to the strong hydrogen bond interaction between the hydroxyl group and the carbonyl on the amide bond. This crystal enabled us to finally assign the absolute stereochemistry of the sterically bulky, activated model system product **190** to be the *S,S* enantiomer of the *cis* diastereomer.

Growing a crystal for substrates **193-194** was easier and served a dual purpose (Figure 1.29). Since the *trans* (**193**) and *cis* (**194**) diastereomers could not be separated by column chromatography, derivatization enabled the separation of the two diastereomers and created a crystalline product for x-ray crystallography to obtain absolute stereochemistry.

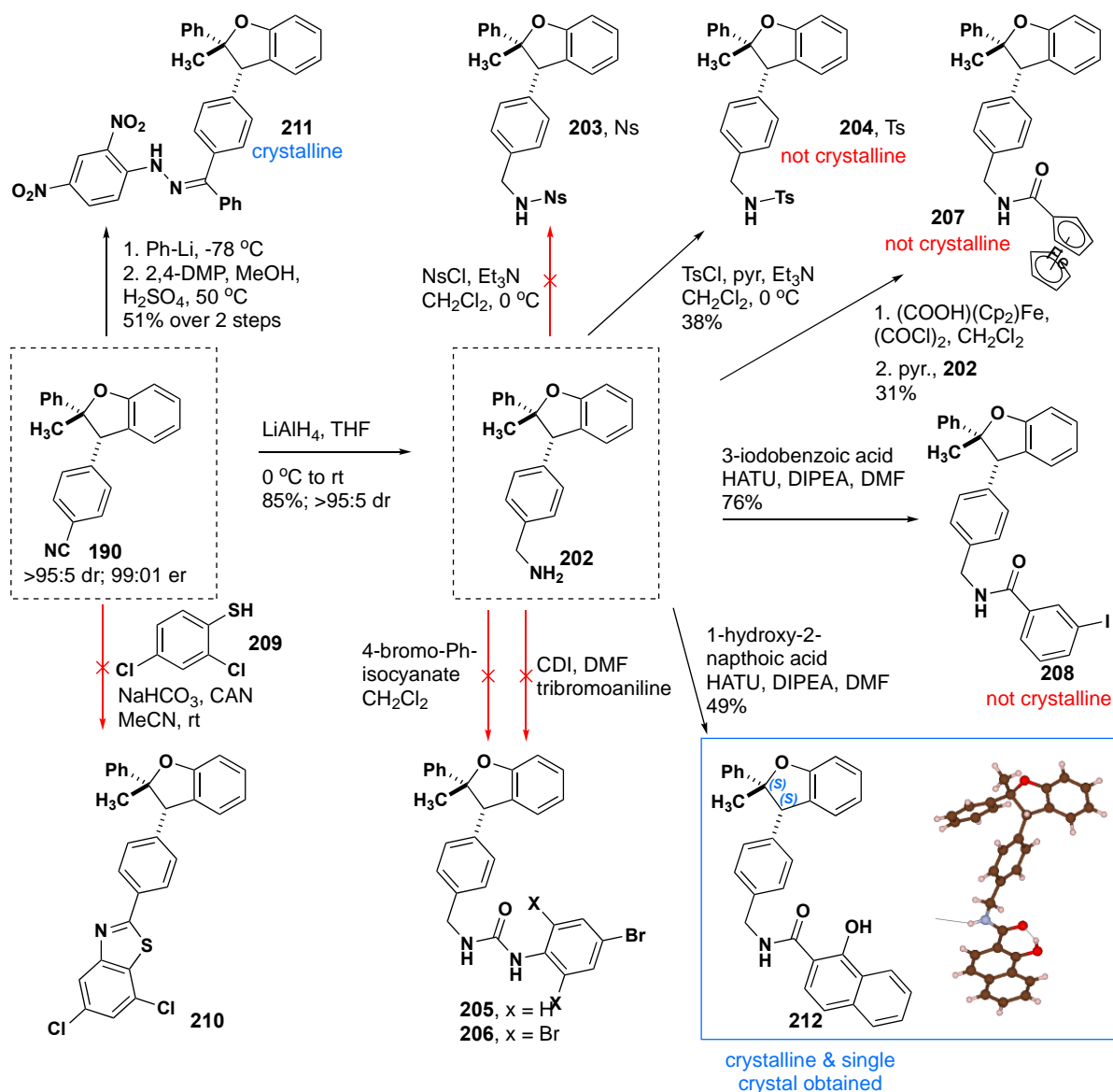


Figure 1.28 Synthesis of cyano derivatives (final crystal + failed crystal couplings).

First, the alkene on **193-194** was oxidatively cleaved using sodium periodate and catalytic ruthenium (II) chloride to yield carboxylic acid **213**, which could rapidly be functionalized.¹⁰¹

First, a third stereocenter was added to the molecule by coupling (*S*)-phenylethan-1-amine (**214**) with **213** through acyl chloride formation and nucleophilic addition. This produced **215** in a low 19% yield, and the two diastereomers were inseparable. Next, *p*-anisidine and DPPA were used to create urea⁹⁶ **216** in a moderate 56% yield from carboxylic acid **213**. Fortunately, the diastereomers of **216** could be separated, but both were a chalky powder morphology that

a single crystal could never successfully be grown from. Finally, carboxylic acid **213** was coupled to 4-iodoaniline using HATU and DIPEA to yield a mixture of diastereomers in 57% yield, which could easily be separable from each other by column chromatography. Both the *trans* diastereomer (**217**) and *cis* diastereomer (**218**) of the crystal derivative were derived from enantiopure hydrazone (**192**); therefore, each crystal was a single enantiomer.

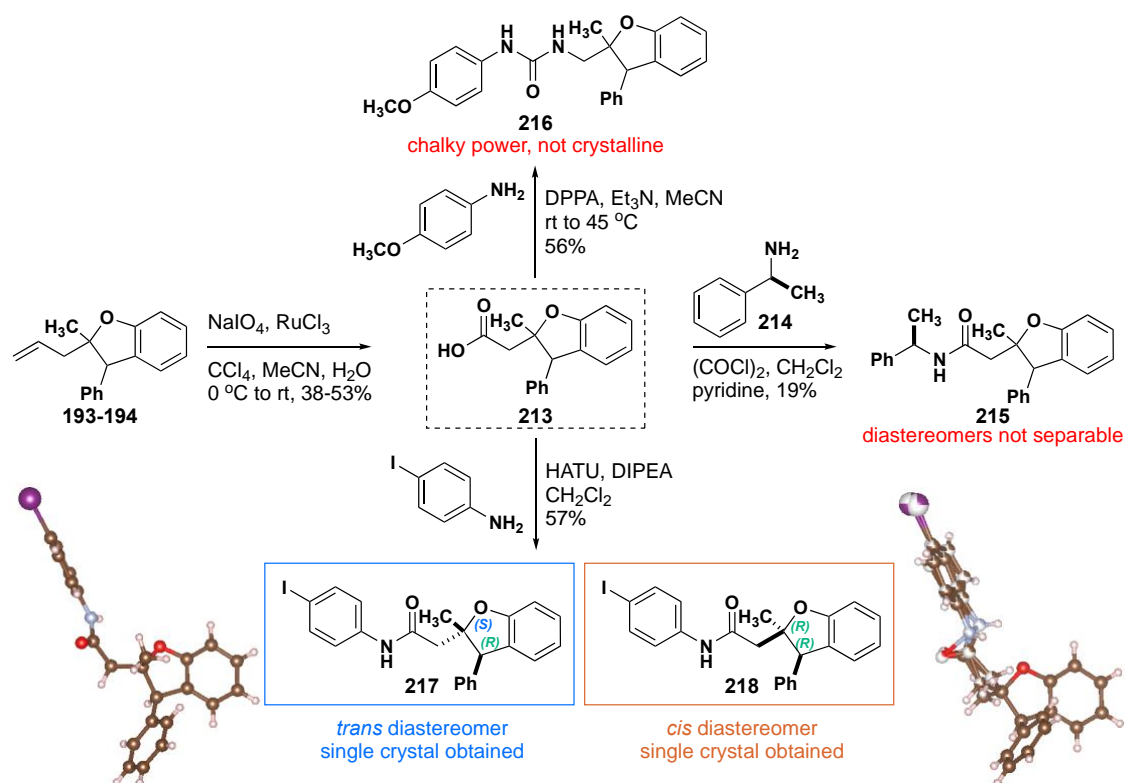


Figure 1.29 Synthesis of alkene oxidative cleavage derivatives (final crystals + failed crystal couplings).

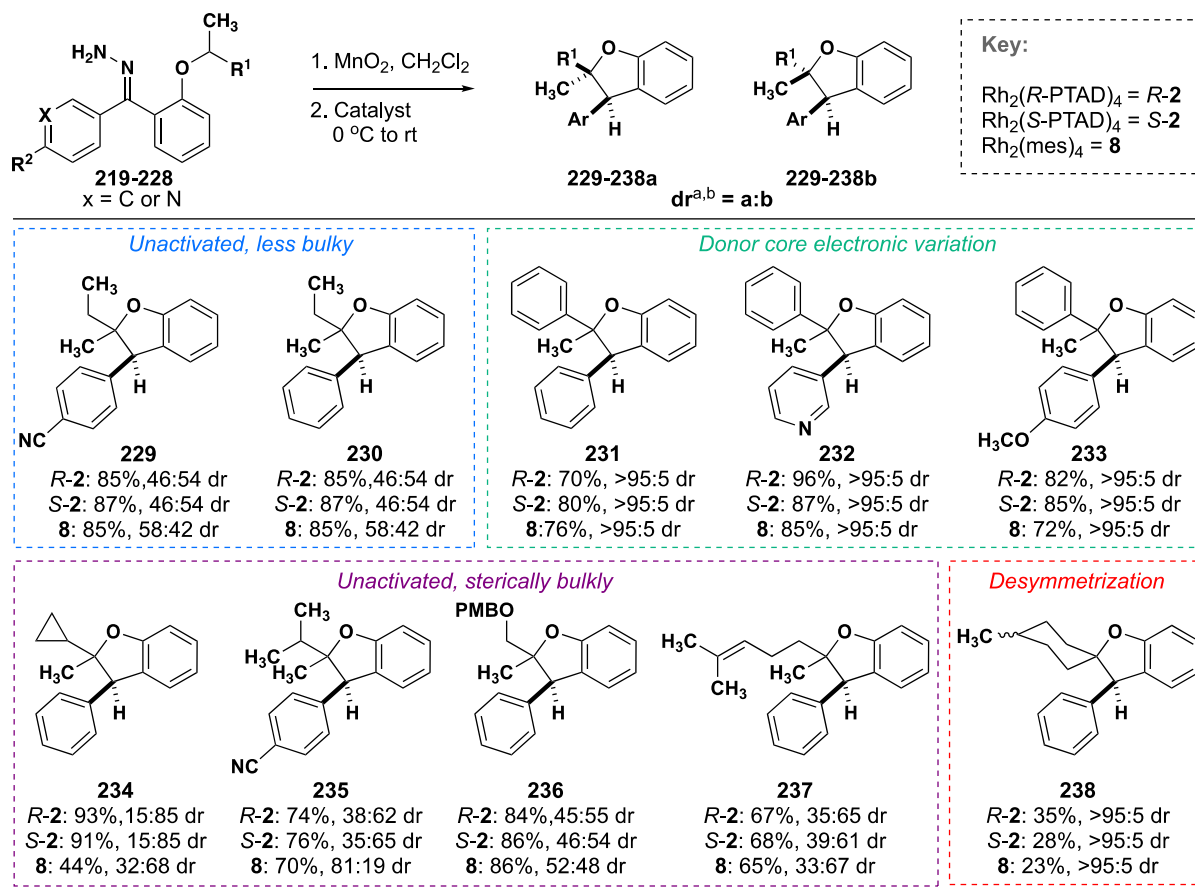
These iodoaniline derivatives grew single crystals (often crashing out as needle-like crystals in the column fraction tubes), and X-ray crystallography from Jim Fettinger showed the absolute stereochemistry of the *trans* diastereomer **217** to be the (*S,R*) enantiomer and the *cis* diastereomer **218** to be the (*R,R*) enantiomer. With two enantiomers confirmed by X-ray crystallography, the absolute stereochemistry of two peaks on the HPLC trace described earlier (Figure 1.27) could be identified, and the other two were assigned via the process of elimination to give us a fully characterized and assigned mixture of stereoisomers.

1.2.8 Substrate scope

We could make two key conclusions about stereoselectivity from the two model systems discussed in sections 1.23 and 1.24. First, the enantioselectivity would always be under substrate control, meaning the enantiomer of starting material used would determine the enantiomer of the product obtained. On the other hand, the diastereoselectivity could be under catalyst control based on how bulky and electronically activated the C–H insertion center was. However, these diastereoselectivity trends were observed between two groups on opposite ends of the spectrum, sterically occluded and electronically activated versus less sterically hindered and minimal electronic activation of the C–H bond. Therefore, we wanted to investigate further how a spectrum of substrates falling between these two model systems would affect the diastereoselectivity. Based on the previous findings, only racemic starting material was needed, and if the dr was about 50:50, that suggested high match/mismatched pairings and high catalyst control over the dr. In contrast, higher drs and/or no reversal in the dr ratios between enantiomers of the catalyst suggested high substrate control over the dr. Overall, four main groupings of 10 substrates were synthesized (Figure 1.30) to probe how the following affected the diastereoselectivity:

1. Similarity between the two substituents off the stereogenic center
2. Donor core electronic variation
3. Variations in bulk for inactivated C–H centers
4. Desymmetrization and remote stereogenic centers.

The ethyl substrates (**229-230**) behave much like the unactivated, less bulky substrate **192**, exhibiting high catalyst control over the dr even when there is such a small difference between the methyl and ethyl groups. Similarly, **231-233** match the trends observed for sterically bulky, highly activated substrate **190**, where they are all under substrate control demonstrated by the high dr regardless of the catalyst employed.



^a dr determined by ¹H NMR analysis of unpurified reaction mixtures

^b assigned diastereomers determined from analogous compound NMR shifts

*isolated yield after column chromatography

Figure 1.30 Substrate scope.

Excitingly, heterocycles are tolerated without any decline in yield or stereoselectivity (**232**)! The caveat is that the pyridine is Lewis basic and can bind the dirhodium unproductively and slow the reaction rate. In this case, upon catalyst addition, the reaction with the pyridine substrate to make **232** took about 8 hours compared to the reactions with the phenyl group to make **231** or **233** only took 5-15 minutes, depending on the solution dilution.

Next, the effect of steric bulk on delineating between catalyst and substrate control over the dr was accessed. It was observed that if the steric bulk is pushed far enough away from the C–H insertion center, such as the -OPMB group in **236**, then we maintain

catalyst control over the dr. However, as soon as we increased the steric interactions around the C–H insertion with a branched alkyl group (**235**, R¹ = isopropyl), it switched to substrate control, preferring the trans diastereomer in about 65:35 dr for both enantiomers of Rh₂(PTAD)₄ (**2**), contrary to the preferred cis diastereomer with an achiral catalyst (**8**). An even longer branch alkyl substrate (**237**, R¹ = prenyl) is analogous to **235**, where there is a slight substrate preference for the trans diastereomer in about a 65:35 dr too. Interestingly, when R¹ = cyclopropyl (**234**), the dr remains under substrate control due to the increased steric bulk, but the magnitude of the dr increases to an 85:15 dr preferring the trans diastereomer due to the increased electronic activation of the C–H bond. Lastly, an attempt at a desymmetrization C–H insertion into methylcyclohexane gave a single diastereomer of product **238** regardless of the catalyst employed.

From this substrate scope, we can conclude some key features of substrates that elicit catalyst control over the dr versus substrates that maintain substrate control over the dr. First, steric bulk is the main component that delineates these two modes of diastereocontrol. Linear alkyl chains or alkyl chains with bulky groups pushed multiple carbons away from the C–H insertion center (**229-230** & **236**) enable productive match/mismatch substrate-catalyst pairings where the enantiomer of the catalyst controls the preferred diastereomer. However, as soon as the steric hindrance around the insertion center is increased, there is inherent substrate control over the diastereoselectivity that cannot easily be overcome by different enantiomers of the catalyst (**231-233** & **234-235**, **237-238**). For these substrates, electronic activation of the C–H bond by R¹ appears to increase the magnitude of the dr with unactivated substrates exhibiting low dr (**235** & **237**) versus more activated substrates exhibiting moderate to very high drs (**234** & **231-233** respectively). We cannot rule out that the increased

electronic activation of the C–H bond changed the mechanism from a stepwise to a concerted, asynchronous process, thereby accounting for the huge jump in diastereoselectivity.

1.2.9 Mechanistic DFT calculation collaboration with Tantillo Lab

A collaboration with the Tantillo lab was established to model the stepwise mechanism hypothesis and elucidate the stereoelectronic factors that controlled the stereoselectivity of the C–H insertion methodology discussed in this chapter. Initial experimental evidence gave three key parameters as a starting place for the DFT calculations undertaken by Croix Laconsay in the Tantillo Lab (see CJL dissertation: chapter 5 for expert discussion of the DFT models built for this system¹⁰²). First, the system needed to be modeled with the full Rh₂(*R/S*-PTAD)₄ catalyst (**2**) since the control over diastereoselectivity was not observed with the smaller achiral Rh₂(mes)₄ catalyst (**8**). Second, the stereoselectivity data found for the homoallylic C–H insertion products (**193-194**) highly suggested a stepwise mechanism due to the disentanglement of the enantioselectivity from the diastereoselectivity throughout the match/mismatch pairings. Therefore, Croix was tasked with first modeling the hypothesized hydride transfer intermediate and then finding transition states that lead to that intermediate, as well as separate transition states that lead from that intermediate to all four possible stereoisomer outcomes. Third, the solvent screen (Table 5) showed that solvent effects did not have any significant bearing on the stereoselective outcome, thereby helping greatly simplify needed DFT calculations.

Computational experiments took a great deal of time due to the size of the system being modeled, as well as the level of theory needed for a system where we are trying to differentiate between free energies of only a couple of kcal/mol. While extensive discussion of the troubleshooting done for this system can be found in CJL's dissertation and all optimized

structure coordinates are reported on the ioChem-BD database¹⁰³, the following two points will be discussed briefly since they significantly shaped the final conclusions we could make about the mechanism.

1. The catalyst used for published DFT models is a truncated version of $\text{Rh}_2(\text{R-PTAD})_4$ (2), where the adamantyl group is replaced with a methyl group to reduce the computational time needed for every calculation (1+ week to 1-2 days).

Computational DFT modeling of full dirhodium catalysts has been done before but is rarely used due to the difficulty, time, and cost needed to undertake such a project.^{104–109} These previously reported methods were a starting point for the development of the DFT methods by Croix Laconsay used in this paper. Eventually, the optimal DFT method with the truncated $\text{Rh}_2(\text{R-PTAD})_4$ as well as all final reported energies and lowest frequencies used the (PCM-(CH_2Cl_2)-B3LYP-D3(BJ)/SDD[6-31+G(d,p)]//PCM(CH_2Cl_2)-B3LYP-D3(BJ)/LANL2DZ[6-31G(d)]) level of theory.

2. The free energy differences fall within 1-2 kcal/mol, which is all within typical DFT error, making the computational findings more qualitative than quantitative regarding the exact energies. However, this doesn't call into question the key conclusions about the nature of the bond-making and bond-breaking events in the C–H insertion mechanism.

Due to working on the cusp of current DFT theory margins of error for reported free energies, Croix made a More O'Ferrall-Jencks plot^{36,110,111} to depict all the possible mechanistic possibilities for hydride shift and C–C bond closure events (Figure 1.31). This plot showed that the stepwise mechanism we report for this methodology exists very close (but not within) to the border area between a stepwise and a concerted, highly asynchronous mechanism.

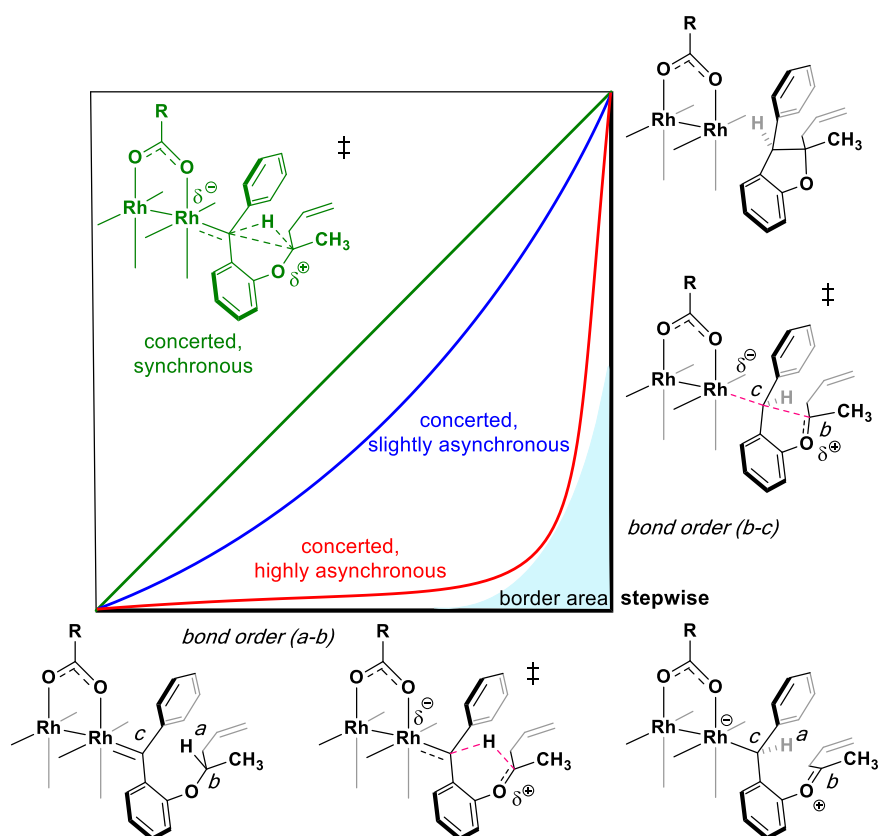


Figure 1.31 Qualitative More O'Ferrall-Jencks plot.

From these two DFT calculation adjustments discussed above, we were able to obtain a full potential energy surface starting from the (*S*)-homoallylic carbene hydrazone precursor (**192**) and using $\text{Rh}_2(\text{R-PTAD})_4$ (**2-truncated**) to map to all four potential stereoisomers (**193a-b** and **194a-b**) (Figures 1.33 & 1.34). The findings from these reaction coordinate diagrams can be distilled down into a representative mechanistic figure that highlights the unique structural components of this mechanism that lend itself to the observed experimental stereoselectivity (Figure 1.32). Figure 1.32 shows a stepwise mechanism where hydride transfer results in a short-lived zwitterionic intermediate (**241**), similar to what was hypothesized previously for C–H insertions of donor/donor carbenes, followed by C–C bond closure to give to observed products (**193a** & **194b**).

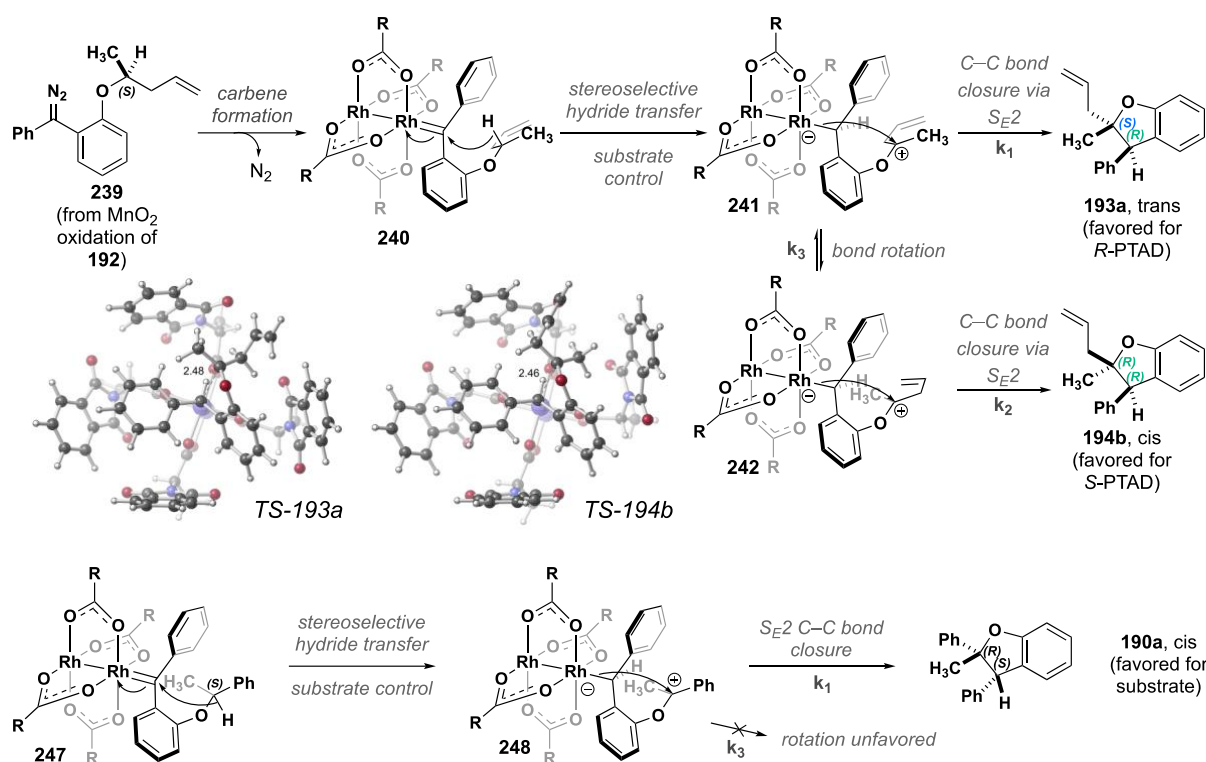


Figure 1.32 Proposed stepwise mechanism.

Further insights into this stepwise mechanism are illustrated by the reaction coordinate diagrams showing the pathways to all four possible stereoisomers. For clarity, the mechanism for the formation of the four stereoisomers from the pairing of the *S* enantiomer of diazo (**239**) with the *R* enantiomer of the catalyst (**2**) is broken up into two coordinate diagrams. The first shows the pathway to the experimentally observed stereoisomers **193a** and **194b** (Figure 1.33), and the second shows the pathway to the unobserved stereoisomers **193b** and **194a** (Figure 1.34).

First, the addition of $\text{Rh}_2(\text{R-PTAD})_4$ (**2**) to a solution of diazo **239** results in catalyst binding and extruding N_2 in a highly exergonic process ($\Delta G = -38.4$ kcal/mol) to form one major rotamer of the highly stabilized Rh carbene **240**. From **240**, a hydride shift occurs from the tertiary C–H bond to the carbene center to form the oxocarbenium ion intermediate **241**. This step is the rate-limiting step ($\Delta G = +13.4$ kcal/mol) and occurs with high stereochemical fidelity accounting for the high selectivity for the newly formed stereogenic center at the former

carbene center. Therefore, this step is responsible for setting the enantioselectivity of the reaction.

From intermediate **241**, there are two separate pathways that led to the two observed products. First, a C–C bond closure that goes through a novel S_E2 mechanism could occur to yield the major product, the (*S,R*) trans diastereomer (**193a**). S_E2 mechanisms are unusual and sparsely reported in the literature and haven't been reported for systems involving Rh.

Reaction Coordinate Diagram for experimentally observed hydride shift/enantiomer

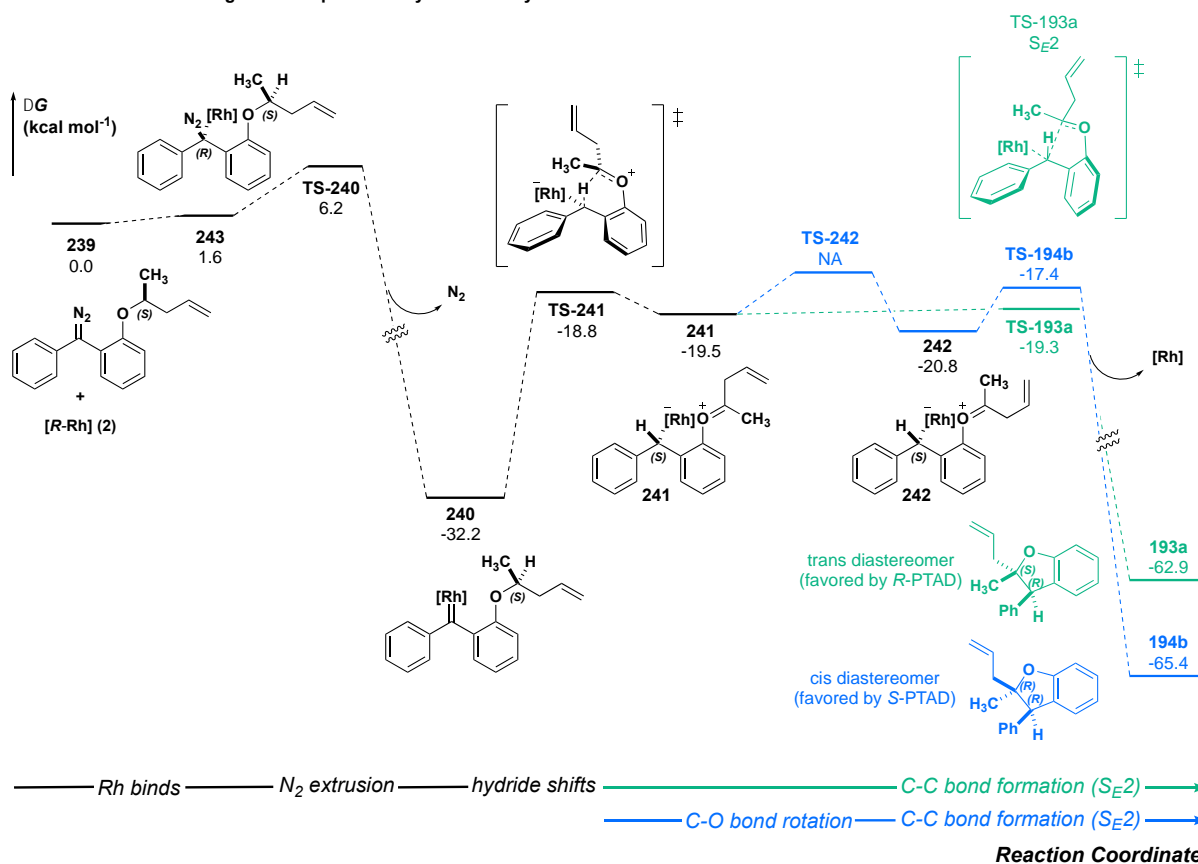


Figure 1.33 Pathway for Rh₂(*R*-PTAD)₄ and (*S*)-homoallylic carbene precursor to observed products **193a** and **194b**.

S_E2 mechanisms have been reported before in electrophilic cleavages of organomercurial compounds^{112,113} exhibiting S_E2 retention of configuration and organotin compounds,^{114,115} which exhibit S_E2 inversion of configuration at carbon. In this case, the S_E2 mechanism results in the inversion of the *S* stereochemistry of the carbon in **241** to the *R* stereochemistry of that carbon in **193a**. During this first pathway, the prochiral face exposed in intermediate **241** forms

the trans diastereomer **193a** during nucleophile attack from the Rh–C bond to the oxocarbenium ion.

The second pathway is where intermediate **241** can rotate about the C_{aryl}–O bond to expose the opposite prochiral face to give intermediate **242**. **242** can then undergo the same S_E2 C–C bond closure to give the (*R,R*) cis diastereomer **194b**. Although we successfully identified transition states leading from **241** to **193a** and from **242** to **194b**, the transition state for **241** to **242** remains elusive. This bond rotation step accounts for the diastereomeric ratio observed. It shows that the rate of C–C bond closure versus the rate of bond rotation is responsible for controlling the diastereoselectivity of the reaction. The relative energies of transition states TS-**193a** and TS-**194b**, as well as the TS-**242**, could all be influencing the diastereoselectivity and be dependent on the catalyst used in the reaction.

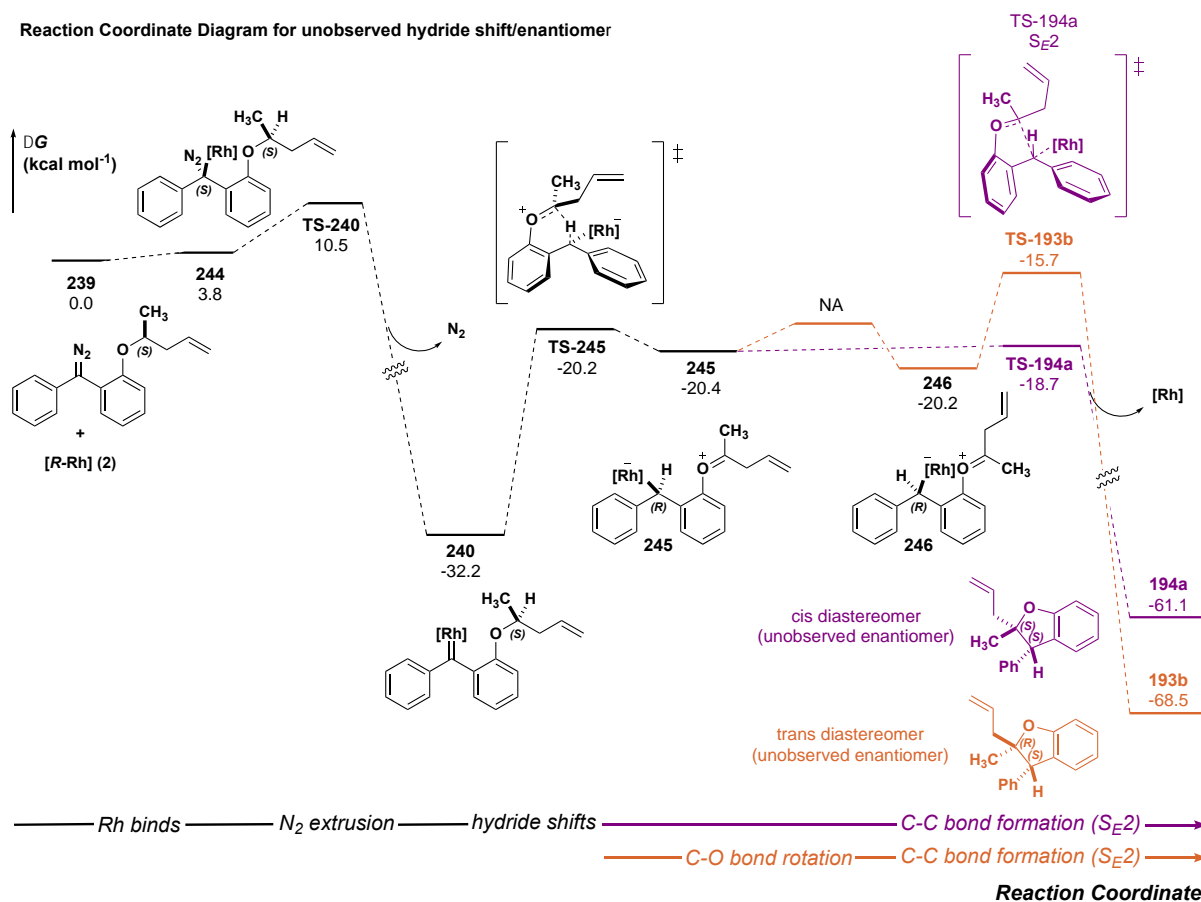


Figure 1.34 Pathway for Rh₂(*R*-PTAD)₄ and (*S*)-homoallylic precursor to **193b**/**194a**.

This stepwise pathway can be used to hypothesize a similar mechanism for forming **190a** (Figure 1.35). Oxidation of (*S*)-**189** to diazo followed by the addition of catalyst will form Rh carbene **247**. This intermediate will undergo the same highly stereoselective hydride transfer to form a single oxocarbenium ion intermediate **248**. Rotating about the C_{aryl}–O bond in **248** to expose the other prochiral oxocarbenium ion face is kinetically unfavorable due to increased steric bulk, contributing to a high energetic cost to rotate in the chiral cavity. Our computational results from an energy surface scan with an achiral catalyst (**6**) indicate that rotation about the C_{aryl}–O bond in **248** indeed requires more energy (>4 kcal/mol) than C–C bond formation. Therefore, **248** rapidly closes to form a new C–C bond by an S_E2 mechanism yielding **190a** as a single enantiomer and single diastereomer of the product. The computed pathway for the sterically bulky, highly activated substrate **189** reacting with Rh₂(OAc)₄ also supports a stepwise mechanism for the C–H insertion reaction.

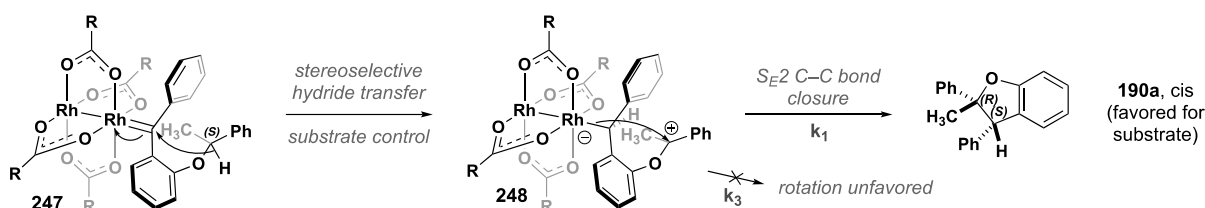


Figure 1.35 Proposed mechanism for the formation of **190a**.

1.3 Conclusion

In summary, we have developed a method and stereochemical rationale for intramolecular C–H insertion reactions with donor/donor carbene systems possessing chiral ethers (Figure 1.36). This enables the generation of two contiguous stereogenic centers in a single step, yielding a trisubstituted benzodihydrofuran core. Exploration of chiral substrates with two enantiomers of a chiral catalyst revealed stereoselectivity patterns not observed with other types of carbene C–H insertion systems. High enantioselectivity can be achieved and controlled based on the enantiomer of starting material used. High diastereoselectivity emerges from substrate control, irrespective of

the catalyst used for sterically hindered and highly activated C-H insertion centers. Less sterically demanding and less activated C-H insertion centers exhibit high diastereoselectivity that is controlled based on the enantiomer of catalyst employed in the reaction. Our DFT studies with a truncated variant of the chiral $\text{Rh}_2(\text{R-PTAD})_4$ catalyst demonstrate that the highly stereoselective hydride transfer controls enantioselectivity outcomes, whereas a zwitterionic intermediate undergoes diastereoselective ring closure through an $\text{S}_{\text{E}}2$ mechanism. These studies demonstrate that donor/donor carbenes are capable of unique levels of stereocontrol not previously seen with acceptor-containing carbenes.

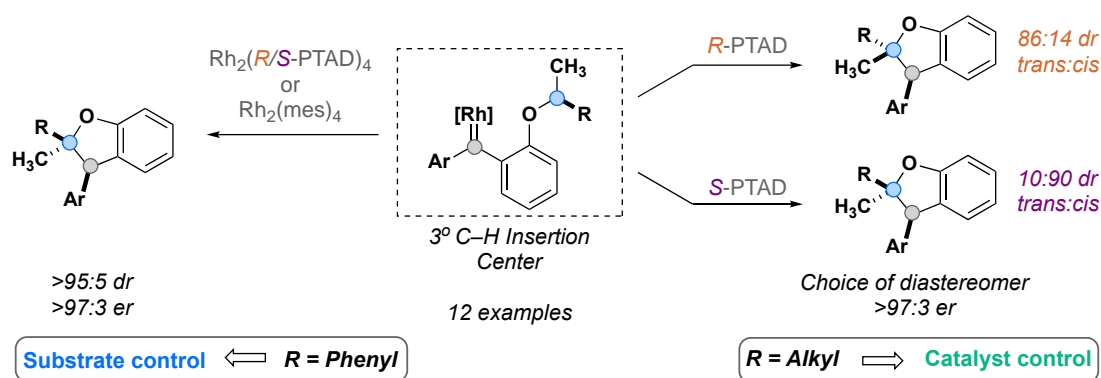


Figure 1.36 Graphic summary of C-H insertions into chiral ethers.

1.4 Experimental Section

1.4.1 General Procedures

General Comments. Chemicals were purchased and used without further purification unless otherwise specified. All reactions using anhydrous solvents were carried out under an atmosphere of industrial argon in flame-dried glassware with magnetic stirring. Anhydrous solvent was dispensed from a solvent purification system that passes solvent through two columns of dry neutral alumina. Reactions were monitored by thin layer chromatography (TLC, Merck), and detected by examination under UV light (254 nm and 365 nm). Flash column chromatography was performed using silica gel [230–400 mesh (40–63 μm)].

Extracts were concentrated in vacuo using both a rotary evaporator (bath temperatures up to 40 °C) at a pressure of either 15 mmHg (diaphragm pump) or 0.1 mmHg (oil pump), as appropriate. ¹H and proton-decoupled ¹³C spectra were measured in CDCl₃ at 400, or 600 MHz, and 101 or 151 MHz respectively unless otherwise noted. All spectra in CDCl₃ were referenced at TMS = 0 ppm. High-resolution mass spectrometry was performed on positive mode and ESI/Orbitrap™, ESI/TOF, and CI/TOF techniques were generally used. For substrates 24 and 25 high-resolution mass spectrometry using the aforementioned techniques was not achieved; low-resolution mass spectrometry using an Advion© ASAP-APCI-MS was achieved and the corresponding data is reported for those. Melting points were taken on an EZ-melting apparatus and were uncorrected. Infrared spectra were taken on a Bruker Tensor 27 spectrometer.

General Procedure A (Mitsunobu reaction). To a flame-dried 100 mL round bottom flask under argon atmosphere was added phenol (1.0 equiv), alcohol (1.1 equiv), and THF (0.1 M). The reaction was cooled to 0 °C, then triphenylphosphine (1.3 equiv) and diisopropyl azodicarboxylate (1.3 equiv) were added sequentially. After stirring overnight and allowing the reaction to warm to room temperature, the reaction was concentrated *in vacuo* and purified by flash column chromatography to yield the desired ether.

General Procedure B (Benzophenone formation). To a flame-dried 100 mL round bottom flask under argon atmosphere was added aryl bromide (1.0 equiv) and THF (0.25 M). The reaction was cooled to -78 °C, then n-BuLi (1.2 equiv) was added and the reaction was stirred at -78 °C for two hours. A solution of weinreb (1.0 equiv) in THF (0.8 M) was added to the reaction mixture, then the reaction was stirred overnight while allowing it to warm to room temperature. The reaction was cooled back down to -78 °C and quenched with saturated NH₄Cl aqueous

solution. The mixture was extracted three times with EtOAc, then the combined organic layers were dried over Na₂SO₄, concentrated *in vacuo*, and purified by flash column chromatography to yield the desired ketone.

General Procedure C (Hydrazone formation). Following a literature precedent¹, to an oven-dried 10-20 mL microwave vial under argon atmosphere was added the desired alkylated benzophenone (1.0 equiv) in anhydrous EtOH (0.1 M). Glacial acetic acid (2.0 equiv) and anhydrous hydrazine (8.0 equiv) were added dropwise to the solution. The reaction was heated to 80 °C for 3-12 hours until the starting material fully converted by TLC. After the reaction was cooled, it was diluted in diethyl ether (25 mL) then washed with water (2 x 10 mL) and brine (1 x 10 mL). The organic layer was dried over Na₂SO₄, concentrated *in vacuo*, and purified by flash column chromatography to yield the desired hydrazone.

Note: Hydrazones were isolated as a mixture of E/Z isomers or used without further purification. As such ¹H peaks have been reported only for selected examples.

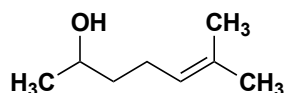
General Procedure D (One-pot sequential C-H insertion). To a flame-dried 20 mL scintillation vial under argon atmosphere was added a solution of hydrazone (1.0 equiv) in anhydrous CH₂Cl₂ (0.01 M). To the solution was added MnO₂ (8.0 equiv), and the suspension was stirred until full conversion of the starting material to diazo was observed by TLC. A color change of the solution from clear to magenta was observed from the formation of the diazo. The reaction was cooled to 0 °C then the desired dirhodium catalyst was added (1 mol %), and the reaction was stirred while allowing it to warm to room temperature until full conversion of diazo to the desired product was observed. The crude reaction mixture was filtered over Celite to remove

MnO₂, concentrated *in vacuo*, and purified by flash column chromatography to yield the desired insertion product.

Note: it is necessary that the MnO₂ used for the oxidation of hydrazones be ~85% pure with an average particle size of 2 microns, appearing as a fine black powder (e.g. Oakwood Chemical, CAS #: 1313-13-9, cat. #: 094454, lot #: 094454K03K).

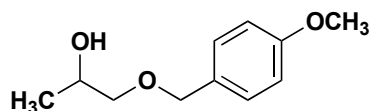
General Procedure E (synthesis of Weinreb amide). To a flame-dried round bottom flask was added the substituted benzoic acid (1.0 equiv) in DCM (0.3 M) and oxalyl chloride (2.0 equiv). DMF (1.3 equiv) was added dropwise, and the solution was stirred for 1 h. The solution was then concentrated *in vacuo* and re-diluted in DCM (30 mL). To a separate flame-dried round bottom flask were added *N,O*-dimethylhydroxylamine hydrochloride (1.5 equiv), Et₃N (3.0 equiv), and DCM (0.3 M) and the solution was stirred for 10 min. The Weinreb salt solution was cooled down to 0 °C, then the acyl chloride solution was added dropwise and stirred at rt overnight. Upon completion, the reaction was quenched with sat. aq. NaHCO₃ (50 mL) and the mixture was extracted with CH₂Cl₂ (3 x 50 mL). The combined organic layers were washed with H₂O (2 x 30 mL) and brine (30 mL). The organic layer was dried over Na₂SO₄, filtered, and concentrated *in vacuo*. The crude reaction mixture was purified by flash column chromatography to yield the desired Weinreb amide.

1.4.2 Alcohol substrates



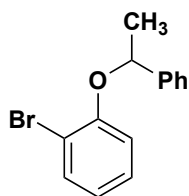
(171e) 6-methylhept-5-en-2-ol was synthesized according to reported literature procedure¹¹⁶ using 6-methylhept-5-en-2-one (5.0 g, 39.6 mmol), sodium borohydride (0.749 g, 19.8 mmol) with EtOH (132 mL, 0.3 M) and H₂O (40 mL, 0.5 M with NaBH₄). After workup no further purification was needed to yield **171e** as a clear oil (4.13g, 81%). ¹H NMR (400 MHz, CDCl₃)

δ 5.13 (t, $J = 8.0$ Hz, 1H), 3.81 (q, $J = 6.4$ Hz, 1H), 2.08 (hept, $J = 7.3$ Hz, 2H), 1.69 (s, 3H), 1.63 (s, 3H), 1.53 – 1.44 (m, 3H), 1.19 (d, $J = 6.1$ Hz, 3H). ^1H NMR data was consistent with literature values.¹¹⁶



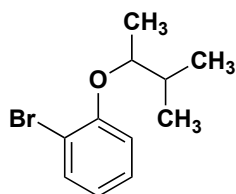
(171f) 1-((4-methoxybenzyl)oxy)propan-2-ol was synthesized according to reported literature procedure¹¹⁷ using propene oxide (1.00 g, 17.2 mmol), NaH (0.798 g, 19.8 mmol, 57% dispersion in mineral oil) with anhydrous DMF (27 mL, 0.7 M) and 4-methoxybenzyl alcohol (4.76 g, 34.4 mmol) with anhydrous DMF (17.2 mL, 2.0 M). The crude product was purified by flash column chromatography (40:60 EtOAc:Hexanes) affording alcohol **171f** as a clear oil (2.56 g, 76%): ^1H NMR (400 MHz, CDCl_3) δ 7.37 – 7.19 (m, 2H), 6.97 – 6.82 (m, 2H), 4.62 (s, 1H), 4.49 (s, 1H), 3.81 (s, 4H), 3.45 (dd, $J = 9.4, 3.1$ Hz, 1H), 3.25 (t, $J = 8.8$ Hz, 1H), 2.37 (br, 1H), 1.14 (d, $J = 6.4$ Hz, 2H). ^1H NMR data was consistent with literature values.¹¹⁷

1.4.3 Bromo-ether substrates

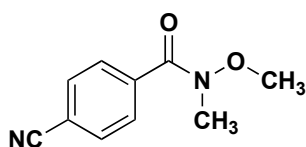


(182a) 1-bromo-2-(1-phenylethoxy)benzene was synthesized according to general procedure A, 2-bromophenol (1.14 mL, 9.83 mmol), 1-phenylethan-1-ol (1.00 mL, 8.19 mmol), triphenylphosphine (2.79 g, 10.65 mmol), and DIAD (2.09 mL, 10.65 mmol) with anhydrous THF (82 mL) were used. The crude product was purified by flash column chromatography (10:90 EtOAc:hexanes) affording ether **182a** as a light yellow oil (2.16 g, 95%): ^1H NMR (600 MHz, CDCl_3) δ 7.50 (d, $J = 7.8$ Hz, 1H), 7.41 – 7.36 (m, 2H), 7.32 (t, 2H), 7.24 (t, 1H), 7.06 (t, $J = 7.8$ Hz, 1H), 6.76 – 6.70 (m, 2H), 5.34 (q, $J = 6.4$ Hz, 1H), 1.67 (d, $J = 6.5$ Hz, 3H). ^{13}C

NMR (151 MHz, CDCl₃) δ 154.43, 142.68, 133.45, 128.76(2), 128.26, 127.74, 125.71(2), 122.01, 115.60, 113.18, 77.41, 24.49; IR (thin film) 3063, 1584, 1494 cm⁻¹; TLC (20:80, EtOAc:hexanes) R_F = 0.85. Low-resolution MS (Advion ASAP-APCI) m/z calcd for C₁₄H₁₄BrO⁺[M+H]⁺ 277.0173, found 277.0. $[\alpha]_D^{23} = +32.0$ (c = 0.30, CHCl₃).

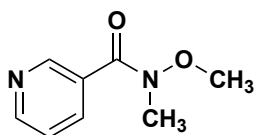


(182h) 1-bromo-2-((3-methylbutan-2-yl)oxy)benzene was synthesized according to general procedure A, 2-bromophenol (3.35 mL, 28.9 mmol), 3-methyl-2-butanol (3.43 mL, 31.8 mmol), triphenylphosphine (9.10 g, 34.7 mmol), diisopropyl azodicarboxylate (6.81 mL, 34.7 mmol), and anhydrous THF (150 mL) were used. The crude product was purified by flash column chromatography (90:10, hexanes:EtOAc) affording ether **182h** as a clear oil (3.97 g, 56%): ¹H NMR (599 MHz, CDCl₃) δ 7.52 (d, $J = 7.9$ Hz, 1H), 7.21 (t, $J = 7.8$ Hz, 1H), 6.87 (d, $J = 8.3$ Hz, 1H), 6.78 (t, $J = 7.6$ Hz, 1H), 4.20 (p, $J = 6.0$ Hz, 1H), 1.97 (hd, $J = 6.8, 5.1$ Hz, 1H), 1.26 (d, $J = 6.3$ Hz, 3H), 1.03 (d, $J = 6.8$ Hz, 3H), 1.01 (d, $J = 6.8$ Hz, 3H); ¹³C NMR (150 MHz, CDCl₃) δ 154.92, 133.59, 128.35, 121.51, 114.90, 113.58, 80.03, 77.37, 77.16, 76.95, 33.26, 18.29, 18.04, 16.10.; IR (thin film) 3184, 1773, 1704 cm⁻¹; Low-resolution MS (Advion ASAP-APCI) m/z calcd for C₁₁H₁₆BrO⁺[M+H]⁺ 243.0379.1307 found 243.0.



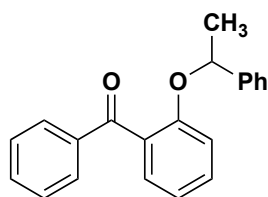
(183a) 4-cyano-N-methoxy-N-methylbenzamide was synthesized according to general procedure E using 4-cyanobenzoic acid (8.00 g, 54.5 mmol) in CH₂Cl₂ (181 mL), oxalyl chloride (9.3 mL, 108.7 mmol), DMF (5.46 mL, 70.75 mmol), Et₃N (22.8 mL, 163.2 mmol), and *N,O*-dimethylhydroxylamine hydrochloride (7.96 g, 81.6 mmol) in CH₂Cl₂ (181 mL). The crude product was extracted from NaHCO₃ (150 mL) with CH₂Cl₂ (3 x 100 mL) and the

combined organic layers were washed with NaHCO₃ (2 x 50 mL) and brine (1 x 50 mL). The crude product was purified by flash column chromatography (90:10, hexanes:EtOAc) affording **183a** as a clear oil (7.86 g, 76%). ¹H NMR (400 MHz, CDCl₃) δ 7.78 (d, *J* = 7.6 Hz, 2H), 7.71 (d, *J* = 8.1 Hz, 2H), 3.53 (s, 3H), 3.38 (s, 3H). ¹H NMR data was consistent with literature values.¹¹⁸

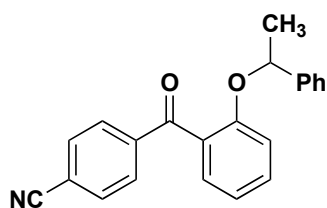


(183c) N-methoxy-N-methylnicotinamide was synthesized by preparing a suspension of N-methoxy-N-methylamine•HCl (1.317 g, 13.50 mmol, 1.2 equiv.) in CH₂Cl₂ (45.0 mL), following a modified literature procedure.⁴ This suspension was cooled to 0 °C and triethylamine (6.25 mL, 44.8 mmol, 3.9 equiv) was added slowly over 20 minutes, the resulting solution was cooled to 0 °C. To the solution was added nicotinoyl chloride•HCl (2.032 g, 11.41 mmol, 1.0 equiv) and the mixture was allowed to warm to rt and stirred for 23 h, The reaction mixture was quenched with sat. aq. NaHCO₃ (10 mL), and the organic layer was separated. The aqueous layer was then neutralized with 1 M HCl and extracted with CH₂Cl₂ (3 X 50 mL); the combined organic layers were washed with brine (2 X 100 mL) and dried over Na₂SO₄. The resulting solution was concentrated in vacuo and the crude product was purified using flash column chromatography (95:5, CH₂Cl₂:CH₃OH), affording **183c** as a yellow oil (1.568 g, 83%). ¹H NMR (400 MHz, CDCl₃) δ 8.96 (d, *J* = 1.2 Hz, 1H), 8.69 (dd, *J* = 4.9, 1.7 Hz, 1H), 8.03 (dt, *J* = 7.9, 1.9 Hz, 1H), 7.37 (ddd, *J* = 7.9, 4.9, 0.9 Hz, 1H), 3.56 (s, 3H), 3.40 (s, 3H). ¹H NMR data was consistent with literature values.¹¹⁸

1.4.4 Ketone substrates

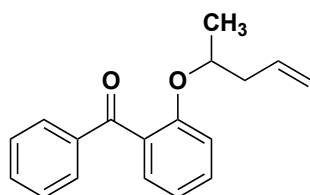


(172a) Phenyl(2-(1-phenylethoxy)phenyl)methanone was synthesized according to general procedure A, 2-hydroxyphenyl(phenyl)methanone (1.00 g, 5.04 mmol), 1-phenylethan-1-ol (0.607 mL, 5.04 mmol), triphenylphosphine (1.59 g, 6.05 mmol), and DIAD (1.19 mL, 6.05 mmol) with anhydrous THF (50 mL) were used. The crude product was purified by flash column chromatography (10:90 EtOAc:hexanes) affording ketone **172a** as a clear oil (1.26 g, 83%): $^1\text{H NMR}$ (600 MHz, CDCl_3) δ 7.86 (d, $J = 8.5$ Hz, 2H), 7.70 (d, $J = 6.7$ Hz, 2H), 7.48 (d, $J = 7.6$ Hz, 1H), 7.40 – 7.34 (m, 1H), 7.28 – 7.22 (m, 4H), 7.06 – 7.00 (m, 3H), 6.83 (d, $J = 8.4$ Hz, 1H), 5.20 (q, $J = 7.0, 6.4$ Hz, 1H), 1.25 (d, $J = 6.5$ Hz, 3H).; $^{13}\text{C NMR}$ (150 MHz, CDCl_3) δ 195.81, 156.20, 142.33, 142.16, 133.17, 132.12(2), 130.41, 129.76(2), 128.76(2), 128.31, 127.93(2), 125.41, 121.12, 118.39, 115.67, 114.08, 77.37, 77.20, 77.16, 76.95, 23.77.; IR (thin film) 3018, 2361, 2339, 1664 cm^{-1} ; TLC (10:90, EtOAc:hexanes) $R_F = 0.2$. AMM (ESI) m/z calcd for $\text{C}_{21}\text{H}_{19}\text{O}_2^+[\text{M}+\text{H}]^+$ 327.1259; $[\alpha]_D^{23} = +124.4$ ($c = 1.4$, CHCl_3).

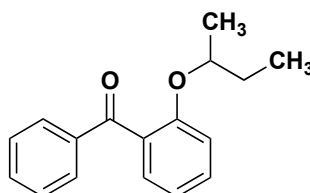


(184a) 4-(2-(1-phenylethoxy)benzoyl)benzonitrile was synthesized according to general procedure B, 1-bromo-2-(1-phenylethoxy)benzene (5.00 g, 18.04 mmol) with anhydrous THF (60 mL), *n*-BuLi (2.28 M, 21.64 mmol, 9.50 mL), para-cyano Weinreb (4.12 g, 21.65 mmol) with anhydrous THF (27 mL) were used. The crude product was purified by flash column chromatography (30:70, EtOAc:hexanes) affording ketone **184a** as a light yellow oil (2.66 g, 45%): $^1\text{H NMR}$ (600 MHz, CDCl_3) δ 7.86 (d, $J = 8.4$ Hz, 2H), 7.71 (d, $J = 8.5$ Hz, 2H), 7.48 (d, $J = 7.6$ Hz, 1H), 7.37 (t, 1H), 7.28 – 7.22 (m, 4H), 7.07 – 7.00 (m, 3H), 6.83 (d, $J = 8.4$ Hz,

1H), 5.20 (q, $J = 6.6$ Hz, 1H), 1.25 (d, $J = 6.4$ Hz, 3H); ^{13}C NMR (150 MHz, CDCl_3) δ 195.81, 156.20, 142.33, 142.16, 133.16, 132.12(2), 130.41, 129.76,(2) 128.75(2), 128.31, 127.93, 125.41(2), 121.12, 118.39, 115.67, 114.08, 77.20, 23.77; IR (thin film) 2977, 2229, 1662, 1448, 1236 cm^{-1} ; TLC (40:60, EtOAc:hexanes) $R_F = 0.45$. AMM (ESI) m/z calcd for $\text{C}_{22}\text{H}_{18}\text{NO}_2^+[\text{M}+\text{H}]^+$ 328.1332, found 328.1333; $[\alpha]_D^{23} = +85.4$ ($c = 0.62$, CHCl_3)

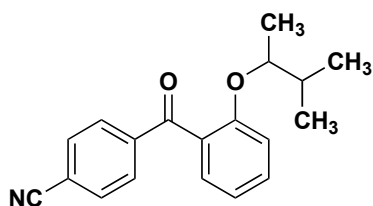


(172c) (2-(pent-4-en-2-yloxy)phenyl)(phenyl)methanone was synthesized according to general procedure A, (2-hydroxyphenyl)(phenyl)methanone (5.51 g, 27.80 mmol), pent-4-en-2-ol (2.39 mL, 23.20 mmol), triphenylphosphine (7.92 g, 30.20 mmol), diisopropyl azodicarboxylate (5.93 mL, 30.20 mmol), and anhydrous THF (57 mL) were used. The crude product was purified by flash column chromatography (40:60, CH_2Cl_2 :hexanes) affording ketone **172c** as a light yellow oil (5.00 g, 81%): ^1H NMR (600 MHz, CDCl_3) δ 7.78 (d, $J = 8.2$ Hz, 2H), 7.52 (t, $J = 7.4$ Hz, 1H), 7.45 – 7.36 (m, 4H), 7.01 (t, $J = 7.4$ Hz, 1H), 6.93 (d, $J = 8.3$ Hz, 1H), 4.25 (h, $J = 6.0$ Hz, 1H), 1.47 – 1.31 (m, 2H), 1.07 (d, $J = 6.1$ Hz, 3H), 0.67 (t, $J = 7.5$ Hz, 3H); ^{13}C NMR (100 MHz, CDCl_3) δ 198.47, 149.25, 137.96, 133.82, 132.74, 131.93, 130.21, 130.01, 129.72(2), 128.18(2), 122.15, 118.40, 113.74, 74.24, 41.07, 18.01; IR (thin film) 3063, 2978, 1692, 1584, 1493 cm^{-1} ; AMM (ESI) m/z calcd for $\text{C}_{18}\text{H}_{18}\text{O}_2^+[\text{M}+\text{H}]^+$ 266.1307 found 267.1378; $[\alpha]_D^{23} = +95.5$ ($c = 0.35$, CHCl_3)

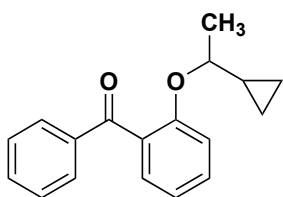


(172b) (2-(sec-butoxy)phenyl)(phenyl)methanone was synthesized according to general procedure A, (2-hydroxyphenyl)(phenyl)methanone (0.50 g, 2.52 mmol), 2-butanol (0.26 mL,

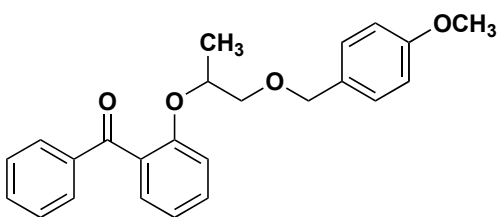
2.77 mmol), triphenylphosphine (0.86 g, 3.28 mmol), diisopropyl azodicarboxylate (0.64 mL, 3.28 mmol), and anhydrous THF (25 mL) were used. The crude product was purified by flash column chromatography (40:60, CH₂Cl₂:hexanes) affording ether **172b** as a light yellow oil (0.574 g, 90%): ¹H NMR (600 MHz, CDCl₃) δ 7.78 (d, *J* = 8.1 Hz, 2H), 7.52 (t, *J* = 7.4 Hz, 1H), 7.45 – 7.37 (m, 4H), 7.01 (t, *J* = 7.4 Hz, 1H), 6.93 (d, *J* = 8.3 Hz, 1H), 4.25 (h, *J* = 6.0 Hz, 1H), 1.47 – 1.38 (m, 1H), 1.39 – 1.30 (m, 1H), 1.07 (d, *J* = 6.1 Hz, 3H), 0.67 (t, *J* = 7.4 Hz, 3H); ¹³C NMR (150 MHz, CDCl₃) δ 197.41, 155.99, 138.53, 132.70, 131.89, 130.14, 129.93, 129.70(2), 128.15(2), 120.37, 113.59, 77.37, 77.16, 76.95, 75.38, 28.91, 18.63, 9.31. IR (thin film) 3020, 2975, 2361, 1776, 1664 cm⁻¹; AMM (ESI) *m/z* calcd for C₁₇H₁₈O₂⁺[M+H]⁺ 255.1380 found 255.1379; [α]_D²³ = -43.6 (c = 1.29, CHCl₃)



(184h) 4-(2-((3-methylbutan-2-yl)oxy)benzoyl)benzonitrile was synthesized according to general procedure B, 1-bromo-2-((3-methylbutan-2-yl)oxy)benzene (1.96 g, 8.06 mmol) with anhydrous THF (56 mL), n-BuLi (1.7 M, 10.48 mmol, 6.16 mL), para-cyano Weinreb (1.89 g, 9.67 mmol) with anhydrous THF (23 mL) were used. The crude product was purified by flash column chromatography (30:70, EtOAc:hexanes) affording ketone **184h** as a light yellow oil (1.37 g, 58%): ¹H NMR (400 MHz, CDCl₃) δ 7.85 (d, *J* = 8.3 Hz, 2H), 7.71 (d, *J* = 8.2 Hz, 2H), 7.54 – 7.43 (m, 2H), 7.04 (t, *J* = 7.4 Hz, 1H), 6.94 (d, *J* = 8.8 Hz, 1H), 4.17 (dt, 1H), 1.61 – 1.51 (m, 1H), 1.02 (d, *J* = 6.2 Hz, 3H), 0.65 – 0.55 (m, 6H); ¹³C NMR (101 MHz, CDCl₃) δ 196.00, 156.31, 142.32, 133.17, 132.11(2), 130.58, 129.81(2), 128.59, 120.65, 118.41, 115.59, 113.19, 79.05, 33.36, 17.59, 17.51, 15.26.; IR (thin film) 3046, 2971 1774 cm⁻¹; AMM (ESI) *m/z* calcd for C₁₉H₂₀NO₂⁺[M-H]⁻ 293.1416, found 293.1809.

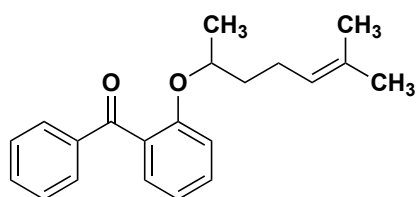


(172d) (2-(1-cyclopropylethoxy)phenyl)(phenyl)methanone was synthesized according to general procedure A, (2-hydroxyphenyl)(phenyl)methanone (0.500 g, 2.52 mmol), 1-cyclopropylethan-1-ol (0.271 mL, 2.77 mmol), triphenylphosphine (0.860 g, 3.28 mmol), diisopropyl azodicarboxylate (0.644 mL, 3.28 mmol), and anhydrous THF (25 mL) were used. The crude product was purified by flash column chromatography (10:90, EtOAc:hexanes) affording ketone **172d** as a pale yellow oil (0.495 g, 74%): $^1\text{H NMR}$ (600 MHz, CDCl_3) δ 7.82 (dd, $J = 8.3, 1.4$ Hz, 2H), 7.59 – 7.54 (m, 1H), 7.47 – 7.41 (m, 4H), 7.06 (td, $J = 7.5, 1.0$ Hz, 1H), 6.98 (d, $J = 9.0$ Hz, 1H), 3.89 (p, $J = 6.2$ Hz, 1H), 1.16 (d, $J = 6.1$ Hz, 3H), 0.79 (tdt, $J = 8.2, 6.7, 5.1$ Hz, 1H), 0.34 (tdd, $J = 8.6, 5.5, 4.2$ Hz, 1H), 0.27 (dddd, $J = 9.2, 7.9, 5.4, 4.3$ Hz, 1H), 0.08 (dtd, $J = 9.4, 5.2, 4.3$ Hz, 1H), 0.05 – -0.00 (m, 1H); $^{13}\text{C NMR}$ (150 MHz, CDCl_3) δ 197.28, 155.96, 138.38, 132.70, 131.84, 130.48, 129.92, 129.73(2), 128.17, 120.79, 114.84, 78.00, 22.04, 19.28, 16.40, 3.11, 1.60; IR (thin film) 2978, 1659, 1596 cm^{-1} AMM (ESI) m/z calcd for $\text{C}_{18}\text{H}_{18}\text{O}_2^+[\text{M}+\text{H}]^+$ 267.1380, found 267.1378.

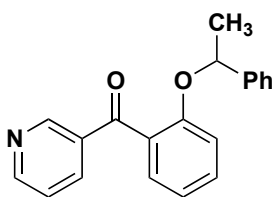


(172f) (2-(((1-(4-methoxybenzyl)oxy)propan-2-yl)oxy)phenyl)(phenyl)methanone was synthesized according to general procedure A, (2-hydroxyphenyl)(phenyl)methanone (1.00 g, 5.04 mmol), 1-((4-methoxybenzyl)oxy)propan-2-ol (1.09 g, 5.55 mmol), triphenylphosphine (1.72 g, 6.55 mmol), diisopropyl azodicarboxylate (1.29 mL, 6.55 mmol), and anhydrous THF (51 mL) were used. The crude product was purified by flash column chromatography (10:90, EtOAc:hexanes) affording ketone **172f** as a pale yellow oil (1.73 g, 92%): $^1\text{H NMR}$ (400 MHz,

CDCl₃) δ 7.78 (d, J = 6.9 Hz, 2H), 7.51 (t, J = 7.4 Hz, 1H), 7.40 (tt, J = 9.8, 6.8 Hz, 4H), 7.11 (d, J = 8.6 Hz, 2H), 7.07 – 6.97 (m, 2H), 6.82 (d, J = 8.6 Hz, 2H), 4.49 (h, J = 6.1 Hz, 1H), 4.27 (d, J = 2.0 Hz, 2H), 3.78 (s, 3H), 3.32 (dd, J = 10.2, 5.7 Hz, 1H), 3.23 (dd, J = 10.2, 4.9 Hz, 1H), 1.09 (d, J = 6.3 Hz, 3H); ¹³C NMR (100 MHz, CDCl₃) δ 197.05, 159.20, 155.79, 138.33, 132.75, 131.88, 130.28, 130.10, 129.79, 129.73(2), 129.23(2), 128.17(2), 120.81, 114.05, 113.77(2), 77.48, 77.16, 76.84, 74.04, 73.04, 72.87, 55.33, 16.78; IR (thin film) 2923, 1663, 1597 cm⁻¹. AMM (ESI) m/z calcd for C₂₄H₂₅O₄⁺[M+H]⁺ 377.1748, found 377.1731.

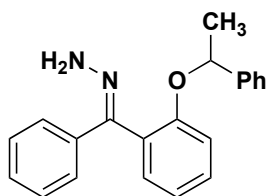


(172e) (2-((6-methylhept-5-en-2-yl)oxy)phenyl)(phenyl)methanone was synthesized according to general procedure A, (2-hydroxyphenyl)(phenyl)methanone (1.00 g, 5.04 mmol), 6-methylhept-5-en-2-ol (0.712 g, 5.55 mmol), triphenylphosphine (1.72 g, 6.55 mmol), diisopropyl azodicarboxylate (1.29 mL, 6.55 mmol), and anhydrous THF (51 mL) were used. The crude product was purified by flash column chromatography (10:90, EtOAc:hexanes) affording ketone **172e** as a pale yellow oil (1.13 g, 73%): ¹H NMR (400 MHz, CDCl₃) δ 7.81 – 7.76 (m, 2H), 7.56 – 7.49 (m, 1H), 7.44 – 7.37 (m, 4H), 7.01 (td, J = 7.5, 0.9 Hz, 1H), 6.92 (d, J = 8.3 Hz, 1H), 4.95 (t, J = 7.2 Hz, 1H), 4.31 (h, J = 6.0 Hz, 1H), 1.79 (dt, J = 7.7, 7.7 Hz, 2H), 1.64 (s, 3H), 1.46 (s, 3H), 1.45 – 1.39 (m, 1H), 1.39 – 1.29 (m, 1H), 1.09 (d, J = 6.0 Hz, 3H); ¹³C NMR (100 MHz, CDCl₃) δ 197.38, 155.95, 138.54, 132.73, 132.17, 131.88, 130.15, 129.92, 129.71(2), 128.18(2), 123.75, 120.36, 113.48, 77.48, 77.16, 76.84, 73.56, 36.25, 25.80, 23.71, 19.16, 17.73; IR (thin film) 2970, 1661, 1595 cm⁻¹ AMM (ESI) m/z calcd for C₂₁H₂₅O₂⁺[M+H]⁺ 309.1849, found 309.1858.



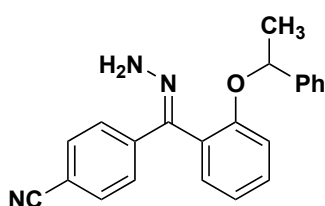
(184c) 2-(1-phenylethoxy)phenyl(pyridin-3-yl)methanone was synthesized according to general procedure B. 1-bromo-2-((3-methylbutan-2-yl)oxy)benzene (0.500 g, 1.80 mmol) with anhydrous THF (6.7 mL), n-BuLi (2.28 M, 2.34 mmol, 1.03 mL), *N*-methoxy-*N*-methylnicotinamide (0.359 g, 2.16 mmol) with anhydrous THF (2.7 mL) were used. The crude product was purified by flash column chromatography (50:50, EtOAc:hexanes) affording ketone **184c** as a yellow oil (0.221 g, 41%): ^1H NMR (400 MHz, CDCl_3) δ 8.96 (d, $J = 1.6$ Hz, 1H), 8.76 (dd, $J = 4.9, 1.7$ Hz, 1H), 8.13 (dt, $J = 7.9, 2.0$ Hz, 1H), 7.49 (dd, $J = 7.5, 1.8$ Hz, 1H), 7.45 – 7.31 (m, 2H), 7.30 – 7.19 (m, 4H), 7.13 – 7.07 (m, 2H), 7.02 (td, $J = 7.5, 0.9$ Hz, 1H), 6.81 (d, $J = 8.6$ Hz, 1H), 5.22 (q, $J = 6.4$ Hz, 1H), 1.25 (d, $J = 6.4$ Hz, 3H); ^{13}C NMR (100 MHz, CDCl_3) δ 195.54, 156.04, 152.79, 151.07, 142.28, 136.33, 134.15, 132.87, 130.19, 128.67(2), 128.42, 127.68, 125.29(2), 123.20, 120.97, 114.07, 77.03, 23.84; IR (thin film) 3032, 2978, 1663, 1596, 1301 cm^{-1} ; AMM (ESI) m/z calcd for $\text{C}_{20}\text{H}_{18}\text{N}_3\text{O}^+[\text{M}+\text{H}]^+$ 304.1332, found 304.1331.

1.4.5 Hydrazone substrates

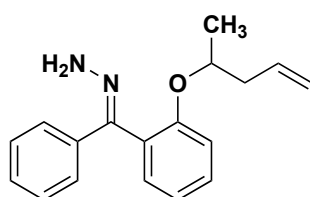


(173a) Phenyl(2-(1-phenylethoxy)phenyl)methylene)hydrazine was synthesized according to general procedure C, phenyl(2-(1-phenylethoxy)phenyl)methanone (0.600 g, 1.98 mmol), hydrazine (0.623 mL, 19.84 mmol), glacial acetic acid (0.230 mL, 3.97 mmol) with anhydrous

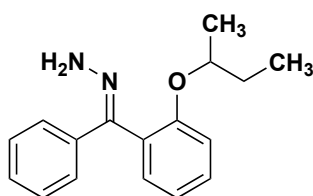
EtOH (6.6 mL) were used. After workup, the mixture was purified by flash column chromatography (30:70, EtOAc:hexanes) affording hydrazone **173a** as a yellow oil (0.478 g, 76%): Note: due to restricted rotation and the mix of isomers many of the ^1H peaks are broadened, see attached spectra ^1H NMR (400 MHz, CDCl_3) δ 7.58 – 7.41 (m, 2H), 7.37 – 7.17 (m, 8H), 7.17 – 7.06 (m, 2H), 7.06 – 6.95 (m, 1H), 6.90 (d, $J = 8.3$ Hz, 1H), 5.45 – 5.14 (m, 2H), 1.37 (s, 3H); IR (thin film) 3015, 2997, 2361, 2339 cm^{-1} ; AMM (ESI) m/z calcd for $\text{C}_{21}\text{H}_{21}\text{N}_2\text{O}^+[\text{M}+\text{H}]^+$ 317.1649, found 317.1651; $[\alpha]_D^{22} = +48.0$ ($c = 1.9$, CHCl_3)



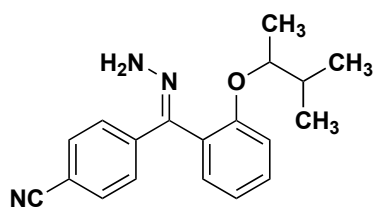
(185a) **4-(hydrazoneylidene(2-(1-phenylethoxy)phenyl)methyl)benzonitrile** was synthesized according to general procedure C, 4-(2-(1-phenylethoxy)benzoyl)benzonitrile (0.423 g, 1.29 mmol), hydrazine (0.324 mL, 10.32 mmol), glacial acetic acid (0.148 mL, 2.58 mmol) with anhydrous EtOH (4.3 mL) were used. After workup hydrazone **183a** was afforded as a mix of two isomers and a light yellow oil (0.348 g, 87%): Note: due to restricted rotation and the mix of isomers many of the ^1H peaks are broadened, see attached spectra. ^1H NMR (600 MHz, CDCl_3) δ 7.65 – 7.47 (m, 3H), 7.37 – 7.17 (m, 5H), 7.17 – 6.97 (m, 3H), 6.97 – 6.81 (m, 1H), 5.80 – 5.53 (m, 2H), 5.36 – 5.16 (m, 1H), 3.70 (qd, $J = 7.0, 0.9$ Hz, 1H), 1.60 – 1.40 (m, 2H), 1.40 – 1.28 (m, 1H), 1.24 (h, $J = 7.2$ Hz, 2H); IR (thin film) 3417, 2977, 2223 cm^{-1} ; TLC (40:60, EtOAc:hexanes) $R_F = 0.85$. AMM (ESI) m/z calcd for $\text{C}_{22}\text{H}_{20}\text{NO}_3^+[\text{M}+\text{H}]^+$ 342.1601, found 342.1603; $[\alpha]_D^{22} = +65.7$ ($c = 1.2$, CHCl_3)



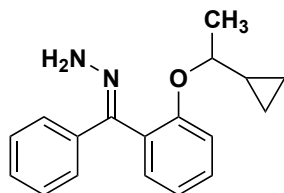
(173c) ((2-(pent-4-en-2-yloxy)phenyl)(phenyl)methylene)hydrazine was synthesized according to general procedure C, (2-(pent-4-en-2-yloxy)phenyl)(phenyl)methanone (0.689 g, 2.59 mmol), hydrazine (0.651 mL, 20.72 mmol), glacial acetic acid (0.296 mL, 5.18 mmol), and anhydrous EtOH (8.6 mL) were used. After workup, hydrazone **173c** was afforded as a light yellow oil (0.629, 87%) and was carried through to the insertion. Note: due to restricted rotation and the mix of isomers many of the ^1H peaks are broadened, see attached spectra: ^1H NMR (600 MHz, CDCl_3) δ 7.50 – 7.45 (m, 2H), 7.45 – 7.38 (m, 1H), 7.35 – 7.23 (m, 3H), 7.19 – 7.11 (m, 1H), 7.11 – 7.03 (m, 2H), 5.44 (s, 2H), 5.13 – 4.82 (m, 2H), 4.40 (s, 1H), 2.47 – 2.07 (m, 2H), 1.38 – 1.00 (m, 3H); IR (thin film) 3404, 3060, 2975, 1641, 1596 cm^{-1} ; AMM (ESI) m/z calcd for $\text{C}_{18}\text{H}_{20}\text{N}_2\text{O}^+[\text{M}+\text{H}]^+$ 281.1649, found 281.1649.



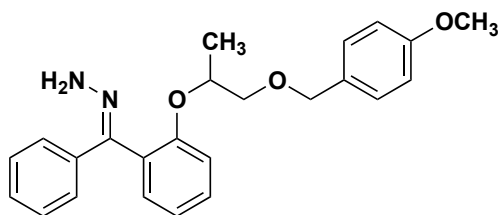
(173b) ((2-(sec-butoxy)phenyl)(phenyl)methylene)hydrazine was synthesized according to general procedure C, (2-(sec-butoxy)phenyl)(phenyl)methanone (0.143 g, 0.563 mmol), hydrazine (0.179 mL, 5.63 mmol), glacial acetic acid (0.064 g, 1.13 mmol), and anhydrous EtOH (1.88 mL) were used. After workup, the mixture was purified by flash column chromatography (20:80, EtOAc:hexanes) affording hydrazone **173b** as a yellow oil (0.116 g, 77%): ^1H NMR (600 MHz, CDCl_3) δ 7.49 – 7.43 (m, 2H), 7.42 – 7.36 (m, 1H), 7.29 – 7.20 (m, 3H), 7.13 (dd, $J = 7.4, 1.8$ Hz, 1H), 7.08 – 6.99 (m, 2H), 5.45 (s, 2H), 4.28 (h, $J = 6.1$ Hz, 1H), 1.72 – 1.35 (m, 2H), 1.35 – 0.97 (m, 4H), 0.97 – 0.55 (m, 3H); IR (thin film) 3023, 2997, 2363, 2337 cm^{-1} AMM (ESI) m/z calcd for $\text{C}_{19}\text{H}_{21}\text{N}_3\text{O}^+[\text{M}+\text{H}]^+$ 308.1758, found 308.1760. $[\alpha]_D^{23} = -10.2$ ($c = 0.53$, CHCl_3)



(185h) 4-(hydrazoneylidene(2-((3-methylbutan-2-yl-oxy)phenyl)methyl)benzoyl)benzonitrile was synthesized according to general procedure C, 4-(2-((3-methylbutan-2-yl)oxy)benzoyl)benzonitrile (1.37 g, 4.65 mmol), hydrazine (1.17 mL, 37.20 mmol), glacial acetic acid (0.532 g, 9.30 mmol), and anhydrous EtOH (15.5 mL) were used. After workup, the mixture was purified by flash column chromatography (50:50, EtOAc:hexanes) affording hydrazone **185h** as an orange oil (0.455 g, 32%): $^1\text{H NMR}$ (400 MHz, CDCl_3) δ 7.54 (s, 3H), 7.42 (t, $J = 7.8$ Hz, 1H), 7.13 (d, $J = 7.4$ Hz, 1H), 7.09 – 6.99 (m, 1H), 5.67 (s, 1H), 4.14 (dt, $J = 14.7, 6.6$ Hz, 1H), 1.25 (td, $J = 6.4, 3.4$ Hz, 1H), 1.21 – 1.09 (m, 1H), 1.00 (td, $J = 7.3, 3.7$ Hz, 2H), 0.89 – 0.58 (m, 4H); IR (thin film) 3021, 2998, 2325 cm^{-1} ; AMM (ESI) m/z calcd for $\text{C}_{19}\text{H}_{21}\text{N}_3\text{O}^+[\text{M}+\text{H}]^+$ 308.1758, found 308.1760.

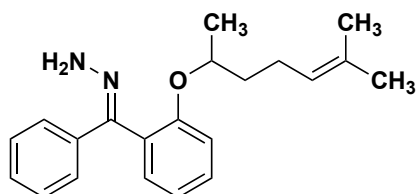


(173d) ((2-(1-cyclopropylethoxy)phenyl)(phenyl)methylene)hydrazine was synthesized according to general procedure C, (2-(1-cyclopropylethoxy)phenyl)(phenyl)methanone (0.363g, 1.36 mmol), hydrazine (0.342 mL, 10.88 mmol), glacial acetic acid (0.156 mL, 2.72 mmol), and anhydrous EtOH (4.5 mL) were used. After workup, the mixture was purified by flash column chromatography (40:60 EtOAc:Hexanes) affording hydrazone **173d** as a yellow oil (0.236g, 62%): $^1\text{H NMR}$ (600 MHz, CDCl_3) δ 7.31 – 7.23 (m, 1H), 7.09 – 7.02 (m, 1H), 3.72 (qd, $J = 7.0, 1.5$ Hz, 1H), 1.43 (s, 1H), 1.29 – 1.20 (m, 3H), 0.51 – 0.07 (m, 1H); IR (thin film) 3400, 2978, 1724, 1484 cm^{-1} ; AMM (ESI) m/z calcd for $\text{C}_{18}\text{H}_{20}\text{N}_2\text{O}^+[\text{M}+\text{H}]^+$ 281.1649, found 281.1649.



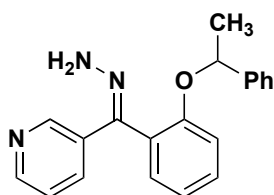
(173f) (2-((1-((4-methoxybenzyl)oxy)propan-2-yl)oxy)phenyl)(phenyl)methylene

hydrazine was synthesized according to general procedure C, (2-((1-((4-methoxybenzyl)oxy)propan-2-yl)oxy)phenyl)(phenyl)methanone (0.181 g, 0.481 mmol), hydrazine (0.121 mL, 3.85 mmol), glacial acetic acid (0.055 mL, 0.962 mmol), and anhydrous EtOH (1.6 mL) were used. After workup, the mixture was purified by flash column chromatography (80:20 EtOAc:Hexanes) affording hydrazone **173f** as a clear oil (0.179 g, 95%): $^1\text{H NMR}$ (400 MHz, CDCl_3) δ 7.52 – 7.44 (m, 2H), 7.43 – 7.35 (m, 1H), 7.31 – 7.22 (m, 3H), 7.21 – 7.04 (m, 5H), 6.91 – 6.76 (m, 2H), 5.43 (s, 2H), 4.56 (q, $J = 5.8$ Hz, 1H), 4.48 – 4.21 (m, 2H), 3.79 (s, 3H), 3.43 (s, 2H), 1.30 – 1.06 (m, 4H); IR (thin film) 3406, 3000, 1511; AMM (ESI) m/z calcd for $\text{C}_{24}\text{H}_{27}\text{N}_2\text{O}_3^+[\text{M}+\text{H}]^+$ 391.2016, found 391.2005.



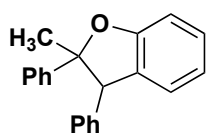
(173e) ((2-((6-methylhept-5-en-2-yl)oxy)phenyl)(phenyl)methylene)hydrazine was synthesized according to general procedure C, (2-((6-methylhept-5-en-2-yl)oxy)phenyl)(phenyl)methanone (0.500 g, 1.62 mmol), hydrazine (0.407 mL, 13.0 mmol), glacial acetic acid (0.185 mL, 3.24 mmol), and anhydrous EtOH (5.4 mL) were used. After workup, the mixture was purified by flash column chromatography (70:30 EtOAc:Hexanes) affording hydrazone **173e** as a clear oil (0.173 g, 87%): $^1\text{H NMR}$ (400 MHz, CDCl_3) δ 7.49 – 7.43 (m, 2H), 7.43 – 7.36 (m, 1H), 7.30 – 7.22 (m, 3H), 7.14 (dd, $J = 7.5, 1.8$ Hz, 1H), 7.08 – 6.99 (m, 2H), 5.43 (s, 2H), 4.97 (s, 1H), 4.35 (h, $J = 6.1$ Hz, 1H), 1.97 (s, 1H), 1.65 (s, 4H),

1.56 (s, 2H), 1.49 – 1.36 (m, 3H), 1.24 – 1.03 (m, 3H); IR (thin film) 3404, 2968, 1595, 1482; AMM (ESI) m/z calcd for $C_{21}H_{27}N_2O^+[M+H]^+$ 323.2118, found 323.2113.



(185c) 3-(hydrazineylidene(2-(1-phenylethoxy)phenyl)methyl)pyridine was synthesized according to general procedure C, (2-(1-phenylethoxy)phenyl)(pyridin-3-yl)methanone (0.200 g, 0.659 mmol), hydrazine (0.180 mL, 5.27 mmol), glacial acetic acid (0.075 mL, 1.32 mmol), and anhydrous EtOH (2.2 mL) were used. After workup, the mixture was purified by flash column chromatography (70:30 EtOAc:Hexanes) affording hydrazone **185c** as a clear oil (0.173 g, 83%): 1H NMR (400 MHz, $CDCl_3$) δ 8.65 (s, 1H), 8.50 (d, $J = 4.8$ Hz, 1H), 7.82 (s, 1H), 7.47 – 7.08 (m, 8H), 7.03 (t, $J = 7.4$ Hz, 1H), 6.92 (d, $J = 8.4$ Hz, 1H), 5.60 (s, 2H), 5.27 (s, 1H), 1.70 – 1.21 (m, 3H); IR (thin film) 3397, 2977, 1663, 1597; AMM (ESI) m/z calcd for $C_{20}H_{20}N_3O^+[M+H]^+$ 318.1601, found 318.1606.

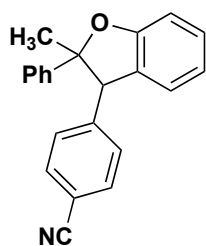
1.4.6 Insertion substrates



(231) 2-methyl-2,3-diphenyl-2,3-dihydrobenzofuran was synthesized according to general procedure D, phenyl(2-(1-phenylethoxy)phenyl)methylenehydrazine (0.035 g, 0.111), manganese(IV) dioxide (0.076 g, 0.885 mmol), $Rh_2(mes)_4$ (0.00095 g, 0.001 mmol) with anhydrous DCM (7.37 mL). After filtration, the crude product was purified by flash column chromatography (10:90, EtOAc:hexanes) affording dihydrobenzofuran **231** as a light yellow oil (0.027 g, 86%):

All catalysts screened ($\text{Rh}_2(\text{R-PTAD})_4$, $\text{Rh}_2(\text{S-PTAD})_4$, $\text{Rh}_2(\text{mes})_4$) with both racemic and enantiopure starting material yielded >95:5 dr of the same, single diastereomer. The racemic standard was never able to be separated on a CSP-HPLC to obtain enantiomeric ratios.

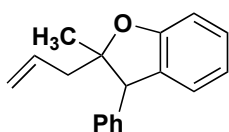
^1H NMR (400 MHz, CDCl_3) δ 7.24 (t, $J = 7.7$ Hz, 1H), 7.06 – 6.92 (m, 10H), 6.87 (t, $J = 7.4$ Hz, 1H), 6.75 – 6.66 (m, 2H), 4.64 (s, 1H), 1.93 (s, 3H); ^{13}C NMR (100 MHz, CDCl_3) δ 159.37, 142.17, 139.85, 130.97, 129.34(2), 128.88, 128.54, 127.87(2), 127.42(2), 126.74, 126.54, 126.05(2), 121.07, 109.79, 93.50, 77.48, 77.16, 76.84, 61.11, 29.40; IR (thin film) 3028, 2967, 1216 cm^{-1} ; AMM (ESI) m/z calcd for $\text{C}_{21}\text{H}_{19}\text{O}^+[\text{M}+\text{H}]^+$ 287.1473, found 287.1471. $[\alpha]_D^{23} = -3.47$ ($c = 1.4$, CHCl_3).



(190) 4-(2-methyl-2-phenyl-2,3-dihydrobenzofuran-3-yl)benzonitrile was synthesized according to general procedure D, 4-(hydrazineylidene(2-(1-phenylethoxy)phenyl)methyl)benzonitrile (0.450 g, 1.32 mmol), manganese(IV) dioxide (0.908 g, 10.56 mol), $\text{Rh}_2(\text{R-PTAD})_4$ (0.021 g, 0.0132 mmol) with anhydrous DCM (88 mL). After filtration, the crude product was purified by flash column chromatography (20:80, EtOAc:hexanes) affording dihydrobenzofuran **190** as a light yellow oil (0.336 g, 82%):

All catalysts screened ($\text{Rh}_2(\text{R-PTAD})_4$, $\text{Rh}_2(\text{S-PTAD})_4$, $\text{Rh}_2(\text{mes})_4$) with both racemic and enantiopure starting material yielded >95:5 dr of the same, single diastereomer. The corresponding enantiomeric ratios can be found in the main text, Table 1.

^1H NMR (600 MHz, CDCl_3) δ 7.30 – 7.24 (m, 3H), 7.08 – 7.00 (m, 6H), 6.94 (d, $J = 7.3$ Hz, 1H), 6.90 (t, $J = 7.4$ Hz, 1H), 6.82 (d, $J = 7.8$ Hz, 2H), 4.64 (s, 1H), 1.93 (s, 3H); ^{13}C NMR (150 MHz, CDCl_3) δ 159.13, 145.99, 141.48, 131.67(2), 129.88(2), 129.84, 129.50, 127.81(2), 127.03, 125.92, 125.79(2), 121.41, 118.93, 110.44, 110.30, 93.38, 60.81, 29.40; IR (thin film) 2974, 2226, 1596, 1497 cm^{-1} ; TLC (10:90, EtOAc:hexanes) $R_F = 0.9$. AMM (ESI) m/z calcd for $\text{C}_{22}\text{H}_{18}\text{NO}^+[\text{M}+\text{H}]^+$ 312.1383, found 312.1376. $[\alpha]_D^{23} = -5.62$ ($c = 0.69$, CHCl_3).

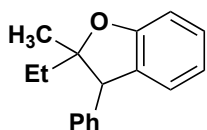


(193-194) 2-allyl-2-methyl-3-phenyl-2,3-dihydrobenzofuran was synthesized according to general procedure D, ((2-(pent-4-en-2-yloxy)phenyl)(phenyl)methylene)hydrazine (0.550 g, 1.96 mmol), manganese(IV) dioxide (1.35 g, 15.68 mmol), $\text{Rh}_2(\text{R-PTAD})_4$ (0.031 g, 0.0196 mmol), and anhydrous CH_2Cl_2 (130.7 mL) were used. After filtration, the mixture was purified by flash column chromatography (10:90, EtOAc:hexanes) affording dihydrobenzofuran **193-194** as a light yellow oil (0.338 g, 77%):

NMR reported is with $\text{Rh}_2(\text{R-PTAD})_4$ and racemic SM yielding a 47:53 dr (trans:cis)(**193:194**). The peaks reported are the major diastereomer of the mixture of two diastereomers, that could not be separate by flash column chromatography or prep-TLC. The singlets at 4.49 and 4.41 are the double benzylic protons at the former carbene center, and used to determine the dr.

^1H NMR (600 MHz, CDCl_3) δ 7.35 – 7.22 (m, 7H), 7.18 (dt, $J = 7.9, 4.0$ Hz, 2H), 7.12 (d, $J = 7.2$ Hz, 2H), 7.09 – 6.97 (m, 4H), 6.91 – 6.81 (m, 4H), 6.01 – 5.90 (m, 1H, minor diastereomer), 5.80 – 5.70 (m, 1H, major diastereomer), 5.25 – 5.18 (m, 2H, minor diastereomer), 5.01 (d, $J = 10.2$ Hz, 1H, major diastereomer), 4.89 (dd, $J = 17.0, 2.0$ Hz, 1H, major diastereomer), 4.49

(s, 1H, minor diastereomer), 4.41 (s, 1H, major diastereomer), 2.63 – 2.53 (m, 2H, minor diastereomer), 2.23 (dd, $J = 14.4, 6.2$ Hz, 1H, major diastereomer), 1.67 (dd, $J = 14.3, 8.2$ Hz, 1H, major diastereomer), 1.54 (s, 4H, major diastereomer), 0.96 (s, 3H, minor diastereomer); ^{13}C NMR (150 MHz, CDCl_3) δ 159.05, 139.16, 133.85, 130.60, 129.43, 128.76, 128.53, 127.39, 126.02, 120.65, 118.23, 110.14, 109.86, 91.00, 77.48, 77.16, 76.84, 59.12, 41.41, 25.94, 0.15; IR (thin film) 3028, 2976, 1640, 1596 cm^{-1} ; AMM (ESI) m/z calcd for $\text{C}_{18}\text{H}_{18}\text{O}_2^+[\text{M}+\text{H}]^+$ 251.1431 found 251.1429.

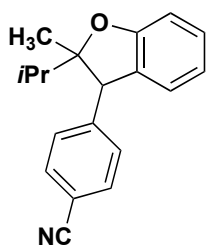


(230) 2-ethyl-2-methyl-3-phenyl-2,3-dihydrobenzofuran was synthesized according to general procedure D, ((2-(*sec*-butoxy)phenyl)(phenyl)methylene)hydrazine (0.025 g, 0.093 mmol), manganese(IV) dioxide (0.064 g, 0.744 mmol), $\text{Rh}_2(\text{S-PTAD})_4$ (0.0015 g, 0.00097 mmol), and anhydrous CH_2Cl_2 (6.2 mL) were used. The filtered mixtures was purified by flash column chromatography (05:95, EtOAc:hexanes) affording insertion **230** as a clear oil (0.020 g, 91%):

NMR reported is with a catalyst yielding a 46:54 dr. The peaks reported are a mixture of two diastereomers, that could not be separate by flash column chromatography or prep-TLC. The singlets at 4.42 and 4.37 are the double benzylic protons at the former carbene center, and used to determine the dr.

^1H NMR (400 MHz, CDCl_3) δ 7.27 (ddt, $J = 14.1, 12.5, 4.6$ Hz, 7H), 7.18 (t, $J = 7.7$ Hz, 2H), 7.08 (ddd, $J = 7.7, 6.1, 1.6$ Hz, 4H), 7.02 (dd, $J = 7.4, 6.0$ Hz, 3H), 6.89 – 6.80 (m, 4H), 4.42 (s, 1H), 4.37 (s, 1H), 1.95 – 1.79 (m, 2H), 1.53 (s, 4H), 1.46 (dt, $J = 14.6, 7.3$ Hz, 1H), 1.06 (t,

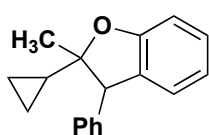
$J = 7.4$ Hz, 3H), 1.03 – 0.97 (m, 1H), 0.93 (s, 3H), 0.83 (t, $J = 7.4$ Hz, 4H); ^{13}C NMR (100 MHz, CDCl_3) δ 159.38, 159.15, 140.29, 139.59, 130.99, 130.61, 129.40, 129.36, 128.67, 128.65, 128.42, 128.37, 127.17, 127.11, 126.13, 126.05, 120.47, 120.42, 110.02, 109.78, 92.43, 91.99, 77.48, 77.36, 77.16, 76.84, 59.21, 56.32, 34.47, 29.85, 29.44, 25.08, 22.13, 8.47, 8.33; IR (thin film) 2973, 1597, 1478 cm^{-1} ; AMM (ESI) m/z calcd for $\text{C}_{17}\text{H}_{19}\text{O}_2^+[\text{M}+\text{H}]^+$ 239.1431 found 239.1426.



(235) 4-(2-isopropyl-2-methyl-2,3-dihydrobenzofuran-3-yl)benzonitrile was synthesized according to general procedure D, 4-(hydrazineylidene(2-((3-methylbutan-2-yl)oxy)phenyl)methyl)benzonitrile (0.030 g, 0.098 mmol), manganese(IV) dioxide (0.067 g, 0.781 mmol), $\text{Rh}_2(\text{mes})_4$ (0.00084 g, 0.00098 mmol), and anhydrous CH_2Cl_2 (6.5 mL) were used. After filtration, the mixtures was purified by preparative TLC (10:90 EtOAC:Hexanes, SiliaPlateTM Preparative, 1,000 μm , 20 x 20 cm, with F254 indicator) affording dihydrobenzofuran **235** as a light yellow oil (0.019 g, 70%):

NMR reported is with the $\text{Rh}_2(\text{mes})_4$ catalyst yielding a 81:19 dr. The peaks reported are a mixture of two diastereomers that could not be separate by flash column chromatography or prep-TLC; with the major diastereomer peaks reported. The singlets at 4.54 and 4.13 are the double benzylic protons at the former carbene center, for each the major and minor diastereomer respectively.

^1H NMR (600 MHz, CDCl_3) δ 7.60 – 7.57 (m, 2H), 7.54 – 7.52 (m, 1H), 7.23 – 7.18 (m, 1H), 7.14 (d, $J = 8.1$ Hz, 2H), 6.94 – 6.90 (m, 1H), 6.85 (ddd, $J = 9.1, 7.6, 1.4$ Hz, 2H), 4.54 (s, 1H), 2.08 (p, $J = 6.8$ Hz, 1H), 1.07 (d, $J = 6.8$ Hz, 3H), 1.02 (d, $J = 6.9$ Hz, 4H), 0.90 (s, 3H); ^{13}C NMR (101 MHz, CDCl_3) δ 158.44, 146.48, 132.43, 132.06(2), 130.24(2), 129.32, 129.16, 125.82, 121.03, 110.72, 109.76, 94.61, 77.48, 77.36, 77.16, 76.84, 31.73, 19.99, 18.31, 17.61; IR (thin film) 2965, 2228, 1597, 1480 cm^{-1} ; AMM (ESI) m/z calcd for $\text{C}_{19}\text{H}_{20}\text{NO}^+[\text{M}+\text{H}]^+$ 278.1540 found 278.1539.

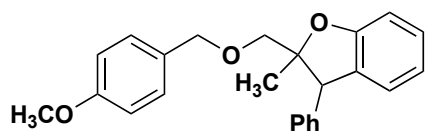


(234) 2-cyclopropyl-2-methyl-3-phenyl-2,3-dihydrobenzofuran was synthesized according to general procedure D, ((2-(1-cyclopropylethoxy)phenyl)(phenyl)methylene) hydrazine (0.025 g, 0.089 mmol), manganese(IV) dioxide (0.061 g, 0.712 mmol), $\text{Rh}_2(\text{mes})_4$ (0.00080 g, 0.00089 mmol), and anhydrous CH_2Cl_2 (5.9 mL) were used. After filtration, the mixtures was purified by flash column chromatography (05:95 EtOAc:Hexanes) affording dihydrobenzofuran **234** as a clear oil (0.099 g, 44%):

NMR reported is with the $\text{Rh}_2(R\text{-PTAD})_4$ catalyst yielding a 15:85 dr. The peaks reported are a mixture of two diastereomers, that could not be separate by flash column chromatography or prep-TLC. The singlets at 4.64 and 4.52 are the double benzylic protons at the former carbene center, for each the minor and major diastereomer respectively with the peaks for the major diastereomer reported below.

^1H NMR (600 MHz, CDCl_3) δ 7.35 – 7.23 (m, 8H), 7.23 – 7.12 (m, 8H), 7.07 – 7.00 (m, 2H), 6.89 – 6.83 (m, 3H), 6.83 – 6.73 (m, 3H), 4.64 (s, 0.32H), 4.52 (s, 1H), 1.53 (s, 3H), 1.34 – 1.22 (m, 1H), 0.91 – 0.86 (m, 4H), 0.59 – 0.47 (m, 4H), 0.39 – 0.27 (m, 5H), 0.19 – 0.06 (m,

4H); ^{13}C NMR (151 MHz, CDCl_3) δ 159.80, 139.70, 130.76, 129.71, 129.43, 128.68, 128.43, 128.18, 127.09, 125.94, 120.45, 109.43, 90.66, 59.49, 26.70, 17.55, 2.35, 0.94; IR (thin film) 3458, 3009, 1477 cm^{-1} ; AMM (ESI) m/z calcd for $\text{C}_{18}\text{H}_{18}\text{O}^+[\text{M}-\text{H}]$ 248.9616 found 248.9616.

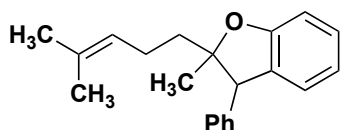


(236) 2-(((4-methoxybenzyl)oxy)methyl)-2-methyl-3-phenyl-2,3-dihydrobenzofuran was synthesized according to general procedure D, (2-((1-((4-methoxybenzyl)oxy)propan-2-yl)oxy)phenyl)(phenyl)methylene)hydrazine (0.025 g, 0.064 mmol), manganese(IV) dioxide (0.044 g, 0.512 mmol), $\text{Rh}_2(\text{R-PTAD})_4$ (0.001 g, 0.00064 mmol), and anhydrous CH_2Cl_2 (4.3 mL) were used. After filtration, the mixture was purified by flash column chromatography (20:80 EtOAc:Hexanes) affording dihydrobenzofuran **236** as a clear oil (0.019 g, 84%, 44:56 dr):

NMR reported is with the $\text{Rh}_2(\text{R-PTAD})_4$ catalyst yielding a 44:56 dr. The peaks reported are a mixture of two diastereomers, that could not be separated by flash column chromatography or prep-TLC. The singlets at 4.67 and 4.39 are the double benzylic protons at the former carbene center, for each the minor and major diastereomer respectively with the peaks for the major and minor diastereomers reported below (the aryl protons are overlapping and therefore cannot be assigned clearly to the major or minor diastereomers).

^1H NMR (400 MHz, CDCl_3) δ 7.31 – 7.23 (m, 8H), 7.22 – 7.16 (m, 2H), 7.10 – 7.00 (m, 7H), 6.92 – 6.84 (m, 5H), 6.82 – 6.77 (m, 2H), 4.67 (s, 1H, minor diastereomer), 4.64 – 4.54 (m, 2H, minor diastereomer), 4.39 (s, 1H, major diastereomer), 4.22 (d, $J = 11.6$ Hz, 1H, major diastereomer), 4.05 (d, $J = 11.6$ Hz, 1H, major diastereomer), 3.81 (s, 2H, minor diastereomer),

3.78 (s, 3H, major diastereomer), 3.59 (s, 2H, minor diastereomer), 3.26 (d, $J = 10.0$ Hz, 1H, major diastereomer), 3.00 (d, $J = 10.0$ Hz, 1H, major diastereomer), 1.62 (s, 3H, major diastereomer), 0.96 (s, 2H, minor diastereomer). ^{13}C NMR (100 MHz, CDCl_3) δ 59.36, 159.28, 159.13, 159.08, 139.84, 138.96, 130.48, 130.45, 130.37, 130.17, 129.49, 129.48, 129.36, 129.13, 128.78, 128.63, 128.40, 128.30, 127.28, 127.14, 126.21, 125.88, 120.80, 120.75, 113.92, 113.68, 110.15, 109.94, 91.35, 90.49, 77.48, 77.16, 76.84, 75.04, 73.37, 73.23, 72.98, 57.72, 55.43, 55.38, 53.38, 24.67, 20.58, 0.14.; IR (thin film) 3003, 1476, 1459 cm^{-1} ; AMM (ESI) m/z calcd for $\text{C}_{24}\text{H}_{25}\text{O}_3\text{Na}$ $[\text{M}+\text{Na}]^+$ 383.1623 found 383.1619.

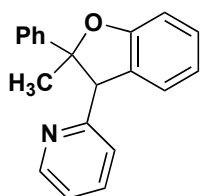


(237) 2-methyl-2-(4-methylpent-3-en-1-yl)-3-phenyl-2,3-dihydrobenzofuran was synthesized according to general procedure D, ((2-((6-methylhept-5-en-2-yl)oxy)phenyl)(phenyl)methylene)hydrazine (0.025 g, 0.078 mmol), manganese(IV) dioxide (0.053 g, 0.620 mmol), $\text{Rh}_2(\text{S-PTAD})_4$ (0.0001 g, 0.0078 mmol), and anhydrous CH_2Cl_2 (5.2 mL) were used. After filtration, the mixtures was purified by flash column chromatography (10:90 EtOAc:Hexanes) affording dihydrobenzofuran **237** as a clear oil (0.016 g, 68%):

NMR reported is with the $\text{Rh}_2(\text{S-PTAD})_4$ catalyst yielding a 39:61 dr. The peaks reported are a mixture of two diastereomers, that could not be separate by flash column chromatography or prep-TLC. The singlets at 4.45 and 4.37 are the double benzylic protons at the former carbene center, for each the minor and major diastereomer respectively with the peaks for the major diastereomer reported below.

^1H NMR (400 MHz, CDCl_3) δ 7.57 – 7.50 (m, 1H), 7.34 – 7.22 (m, 6H), 7.21 – 7.15 (m, 2H), 7.09 (ddt, $J = 9.5, 7.8, 1.6$ Hz, 4H), 7.03 (ddd, $J = 7.6, 2.9, 1.5$ Hz, 2H), 6.85 (tt, $J = 8.0, 2.5$

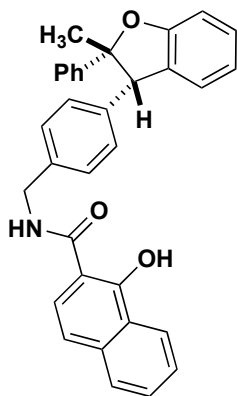
Hz, 4H), 5.15 (t, $J = 7.1$ Hz, 1H, minor diastereomer), 4.85 (t, $J = 7.1$ Hz, 1H, major diastereomer), 4.45 (s, 1H, minor diastereomer), 4.37 (s, 1H, major diastereomer), 2.29 – 2.15 (m, 2H, minor diastereomer), 2.12 – 1.99 (m, 1H), 1.96 – 1.78 (m, 3H), 1.69 (d, $J = 1.5$ Hz, 2H), 1.62 (d, $J = 1.3$ Hz, 1H), 1.57 (s, 6H, major diastereomer), 1.55 (s, 1H), 1.47 (s, 4H), 1.09 – 0.98 (m, 1H), 0.95 (s, 2H, minor diastereomer); ^{13}C NMR (101 MHz, CDCl_3) δ 159.36, 159.11, 140.10, 139.39, 132.10, 131.53, 131.00, 130.73, 130.50, 129.41(2), 129.36(2), 128.69, 128.64, 128.45(2), 128.40(2), 127.21, 127.16, 126.13, 126.01, 124.35, 124.04, 120.48, 120.45, 110.04, 109.84, 92.00, 91.70, 77.48, 77.16, 76.84, 59.35, 56.89, 41.88, 36.57, 25.84, 25.75, 22.81, 22.73, 17.83, 17.67, 0.15; IR (thin film) 3028, 2970, 1597, 1478 cm^{-1} ; AMM (ESI) m/z calcd for $\text{C}_{21}\text{H}_{25}\text{O}^+[\text{M}+\text{H}]^+$ 293.1900 found 293.1903.



(232) 2-(2-methyl-2-phenyl-2,3-dihydrobenzofuran-3-yl)pyridine was synthesized according to general procedure D, 3-(hydrazineylidene(2-(1-phenylethoxy)phenyl)methyl)pyridine (0.015 g, 0.047 mmol), manganese(IV) dioxide (0.033 g, 0.328 mol), $\text{Rh}_2(\text{R-PTAD})_4$ (0.00073 g, 0.00047 mmol) with anhydrous DCM (3.1 mL). After filtration, the crude product was purified by flash column chromatography (40:60, EtOAc:hexanes) affording dihydrobenzofuran **232** as a light yellow oil (0.013 g, 96%): All catalysts screened ($\text{Rh}_2(\text{R-PTAD})_4$, $\text{Rh}_2(\text{S-PTAD})_4$, $\text{Rh}_2(\text{mes})_4$) yielded >95:5 dr of the same, single diastereomer. ^1H NMR (400 MHz, CDCl_3) δ 8.30 – 8.21 (m, 1H), 8.18 (s, 1H), 7.33 – 7.24 (m, 2H), 7.12 – 6.99 (m, 6H), 6.92 (dtd, $J = 15.6, 7.4, 1.3$ Hz, 2H), 6.88 – 6.77 (m, 2H), 4.64 (s, 1H), 1.96 (s, 3H); ^{13}C NMR (100 MHz, CDCl_3) δ 159.26, 150.16, 148.24, 141.65, 136.43, 136.00, 129.96, 129.36, 127.89(2), 126.96, 125.93(2), 125.86, 122.96, 121.37, 110.15,

93.33, 58.27, 29.25; IR (thin film) 2985, 1738, 1372 cm^{-1} ; AMM (ESI) m/z calcd for $\text{C}_{20}\text{H}_{18}\text{NO}^+[\text{M}+\text{H}]^+$ 287.1310 found 288.1380.

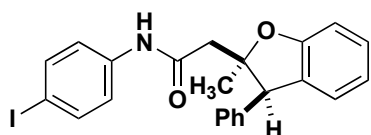
1.4.7 Crystal structure substrates



(212) **1-hydroxy-*N*-(4-((2*R*,3*S*)-2-methyl-2-phenyl-2,3-dihydrobenzofuran-3-yl)benzyl)-2-naphthamide** was synthesized over two steps. First, following a modified literature procedure⁹⁴, lithium aluminum hydride (0.228g, 6.00 mmol, 6.0 equiv) was added to a flame dried round bottom under Ar charged with THF (6.0 mL, 0.1M). The solution was cooled to 0 °C, then a solution of enantiopure **190** (0.313g, 1.00 mmol, 1.0 equiv) in THF (10.0 mL, 0.1M) was added dropwise. The reaction was stirred for 12 hours while being allowed to warm to room temperature. The solution was cooled back down to 0 °C and 0.228 mL of H₂O then 0.228 mL of 15% NaOH(aq) then 0.684 mL of H₂O were added sequentially. The mixture was stirred at room temperature for 15 minutes, then dried over Mg₂SO₄, filtered, and concentrated to afford the primary amine **202** as a light yellow oil and a single diastereomer (0.267g, 85%, >95:5 dr). The compound was not purified forward and carried straight through to the next reaction.

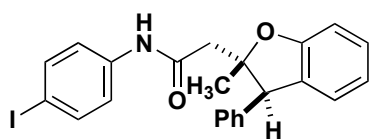
Second, 1-hydroxy-2-naphthoic acid (0.107g, 0.571 mmol, 1.2 equiv), HATU (0.221g, 0.571 mmol, 1.2 equiv), DIPEA (0.176 mL, 1.05 mmol, 2.2 equiv), and DMF (4.76 mL, 0.1M) were added to a flame dried round bottom under Ar and stirred for 10 minutes. Amine intermediate

202 (0.150g, 0.476 mmol, 1.0 equiv) was added and the reaction was stirred overnight. The reaction was diluted in CH₂Cl₂ (10 mL), washed with brine (10 mL x 3), dried over Na₂SO₄, and concentrated. The mixture was purified by flash column chromatography (30:70 CH₂Cl₂:Hexanes) to yield a single diastereomer and single enantiomer of **212** as a white solid (0.113g, 49%). **212** was recrystallized from a mixture of CH₂Cl₂ and Hexanes to afford the crystal structure reported. mp 84-85 °C; ¹H NMR (600 MHz, CDCl₃) δ 13.74 (s, 1H), 8.42 (d, *J* = 7.3 Hz, 1H), 7.73 (d, *J* = 8.1 Hz, 1H), 7.57 (ddd, *J* = 8.2, 6.9, 1.3 Hz, 1H), 7.52 (ddd, *J* = 8.2, 6.8, 1.3 Hz, 1H), 7.27 – 7.19 (m, 3H), 7.06 – 6.97 (m, 8H), 6.97 – 6.92 (m, 1H), 6.87 (td, *J* = 7.4, 1.1 Hz, 1H), 6.72 (d, *J* = 7.8 Hz, 2H), 6.38 (t, *J* = 5.7 Hz, 1H), 4.63 (s, 1H), 4.49 (d, *J* = 5.5 Hz, 2H), 1.92 (s, 3H); ¹³C NMR (150 MHz, CDCl₃) δ 170.32, 160.75, 159.09, 142.00, 139.75, 136.28, 135.77, 130.74, 129.65(2), 128.94, 128.86, 127.38, 127.34(2), 127.30(2), 127.28, 126.46, 125.90(2), 125.83, 125.67, 123.87, 120.98, 120.64, 118.14, 109.80, 106.43, 93.30, 60.54, 43.33, 29.31; IR (thin film) 3432, 3056, 2975, 1620, 1595 cm⁻¹; AMM (ESI) *m/z* calcd for C₃₃H₂₇NO₃⁺[M+H]⁺ 485.1991, found 486.2060. [α]_D²³ = +7.88 (c = 0.38, CHCl₃).



(218) Cis-N-(4-iodophenyl)-2-methyl-3-phenyl-2,3-dihydrobenzofuran-2-yl)acetamide was synthesized over two steps following the prep below. mp 130-132 °C; ¹H NMR (600 MHz, CDCl₃) δ 8.06 (s, 1H), 7.61 (d, *J* = 8.3 Hz, 2H), 7.34 – 7.27 (m, 6H), 7.12 (d, *J* = 7.4 Hz, 1H), 7.07 (d, *J* = 7.2 Hz, 2H), 7.00 – 6.92 (m, 2H), 4.48 (s, 1H), 2.52 (d, *J* = 14.9 Hz, 1H), 1.95 (d, *J* = 15.0 Hz, 1H), 1.72 (s, 3H); ¹³C NMR (100 MHz, CDCl₃) δ 168.64, 157.71, 138.16, 138.01(2), 137.81, 129.76, 129.23(2), 129.21, 128.92(2), 128.00, 126.44, 121.95, 121.89(2), 110.27, 89.97, 87.33, 77.48, 77.16, 76.84, 59.39, 45.86, 25.84; IR (thin film) 3314, 2975, 1667,

1585 cm^{-1} ; AMM (ESI) m/z calcd for $\text{C}_{23}\text{H}_{21}\text{INO}_2^+[\text{M}+\text{H}]^+$ 470.0612, found 470.0608. $[\alpha]_D^{23} = +13.7$ ($c = 0.18$, CHCl_3).



(217) Trans-N-(4-iodophenyl)-2-methyl-3-phenyl-2,3-dihydrobenzofuran-2-yl

acetamide was synthesized over two steps following the prep below. mp 144-145 °C; ^1H NMR (600 MHz, CDCl_3) δ 8.17 (s, 1H), 7.60 (d, $J = 8.2$ Hz, 2H), 7.36 – 7.28 (m, 3H), 7.28 – 7.22 (m, 3H), 7.15 (d, $J = 7.4$ Hz, 2H), 7.09 (d, $J = 7.5$ Hz, 1H), 6.98 – 6.90 (m, 2H), 4.60 (s, 1H), 2.96 (d, $J = 14.8$ Hz, 1H), 2.85 (d, $J = 14.9$ Hz, 1H), 1.06 (s, 3H); ^{13}C NMR (100 MHz, CDCl_3) δ 168.12, 157.76, 138.15, 138.04(2), 137.64, 129.77, 129.34(2), 129.14, 128.74(2), 127.76, 126.54, 121.95(2), 121.92, 110.12, 90.49, 87.57, 56.78, 49.10, 22.48; IR (thin film) 3269, 2926, 1704, 1597 cm^{-1} ; AMM (ESI) m/z calcd for $\text{C}_{23}\text{H}_{21}\text{INO}_2^+[\text{M}+\text{H}]^+$ 470.0612, found 470.0608. $[\alpha]_D^{23} = +23.1$ ($c = 0.17$, CHCl_3).

First following a literature procedure¹⁰¹, **(193-194)** 2-allyl-2-methyl-3-phenyl-2,3-dihydrobenzofuran (0.250g, 0.998 mmol, 1.0 equiv) (derived from enantiopure starting material, and insertion catalyzed by $\text{Rh}_2(\text{R-PTAD})_4$) was added to a solution of carbon tetrachloride (10 mL, 0.1M) in a round bottom. Then acetonitrile (10 mL, 0.1M) and H_2O (15 mL, 0.07M) were added sequentially. The mixture was cooled down to 0 °C then NaIO_4 (1.06g, 4.99 mmol, 5.0 equiv) was added. RuCl_3 (0.0207g, 0.0998 mmol, 0.1 equiv) was added portionwise, then the reaction was stirred overnight while allowing it to warm to room temperature. The reaction was quenched with 2M $\text{NaOH}(\text{aq})$ (5 mL) and extracted with CH_2Cl_2 (10 mL x 1). The aqueous layer was acidified with 1M HCl until a pH <1 was reached, then extracted with CH_2Cl_2 (10 mL x 3). The organic layers were combined, dried over Na_2SO_4 , and concentrated. The mixture was purified by flash column chromatography (90:9.8:0.2

EtOAc:Hex:AcOH) affording carboxylic acid as a clear oil and mixture of diastereomers (0.119g, 44%, 85:15 dr trans:cis).

Second, carboxylic acid was added to a solution of HATU (0.170g, 0.448 mmol, 1.2 equiv), DIPEA (0.137 mL, 0.821 mmol, 2.2 equiv) in CH₂Cl₂ (0.1M). The reaction was stirred for 15 minutes, then 4-iodobenzoic acid (0.105g, 0.448 mmol, 1.2 equiv) was added. The reaction was stirred overnight, then diluted in CH₂Cl₂ and washed with brine (5 mL x 3). The organic layer was dried over Na₂SO₄ and concentrated to yield a mixture of diastereomers of amides **217** & **218** (yield = 57%). The mixture was purified and diastereomers were separated by flash column chromatography (90:10 EtOAc:Hex) affording minor cis diastereomer **218** as a white solid (0.0085g, 5%) and major trans diastereomer **217** as a white solid (0.043, 25%). These enantiomerically pure diastereomers were then recrystallized in a mixture of CH₂Cl₂:Hexanes to afford the crystal structures reported.

1.5 References

- (1) Reproduced from: Dishman, S. N.; Laconsay, C. J.; Fettingner, J. C.; Tantillo, D. J.; Shaw, J. T. Divergent Stereochemical Outcomes in the Insertion of Donor/Donor Carbenes into the C–H Bonds of Stereogenic Centers. *Chem. Sci.* **2022**, *13* (4), 1030–1036. 10.1039/D1SC04622E. <https://doi.org/10.1039/D1SC04622E>. With permission from the Royal Chemical Society.
- (2) Lovering, F.; Bikker, J.; Humblet, C. Escape from Flatland: Increasing Saturation as an Approach to Improving Clinical Success. *J. Med. Chem.* **2009**, *52* (21), 6752–6756. 10.1021/jm901241e.

- (3) Abrams, D. J.; Provencher, P. A.; Sorensen, E. J. Recent Applications of C–H Functionalization in Complex Natural Product Synthesis. *Chem. Soc. Rev.* **2018**, *47* (23), 8925–8967. 10.1039/C8CS00716K.
- (4) Altus, K. M.; Love, J. A. The Continuum of Carbon–Hydrogen (C–H) Activation Mechanisms and Terminology. *Commun Chem* **2021**, *4* (1), 173. 10.1038/s42004-021-00611-1.
- (5) Davies, H. M. L.; Morton, D. Recent Advances in C–H Functionalization. *J. Org. Chem.* **2016**, *81* (2), 343–350. 10.1021/acs.joc.5b02818.
- (6) P. Doyle, M.; Liu, Y.; Ratnikov, M. Catalytic, Asymmetric, Intramolecular Carbon–Hydrogen Insertion. In *Organic Reactions*; John Wiley & Sons, Inc., Ed.; John Wiley & Sons, Inc.: Hoboken, NJ, USA, 2012; pp 1–132. 10.1002/0471264180.or080.01.
- (7) Burke, S. D.; Grieco, P. A. Intramolecular Reactions of Diazocarbonyl Compounds. In *Organic Reactions*; John Wiley & Sons, Inc., Ed.; John Wiley & Sons, Inc.: Hoboken, NJ, USA, 1979; pp 361–475. 10.1002/0471264180.or026.02.
- (8) Davies, H. M. L.; Liao, K. Dirhodium Tetracarboxylates as Catalysts for Selective Intermolecular C–H Functionalization. *Nat Rev Chem* **2019**, *3* (6), 347–360. 10.1038/s41570-019-0099-x.
- (9) Doyle, M. P.; Duffy, R.; Ratnikov, M.; Zhou, L. Catalytic Carbene Insertion into C–H Bonds. *Chem. Rev.* **2010**, *110* (2), 704–724. 10.1021/cr900239n.
- (10) Dutta, S.; Kumar, P.; Yadav, S.; Sharma, R. D.; Shivaprasad, P.; Vimalaswaran, K. S.; Srivastava, A.; Sharma, R. K. Accelerating Innovations in C H Activation/Functionalization through Intricately Designed Magnetic Nanomaterials: From Genesis to Applicability in Liquid/Regio/Photo Catalysis. *Catalysis Communications* **2023**, *175*, 106615. 10.1016/j.catcom.2023.106615.

- (11) Bon, J. L.; Feng, D.; Marder, S. R.; Blakey, S. B. A C–H Functionalization Protocol for the Direct Synthesis of Benzobisthiazole Derivatives. *J. Org. Chem.* **2014**, *79* (16), 7766–7771. 10.1021/jo501416j.
- (12) Jana, R.; Begam, H. M.; Dinda, E. The Emergence of the C–H Functionalization Strategy in Medicinal Chemistry and Drug Discovery. *Chem. Commun.* **2021**, *57* (83), 10842–10866. 10.1039/D1CC04083A.
- (13) Bergstrom, B. D.; Nickerson, L. A.; Shaw, J. T.; Souza, L. W. Transition Metal Catalyzed Insertion Reactions with Donor/Donor Carbenes. *Angew. Chem. Int. Ed.* **2021**, *60* (13), 6864–6878. 10.1002/anie.202007001.
- (14) Mieusset, J.-L.; Brinker, U. H. The Carbene Reactivity Surface: A Classification. *J. Org. Chem.* **2008**, *73* (4), 1553–1558. 10.1021/jo7026118.
- (15) *Transition Metal-Catalyzed Carbene Transformations*, 1st ed.; Wang, J., Che, C., Doyle, M. P., Eds.; Wiley, 2022. 10.1002/9783527829170.
- (16) Taber, D. F.; Petty, E. H.; Raman, K. Enantioselective Ring Construction: Synthesis of (+)- α -Cuparenone. *J. Am. Chem. Soc.* **1985**, *107* (1), 196–199. 10.1021/ja00287a035.
- (17) Taber, D. F.; Raman, K. Enantioselective Carbocyclization: A Facile Route to Chiral Cyclopentanes. *J. Am. Chem. Soc.* **1983**, *105* (18), 5935–5937. 10.1021/ja00356a048.
- (18) Reddy, R. P.; Lee, G. H.; Davies, H. M. L. Dirhodium Tetracarboxylate Derived from Adamantylglycine as a Chiral Catalyst for Carbenoid Reactions. *Org. Lett.* **2006**, *8* (16), 3437–3440. 10.1021/ol060893l.
- (19) Doyle, M. P.; Zhou, Q.-L.; Raab, C. E.; Roos, G. H. P.; Simonsen, S. H.; Lynch, V. Synthesis and Structures of (2,2- *Cis*)-Dirhodium(II) Tetrakis[Methyl 1-Acyl-2-Oxoimidazolidine-4(*S*)-Carboxylates]. Chiral Catalysts for Highly Stereoselective

- Metal Carbene Transformations. *Inorg. Chem.* **1996**, *35* (21), 6064–6073.
10.1021/ic960249a.
- (20) Davies, H. M. L. Finding Opportunities from Surprises and Failures. Development of Rhodium-Stabilized Donor/Acceptor Carbenes and Their Application to Catalyst-Controlled C–H Functionalization. *J. Org. Chem.* **2019**, *84* (20), 12722–12745.
10.1021/acs.joc.9b02428.
- (21) Davies, H. M. L.; Bruzinski, P. R.; Fall, M. J. Effect of Diazoalkane Structure on the Stereoselectivity of Rhodium(II) (S)-N-(Arylsulfonyl)Proline Catalyzed Cyclopropanations. *Tetrahedron Letters* **1996**, *37* (24), 4133–4136. 10.1016/0040-4039(96)00823-4.
- (22) Davies, H. M. L.; Grazini, M. V. A.; Aouad, E. Asymmetric Intramolecular C–H Insertions of Aryldiazoacetates. *Org. Lett.* **2001**, *3* (10), 1475–1477.
10.1021/ol0157858.
- (23) Fu, J.; Ren, Z.; Bacsá, J.; Musaev, D. G.; Davies, H. M. L. Desymmetrization of Cyclohexanes by Site- and Stereoselective C–H Functionalization. *Nature* **2018**, *564* (7736), 395–399. 10.1038/s41586-018-0799-2.
- (24) Soldi, C.; Lamb, K. N.; Squitieri, R. A.; González-López, M.; Di Maso, M. J.; Shaw, J. T. Enantioselective Intramolecular C–H Insertion Reactions of Donor–Donor Metal Carbenoids. *J. Am. Chem. Soc.* **2014**, *136* (43), 15142–15145. 10.1021/ja508586t.
- (25) Wang, H.-X.; Wan, Q.; Low, K.-H.; Zhou, C.-Y.; Huang, J.-S.; Zhang, J.-L.; Che, C.-M. Stable Group 8 Metal Porphyrin Mono- and Bis(Dialkylcarbene) Complexes: Synthesis, Characterization, and Catalytic Activity. *Chem. Sci.* **2020**, *11* (8), 2243–2259.
10.1039/C9SC05432D.
- (26) Reddy, A. R.; Zhou, C.-Y.; Guo, Z.; Wei, J.; Che, C.-M. Ruthenium-Porphyrin-Catalyzed Diastereoselective Intramolecular Alkyl Carbene Insertion into C-H Bonds of

- Alkyl Diazomethanes Generated In Situ from *N*-Tosylhydrazones. *Angew. Chem. Int. Ed.* **2014**, *53* (51), 14175–14180. 10.1002/anie.201408102.
- (27) Cheung, W.-H.; Zheng, S.-L.; Yu, W.-Y.; Zhou, G.-C.; Che, C.-M. Ruthenium Porphyrin Catalyzed Intramolecular Carbenoid C–H Insertion. Stereoselective Synthesis of Cis-Disubstituted Oxygen and Nitrogen Heterocycles. *Org. Lett.* **2003**, *5* (14), 2535–2538. 10.1021/ol034806q.
- (28) Li, Y.; Huang, J.-S.; Zhou, Z.-Y.; Che, C.-M. Isolation and X-Ray Crystal Structure of an Unusual Biscarbene Metal Complex and Its Reactivity toward Cyclopropanation and Allylic C–H Insertion of Unfunctionalized Alkenes. *J. Am. Chem. Soc.* **2001**, *123* (20), 4843–4844. 10.1021/ja003184q.
- (29) Zheng, S.-L.; Yu, W.-Y.; Xu, M.-X.; Che, C.-M. First Synthesis of Naturally Occurring (±)-Epi-Conocarpan. *Tetrahedron Letters* **2003**, *44* (7), 1445–1447. 10.1016/S0040-4039(02)02860-5.
- (30) Zhu, D.; Ma, J.; Luo, K.; Fu, H.; Zhang, L.; Zhu, S. Enantioselective Intramolecular C–H Insertion of Donor and Donor/Donor Carbenes by a Nondiazo Approach. *Angew. Chem. Int. Ed.* **2016**, *55* (29), 8452–8456. 10.1002/anie.201604211.
- (31) Zhu, D.; Chen, L.; Fan, H.; Yao, Q.; Zhu, S. Recent Progress on Donor and Donor–Donor Carbenes. *Chem. Soc. Rev.* **2020**, *49* (3), 908–950. 10.1039/C9CS00542K.
- (32) Nickerson, L. A.; Bergstrom, B. D.; Gao, M.; Shiue, Y.-S.; Laconsay, C. J.; Culberson, M. R.; Knauss, W. A.; Fettinger, J. C.; Tantillo, D. J.; Shaw, J. T. Enantioselective Synthesis of Isochromans and Tetrahydroisoquinolines by C–H Insertion of Donor/Donor Carbenes. *Chem. Sci.* **2020**, *11* (2), 494–498. 10.1039/C9SC05111B.
- (33) Souza, L. W.; Squitieri, R. A.; Dimirjian, C. A.; Hodur, B. M.; Nickerson, L. A.; Penrod, C. N.; Cordova, J.; Fettinger, J. C.; Shaw, J. T. Enantioselective Synthesis of Indolines,

- Benzodihydrothiophenes, and Indanes by C–H Insertion of Donor/Donor Carbenes. *Angew. Chem.* **2018**, *130* (46), 15433–15436. 10.1002/ange.201809344.
- (34) Lamb, K. N.; Squitieri, R. A.; Chintala, S. R.; Kwong, A. J.; Balmond, E. I.; Soldi, C.; Dmitrenko, O.; Castiñeira Reis, M.; Chung, R.; Addison, J. B.; Fettinger, J. C.; Hein, J. E.; Tantillo, D. J.; Fox, J. M.; Shaw, J. T. Synthesis of Benzodihydrofurans by Asymmetric C–H Insertion Reactions of Donor/Donor Rhodium Carbenes. *Chem. Eur. J.* **2017**, *23* (49), 11843–11855. 10.1002/chem.201701630.
- (35) Panish, R.; Chintala, S. R.; Boruta, D. T.; Fang, Y.; Taylor, M. T.; Fox, J. M. Enantioselective Synthesis of Cyclobutanes via Sequential Rh-Catalyzed Bicyclobutanation/Cu-Catalyzed Homoconjugate Addition. *J. Am. Chem. Soc.* **2013**, *135* (25), 9283–9286. 10.1021/ja403811t.
- (36) Nakamura, E.; Yoshikai, N.; Yamanaka, M. Mechanism of C–H Bond Activation/C–C Bond Formation Reaction between Diazo Compound and Alkane Catalyzed by Dirhodium Tetracarboxylate. *J. Am. Chem. Soc.* **2002**, *124* (24), 7181–7192. 10.1021/ja017823o.
- (37) Ledon, H.; Linstrumelle, G.; Julia, S. *Tetrahedron Lett.* **1973**, *1*, 25–28.
- (38) Cane, D. E.; Thomas, P. J. Synthesis of (DI)-Pentalenolactones E and F. *J. Am. Chem. Soc.* **1984**, *106* (18), 5295–5303. 10.1021/ja00330a044.
- (39) Taber, D. F.; Song, Y. Diastereoselective Rh-Mediated Construction of 2,3,5-Trisubstituted Tetrahydrofurans. *J. Org. Chem.* **1996**, *61* (19), 6706–6712. 10.1021/jo960758u.
- (40) Adams, J.; Poupart, M.-A.; Grenier, L. Diastereoselectivity in the Synthesis of 3(2H)-Furanones. Total Synthesis of (+)-Muscarine. *Tetrahedron Letters* **1989**, *30* (14), 1753–1756. 10.1016/S0040-4039(00)99571-6.

- (41) Adams, J.; Frenette, R. Stereoselective Synthesis of Endo-1,3-Dimethyl-2,9-Dioxabicyclo[3,3,1]nonane. 2.
- (42) Doyle, M. P.; Bagheri, V.; Pearson, M. M.; Edwards, J. D. Highly Selective γ -Lactone Syntheses by Intramolecular Carbenoid Carbon-Hydrogen Insertion in Rhodium(II) Carboxylate and Rhodium(II) Carboxamide Catalyzed Reactions of Diazo Esters. **1989**, 7001–7004.
- (43) Taber, D. F.; Ruckle, R. E. Cyclopentane Construction by Dirhodium Tetraacetate-Mediated Intramolecular C-H Insertion: Steric and Electronic Effects. *J. Am. Chem. Soc.* **1986**, 108 (24), 7686–7693. 10.1021/ja00284a037.
- (44) Taber, D. F.; Hennessy, M. J.; Louey, J. P. Rhodium-Mediated Cyclopentane Construction Can Compete with β -Hydride Elimination: Synthesis of (+, -)-Tochuinyl Acetate. *J. Org. Chem.* **1992**, 57 (2), 436–441. 10.1021/jo00028a011.
- (45) Doyle, M. P.; Dyatkin, A. B.; Roos, G. H. P.; Canas, F.; Pierson, D. A.; van Basten, A.; Mueller, P.; Polleux, P. Diastereocontrol for Highly Enantioselective Carbon-Hydrogen Insertion Reactions of Cycloalkyl Diazoacetates. *J. Am. Chem. Soc.* **1994**, 116 (10), 4507–4508. 10.1021/ja00089a062.
- (46) Doyle, M. P.; Kalinin, A. V.; Ene, D. G. Chiral Catalyst Controlled Diastereoselection and Regioselection in Intramolecular Carbon-Hydrogen Insertion Reactions of Diazoacetates. *J. Am. Chem. Soc.* **1996**, 118 (37), 8837–8846. 10.1021/ja961682m.
- (47) Doyle, M. P.; Westrum, L. J.; Wolthuis, W. N. E.; See, M. M.; Boone, W. P.; Bagheri, V.; Pearson, M. M. Electronic and Steric Control in Carbon-Hydrogen Insertion Reactions of Diazoacetates Catalyzed by Dirhodium(II) Carboxylates and Carboxamides. *J. Am. Chem. Soc.* **1993**, 115 (3), 958–964. 10.1021/ja00056a021.

- (48) Taber, D. F.; You, K. K.; Rheingold, A. L. Predicting the Diastereoselectivity of Rh-Mediated Intramolecular C–H Insertion. *J. Am. Chem. Soc.* **1996**, *118* (3), 547–556. 10.1021/ja9515213.
- (49) Wang, J.; Chen, B.; Bao, J. Electronic Effects of Rh(II)-Mediated Carbenoid Intramolecular C–H Insertion: A Linear Free Energy Correlation Study. *J. Org. Chem.* **1998**, *63* (6), 1853–1862. 10.1021/jo971747j.
- (50) Pirrung, M. C.; Liu, H.; Morehead, A. T. Rhodium Chemzymes: Michaelis–Menten Kinetics in Dirhodium(II) Carboxylate-Catalyzed Carbenoid Reactions. *J. Am. Chem. Soc.* **2002**, *124* (6), 1014–1023. 10.1021/ja011599l.
- (51) Wang, P.; Adams, J. Model Studies of the Stereoelectronic Effect in Rh(II) Mediated Carbenoid C-H Insertion Reactions. *J. Am. Chem. Soc.* **1994**, *116* (8), 3296–3305. 10.1021/ja00087a016.
- (52) Pirrung, M. C.; Morehead, A. T. Electronic Effects in Dirhodium(II) Carboxylates. Linear Free Energy Relationships in Catalyzed Decompositions of Diazo Compounds and CO and Isonitrile Complexation. *J. Am. Chem. Soc.* **1994**, *116* (20), 8991–9000. 10.1021/ja00099a017.
- (53) Padwa, A.; Austin, D. J.; Price, A. T.; Semones, M. A.; Doyle, M. P.; Protopopova, M. N.; Winchester, W. R.; Tran, A. Ligand Effects on Dirhodium(II) Carbene Reactivities. Highly Effective Switching between Competitive Carbenoid Transformations. *J. Am. Chem. Soc.* **1993**, *115* (19), 8669–8680. 10.1021/ja00072a021.
- (54) Yoshinori et al. - 1995 - Indole Derivatives, Salts Thereof and Heart Affection Therapeutic Agent Comprising the Same.Pdf.
- (55) Wu, L.; Zhang, Y.-L.; Wang, X.-B.; Zhang, Y.-M.; Yang, M.-H.; Luo, J.; Kong, L.-Y. Viminalins A-O: Diverse [3+2] Hybrids of Acylphloroglucinol and α -Phellandrene from

- the Fruits of *Callistemon Viminalis*. *Tetrahedron* **2017**, *73* (8), 1105–1113. 10.1016/j.tet.2016.12.076.
- (56) Cao, J.-Q.; Tian, H.-Y.; Li, M.-M.; Zhang, W.; Wang, Y.; Wang, L.; Ye, W.-C. Rearranged Phloroglucinol-Monoterpenoid Adducts from *Callistemon Rigidus*. *J. Nat. Prod.* **2018**, *81* (1), 57–62. 10.1021/acs.jnatprod.7b00606.
- (57) Yoshinori, K.; Noboru, S.; Takashi, Y.; Takahiro, K.; Tadaaki, O.; Katsumi, K. Production of Indole Derivative. JP19960036167 19960223.
- (58) Musthapa, I.; Latip, J.; Takayama, H.; Juliawaty, L. D.; Hakim, E. H.; Syah, Y. M. Prenylated Flavones from *Artocarpus Lanceifolius* and Their Cytotoxic Properties against P-388 Cells. *Natural Product Communications* **2009**, *4* (7), 927–930.
- (59) Uemura, H.; Sakamoto, N.; Nakaya, H. Electropharmacological Effects of UK-1745, a Novel Cardiotonic Drug, in Guinea-Pig Ventricular Myocytes. *European Journal of Pharmacology* **1999**, *383* (3), 361–371. 10.1016/S0014-2999(99)00651-2.
- (60) Cao, J.-Q.; Huang, X.-J.; Li, Y.-T.; Wang, Y.; Wang, L.; Jiang, R.-W.; Ye, W.-C. Callistrilones A and B, Triketone–Phloroglucinol–Monoterpene Hybrids with a New Skeleton from *Callistemon Rigidus*. *Org. Lett.* **2016**, *18* (1), 120–123. 10.1021/acs.orglett.5b03360.
- (61) Dethle, D. H.; Nirpal, A. K. Bio-Inspired Enantioselective Total Syntheses of (–)-Viminalins A, B, H, I, and N and Structural Reassignment of (–)-Viminalin M. *Org. Biomol. Chem.* **2019**, *17* (32), 7507–7516. 10.1039/C9OB01426H.
- (62) Suhartati, T.; Achmad, S. A.; Aimi, N.; Hakim, E. H.; Kitajima, M.; Takayama, H.; Takeya, K. Artoindonesianin L, a New Prenylated Flavone with Cytotoxic Activity from *Artocarpus Rotunda*. *Fitoterapia* **2001**, *72* (8), 912–918. 10.1016/S0367-326X(01)00343-4.

- (63) Shigenori et al. - 2000 - Benzofuran Derivatives, Process for the Preparation of the Same and Uses Tehreof.Pdf.
- (64) Chiba, K.; Fukuda, M.; Kim, S.; Kitano, Y.; Tada, M. Dihydrobenzofuran Synthesis by an Anodic [3 + 2] Cycloaddition of Phenols and Unactivated Alkenes. *J. Org. Chem.* **1999**, *64* (20), 7654–7656. 10.1021/jo9908243.
- (65) Wang, X.; Lu, Y.; Dai, H.-X.; Yu, J.-Q. Pd(II)-Catalyzed Hydroxyl-Directed C–H Activation/C–O Cyclization: Expedient Construction of Dihydrobenzofurans. *J. Am. Chem. Soc.* **2010**, *132* (35), 12203–12205. 10.1021/ja105366u.
- (66) Parasram, M.; Iaroshenko, V. O.; Gevorgyan, V. Endo-Selective Pd-Catalyzed Silyl Methyl Heck Reaction. *J. Am. Chem. Soc.* **2014**, *136* (52), 17926–17929. 10.1021/ja5104525.
- (67) Ratushnyy, M.; Parasram, M.; Wang, Y.; Gevorgyan, V. Palladium-Catalyzed Atom-Transfer Radical Cyclization at Remote Unactivated C(Sp³)–H Sites: Hydrogen-Atom Transfer of Hybrid Vinyl Palladium Radical Intermediates. *Angew. Chem. Int. Ed.* **2018**, *57* (10), 2712–2715. 10.1002/anie.201712775.
- (68) Saito, H.; Oishi, H.; Kitagaki, S.; Nakamura, S.; Anada, M.; Hashimoto, S. Enantio- and Diastereoselective Synthesis of Cis-2-Aryl-3-Methoxycarbonyl-2,3-Dihydrobenzofurans via the Rh(II)-Catalyzed C–H Insertion Process. *Org. Lett.* **2002**, *4* (22), 3887–3890. 10.1021/ol0267127.
- (69) Ito, H.; Sato, A.; Taguchi, T. Enantioselective Aromatic Claisen Rearrangement. *Tetrahedron Letters* **1997**, *38* (27), 4815–4818. 10.1016/S0040-4039(97)01040-X.
- (70) Youn, S. W.; Eom, J. I. Ag(I)-Catalyzed Sequential C–C and C–O Bond Formations between Phenols and Dienes with Atom Economy. *J. Org. Chem.* **2006**, *71* (17), 6705–6707. 10.1021/jo061221b.

- (71) Kazushige, H.; Hideki, K.; Akio, M.; Tetsuo, O.; Isao, F. Transition Metal-Catalyzed Cyclized Cyclization of 2-Allylphenol to 2,3-Dihydro-2-Methylbenzofuran without Beta-Elimination. *Chemistry Letters* **1998**, 27 (11), 1083–1084.
- (72) Grant, V. H.; Liu, B. Iridium(III)-Catalyzed Tandem Claisen Rearrangement–Intramolecular Hydroaryloxylation of Aryl Allyl Ethers to Form Dihydrobenzofurans. *Tetrahedron Letters* **2005**, 46 (8), 1237–1239. 10.1016/j.tetlet.2005.01.006.
- (73) Lauer, W. M.; Moe, O. The Rearrangement of Phenyl Allyl Ethers. VIII. Ethyl p-(γ,γ -Dimethylallyloxy)-Benzoate ¹. *J. Am. Chem. Soc.* **1943**, 65 (2), 289–293. 10.1021/ja01242a043.
- (74) Kim, S.; Noda, S.; Hayashi, K.; Chiba, K. An Oxidative Carbon–Carbon Bond Formation System in Cycloalkane-Based Thermomorphic Multiphase Solution. *Org. Lett.* **2008**, 10 (9), 1827–1829. 10.1021/ol8004408.
- (75) Palucki, M.; Wolfe, J. P.; Buchwald, S. L. Synthesis of Oxygen Heterocycles via a Palladium-Catalyzed C–O Bond-Forming Reaction. *J. Am. Chem. Soc.* **1996**, 118 (42), 10333–10334. 10.1021/ja962408v.
- (76) Zhu, D.-X.; Liu, J.-G.; Xu, M.-H. Stereodivergent Synthesis of Enantioenriched 2,3-Disubstituted Dihydrobenzofurans via a One-Pot C–H Functionalization/Oxa-Michael Addition Cascade. *J. Am. Chem. Soc.* **2021**, 143 (23), 8583–8589. 10.1021/jacs.1c03498.
- (77) Swamy, K. C. K.; Kumar, N. N. B.; Balaraman, E.; Kumar, K. V. P. P. Mitsunobu and Related Reactions: Advances and Applications. *Chem. Rev.* **2009**, 109 (6), 2551–2651. 10.1021/cr800278z.
- (78) Nam, N.-H.; Sardari, S.; Parang, K. Reactions of Solid-Supported Reagents and Solid Supports with Alcohols and Phenols through Their Hydroxyl Functional Group. *J. Comb. Chem.* **2003**, 5 (5), 479–546. 10.1021/cc020106l.

- (79) But, T. Y. S.; Toy, P. H. Organocatalytic Mitsunobu Reactions. *J. Am. Chem. Soc.* **2006**, *128* (30), 9636–9637. 10.1021/ja063141v.
- (80) Tsunoda, T.; Ozaki, F.; Itô, S. Novel Reactivity of Stabilized Methylenetriethylphosphorane: A New Mitsunobu Reagent. *Tetrahedron Letters* **1994**, *35* (28), 5081–5082. 10.1016/S0040-4039(00)73326-0.
- (81) Itô, S. Development of New Synthetic Reagents in Mitsunobu-Type Reaction. *YAKUGAKU ZASSHI* **2001**, *121* (8), 567–583. 10.1248/yakushi.121.567.
- (82) Tsunoda, T.; Yamamiya, Y.; Kawamura, Y.; Itô, S. Mitsunobu Acylation of Sterically Congested Secondary Alcohols by N,N,N',N'-Tetramethylazodicarboxamide-Triethylphosphine Reagents. *Tetrahedron Letters* **1995**, *36* (14), 2529–2530. 10.1016/0040-4039(95)00299-R.
- (83) Adly, F. On the Structure of Chiral Dirhodium(II) Carboxylate Catalysts: Stereoselectivity Relevance and Insights. *Catalysts* **2017**, *7* (11), 347. 10.3390/catal7110347.
- (84) Shimada, N.; Hanari, T.; Kurosaki, Y.; Takeda, K.; Anada, M.; Nambu, H.; Shiro, M.; Hashimoto, S. Catalytic Asymmetric Synthesis of the *Endo* -6-Aryl-8-Oxabicyclo[3.2.1]Oct-3-En-2-One Natural Product from *Ligusticum Chuanxing* via 1,3-Dipolar Cycloaddition of a Formyl-Derived Carbonyl Ylide Using Rh₂ (S-TCPTTL) *4*. *J. Org. Chem.* **2010**, *75* (17), 6039–6042. 10.1021/jo101175b.
- (85) Boruta, D. T.; Dmitrenko, O.; Yap, G. P. A.; Fox, J. M. Rh₂(S-PTTL)3TPA—a Mixed-Ligand Dirhodium(I) Catalyst for Enantioselective Reactions of α -Alkyl- α -Diazoesters. *Chem. Sci.* **2012**, *3* (5), 1589. 10.1039/c2sc01134d.
- (86) Yang, S.; Zhang, Y. Pd-Catalyzed Alkene-Relayed Intermolecular C–H Alkylation Using Aryl Halide Substrates. *Org. Lett.* **2022**, *24* (49), 9060–9064. 10.1021/acs.orglett.2c03699.

- (87) Adly, F. G.; Maddalena, J.; Ghanem, A. Rh₂ (S-1,2-NTTL)₄: A Novel Rh₂ (S-PTTL)₄ Analog With Lower Ligand Symmetry for Asymmetric Synthesis of Chiral Cyclopropylphosphonates: Aymmetric Synthesis of Chiral Cyclopropylphosphonates.. *Chirality* **2014**, *26* (11), 764–774. 10.1002/chir.22349.
- (88) Wang, X.; Weigl, C.; Doyle, M. P. Solvent Enhancement of Reaction Selectivity: A Unique Property of Cationic Chiral Dirhodium Carboxamidates. *J. Am. Chem. Soc.* **2011**, *133* (24), 9572–9579. 10.1021/ja202676a.
- (89) Laconsay, C. J.; Pla-Quintana, A.; Tantillo, D. J. Effects of Axial Solvent Coordination to Dirhodium Complexes on the Reactivity and Selectivity in C–H Insertion Reactions: A Computational Study. *Organometallics* **2021**, *40* (24), 4120–4132. 10.1021/acs.organomet.1c00574.
- (90) Green, A. I.; Tinworth, C. P.; Warriner, S.; Nelson, A.; Fey, N. Computational Mapping of Dirhodium(II) Catalysts. *Chem. Eur. J.* **2021**, *27* (7), 2402–2409. 10.1002/chem.202003801.
- (91) Sharland, J. C.; Dunstan, D.; Majumdar, D.; Gao, J.; Tan, K.; Malik, H. A.; Davies, H. M. L. Hexafluoroisopropanol for the Selective Deactivation of Poisonous Nucleophiles Enabling Catalytic Asymmetric Cyclopropanation of Complex Molecules. *ACS Catal.* **2022**, *12* (20), 12530–12542. 10.1021/acscatal.2c03909.
- (92) Wang, Y.; Wolf, J.; Zavalij, P.; Doyle, M. P. Cationic Chiral Dirhodium Carboxamidates Are Activated for Lewis Acid Catalysis. *Angew. Chem. Int. Ed.* **2008**, *47* (8), 1439–1442. 10.1002/anie.200704618.
- (93) Trindade, A. F.; Coelho, J. A. S.; Afonso, C. A. M.; Veiros, L. F.; Gois, P. M. P. Fine Tuning of Dirhodium(II) Complexes: Exploring the Axial Modification. *ACS Catal.* **2012**, *2* (3), 370–383. 10.1021/cs200597a.

- (94) Bernardes, G. J. L.; Casi, G.; Trüssel, S.; Hartmann, I.; Schwager, K.; Scheuermann, J.; Neri, D. A Traceless Vascular-Targeting Antibody-Drug Conjugate for Cancer Therapy. *Angew. Chem. Int. Ed.* **2012**, *51* (4), 941–944. 10.1002/anie.201106527.
- (95) Ito, S.; Okuno, M.; Asami, M. Differentiation of Enantiomeric Anions by NMR Spectroscopy with Chiral Bisurea Receptors. *Org. Biomol. Chem.* **2018**, *16* (2), 213–222. 10.1039/C7OB02318A.
- (96) Yu, R. T.; Rovis, T. Asymmetric Synthesis of Bicyclic Amidines via Rhodium-Catalyzed [2+2+2] Cycloaddition of Carbodiimides. *J. Am. Chem. Soc.* **2008**, *130* (11), 3262–3263. 10.1021/ja710065h.
- (97) Burns, A. S.; Rychnovsky, S. D. Total Synthesis and Structure Revision of (–)-Illisimonin A, a Neuroprotective Sesquiterpenoid from the Fruits of *Illicium Simonsii*. *J. Am. Chem. Soc.* **2019**, *141* (34), 13295–13300. 10.1021/jacs.9b05065.
- (98) Tale, R. H. Novel Synthesis of 2-Arylbenzothiazoles Mediated by Ceric Ammonium Nitrate (CAN). *Org. Lett.* **2002**, *4* (10), 1641–1642. 10.1021/ol020027i.
- (99) Li, S.-S.; Wu, L.; Qin, L.; Zhu, Y.-Q.; Su, F.; Xu, Y.-J.; Dong, L. Iridium(III)-Catalyzed Tandem [3 + 2] Annulation: Synthesis of Spirocyclic Phosphoramidate Derivatives. *Org. Lett.* **2016**, *18* (17), 4214–4217. 10.1021/acs.orglett.6b01895.
- (100) Morgan, L. R.; Thangaraj, K.; LeBlanc, B.; Rodgers, A.; Wolford, L. T.; Hooper, C. L.; Fan, D.; Jursic, B. S. Design, Synthesis, and Anticancer Properties of 4,4'-Dihydroxybenzophenone-2,4-Dinitrophenylhydrazone and Analogues. *J. Med. Chem.* **2003**, *46* (21), 4552–4563. 10.1021/jm0301080.
- (101) Murakata, M.; Ikeda, T. Stereoselective Synthesis of the Viridifungin Analogue NA808 from a Chiral Tetrahydrofuran-Carboxylic Acid. *Org. Biomol. Chem.* **2017**, *15* (31), 6632–6639. 10.1039/C7OB01608E.

- (102) Laconsay, C. J. Theoretical Models of Dirhodium Catalyzed Reactions and Divergent Heterolytic Fragmentations, UC Davis, 2022. <https://escholarship.org/uc/item/3qm9r76q>.
- (103) Laconsay, C.; Dishman, S.; Fettinger, J.; Tantillo, D.; Shaw, J. Stereochem_Rh_carbenes, 2021. 10.19061/iochem-bd-6-94.
- (104) Hansen, J.; Autschbach, J.; Davies, H. M. L. Computational Study on the Selectivity of Donor/Acceptor-Substituted Rhodium Carbenoids. *J. Org. Chem.* **2009**, *74* (17), 6555–6563. 10.1021/jo9009968.
- (105) Sperger, T.; Sanhueza, I. A.; Schoenebeck, F. Computation and Experiment: A Powerful Combination to Understand and Predict Reactivities. *Acc. Chem. Res.* **2016**, *49* (6), 1311–1319. 10.1021/acs.accounts.6b00068.
- (106) Vogiatzis, K. D.; Polynski, M. V.; Kirkland, J. K.; Townsend, J.; Hashemi, A.; Liu, C.; Pidko, E. A. Computational Approach to Molecular Catalysis by 3d Transition Metals: Challenges and Opportunities. *Chem. Rev.* **2019**, *119* (4), 2453–2523. 10.1021/acs.chemrev.8b00361.
- (107) Sperger, T.; Sanhueza, I. A.; Kalvet, I.; Schoenebeck, F. Computational Studies of Synthetically Relevant Homogeneous Organometallic Catalysis Involving Ni, Pd, Ir, and Rh: An Overview of Commonly Employed DFT Methods and Mechanistic Insights. *Chem. Rev.* **2015**, *115* (17), 9532–9586. 10.1021/acs.chemrev.5b00163.
- (108) Ahn, S.; Hong, M.; Sundararajan, M.; Ess, D. H.; Baik, M.-H. Design and Optimization of Catalysts Based on Mechanistic Insights Derived from Quantum Chemical Reaction Modeling. *Chem. Rev.* **2019**, *119* (11), 6509–6560. 10.1021/acs.chemrev.9b00073.
- (109) Pidko, E. A. Toward the Balance between the Reductionist and Systems Approaches in Computational Catalysis: Model versus Method Accuracy for the Description of Catalytic Systems. *ACS Catal.* **2017**, *7* (7), 4230–4234. 10.1021/acscatal.7b00290.

- (110) Tantillo, D. J. Recent Excursions to the Borderlands between the Realms of Concerted and Stepwise: Carbocation Cascades in Natural Products Biosynthesis. *J. Phys. Org. Chem.* **2008**, *21* (7–8), 561–570. 10.1002/poc.1320.
- (111) O’Ferrall, R. A. M. Relationships between E2 and E1cB Mechanisms of β -Elimination. *J. Chem. Soc. B* **1970**, *0* (0), 274–277. 10.1039/J29700000274.
- (112) Jensen, F. R.; Rickborn, B. *Electrophilic Substitution of Organomercurials*; McGraw-Hill: New York, 1968.
- (113) Jensen, F. R.; Gale, L. H. Electrophilic Aliphatic Substitution. I. Electrophilic Substitution Studies with Cis- and Trans-4-Methylcyclohexylmercuric Bromides. *Journal of the American Chemical Society* **1959**, *81*, 1261.
- (114) Fukuto, J. M.; Jensen, F. R. Mechanisms of SE2 Reactions: Emphasis on Organotin Compounds. *Acc. Chem. Res.* **1983**, *16* (5), 177–184. 10.1021/ar00089a005.
- (115) Fleming, I.; Rowley, M. The Stereochemistry of the Intramolecular Electrophilic Attack of an Aldehyde on a Carbon-Tin Bond. *Tetrahedron* **1986**, *42* (12), 3181–3198. 10.1016/S0040-4020(01)87383-X.
- (116) Curini, M.; Epifano, F.; Marcotullio, M. C.; Montanari, F. Oxone[®]-KI Induced Lactonization and Etherification of Unsaturated Acids and Alcohols: A Formal Synthesis of Mintlactone. *Synlett* **2004**, No. 2, 0368–0370. 10.1055/s-2003-45009.
- (117) Pilli, R. A.; Victor, M. M.; de Meijere, A. First Total Synthesis of Aspinolide B, a New Pentaketide Produced by *Aspergillus ochraceus*. *J. Org. Chem.* **2000**, *65* (19), 5910–5916. 10.1021/jo000327i.
- (118) Niu, T.; Wang, K.-H.; Huang, D.; Xu, C.; Su, Y.; Hu, Y.; Fu, Y. One-Pot Transition-Metal-Free Synthesis of Weinreb Amides Directly from Carboxylic Acids. *Synthesis* **2013**, *46* (03), 320–330. 10.1055/s-0033-1340317.

Chapter 2

Targeted Synthesis of Dihydrobenzoxanthenes: *cycloartobiloxanthere* and *artoindonesianin Z-2*

2.1 Introduction

Natural products have long served as an essential component of the drug discovery process. The large structural complexity of natural product families opens unexplored areas of chemical space that typical synthetic small molecule libraries fail to reach.^{1,2} Throughout each natural product class arises an evolutionarily optimized scaffold modified to target well-defined biological functions. The biosynthetic pathway from which each family originates yields sequentially modified versions of a privileged scaffold. These related analogs often bind different protein targets within a biological signaling pathway. Notably, since natural products are already made within living systems to target living organisms, they usually possess intrinsic bioavailability, making them great starting points for a drug discovery program. The use of natural products in natural medicines also offers critical insights into their possible disease indications. Therefore, developing synthetic strategies toward natural product families is not only a challenging intellectual exercise but can serve as a structural confirmation and starting point for an entire drug discovery program. The key when designing a natural product synthetic strategy is to heed the information already given by nature. Identifying the core scaffold shared across all analogs of the natural product class is key. This core highlights the main framework the synthetic plan must focus on constructing and identifies the areas of divergence that would optimally be tolerated.³

2.1.1. Isolation of furanodihydrobenzoxanthenes

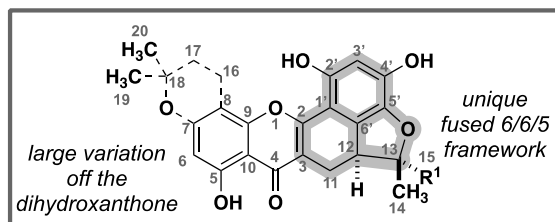
Based on our publication on the C–H insertion of donor/donor carbenes into stereogenic centers⁴ (see Chapter 1), we identified a unique tetrahydronaphthol[1,8*bc*]furan core that could be accessed stereoselectivity using our methodology. We discovered that this fused 6/6/5

framework (Figure 2.1A) was prevalent in three main natural product families: the opioid family⁵, the sesquiterpene family⁶⁻⁸, and the furanodihydrobenzoxanthone family⁹. The furanodihydrobenzoxanthones are an underexplored subclass of xanthone natural products isolated from the bark of plants in the *Artocarpus* genus.⁹ They are characterized by their fused benzodihydrofuran tricyclic core containing one to two stereocenters and have vast variations off the aryl ring of the dihydrobenzoxanthone core (Figure 2.1A). Unlike the opioid and sesquiterpene natural product families, the dihydrobenzoxanthone family has never been synthesized. The vast biological activity possessed by dihydrobenzoxanthones makes them an interesting synthetic target.

Many individual furanodihydrobenzoxanthones family members are isolated from a single species of the *Artocarpus* genus. However, one family member, cycloartobiloxanthone (**1**), is isolated abundantly across the entire genus (Figure 2.1A).¹⁰ Cycloartobiloxanthone (**1**) was first isolated in 1989 by the Surendrakumar group from *Artocarpus nobilis*, a plant native to Sri Lanka.¹¹ Excitingly, it was the first reported occurrence of a dihydrobenzoxanthone isolated from plants and is hypothesized to arise from the flavonoid biosynthetic pathway (see Section 2.1.2). At the time of the initial isolation, cycloartobiloxanthone (**1**) was reported without any stereochemistry assigned. In 2010 the Douglas group characterized cycloartobiloxanthone as a single enantiomer.¹² Artoindonesianin Z-2 (**2**), a very closely related analog, was isolated in 2005 from *A. lanceifolius* and varied only at the C13 position where oxidation of one of the methyl groups created a second stereocenter on the benzodihydrofuran core.¹³ Only the relative stereochemistry of artoindonesianin Z-2 (**2**) was assigned. Still, it was assumed artoindonesianin Z-2 (**2**) most likely has the same absolute configuration as cycloartobiloxanthone (**1**) since both natural products are derived from the same biosynthetic pathway. Notably, the structure drawn for artoindonesianin Z-2 (**2**) (Figure 2.1A) was the structure assigned by the Hakim group in the original isolation paper, where they named the

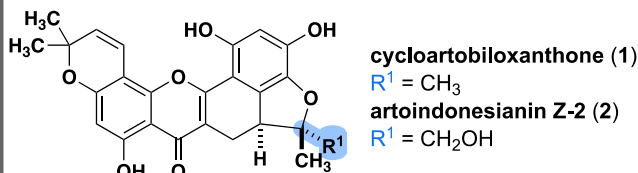
natural product artoindonesianin Z-2. While the closely related pyranodihydrobenzoxanthone was also isolated in the same paper and named artoindonesianin Z-1.¹³

A. Dihydrobenzoxanthenes Natural Product Family

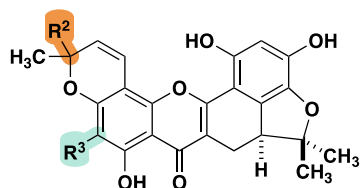


our focus

C13 Substitution

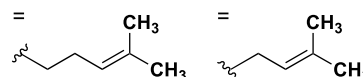
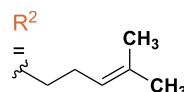


B. C6 & C20 Substitution

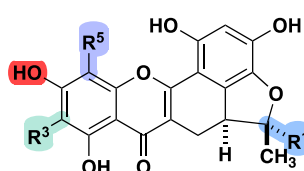


artoriginone B (3)

artoinin W (4)

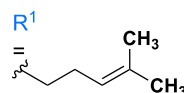


C. C6, C8, C13, O7 Substitution

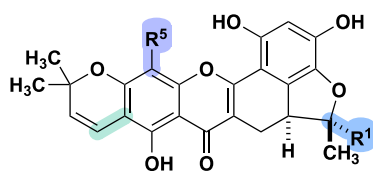


artorigin B (5)

artocarpone B (6)



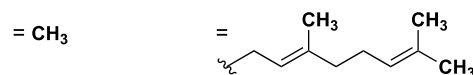
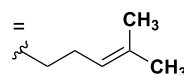
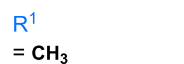
D. C6, C8 & C13 Substitution



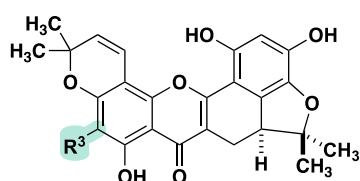
artoinin A (7)

artoinin M (8)

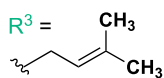
artoindonesianin A (9)



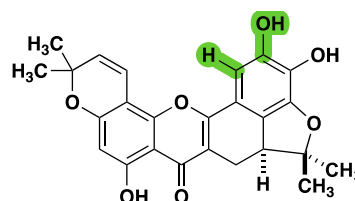
E. C6 Substitution



artoinin F (10)

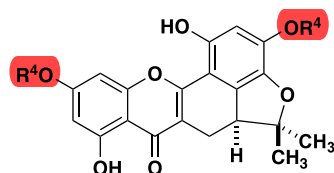


C2' & C3' Substitution



artomandin (11)

O4' & O7 Substitution



artoindonesianin P (12) $R^4 = \text{H}$

artoindonesianin M (13) $R^4 = \text{OCH}_3$

Figure 2.1 Furanodihydrobenzoxanthenes natural product subclass.

However, in a subsequent review published a year later in 2006⁹ by the same group as well as conference proceedings in 2015¹⁴, Hakim and co-workers refer to the furanodihydrobenzoxanthone (**2**) as “artoindonesianin Z-1” and the pyranodihydrobenzoxanthone as “artoindonesianin Z-2”. A similar naming switch has been seen in later publications from other groups citing the 2006 review by Hakim.¹⁵ From this point forward in this dissertation, the furanodihydrobenzoxanthone (**2**) will be referred to as artoindonesianin Z-2, defaulting to the name given upon the initial isolation of the compound.

Artoindonesian Z-2 (**2**) is the only reported family member with just C13 structural variation from cycloartobiloxanthone (**1**) (Figure 2.1A). The rest of the related family members possess structural variation around the 2*H*-chromene core of the main framework in cycloartobiloxanthone (**1**). First, artorigidinone B¹⁶ (**3**) and artonin W¹⁷ (**4**) have a 6-carbon chain rather than a methyl group at the C20 position (Figure 2.1B). This is the biosynthetic result of farnesylation at the C8 position, rather than prenylation, followed by cyclization to afford the 2*H*-chromene core. Artonin W (**4**) is also prenylated at the C6 position.

Artocarpone B (**6**) was isolated in 2007 from *Artocarpus champeden* and is the uncyclized chromene derivative of cycloartobiloxanthone (**1**) with prenylation at the C8 position (Figure 2.1C).¹⁸ Most likely, artocarpone B is a biosynthetic intermediate *en route* to the final fused 6-ring scaffold of cycloartobiloxanthone (**1**). Similarly, artorigidin B (**5**) lacks the chromene core and possesses substitution at the C13 position giving it two chiral centers.¹² The relative stereochemistry has been assigned to be the *trans* diastereomer, the same as artoindonesianin Z-2 (**2**), suggesting a conserved biosynthetic mechanism for furan formation.

Artonin A¹⁹ (**7**), artonin M²⁰ (**8**), and artoindonesianin A²¹ (**9**) possess the C6 regioisomer of the 2*H*-chromene core (Figure 2.1D). In addition, artonin M (**8**) has a prenyl chain at the C13 position in the same *trans* configuration as artorigidin B (**5**). Artoindonesianin A (**9**) is one of the larger family members due to the farnesyl chain at the C8 position.²¹

Artonin F^{22,23} (**10**) has been isolated from *A. communis* and is the C6-prenylated analog of cycloartobiloxanthone (**1**) (Figure 2.1E). Artomandin (**11**) is an interesting family member since it has an ortho phenol substitution pattern on the fused tricycle ring rather than the meta substitution pattern exhibited by all the other family members.²⁴ This indicates that the species it was isolated from possesses a unique oxidation enzyme that can perform this unique C–H oxidation pattern. Artoindonesianin P^{17,25} (**12**) is the biosynthetic intermediate before functionalization occurs at the C6 or C8 positions. Interestingly, the methylated version of the O4' and O7 phenols, artoindonesianin M (**13**), has been isolated specifically from *Artocarpus champeden*.²⁶

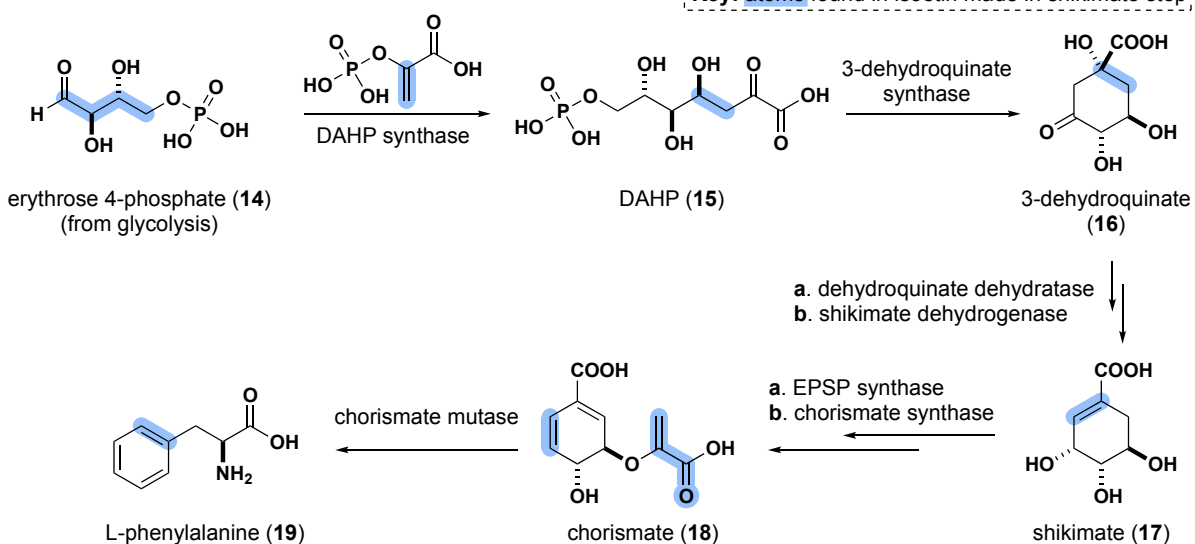
2.1.2. Biosynthetic route

The large array of related dihydrobenzoxanthone natural products isolated and discussed above is due to an extensively connected and divergent biosynthetic pathway. The core biosynthetic intermediate structure from which all these natural products diverge is a flavone, specifically isoetin (**23**) (Figure 2.2). This specific highly oxygenated substitution pattern leads to cycloartobiloxanthone (**1**), artoindonesianin Z-2 (**2**), and related natural products. Isoetin (**23**) is derived from naringenin (**21**) through the intermediate norartocarpetin (**22**).²⁶ These flavones are made from the intersection of the phenylpropanoid, polyketide, and shikimate biosynthetic pathways.

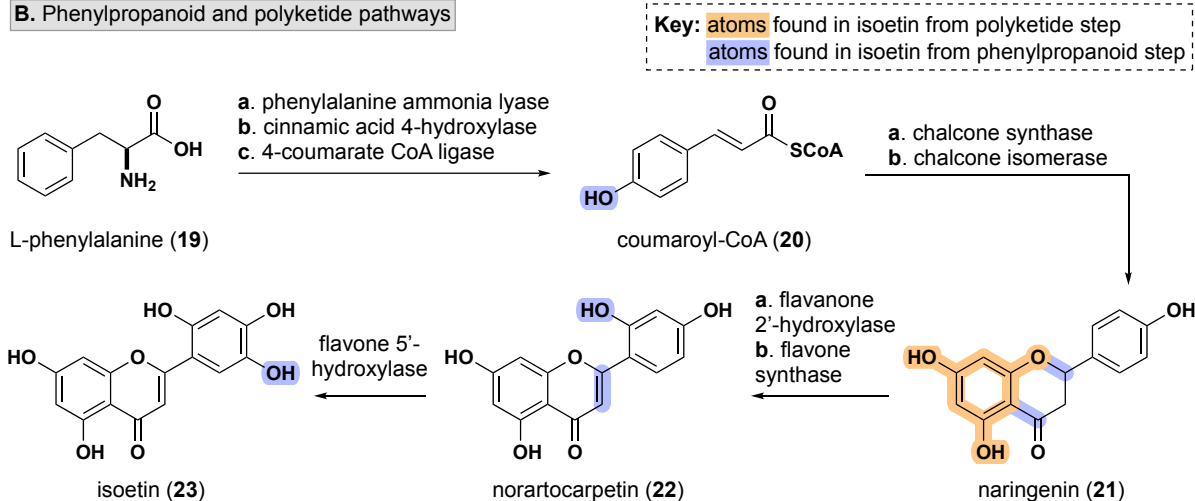
To start, the shikimate pathway takes erythrose 4-phosphate (**14**), sourced from glycolysis, and over four enzymatic steps makes shikimate (**17**) (Figure 2.2).²⁷ Then shikimate (**17**) is alkylated and dehydrated to give L-phenylalanine (**19**), which serves as the building block of ring B and the linking chain in ring C of isoetin (**23**) (Figure 2.2C). Then the phenylpropanoid pathway takes L-phenylalanine (**19**) and, over three steps, makes coumaroyl-CoA (**20**). Three malonyl-CoA molecules (**24**), derived from glucose, sourced from the polyketide pathway are then used to undergo successive Claisen condensations by chalcone synthase to make ring A

and link it to ring B in isoetin (**23**).²⁸ Chalcone isomerase can catalyze the intramolecular cyclization reaction to yield the flavanone, naringenin **22**.

A. Shikimate pathway



B. Phenylpropanoid and polyketide pathways



C. Biosynthetic pathway mapping

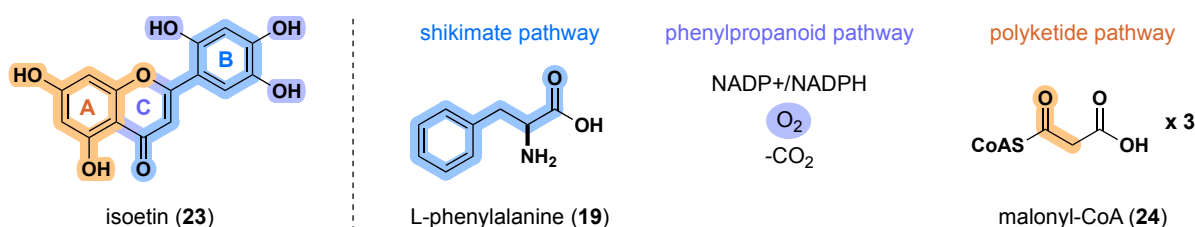


Figure 2.2 Proposed biosynthetic route for the formation of the flavone isoetin: **A.** Shikimate pathway steps **B.** Phenylpropanoid and polyketide pathway steps **C.** Biosynthetic pathway mapping onto isoetin.

Subsequent oxidation reactions to hydroxylate ring B and a dehydration reaction on ring C of the flavanone give the key flavone precursor, isoetin (**23**).^{28,29} Mapping the individual building blocks from the three biosynthetic pathways onto isoetin (**23**) can be seen in Figure 2.2C.²⁸ The transformation of L-phenylalanine (**19**) to coumaroyl-CoA (**20**) is the point of divergence in the biosynthetic pathway for dihydrobenzoxanthenes to be made, rather than other xanthone natural product subclasses. These other subclasses of xanthone natural products convert L-phenylalanine (**19**) to cinnamoyl-CoA, leading to benzaldehyde formation. Benzaldehyde can then go on to eventually make many of the commonly known related xanthone natural products and some tetrahydroxanthenes.^{30,31}

Isoetin (**23**) can be further functionalized downstream in the biosynthetic pathway to eventually make cycloartobiloxanthone (**1**) and artoindonesianin Z-2 (**2**). Figure 2.3 shows the proposed biosynthetic pathways for both these natural products from isoetin (**23**),^{9,11,26,32} where many of the intermediates along the pathway have also been isolated from *Artocarpus* plants and fully characterized as individual natural products (Figure 2.1).^{22,25,33–36} Starting from isoetin (**23**), the flavone is prenylated in the C-3 position to give the 3-prenylflavone (**27**), from which two main routes can occur (Figure 2.3). The first route is addition across the alkene leading to the furanodihydrobenzoxanthenes: artoindonesianin P (**12**)²⁵ and artoindonesianin M (**13**).²⁶ The second route further functionalizes the A ring of the flavone. In this route, prenylation at C-8 gives artochamin D (**28**),³³ which then undergoes oxidization (**29**) and cyclization to make artonin E (**30**).²² Artonin E (**30**) will then undergo oxidative coupling to make the fused three-member ring of cycloartobiloxanthone (**1**) through the intermediate artobiloxanthone (**31**).

There are two proposed mechanisms for the formation of the fused tricyclic core (Figure 2.4). Uvais and co-workers, in the original isolation paper in 1989,¹¹ proposed three

mechanistic steps to go from the 3-prenylflavone (**27** or **30**) to the furanodihydrobenzoxanthone core (**12**).

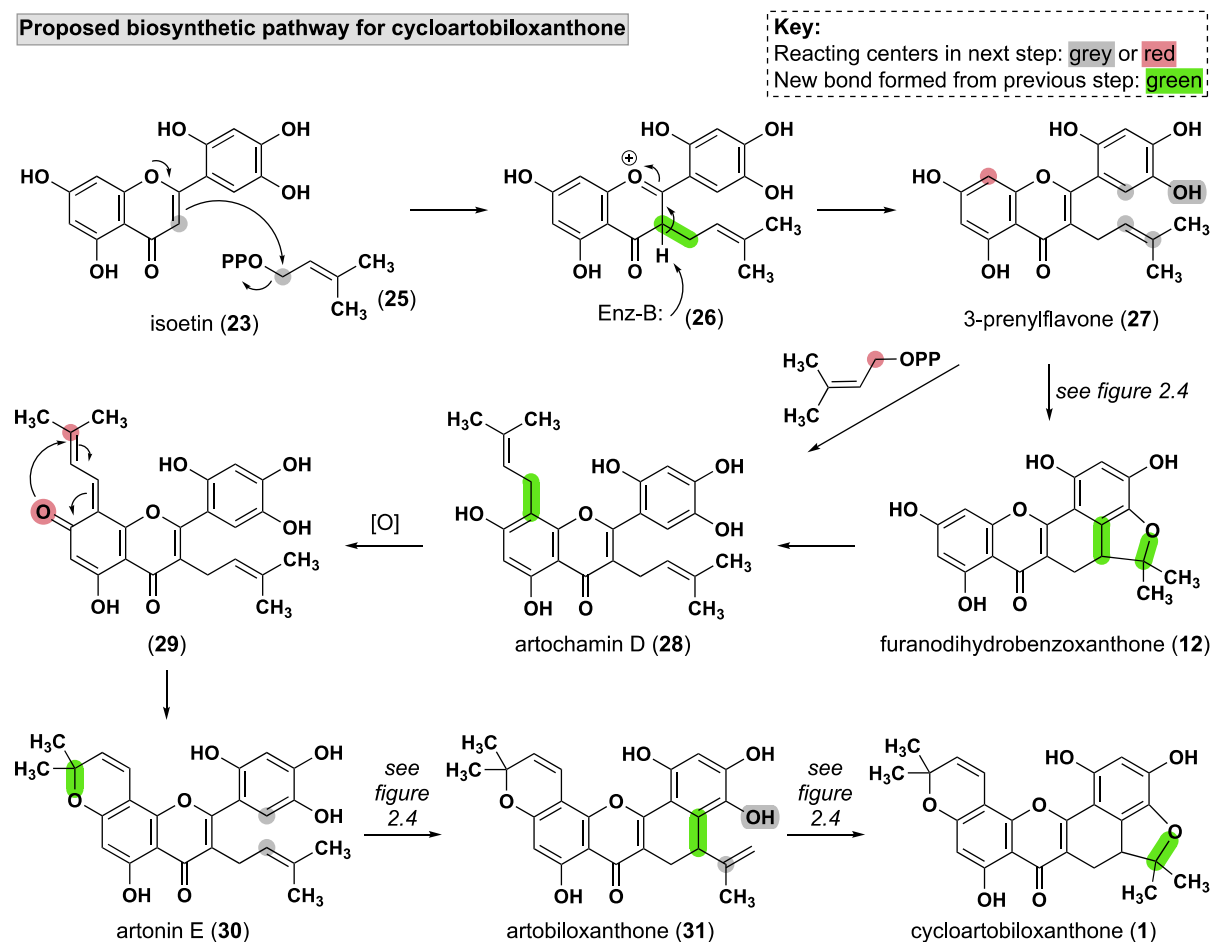


Figure 2.3 Proposed biosynthetic route for cycloartobiloxanthone from isoetin.

First, the alkene in **27** is epoxidized to form **32**. Second, the epoxide (**32**) undergoes intramolecular electrophilic aromatic substitution to form the dihydrobenzoxanthone intermediate (**34** or **31**). Third, oxidative cyclization between the phenol and the alkene in the dihydrobenzoxanthone core yields the fused tricyclic core (**12**). There is indirect evidence for the formation of artobiloxanthone (**31**) in the biosynthetic pathway since it has been isolated from the same plants from which cycloartobiloxanthone (**1**) has been isolated.

However, in 1996 Aida and co-workers³² challenged Uvais' mechanism by stating that the fused tricycle core could be formed from 3-prenylflavone (**27**) through a radical cascade. In

this radical mechanism, the 3-prenylflavone (**27** or **30**) undergoes an aryl H atom abstraction to place a radical on ring B of the flavone (**35**). This radical reacts with the alkene to form a new C–C bond, leaving a tertiary-centered radical (**36**). The ternary radical can either undergo oxidative cyclization with the phenol to form the C–O bond in furanodihydrobenzoxanthone (**1** or **12**) or undergo H atom abstraction yielding the alkene in artobiloxanthone (**31**).

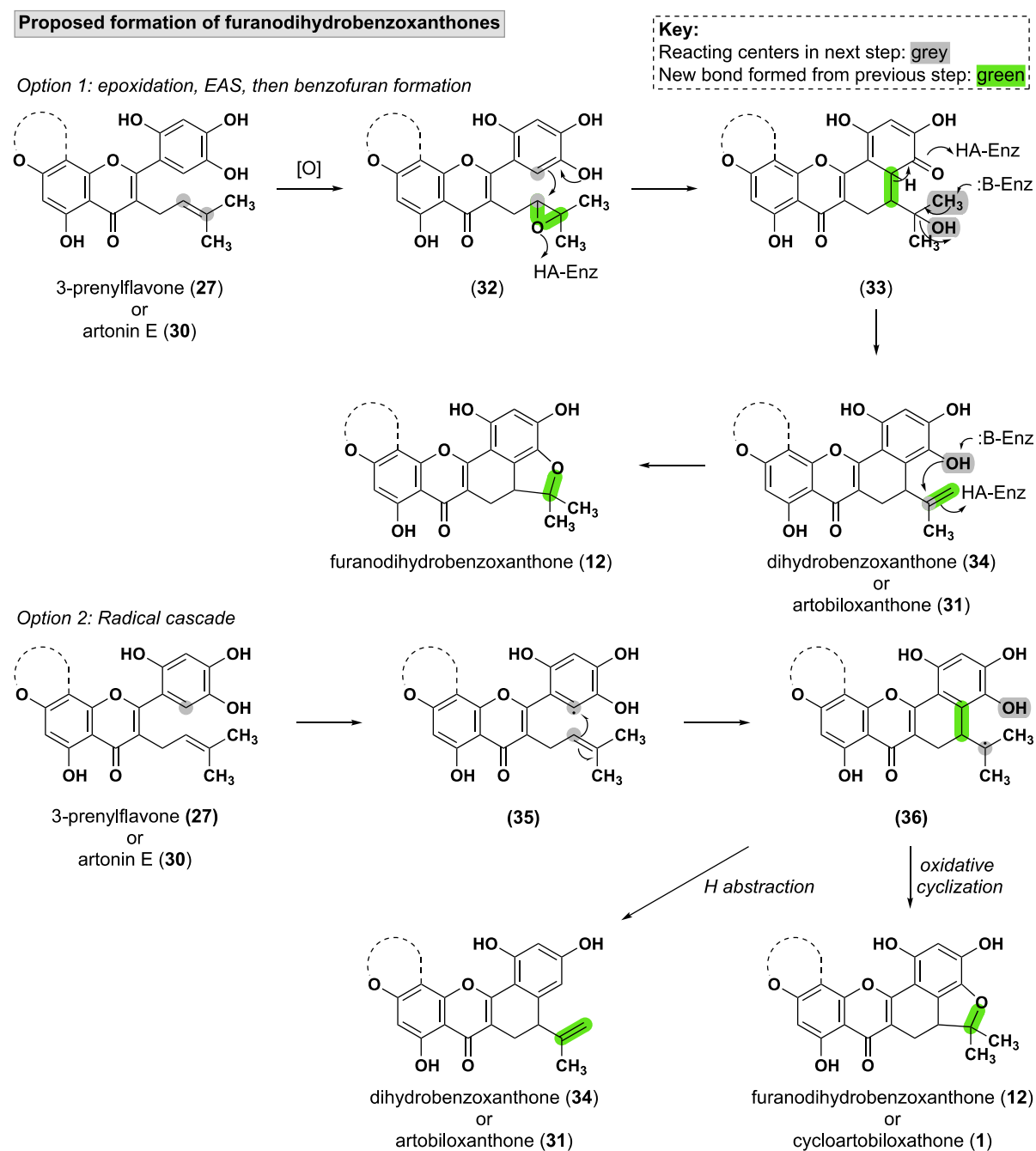


Figure 2.4 Proposed possible formation mechanisms of furanodihydrobenzoxanthones.

While plenty of known enzymes and cofactors can readily perform H atom abstractions and similar radical cascades,³⁷ Aida and co-workers wanted to demonstrate the feasibility of artonin E (**30**) undergoing this specific radical cascade. Therefore, they treated artonin E (**30**) with the stable free radical compound 2,2-diphenyl-1-picrylhydrazyl (DPPH) at room temperature in the presence of chloroform and ethanol. After four days, the reaction yielded artobiloxanthone (**31**) and cycloartobiloxanthone (**1**) in 33% and 6%,³² respectively, supporting the idea that dihydrobenzoxanthenes are biologically derived from 3-prenylflavones through oxidative radical cyclization. Analogous results also showed that irradiation of morusin, the same flavone structure at artonin E except missing the 5' hydroxyl group, yielded morusin hydroperoxide. The peroxide underwent radical cyclization with the 2' phenol to form an oxepinoflavone.^{9,26,32} These results further support the propensity of these 3-prenylflavones to undergo oxidative cyclization via radical cascade mechanism.

The biosynthesis of artoindonesianin Z-2 (**2**) has yet to be explored but based on the proposed pathways for cycloartobiloxanthone (**1**), a potential biosynthesis is proposed in Figure 2. From artonin E (**30**), allylic oxidation can occur to form 14-hydroxyartonin E (**37**), which has been isolated from *Artocarpus lanceifolius* and fully characterized.³⁵ 14-hydroxyartonin (**37**) then undergoes the same radical cascade previously discussed (Figure 2.4) to form artoindonesianin Z-2 (**2**) through ternary radical intermediate **38**.

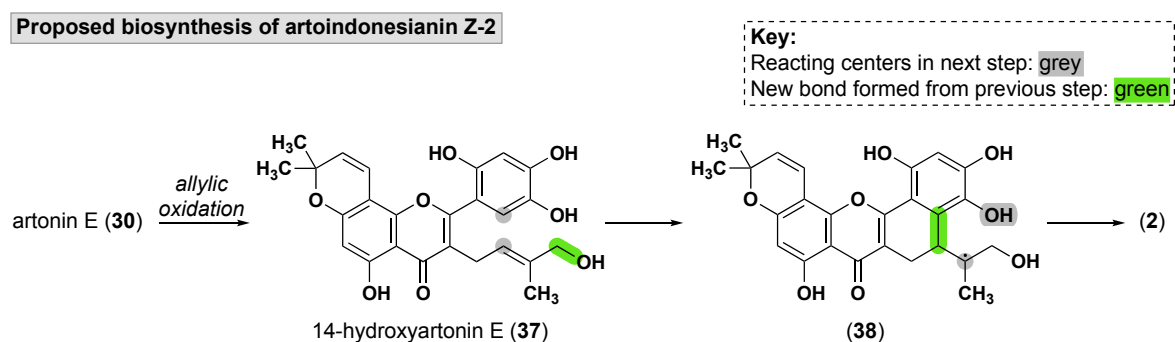


Figure 2.5 Possible biosynthetic pathway for artoindonesianin Z-2.

2.1.3. Biological testing of furanodihydrobenzoxanthenes

The dihydrobenzoxanthone natural product family possesses an extremely wide variety of biological activity. This large activity has historically been reflected in the many traditional medicines that utilize the *Artocarpus* plants.¹⁵ The reported potential biological indications range from anti-cancer, anti-malarial, and anti-microbial activity to inflammation and diabetes treatments (Table 2.1).

Cytotoxic activity against cancer cell lines is the most common biological activity of the dihydrobenzoxanthenes in the literature. Cycloartobiloxanthone (**1**) possesses the most reported biological activity of all the natural products in the family because it is the most abundant natural product and therefore is isolated the most often. First, cycloartobiloxanthone (**1**), artoindonesianin Z-2 (**2**), artoindonesianin A (**9**), artonin M (**8**), and artoindonesianin P (**12**) all possess activity against lymphoma P388 cells in the low micromolar range.^{9,21,25,26,38,39} The diphenol regioisomer, artomandin (**11**), also shows promising low micromolar activity against HL-60 leukemia cells.²⁴ Artorigidinone B (**3**) was tested against multiple cancer cell lines in its isolation paper. **3** had cytotoxic activity against melanoma SK-MEL-28 cells and chondrosarcoma SW1353 cells with IC₅₀ values of 3.37 μM and 5.63 μM, respectively. These values are promising when compared to the standard-of-care doxorubicin with an IC₅₀ of 1.74 μM for both cell lines.¹⁶ Cycloartobiloxanthone (**1**) and artorigidin B (**5**) also had moderate activity against HT-29 colon cancer cells, albeit an order of magnitude less potent than the current paclitaxel treatment.¹² Similarly, cycloartobiloxanthone (**1**) and artomandin (**11**) showed comparable activity to the standard of care, ellipticine, for breast cancer cell lines.^{23,24}

The Chanvorachote group discovered that cycloartobiloxanthone (**1**) had moderate cytotoxic activity for H460 lung cancer cells.⁴⁰ They investigated the potential mode of action and found that cycloartobiloxanthone (**1**) inhibits filopodia formation, a key mechanism in cancer cell metastasis. Furthermore, treatment of H460 cells with cycloartobiloxanthone (**1**)

suppressed cellular levels of cell division cycle protein 42 (Cdc42) signaling, which plays a key role in filopodia formation.

Table 2.1 Reported biological activities for dihydrobenzoxanthenes.

Biological indication	Natural product	Biological activity (IC ₅₀)
lymphoma (cytotoxic against P388 cells)	cycloartobiloxanthone (1)	4.6 µg/mL
	artoindonesianin Z-2 (2)	5.9 µg/mL
	artoindonesianin A (9)	21.0 µg/mL
	artoinin M (8)	7.9 µg/mL
	artoindonesianin P (12)	5.0 µg/mL
leukemia (inhibition of HL-60 cells)	artomandin (11)	2.4 µg/mL
melanoma (cytotoxic against SK-MEL-28 cells)	artorigidinone B (3)	3.37 µg/mL
chondrosarcoma (cytotoxic against SW1353 cells)	artorigidinone B (3)	5.63 µg/mL
colon cancer (cytotoxic against HT-29 cells)	cycloartobiloxanthone (1)	3.7 µM (ED ₅₀)
	artorigidin B (5)	3.4 µM (ED ₅₀)
lung cancer metastasis (cytotoxic against H460 cells) (CDC42 suppression signaling) (filopodia formation inhibition)	cycloartobiloxanthone (1)	61.8 µM
breast cancer (cytotoxic against human BC cells) (cytotoxic against MCF-7 cells)	cycloartobiloxanthone (1)	4.23 µg/mL
	artomandin (11)	3.1 µg/mL
antioxidant (radical scavenging activities)	cycloartobiloxanthone (1)	190 µM
antimalarial (<i>Plasmodium falciparum</i>)	artocarpone B (6)	0.18 µM/L
	cycloartobiloxanthone (1)	3.7 µg/mL
	artoinin F (10)	2.4 µg/mL
antimicrobial (bacterial neuraminidase (BNA) inhibition)	cycloartobiloxanthone (1)	1.3 µM
	artoinin W (4)	0.5 µM
	artorigidinone B (3)	1.1 µM
	artoindonesianin P (12)	3.9 µM
inflammation (human neutrophil elastase (HNE) inhibition)	cycloartobiloxanthone (1)	20.8 µM
	artoindonesianin P (12)	28.7 µM
diabetes & obesity (α-glucosidase inhibition)	cycloartobiloxanthone (1)	9.6 µM
	artoindonesianin P (12)	25.4 µM

Cdc42 is a GTPase that is upstream in the integrin signaling pathway. Integrins are responsible for mediating cellular adhesion by stabilizing filopodia.⁴¹ Often, filopodia formation is upregulated in Ras-related cancer cells allowing for rapid cancer metastasis.

Therefore down-regulation of Cdc42 has been investigated as a therapeutic target for treating these cancers.⁴² The Ganesan group at the University of Irvine recently published extensive structure-based design studies of a small molecular Cdc42 effector interaction inhibitor for cancer treatment.⁴³ The ability of cycloartobiloxanthone (**1**) to down-regulate Cdc42 is notable because a structurally related natural product family, the pseudorigols, possesses inhibitory activity against Cdc25.⁶ Cdc25 is a guanine nucleotide exchange factor (GEF) in the Dbl family.⁴⁴ GEFs are in the Ras signaling pathway directly upstream of Cdc42 and other Rho family GTPases.⁴⁵ Therefore, one possible hypothesis is that the fused tricyclic core, found in cycloartobiloxanthone (**1**) and pseudorigol A/B, is the pharmacophore binding and inhibiting the Cdc25 protein. Effectively downregulating Cdc42 activity and subsequent cellular proliferation pathways.^{46,47}

Aside from possible anticancer activity, the dihydrobenzoxanthenes possess activity for multiple other biological indications (Table 2.1). Cycloartobiloxanthone (**1**) has reported antioxidant activity tested through DPPH (2,2-diphenyl-1-picrylhydrazyl) radical scavenging assays, most likely due to the presence of the dihydroxanthone core.^{48,49} However, the Likhitwitayawuid group contradicted these findings in 2010, showing that cycloartobiloxanthone (**1**) has low free-radical scavenging activity. Especially when the natural product is compared to the non-fused dihydroxanthone cores of earlier biosynthetic intermediates *en route* to cycloartobiloxanthone (**1**).³⁴

Artocarpone B (**6**), cycloartobiloxanthone (**1**), and artonin F (**10**) all show antimalarial/antiplasmodial activity. Artocarpone B (**6**) has the best inhibitory activity for *Plasmodium falciparum* of the three natural products with an IC₅₀ of 180 nM. Comparatively, the well-known malarial drug chloroquine has an IC₅₀ of 6.3 nM.^{18,23}

The Park group from Gyeongsang National University has investigated the antimicrobial, inflammation, and diabetes treatment applications of dihydrobenzoxanthenes from *Artocarpus*

isolations (Table 1). Using molecular docking studies, they have studied dihydrobenzoxanthone modes of binding. First, the group showed that cycloartobiloxanthone (**1**), artonin W (**4**), artorigidinone B (**3**), and artoindonesianin P (**12**) all possessed antimicrobial activity specifically for bacterial neuraminidase (BNA). BNA plays a key role in bacterial pathogenesis, where many bacteria can only infect the host cell in the presence of BNA. BNA recognizes and cleaves sialic acid residues enabling bacterial infection into a host cell. Baiseitova and co-workers used Lineweaver-Burk plots to investigate the inhibitory mechanism and found that the four dihydrobenzoxanthones (**1**, **4**, **3**, **12**) were reversible, non-competitive inhibitors of BNA. Specifically, molecular docking studies with BNA illuminated that cycloartobiloxanthone (**1**) and artonin W (**4**) have unique interactions with Tyr435 of the BNA active site.¹⁷ Ban and co-workers demonstrated that cycloartobiloxanthone (**1**) and artoindonesianin P (**12**) inhibit human neutrophil elastase (HNE) in a dose-dependent manner. HNE is a serine protease with implications for the immune system response due to its large expression in the bone marrow and migration to primary granules. Both **1** and **12** were classified as mixed type I inhibitors of HNE, meaning they bind to the free enzyme better than the enzyme-substrate complex. Molecular docking studies showed that alkyl groups on the flavone core, such as the fused tricyclic core, were crucial in inhibiting HNE.⁵⁰ Finally, the Park group also found that cycloartobiloxanthone (**1**) and artoindonesianin P (**12**) served as moderate α -glucosidase inhibitors. α -glucosidase receptors are highly studied for diabetes and obesity treatments due to their ability to reduce blood sugar levels when inhibited. Phenolic compounds that bind α -glucosidase are rare, and molecular dockings classified compounds **1** and **12** as competitive inhibitors.

2.1.4 Previous synthetic methods to make 6/6/5 tricyclic framework

There has been a multitude of reported synthetic methods to make the 6/6/5 tricyclic framework found in furanodihydrobenzoxanthenes, also known as the 2a,3,4,5-tetrahydro-2H-naphtho[1,8-bc]furan core (**39**) (Figure 2.6). Most of the previously published work on the 6/6/5 core targets accessing the opioid family^{51,52} and unnatural ergoline analogs.^{53–56} These natural product scaffolds hinge on having access to substitution at the bridgehead (2a-position) of the fused dihydrobenzofurans and the 3- and 4-positions of the tetralone. For example, this specific substitution pattern on the 6/6/5 framework is found in morphine (**40**) and is notoriously difficult to make stereoselectively.

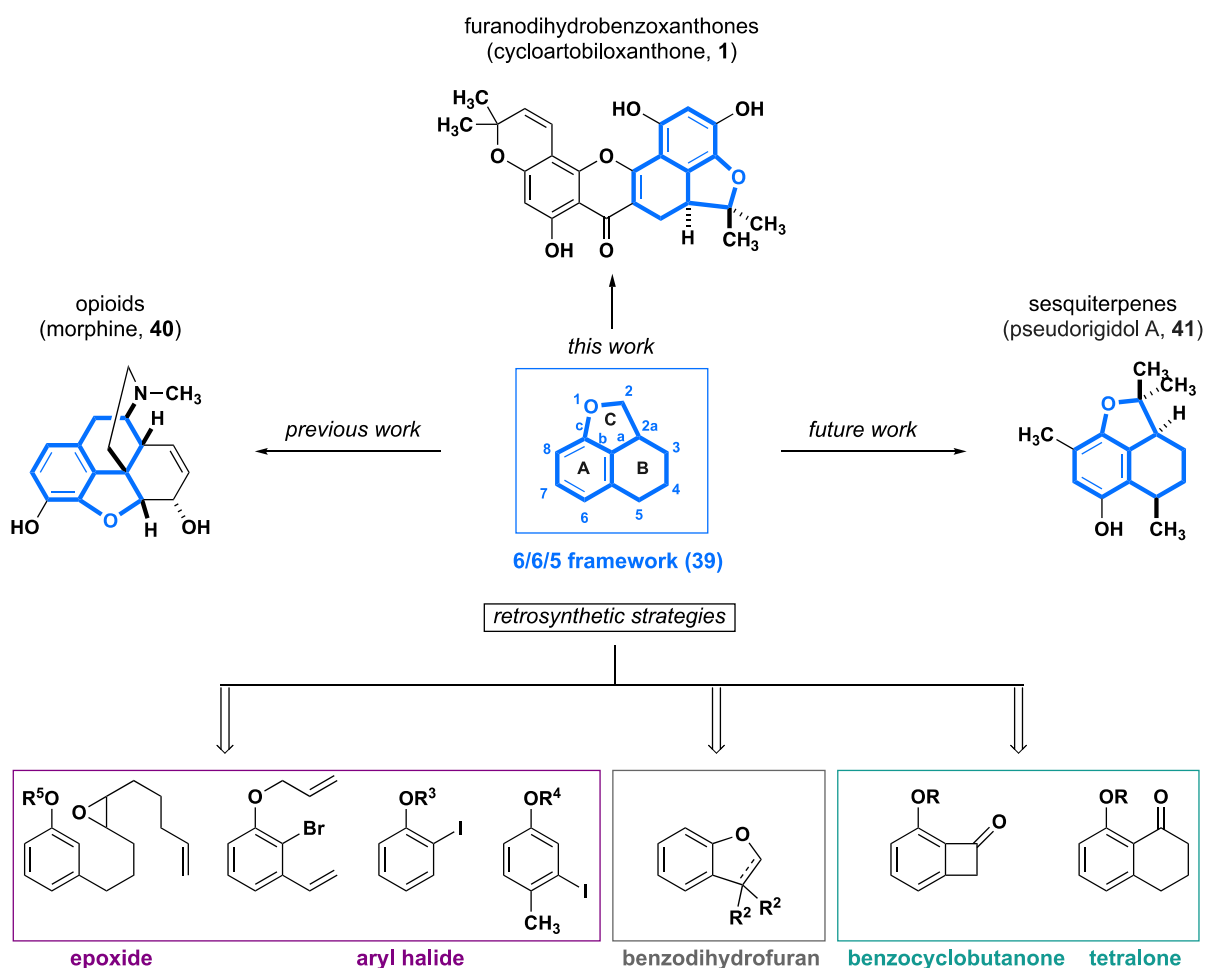


Figure 2.6 Natural product families with 6/6/5 framework and three main retrosynthetic strategies to access it.

In comparison, the subsequent work described in this chapter showcases the development of stereoselective methods to access different substituents at the 2-position of the dihydrobenzofuran. The 2-position is widely substituted in the dihydrobenzoxanthenes natural product family (**1**) and the sesquiterpene (**41**) family. The current work discussed in this chapter will focus on applying these stereoselective methods to the dihydrobenzoxanthone family. Future work in the Shaw group will enable stereoselective access to substitution at both the 2-position of the dihydrobenzofuran and the 5-position of the tetralone to make more recently discovered sesquiterpene (**41**) natural products.^{6,57}

Previously developed synthetic strategies to access the fused 6/6/5 scaffold (A, B, & C rings) (**39**) can be broken down into three categories. The first category is cascade reactions that start from substituted phenyl rings (A ring) and rapidly assemble the B and C rings in a single step. The second strategy makes the benzodihydrofuran core first (A & C rings) then the B ring is assembled through intramolecular Lewis acid-catalyzed annulation reactions. The third strategy synthesizes the tetralone core first (A & B rings), followed by C–H and C–C functionalization methods to assemble the C ring.

2.1.4.1 Cascade reactions

In 1991, Taylor and co-workers attempted to develop an intramolecular oxidative coupling of diarylbutane substrates (**42**) to make oxoeupodienone-1 (Figure 2.7).⁵⁸ Surprisingly, the oxidative coupling did not produce the desired oxoeupodienone product. Rather stirring the diarylbutane (**42**) in a biphasic chloroform and aqueous sodium bicarbonate solution with potassium ferricyanide afforded the oxaspirodienone (**46**). The iron oxidant formed the diradical intermediate (**43**) that undergoes an intramolecular hydrogen transfer to yield the quinone methide (**44**). Radical cyclization between the two unsaturated systems affords the tetralin intermediate (**45**). Then oxidative coupling forms the benzodihydrofuran C–O bond resulting in the final fused 6/6/5 ring system (**46**).

Taylor, 1991

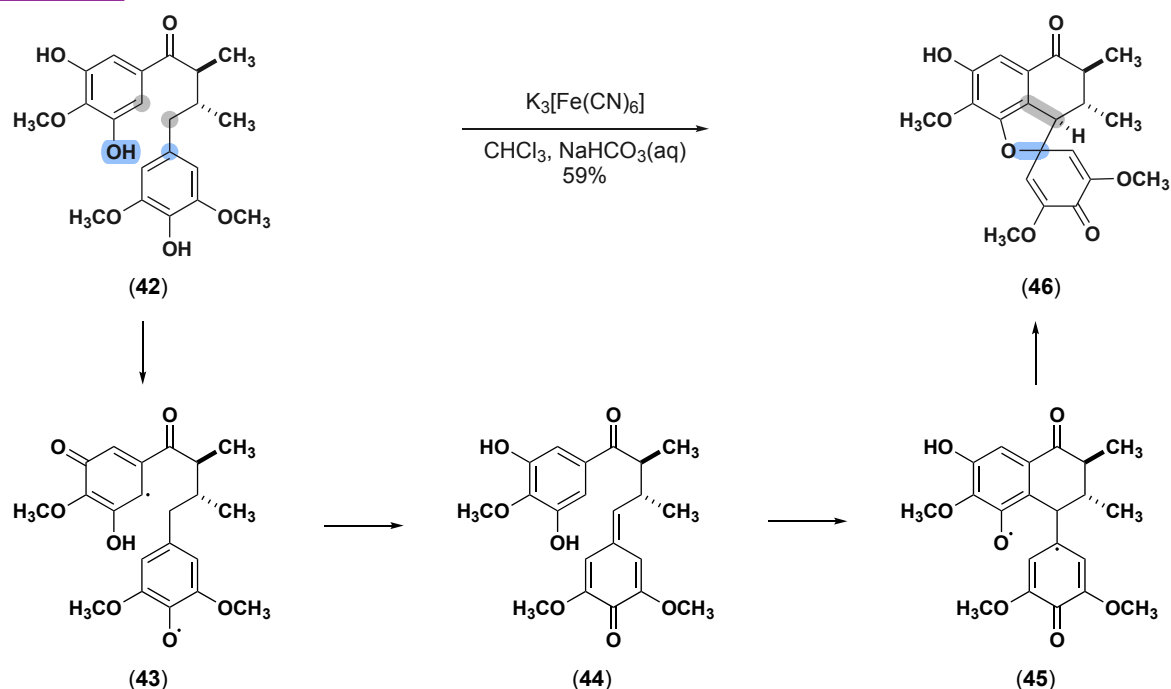


Figure 2.7 Intramolecular oxidative coupling of diphenolic substrates.

Subsequently, Stansby and co-workers were investigating the regioselectivity of Lewis acid-mediated intramolecular epoxide cyclizations (Figure 2.8).⁵⁹ The study aimed to determine if donating substituents affected the regiochemical preference between aromatic rings and alkenes. They found that when the epoxide cyclization can occur on either an aromatic ring or alkene double bond in the starting material (47), the exo cyclization will predominate (48). When a methoxy substituent was used the fused tetrahydronaphofuran core (50) resulted as a byproduct in 12% yield.

Stansby, 1996

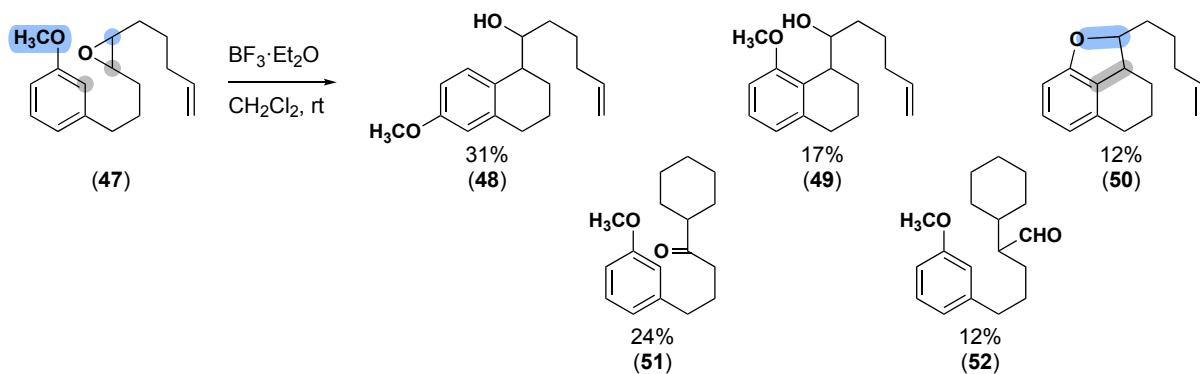


Figure 2.8 Regioselective intramolecular epoxide cyclizations.

The first time the tetrahydronaphthofuran core was intentionally targeted using a cascade reaction was by the Lautens group in a short communication in 2007⁶⁰, followed by a full paper in 2009⁶¹ (Figure 2.9). The Catellani reaction inspired a palladium-catalyzed tandem intramolecular aryl alkylation/Heck reaction sequence.⁶² The palladium-norbornene system enabled the formation of the fused tricyclic ring system (**54**) in a single step.

Lautens, 2007 & 2009

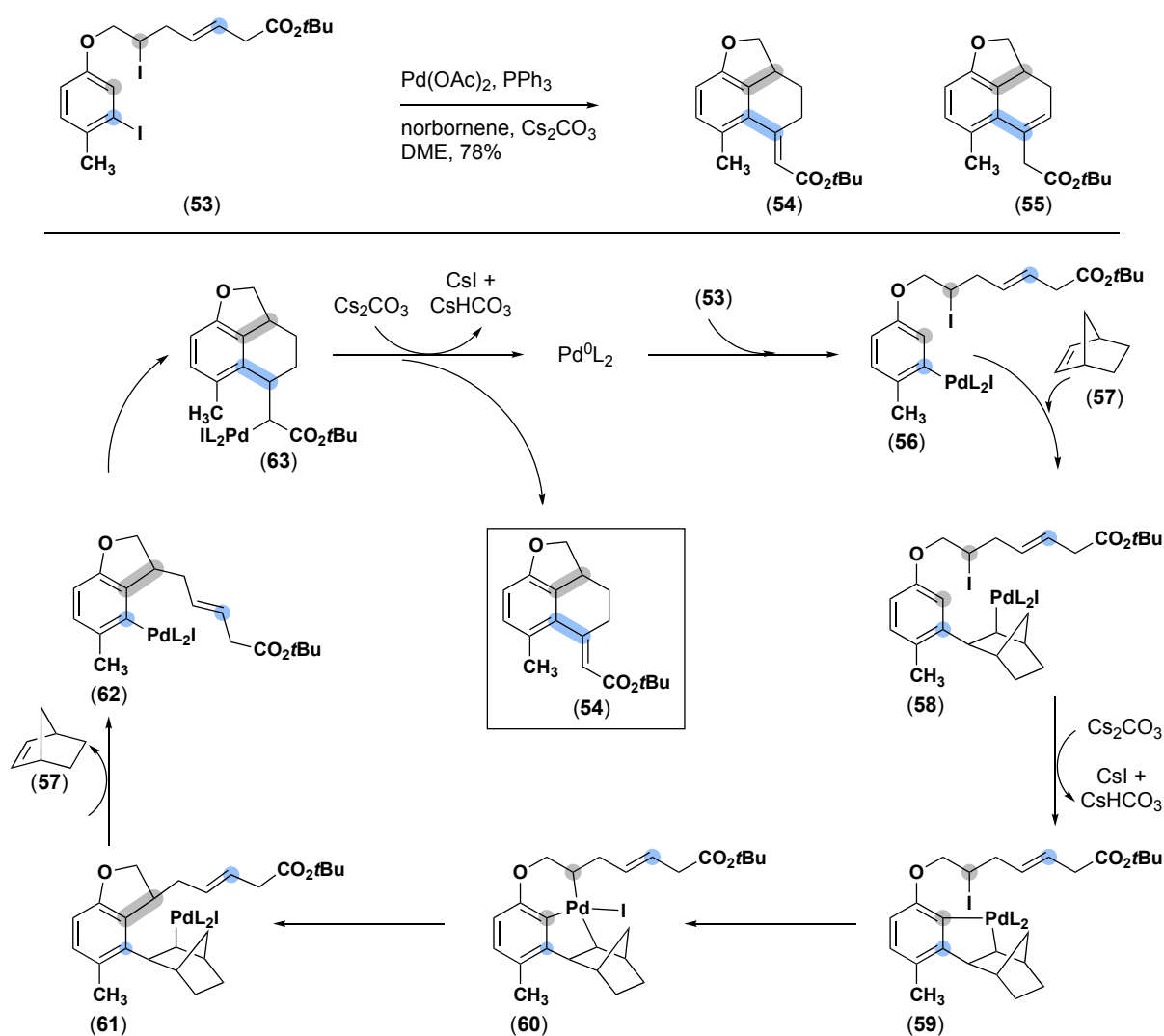


Figure 2.9 Palladium-catalyzed norbornene-mediated domino process to make polycyclic heterocycles.

The reaction starts with mixing the palladium(II) acetate and triphenylphosphine precatalyst system to form an active Pd^0 catalyst. Then oxidative addition of the active catalyst to the aryl C–I bond affords the aryl-palladium iodide intermediate **56**. The complex undergoes

carbopalladation with norbornene to form the *cis*-, *exo*-complex **58**. Next, C_{sp2}-H activation of the ortho C-H bond forms the palladacycle **59**. This C-H activation step is preferred since there are no *syn*-β-hydrogens available that can undergo the often highly favored β-hydride elimination step. Then oxidative addition of palladacycle **59** to the alkyl iodide affords the Pd^{IV} intermediate **60**. Reductive elimination occurs rapidly to form the first C-C bond and the benzodihydrofuran core **61** (A and C rings). Norbornene is then extruded from the complex to yield intermediate **62**. The Pd^{II} intermediate **62** is then primed to undergo a Heck reaction to form the second C-C bond, which affords the final C ring of the fused tricyclic complex (**63**). The Lautens group showed that the reaction had a wide scope too, tolerating large variations of substituents on the aryl ring and the alkene in the starting material.

The Lautens groups' methodology allowed for substitution on the A and B rings of the tricycle core, but never on the C ring. In 2017, the Shi group developed a radical cascade cyclization that enabled C ring substitution using substituted aryl ether groups (Figure 2.10).⁶³

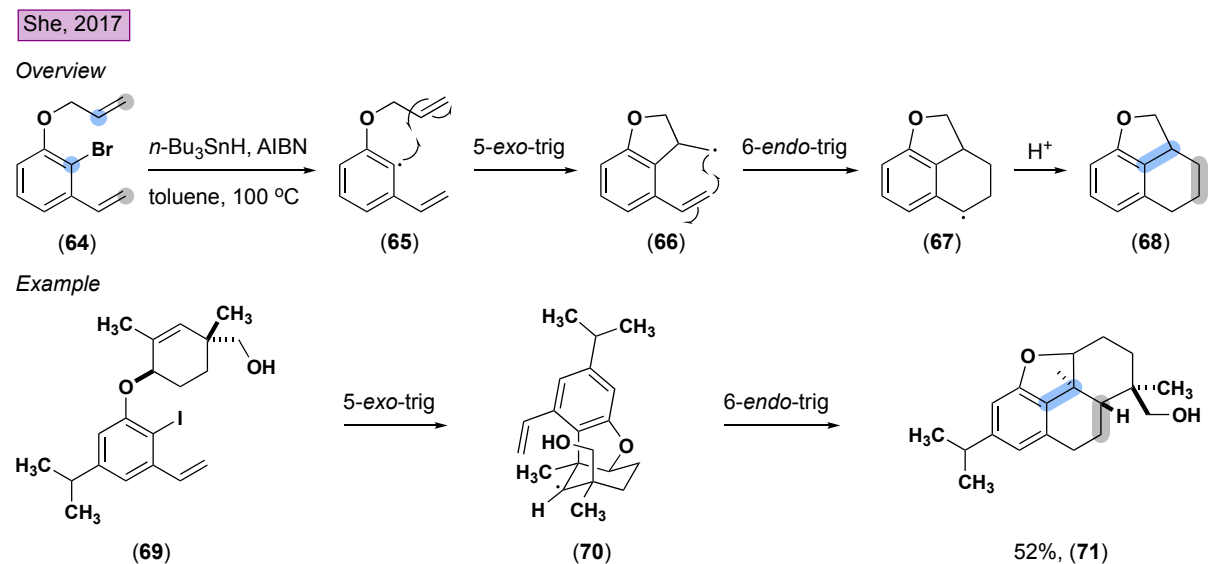


Figure 2.10 Tandem radical annulation to assemble the 6/6/5 fused tricyclic scaffold and application to the synthesis of 5-*epi*-7-deoxy-isoabietenin A (**71**).

The reaction cascade is initiated on a tri-substituted aryl halide starting material (**64**) using tributyltin and AIBN to form aryl radical (**65**). The radical intermediate (**65**) undergoes a 5-

exo-trig cyclization with the allylic ether to form the benzodihydrofuran intermediate (**66**). Radical intermediate **66** then reacts with the styrene through a 6-*endo*-trig ring closure followed by reductive trapping to yield the tricyclic core (**68**). A wide variation of allylic ether substitution patterns was tolerated in the reaction, which is showcased by the reaction of **69** to form 5-*epi*-7-deoxy-isoabietenin A (**71**) in 52% yield.

C–H activation methods developed by the He⁵³ and Lin⁵⁴ groups in 2017 and 2019 combined elements of the previously described methods to make ergoline-like scaffolds (Figure 2.11). The methods from both groups utilized palladium catalysts to first build the benzodihydrofuran bicycle (A and C rings) from an allylic ether. Then the final C–C bonds were made to form the B ring of the tricyclic core in the same pot. The He group's cascade process starts with the oxidative addition of aryl halide (**72**) to Pd⁰ (Figure 2.11A). The aryl palladium intermediate then goes through an intramolecular 5-*exo*-trig cyclization with the allylic ether to form the benzodihydrofuran ring. Aryne generated *in situ* from **73** undergoes carbopalladation to form the second C–C bond of the B ring. This is followed by another C–H functionalized by base-induced palladation and reductive elimination to make the reaction's third C–C bond affording product (**74**).

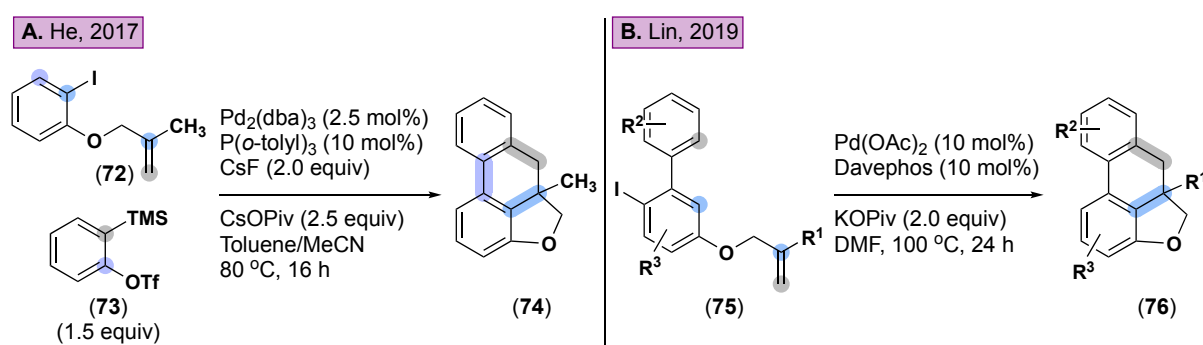


Figure 2.11 Cascade reactions to form LSD analog scaffolds.

In comparison, the Lin group starts with the Csp²–Csp² bond already formed in the starting material (**75**) (Figure 2.11B). The starting material (**75**) undergoes a sequential 1,4-palladium migration to remotely activate the C–H bond ortho to the ether. Alkene insertion of the aryl

palladium intermediate with the allylic ether forms the benzodihydrofuran core. Then C–H activation of the second aryl ring, followed by reductive elimination, makes the second C–C bond yielding the final product (**76**).

2.1.4.2. Benzodihydrofuran bicyclic to fused tricyclic core

Although, cascade reactions provide a rapid way to build the tricyclic core they cannot obtain the core stereoselectively. One solution to this problem is breaking up tricyclic ring formation into two steps. First, the benzodihydrofuran is formed (A & C rings) then the B ring can be formed mainly using Lewis acid-catalyzed annulation reactions.

One of the first examples of this strategy was Uyeo and co-workers' total synthesis of (\pm)-lycoramine in 1968 (Figure 2.12A).⁶⁴ The fused benzodihydrofuran with the carboxylic acid chain (**77**) was synthesized over 12 steps. The carboxylic acid (**77**) was heated with tin chloride and phosphorous pentachloride in benzene to afford the 6/6/5 framework in near quantitative yield. Similarly, the Abe group in 1976 used a mono-substituted benzodihydrofuran (**79**) with polyphosphoric acid (PPA) to undergo the Lewis acid-catalyzed annulation yielding the fused tricyclic core (**80**) in moderate yield (Figure 2.12B).⁶⁵ At the time of publication, PPA was a well-known reagent for catalyzing annulation reactions⁶⁶, and it became a commonly used strategy for intramolecular tetralone formation.⁶⁷ PPA was even used again a decade later by Klöppner and co-workers to make the enantiopure tricyclic core (**86**) from an enantiopure benzodihydrofuran intermediate (**84**) (Figure 2.12D).⁶⁸

David Nichols became interested in the tetrahydronaphofuran 6/6/5 framework as hybrid molecules for the two major hallucinogenic drug classes, phenethylamines and ergolines. His group's first synthetic strategy⁵⁵ was to make a benzofuranone from intramolecular cyclization with diazomethyl ketone. The benzofuranone underwent a Wittig reaction, reduction, hydrolysis, and diazo transfer to yield the desired benzodihydrofuran diazomethyl ketone intermediate (**81**).

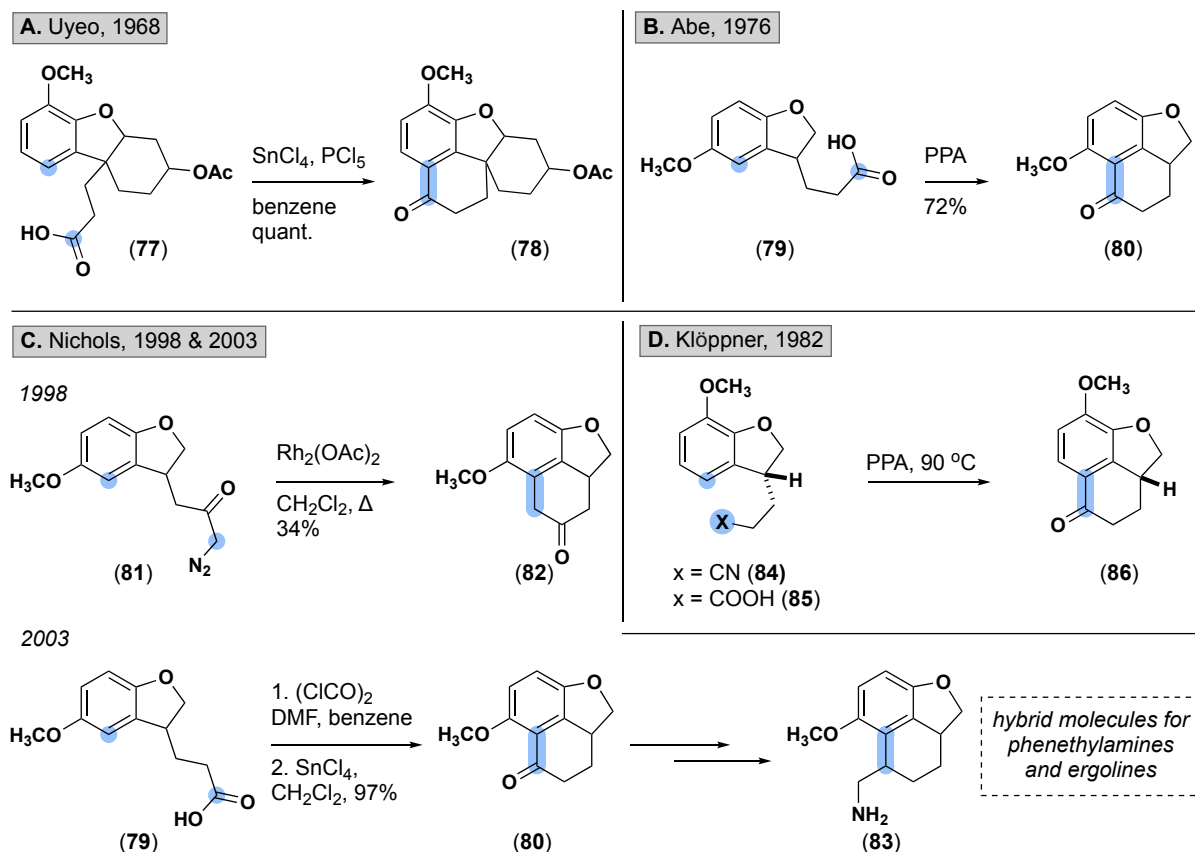


Figure 2.12 A. 6/6/5 framework assembly in Uyeo's total synthesis of (\pm)-lycoramine B. Cyclization of 3-(benzofuran-3-yl)-propionic acid derivatives C. Nichols' synthesis of hydride phenethylamine and ergoline analogs D. Synthesize of enantiopure fused tricyclic core.

The diazomethyl ketone (**81**) was mixed with dirhodium acetate ($\text{Rh}_2(\text{OAc})_4$) and underwent the sp^2 C–H insertion originally developed by McKervery (Figure 2.12C).⁶⁹ Although the C–H insertion reaction was low yielding, it afforded the desired tricyclic core (**82**) with the ketone in the homobenzylic position. A couple of years later, the Nichols group wanted to make the analogous tricyclic core with the ketone in the benzylic position (**80**).⁵⁶ This time the benzodihydrofuran intermediate (**79**) contained a carboxylic acid chain. The carboxylic acid was transformed into acyl chloride and subjected to tin chloride, similar to Uyeo's original conditions,⁶⁴ to yield the fused tricyclic core in 97% yield (Figure 2.12C).

The Lewis acid-catalyzed annulation reactions (Figure 2.12) described above were effective ways to make the 6/6/5 framework from a benzodihydrofuran intermediate. However, the strategies only provided enantiopure product if the benzodihydrofuran intermediate was enantiopure through a chiral chromatography or crystallization step.

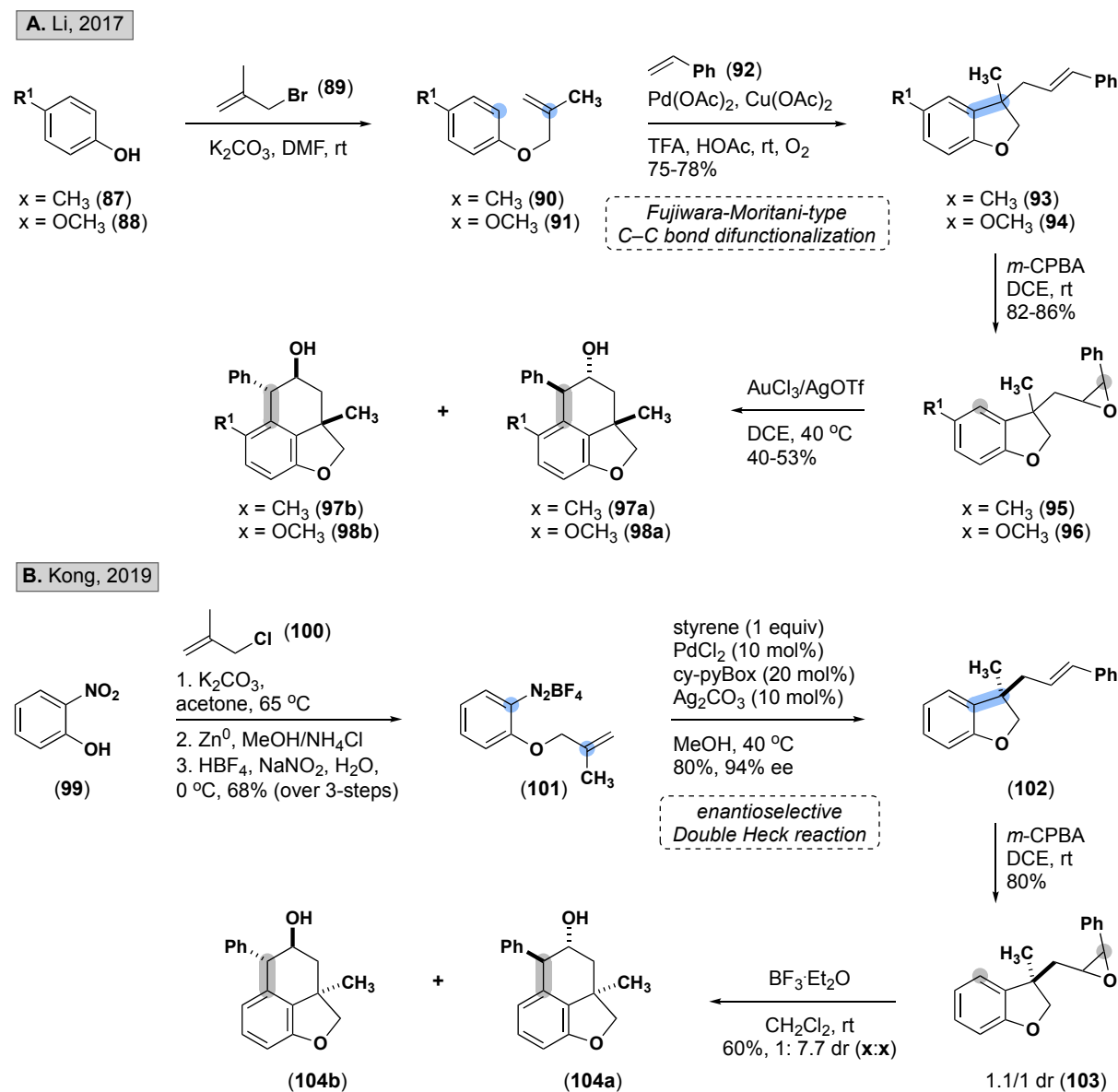


Figure 2.13 A. Li group tricyclic synthetic strategy using a Fujiwara-Moritani-type C–C bond difunctionalization with styrene to afford the 3,3-disubstituted benzodihydrofuran **B.** Kong group’s enantioselective synthetic strategy using a double Heck reaction.

The Kong group sought to solve this problem by first making the enantiopure 3,3-disubstituted benzodihydrofuran (**102**) and then sending it through an intramolecular Lewis

acid-catalyzed cyclization (Figure 2.13B).⁵² The precedent for this effective strategy came from the Li group in 2017 (Figure 2.13A).⁵¹ The Li group started with commercially available phenols (**87-88**). These phenols were alkylated to yield allylic ether intermediates (**90-91**). The ethers (**90-91**) then undergo a Fujiwara-Moritani-type C–C bond difunctionalization with styrene (**92**) to afford the 3,3-disubstituted benzodihydrofurans (**93-94**). Next, an epoxidation reaction with *m*-CPBA makes the epoxide intermediates (**95-96**). The epoxides undergo an intramolecular Au³⁺ catalyzed cyclialkylation reaction developed by the He group for electron-rich arenes.⁷⁰ Cyclization yields two diastereomers (**97a/b-98a/b**) of the fused tricyclic core.

Two years later, the Kong group improved upon this strategy by developing an enantioselective double Heck reaction between an arenediazonium salt (**101**) and alkene to afford the enantiopure 3,3-disubstituted benzodihydrofuran (**102**) (Figure 2.13B). The benzodihydrofuran (**102**) was epoxidized (**103**), and then underwent a highly diastereoselective cyclialkylation reaction catalyzed by BF₃-etherate. Using this synthetic strategy, the 6/6/5 framework could be obtained diastereo- and enantioselectively with substitution at the 2a, 4, and 5 positions (**104a/b**). This substitution pattern was very useful in making progress toward the synthesis of the natural product parviflorene J.

2.1.4.3. Benzylic ketone bicycle to fused tricyclic core

The final synthetic strategy to access the 6/6/5 framework builds the tetralone core (A & B rings) first, followed by the C ring. A couple of groups have made the final C ring through C–H functionalization of activated ether C–H bonds using free carbenes or radical cyclizations (Figure 2.14). Pang and co-workers did this first in 1984 when they made the tetralone core and condensed tosyl hydrazine onto the ketone to get their desired tosyl hydrazone precursor (**105**) (Figure 2.14A).⁷¹ The hydrazone (**105**) was then heated in a sealed reaction vessel to undergo gas phase pyrolysis to form the free carbene. The aryl/alkyl carbene immediately

underwent C–H insertion to afford the desired tricyclic core as a mixture of diastereomers (**107a**, 23%; **107b**, 16%) as well as the Bamford-Stevens alkene byproduct (**106**, 63%). Similarly, the Horaguchi and Sharshira groups independently developed photocyclization reactions from the tetralone core with an ester-substituted ether⁷² (**108**) and a nitrile-substituted ether⁷³ (**111**), respectively (Figure 2.14B-C). Irradiation of ester (**108**) created a 1,5-biradical intermediate that immediately undergoes intramolecular cyclization to afford the tetrahydronaphtho[1,8*bc*]furanols (**109a/b**) in moderate yield (Figure 2.14B). Similarly, the irradiation of nitrile (**111**) in methanol produces a stabilized 1,5-biradical intermediate that undergoes intramolecular cyclization to afford a mixture of furanols (**111**) and their elimination byproduct (**112**) (Figure 2.14C).

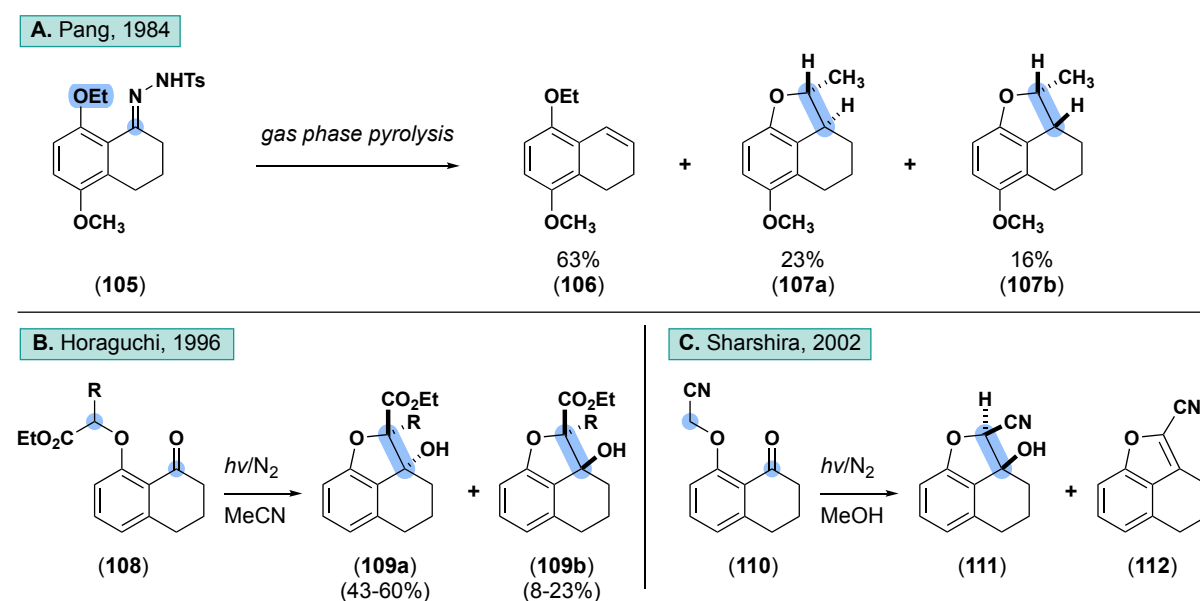


Figure 2.14 A. C–H insertion with free carbene to form tricyclic core B. Photocyclization with ester stabilized biradical intermediate to make tetrahydronaphtho[1,8*bc*]furanols C. Photocyclization with nitrile stabilized biradical intermediate to make tetrahydronaphtho[1,8*bc*]furanols.

In 1994, Dufresne and co-workers devised a novel way to make the fused A-B ring bicycle (Figure 2.15A).⁷⁴ 4-(3-hydroxyphenyl)butanal (**113**) is mixed with phenyl boronic acid

(PhB(OH)₂) to form a benzodioxaborin intermediate (**114**). Intermediate **114** is treated with BF₃ etherate forming the bicyclic orthoquinone methide. The quinone methide then reacts with allyl trimethylsilane (**115**), affording the bicyclic phenol (**116**) in 70% yield. Intramolecular cyclization of the phenol on the olefin using TFA makes the C–O bond and the final fused ring system (**117**) in a moderate 67% yield. In contrast to the acid-cyclization conditions, the Suzuki group developed base cyclization conditions to form the fused ring system (Figure 2.15B).⁷⁵ Starting from tetralone (**118**), the phenol is alkylated by ethyl bromoacetate with potassium carbonate at 120 °C. Then potassium hydroxide is added to form the enolate, which undergoes a Claisen condensation to yield the unsaturated naphthol[1,8*bc*]furan core (**119**) in 41-71% yield, depending on the electronics of the aryl ring. A simple hydrogen and palladium on carbon reduction of **119** yields the desired saturated fused tricyclic ring system (**120**) quantitatively.

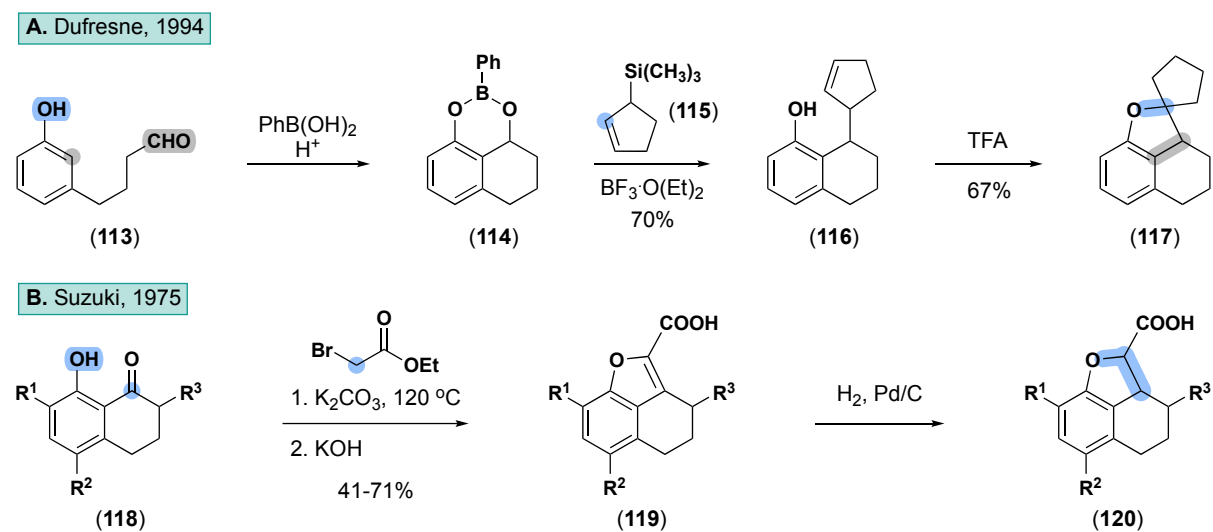


Figure 2.15 A. Tricycle framework via novel benzodioxaborin intermediate B. Synthesis of naphthol[1,8*bc*]furans *en route* to tetrahydronaphthol[1,8*bc*]furans.

Finally, the Dong group in 2012 published an enantioselective “cut-and-sew” method to access the fused 6/6/5 framework from a benzocyclobutanone (**121**) (Figure 2.16).^{76,77} This unique method uses a Rh(I)/Rh(III) system to oxidatively add to a relatively inert C–C bond. The proposed catalytic cycle begins with catalyst activation between [Rh(cod)Cl₂] and (*R*)-

DTBM-Segphos to form the active $[\text{Rh}^{\text{I}}]$ catalyst. Oxidative addition of the rhodium catalyst into the $\text{C}_1\text{--C}_2$ bond of **121** affords the 5-membered rhodacycle (**124**). The olefin on the starting material serves as a strong direction group for the rhodium catalyst to add into the $\text{C}_1\text{--C}_2$ over the distal $\text{C}_1\text{--C}_8$ bond. Then syn migratory insertion leads to a seven-membered rhodacycle (**125**) and is the enantio-determining step of the mechanism. Reductive elimination of the $[\text{Rh}^{\text{III}}]$ complex (**125**) affords the final fused tricyclic product (**122**) in 98% ee and 77% yield.

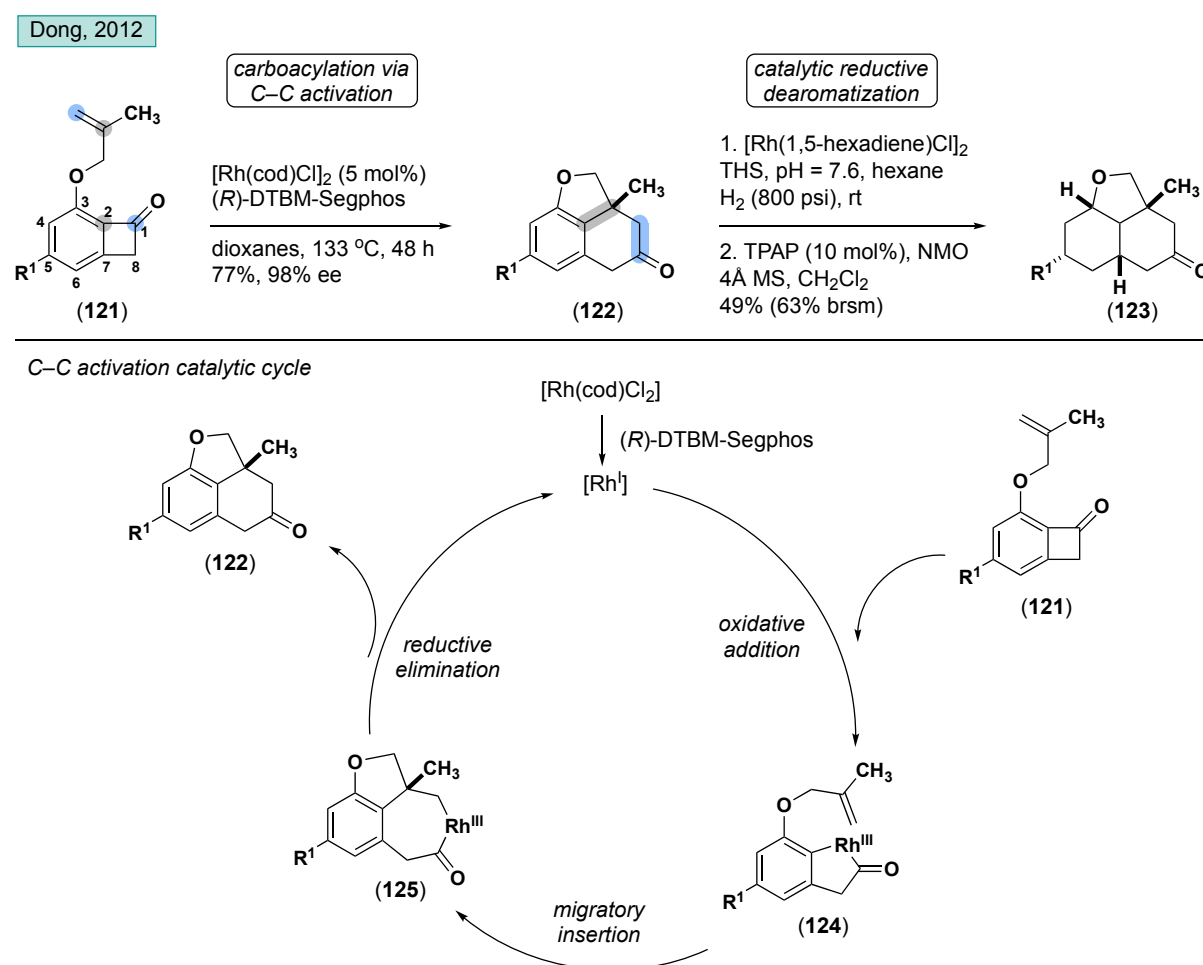


Figure 2.15 Cut-and-sew method for carboacylation of benzocyclobutanones via C–C activation and proposed catalytic cycle.

In addition to making the tetrahydronaphtho[1,8*bc*]furan (**122**), the Dong group went one step further to make the fully saturated fused ring system (**123**). They developed a catalytic reductive dearomatization reaction that used rhodium under phase transfer and neutral conditions at high pressure. During this hydrogenation reaction, the ketone was partially

reduced to the alcohol. Therefore, a subsequent Ley oxidation was performed on the hydrogenation reaction mixture to afford only the ketone-containing saturated fused ring system (**123**). Notably, the hydrogenation proceeded stereoselectively on the convex face of the tricycle, determined by the quaternary stereocenter, to afford a single diastereomer of the product (**123**).

2.2 Results and discussion: first-generation route

2.2.1 Retrosynthesis

To assemble the dihydrobenzoxanthenes, we envisioned a convergent synthesis that would split the molecule into two halves: a left hemisphere and a right hemisphere (Figure 2.17).

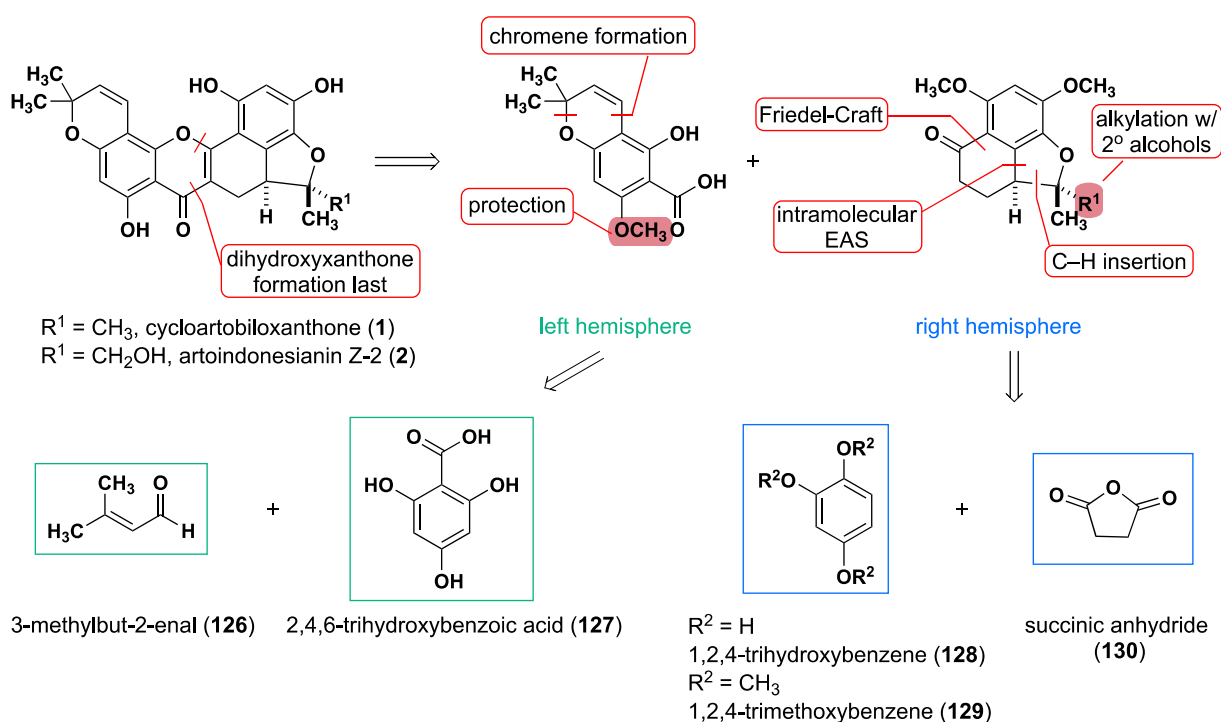


Figure 2.17 First-generation route retrosynthesis.

Splitting into these two hemispheres was ideal since it enabled a modular synthesis where multiple natural product family members could be made with only slight variations in the main route. The left hemisphere could be made from 2,4,6-trihydroxybenzoic acid (**127**), where

swapping protecting group steps around would allow us to access both *2H*-chromene isomers of the left half. The right hemisphere could be synthesized from 1,2,4-trihydroxybenzene (**128**) or 1,2,4-trimethoxybenzene (**129**), where alkylation of a phenol on the tetralone core would allow for rapid variation of the R groups on the fused tricyclic core. A C–H insertion using a donor/donor carbene would serve as the key stereoselective step enabling the synthesis of both the natural and unnatural stereoisomers of the natural products.

2.2.2 Right hemisphere: forward synthesis to insertion core

2.2.2.1 Isopropyl protecting groups strategy

Initially, 1,2,4-trihydroxybenzene (**128**) was selected as the starting material that could be protected and then undergo a Friedel-Crafts acylation, ketone reduction, and Friedel-Crafts cyclization to make the desired tetralone scaffold (Figure 2.18).^{78,79} Isopropyl groups were initially chosen as the ideal phenol-protecting groups due to the mild conditions that could be used to install and remove them. In addition, the isopropyl group provides the correct C–H insertion center we need later in the synthesis. However, difficulty tri-protecting **128** led to 3,4-dihydroxybenzaldehyde (**131**) being selected as the starting material. Following a procedure already optimized by Christine Dimirjian (see CAD dissertation Scheme 3.3), 3,4-dihydroxybenzaldehyde (**131**) was isopropylated, giving **132** in nearly quantitative yield. A Dakin oxidation⁸⁰ was performed on the aldehyde (**132**) to take it to the phenol (**133**) in good yield. The phenol was then isopropylated with the same conditions as step 1 to give **134**. Intermediate **134** then underwent a Friedel-Crafts acylation to afford the carboxylic acid **135**. The carboxylic acid (**135**) was worked up and carried directly into a mild ketone reduction with triethylsilane and trifluoroacetic acid (TFA) to yield **136** in 59% over two steps.

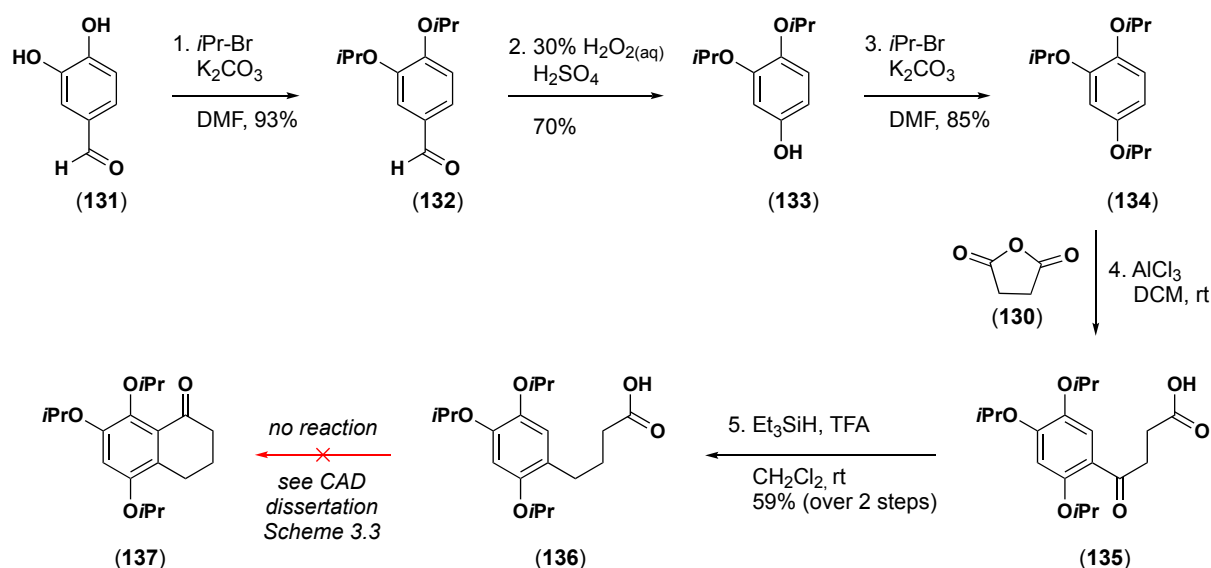


Figure 2.18 Failed isopropyl-protecting group route.

At the time, I was working on this route to bring up material for Christine Dimirjian to attempt intramolecular Friedel-Crafts conditions to form the tetralone core (**137**). However, Christine could not get the Friedel-Crafts to go after trying multiple different conditions (see CAD dissertation page 144). It was hypothesized that the reaction could not occur due to the large steric bulk from the ortho isopropyl group.^{81–83} Therefore, we decided to re-route using methyl-protecting groups for the phenols. Luckily, 1,2,4-trimethoxybenzene (**129**) was commercially available, which would end up saving two overall linear steps in the right hemisphere synthesis.

2.2.2.2. Methoxy protecting groups strategy

To start the minor re-route, 1,2,4-trimethoxybenzene (**129**) can undergo a Friedel-Crafts cyclization with either succinic anhydride (**130**) or an acyl chloride (**140**) to afford **138** and **139**, respectively (Figure 2.19). Originally, the Friedel-Crafts reaction with succinic anhydride to make **138** was variable yielding after isolation via column chromatography, with 30–39% yield. Therefore, the ester route was developed since intermediate **139** could be readily isolated on a large scale after column in 89% yield. The benzylic ketone on ester **139** is then reduced

selectively using the mild reducing agent triethylsilane with trifluoroacetic acid yielding the ester **142**. Reducing this ketone to the alkane is necessary to avoid a regiochemistry issue later in the synthesis during hydrazone formation. (Figure 2.19). The ester **142** could then be hydrolyzed efficiently in 30 minutes to the carboxylic acid **141** using 1M NaOH in methanol.

Before proceeding with the synthesis, we revisited the succinic anhydride Friedel-Crafts reaction. If the yield of this reaction could be optimized, then it would save us a linear step from the ester hydrolysis and another two steps required to make the acyl chloride **140** from succinic anhydride (**130**). The ¹H NMR spectrum of the succinic anhydride Friedel-Crafts reaction after an acid-base workup showed very clean product, and the crude had almost full mass recovery. Therefore, a 2D TLC experiment and a control experiment of stirring **138** with silica for 20 minutes demonstrated that intermediate **138** was degrading on the column. Switching the purification technique to a short alumina plug to get rid of excess AlCl₃ afforded **138** in nearly quantitative yield. Reduction of **138** with triethylsilane and trifluoroacetic acid proceeded smoothly to make the carboxylic acid **141** in high yield. Therefore, the succinic anhydride Friedel-Crafts and mild ketone reduction became the most efficient way to access intermediate **141**, and we could move forward in our synthesis of the right hemisphere.

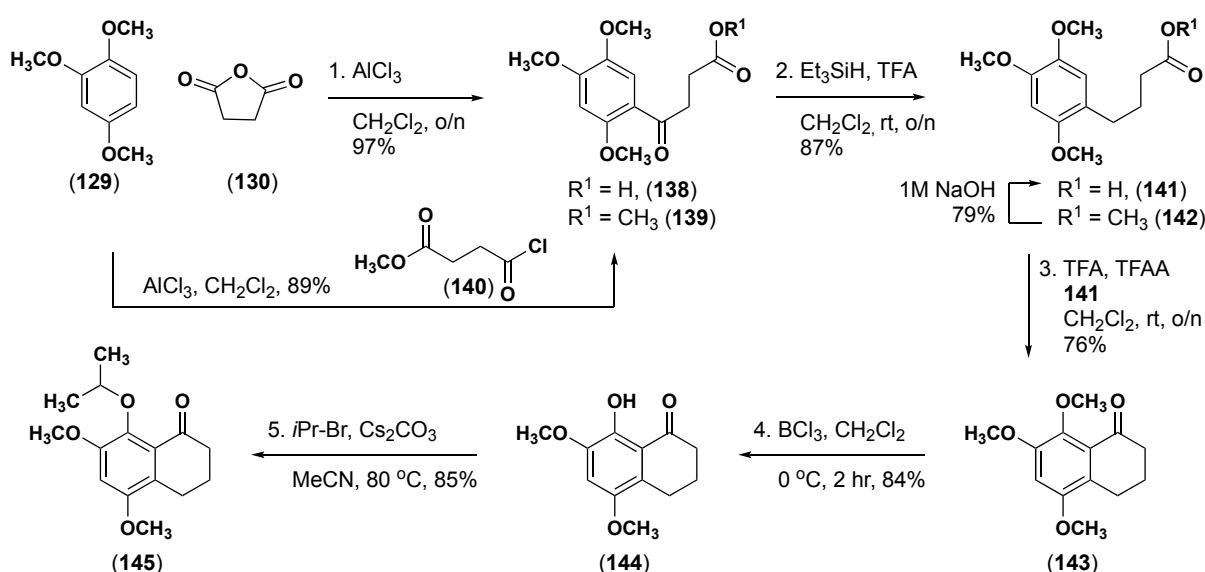


Figure 2.19 Trimethoxybenzene route to the desired tetralone core (**146**).

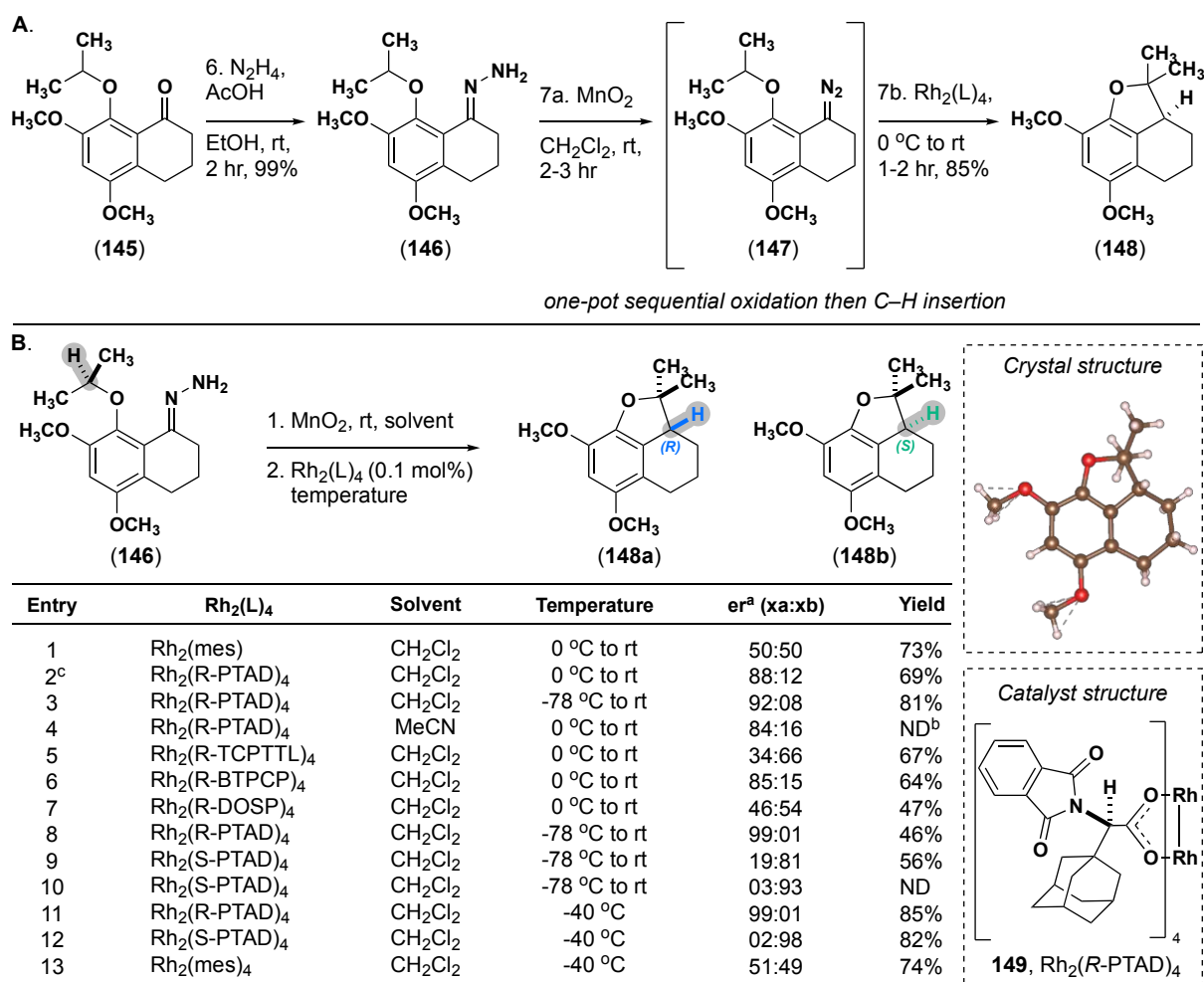
Intramolecular electrophilic aromatic substitution (EAS) on the carboxylic acid **141** formed tetralone **143** in 76% yield. Trifluoroacetic acid (TFA) and trifluoroacetic anhydride (TFAA) were found to promote the EAS reaction best.⁸⁴⁻⁸⁶ Notably, the TFA/TFAA conditions were easy to set up, required no heating, and were reproducible on a 20 g scale. While other commonly used cyclization conditions, such as polyphosphoric acid (PPA), require refluxing conditions and are more difficult to handle reagents.⁸⁷ Further discussion on the EAS conditions screened for the tetralone formation can be found in CAD's dissertation.

Excitingly, when we began conducting large scale-ups to access the tetralone intermediate (**143**), we discovered we did not need to run any column chromatography across the first three steps of the synthesis. It was discovered that the Friedel-Crafts reaction mixture of **138** after workup could be telescoped straight into the mild ketone reduction. The reduction reaction mixture of **141** could also be telescoped into the tetralone formation step. It is important to note that to be able to telescope the crude mixture after reduction to the cyclization step, care must be taken to make sure all the triethylsilane has been removed, or else it significantly drops the yield of the cyclization step from 76% to 14-25% yield.

After the tetralone **143** was acquired, the ortho methoxy needed to be removed and replaced with an isopropyl group that would serve as the needed tertiary ether C-H insertion center. This was done using boron trichloride to selectively chelate to the ketone on **143** and remove the methyl group ortho to the ketone to yield phenol (**144**). The phenol (**144**) was then alkylated using isopropyl bromide and cesium carbonate in acetonitrile at reflux to afford the desired tetralone (**145**).

From tetralone (**145**), hydrazine condenses onto the ketone to form hydrazone (**146**) (Figure 2.20A). Hydrazone (**146**) is the carbene precursor for the C-H insertion step. Using our group's previously reported C-H insertion method,⁴ one-pot sequential oxidation and C-H insertion was performed. The extremely mild oxidant MnO₂ oxidizes the hydrazone up to diazo at room

temperature. Once all the hydrazone (**146**) has converted to diazo (**147**), the reaction can be cooled down to any desired temperature, and a dirhodium catalyst can be added. The addition of catalyst will extrude nitrogen to form the metal carbene, which rapidly undergoes intramolecular C–H insertion with the tertiary ether C–H bond to form the fused tetrahydronaphtho(1,8)furan ring system (**148**). This C–H insertion proceeded smoothly in 85% yield without any observed β -hydride elimination, azine, imine, or ketone byproducts.



^aer determined by chiral HPLC

^bND = yield not determined

^cabsolute stereochemistry of major enantiomer determined by X-ray crystallography

Figure 2.20 Methoxy route **A**. Tetralone to insertion core **B**. Enantioselectivity screening for the C–H insertion step.

Notably, something about the fused tetrahydronaphthone core enables this intramolecular C–H insertion to occur over 1,2-hydride shift to form alkene byproduct. The analogous aryl/alkyl carbene C–H insertion on an acyclic system exclusively forms the alkene byproduct from a 1,2-hydride shift.

Initially, the C–H insertion reaction yielded **148** in 88:12 er with Rh₂(*R*-PTAD)₄ (Figure 2.20B entry 2). Changing the solvent to acetonitrile or changing the catalyst did not increase er (Figure 2.20B entries 4-7). Dropping the temperature to –78 °C and allowing it to warm to room temperature slightly increased the enantioselectivity to 92:08 er (Figure 2.20B entry 3). Repeating these temperature conditions but slowing the rate of the reaction warming to room temperature gave a single enantiomer of the product with Rh₂(*R*-PTAD)₄ (Figure 2.20 B entry 8). However, shortly after this er was obtained, X-ray crystallography discovered that Rh₂(*R*-PTAD)₄ favored the unnatural enantiomer of the natural product (**148a**). When the reaction was repeated with Rh₂(*S*-PTAD)₄, the natural enantiomer (**148b**) was favored. Variability in reaction warming time due to the changes in the room temperature throughout the day and the amount of dry ice used each time gave different er results. For example, the first time the C–H insertion was tried with Rh₂(*S*-PTAD)₄, the er was 81:19, while the second attempt gave an er of 93:3 (Figure 2.20B entry 9-10). Therefore, it was concluded that a more exact temperature for the reaction needed to be used, where the reaction could be held at that temperature until it was fully complete. Due to qualitative color change observations, it was predicted that the C–H insertion began to go at –40 °C. When the C–H insertion was repeated at –40 °C, Rh₂(*R*-PTAD)₄ gave a single enantiomer of the unnatural product (**148a**) (Figure 2.20B entry 11), and Rh₂(*S*-PTAD)₄ yielded the natural occurring enantiomer (**148b**) in 98:02 er (Figure 2.29B entry 12).

2.2.3 Right hemisphere: benzylic oxidation attempts

Now that the fused tricyclic core (**148**) has been made, we envisioned that oxidation of the secondary benzylic position to the ketone would afford us the best functional group handle to begin assembly of the two hemispheres. What was originally believed to be a relatively facile oxidation with considerable precedent for oxidation of tetrahydronaphthalene to alpha tetralone turned out to be very difficult due to the electron-rich character of the ring system (Figure 2.21). The maximum yield obtained for the desired ketone (**150**) was 18% using DDQ as the oxidant (Table 2.2, entries 13-14). However, these conditions could never be scaled up, and the yield dropped to 7% when the scale was above 100 mg. The most common byproducts of the reaction were oxidation to quinone methides (**153a/b**). These quinone species showed up as bright blue UV active spots by TLC. If the reaction was worked up in neutral conditions and a ^1H NMR spectrum was taken immediately, not in acidic deuterated solvents (i.e., taken in CD_2Cl_2 not CDCl_3), then the quinones could be transiently observed by ^1H NMR spectroscopy.

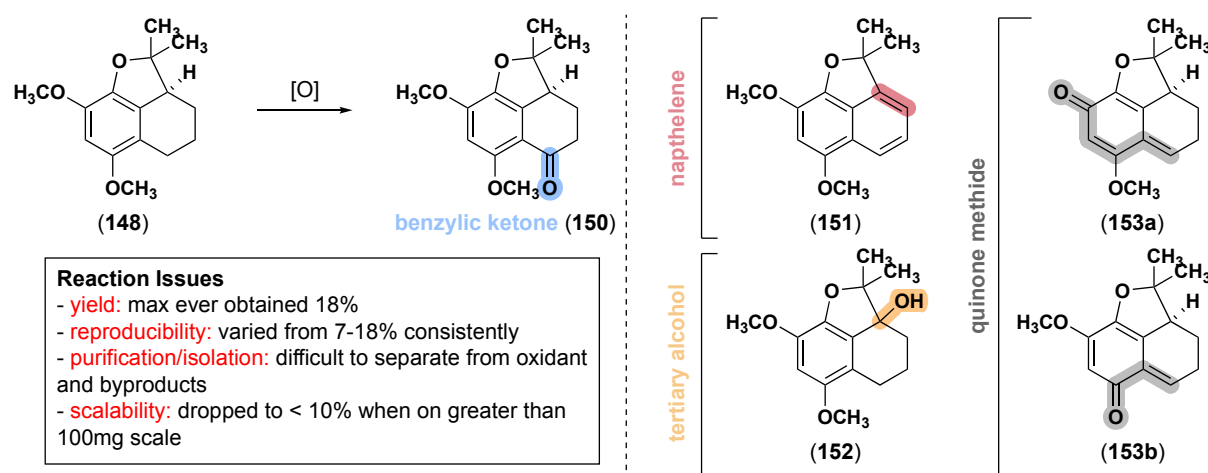


Figure 2.21 Benzylic oxidation desired product and byproducts.

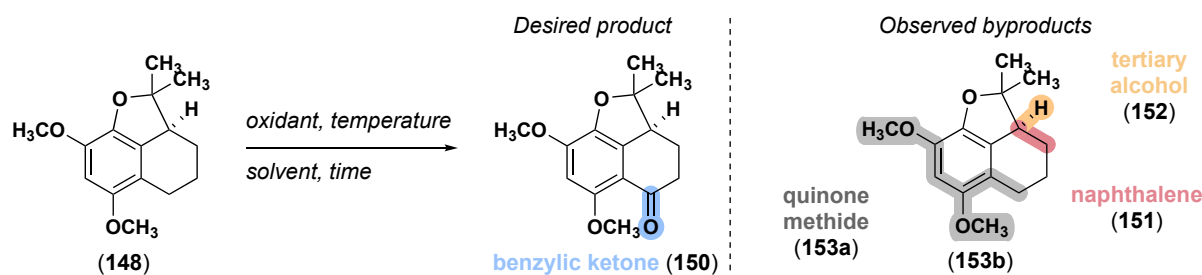
The ^1H NMR spectra for the quinone byproducts showed all the signals from the insertion core (**148**) except one of the methoxy peaks. As well as, both benzylic sp^3 C–H peaks were missing, and a new alkene peak could be observed. These quinone species (**153a/b**) would rapidly

degrade after 1-5 minutes, and they could never be isolated since they were completely unstable on silica or alumina columns. Two other common byproducts observed in the reaction were the oxidation of the tertiary benzylic position to the alcohol (**152**) or the elimination of the tertiary benzylic C–H to form the naphthalene core (**151**). Lastly, most often, oxidative conditions would lead to the degradation of the starting material (**148**), yielding a structurally indiscernible mixture by ¹H NMR spectrum or LCMS trace. The path to degradation is hypothesized to be due to oxidative cleavage or over oxidation to quinone (**153**), which then rapidly decomposes.

Initial optimization of the benzylic oxidation was conducted by Christine Dimirjian (Table 2.2). *Tert*-butyl hydroperoxide and catalytic CuI in MeCN at 60 °C were the first oxidation conditions attempted. These conditions were successful and high-yielding for oxidation on a closely related dimethoxy-substituted tetralin system to a tetralone reported by Huang and coworkers.^{88,89} However, these conditions only afforded quinone (**153**) as the major product and degraded the remainder of the starting material (Table 2.2, entry 1). Next, attempts at sequential benzylic bromination and substitution to form the benzylic alcohol *in situ*, followed by oxidation to the ketone, were unsuccessful (Table 2.2, entry 2).⁹⁰ All attempts resulted in bromination of the aryl ring at room temperature before the benzylic position could be functionalized. Traditional oxidants, such as CAN, IBX, KMnO₄, PCC, and CrO₃, did not work either. Rather these oxidants favored quinone (**153**) as the sole product or degradation of the starting material (Table 2.2, entries 3-9). A couple of literature precedents using DDQ as an oxidant^{91,92} to selectively oxidize tetralin to tetralone rather than enone gave us hope, but repeating these conditions on our system only gave us degradation of the starting material (Table 2.2, entries 10-12). Excitingly, during optimization of the DDQ conditions, Christine discovered that adding acid into the reaction with DDQ in the form of formic acid or CHCl₃ yielded the desired ketone (**150**) in 18% yield (Table 2.2, entries 13-14). Unfortunately, it was

discovered that when these DDQ conditions were repeated on a scale larger than 100 mg, the yield dropped below 10% every time. It was impossible to isolate pure ketone (**150**) from the excess DDQ and reduced DDQ byproduct. Therefore, I continued screening for new benzylic oxidation conditions.

Table 2.2 Oxidation screening conducted by Christine Dimirjian.



Entry	Conditions	Temperature	Major product	Yield
1	TBHP/CuI	60 °C	quinone (153)	NR**
2	1. NBS, dibenzoyl peroxide 2. MnO ₂	80 °C	aryl bromination	73%
3	CAN	rt	ND*	-
4	IBX, DMSO	85 °C	quinone (153)	28%
5	KMnO ₄ /FeCl ₃	0 °C to rt	ND	-
6	KMnO ₄ /CuSO ₄	rt then sonicate	ND	-
7	PCC (1 equiv)	rt	quinone (153)	22%
8	CrO ₃ (2.2 equiv), AcOH	0 °C	quinone (153)	NR**
9	CrO ₃ (10 equiv), 3,5-dimethylpyrazole	-10 °C	quinone (153)	NR**
10	DDQ, dioxanes/phosphate buffer	rt	ND	-
11	DDQ, dioxanes, formic acid (cat.)	30 °C, sonicate	no conversion	0%
12	DDQ, dioxanes, H ₂ O, formic acid (cat)	rt	ND	-
13	DDQ, dioxanes, H ₂ O, formic acid (1M)	120 °C, mW	ketone (150)	18%
14	DDQ, CHCl ₃ , H ₂ O	rt	ketone (150)	18%
15	DDQ, DCE, H ₂ O, formic acid (1M)	120 °C, mW	ND	-
16	DDQ, CHCl ₃ , H ₂ O, formic acid (1M)	65 °C	ketone (150)	7%

[†]See CAD dissertation Table 3.2 & corresponding discussion

* ND = major product not determined due to messy reaction and inability to purify

**NR = not reported by CAD in dissertation or notebooks

Further DDQ conditions were initially screened to exhaustively determine that the reaction could not be optimized for higher ketone yields (**150**).⁹³ None of the new conditions were successful (Table 2.3, entries 17-24), but the use of DDQ in a 1:1 mix of CHCl₃ and H₂O yielded the naphthalene (**151**) core cleaning in 53% yield (Table 2.3, entry 19). The less reactive benzoquinone oxidant showed no conversion (Table 2.3, entry 25). Selenium dioxide did not react with the starting material at all, even in large excess and at high temperatures (Table 2.3, entries 26-27). Co-oxidants with KMnO₄ meant to temper the reactivity of the oxidant only lead to degradation or trace ketone (Table 2.3, entries 28-31). However, using

only the mild co-oxidants, such as MnO₂, CuSO₄, or oxone, gave little to no conversion of starting material (Table 2.3, entries 32-33). Reducing the equivalents of CrO₃ and lowering the temperature from the conditions used by Christine gave ketone (**150**) in 2% yield (Table 2.3, entries 34-35). Combining PCC with celite as a solid support and heating to reflux in benzene yielded the ketone (**150**) in 8% yield (Table 2.3, entry 36). Adjusting the equivalents of IBX used still only afforded quinone (**153**).⁹⁴ Meanwhile, DMP gave no conversion at all. Surprisingly, a PIDA and oxone co-oxidant system did not afford any product or byproduct when usually hypervalent iodides are commonly known to be used for quinone formation for phenolic systems.⁹⁵

Table 2.3 Benzylic oxidation screening for benzylic ketone (**150**) formation.

Benzylic oxidation screening: benzylic site w/ortho methoxy group

Starting material (**148**) $\xrightarrow[\text{solvent, time}]{\text{oxidant, temperature}}$ benzylic ketone (**150**)

Desired product

benzylic ketone (**150**)

Observed byproducts

quinone methide (**153a**)
tertiary alcohol (**152**)
naphthalene (**151**)

Entry	Oxidant	Temperature	Solvent	Time	Major product	Yield
17	DDQ, formic acid	100 °C, mW	dioxanes/H ₂ O	0.5 hr	quinone (153)	ND*
18	DDQ pre-stir in H ₂ O	65 °C	CHCl ₃ /H ₂ O	12 hr	quinone (153)	ND*
19	DDQ	rt	CHCl ₃ /H ₂ O	0.1 hr	naphthalene (152)	53%
20	DDQ	rt	formic acid/H ₂ O	0.05 hr	quinone (153)	ND*
21	DDQ	rt	dioxanes	0.1 hr	ketone (150)	7%
22	DDQ	rt	CH ₂ Cl ₂	12 hr	quinone (153)	ND*
23	DDQ, Mn(OAc) ₃	rt	CH ₂ Cl ₂	0.5 hr	ketone (150)	9%
24	DDQ, pyr	rt	CH ₂ Cl ₂	0.05 hr	quinone (153)	0%**
25	benzoquinone	rt to 40 °C	formic acid/H ₂ O	15 hr	no conversion	-
26	SeO ₂	100 °C	dioxanes	10 hr	no conversion	-
27	SeO ₂ , KHPO ₄	90 °C	dioxanes	14 hr	no conversion	-
28	KMnO ₄ /MnO ₂	rt	CH ₂ Cl ₂	11 hr	no conversion	-
29	KMnO ₄ /MnO ₂	40 °C, mW	CH ₂ Cl ₂	10 hr	trace ketone (150)	-
30	KMnO ₄ /FeCl ₃	rt	CH ₂ Cl ₂	24 hr	degradation	-
31	KMnO ₄ /CuSO ₄	rt	CH ₂ Cl ₂	24 hr	degradation	-
32	CuSO ₄ , oxone, MnO ₂	60 °C	MeCN	6 hr	degradation	-
33	MnO ₂	40 °C	CH ₂ Cl ₂	8 hr	no conversion	-
34	CrO ₃	rt	AcOH	3 hr	quinone (153)	2%
35	CrO ₃	-20 °C	3,5-dimethylpyrazole	3 hr	quinone (153)	2%
36	PCC/celite	80 °C	benzene	12 hr	ketone (150)	8%
37	IBX	85 °C	DMSO	6 hr	quinone (153)	0%**
38	DMP	60 °C	CH ₂ Cl ₂	24 hr	no conversion	-
39	PIDA/oxone	40 °C	CH ₂ Cl ₂	4 hr	no conversion	-

* ND = yield not determined due to messy reaction and inability to purify

** quinone degrades on column

At this point, many of the traditional oxidants and less complex oxidant systems had been exhausted with no promising improvements in yield. Therefore, transition metal-catalyzed, photochemical, and radical-based systems began to be explored (Table 2.4).

Table 2.4 Benzylic oxidation screening for benzylic ketone (**150**) formation.

Benzylic oxidation screening: benzylic site w/ortho methoxy group

Desired product
benzylic ketone (**150**)

Observed byproducts

quinone methide (**153a**)
tertiary alcohol (**152**)
naphthalene (**151**)

Entry	Oxidant	Temperature	Solvent	Time	Major product	Yield
40	Rh ₂ (cap) ₄ , NaHCO ₃ , <i>t</i> BuOOH	40 °C	DCE	4 hr	degradation	-
41	CuI, TBHP (70% in H ₂ O)	rt	MeCN	0.5 hr	quinone (153)	0%**
42	CuSO ₄ , K ₂ S ₂ O ₈	60 °C	MeCN	12 hr	no conversion	-
43	RuCl ₃ , K ₂ S ₂ O ₈ , iodobenzene	rt	MeCN/H ₂ O	24 hr	degradation	-
44	RuCl ₂ (PPh) ₃ , TEMPO, O ₂	rt	toluene	24 hr	no conversion	-
45	K ₂ S ₂ O ₈ , pyr	0 °C to 60 °C	MeCN	48 hr	no conversion	-
46	oxone, pyr, MnO ₂	60 °C	MeCN	12 hr	trace ketone	ND*
47	oxone, pyr, Pd(OAc) ₂	100 °C	toluene	24 hr	no conversion	-
48	1. oxone, pyr 2. DMP	60 °C	MeCN	18 hr	no conversion	-
49	1. oxone, pyr 2. CuSO ₄	60 °C	MeCN	18 hr	degradation	-
50	KBr, oxone	50 °C	MeNO ₂	24 hr	no conversion	-
51	KBr, oxone	rt, <i>hν</i>	MeCN/H ₂ O	24 hr	degradation	-
52	KBr, oxone	rt, <i>hν</i>	CH ₂ Cl ₂ /H ₂ O	2 hr	no conversion	-
53	[Co ^{III}], Mes-Acr ⁺ , LiNO ₃	rt, <i>hν</i>	MeCN/H ₂ O	6 hr	degradation	-
54	Fe(TPP)Cl, PhI(O)	80 °C	MeCN/H ₂ O	24 hr	degradation	-
55	CuBr ₂ , TEMPO, KO ^t Bu	80 °C	MeCN/H ₂ O	24 hr	degradation	-
56	TEMPO, CAN, O ₂	80 °C	MeCN	14 hr	no conversion	-
57	TEMPO, CAN, O ₂	80 °C	MeCN	24 hr	no conversion	-
58	TEMPO, NaClO, Co(OAc) ₂	rt	CH ₂ Cl ₂	24 hr	degradation	-
59	CAN, O ₂	80 °C	MeCN/H ₂ O	18 hr	ketone	11%
60	DMDO	40 °C	acetone	72 hr	tertiary alcohol (152)	23%
61	TBHP, O ₂	rt	DMSO	0.5 hr	degradation	-
62	TBHP, Bi, picolinic acid	100 °C	pyr/AcOH (10:1)	1 hr	degradation	-
63	Phthaloyl peroxide, NaHCO ₃	50 °C	HFIP, MeOH	24 hr	no conversion	-

* ND = yield not determined due to messy reaction and inability to purify

** quinone degrades on column

Dirhodium-catalyzed benzylic oxidation⁹⁶ with *tert*-butyl peroxide only led to degradation, confirming that any use of peroxide oxidants immediately degraded the insertion core (Table 2.4, entry 40). Ruthenium tandem catalytic systems with either TEMPO or oxone as the co-oxidant gave no conversion (Table 2.4, entries 43-44).^{97,98} Both thermal and photochemical conditions with KBr and oxone that aimed to brominate the benzylic position and oxidize to the ketone rapidly also gave no conversion (Table 2.4, entries 50-52).⁹⁹ A photoredox cobalt

catalytic oxygenation system developed by the Nicewicz group,¹⁰⁰ and the well-known iron porphyrin catalyst first reported by the White group only degraded the starting material (Table 2.4, entries 53-54). Catalytic TEMPO conditions also were found to be fruitless.¹⁰¹ Catalytic CAN conditions with an oxygen atmosphere to recycle the catalyst in aqueous MeCN at 80 °C yielded ketone (**150**) but only in 11% yield (Table 2.4, entry 59). Synthesis of fresh DMDO and its immediate use afforded the tertiary alcohol exclusively in 23% yield (Table 2.4, entry 60).¹⁰² Very mild peroxide conditions with a bismuth catalyst¹⁰³ or phthaloyl peroxide,¹⁰⁴ which had to be made in-house, were attempted in a last-ditch effort but did not yield any of the desired ketone (**150**) (Table 2.4, entries 62-63).

Reaction conditions to go directly from alkane to ketone proved unsuccessful, so options for functionalizing the benzylic position were explored (Table 2.5). Sp³ C–H acetoxylation reactions with lead acetate gave no reaction. DDQ with acetic acid and PIDA with acetic acid yielded quinone (**153**) (Table 2.5, entries 64-66).¹⁰⁵ Both thermal and photochemical radical benzylic bromination conditions were attempted, yet they only degraded the starting material (Table 2.5, entries 67-69).

Table 2.5 Benzylic oxidation screening for a functionalized benzylic position.

Benzylic oxidation screening: benzylic site w/*ortho* methoxy group

The reaction scheme shows starting material **(148)** reacting with an oxidant at a certain temperature in a solvent over time. The desired product is a functionalized benzylic position (**154a-b**), where the benzylic carbon is oxidized to a ketone (R¹). Observed byproducts include quinone methide (**153a**), a tertiary alcohol (**152**), and naphthalene (**151**).

Entry	Oxidant	Temperature	Solvent	R ¹	Major product	Yield
64	Pb ₃ O ₄ , AcOH	80 °C	benzene	-OC(O)CH ₃	no conversion	ND*
65	DDQ, AcOH	60 °C	CHCl ₃	-OC(O)CH ₃	quinone (153)	ND*
66	PIDA, NaBr, AcOH	40 °C	CH ₂ Cl ₂	-OC(O)CH ₃	quinone (153)	ND*
67	NBS then silica	30 °C	dioxanes	-Br	degradation	ND*
68	NBS then KOH	rt, <i>hν</i>	CH ₂ Cl ₂	-Br	degradation	ND*
69	NBS then NaOtBu	rt, <i>hν</i>	CH ₂ Cl ₂	-Br	degradation	ND*

* ND = yield not determined due to messy reaction and inability to purify

In conclusion, after screening about seventy different benzylic oxidation conditions, the best conditions could only afford ketone (**150**) in 18% yield on a 50 mg scale. This was determined to be an insurmountable obstacle for this initial route. Therefore, alternative re-routes that could enable alternative pathways around this oxidation problem began to be explored.

2.2.4. Right hemisphere: Vilsmeier-Haack reaction

Even though it was determined that an alternative strategy needed to be found to circumvent the benzylic oxidation issue, there was still enough material to test late-stage transformations, a Claisen reaction with the late-stage ketone (**150**) and an ester version of the left hemisphere (**162**) was attempted once on a very small scale (see CAD dissertation), but it did not yield the desired dicarbonyl. Other xanthone formation conditions directly from the late-stage ketone (**150**) were explored by Christine, too, without any luck. Therefore, we tried a Vilsmeier-Haack-Arnold (VHA) reaction on the late-stage ketone (**150**), which would form the β -chloro-cinnamaldehyde (**155**). The formylation step in this mechanism would make the C–C bond on the dihydroxanthone core that the Claisen reaction could not.

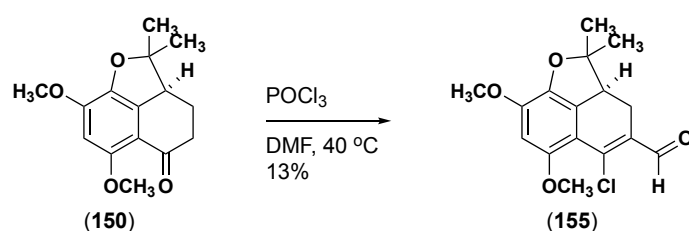


Figure 2.22 Vilsmeier-Haack-Arnold reaction.

Small amounts of ketone (**150**) obtained from oxidation with DDQ in $\text{CHCl}_3/\text{H}_2\text{O}$ were used in the VHA reaction to afford (**155**) in 13% yield. Notably, there was extreme difficulty in purifying the DDQ and its byproducts away from the ketone due to strong π -stacking occurring between the highly electron-rich product and highly electron-deficient DDQ. This problem ensured that the ketone (**150**) was never close to being a completely pure product by ^1H NMR spectroscopy. Therefore, the low yield in the VHA reaction could be due to impure starting

material (**150**) and unproductive interactions between the POCl₃ and DDQ. Albeit in low yields, the β -chloro-cinnamaldehyde (**155**) could be columned and isolated as a single pure product. The aldehyde (**155**) was then handed off to Christine to try initial attempts at joining the right hemisphere with a phenol version of the left hemisphere (**168**).

2.2.5. Left hemisphere

The left hemisphere is a highly substituted *2H*-chromene core, an incredibly common heterocycle in natural products derived from the polyketide pathway.¹⁰⁶ There are multiple intra- and intermolecular routes to *2H*-chromene formation, but they can all suffer from regioselectivity problems when there is high substitution on the aryl ring. However, in our synthetic strategy, poor regioselectivity would not be the worst outcome if the isomers were separable. Many of the natural product family members are only regioisomers of each other at the chromene core, and therefore our synthetic design could utilize both chromene isomers formed.

2.2.5.1. Initial route: ester functionality

The first left hemisphere was designed as a *2H*-chromene core with an ester and aryl triflate group. The ester could be used in a Claisen reaction with the late-stage ketone (**150**) on the right hemisphere to form the C–C bond of the dihydroxanthone core. The triflate group could be employed in an intramolecular coupling reaction to make the C–O bond of the dihydroxanthone.

To start, 2,4,6-trihydroxybenzoic acid (**156**) was acetal protected to form **157**. This initial protection would enable selective triflation and methylation later in the synthesis (Figure 2.23). Next, benzopyran (**157**) was formed from a Lewis acid-catalyzed tandem aldol reaction and S_N2' cyclization between **157** and 3-methyl-2-butenal (**159**).¹⁰⁷ Initial attempts using reported conditions resulted in a mix of regioisomers (**158a** and **158b**).^{108,109}

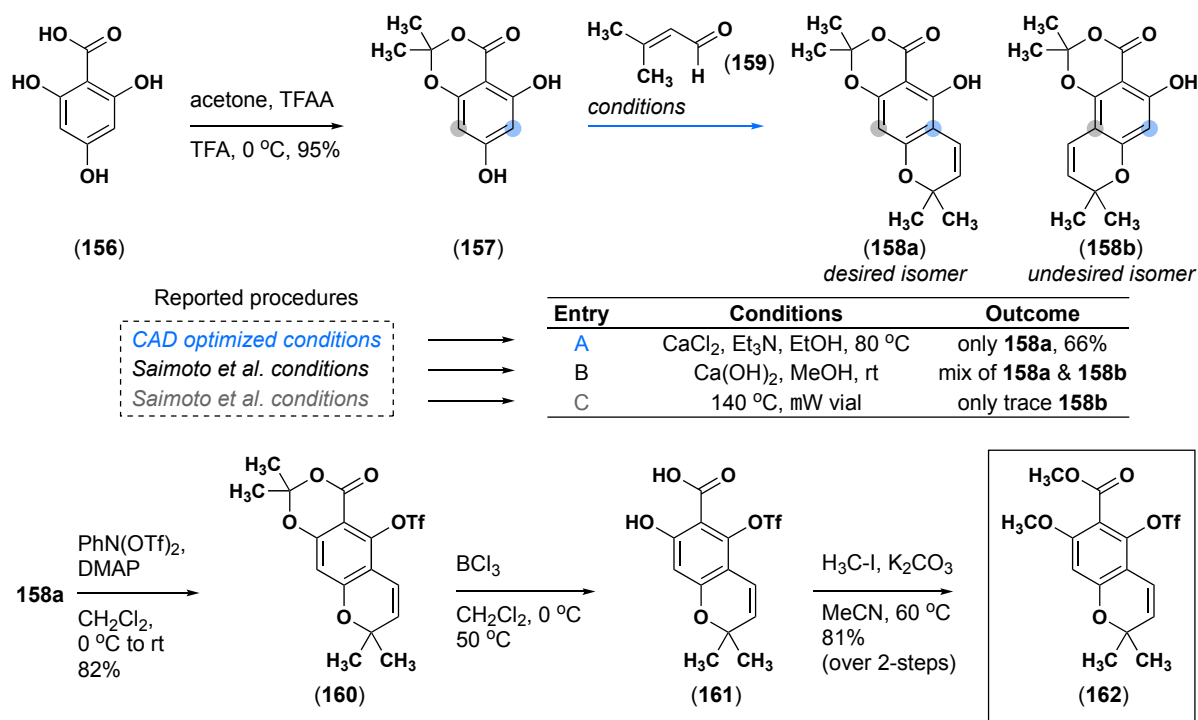


Figure 2.23 Left hemisphere initial route.

Optimization by Christine Dimirjian and Jenna Molas found that refluxing in EtOH with CaCl₂ yielded the desired regioisomer (**158a**) matching a previously published ¹H NMR spectrum.¹¹⁰ Triflation of the free phenol¹¹¹ afforded **160**, whose acetal could be cleaved with BCl₃ without clipping the triflate group to give **161** (see Christine Dimirjian's dissertation scheme 3.7). Finally, methylation of phenol and carboxylic acid yielded the desired left hemisphere (**162**).¹¹² Unfortunately, the model system attempts to form the dihydroxanthone C–C bond using α -tetralone and **162** through a Claisen reaction or enolate addition did not work well (see Christine Dimirjian's dissertation). Therefore, we designed a re-route to a left hemisphere lacking the ester functional group (section 2.2.5.2). The new left hemisphere could serve as a nucleophile and undergo Michael addition to the Vilsmeier-Haack-Arnold product (**155**).

2.2.5.2. Re-route: phenol functionality

The ester functional handle found on **162** was no longer needed due to the formylation that installs it on the right hemisphere (see Figure 2.22). Therefore, the 5-hydroxy-7-methoxyl *2H*-chromene (**168**) needed to be selectively accessed (Figure 2.24).

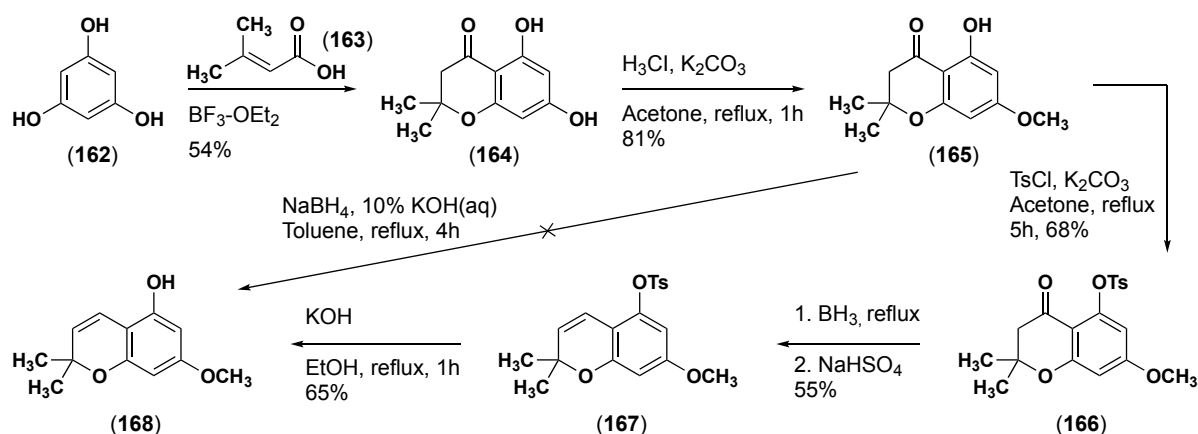


Figure 2.24 Left hemisphere re-route.

From phloroglucinol (**162**), addition and cyclization with 3-methylbut-2-enoic (**163**) acid yields the flavanone (**164**).^{113,114} Following a literature precedent,¹¹⁴ the 7-hydroxy group can be selectively methylated in 81% yield (**165**). The same literature precedent reported that from flavanone **165**, NaBH₄ with 10% aqueous KOH at reflux in toluene could yield the 2*H*-chromene core (**168**). However, upon repeating these results, no chromene (**168**) was obtained, only degradation of the starting material (**165**). Luckily, another route reported by Trost¹¹⁵ on a similar system showed you could protect the phenol ortho to the ketone and then undergo the reduction and elimination reaction to get chromene. Applying these protection conditions to our substrate, **165** afforded the tosylated flavanone (**166**) in decent yield. Refluxing **166** in boron then reduced the ketone to the alcohol, which could be isolated or sequential addition of NaHSO₄ would eliminate the alcohol to form the protected chromene core (**167**). Finally, removal of the tosyl group yielded the desired phenol (**168**) in a moderate 65% yield.¹¹⁶

2.3 Results and Discussion: route scouting

The low yields from the benzylic oxidation and inability to scale the reaction was a roadblock that needed to be addressed before continuing late-stage attempts at joining the two hemispheres of the molecule. It was hypothesized that the low yields were due to the high

electronic activation of the ring system since it possessed three ether-donating groups on the ring. Two possible solutions were to either temper the electronics of the ring system or protect the ketone rather than reducing it to the alkane in the second step of the synthesis so no late-stage oxidation step would be needed.

2.3.1. Protection of the benzylic ketone: acetal and thioacetal attempts

Although not previously reported by our group in any manuscript or dissertation, Christine Dimirjian and a former undergraduate student Jose Maldonado attempted to protect the benzylic ketone rather than reducing it to the alkane in the second step of the synthesis (Figure 2.25).

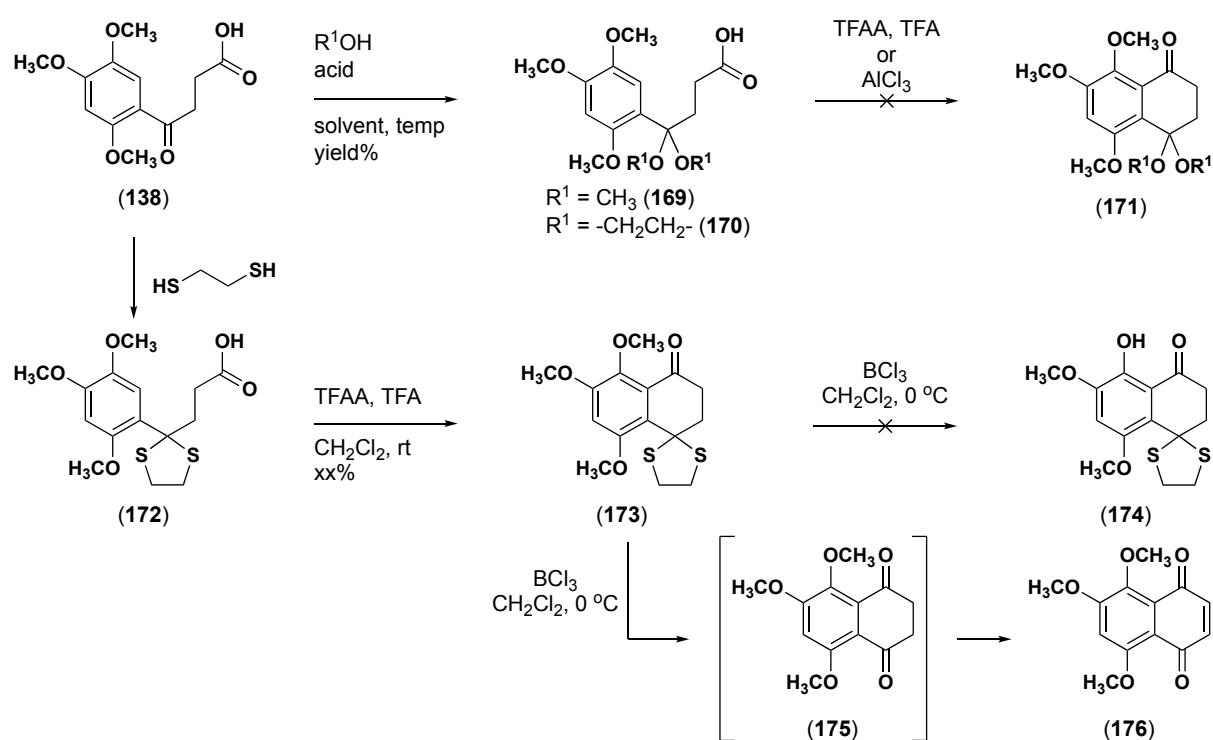


Figure 2.25 Benzylic ketone protection.

Many possible protecting groups for ketones could be selected¹¹⁷. Acetal protection was the initial choice due to the ease with which acetals are installed and removed without disrupting late-stage functionalities.^{118–123} The Friedel-Crafts intermediate (148) was protected with both acyclic (169) and cyclic acetals (170). However, neither acetal survived cyclization conditions

to form the tetralone core. Jose then found conditions to thioacetal protect **138** to afford **172**. The thioacetal (**172**) survived cyclization conditions to form tetralone (**173**), albeit in very poor yield. However, as soon as the tetralone **173** was placed in ortho-deprotection conditions with BCl_3 , the thioacetal was cleaved immediately to the 2,3-dihydro-1,4-naphthoquinone (**175**) and then oxidized up to the 1,4-naphthoquinone (**176**).

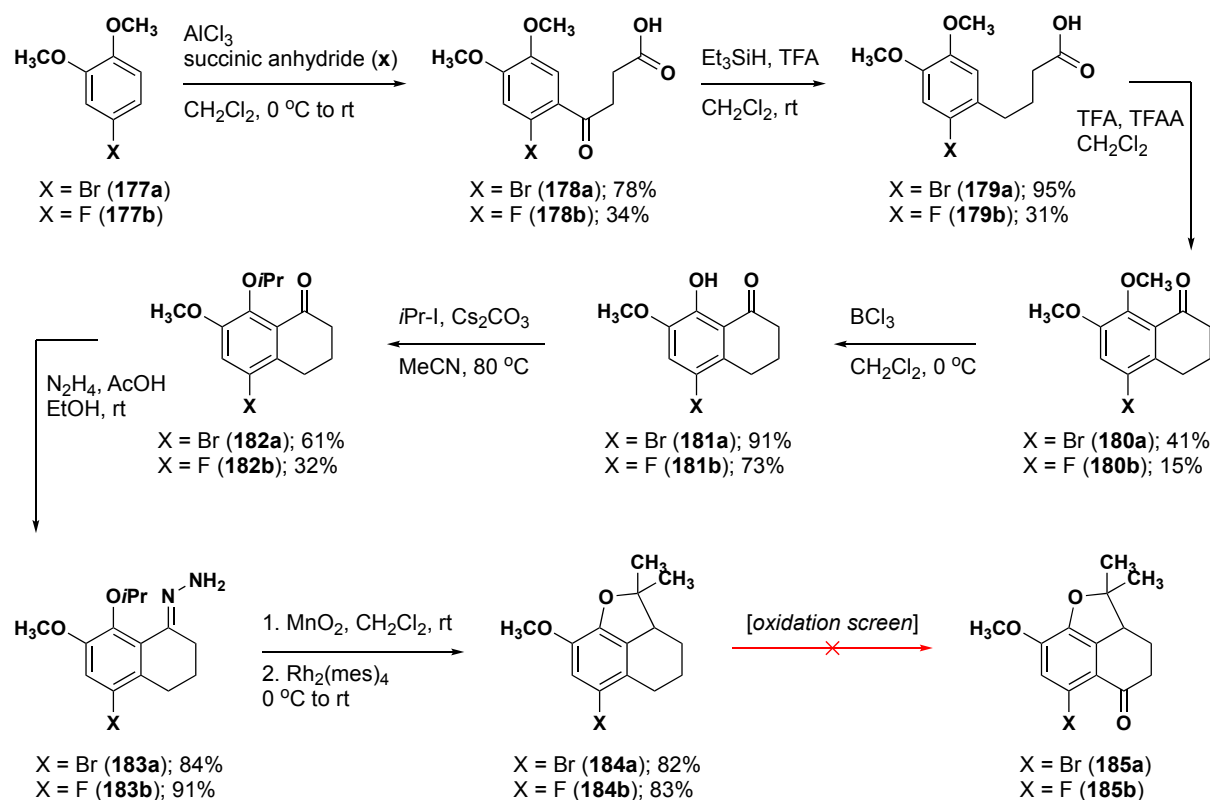
2.3.2. Tempering of the ring system electronics: synthesis of ortho-bromine and ortho-fluorine derivatives

Since the protection of the benzylic ketone was fruitless, I moved on to synthesizing less electronically activated ring systems. Any methoxy group we replaced with a less electronically donating group needed to transform back into a phenol group for the final target. Therefore, considering linear step count and what was commercially available, we decided to see if replacing a single methoxy group with a halogen in the position ortho to the benzylic ketone would enable a successful oxidation reaction. The 4-fluoro-1,2-dimethoxybenzene (**183b**) and 4-bromo-1,2-dimethoxybenzene (**183a**) were commercially available and relatively cheap. The aryl bromide could be transformed to the phenol directly or indirectly through many different coupling reactions.^{124–131} Meanwhile, the aryl fluoride could be a good $\text{S}_{\text{N}}\text{Ar}$ partner to reinstall the desired phenol group.¹³²

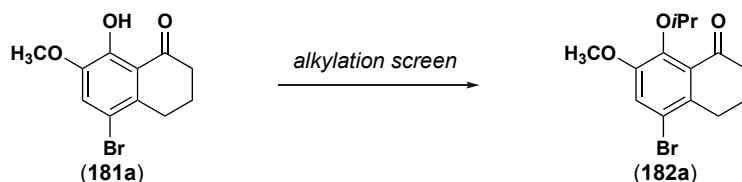
The 4-fluoro-(**177b**) and 4-bromo-(**177a**) 1,2-dimethoxybenzene rings were taken through the first-generation synthesis developed for the right hemisphere with little reaction optimization (Figure 2.26A). If either analog proved successful in the benzylic oxidation, the steps with lower yields would be optimized afterward. Due to decreased substrate reactivity, the first Friedel-Crafts acylation step in the synthesis took a hit in yield for both analogs, 78% (**178a**) and 34% (**178b**). While this was not ideal for bringing up starting material, it did suggest significant changes in electronic activation at the 5-position, which is exactly what we hoped

for. Reduction of the ketone to the alkane worked well for the bromine analog (**179a**), but the yield declined significantly with the fluorine analog (**179b**).

A. Synthesis of halogen analogs



B. Bromine analog alkylation screening



Entry	Electrophile	Base	Solvent	Temperature	Yield
1	<i>i</i> Pr-Br (2.0 equiv)	Cs ₂ CO ₃ (3.0 equiv)	MeCN	80 °C	25%
2	<i>i</i> Pr-Br (2.0 equiv)	K ₂ CO ₃ (2.0 equiv), NaI (10 mol%)	DMF	100 °C	0%
3	<i>i</i> Pr-Br (1.3 equiv)	NaH (3.0 equiv)	THF	25 °C	0%
4	<i>i</i> Pr-Br (1.3 equiv)	NaH (3.0 equiv)	DMF	25 °C	0%
5	<i>i</i> Pr-OTs (2.0 equiv)	Cs ₂ CO ₃ (3.0 equiv)	MeCN	80 °C	tosylated phenol
6	<i>i</i> Pr-I (3.0 equiv)	Cs ₂ CO ₃ (3.0 equiv)	MeCN	80 °C	52%
7	<i>i</i> Pr-I (4.0 equiv)	Cs ₂ CO ₃ (5.0 equiv)	MeCN	80 °C	61%

Figure 2.26 A. Synthesis of bromine and fluorine analogs **B.** Bromine analog alkylation screening.

Similarly to the Friedel-Crafts acylation, the TFA/TFAA cyclization to form tetralone was low yielding. The fluorine analog could only yield the desired tetralone (**180b**) in a 15% yield on a

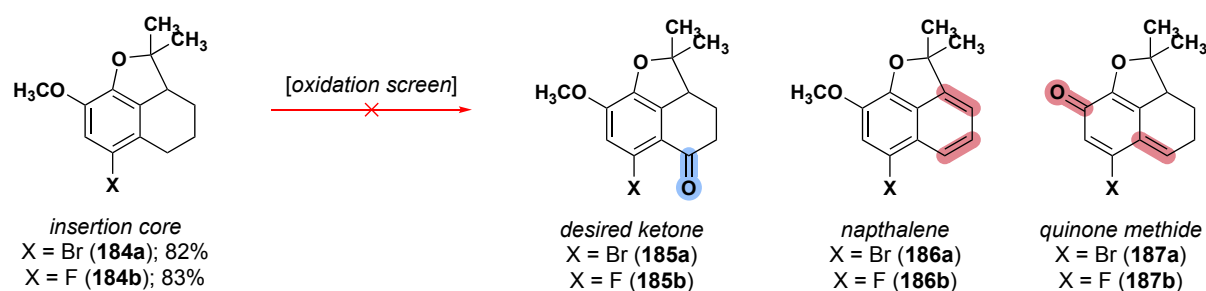
2.0 g scale. Ortho deprotection of the tetralone analogs (**180a-b**) with BCl_3 proceeded smoothly to afford **181a** and **181b**.

Shockingly, alkylation with isopropyl bromide and Cs_2CO_3 yielded no desired ether (**182a** or **182b**) (Figure 2.26B entry 1) even though the same conditions gave the analogous ether (**145**) on the triphenolic system near quantitatively (Figure 2.20). Different bases and solvents did not amount to any conversion from the phenol (Figure 2.26B entries 2-4). Therefore, different electrophiles were screened in the reaction. The use of a tosylate leaving group had proved to be very effective in forming the more complex, hindered ether for artoindonesianin Z-2 (**2**) (see section 2.6). Therefore, the isopropyl tosylate was synthesized. The phenol was completely consumed overnight after subjecting the tosylate to the alkylation conditions with Cs_2CO_3 . However, it was quickly discovered that the phenol (**181a**) was tosylated in near quantitative yield (Figure 2.26B entries 5). Luckily, the use of isopropyl iodide gave a more reactive electrophile resulting in the alkylation of the phenol (**181a**). The use of two equivalents of isopropyl iodide yielded ether **182a** in 52% yield (Figure 2.26B entry 6). Increasing isopropyl iodide equivalents to four increased the isolated yield to 61% (Figure 2.26B entry 7). Using the optimized conditions from entry 7 with the fluoro-phenol analog (**181b**) afforded the fluoro-ether (**182b**) in 32% yield.

Finally, hydrazone formation (**183a-b**) and one-pot sequential oxidation and C–H insertion yielded both the 4-bromo (**184a**) and 4-fluoro (**184b**) analogs of the insertion core with no drops in yield over those two steps when compared to the original substrate.

2.3.2.1. Benzylic oxidation attempts

Now that the modified insertion cores were in hand, a small screen of the best-yielding benzylic oxidation conditions for the original substrate (**148**) was tested against the less electron-rich analogs (Table 2.6). Unfortunately, neither the bromine (**184a**) nor the fluorine (**184b**) containing analogs produced any desired ketone (**185a-b**). DDQ conditions, which

Table 2.6 Benzylic oxidation screening of bromine and fluorine analogs.

Entry	Starting Material	Conditions	Outcome
1	X = Br (184a)	DDQ, CHCl ₃ /H ₂ O	quinone methide (187a) + naphthalene (186a)
2	X = Br (184a)	PCC/celite, benzene, 80 °C	quinone methide (187a)
3	X = Br (184a)	oxone, pyr, MnO ₂ , MeCN, 60 °C	no conversion
4	X = Br (184a)	KMnO ₄ /MnO ₂ , DCE, 80 °C	no conversion
5	X = Br (184a)	1. PCC/celite 2. POCl ₃ , DMF	degradation
6	X = Br (184a)	PIDA, NaBr, AcOH, 40 °C	degradation
7	X = F (184b)	DDQ, CHCl ₃ /H ₂ O	quinone methide (187b) + naphthalene (186b)
8	X = F (184b)	PCC/celite, benzene, 80 °C	quinone methide (187b)
9	X = F (184b)	KMnO ₄ /MnO ₂ , DCE, 80 °C	degradation

afforded ketone in 18% with the 4-methoxy substrate, gave only quinone methide (**187a-b**) and naphthalene (**186a-b**) byproducts for both analogs (Table 2.6, entries 1, 7). PCC mixed with celite yielded exclusively quinone methide (**187a-b**) in <10% (Table 2.6, entries 2, 8). All other oxidation conditions either did not convert the starting material to anything or rapidly degraded both molecules (Table 2.6, entries 2-6, 9). It was hypothesized that the PCC conditions with the analogs could be generating alcohol and ketone *in situ*, but upon workup, they were getting oxidized to quinone or degrading. Therefore, a one-pot sequential method was attempted to telescope the ketone directly into the Vilsmeier-Haack reaction. Only degraded starting material was observed by ¹H NMR spectroscopy with this method (Table 2.6, entry 5).

2.3.3. Tosyl protection of phenols

Swapping one methoxy group out for bromine or fluorine did not improve the benzylic oxidation success. Therefore, we next wanted to swap both methoxy-protecting groups for electron-withdrawing tosyl-protecting groups. Switching from electron-donating groups on the ring to two electron-withdrawing groups would significantly change the electronics of the ring

system. This change would give further insight into the role that electronic activation of the ring played in the overoxidation of the insertion core (**148**) to unwanted byproducts.

The benzylic oxidation screens on the insertion core (**148**) (Figures 2.27) showcased the high acid sensitivity the tricyclic core had and the propensity for the aryl ring to be brominated even at cryogenic temperatures. Therefore, when we selected the initial demethylation conditions, the classic boron tribromide (BBr_3) reagent was avoided since it generates the strong acid, HBr , and the robust bromination reagent, Br_2 . Conversely, sodium ethane thiolate (NaSEt) is often used for demethylation reactions for base-stable molecules.¹³³ Lower temperature conditions with NaSEt were attempted initially. First, the Lewis acid AlCl_3 was added to a solution of **148** in CH_2Cl_2 at $0\text{ }^\circ\text{C}$ to coordinate with the ether oxygen. Then NaSEt was added to demethylate **148** through an $\text{S}_{\text{N}}2$ attack.¹³⁴ Unfortunately, as soon as AlCl_3 was added to the solution of **148** in CH_2Cl_2 , the reaction went from a light yellow to black. Reaction work-up and ^1H NMR spectrum elucidated that the Lewis acid immediately degraded the starting material (**148**) (Figure 2.27 entry 1). Since we knew BCl_3 did not degrade the molecule earlier in the synthesis, conditions were attempted that combined BCl_3 and tetrabutylammonium iodide (TBAI) at $-78\text{ }^\circ\text{C}$ and allowed the reaction to slowly warm to room temperature. After the reaction workup, the ^1H NMR spectrum was indiscernible and was missing the expected aryl peak from the starting material or the product (Figure 2.27 entry 2). Next, higher temperature conditions were attempted. Ten equivalents of NaSEt in DMF at $140\text{ }^\circ\text{C}$ did not demethylate any starting material (**148**) (Figure 2.27 entry 3). Using the same conditions while increasing the equivalents of NaSEt to fifteen yielded the mono-demethylated product (**188**) (Figure 2.27 entry 4).⁵⁷ This was not surprising since regioselective aryl ether demethylation with NaSEt has been observed before.^{135,136} Modifying the reaction conditions to heat at $140\text{ }^\circ\text{C}$ in the microwave in 30 min intervals yielded both mono- (**188**) and di- (**189**) demethylated products after 1.5 hours (Figure 2.27 entry 5).

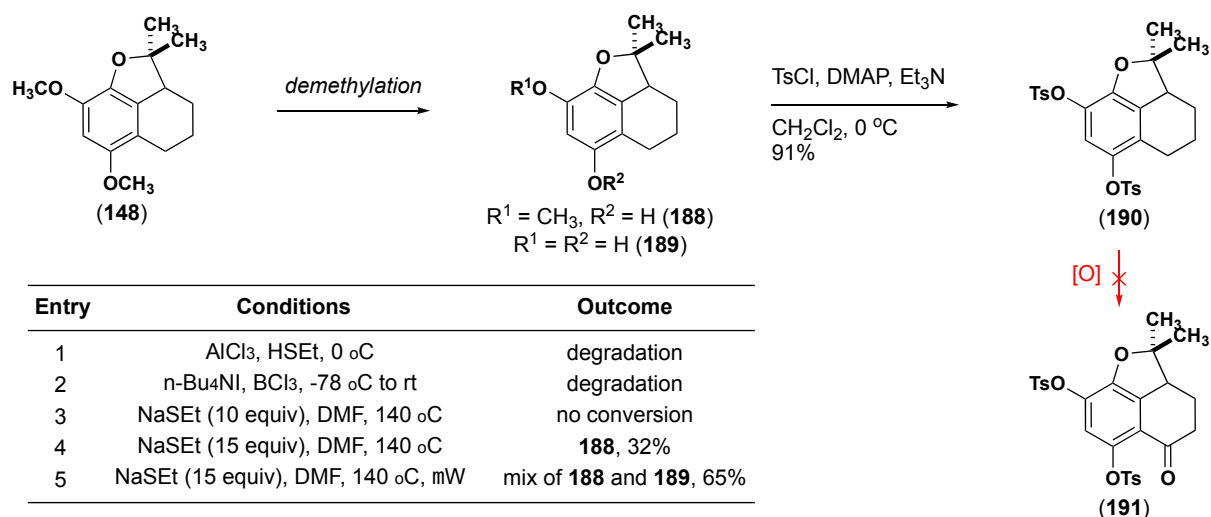


Figure 2.27 Protecting group swap from methoxy to tosyl on insertion core **148**.

Column chromatography separated the mono-demethylated product (**188**) from the di-demethylated product (**189**). The dihydroxy product (**189**) was then tosylated easily to yield about 20 mg of **190** and complete the protecting group swap. The 20 mg of **190** was split into two benzylic oxidation test reactions. PCC/celite in benzene at 80 °C and DDQ in dioxanes were tested since these were the top two oxidation conditions for the methoxy-protected substrate (**148**). However, both oxidative conditions only degraded the starting material (**190**), where no starting material (**190**) or desired ketone (**191**) was observed in the ¹H NMR spectrum after workup.

2.3.4. Unsubstituted ortho position

Adjusting the electronic activation of the aromatic ring on the fused tricyclic core did not aid the benzylic oxidation at all. Therefore, the hypothesis that electronics solely contributed to the overoxidation problem was ruled out, and a steric argument began to be explored. Potentially, the formation of the benzylic of the ketone could be disfavored over byproduct formation due to poor steric interactions between the benzylic ketone and the substituent at the 4-position on the aryl ring. Leaving the 4-position unsubstituted and screening benzylic oxidation conditions would quickly test this hypothesis.

At the time of the hypothesis, the bromo-analog insertion core (**184a**) was readily available. The aryl bromide (**184a**) was rapidly de-brominated in 30 minutes using H₂, Pd/C in methanol at room temperature, giving the unsubstituted 4-position (**192**) in nearly quantitative yield (Figure 2.28).

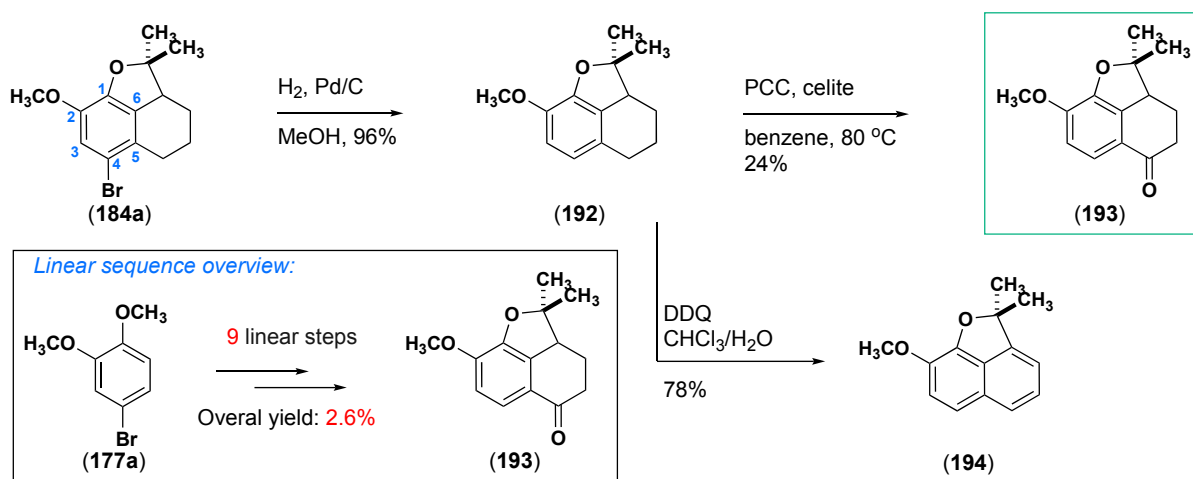


Figure 2.28 Initial formation and benzylic oxidation of unsubstituted fused tricyclic core.

The fused tricyclic core (**192**) was then oxidized using DDQ in chloroform and water. First, the DDQ was stirred in water and chloroform and heated to 65 °C for 10 minutes turning the solution orange to red. The solution was cooled to 0 °C, then the starting material (**192**) was added, and the solution immediately turned a deep blue color. After 5 minutes, all the starting material was completely consumed by TLC, and the solution had changed color to a clear/black heterogeneous mixture. TLC showed spot-to-spot conversion of the starting material. However, ¹H NMR spectrum revealed that the insertion core (**192**) had cleanly converted to the naphthalene byproduct (**194**) in 78% isolated yield. Next, PCC with celite was tried as an oxidant. Refluxing the starting material with PCC and celite in benzene overnight afforded the desired ketone (**193**) in 24% yield. This was the highest reported yield for the benzylic oxidation at the time. More importantly, the reaction yield was reproducible, and the crude

mixture was easy to purify, unlike the best DDQ conditions for the previous system (**148**) (Table 2.2).

The PCC oxidation results with **192** lead us to believe that the overoxidation problem was caused by high electronic activation and unfavorable steric interactions between the desired ketone and any substituent at the 4-position on the aryl ring. Therefore, optimizing the benzylic oxidation on the unsubstituted tricyclic core (**192**) could theoretically yield the desired ketone in greater than 50% yield. However, the initial route to access the unsubstituted core (**192**) was not optimal. Starting from the 4-bromo-1,2-dimethoxybenzene (**177a**), it took nine linear steps to reach the desired ketone (**193**) in an overall yield of only 2.6%. The low yield made it difficult to bring up enough material to try subsequent reactions after oxidation. Also, the linear step count would continue to increase since the phenol in the 4-position had to be reinstalled. To reinstall this group, one probable method would be the bromination of the aryl ring followed by one of the transition metal-catalyzed C–O bond formation conditions mentioned earlier. Removing the bromine group to oxidize the benzylic center to only immediately reinstall the bromine group had a very poor atom economy, analogous to a protecting group swap.

Going back to the beginning of the synthesis and starting with 1,2-dimethoxybenzene (**195**) was briefly considered as an option. However, the tetralone formation reaction would favor the incorrect regioisomer of tetralone (**198**) (Figure 2.29).

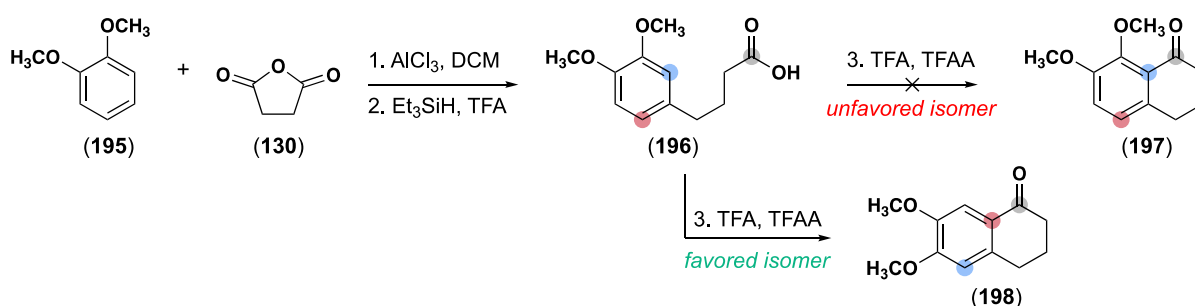


Figure 2.29 Incorrect regioselectivity if 1,2-dimethoxybenzene is used as the starting material.

For due diligence, the intramolecular cyclization of **196** with the TFA/TFAA system was attempted. If the regioselectivity was poor and gave a mix of separable tetralones **197** and **198**,

this route could bring up the unsubstituted tricyclic core (**197**) in higher yields than the bromination route. Then, late-stage reactions after ketone formation could continue to be explored while a re-route to the unsubstituted core (**197**) was developed. Unfortunately, the intramolecular cyclization of the carboxylic acid **196** favored the undesired isomer (**198**) almost exclusively.

With all these results in hand, we decided that the initial “Friedel-Crafts” route had to be abandoned, and completely new routes to access the disubstituted tetralone (**197**) began to be explored. After searching the literature, two promising routes emerged for accessing the 8-isopropoxy-7-methoxy-tetralone (**199**) (Figure 2.30).

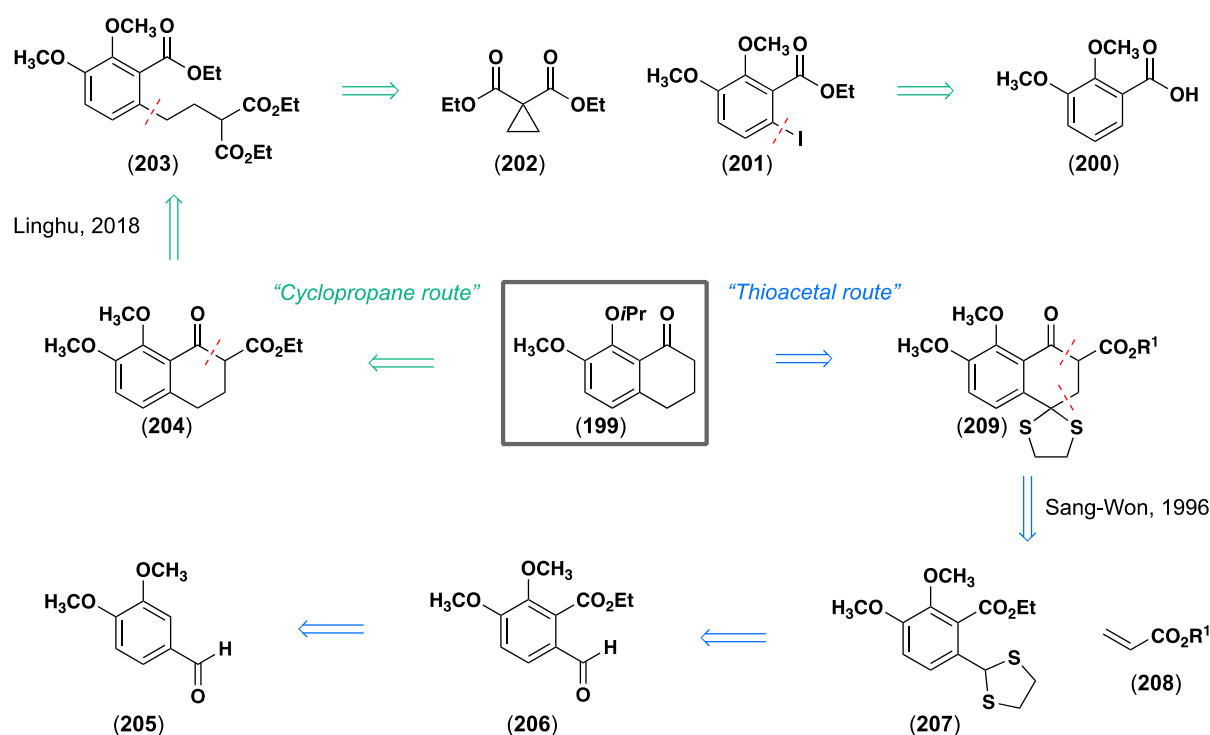


Figure 2.30 Retrosynthetic analysis for new ways to access the tetralone **199**.

The first route, the “thioacetal route”, was where the tetralone scaffold (**209**) is assembled by a tandem Michael-Claisen condensation between a benzylic thioacetal (**207**) and an acrylate (**208**). This reaction also leaves a thioacetal in the benzylic position, which could be hydrolyzed later in the synthesis to afford the benzylic ketone. The thioacetal (**207**) could be derived from commercially available 3,4-dimethoxy-benzaldehyde (**205**). The second route, the

“cyclopropane route”, built the desired tetralone scaffold (**204**) through a homoconjugate addition of an aryl Grignard to diethyl cyclopropane-1,1-dicarboxylate (**202**) followed by a decarboxylative Dieckmann annulation. The aryl Grignard would be formed from an aryl-iodide (**201**) mixed with a Turbo Grignard. The aryl-iodide (**201**) could be derived from commercially available 2,3-dimethoxybenzoic acid (**200**).

2.3.5 Thioacetal route

Starting from 3,4-dimethoxy-benzaldehyde (**205**), the aldehyde must be protected to prevent self-addition in the next lithiation step (Figure 2.31A). Refluxing the aldehyde (**205**) with ethylene glycol and catalytic para-toluenesulfonic acid in toluene at 130 °C and a D.S. trap did not form any cyclic acetal (**210a**) (Figure 2.31B, entry 1). Keeping the same conditions but increasing the temperature to 170 °C helped push the reaction and afforded cyclic acetal (**210a**) in 68% yield. We attempted to make the acyclic acetal (**210b**) to see if it could be a more suitable substrate for the ortho lithiation step. However, switching to methanol and refluxing in benzene only gave acyclic acetal (**210b**) in 17% yield (Figure 2.31B entry 2). Adding trimethoxymethane as a dehydrating reagent and refluxing the aldehyde (**205**) in methanol increased the yield of the acyclic acetal (**210b**) to 36% (Figure 2.31B, entry 3).

Next, an ortho lithiation with *n*-butyl lithium (*n*-BuLi) was attempted to install the ester group in the 2-position (**206**). The acyclic acetal (**210b**) was subjected to *n*-BuLi at -78 °C to form the lithiate, then either methyl chloroformate or ethyl chloroformate was added. Both reactions exclusively gave unprotected aldehyde starting material (**205**) (Figure 2.31C, entries 1-2).

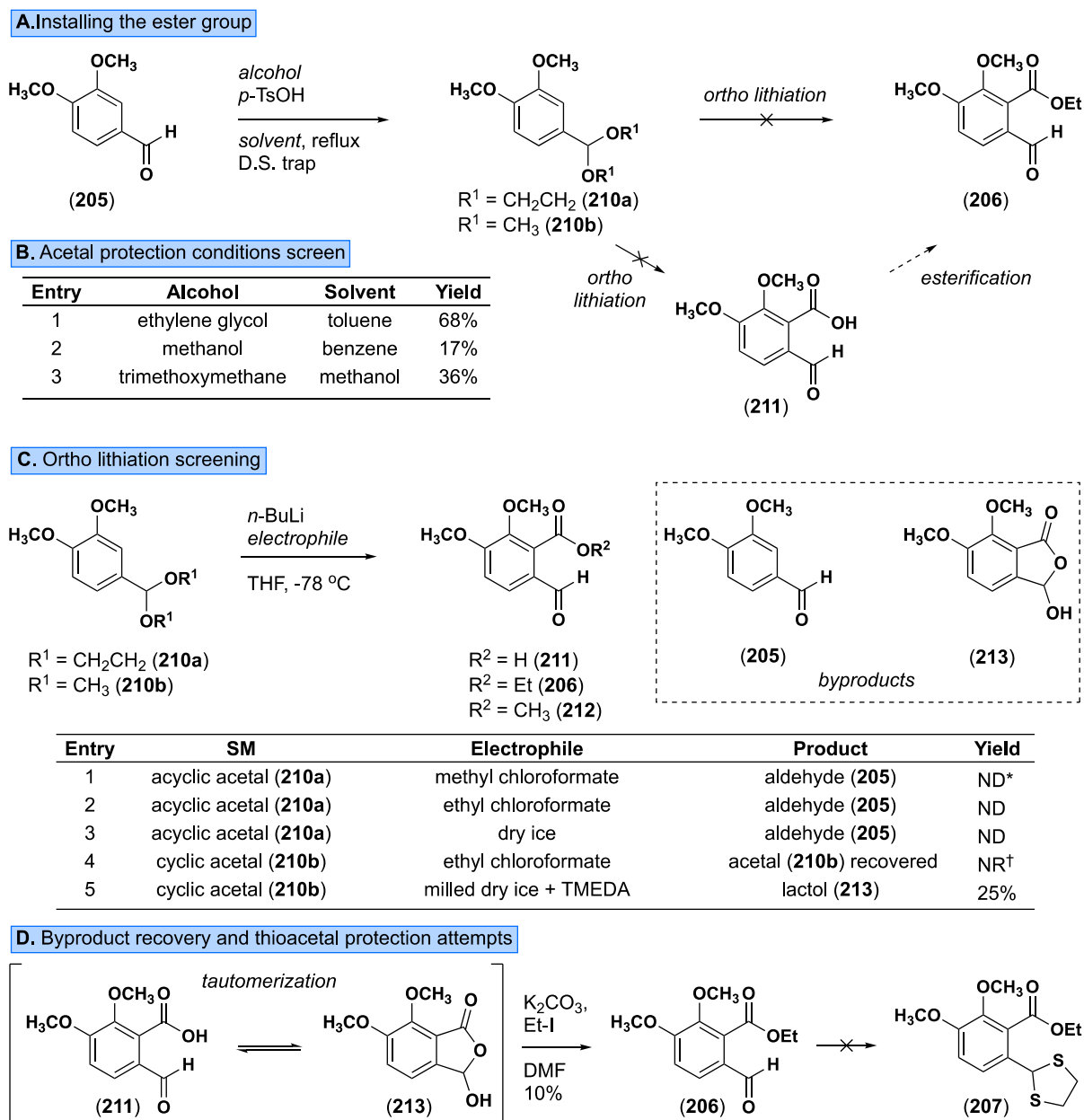


Figure 2.31 Accessing the starting material acetal: **A.** Installing the ester group **B.** Acetal protection screening **C.** Ortho lithiation screening **D.** Byproduct recovery.

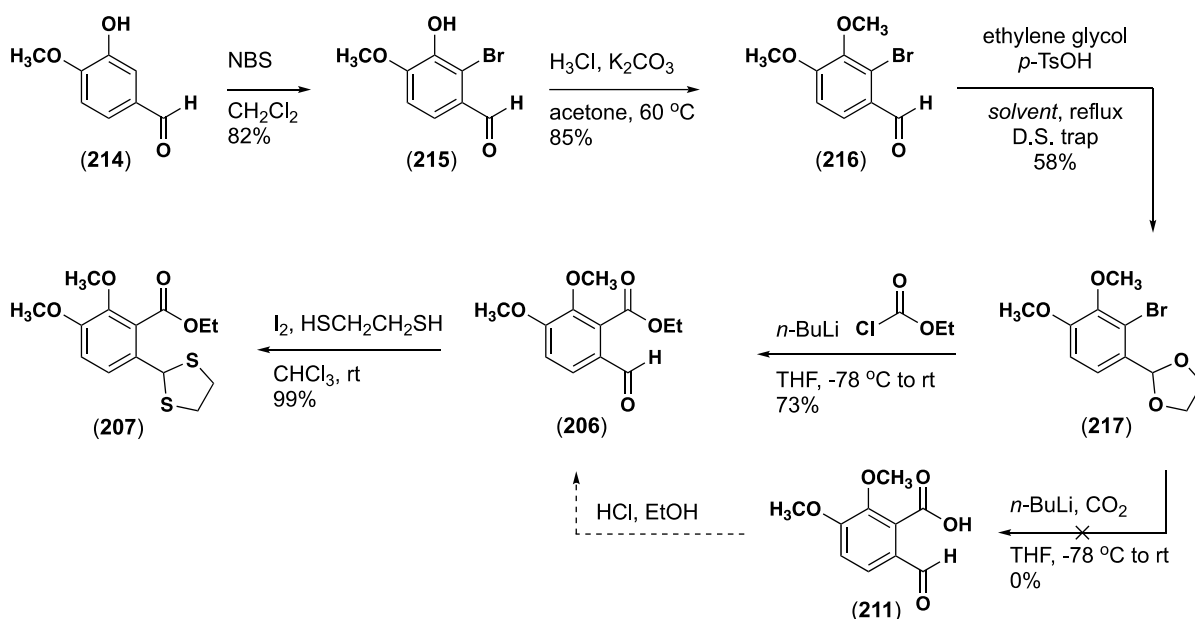
Quenching the reaction after lithiate formation and before adding any electrophile yielded only starting acetal (**205**). Methyl and ethyl chloroformate are known to possess large amounts of HCl and H₂O as they age and degrade over time, and the lab bottles were over 7 years old. It was hypothesized that the presence of additional water contributed to the conversion of acetal (**210a**) back to aldehyde (**205**). Therefore, acid-free and lower water content conditions were

explored by adding the lithiate to CO₂ using crushed dry ice. These conditions also yield only aldehyde (**205**) (Figure 2.31C, entry 3), suggesting it was a substrate issue.

We switched to a different substrate, the cyclic acetal (**210b**). Lithiate formation and addition to a brand-new bottle of ethyl chloroformate gave no reaction, and there was a complete mass recovery of the starting acetal (**210b**) (Figure 2.31C, entries 4). Finally, tetramethylethylenediamine (TMEDA) was added to increase the rate of metalation then milled dry ice washed with THF was added to the reaction.¹³⁷ There was a successful addition to CO₂ and the formation of the carboxylic acid (**211**), but the carboxylic acid immediately tautomerized to the lactol (**213**). The lactol (**213**) was the final compound isolated from the reaction in 25% yield (Figure 2.31C, entry 5). A reported reaction with K₂CO₃ and iodoethane in DMF was attempted to transform the lactol (**213**) to the desired ester (**206**) but only afforded the product in 10% yield.¹³⁸ The small amount of ester material (**206**) isolated from the previous reaction was pushed forward into thioacetal protection. However, reported conditions using ZnCl₂ and 1,2-ethanedithiol did not afford any of the desired product (**207**) (Figure 2.31D).^{139,140}

The ortho lithiation reaction was not working well, so we re-routed to brominating the 2-position first to make a better lithiation substrate (Figure 2.32A). Starting from isovanillin (**214**), NBS in dichloromethane regioselectively brominates the 2-position (**215**).¹⁴¹ The free phenol can be methylated with K₂CO₃ and methyl iodide in 85% yield (**216**), followed by the previously optimized acetal formation conditions to give cyclic acetal (**217**) in 58% yield. Now lithium-halogen exchange with the bromine (**217**) and addition to ethyl chloroformate affords the desired ester (**206**) in 73% yield. Surprisingly, adding the lithiate to dry ice gave no desired carboxylic acid (**211**) or its corresponding lactol tautomer (**213**). Thioacetal protection conditions using iodide and 1,2-ethanedithiol in chloroform yielded the desired cyclic thioacetal (**207**) quantitatively.¹⁴²

A. Switch to ortho bromine substrate



B. Thioacetal annulation reaction: initial results

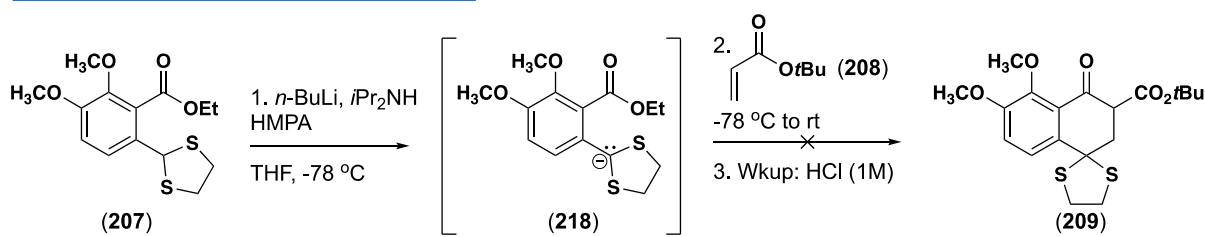


Figure 2.32 A. Switching to an aryl bromide for Li-X exchange B. Initial attempts at thioacetal annulation reaction.

With the thioacetal starting material (207) in hand, the thioacetal annulation conditions could finally be attempted (Figure 2.32B).¹⁴³ First, a solution of the thioacetal (207) in THF is cooled down to -78 °C, and hexamethylphosphoramide (HMPA) and diisopropylamine (*i*Pr₂NH) were added. Then the addition of *n*-BuLi deprotonates the benzylic proton to form the thioacetal anion (218) *in situ*. An acrylate, in this case, tert-butyl acrylate (208), is added at -78 °C, and the reaction is allowed to warm slowly to room temperature as the substrates undergo the tandem reaction. The thioacetal anion will undergo Michael addition with the α,β -unsaturated system in the acrylate, followed immediately by a Claisen condensation between the generated ester enolate and the ester in the 2-position affording the tetralone (209). However, it was discovered upon work-up that the reaction did not work. At this point, the

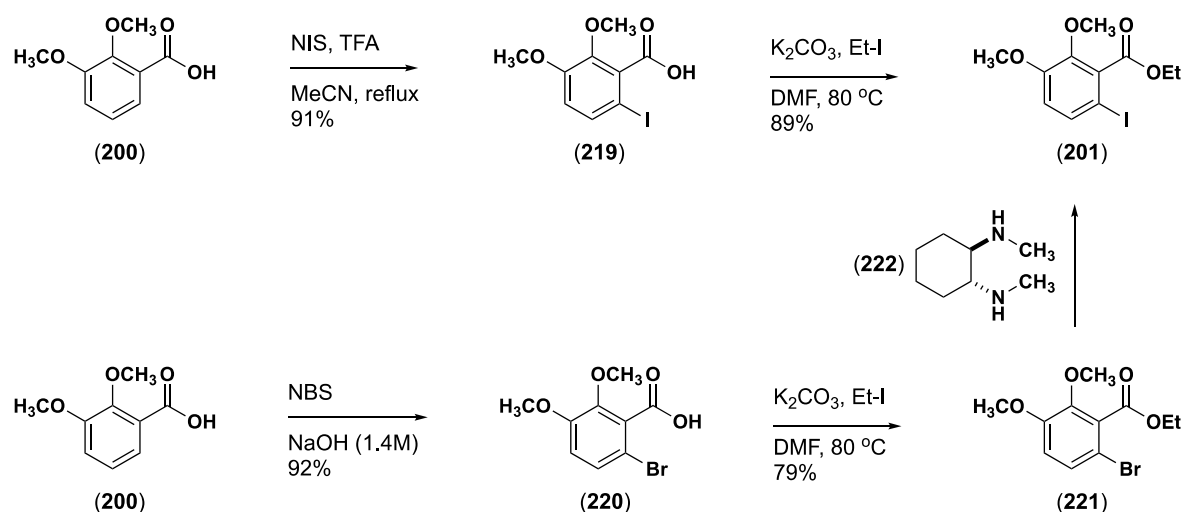
“thioacetal route” troubleshooting and optimization was handed over to graduate student Andy Hsieh. Andy later discovered that the cyclic thioacetal (**207**) could not successfully undergo the annulation reaction, but switching to an acyclic thioacetal solved the issue. After some short screening, Andy also found successful decarboxylation conditions. At this point, though, the “thioacetal route” possessed a very low-yielding, long linear step sequence, and the insertion core had not even been successfully accessed from it yet. The route was abandoned, and efforts were put into optimizing the more promising “tetralone route,” which evolved into the current second-generation route for the right hemisphere.

2.3.6 Cyclopropane route

Another route to the disubstituted tetralone core (**199**) was explored simultaneously with the optimization of the thioacetal route. This “cyclopropane” route hinged on a key homoconjugate addition followed by a decarboxylative Dieckmann annulation strategy to access the tetralone core (Figure 2.30).¹⁴⁴ The homoconjugate addition step required Grignard formation from an aryl iodide, while the Dieckmann annulation needed an aryl ester present. This iodo-ester (**201**) intermediate could be accessed in two steps from the commercially available 2,3-benzoic acid (**200**). Moving forward, stirring **200** with *N*-iodosuccinimide and TFA in acetonitrile at reflux afforded the mono-iodination product (**219**) (Figure 2.33A). The benzoic acid acts as a directing group to selectively iodinate the ortho position to the carboxylic acid.¹⁴⁵ From there, the carboxylic acid (**219**) can be esterified to give desired ester intermediate (**201**). Surprisingly, the initial esterification conditions tried gave only low yields of the ester (**201**). Specifically, Fischer esterification with H₂SO₄ and ethanol at 70 °C afforded only 10% of the desired ester (**201**) (Figure 2.33B entry 1). While refluxing in thionyl chloride and ethanol yielded no product (Figure 2.33B entry 2). Stirring the carboxylic acid with oxalyl chloride in a 1:1 mixture of dimethylformamide and dichloromethane to pre-form the acyl

chloride, then adding ethanol and triethylamine and stirring overnight increased the isolated yield to 33% (Figure 2.33B entry 3). Finally, deprotonation of the carboxylic acid (**219**) with potassium carbonate and then S_N2 addition to iodoethane afforded the ester (**201**) in 89% yield (Figure 2.33B entry 4).

A. "Cyclopropane" route: accessing the iodo-ester



B. Esterification screening

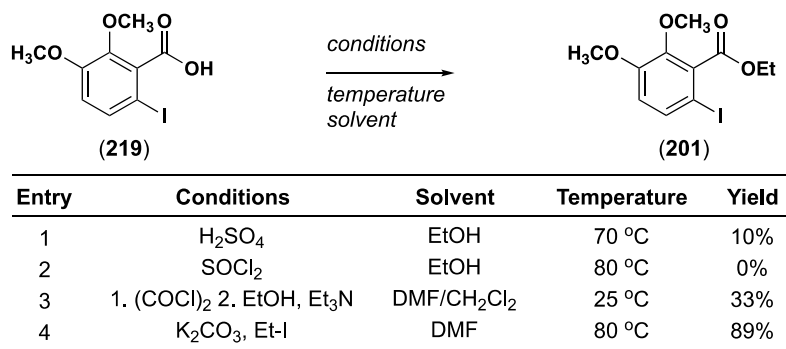


Figure 2.33 A. Accessing the iodo-ester (**201**) intermediate **B.** Esterification condition optimization.

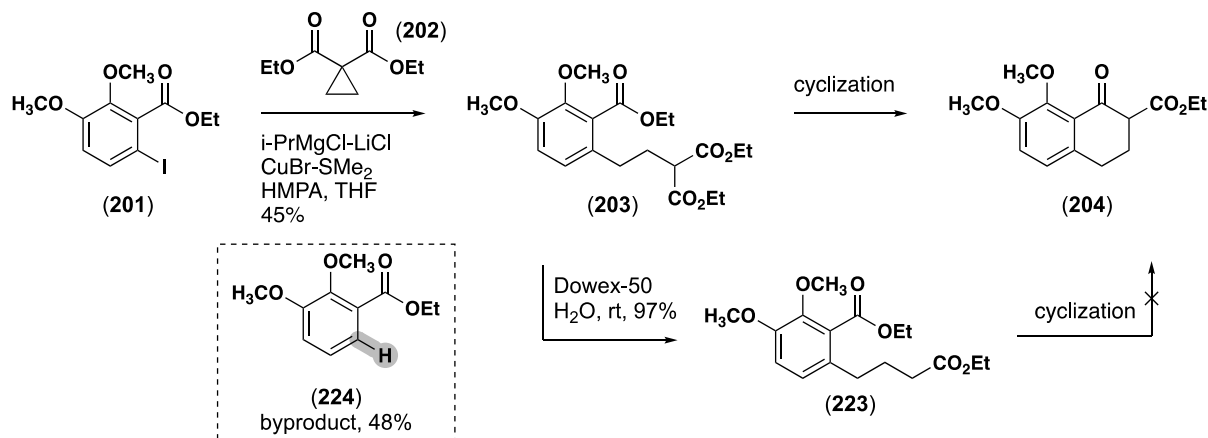
Since the initial esterification was low yielding, another route to the iodo-ester (**201**) was explored. The hypothesis for the poor yielding esterification was that the large aryl iodine increased steric congestion around the electrophilic carbonyl site, thereby disfavoring nucleophilic attack by ethanol. Therefore, switching to an aryl bromide with a smaller atomic

radius may help increase the yield of the esterification (Figure 2.33A). The aryl bromide could subsequently be transformed into the aryl iodide through a Finkelstein reaction. Stirring 2,3-dimethoxy-benzoic acid (**200**) in 1.4 M NaOH solution with *N*-bromosuccinimide (NBS) regioselectively gave the mono-brominated ortho product (**220**) in 92% yield.¹⁴⁶ As soon as this aryl bromide-carboxylic acid (**220**) was made, the high-yielding K₂CO₃ with iodoethane esterification conditions with the aryl iodo-carboxylic acid (**219**) was discovered. However, in case the aryl bromide analog would be needed for troubleshooting the homoconjugate addition step, it was pushed forward through esterification. The same K₂CO₃ with iodoethane conditions gave the aryl bromide-ester (**221**) intermediate in 79% yield. Some of that material was set aside, and the rest was transformed from the aryl bromide (**221**) to the aryl iodide (**201**). The optimal Finkelstein reaction used oven-dried sodium iodide, catalytic copper iodide, and catalytic *N,N*-dimethylcyclohexane-1,2,-diamine refluxing in dioxanes to afford the aryl iodide (**201**) in 80% yield.

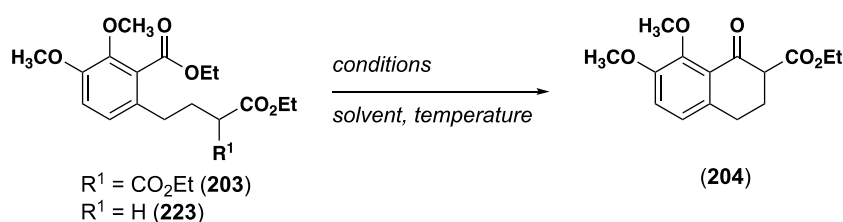
Now that the iodo-ester (**201**) intermediate was in hand, the homoconjugate addition could be attempted (Figure 2.34A). The aryl iodide (**201**) was pre-stirred with Turbo Grignard™ in THF at -78 °C for 30 minutes. Then a heterogeneous mixture of copper (I) bromide dimethyl sulfide complex in THF and HMPA was added, followed by in-house synthesized¹⁴⁷ diethyl cyclopropane-1,1-dicarboxylate (**202**). The reaction was left to stir overnight while allowing it to warm to room temperature. However, after 24 hours, the reaction had not converted to any of the desired product only the starting material (**201**) and proto-deiodination byproduct (**224**) was re-isolated. It was believed that the in-house synthesized cyclopropane must have possessed impurities that were interfering with the reaction. Therefore, after waiting a couple of weeks for the commercially available diethyl cyclopropane-1,1-dicarboxylate (**202**) to arrive, the reaction was attempted again and gave the desired dicarbonyl intermediate (**203**), and the proto-deiodination byproduct (**224**) in 45% and 48% yield, respectively. The

homoconjugate addition was not optimized further since the focus shifted to attempting to get the Dieckmann annulation to work.

A. Homoconjugate addition and cyclization



B. Cyclization screening



Entry	Starting Material	Conditions	Solvent	Temperature	Yield
1	dicarbonyl (203)	MgBr , Et_3N	Me-THF	$60\text{ }^\circ\text{C}$	NR*
2	dicarbonyl (203)	MgBr , Et_3N	Me-THF	μW , $80\text{ }^\circ\text{C}$	NR
3	ester (223)	MgBr , Et_3N	Me-THF	$60\text{ }^\circ\text{C}$	NR
4	dicarbonyl (203)	NaOEt , Et_3N	THF	$60\text{ }^\circ\text{C}$	NR
5	ester (223)	NaOEt , Et_3N	THF	$60\text{ }^\circ\text{C}$	NR
6	dicarbonyl (203)	NaH	THF	$60\text{ }^\circ\text{C}$	NR
7	ester (223)	NaH	THF	$60\text{ }^\circ\text{C}$	NR
8	dicarbonyl (203)	AlCl_3 , Et_3N	THF	$60\text{ }^\circ\text{C}$	98%
9	ester (223)	AlCl_3 , Et_3N	THF	$60\text{ }^\circ\text{C}$	NR

* NR = no reaction, only starting material reisolated

C. Decarboxylation

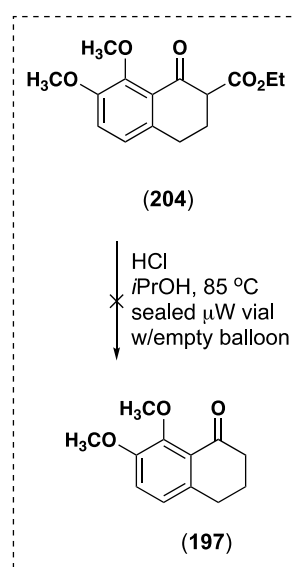


Figure 2.34 A. B-ketoester synthesis B. Decarboxylative Dieckmann annulation screening C. α -decarboxylation on tetralone core.

The dicarbonyl ester (203) intermediate could undergo a Dieckmann annulation to yield the desired tetralone core (204). However, the mild conditions reported in the paper utilizing magnesium bromide with triethylamine in Me-THF at reflux did not give any reaction on our substrate (203) (Figure 2.34B entry 1).¹⁴⁴ Trying to force the reaction in the microwave also gave no reaction (Figure 2.34B entry 2). In the published paper on the cyclization conditions,

none of the substrates possessed an electron-donating substituent ortho to the ester electrophile. We hypothesized that the decrease in electrophilicity of the ester, as well as the increased steric interactions in the product from this substitution pattern, was causing issues. Therefore, the di-carbonyl intermediate (**203**) was decarboxylated using Dowex-50 resin in water to yield the mono-ester intermediate (**223**) quantitatively. Then both the mono- and di-carbonyl intermediates were screened against harsher annulation conditions to see if tetralone (**204**) could be formed (Figure 2.34B). Using stronger bases, sodium ethoxide, and sodium hydride, with heat, gave no reaction for either substrate (Figure 2.34B entries 4-7). Switching to the Lewis acid AlCl_3 with triethylamine enabled the intramolecular annulation to proceed in high yield with the di-carbonyl intermediate (**203**) (Figure 2.34B entry 8).

Finally, all that was left was to decarboxylate the alpha position on the tetralone (**204**) to give the desired tetralone intermediate to push forward to C-H insertion. However, the reported decarboxylation conditions with HCl refluxing in isopropanol only degraded the starting material (**204**) (Figure 2.34C). The failed decarboxylation, coupled with very limited precedent for other decarboxylation conditions, eventually led us to abandon this route in favor of proceeding forward with the promising “tetralone” route.

2.3.7 7-methoxytetralone route

Taking a step back to evaluate the pros and cons of the Friedel-Crafts route with halogen analogs route, the thioacetal annulation route, and the cyclopropane addition/decarboxylative annulation route, all three routes explored had one common roadblock. The formation of the tetralone with the *ortho*-methoxy already installed was proving difficult and low-yielding. Therefore, we began exploring whether we could start with the tetralone already formed and then install the aryl functionality *en route* to the fused tricyclic core (Figure 2.35). Once we stopped restricting ourselves to routes where the methoxy ortho to the ketone was pre-installed, it opened many more route options. Excitingly, I discovered that the 7-methoxytetralone (**225**)

was commercially available. From the 7-methoxytetralone (**225**), only the ortho C–O bond would need to be installed to access the desired tetralone (**199**) C–H insertion precursor.

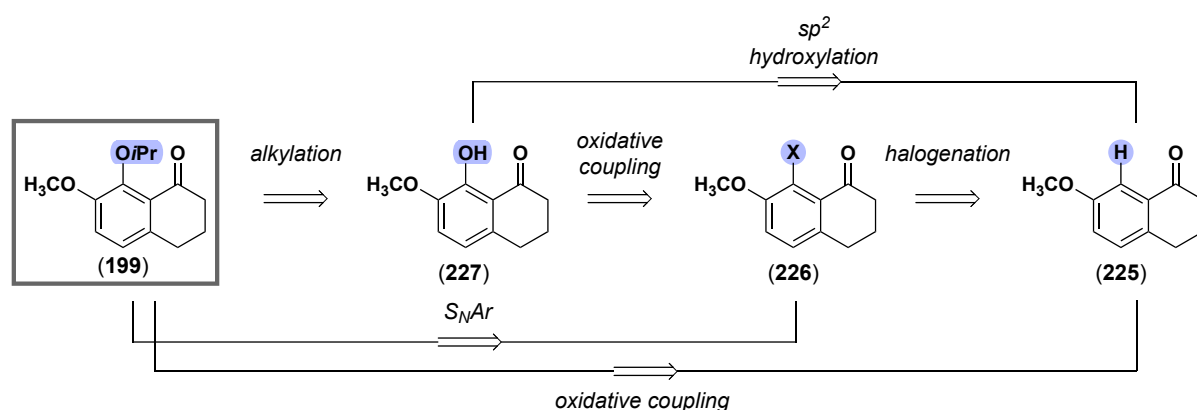


Figure 2.35 Retrosynthesis of tetralone (**199**) intermediate to 7-methoxytetralone (**225**).

C–O bond formation could be done in one step from 7-methoxytetralone (**225**) by an oxidative coupling to give the sp^2 alkoxylation product (**199**). However, the literature precedent was extremely limited and not feasible to be able to access other ether C–H insertion centers for related natural products in the sub-family.^{148–151} Another option would be direct sp^2 hydroxylation of tetralone **225** to form the phenol **227**. Although there are many options for the hydroxylation of a benzene ring, most methods aren't selective for the more hindered position on the aryl ring.^{152–161} Directing groups are usually needed to be selective for this position,^{162–164} however, the tetralone ketone isn't an ideal directing group. The carbonyl oxygen is a weaker sigma donor than oximes, amides, carboxylic acids, and ester directing groups.¹⁶⁵ Also, many of the oxidation reactions require harsh oxidants prone to undesirable side reactions with the enolizable alpha protons on the tetralone or the alpha C–C bond, such as Baeyer-Villiger oxidation.¹⁶⁶

A third option was the halogenation of the starting tetralone (**225**), which had direct precedent for regioselective fluorination^{167,168} and bromination^{169,170} of 7-methoxytetralone (**225**) to our desired halogenation 8-position (**226**). From the halogenated tetralone (**226**), the desired ether (**199**) could be directly formed through an *S_NAr* reaction, where there are

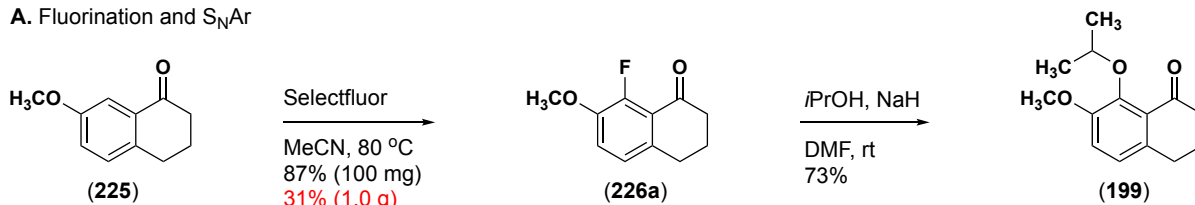
analogous examples with hindered secondary alcohol nucleophiles and aryl rings possessing enolizable protons.^{169,171–173} Due to all the above factors, the halogenation to S_NAr route was chosen to be explored first since it had the most robust and direct literature precedent.

2.3.7.1 Fluorination of the 7-methoxytetralone

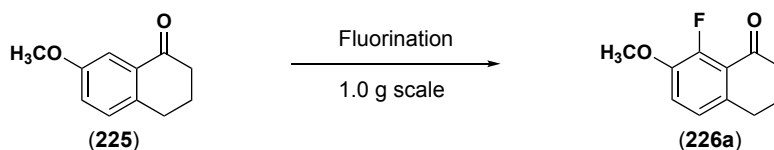
We decided first to fluorinate 7-methoxytetralone (**225**) since there was direct literature precedent,¹⁶⁷ and fluorine would serve as the best leaving group for the subsequent S_NAr reaction. Selectfluor in acetonitrile at 80 °C overnight regioselectively fluorinated the tetralone (**224**) in the 8-position yielding 7-methoxy-8-fluoro-tetralone (**226a**) in 87% yield (Figure 2.36A). However, the 87% yield was obtained from a 100 mg scale reaction. Whenever the reaction was repeated on a gram scale or above, the reaction yield dropped to 31% (Figure 2.36B entry 1). Interestingly, the remainder of the mass recovery was solely unreacted starting material. The fluorination reaction was the first reaction of the synthesis. Therefore it needed to be able to be run on a 10-20 gram scale ideally and minimally a 1 gram scale that could be run in a high-throughput batch set-up to bring material up. Since the starting material ceased converting on a larger scale, we hypothesized that aggregation of the DABCO scaffold of the Selectfluor byproduct with either Selectfluor or the starting tetralone (**225**) interfered with the reaction.¹⁷⁴ Reducing the temperature of the reaction to 60 °C and sonicating the reaction to help break up aggregates did not change the yield or conversion at all (Figure 2.36B entry 2). Portion-wise addition of Selectfluor over time only slowed the reaction rate and dropped the overall isolated yield (Figure 2.36B entry 3). Further solvent and temperature screens were conducted by Andy Hsieh, but these showed no improvement in yield. This was in agreement with reported process chemistry routes using Selectfluor, where acetonitrile was the optimal solvent, and the ideal temperature range for conversion was between 60 °C to 80 °C.¹⁷⁵ Switching to N-fluorobenzenesulfonimide (NFSI), a different electrophilic fluorine source,

gave no conversion of the starting material (**225**) (Figure 2.36B entry 4). Even Pd(OAc)₂ and AgNO₃ catalyzed conditions with NSFI showed no reaction with the tetralone core (**225**) (Figure 2.36B entry 5).¹⁷⁶

A. Fluorination and S_NAr



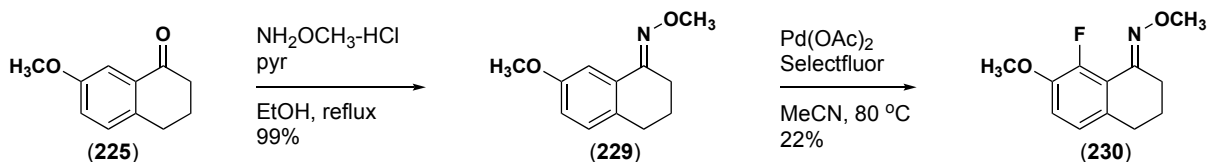
B. Fluorination scaling optimization



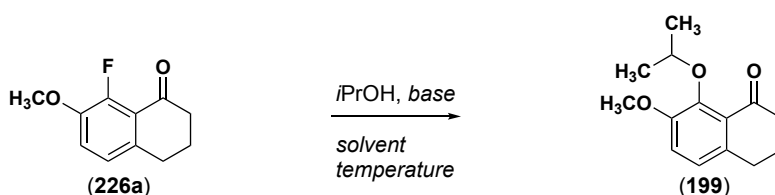
Entry	Fluorination Reagent	Conditions	Solvent	Temperature	Yield
1	Selectfluor	-	MeCN	80 °C	31%
2	Selectfluor	-	MeCN	60 °C, sonication	30%
3	Selectfluor	portion-wise addition	MeCN	80 °C	14%
4	NFSI	Ag ₂ CO ₃	CH ₂ Cl ₂	85 °C	no conversion
5	NFSI	Pd(OAc) ₂ , AgNO ₃	MeCN	80 °C	no conversion

(228)

C. Directed fluorination



D. S_NAr screening



Entry	Base	Solvent	Temperature	Yield
1	K ₂ CO ₃	MeCN	80 °C	0%
2	CS ₂ CO ₃	MeCN	80 °C	0%
3	NaH	DMF	80 °C	45%
4	NaH	DMF	40 °C	65%
5	NaH	DMF	25 °C	66%
6	NaH	DMF	25 °C	73%

(prestir with *i*PrOH)

Figure 2.36 **A.** Initial fluorination and S_NAr on tetralone core **B.** Scalable fluorination conditions screening **C.** Directed fluorination attempt **D.** S_NAr optimization.

The ketone on the tetralone (**225**) was cleanly converted into the methyl-oxime (**229**), which would serve as a stronger directing group. The oxime (**299**) was subjected to palladium-catalyzed directed fluorination with Selectfluor in acetonitrile at 80 °C. Unfortunately, these conditions only afforded the desired fluorinated oxime (**230a**) in 22% on a 1 gram scale (Figure 2.36C).

While the scalable fluorination conditions were being screened, the subsequent S_NAr step was explored (Figure 2.36D). Initially, fluorinated tetralone (**226a**) was stirred at reflux in acetonitrile with isopropanol and K₂CO₃ or Cs₂CO₃, resulting in no conversion (Figure 2.36D entries 1-2). The base in the S_NAr reaction was switched out for the stronger base, sodium hydride (NaH), and the desired ether (**199**) was obtained in 45% yield (Figure 2.36D entry 3). It was discovered that dropping the reaction temperature from 80 °C to room temperature slowed the starting material (**226a**) degradation pathway with NaH and increased the isolated yield to 66% (Figure 2.36D entries 4-5). Furthermore, pre-stirring NaH and isopropanol for 30 minutes before adding the fluorinated tetralone (**226a**) gave the highest yield for the S_NAr at 73% (Figure 2.36D entry 6).

However, even though the S_NAr was working well, the inability of the fluorination reaction to be optimized on a 1 g scale or larger led us to abandon the fluorinated substrate and explore other halogenation reactions.

2.3.7.2 Bromination and chlorination of the 7-methoxytetralone

Once the fluorinated tetralone (**226a**) was abandoned, we attempted to access the chlorinated, brominated, and iodinated versions of the tetralone. 7-methoxytetralone (**225**) can be stirred at room temperature with NBS in acetonitrile to yield the regioselective bromination product (**226c**). However, the analogous reaction with NCS or with NIS in TFA gave no reaction. Therefore, the tetralone (**225**) was converted to the *O*-methyl oxime (**229**). The oxime

(**229**) could then direct the palladium-catalyzed bromination or chlorination of the tetralone to yield the 8-bromo (**230c**) or 8-chloro (**230b**) substrates in 78% and 88%, respectively.¹⁷⁷ The oxime (**230**) could be hydrolyzed back to the ketone by refluxing it with 2M HCl (aq) in dioxanes for 3 hours (Figure 2.37). All the bromination and chlorination yields replicated on a 10-gram scale, allowing us to push forward to the ether formation step.

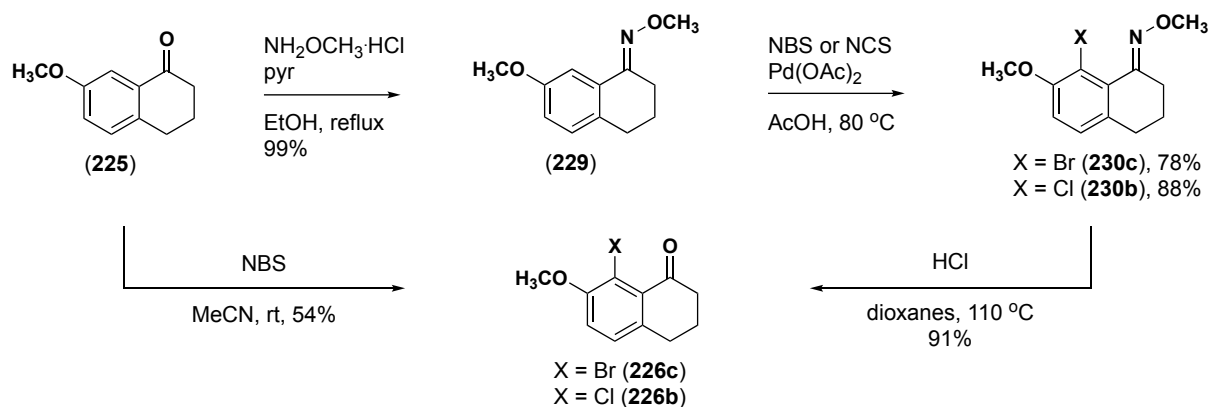
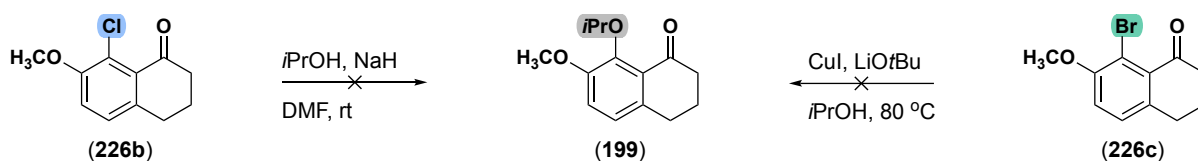


Figure 2.37 Bromination and chlorination of the 7-methoxytetralone (**225**).

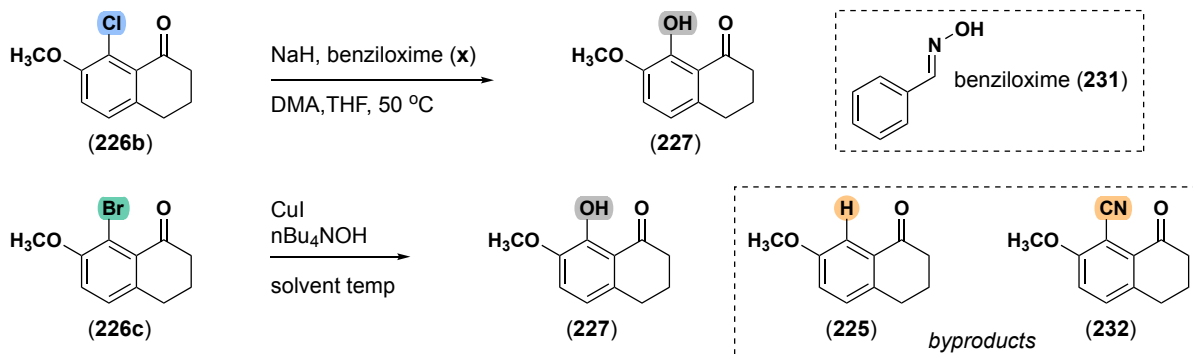
With the 8-bromo (**226c**) and 8-chloro (**226b**) tetralones in hand, we first attempted the working $\text{S}_{\text{N}}\text{Ar}$ conditions used with the 8-fluoro tetralone (**226a**). However, NaH with *i*PrOH in DMF failed to yield any product with either halogen analog. Reported etherification conditions¹⁷⁸ with the aryl bromide (**226c**) and CuI, lithium tert-butoxide, and isopropanol also only degraded the starting material (Figure 2.38A).

Since direct isopropylation conditions weren't working, hydroxylation conditions were tried next. This would only add one step to the synthesis, and we already knew the alkylation of phenol (**227**) to get ether (**199**) worked well. First, literature precedent on quinone derivatives showed that an aryl chloride ortho to the quinone ketone could be selectively hydroxylated using NaH and benziloxime (**231**) in a dimethylacetamide and THF mixture at 50 °C.¹⁷⁹ Applying this system to the 8-chlorotetralone (**226b**) gave no conversion.

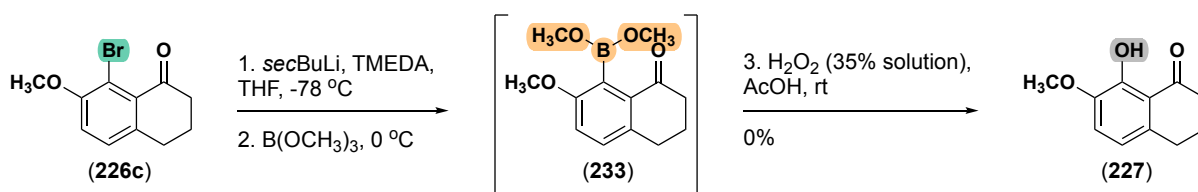
A. Isopropylation



B. Hydroxylation



Entry	Cu Catalyst	Solvent	Temperature	Major Product	Yield of X
1	CuI (powdered), 50 mol%	H ₂ O	80 °C	phenol 227	0%
2	CuI (powdered), 50 mol%	H ₂ O	90 °C	debromination 225	21%
3	CuI (powdered), 50 mol%	H ₂ O	100 °C	debromination 225	19%
4	CuI (powdered), 5 mol%	H ₂ O	100 °C	debromination 225	0%
5	CuI (powdered), 1 equiv	H ₂ O	100 °C	phenol 227	33%
6	CuI (powdered), 1 equiv	<i>n</i> Bu ₄ NOH	100 °C	phenol 227	24%
7	CuI (powdered), 20 mol%	H ₂ O:MeCN	100 °C	cyano 232	0%
8	CuI (np110), 20 mol%	H ₂ O	100 °C	phenol 227	10%



C. Methoxylation

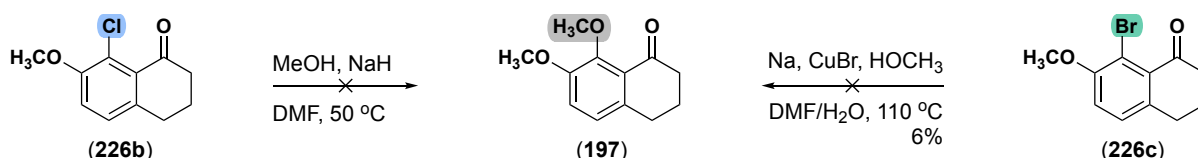


Figure 2.38 A. S_NAr attempts B. Hydroxylation attempts C. Methoxylation attempts

Next, a copper (I) iodide catalyzed hydroxylation was screened that used tertbutylammonium hydroxide (*n*-Bu₄NOH) as the hydroxide source.¹⁸⁰ The copper(I) iodide (CuI) could either be in a finely ground powder, or the optimal form were in synthesized nanoparticles with a radius of 110 nm. The increased surface area on the nanoparticles enabled

better catalysis at a lower mol loading (5 mol%). The finely ground CuI required higher loadings ranging from 20 mol% to a full stoichiometric equivalent based on the substrate. Half of an equivalent of powdered CuI was used first in H₂O at 80 °C, but no reaction occurred (Figure 2.38B, entry 1). Increasing the temperature to 90 °C afforded the desired phenol (**x**) in 21% yield but gave a significant amount of the debromination byproduct (**225**) (Figure 2.38B, entry 2). Increasing the temperature to 100 °C did not improve the yield at all and only increased the rate of byproduct formation (Figure 2.38B, entry 3). Increasing the loading of the CuI to one equivalent only marginally increased the isolated yield of the phenol (**227**) to 33% (Figure 2.38B, entry 5). Running the reaction neat in only tetrabutylammonium hydroxide with 1 equivalent of CuI showed no yield improvement (Figure 2.38B, entry 6). Because the reaction was run in aqueous conditions, the solvent system was switched to a 1:1 mixture of water and acetonitrile to help improve starting material (**226c**) solubility. Surprisingly, this led to full conversion to the 8-cyano tetralone (**232**) byproduct (Figure 2.38B, entry 7). Finally, the nanoparticles were synthesized according to the procedure published in the paper and employed in the reaction. Still, they gave the lowest yield thus far for the desired phenol (**227**) (Figure 2.38B, entry 8).

Another route from the 8-bromo (**226c**) starting material to the phenol (**227**) used *sec*-butyl lithium and TMEDA to undergo lithium-halogen exchange to form the aryl lithiate at -78 °C. Trimethoxyborane was then added to the lithiate solution. The reaction was warmed to 0 °C until the lithiate fully converted the aryl borate intermediate (**233**) *in situ*. Then hydrogen peroxide and acetic acid could be added to oxidize the borate (**233**) to the phenol (**227**) (Figure 2.38B).¹⁸¹ After working up the reaction, only the debromination byproduct was observed (**225**), suggesting that the lithium-halogen exchange occurred, but an addition to trimethoxyborane never occurred.

Finally, since the direct isopropylation and hydroxylation on the 8-bromo (**226c**) and 8-chloro (**226b**) substrates weren't working well, methoxylation reactions were screened (Figure 2.38C). S_NAr with methanol and NaH on the 8-chloro tetralone (**226b**) only led to the degradation of the starting material. Shockingly, reported conditions¹⁶⁹ that transformed the 8-bromo tetralone (**226c**) to the dimethoxytetralone (**197**) in near quantitative yield with sodium, copper (I) bromide, and methanol only afforded 6% of the desired product (**197**).

2.3.7.3 Accidental discovery of direct hydroxylation of 7-methoxytetralone

Another possible route for functionalizing the tetralone (**225**) was direct sp² hydroxylation in the 8-position (Figure 2.39). There was strong precedent for ortho hydroxylation to a ketone^{182,183} or other directing groups,^{155,162,184,185} but far less precedent for when the C–H bond of interest had two ortho substituents. One-step or one-pot sequential hydroxylation methods across various modes of C–H activation were attempted first, with the ketone on **225** serving as the directing group. Near quantitative reported conditions¹⁵⁴ with a di-ortho substituted flavanone and IBX were attempted but gave no conversion from 7-methoxytetralone (**225**) (Figure 2.39 entry 1). Next, ketone-directed palladium-catalyzed hydroxylation conditions with potassium persulfate as the oxidant in TFA at 50 °C also gave no conversion (Figure 2.39 entry 2). In this reported reaction, the aryl ring is acetoxyated with trifluoroacetate from TFA, which cleaves to the phenol upon workup.¹⁸³ However, neither the acetoxyated intermediate nor the desired phenol (**227**) were observed in the ¹H NMR spectrum after work-up. Ortho lithiation with *sec*-butyl lithium and TMEDA, followed by an attack on trimethoxyborane, and oxidation of the borate to the phenol (**227**) only yielded starting material (**225**) (Figure 2.39 entry 3).¹⁵² This result suggested that either the lithiate was not forming in the first place or the lithiate could not attack trimethoxyborane due to steric hindrance. Diradical C–H activation conditions using phthaloyl peroxide (**234**) can oxidize the phenyl ring through a reverse-rebound mechanism at low temperatures.¹⁵⁷ However, phthaloyl peroxide (**234**) did not react with 7-

methoxytetralone (**225**) (Figure 2.39 entry 4). The reaction could not be heated to higher temperatures due to known safety concerns with the peroxide (**234**). Finally, direct borylation with an iridium catalyst and silyl-ligand (**235**) never yielded the desired borate (Figure 2.39 entry 5).^{186,187}

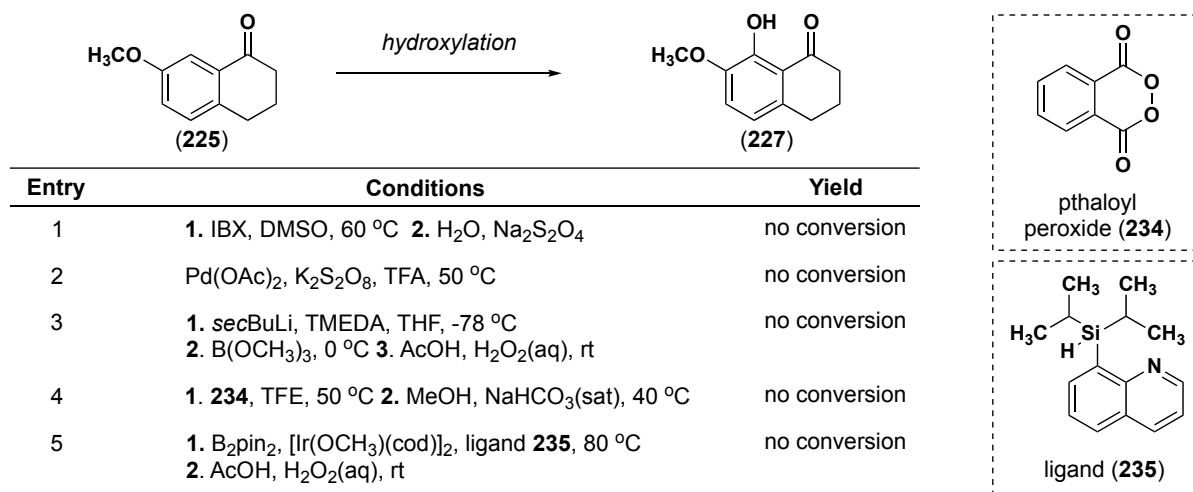


Figure 2.39 Direct hydroxylation attempts on tetralone (**225**).

Around the same time the direct hydroxylation attempts were being made (Figure 2.39), we were working on making the fluorination of 7-methoxytetralone (**225**) scalable (Figure 2.36B). One of the conditions we tried was a direct fluorination where 7-methoxytetralone (**225**) was converted into the *O*-methyl oxime (**229**). The oxime (**229**) was subjected to fluorination conditions consisting of palladium(II) acetate (5 mol%), Selectfluor (serving as the electrophilic fluorinating reagent), and acetic acid at reflux. However, these conditions only yielded the desired 8-fluoro oxime (**230a**) in 19% yield. We did notice a second product spot by TLC in the organic layer after the work-up. Since the reaction was conducted on a one-gram scale, it was easy to isolate the unknown compound. ¹⁹F NMR spectrum revealed that the isolated compound possessed no fluorine atoms, and the ¹H NMR spectrum confirmed that only the 8-position on the tetralone had been functionalized, and a phenol proton appeared to be present. We hypothesized that the substrate had undergone a palladium-catalyzed acetoxylation with acetic acid, where Selectfluor served as the oxidant to recycle the palladium

catalytic cycle.¹⁶⁷ The acetyl group was then hydrolyzed *in situ* from water present in the acetic acid yielding the phenol (**236**) in 10% yield (Table 2.7, entry 1). The use of Selectfluor as an oxidant in a palladium-catalyzed C–H hydroxylation isprecedented.¹⁸⁸ In the reported conditions, a nine-to-one mixture of trifluoroacetic acid (TFA) and trifluoroacetic anhydride (TFAA) is used as the solvent system. The more acidic solvent system helped increase reaction conversion significantly. Therefore, we re-attempted the palladium acetate and Selectfluor conditions but swapped out acetic acid for the TFA/TFAA system. The solvent swap gave exclusively phenol (**236**) product in 23% yield (Table 2.7, entry 2). We also tried using NFSI since it has a similar oxidant potential as Selectfluor, but it did not yield any fluorinated or hydroxylated tetralone (Table 2.7, entries 3-5).

Table 2.7 Discovery of hydroxylated oxime as a byproduct of directed fluorination conditions.

Entry	Catalyst	Fluorinating Reagent	Solvent	Temperature	Yield (230a)	Yield (236)
1	Pd(OAc) ₂	Selectfluor	AcOH	80 °C	19%	10%
2	Pd(OAc) ₂	Selectfluor	TFA/TFAA (9:1)	50 °C	0%	23%
3	Pd(OAc) ₂	NFSI	AcOH	80 °C	0%	0%
4	Pd(DBA) ₂	NFSI	AcOH	80 °C	NR	NR
5	Pd(TFA) ₂	NFSI	TFA	70 °C	0%	0%

The discovery of the hydroxylated byproduct gave us insight into why the previously discussed hydroxylation reactions weren't working (Figure 2.39). A stronger directing group, in this case the *O*-methyl oxime, must be needed to facilitate oxidative addition. The quick optimization to preference for the phenol byproduct (**236**) over the fluorinated product (**230a**) gave us hope that the hydroxylation reaction yield could be optimized.

2.4. Results and Discussion: second-generation route

Once we realized we needed a stronger directing group to form the desired C–O bond, our retrosynthetic strategy changed slightly (Figure 2.40) from our exploratory retrosynthetic

strategies (Figure 2.35). Luckily, this retrosynthesis ended up being our final route toward the dihydroxybenzoxanthone natural product family. The isopropyl ether intermediate (**199**) can come from the alkylation of phenol (**227**). The phenol (**227**) can be derived in two steps from C–H oxidation of the oxime (**229**) followed by hydrolysis of the oxime back to the ketone. The oxime (**229**) can easily be synthesized from the condensation of hydroxylamine on the ketone of 7-methoxytetralone (**225**).

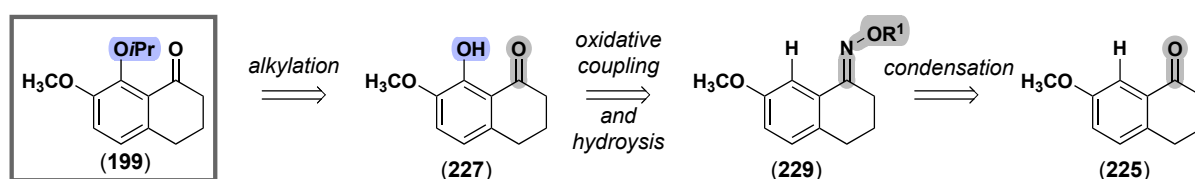
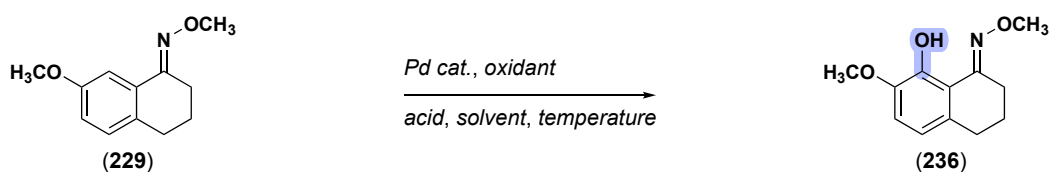


Figure 2.40 Revised retrosynthesis strategy.

2.4.1 Directed hydroxylation attempts and screening

Reaction optimization for the directed hydroxylation of the *O*-methyl oxime (**229**) began by screening different terminal oxidants, solvent systems, and -OH sources. The initial hit had used Selectfluor in a nine-to-one TFA/TFAA solvent mixture but only afforded phenol (**236**) in 23% (Table 2.8, entry 1). Doubling the catalyst loading had negligible effects on the yield (Table 2.8, entry 2). In the paper where the Rao group reported the TFA/TFAA conditions¹⁸⁸, oxone (potassium persulfate) was also an effective terminal oxidant. However, using K₂S₂O₈ did not afford any conversion of oxime (**229**) across multiple different solvent systems (Table 2.8 entries 3-5). Switching two other oxidants, *N*-fluorobenzenesulfonimide (NFSI) and [bis(trifluoroacetoxy)iodo]benzene (PhI(OTFA)₂), did not give any reaction conversion either, even with varying the temperature, catalyst, and solvent system (Table 2.8 entries 7-13). The exception was NFSI in acetic acid (AcOH). Where this combination of oxidant and solvent with Pd(OAc)₂ and Pd₂(dba)₃ gave a 16% and 23% yield of the desired product (**236**), respectively (Table 2.8, entries 6 & 14). A Wacker-type oxidation where copper (I) chloride served as the oxidant only afforded trace amounts of product (**236**) (Table 2.8, entries 16-17).

Table 2.8 Directed hydroxylation initial oxidant screen.

Entry	Catalyst	mol%	Oxidant	Solvent	Acid	Temp	Yield
1	Pd(OAc) ₂	5 mol%	Selectfluor	TFA:TFAA (9:1)	-	50 °C	23%
2	Pd(OAc) ₂	10 mol%	Selectfluor	TFA:TFAA (9:1)	-	50 °C	27%
3	Pd(OAc) ₂	5 mol%	oxone	AcOH	-	80 °C	0%
4	Pd(OAc) ₂	5 mol%	oxone	TFA	-	50 °C	0%
5	Pd(OAc) ₂	5 mol%	oxone	TFA:TFAA (9:1)	-	50 °C	0%
6	Pd(OAc) ₂	5 mol%	NFSI	DCE	AcOH	50 °C	16%
7	Pd(OAc) ₂	5 mol%	NFSI	MeCN	AcOH	50 °C	0%
8	Pd(TFA) ₂	5 mol%	NFSI	TFA	-	70 °C	0%
9	Pd(TFA) ₂	5 mol%	PhI(OTFA) ₂	DCE	-	50 °C	0%
10	Pd(TFA) ₂	5 mol%	PhI(OTFA) ₂	DCE	TFA	50 °C	0%
11	Pd(TFA) ₂	5 mol%	NFSI	TFA:TFAA	-	50 °C	0%
12	Pd(TFA) ₂	5 mol%	NFSI	DCE	TFA:TFAA	80 °C	0%
13	Pd(TFA) ₂	5 mol%	selectfluor	DCE	TFA:TFAA	80 °C	0%
14	Pd ₂ (dba) ₃	5 mol%	NFSI	AcOH	-	80 °C	22%
15	Pd ₂ (dba) ₃	5 mol%	selectfluor	AcOH	-	50 °C	9%
16	PdCl ₂	50 mol%	CuCl, air	AcOH	-	rt	5%
17	PdCl ₂	50 mol%	CuCl, air	DMF:H ₂ O	AcOH	rt	2%

The fact that oxone as an oxidant was not working for our reaction seemed odd, given how closely the reaction precedent was with oxone.^{185,188} However, upon closer investigation of one of those precedents, we noticed in the footer of a table that the Sanford group stated, “for most substrates, Oxone and K₂S₂O₈ afforded similar results; however, in some cases, significantly better yields were obtained with K₂S₂O₈. The reasons for this difference in reactivity are unclear at this time”.¹⁸⁵ The only difference between oxone and K₂S₂O₈ is that oxone is the monomer, and K₂S₂O₈ is the dimer of potassium persulfate. Therefore, we immediately re-tried the hydroxylation conditions with K₂S₂O₈ rather than oxone, yet we still obtained no reactivity (Table 2.9, entries 1-3). Interestingly, we found direct hydroxylation conditions from the Jiao group that also only used K₂S₂O₈ according to their SI and email correspondence, even though they refer to their oxidant as oxone in their paper.¹⁸⁹ In their paper, they needed a ligand, either triphenylphosphine (PPh₃) or diethyl azodicarboxylate (DEAD), in addition to palladium (II) acetate and a terminal oxidant to help catalyze the reaction. Adding PPh₃ or DEAD to the reaction in DCE did not improve reactivity (Table 2.9, entries 4-6). Instead, switching the

solvent to TCE so the reaction could be heated to higher temperatures proved successful. The addition of 5 mol% Pd(OAc)₂, 10 mol% of PPh₃, with K₂S₂O₈ in TCE at 100 °C afforded the hydroxylated product in 25% yield (Table 2.9, entry 11). However, the 25% yield was not any improvement on the original conditions with Selectfluor. Excitingly, doubling the catalyst and ligand loading doubled the reaction yield to 47% on a 500 mg scale (Table 2.9, entry 12).

Table 2.9 Second round of hydroxylation reaction condition screening.

Entry	Catalyst Loading	Oxidant	Ligand	Ligand Loading	Solvent	Temperature	Yield	Reaction scale
1	5 mol%	K ₂ S ₂ O ₈	-	-	TFA/TFAA (9:1)	50 °C	0%	50 mg
2	5 mol%	K ₂ S ₂ O ₈	-	-	AcOH	80 °C	0%	50 mg
3	5 mol%	K ₂ S ₂ O ₈	-	-	DCE	80 °C	0%	50 mg
4	30 mol%	DIAD	-	-	DCE	80 °C	0%	50 mg
5	5 mol%	K ₂ S ₂ O ₈	PPh ₃	10 mol%	DCE	80 °C	0%	50 mg
6	30 mol%	K ₂ S ₂ O ₈	DEAD	30 mol%	DCE	80 °C	0%	50 mg
7	5 mol%	PhI(OTFA) ₂	-	-	DCE	80 °C	0%	50 mg
8	5 mol%	PhI(OTFA) ₂	PPh ₃	10 mol%	DCE	80 °C	0%	50 mg
9	5 mol%	K ₂ S ₂ O ₈	PPh ₃	10 mol%	TCE	80 °C	0%	50 mg
10	5 mol%	oxone	PPh ₃	20 mol%	TCE	100°C	0%	200 mg
11	5 mol%	K ₂ S ₂ O ₈	PPh ₃	20 mol%	TCE	100°C	25%	500 mg
12	10 mol%	K ₂ S ₂ O ₈	PPh ₃	20 mol%	TCE	100 °C	47%	425 mg
13	5 mol%	K ₂ S ₂ O ₈	PPh ₃	10 mol%	MeCN	90 °C	51%	700 mg
14	5 mol%	K ₂ S ₂ O ₈ *	PPh ₃	10 mol%	MeCN	90 °C	16%	50 mg
15	5 mol%	K ₂ S ₂ O ₈	PPh ₃	20 mol%*	MeCN	90 °C	35%	1.0 g
16	5 mol%	K ₂ S ₂ O ₈	PPh ₃	20 mol%	MeCN	90 °C	30%	1.0 g
17	10 mol%	K ₂ S ₂ O ₈	PPh ₃	20 mol%	MeCN	90 °C	28%	1.0 g
18	15 mol%*	K ₂ S ₂ O ₈	PPh ₃	30 mol%	MeCN	90 °C	22%	5.0 g
19	10 mol%	K ₂ S ₂ O ₈	PPh ₃	20 mol%	TCE, hexafluoropropanol	90 °C	19%	100 mg
20	5 mol%	K ₂ S ₂ O ₈	BINAP	10 mol%	MeCN	90 °C	16%	50 mg
21	10 mol%	K ₂ S ₂ O ₈	PPh ₃	20 mol%	tert-BuCN	100 °C	28%	50 mg
22	10 mol%	K ₂ S ₂ O ₈	BINAP	20 mol%	tert-BuCN	100 °C	17%	50 mg

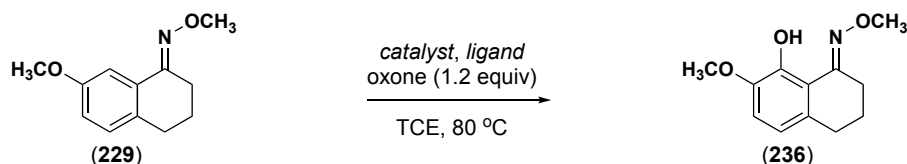
* portionwise addition of the reagent over 24 hours

A solvent screen found that acetonitrile marginally improved the yield to 51% of the desired product (**236**) and could do so on a relatively large scale (Table 2.9, entry 13). Unfortunately, as soon as the reaction was conducted on a one-gram scale or larger in acetonitrile, the yield of the reaction decreased significantly back to 22-30% (Table 2.9, entries 15-18).

At this point, we hypothesized that the slow reaction conversion was due to issues with the reductive elimination step of the catalytic cycle. The reductive elimination step tends to be the

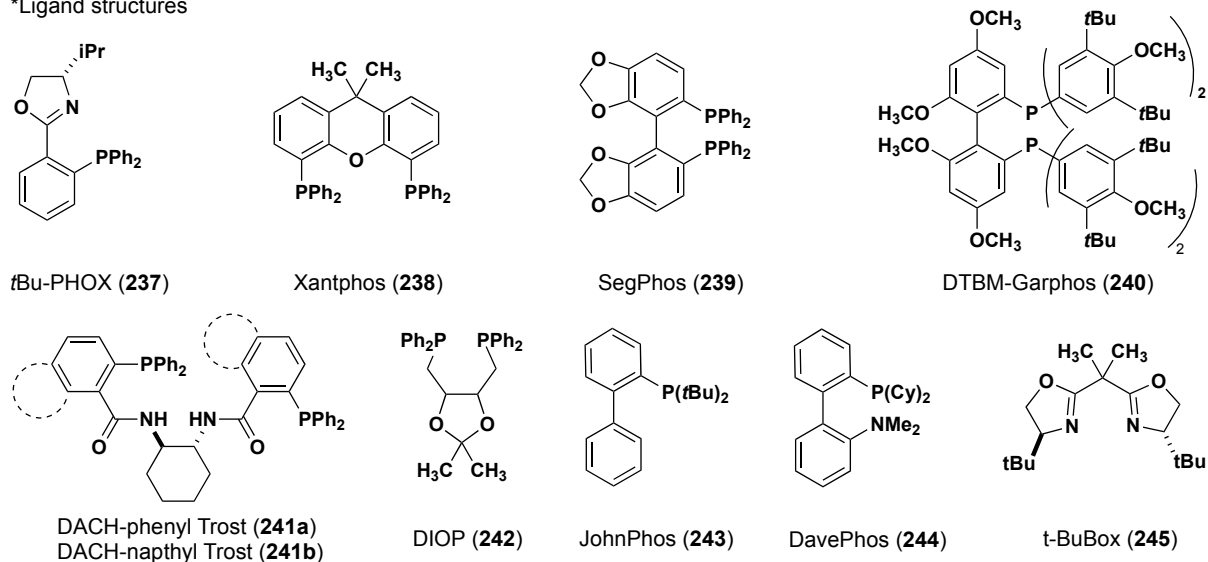
highest energy step and is aided by increasing the electron density donated from the ligands on palladium. A wide variety of ligands were screened in place of triphenylphosphine.

Table 2.10 Ligand screening.



Entry	Catalyst	Catalyst Loading	Ligand*	Yield
1	Pd(OAc) ₂	5 mol%	(<i>R</i>)-Segphos (239)	28%
2	Pd(OAc) ₂	5 mol%	P(OMe-Ph) ₃	37%
3	Pd(OAc) ₂	5 mol%	Xantphos (238)	27%
4	Pd(OAc) ₂	5 mol%	(+)-DIOP (242)	no reaction
5	Pd(OAc) ₂	5 mol%	BINAP	19%
6	Pd(OAc) ₂	5 mol%	TolBINAP	21%
7	Pd(OAc) ₂	5 mol%	(<i>R</i>)-DTBM-Garphos (240)	no reaction
8	Pd(OAc) ₂	5 mol%	(<i>R,R</i>)-DACH-phenyl-Trost (241a)	no reaction
9	Pd(OAc) ₂	5 mol%	(<i>R,R</i>)-DACH-naphthyl (241b)	no reaction
10	Pd(OAc) ₂	5 mol%	<i>t</i> Bu-Box (245)	34%
11	Pd(OAc) ₂	5 mol%	DavePhos (244)	28%
12	Pd(OAc) ₂	5 mol%	JohnPhos (243)	31%
13	Pd(PPh ₃) ₄	5 mol%	-	24%
14	Pd(PPh ₃) ₄	5 mol%	PPh ₃	22%
15	Pd(PPh ₃) ₄	10 mol%	PPh ₃	25%
16	Pd(PPh ₃) ₄	5 mol%	(<i>S</i>)- <i>t</i> Bu-PHOX (237)	29%
17	Pd(PPh ₃) ₄	10 mol%	(<i>S</i>)- <i>t</i> Bu-PHOX (237)	36%
18	Pd(PPh ₃) ₄	5 mol%	P(OMe-Ph) ₃	no reaction
19	Pd(PPh ₃) ₄	10 mol%	P(OMe-Ph) ₃	no reaction

*Ligand structures



The bulkier DTBM-Garphos (**240**) and DACH-phenyl/naphthyl Trost (**241a-b**) ligands gave no reaction (Table 2.10, entries 7-9). The bidentate Xantphos (**238**), Segphos (**239**), and *t*-

BuBox (**245**) ligands afforded analogous yields compared to PPh₃ (Table 2.10, entries 1, 3, 10). Tris(*p*-methoxyphenyl)phosphine gave the highest overall yield of hydroxylated product (**236**), but at only 37% (Table 2.10, entry 2), the reaction was still far from ideal.

2.4.1.1. Product inhibition theory

The inability to push the hydroxylation reaction past a 20-30% yield across dozens of reaction conditions led us to hypothesize that the reaction was undergoing product inhibition. The proposed catalytic cycle by Liang and coworkers¹⁸⁹ first has the triphenylphosphine ligand and Pd(OAc)₂ combination forming the active Pd^{II} catalyst (**246**) (Figure 2.41). The coordination of the nitrogen on the *O*-methyl oxime (**229**) followed by C–H activation of the 8-position of the tetralone produced intermediate **247**. Intermediate **247** is oxidized by the active oxidant peroxymonosulfate (**248**) derived from K₂S₂O₈ to form the Pd^{IV} species **249**. The Pd^{IV} complex (**249**) undergoes reductive elimination to afford the desired hydroxylated product (**236**) and regenerate the active Pd^{II} complex (**246**). We propose that once the product reaches a certain concentration in solution, it effectively inhibits the palladium catalyst. The paper reports a high-yielding reaction with an unsubstituted α -tetralone oxime. Still, the key difference with our substrate is the highly electron-donating methoxy substituent ortho to the phenol in the product (**236**). The increase in electron density in the ring system would make the phenol a stronger Lewis basic site primed to coordinate to the palladium complex. The phenol, combined with the strong nitrogen coordination site on the oxime, must bind at a competitive rate to the starting oxime (**229**) and ligands in the solution. It is possible that product coordination to the palladium complex could also catalyze a degradation pathway for the product (**236**). Hence poor mass recovery was observed across many of the screening reactions even after full starting material (**229**) consumption.

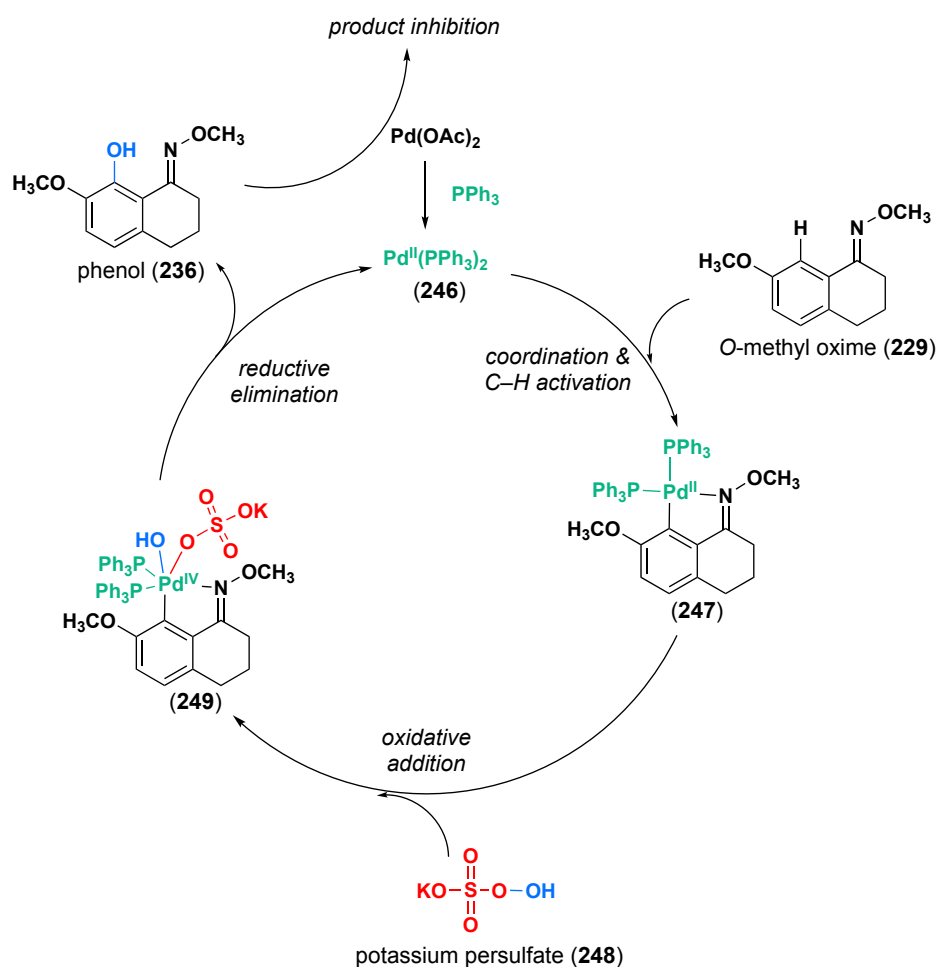


Figure 2.41 Directed hydroxylation catalytic cycle.

The product inhibition could occur at multiple stages of the catalytic cycle. A few control experiments run during the previously mentioned optimization (Table 2.8) can help point toward the more likely stages. Portion-wise addition of two equivalents of K₂S₂O₈ over 6 hours decreased the yield and conversion of the reaction (16%, Table 2.8 entry 14). The slow addition of 15 mol% Pd(OAc)₂ over 12 hours did not affect the yield or conversion of the reaction (22%, Table 2.8 entry 18). However, the portion-wise addition of 20 mol% PPh₃ ligand over 12 hours slightly increased the overall yield of the reaction (35%, Table 2.8 entry 15). Therefore, the addition of ligand over time suggests that extra PPh₃ is helping to outcompete the unproductive product coordination to Pd(OAc)₂. The definitive answer for where product inhibition occurs in the catalytic cycle remains unresolved.

2.4.2 Directed acetoxylation solution to product inhibition

The direct hydroxylation reaction capped out at 30% yield due to product inhibition from the tight binding of the newly formed phenol and *O*-methyl oxime in the product (**236**). One solution would be to acetylate the 8-position rather than hydroxylate (Figure 2.42). Therefore, the ester oxygen would not be as Lewis basic as the phenol and shouldn't exhibit the same product inhibition.¹⁹⁰ The acetyl group and oxime can then be hydrolyzed in the same step to afford the desired tetralone (**227**). This re-route would add no extra steps and can still be done in a one-pot sequential method from C–H functionalization to hydrolysis.

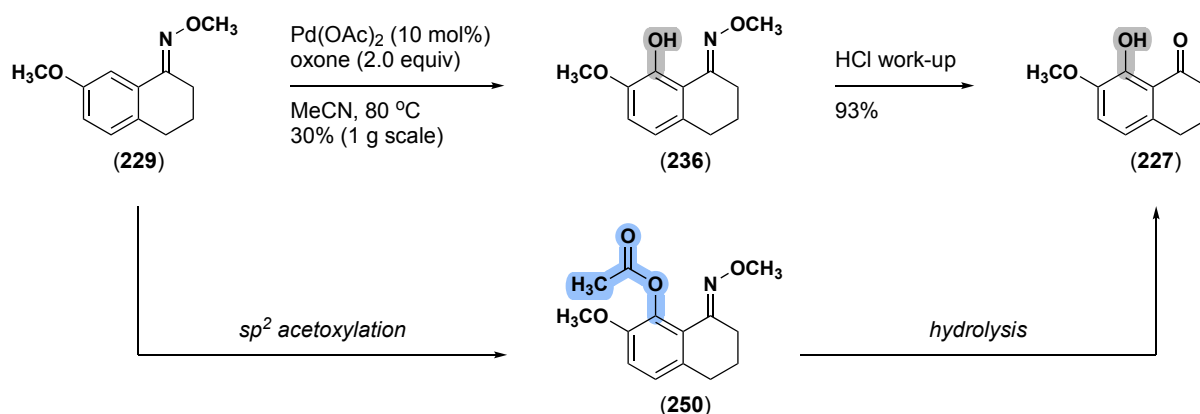


Figure 2.42 Directed acetoxylation workaround for product inhibition problem

There was good precedent for a palladium-catalyzed sp^2 acetylation with a benzylic *O*-methyl oxime or free oxime from the Sanford group^{185,191–193} and nitrogen directing groups from Jin-Quan Yu's group.¹⁹⁴ There were also reports of oxime directed sp^2 acetylation on a tetralone core from the He group¹⁹⁵ and the Sanford group.¹⁹⁶ As well as sp^2 acylation on a tetralone core from Wing-Yiu Yu's group.¹⁹⁷ Throughout these reports, *O*-methyl oxime directing groups had the highest yields, and almost every single procedure used bis(trifluoroacetoxy)iodobenzene (PIFA) or (diacetoxyiodo)benzene (PIDA) as the oxidant (Figure 2.43).

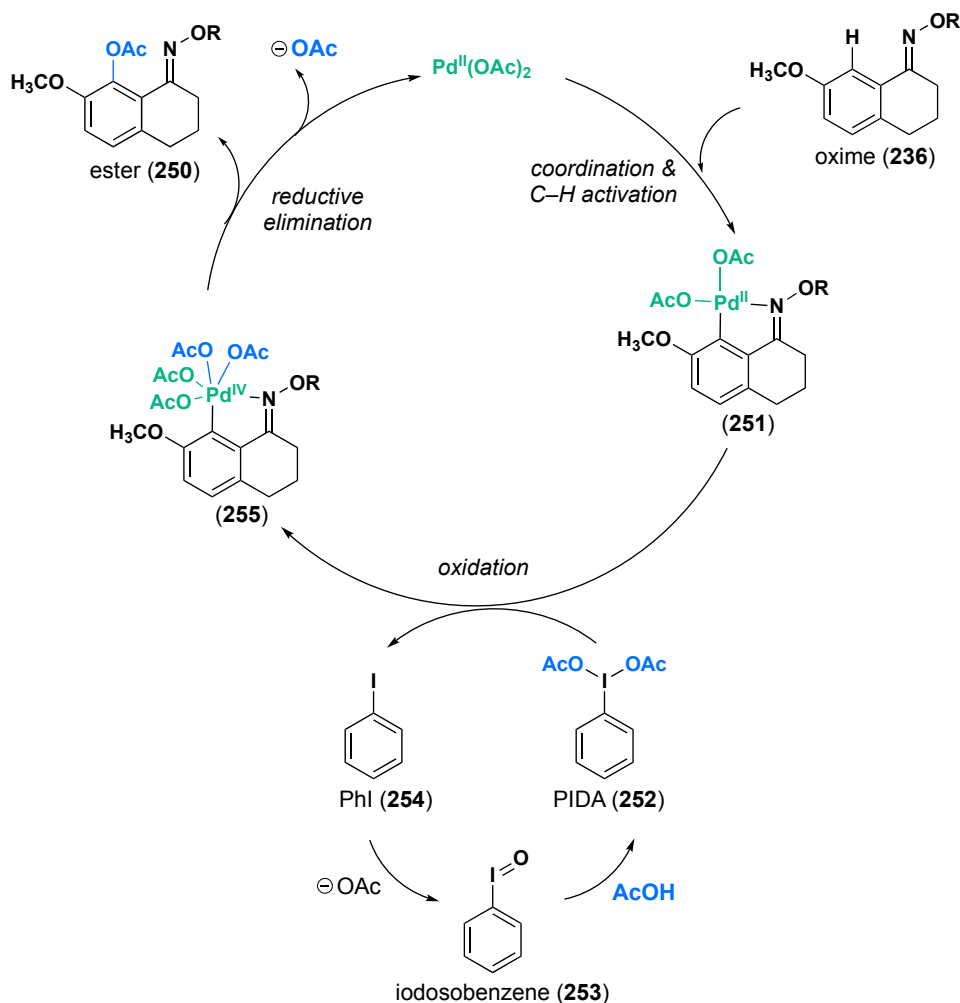


Figure 2.43 Palladium(II) acetate and PIDA oxime direct sp^2 acetoxylation catalytic cycle.

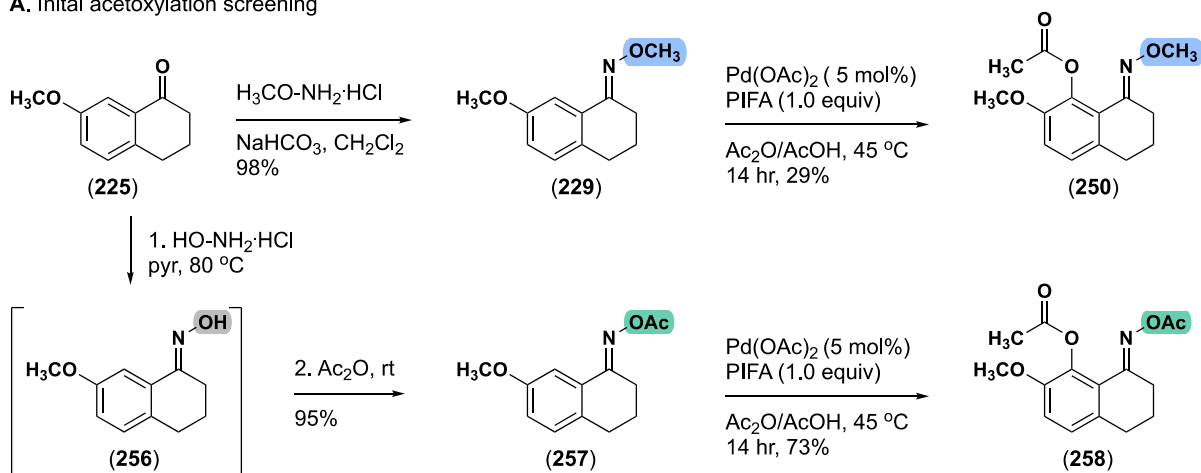
7-methoxytetralone (**225**) was quantitatively transformed into the O-methyl oxime (**229**). The oxime (**229**) was then subjected to acetoxylation conditions with 5 mol% palladium (II) acetate and one equivalent of PIFA in a 1:1 mixture of acetic anhydride (Ac_2O) and acetic acid ($AcOH$) at 45 °C. However, this reaction only yielded the desired acetoxyated oxime (**250**) in 29% yield (Figure 2.44A). Right around the time that these test reactions were conducted, the Sarpong group published a string of natural product papers that used oxime-directed palladium-catalyzed acetoxylation reactions in their syntheses of cephanolides A-D¹⁹⁸ and longiborneol sesquiterpenoids.^{199,200} However, the oximes used were *O*-acetyl oximes. Adapting the procedure from Lusi and co-workers,¹⁹⁹ 7-methoxytetralone (**225**) was transformed to the *O*-acetyl oximes (**257**) in 95% yield. The *O*-acetyl oxime (**257**) was then subjected to the same

acetoxylation conditions used with the *O*-methyl oxime (**229**). Gratifyingly this time, it afforded the desired acetoxyated product (**258**) in 73% yield. To confirm that the low yield for the hydroxylation reaction was indeed due to product inhibition and not the use of the wrong oxime, the *O*-acetyl oxime (**257**) was subjected to the best hydroxylation conditions. However, the reaction gave zero conversion of the starting material to the hydroxylated product.

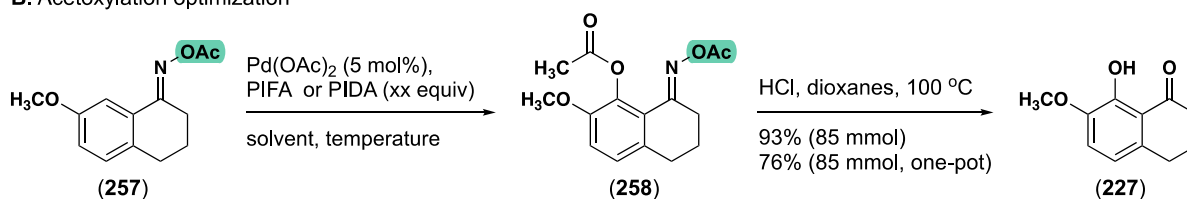
The acetoxylation reaction was screened to get the yield as high as possible (Figure 2.44B). First, the equivalents of PIFA were varied, and it was found that 0.9 equivalents of PIFA gave the highest best conversion and highest isolated yield affording product (**258**) in 83% yield on 85 mmol scale (Figure 2.44B, entries 1-6). Cutting the 1:1 Ac₂O:AcOH solvent system with additional solvents was attempted to make large-scale work-ups easier. However, the original solvent system maintained the highest yield (Figure 2.44B, entries 7-9). Decreasing the temperature to room temperature gave little to no conversion of the starting material (**257**) (Figure 2.44B, entry 10). Increasing the temperature of the reaction to 70 °C decreased the reaction yield to 43%, where the rest of the mass recovery was oxime (**257**) hydroxylzed back to the tetralone (**225**) (Figure 2.44B, entry 11).

PIDA was also screened as a possible oxidant in the catalytic cycle. However, in a 1:1 mixture of AcOH/Ac₂O, both 0.9 and 1.5 equivalents of PIDA only gave 29% and 45% yield, respectively (Figure 2.44B, entries 12-13). Switching to a 10:1 ratio of AcOH/Ac₂O as the solvent system and using 1.5 equivalents of PIDA at 70 °C gave a comparable 85% yield to the PIFA conditions (Figure 2.44B, entry 14). These conditions were also scalable, and the yield was repeated on an 85 mmol scale.

A. Initial acetoxylation screening



B. Acetoxylation optimization



Entry	PIFA	PIDA	HCl	solvent	temperature	yield (258)	yield (227)
1	0.2 equiv	-	-	AcOH/Ac ₂ O (1:1)	50 °C	22%	-
2	0.5 equiv	-	-	AcOH/Ac ₂ O (1:1)	50 °C	34%	-
3	0.9 equiv	-	-	AcOH/Ac ₂ O (1:1)	50 °C	83%	-
4	1.0 equiv	-	-	AcOH/Ac ₂ O (1:1)	50 °C	73%	-
5	1.2 equiv	-	-	AcOH/Ac ₂ O (1:1)	50 °C	33%	-
6	1.4 equiv	-	-	AcOH/Ac ₂ O (1:1)	50 °C	17%	-
7	0.9 equiv	-	-	AcOH/Ac ₂ O/MeCN (1:1:1)	50 °C	56%	-
8	0.9 equiv	-	-	AcOH/Ac ₂ O/EtOAc (1:1:1)	50 °C	72%	-
9	0.9 equiv	-	-	AcOH/Ac ₂ O/THF (1:1:1)	50 °C	28%	-
10	0.9 equiv	-	-	AcOH/Ac ₂ O (1:1)	25 °C	5%*	-
11	0.9 equiv	-	-	AcOH/Ac ₂ O (1:1)	70 °C	43%**	-
12	-	0.9 equiv	-	AcOH/Ac ₂ O (1:1)	50 °C	29%	-
13	-	1.5 equiv	-	AcOH/Ac ₂ O (1:1)	50 °C	45%	-
14	-	1.5 equiv	-	AcOH/Ac ₂ O (10:1)	70 °C	85%	-
15	-	1.5 equiv	-	AcOH/Ac ₂ O (10:1)	90 °C	76%	-
16	-	1.5 equiv	-	AcOH/Ac ₂ O (10:1)	70 °C to 100 °C [†]	17%	47%
17	-	1.5 equiv	20 equiv	AcOH/Ac ₂ O (10:1)	70 °C to 100 °C [†]	0%	54%
18	-	1.5 equiv	20 equiv	AcOH/Ac ₂ O (10:1)	70 °C to 70 °C [†]	0%	76%

*mass recovery = unreacted starting material

**mass recovery = hydrolyzed oxime

[†]acetoxylation reaction set up as normal, once starting material was consumed the indicated amount of HCl was added and the reaction temperature was increased to the indicated value

Figure 2.44 A. *O*-methyl oxime (**229**) and *O*-acetyl oxime (**247**) directed acetoxylation **B.**

Two-step and one-pot sequential sp² acetoxylation and hydrolysis.

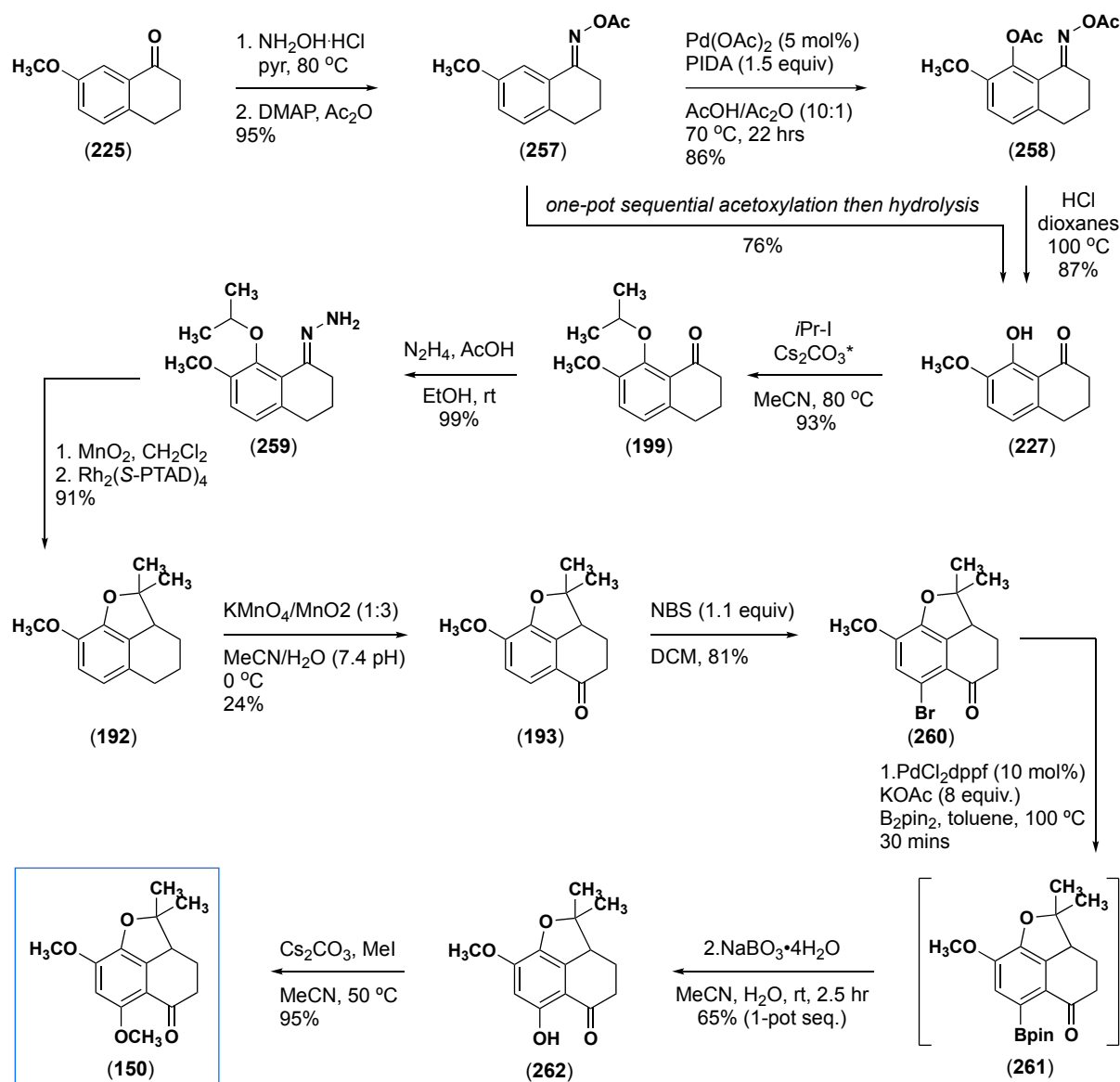
Excitingly, the new 10:1 AcOH/Ac₂O ratio was amendable to one-pot acetoxylation then hydrolysis conditions. On an 15g scale, the starting material (**257**) was subjected to the optimized acetoxylation conditions and heated overnight until the starting material was fully consumed to the product by TLC. Then 20 equivalents of HCl were added, and the reaction

was continued to be heated at 70 °C until all the acetoxylated product (**258**) was cleaved to the desired phenol (**227**). The one-pot sequential reaction afforded the desired phenol (**227**) in 76% yield, compared to the two-step procedure that gave a 79% yield over two steps. The caveat is that the one-pot sequential procedure is a more onerous work-up on a larger scale due to the PIDA byproducts and palladium (II) acetate mixing with HCl.

2.4.3 Right hemisphere: forward synthesis to insertion core

Now that the desired phenol intermediate (**227**) can be accessed reliably on a large scale in good yield, the synthesis of the right hemisphere could be continued (Figure 2.44). The phenol (**227**) was alkylated with isopropyl iodide and Cs₂CO₃ in MeCN at reflux to afford the ether (**199**) in a 93% yield. Next, condensation with hydrazine and acetic acid in ethanol at room temperature yielded hydrazone (**259**) quantitatively. Using the one-pot sequential C–H insertion method, the hydrazone (**259**) was oxidized to diazo with MnO₂ over 2 hours. The reaction was cooled to 0 °C, and a dirhodium catalyst was added to form metal carbene. The C–H insertion reaction is very fast and proceeds fully to completion in 5 minutes on a small scale and 30 minutes on a larger scale, affording the fused tricyclic core (**192**) enantioselectivity in 91% yield. See section 2.4.4 for further discussion on stereoselectivity optimization. The fused tricyclic core can then be oxidized by a KMnO₄/MnO₂ (1:3 w/w) mixture to afford ketone (**193**) in 24% on a multi-gram scale. See section 2.4.5 for further discussion on benzylic oxidation screening. From the ketone (**193**), a selective ortho bromination with NBS affords the aryl bromide (**260**) in 81% yield. Then, through a two-step or one-pot procedure, the bromine is transformed into the aryl Bpin (**261**), followed by oxidation to the phenol (**262**). The one-pot method affords the phenol (**262**) in a moderate 65% yield. The phenol (**262**) is then methylated near quantitatively to give the final desired right hemisphere (**150**) in 9 linear steps with an

overall yield of 7%. Further discussion of late-stage methods screened to install the methoxy group can be found in section 2.4.6.



* Cs_2CO_3 was ground up to a fine powder with a mortar and pestle and oven-dried overnight

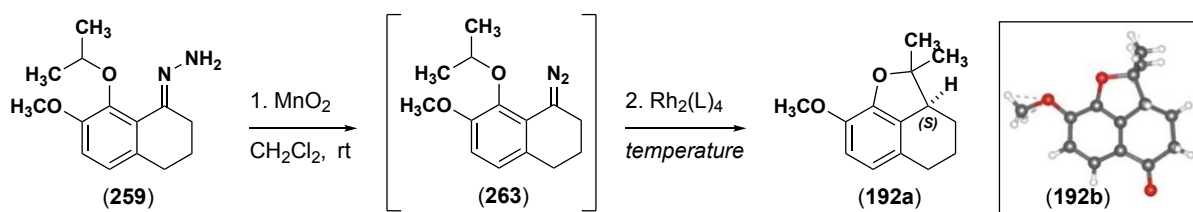
Figure 2.45 Forward route from 7-methoxytetralone (225) to the right hemisphere (150).

2.4.3.1 C–H insertion stereoselectivity optimization

Following the original right hemisphere conditions, the one-pot sequential C–H insertion reaction worked well on the new hydrazone precursor (259) (Figure 2.45). Gratifyingly, the reaction remained high yielding, affording the fused tricyclic core (192) in 91% yield on a multi-gram scale with 1 mol% of catalyst. On a multi-gram scale, the catalyst loading could be

dropped down to 0.01 mol%, and the yield only dipped to 76%. Like the previous route, a crystal structure of the ketone intermediate (**192**) after insertion was obtained and showed that the *R*-enantiomer of Rh₂(PTAD)₄ afforded the unnatural isomer (**192a**) (*R* stereocenter) (Table 2.11). Therefore, optimization for the enantioselectivity began with Rh₂(*S*-PTAD)₄.

Table 2.11 Enantioselectivity optimization for C–H insertion reaction.



Entry	Catalyst	Temperature	Time for C–H insertion	Yield (192)	er (<i>S</i> : <i>R</i>)*
1	Rh ₂ (mes) ₄	0 °C	10 min	53%	47:53
2	Rh ₂ (<i>R</i> -PTAD) ₄	0 °C	<1 min	83%	10:90
3	Rh ₂ (<i>R</i> -PTAD) ₄	-78 °C	5 min	88%	01:99
4	Rh ₂ (<i>S</i> -PTAD) ₄	0 °C	<1 min	89%	89:11
5	Rh ₂ (<i>S</i> -PTAD) ₄	-5 °C	<1 min	85%	87:13
6	Rh ₂ (<i>S</i> -PTAD) ₄	-40 °C	5 min	90%	94:06
7	Rh ₂ (<i>S</i> -PTAD) ₄	-78 °C	5 min	88%	96:04
8	Rh ₂ (<i>R</i> -BTCP) ₄	0 °C	1 min	82%	12:88
9	Rh ₂ (<i>S</i> -BTCP) ₄	0 °C	1 min	75%	88:12
10	Rh ₂ (<i>S</i> -TCPTTL) ₄	0 °C	<1 min	68%	67:33
11	Rh ₂ (<i>S</i> -PTTL) ₄	0 °C	<1 min	84%	94:06
12	Rh ₂ (<i>S</i> -PTTL) ₄	-78 °C	5 min	88%	99:01
13	Rh ₂ (<i>S</i> -PhenTTL) ₄	0 °C	<1 min	72%	89:11

* er determined by chiral HPLC

At 0 °C, Rh₂(*S*-PTAD)₄ afforded the desired *S* enantiomer of **192** as the major enantiomer in 89:11 er (Table 2.11, entry 4). Dropping the temperature to -40 °C increased the er to 94:06, but decreasing the temperature to -78 °C only led to a slight increase to 96:04 er (Table 2.11, entries 6-7). Next, other dirhodium catalysts were screened, and excitingly Rh₂(*S*-PTTL)₄ afforded the desired enantiomer of **192a** in 94:06 er at 0 °C (Table 2.11, entry 11). Decreasing the temperature of the reaction to -78 °C yielded the fused tricyclic core (**192a**) as a single enantiomer without affecting the yield (Table 2.11, entry 12).

2.4.4 Right hemisphere: benzylic oxidation attempts and screening

The purpose of re-routing the left hemisphere synthesis was to access a fused tricyclic core that could undergo benzylic oxidation reliably on a large scale and in a moderate to good yield.

However, the benzylic oxidation on the new substrate (**192**) exhibited many of the same issues as before (section 2.2.2). The fused tricyclic core was prone to overoxidation, where oxidants would afford the naphthalene core (**194**), the tertiary alcohol (**264**), or the quinone methide (**265**) rather than the desired ketone (**193**) (Figure 2.46). Also, scaling the reaction proved difficult, where moderate yields were obtained with some conditions on the screening scale (25mg), but those yields did not repeat on a larger scale (1 gram). Finally, many of the oxidants screened degraded either the starting material or the products. Therefore, even when ketone (**193**) was very cleanly obtained as the major product, there was never any mass recovery resulting in low yields.

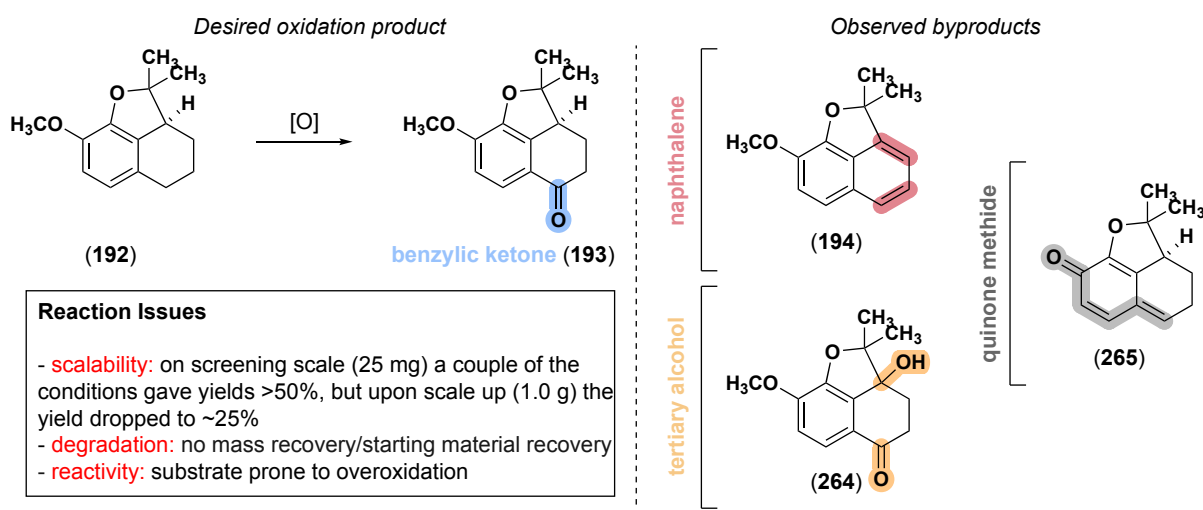


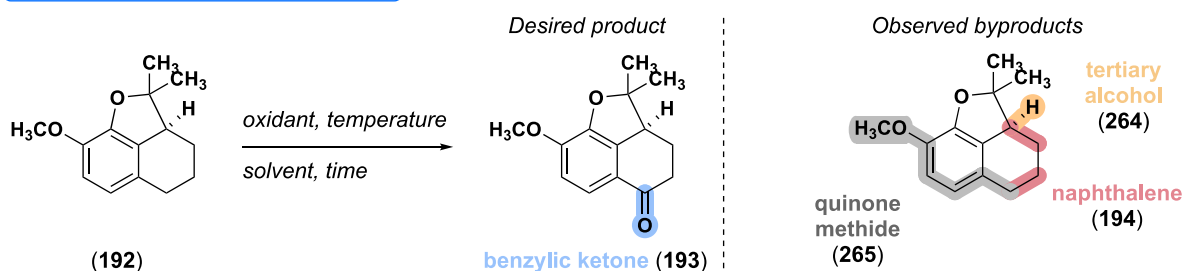
Figure 2.46 Overview of the benzylic oxidation reaction for fused tricyclic core **192**.

Starting with some of the best benzylic oxidation conditions on the old substrate (section 2.2.3), a multitude of oxidants were screened. PCC with celite afforded ketone (**193**) in 24% yield with no mass recovery (Table 2.12, entry 1). Decreasing the equivalents of PCC and the reaction temperature did not improve yield or mass recovery (Table 2.12, entry 2). We knew from previous experiments that the insertion core (**192**) was acid-sensitive, and acid generated in the PCC reaction might be leading to the degradation pathways. Therefore, less acidic chromium oxidizing conditions were attempted by using a neutralizing reagent or PDC with mol sieves (Table 2.12, entries 3-4).¹⁹⁸ However, neither condition gave any improvements in

yield and mass recovery. Iodosobenzene and KBr conditions gave ketone (**193**), but only in 10% yield (Table 2.12, entry 5).²⁰¹ IBX afforded ketone (**193**) in a comparable yield to PCC, 21% yield, but there was no mass recovery (Table 2.12, entry 8). Changing the work-up to sodium sulfite or switching to the catalytic generation of IBX *in situ* did not yield any desired product (Table 2.12, entries 9-11).²⁰²

Table 2.12 Screening of oxidants for the benzylic oxidation of **193**.

Benzylic oxidation conditions screened



Entry	Oxidant	Solvent	Temperature	Major product	Yield
1	PCC(10 equiv)/celite	benzene	80 °C	ketone (193)	24%
2	PCC (5 equiv)/celite	benzene	rt	ketone (193)	21%
3	PCC (5 equiv), NH ₄ OAc	DCE	80 °C	ketone (193)	trace
4	PDC, 4Å MS	CH ₂ Cl ₂ /DMF	rt	ketone (193)	26%
5	PhIO, KBr	H ₂ O	rt	ketone (193)	10%
6	Dess-Martin	THF	rt	ND*	-
7	DDQ	CH ₂ Cl ₂ /H ₂ O	rt	quinone methide (265)	-
8	IBX (2 equiv)	EtOAc	80 °C	ketone (193)	21%
9	IBX (3 equiv), Na ₂ SO ₃ wkup	EtOAc	80 °C	ND*	-
10	2-iodobenzoic acid, oxone	MeCN	rt	NR**	-
11	2-iodobenzoic acid, TBAH, oxone	MeCN	rt to 60 °C	NR**	-
12	CuSO ₄ ·H ₂ O, oxone	MeCN	60 °C	ND*	-
13	RuCl ₃ , oxone, PhI	MeCN/H ₂ O	rt	ND*	-
14	KBr, oxone	MeNO ₂	50 °C	NR**	-
15	KBr, oxone	CH ₂ Cl ₂ /H ₂ O	purple LEDS	NR**	-
16	KMnO ₄ /MnO ₂ (1:3 w/w)	CH ₂ Cl ₂	rt	ketone (193)	17% (90% brsm)
17	KMnO ₄ , MgSO ₄	acetone	rt	ketone (193)	22%
18	Mn(OAc) ₃ ·H ₂ O	DMSO	50 °C	NR**	-
19	Mn(OAc) ₃ ·H ₂ O	AcOH	50 °C	NR**	-
20	KMnO ₄ , Mn(OAc) ₃ ·H ₂ O	DMSO	70 °C	NR**	-
21	KMnO ₄ /CuSO ₄ ·H ₂ O	CH ₂ Cl ₂	sonicate, rt	ND*	-
22	CuCl, NHPI, O ₂	PhCN	30 °C	ND*	-
23	TEMPO, CAN, O ₂	MeCN	90 °C	ketone (193)	63% (86% brsm)
24	CeCl ₃ ·7H ₂ O, NaHCO ₃ , air	MeCN	blue LEDS	NR**	-
25	SeO ₂ , KH ₂ PO ₄	dioxanes/H ₂ O	110 °C	NR**	-
26	RuCl ₃ ·H ₂ O, KBrO ₃ , pyr	MeCN/H ₂ O	60 °C	naphthalene (194)	-
27	CoCl ₂ , <i>i</i> PrCHO, O ₂	DCE	rt	NR**	-
28	HCl (15 mol%), air	MeCN	visible light	NR**	-
29	Fe(NO ₃) ₃ ·H ₂ O, NHSI, O ₂	PhCN	90 °C	nitrated byproduct (266)	-
30	Fe(OAc) ₃ , NHSI, O ₂	PhCN	90 °C	ND*	-
31	Rose bengal (1 mol%), Al ₂ O ₃	PhCl	90 °C	NR**	-
32	Rose bengal (1 mol%), Al ₂ O ₃	MeCN/CH ₂ Cl ₂	blue LEDS	ketone (193)	trace
33	tert-butyl nitrile, NHPI, O ₂	MeCN/acetone	90 °C	NR**	-
34	Rh ₂ (cap) ₄ , NaHCO ₃ , tBuOOH	DCE	40 °C	ND*	-
35	Fe(PDP), AcOH, H ₂ O ₂	MeCN	rt	ND*	-

* ND = major product not determined due to messy reaction/degradation

** NR = no reaction

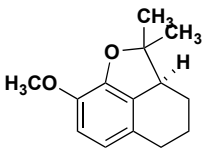
Many mild oxidations of tetralin use oxone; however, when those oxone conditions were screened, they gave no reaction or degradation (Table 2.12, entries 12-15).^{97,99,203,204} Excitingly, when a mixture of ground $\text{KMnO}_4/\text{MnO}_2$ (w/w) was used as a heterogenous oxidant in CH_2Cl_2 , ketone (**193**) was yielded in 17%, and the starting material (**192**) was fully recovered (Table 2.12, entry 16).²⁰⁵ Interestingly, these oxidations conditions gave no reaction on the old insertion core (**192**). Switching out the MnO_2 for MgSO_4 afforded ketone in 22% yield but gave no starting material recovery (Table 2.12, entry 17). Other potassium permanganate and manganese-based oxidant systems afford no ketone (Table 2.12, entries 18-21).²⁰⁶⁻²⁰⁹ A ruthenium-catalyzed sp^3 hydroxylation system by the Du Bois group²¹⁰ was attempted, but it cleanly afforded naphthalene byproduct (**194**) (Table 2.12, entry 26). A cobalt-catalyzed singlet oxygen system by the Powers group,²¹¹ a catalytic HCl aerobic oxidation,²¹² and a Rose bengal photosensitizer singlet oxygen system²¹³ all reported high yields for oxidation of tetralin to tetralone but afforded no reaction on our insertion core (**192**) (Table 2.12, entries 27-28, 31-32). Iron-catalyzed systems such as the White-Chen aliphatic C–H oxidation catalyst²¹⁴ (Table 2.12, entry 35) and the Ir(III)-NHSI tandem oxidant system²¹⁵ (Table 2.12, entries 29-30) only led to degradation. Finally, a tandem TEMPO/Ceric Ammonium Nitrate (CAN) aerobic oxidation method gave the best yield to date.²¹⁶ The reaction afforded the desired ketone in 63% isolated yield and 86% based on recovered starting material (Table 2.12, entry 23).

The TEMPO/CAN oxidant system was promising on a small scale (40 mg), affording the ketone (**193**) in 63%, the nitration byproduct (**266**) in 13%, and the rest of the mass recovery being unreacted starting material (**192**) (Table 2.13, entry 2). However, when the results were repeated on the same scale, only the nitrated byproduct was isolated (Table 2.13, entry 3). CAN is reported to nitrate electron-rich aromatic rings at room temperature. It was hypothesized that in the first reaction addition of CAN occurred while the reaction was already close to 90 °C, and in the second reaction, CAN addition occurred at room temperature. Therefore, the

nitration pathway was favored over oxidation. The reaction was repeated on a larger scale, and CAN was added once the reaction had reached 90 °C. However, these conditions still gave the nitrated byproduct (**266**) as the major product in 50% yield, and the ketone was the minor product in 37% yield (Table 2.13, entry 4). The reaction was attempted without CAN since, feasibly, O₂ is a strong enough oxidant to re-oxidize TEMPO. The absence of the secondary oxidant, CAN, gave no reaction (Table 2.13, entry 5). Alternative secondary oxidants were then screened, ranging from I₂²¹⁷, cerium(IV) ammonium sulfate (CAS), cerium(III) chloride, and many others. Unfortunately, none of these secondary oxidants gave any reaction (Table 2.13, entries 6-14).

Table 2.13 TEMPO/CAN reaction optimization.

Co-oxidants screened for conversion



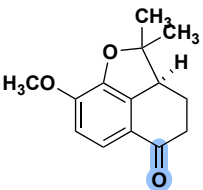
(192)

TEMPO (equiv)
co-oxidant, O₂

→

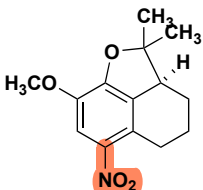
temperature
solvent, time

Desired product



benzylic ketone (193)

Observed byproduct



nitration (266)

Entry	TEMPO equivalents	Co-oxidant	Solvent	Temperature	Reaction scale	Yield (193)	Yield (266)
1	10 mol%	CAN (20 mol%)	MeCN	rt to 90 °C	15 mg	0%	25%
2	20 mol%	CAN (40 mol%)	MeCN	90 °C	40 mg	63%	13%
3	20 mol%	CAN (40 mol%)	MeCN	90 °C	38 mg	0%	43%
4	20 mol%	CAN (40 mol%)	MeCN	90 °C	280 mg	37%	50%
5	20 mol%	-	MeCN	90 °C	50 mg	NR*	-
6	20 mol%	I ₂ (2 equiv), NaHCO ₃	toluene	rt to 100 °C	50 mg	NR*	-
7	20 mol%	CAN (1 mol%)	MeCN	90 °C	25 mg	0%	6%
8	20 mol%	CAS (40 mol%)	MeCN	90 °C	50 mg	0%	0%
9	-	CAS (1 equiv)	MeCN/H ₂ O	90 °C	42 mg	NR*	-
10	20 mol%	phenol (2 equiv)	PhCl	100 °C	25 mg	NR*	-
11	20 mol%	thiophenol (2 equiv)	PhCl	100 °C	25 mg	NR*	-
12	20 mol%	CeCl ₃ (2 equiv)	PhCl	100 °C	25 mg	NR*	-
13	20 mol%	Mn(OAc) ₃ (2 equiv)	PhCl	100 °C	25 mg	NR*	-
14	20 mol%	PIFA (2 equiv)	PhCl	100 °C	25 mg	ND**	-
15	1 equiv	-	PhCl	120 °C	25 mg	6%	-

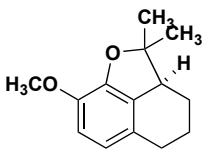
*NR = no conversion from starting material

The TEMPO/CAN system optimization was abandoned, and optimization of the KMnO₄/MnO₂ conditions began since it was one of the few oxidations screened that gave close to full mass recovery (Table 2.14). The main issue with the oxidation system was the poor

conversion of the starting material (**192**) to ketone (**193**). Leaving the reaction for an extended amount of time was not ideal because, over time, the KMnO_4 would no longer be active, or the ketone (**193**) would continue to be oxidized to the tertiary alcohol byproduct (**264**). The ratio of KMnO_4 to MnO_2 is by weight, and the reported conditions use a 1:3 ratio.²⁰⁵ Therefore, the ratio of KMnO_4 to MnO_2 was varied across multiple different organic solvent systems (Table 2.14, entries 1-22).

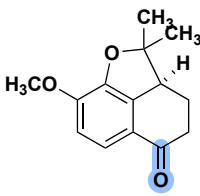
Table 2.14 $\text{KMnO}_4/\text{MnO}_2$ oxidation optimization.

KMnO₄/MnO₂ Optimization

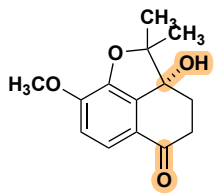


(192)

$\xrightarrow[\text{solvent, time}]{\text{KMnO}_4/\text{MnO}_2 \text{ (ratio)}}$



benzylic ketone (193)



tertiary alcohol (264)

Entry	$\text{KMnO}_4:\text{MnO}_2$ (w/w)	Solvent	Temperature	Time	Product Ratio (192:193:264)
1	6:1	MeCN	rt	24 h	5 : 1 : 0.25
2	5:2	MeCN	rt	24 h	1 : 1 : 1
3	5:2	CH_2Cl_2	rt	48 h	13 : 1 : 0.5
4	1:1	MeCN	rt	48 h	1.25 : 1 : 0.64
5	2:5	MeCN	rt	48 h	3 : 1 : 0.27
6	1:6	MeCN	rt	24 h	7 : 1 : 0.22
7	1:6	MeCN	60 °C	48 h	23 : 1 : 0
8	1:6	hexanes	rt	48 h	28 : 1 : 0
9	1:6	EtOAc	rt	48 h	6 : 1 : 0.42
10	1:6	CH_2Cl_2	rt	48 h	4 : 1 : 0.23
11	1:6	benzene/TFA	rt	1 min	ND*
12	2 equiv KMnO_4	MeCN	rt	48 h	28 : 0 : 1
13	2 equiv KMnO_4	H_2O (pH = 13)	rt	12 h	1 : 0 : 0
14	1:3	neat, sonication	rt	12 h	1 : 0 : 0.7
15	1:3	MeCN	0 °C	3 h	7%†
16	1:3	MeCN	-78 °C	24 h	NR**
17	1:3	MeCN	-5 °C	12 h	32%†: 14%†: 0%
18	1:3	EtOH, pyr	-78 °C to rt	48 h	NR**
19	1:3	CH_2Cl_2	rt	24 h	3 : 1 : 0.5
20	1:3	THF	rt	24 h	NR**
21	1:3	MeOH	rt	24 h	NR**
22	1:3	benzene	rt	24 h	NR**
23	1:3	dioxanes/ H_2O	rt	4 h	0 : 0 : 1
24	1:3	MeCN/ H_2O (pH = 7.4)	0 °C	1 h	0 : 1 : 1

* ND = conversion not determined due to messy reaction and decomposition as major pathway

**NR = no reaction/conversion

† After workup there was very poor mass recovery, no starting material present in the ^1H NMR

Unfortunately, the conditions that increased the conversion of starting material (**192**) to ketone (**193**) also significantly increased the conversion of ketone (**193**) to byproduct (**264**). Using only organic solvents meant the reaction was a heterogenous reaction dependent on surface

chemistry. Therefore, many other factors, such as the reaction vessel and stir bar surface area contact, could contribute to poor conversion.

Miscible organic/aqueous solvent systems were then attempted to allow the starting material to be fully soluble and the KMnO_4 . This strategy significantly decreased the reaction time. A dioxanes/water solvent system resulted in full starting material consumption after 4 hours but exclusively afforded the overoxidation byproduct (264) (Table 2.14, entry 23). Acetonitrile as one of the better solvents for conversion in the earlier screens, therefore a MeCN/ H_2O solvent system was selected. After an extensive screen (not shown) it was found that decreasing the temperature to $0\text{ }^\circ\text{C}$ and buffering the reaction pH to temper the reactivity of the KMnO_4 gave full starting material consumption after 1 hour.

Next, the optimized oxidation conditions were repeated to obtain isolated yields (Figure 2.47). On a small scale (20.2 mg), the ketone (193) was isolated in 61% yield and the byproduct (264) in only 13% yield. However, as the oxidation scale increased and the overall reaction time increased, the mass recovery from the reaction declined. This meant that even though the starting material was fully consumed after a couple of hours, a degradation pathway destroyed the fused tricyclic core. No degradation byproducts were ever able to be isolated from the reaction. It is hypothesized that adding water as a solvent enables an oxidative cleavage degradation pathway of the starting material and product by KMnO_4 .

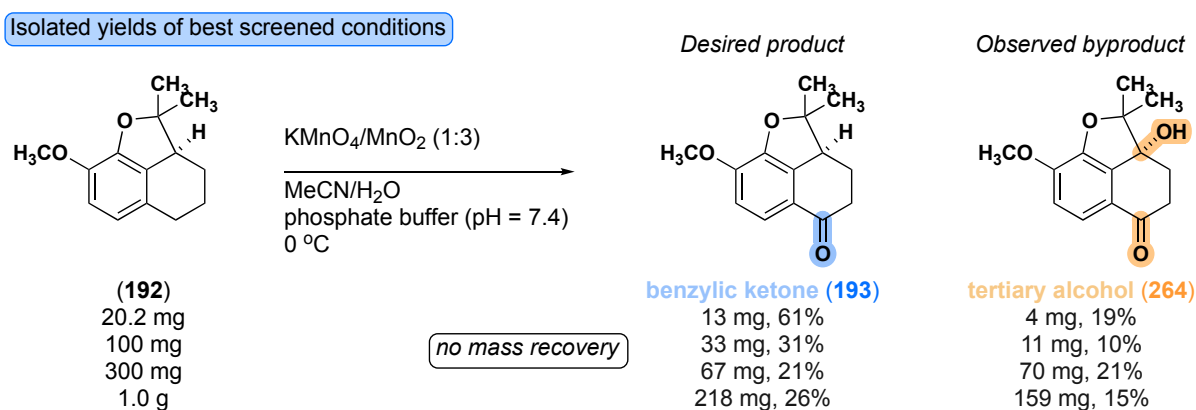


Figure 2.47 Poor mass recovery as $\text{KMnO}_4/\text{MnO}_2$ reaction scale increases.

Currently, the $\text{KMnO}_4/\text{MnO}_4$ (1:3 w/w) in MeCN/phosphate buffer_(aq) conditions are the best oxidations conditions on a gram scale to convert the insertion core (**192**) to the benzylic ketone (**193**). These conditions on a 1 to 5-gram scale consistently afford the benzylic ketone (**193**) in ~25% yield and the tertiary alcohol byproduct (**264**) in ~15% yield. So far, mild deoxygenation conditions haven't successfully taken the tertiary alcohol (**264**) back to the desired ketone (**193**).^{218–220} Rather, the conditions led to naphthalene (**194**) formation or degradation.

We screened over 200 different benzylic oxidations conditions (150 conditions shown in this dissertation), and the highest yield of ketone (**193**) obtained on a gram scale was 25%. Other groups have reported similar difficulty oxidizing a complex tetralin core in a natural product and haven't been able to get above a 50% yield for the oxidation.^{87,198,206,221,222} Chemical oxidants did not seem to hold the solution to this problem, but there are many highly selective enzymatic C–H oxidations that could successfully oxidize the fused tricyclic core (**192**).^{223–226} We currently have a collaboration underway with Dr. Mike Di Maso at Merck-Process to do a high-throughput screen across their large enzyme library to assess if enzymatic oxidation will be effective.

2.4.5 Late-stage sp^2 methoxylation

The final bond to make on the right hemisphere was oxidizing the aryl C_{sp^2} –H bond ortho to the ketone (**193**) (Figure 2.48). Theoretically, many of the same methods explored for the first step of the right hemisphere re-route could be used again to install the needed C–O bond. We began by attempting the most direct functionalization. From the ketone (**193**), reported palladium-catalyzed methoxylation¹⁸⁵ and hydroxylation¹⁸³ conditions were attempted, but none gave any reaction. Next, the late-stage ketone (**193**) was transformed into the *O*-methyl oxime (**267a**) and the *O*-acetyl oxime (**267b**) in 99% and 89% yield, respectively. The highest-yielding hydroxylation conditions from our earlier screenings were attempted (Table 2.8, entries 12 & 13) but afforded no product (**268**). Both oximes (**267a-b**) were subjected to the

2.5 Results and Discussion: final steps to join two hemispheres

2.5.1 Claisen strategy

One strategy to combine the left and right hemispheres is first to make the dihydroxanthone C–C bond through a Claisen reaction, then form the C–O bond using a coupling or addition reaction. Right hemisphere (**150**) was stirred with NaH in THF at $-40\text{ }^{\circ}\text{C}$ for 30 minutes to form the enolate (Figure 2.49). Then left hemisphere (**162**) was added, and the reaction was stirred for 1 hour at $-40\text{ }^{\circ}\text{C}$. No addition to the ester occurred after one hour. Therefore, the reaction was allowed to warm to room temperature over 3 hours. However, after 3 hours no reaction had happened. The reaction was heated up to $50\text{ }^{\circ}\text{C}$, and bubbling was observed. This suggested that the NaH had not reacted with the ketone (**150**) to form the enolate at $-40\text{ }^{\circ}\text{C}$, and enolate formation with NaH required heating. After the bubbling was observed, two new spots on TLC were observed. The reaction was stirred until the left hemisphere (**162**) was fully consumed by TLC and worked up. One of the newly formed spots by TLC was the desired 1,3-dicarbonyl (**272**), which was isolated in 13% yield. The other spot was the left hemisphere (**162**), with the triflate group cleaved back to the phenol. The small amount of dicarbonyl (**272**) isolated also had the triflate group cleaved. The product (**272**) was pushed forward to C–O bond formation using a pyrrolidine-catalyzed addition, yet none of the desired dihydroxanthone core (**273**) was isolated.

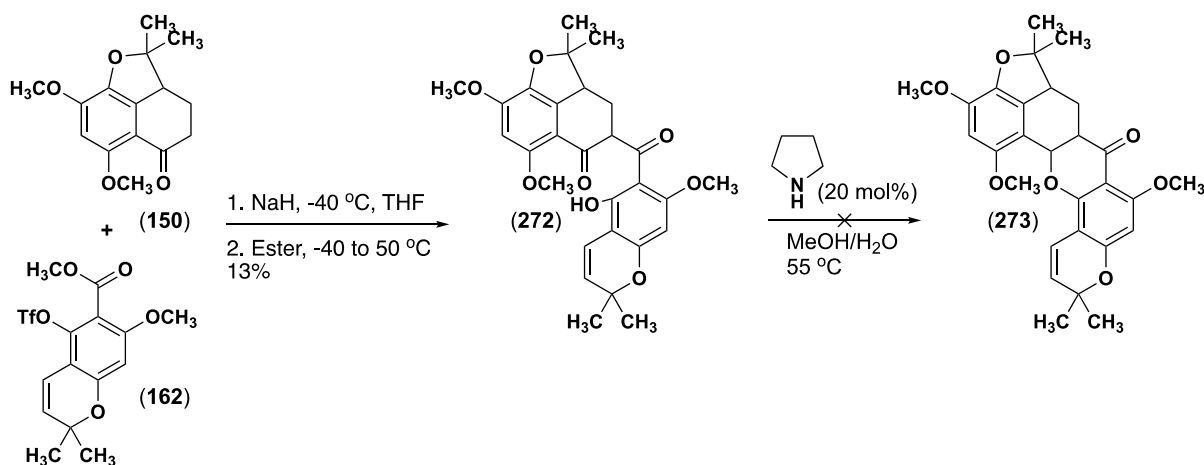


Figure 2.49 Claisen reaction attempt with left (**162**) and right (**150**) hemispheres

2.5.2 1,4-addition strategy

Another strategy to make the desired dihydroxanthone core is first to form the C–O bond using a 1,4-addition followed by a Friedel-Crafts-like acylation to make the C–C bond. To start, the right hemisphere ketone (**150**) can undergo a Vilsmeier-Haack-Arnold (VHA) reaction to afford the α,β -unsaturated aldehyde (**155**). The VHA reaction is prone to byproduct formation, specifically, the vinyl chloride (**277**) resulting from chloride anion attacking the activated VHA intermediate before formylation can occur (Table 2.15).

Table 2.15 Vilsmeier-Haack-Arnold reaction optimization

Reaction scheme: **150** (ketone) $\xrightarrow[\text{solvent, temperature}]{\text{POCl}_3 \text{ (equiv)}, \text{DMF (equiv)}}$ **155** (desired product, α,β -unsaturated aldehyde) + **277*** (byproduct, vinyl chloride).

Entry	Cl Source	DMF equivalent	Temperature	Solvent	Order of addition	Yield (155)
1	POCl ₃ (2 equiv)	0.1M	rt to 40 °C	-	all at once then heat	31%
2	POCl ₃ (1.3 equiv)	0.3M	rt to 40 °C	-	all at once then heat	23%
3	POCl ₃ (1.3 equiv)	0.3M	40 °C	-	150 in DMF, heat, then POCl ₃	45%
4	POCl ₃ (10 equiv)	50 equiv	40 °C	-	150 in DMF, heat, then POCl ₃	76%
5	(COCl) ₂ (1.2 equiv)	2 equiv	0 °C to rt	CH ₂ Cl ₂	(COCl) ₂ in DMF, then 150 in CH ₂ Cl ₂	0%

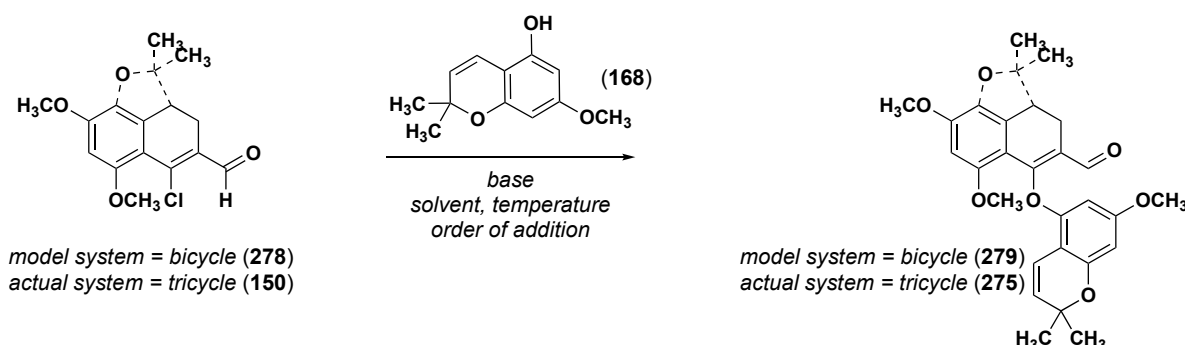
*Product degrades quickly, especially on column. Pure ¹H NMRs of the product come from ¹H NMRs immediately after workup.

Optimization for the desired product (**155**) proved to be temperature dependent. First, the addition of the ketone (**150**), 2 equivalents of phosphorous (V) chloride (POCl₃), and DMF to a vial, then heating the reaction to 40 °C afforded the desired product (**155**) in 31% yield (Table 2.15, entry 1). Decreasing the equivalents of POCl₃ decreased the reaction yield to 23% (Table 2.15, entry 2). Next, adding the ketone (**150**) and DMF to the reaction vessel first, heating the solution to 40 °C, then adding 1.3 equivalents of POCl₃ increased the yield to 45% (Table 2.15, entry 3). Maintaining this order of addition strategy but increasing the amount of POCl₃ in the reaction to 10 equivalents increased the yield even further to afford the desired product in 76% yield (Table 2.15, entry 4). Notably, attempts to pre-form the Vilsmeier reagent first and then

add the ketone (**150**) to the solution failed to yield any desired product (**155**). Instead, this order of addition exclusively afforded the vinyl chloride byproduct (**277**) (Table 2.15, entry 5).

Now that the α,β -unsaturated aldehyde (**155**) could be readily accessed, we attempted the 1,4-addition reaction (Table 2.16). First, one equivalent of tricyclic aldehyde (**150**) was heated with excess left hemisphere (**168**) and potassium carbonate in DMF (Table 2.16, entries 1-2). Only trace product (**275**) was detected by LC-MS but was not isolated due to difficulty separating the product from the large excess of the left hemisphere (**168**). Rather than waste precious late-stage material (**150**), a bicyclic model system (**278**) was synthesized to screen reactions.

Table 2.16 1,4-addition optimization



Entry	Starting Material	Nucleophile (168) equivalents	Base	Additive	Solvent	Temperature	Order of Addition	Yield
1	150	6.0	K ₂ CO ₃	-	DMF	100 °C	one-pot	trace
2	150	4.0	K ₂ CO ₃	-	DMF	80 °C	one-pot	trace
3	278	2.0	Cs ₂ CO ₃	-	MeCN	90 °C	one-pot	24%
4	278	1.2	NaH	-	DMF	rt	base + phenol pre-stir (30 min)	0%
5	278	1.2	Cs ₂ CO ₃	-	MeCN	60 °C	base + phenol pre-stir (30 min)	62%
6	150	1.2	Cs ₂ CO ₃	-	MeCN	60 °C	base + phenol pre-stir (30 min)	23%
7	150	1.2	Cs ₂ CO ₃	AgNO ₃	MeCN	60 °C	one-pot	50%

The bicyclic starting material (**278**) was stirred with cesium carbonate (Cs₂CO₃) and 2 equivalents of phenol (**168**) in MeCN at 90 °C, yielding the desired ether (**279**) in 24% yield (Table 2.16, entry 3). Next, 1.2 equivalents phenol (**168**) was pre-stirred with Cs₂CO₃ for 30 minutes in MeCN. Then the model system (**278**) was added, and the reaction was heated to 90 °C (Table 2.16, entry 5). Excitingly, this afforded the desired model system ether (**279**) in 63% yield. These conditions were immediately repeated on the tricyclic core (**150**). However, only

the desired ether (**275**) was isolated in 23% yield (Table 2.16, entry 7). I hypothesized that the reaction equilibrium favored the reverse reaction. Therefore, one way to push the equilibrium forward would be to remove the chloride anions from the solution after they are displaced. To test this hypothesis, 1.0 equivalent of silver nitrate (AgNO_3) was added to the reaction. The silver nitrate would react with the chloride anions to form silver chloride (AgCl) salts that would immediately crash out of the reaction mixture, thereby driving the reaction forward. Gratifying, adding 1.0 equivalent of AgNO_3 increased the reaction yield to 50% (Table 2.16 entry 7).

Starting from the right hemisphere ketone (**150**), a VHA reaction afforded the α,β -unsaturated aldehyde (**155**) in 76% yield (Figure 2.50). The left hemisphere phenol (**168**) and its bromine analog (**274**) were added to the aldehyde (**155**) to afford ethers **275** and **276** in 50% and 53% yield, respectively. Current efforts focus on screening reaction conditions to make the final C–C bond (**273**).

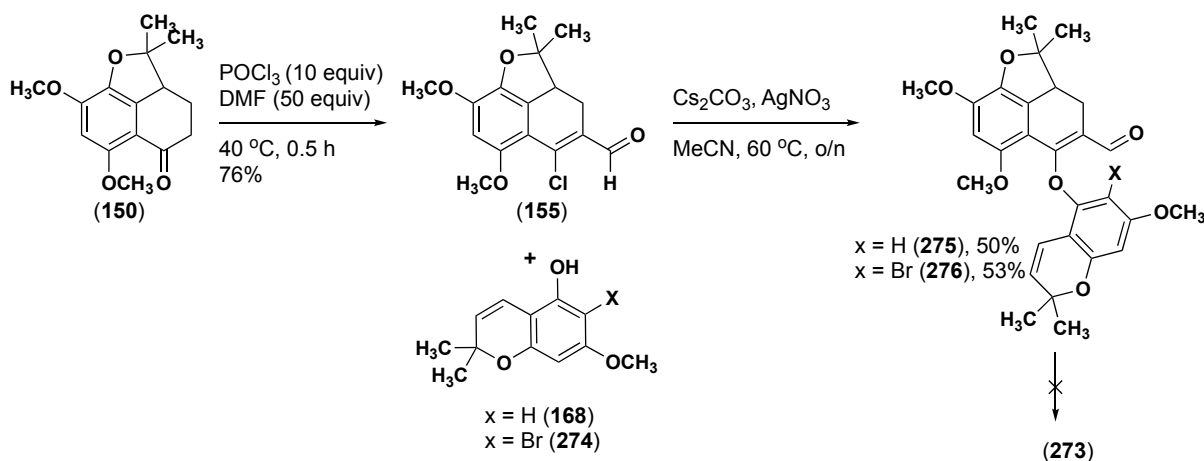


Figure 2.50 1,4-addition dihydroxanthone formation strategy.

2.6 Results and Discussion: synthesis of artoindonesianin Z-2

Artoindonesianin Z-2 (**2**) was envisioned to be made from the same synthetic route as cycloartobiloxanthone (**1**), with one divergence during the alkylation of the phenol

intermediate (Figure 2.51). Instead of using isopropyl iodide to make the achiral ether (**199**) for cycloartobiloxanthone (**1**), a chiral electrophile could be alkylated onto a phenol intermediate (**144**) in an S_N2 fashion to afford an enantiopure chiral ether (**281**).

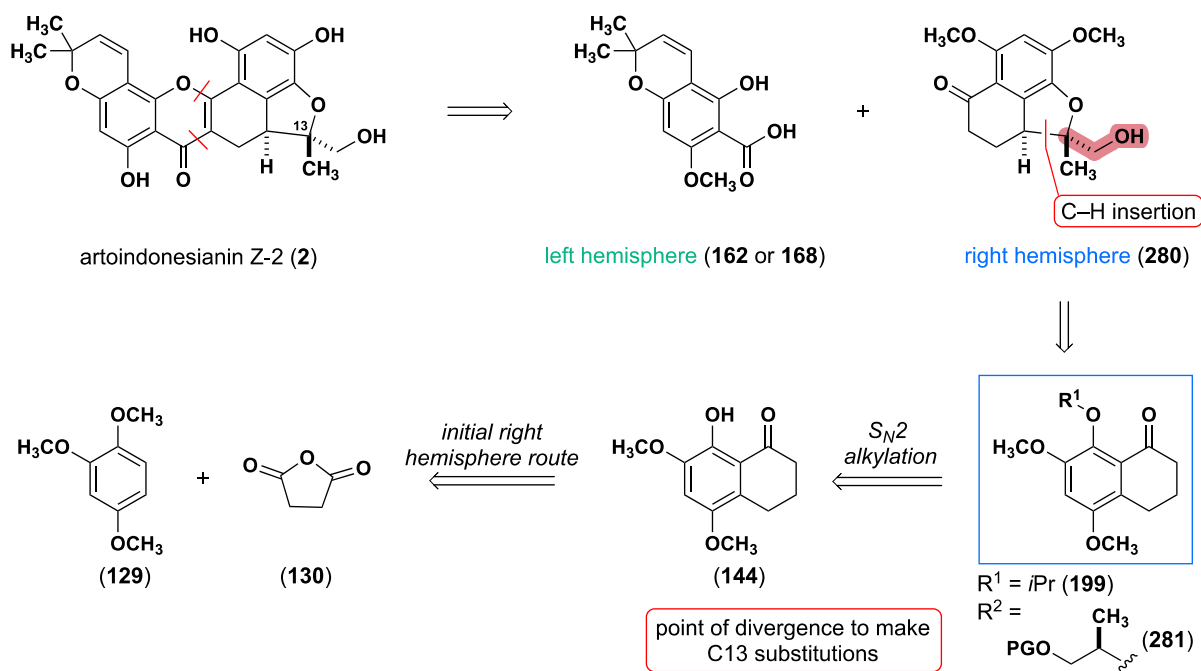


Figure 2.51 Retrosynthesis for artoindonesianin Z-2 (**2**).

2.6.1. Synthesis of enantiopure ether

Using the first right hemisphere route, the same Friedel-Crafts acylation with succinic anhydride (**130**) gave intermediate **138**. A mild ketone reduction on intermediate **138** afforded carboxylic acid **141**. The carboxylic acid (**141**) then undergoes a Lewis acid-mediated cyclization to yield tetralone (**143**). An ortho methoxy deprotection of tetralone **143** yields the common phenol intermediate (**144**) (Figure 2.52). From there, we envisioned the isopropyl iodide used in the main route could be swapped out with chiral ether electrophiles. However, this alkylation to make the chiral ether intermediate (**282**), which we initially believed would be straightforward, turned out to be much more difficult.

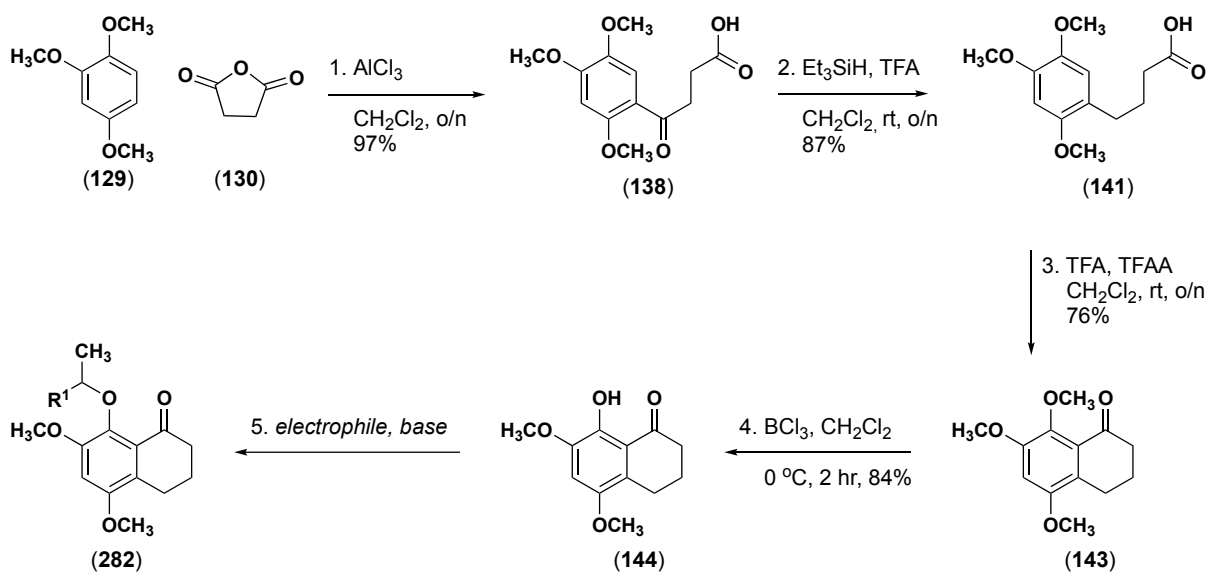
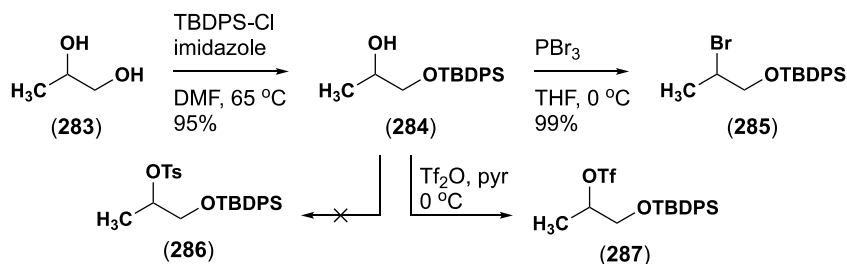


Figure 2.52 Initial top half route to artoindonesianin Z-2 alkylation.

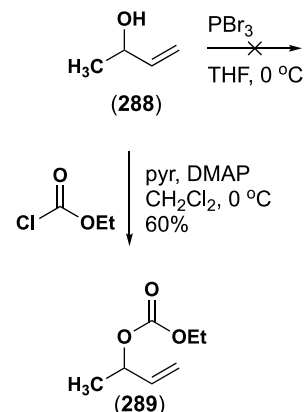
The di-ortho substituted ether created a highly hindered nucleophile and subsequent ether (**282**). Therefore, finding a reactive enough electrophile that was not too sterically hindered took extensive screening (Figure 2.53). Propane-1,2-diol (**283**) was initially selected since its enantiopure versions were commercially available. Following literature precedent,^{231,232} the primary alcohol on **283** was selectively TBDPS protected to yield **284**. The alcohol (**284**) was then used in a Mitsunobu reaction with phenol (**144**), but no reaction occurred, and only unreacted starting material was obtained back after the work-up (Figure 2.53B, entries 1-2). It was hypothesized that the TBDPS electrophile (**284**) was too bulky. Using a more reactive alkyl phosphine was also unsuccessful (Figure 2.53B, entry 3).²³³ Therefore, the Mitsunobu was attempted again with the smaller allylic alcohol, but-3-en-2-ol (**288**), and the alkynal alcohol, but-3-yn-2-ol (**290**). However, no reaction was obtained again (Figure 2.53B, entries 4-5), even with reported sonication conditions for hindered ether formation (Figure 2.53B, entries 6-7).²³⁴ Changing the solvent in the reaction from THF to a 1:1 mix of THF:toluene afforded a small amount of ether **282b** in a 4:1 ratio of starting material:product (Figure 2.53B, entry 8). It was concluded that the Mitsunobu to form a sterically hindered ether was not favorable on phenol **144**, a commonly known reaction limitation.^{235,236}

A. Electrophile synthesis

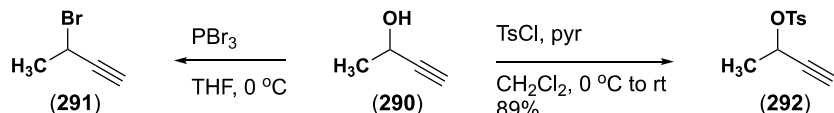
Diol electrophiles



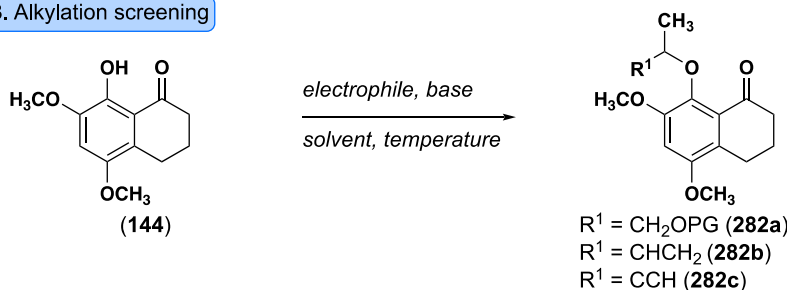
Alkyne electrophiles



Allylic electrophiles



B. Alkylation screening



Entry	Electrophile	Product	Conditions	Solvent	Temperature	Yield
1	A	282a	PPh ₃ , DIAD	THF	0 °C to rt	NR
2	(R)-A	282a	PPh ₃ , DIAD	THF	0 °C to rt	NR
3	A	282a	PBu ₃ , DIAD	THF	0 °C to rt	NR
4	B	282b	PPh ₃ , DIAD	THF	0 °C to rt	NR
5	F	282c	PPh ₃ , DIAD	THF	0 °C to rt	NR
6	F	282c	PPh ₃ , DIAD, sonication	THF	rt	NR
7	B	282b	PPh ₃ , DIAD, sonication	THF	rt	NR
8	B	282b	PPh ₃ , DIAD	THF:Tol	0 °C to rt	20%
9	C	282a	Cs ₂ CO ₃	MeCN	60 °C	0%
10	C	282a	K ₂ CO ₃ , NaI	DMF	60 °C	0%
11	D	282a	Cs ₂ CO ₃	MeCN	60 °C	0%
12	E	282b	1. NaHMDS 2. Rh(PPh ₃) ₃	THF	0 °C to rt	0%
13	G	282c	1. DBU, TFAA 2. CuCl ₂	MeCN	-20 °C	NR
14	H	282c	Cs ₂ CO ₃	MeCN	80 °C	16%
15	H	282c	Cs ₂ CO ₃ , seq. add.	MeCN	80 °C	53%

Electrophiles

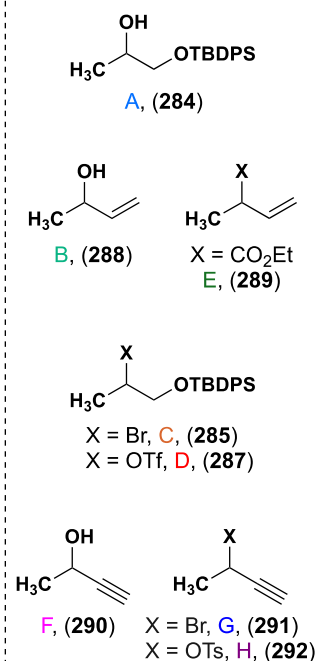


Figure 2.53 A. Electrophile synthesis B. Chiral ether formation screening

Next, the TBDPS alcohol (**284**) was converted to the bromide (**285**) using PBr₃. This bromide (**285**) was used in an alkylation reaction with phenol (**144**), but only phenol (**144**) and alcohol (**284**) were isolated after the work-up (Figure 2.53B, entries 9-10). The triflate version of the TBDPS alcohol (**287**) was also used but only afforded phenol and desilylated alcohol (Figure 2.53B, entry 11). Attempts to make the tosylated version of the TBDPS alcohol (**286**) were unsuccessful.

A reported procedure²³⁷ for rhodium-catalyzed allylic etherification with ortho-substituted phenols appeared promising. After making the needed carbonate (**289**) from allylic alcohol (**288**), this reaction was attempted, but only starting material and unidentified byproducts were obtained from the reaction (Figure 2.53B, entry 12).²³⁸ CuCl₂ and catalyzed ether formation with but-3-yn-2-ol (**x**) also did not give any reaction (Figure 2.53B, entry 13).

Finally, but-3-yn-2-ol (**290**) was tosylated to yield **292** in 89% yield. **292** was then successfully alkylated onto phenol (**144**) with Cs₂CO₃ in MeCN at reflux, affording ether (**282c**) in 16% yield (Figure 2.53B, entry 14). The low yield was due to the tosylate (**292**) being fully consumed before reacting with the phenol (**144**). Therefore, after some optimization, it was found that the sequential addition of 3.0 equiv of the tosylate over 3 hours helped push the reaction to full conversion. The alkyne ether (**282c**) was isolated in 53% yield (Figure 2.53B, entry 15). Now that a chiral ether could be made, the alkyne must be transformed to the -CH₂OH found in artoindonesianin Z-2. One route would be to take **282c** through C–H insertion, then reduce and oxidatively cleave the alkyne to the needed -CH₂OH group. However, attempts at hydrazone formation to make **293** from **282c** were unsuccessful (Figure 2.54). The second route would be to reduce and oxidatively cleave the alkyne to the -CH₂OH group, then push it through C–H insertion. Reduction of the alkyne with Lindlar's catalyst afforded the desired alkene in 29% yield, but it co-eluted with the over-reduced alkane byproduct and cleavage byproduct to the phenol.

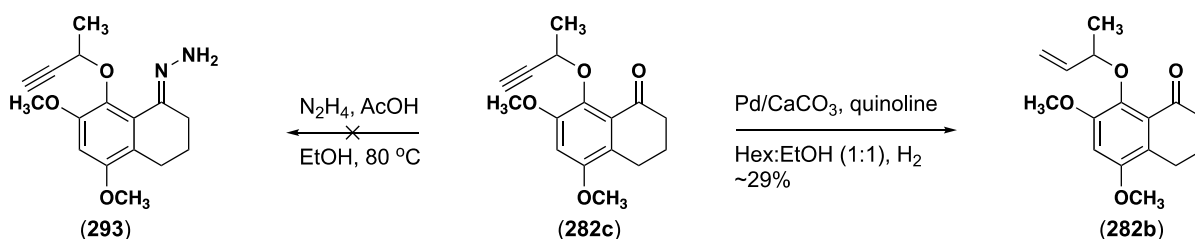


Figure 2.54 Alkyne ether functionalization.

The inability to functionalize the alkyne meant that this route had to be abandoned, even though it was the first successful formation of a chiral ether on the phenol core. Therefore, I

returned to the drawing board and hypothesized that the alkylation with the tosyl-alkyne electrophile (**292**) was successful due to the stability of the tosylated and the small steric bulk offered by the alkyne group. To test this hypothesis, a protected diol electrophile was designed where the primary alcohol was methylated then the secondary alcohol was tosylated to form the good leaving group (**296**) (Figure 2.55A). Phenol **144** was successfully alkylated with this electrophile (**295**) in nearly quantitative yield (98%) using Cs₂CO₃ in MeCN reflux and sequentially adding the electrophile over 3-4 hours.

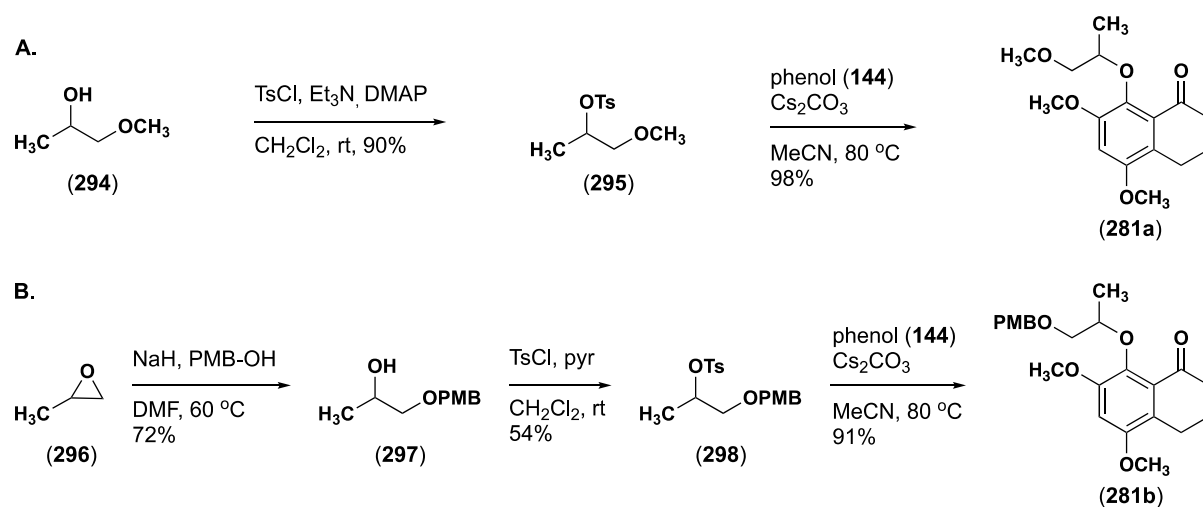


Figure 2.55 Synthesis of protected diol electrophiles: **A.** Methyl protected primary alcohol **B.** PMB-protected primary alcohol.

While the discovery of high-yielding alkylation conditions to form the highly sterically hindered ether was exciting, the methyl-protected electrophile (**281a**) was not ideal since it was not available commercially as a single enantiomer and deprotection of the methyl group would be very difficult. However, 2-methyloxirane (**296**) was cheap and available commercially as the racemic mix, the single *R* enantiomer, and the single *S* enantiomer. The epoxide could be opened under basic conditions with any alcohol nucleophile we chose without eroding the stereocenter. PMB-alcohol was selected as the initial nucleophile since the PMB group provided two mild orthogonal deprotection conditions that would be needed later in the

synthesis. The addition of PMB alcohol to 2-methyloxirane (**296**) proceeded smoothly and was easily scalable (5 g scale), affording the diol (**297**) in 72% yield. **297** could then be tosylated (**298**, 54% yield) and used in the previous alkylation conditions to give ether **281b** in 91% yield (Figure 2.55B). It was discovered that the tosylate (**298**) was not bench stable past 2-3 days and decomposed back to the alcohol (**297**). Therefore, moving forward, the material was kept at the alcohol stage (**297**) and only tosylated when it could be used immediately after purification in the alkylation step.

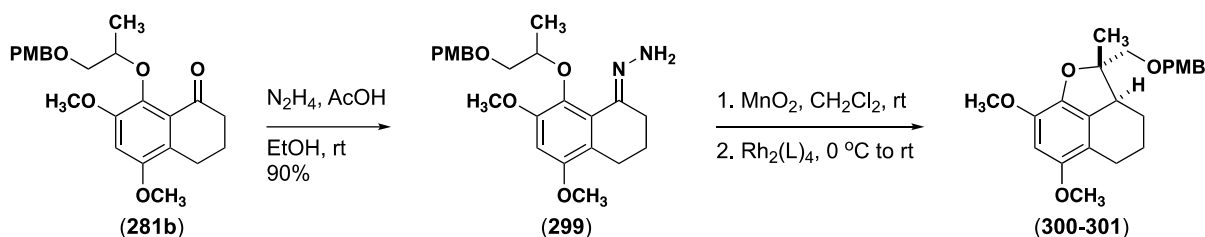
2.6.2. C–H Insertion stereoselectivity data from first-generation route

Now that the chiral ether insertion center could be obtained, the ether (**281b**) was pushed forward to access if the stereoselectivity trends observed for the reported C–H insertion into stereogenic centers methodology⁴ would hold true for a more complex substrate. Hydrazone formation conditions from previously reported papers from the group used hydrazine and acetic acid in ethanol at 80 °C over 12 hours to condense hydrazine onto a ketone. Applying these conditions to ketone (**281b**) only afforded hydrazone (**299**) in 43-57% yield. Reducing the temperature to room temperature afforded hydrazone (**299**) in 90% yield in 2 hours (Figure 2.56A). Similar increases in yield were observed for the formation of hydrazones for analogous aryl-alkyl ketones.²³⁹

When hydrazone **299** was subjected to the one-pot sequential C–H insertion conditions, similar stereoselectivity trends were observed to our previously published methodology.⁴ Racemic hydrazone (**299**) with Rh₂(*R*-PTAD)₄ gave about a 1:1 mix of diastereomers in moderate yield (Figure 2.56 entry 1). Racemic starting material (**299**) with the achiral catalyst Rh₂(mes)₄ preferred the *cis* diastereomer (80:20 dr, Figure 2.56, entry 2) in high yield. All racemic hydrazone (**299**) led to racemic products (**300-301**). Enantiopure hydrazone (*R*-**299**) yielded enantiopure product, always with the *S* stereochemistry at the fused carbon, regardless

of the catalyst used (Figure 2.56 entries 3-4). The *R* enantiomer of hydrazone (*R*-**299**) appeared to be the “match” with $\text{Rh}_2(\text{R-PTAD})_4$, preferring the *cis* diastereomer in 83:17 dr and 79% yield (Figure 2.56, entry 3). Meanwhile, the *R* enantiomer of hydrazone (*R*-**299**) appeared to be the “mis-match” with $\text{Rh}_2(\text{S-PTAD})_4$, preferring the *trans* diastereomer in 19:81dr and a much lower yield of 56% yield (Figure 2.56, entry 4).

A. Chiral C–H insertion synthesis



B. Chiral C–H insertion stereoselectivity data

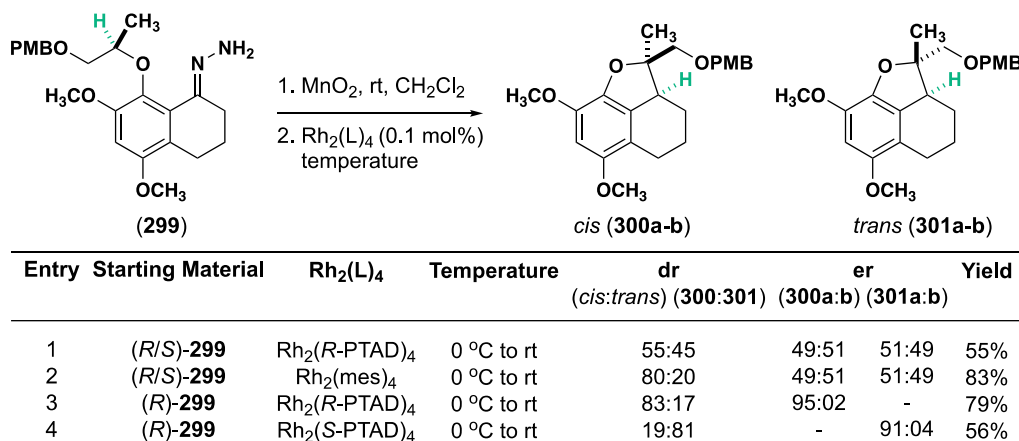


Figure 2.56 A. Chiral C–H insertion core synthesis with PMB-protected alcohol B. Stereoselectivity data for C–H insertion.

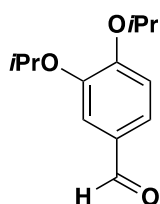
2.7 Conclusion

I have developed a unifying convergent synthetic strategy to access the furanodihydrobenzoxanthone natural product family. A key donor/donor C–H insertion forms the unique fused 6/6/5 tricyclic core stereoselectively and enables the rapid synthesis of the natural and unnatural stereoisomers. Current work on the total synthesis of cycloartobiloxanthone (**1**) and artoindonesianin Z-2 (**2**) focuses on finding conditions to make the final bond of the dihydroxanthone core. If those conditions are found, then global

deprotection would afford the final natural products. Synthetic access to this natural product family will enable future collaborative efforts to test the natural products, and their fused tricyclic pharmacophore for that many reported biological activities.

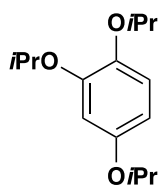
2.8 Experimental section

2.8.1 Right hemisphere: first-generation route



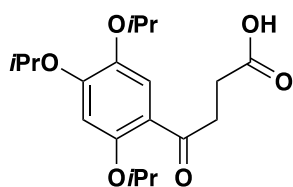
(131) 3,4-Diisopropoxybenzaldehyde

Following literature procedure, to a solution of 3,4-dihydroxybenzaldehyde (2.5 g, 18.4 mmol) in CH₃CN (92 mL, 0.2 M) was added K₂CO₃ (7.6 g, 55.2 mmol) and isopropyl bromide (8.6 mL, 92 mmol). The solution was heated at 80 °C overnight when an additional portion of isopropyl bromide (1.8 mL) was added. The solution was cooled, filtered, and concentrated in vacuo. The crude residue was purified by flash column chromatography on silica gel (80:20 hexanes:EtOAc) to afford the product (3.8 g, 93%): ¹H NMR (599 MHz, CDCl₃) δ 9.83 (s, 1H), 7.44 (d, *J* = 5.1 Hz, 2H), 6.99 (d, *J* = 8.6 Hz, 1H), 4.64 (dd, *J* = 12.1, 6.0 Hz, 1H), 4.54 (dd, *J* = 12.1, 6.0 Hz, 1H), 1.46–1.36 (m, 6H), 1.36 (s, 6H). ¹H NMR data of purified compound was consistent with the reported literature values.⁸⁰



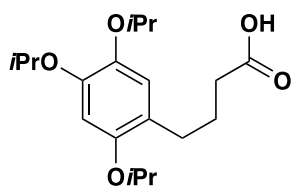
(134) 1,2,4-triisopropoxybenzene

To a solution of **133** (431 mg, 2.0 mmol) in CH₃CN (20 mL, 0.1 M) was added Cs₂CO₃ (1.3 g, 4.0 mmol) and isopropyl bromide (0.28 mL, 3.0 mmol). The solution was heated at 80 °C overnight, and then cooled, filtered and concentrated *in vacuo*. The crude residue was purified by flash column chromatography on silica gel (95:5 hexanes:EtOAc) to afford the product (3420 mg, 81%): ¹H NMR (599 MHz, CDCl₃) δ 6.83 (d, *J* = 8.7 Hz, 1H), 6.49 (d, *J* = 2.4 Hz, 1H), 6.40 (dd, *J* = 8.6, 2.5 Hz, 1H), 4.56 – 4.36 (m, 2H), 4.29 (dt, *J* = 12.1, 6.1 Hz, 1H), 1.51 – 1.11 (m, 17H). ¹H NMR data of purified compound was consistent with the reported literature values.⁸⁰



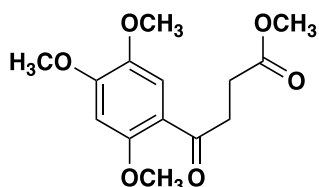
(135) 4-oxo-4-(2,4,5-triisopropoxyphenyl)butanoic acid

A solution of **134** (252 mg, 1.0 mmol) in CH₂Cl₂ (5 mL, 0.05 M) and nitrobenzene (5 mL, 0.05 M) was cooled to 0 °C. Succinic anhydride (110 mg, 1.1 mmol) was added, followed by AlCl₃ (332 mg, 2.5 mmol). The solution was allowed to warm to room temperature and then cooled before quenched with ice-cold DI H₂O (50 mL). The solution was then acidified with 1M HCl (2 mL) to pH = 1. The organic was then extracted with Et₂O (70 mL), dried over Na₂SO₄ and concentrated *in vacuo*. The product was carried to the next reaction with no further purification: ¹H NMR (400 MHz, CDCl₃) δ 7.49 (s, 1H), 6.47 (s, 1H), 4.66- 4.49 (m, 2H), 4.46 – 4.23 (m, *J* = 6.3 Hz, 1H), 3.33 (t, *J* = 6.6 Hz, 2H), 2.72 (t, *J* = 6.6 Hz, 2H), 1.40 (d, *J* = 6.0 Hz, 6H), 1.37 (d, *J* = 6.0 Hz, 6H), 1.30 (d, *J* = 6.0 Hz, 7H).



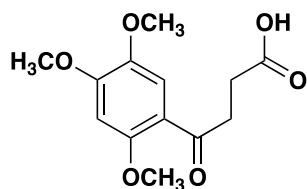
(136) 4-(2,4,5-triisopropoxyphenyl)butanoic acid

To a solution of **135** (143.6 mg, 0.41 mmol) in CH₂Cl₂ (4.1 mL, 0.1 M) was added TFA (0.31 mL, 4.1 mmol) followed by Et₃SiH (0.19 mL, 1.2 mmol). Upon completion, the solution was diluted with CH₂Cl₂ (20 mL) and DI H₂O (20 mL). The solution was basified by adding 10% NaOH (2 mL), and the aqueous was separated and then basified by 1 M HCl. The organic product was extracted with CH₂Cl₂ (5 x 10 mL), dried over Na₂SO₄, and concentrated *in vacuo* and used without further purification (80.8 mg, 59%). ¹H NMR (400 MHz, CDCl₃) δ 6.70 (s, 1H), 6.48 (s, 1H), 4.35-4.22 (m, 3H), 2.57 (t, *J* = 7.2 Hz, 2H), 2.35 (t, *J* = 7.3 Hz, 2H), 1.89 (p, *J* = 7.2 Hz, 2H), 1.29-1.20 (m, 18H).



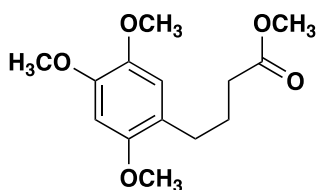
(139) methyl 4-oxo-4-(2,4,5-trimethoxyphenyl)butanoate

To a solution of 1,2,4-trimethoxybenzene (3.4 mL, 22.8 mmol, 1.0 equiv) dissolved in CH₂Cl₂ (114 mL, 0.2 M) was added methyl 4-chloro-4-oxobutanoate (4.1 g, 27.4 mmol, 1.2 equiv). The solution was cooled to 0 °C and solid crystalline AlCl₃ (3.6 g, 27.4 mmol, 1.2 equiv) was crushed and added over two portions. The solution was allowed to warm to room temperature overnight. A color change from dark brown to dark green was observed. The solution was quenched with 1 M HCl (50 mL) and extracted with CH₂Cl₂ (3 x 100 mL). Extracts change from olive green to pink in color. The combined organic extracts were dried over Na₂SO₄ and concentrated *in vacuo*. The crude residue was purified by flash column chromatography on silica gel (66:34 hexanes:EtOAc) to afford the product **139** (6.7 g, 97%): ¹H NMR (599 MHz, CDCl₃) δ 7.47 (s, 1H), 6.50 (s, 1H), 3.95 (d, *J* = 13.8 Hz, 6H), 3.87 (s, 3H), 3.71 (s, 3H), 3.32 (t, *J* = 6.1 Hz, 2H), 2.70 (t, *J* = 6.2 Hz, 2H).



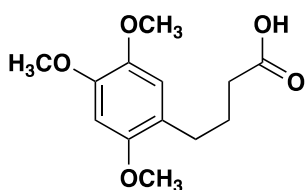
(138) 4-oxo-4-(2,4,5-trimethoxyphenyl)butanoic acid

To a flame dried round bottom flask backfilled with argon was added CH_2Cl_2 (150 mL, 0.2 M), 1,2,4- trimethoxybenzene (4.5 mL, 30.1 mmol, 1 equiv), and freshly recrystallized succinic anhydride (3.6 g, 36.1 mmol, 1.2 equiv). The solution was cooled to 0 °C and solid crystalline AlCl_3 (9.6 g, 72.2 mmol, 2.4 equiv) was crushed and added over three portions. The solution was allowed to warm to room temperature overnight and then was acidified with 1 M HCl (50 mL) and the flask was washed with DI H_2O . The organic product was extracted with CH_2Cl_2 (5 x 50 mL) and then organic solvent was reduced to half by concentration *in vacuo*. The remaining organic layer was made basic with 10% NaOH (150 mL) and the aqueous layer was separated and acidified with 1 M HCl (350 mL). The organic product was extracted with CH_2Cl_2 (5 x 150 mL), dried over Na_2SO_4 , and concentrated *in vacuo*. The resulting tan colored solid **138** was used without further purification (5.7 g, 71%): ^1H NMR (400 MHz, CDCl_3) δ 7.48 (s, 1H), 6.50 (s, 1H), 3.96 (s, 3H), 3.93 (s, 3H), 3.87 (s, 3H), 3.32 (t, $J = 6.5$ Hz, 2H), 2.74 (t, $J = 6.5$ Hz, 2H); ^{13}C NMR (101 MHz, CDCl_3) δ 197.2, 178.8, 155.8, 154.2, 143.1, 118.0, 112.5, 96.2, 56.2, 56.1, 56.1, 38.7, 28.8; AMM m/z calcd for $\text{C}_{13}\text{H}_{17}\text{O}_6^+$ ($\text{M} + \text{H}$) $^+$ 269.1020, found 269.1017.



(142) methyl 4-(2,4,5-trimethoxyphenyl)butanoate

To a flame dried round bottom flask backfilled with argon was added a solution of methyl 4-oxo-4-(2,4,5-trimethoxyphenyl)butanoate **139** (380.9 mg, 1.3 mmol, 1 equiv) in CH₂Cl₂ (13.0 mL, 0.1 M). Trifluoroacetic acid (TFA, 1.0 mL, 13.0 mmol, 10.0 equiv) was slowly added and a color change was observed from red to dark purple. Triethylsilane (5.1 mmol, 4.5 equiv) was added dropwise, and a reversal in color change from dark purple to red was seen. Upon competition, the reaction was quenched with DI H₂O (15 mL) and extracted with CH₂Cl₂ (3 x 25 mL), dried over Na₂SO₄, and concentrated *in vacuo*. The crude residue was purified by flash column chromatography on silica gel (66:34 hexanes:EtOAc) to afford a clear oil (276.0 mg, 76%): ¹H NMR (599 MHz, CDCl₃) δ 6.68 (s, 1H), 6.51 (s, 1H), 3.88 (s, 3H), 3.83 (s, 3H), 3.79 (s, 3H), 3.67 (s, 3H), 2.59 (t, *J* = 6.6 Hz, 2H), 2.33 (t, *J* = 6.5 Hz, 2H), 1.89 (t, *J* = 7.1 Hz, 2H).

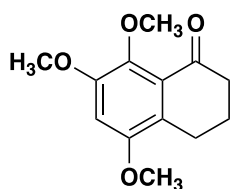


(141) 4-(2,4,5-trimethoxyphenyl)butanoic acid

From **142**: To a solution of **142** (272.3 mg, 1.0 mmol) in methanol (2.5 mL, 0.4 M), was added dropwise 1 M NaOH solution (2.5 mL). The solution was allowed to stir for 1 hour, and then was acidified with 1 M HCl (5 mL), extracted with CH₂Cl₂ (3 x 10 mL), dried over Na₂SO₄, and concentrated *in vacuo*. The resulting solid was used without further purification (244.3 mg, 96%).

From **138**: To a flame dried round bottom flask backfilled with argon was added a solution of **138** (4.75 g, 17.7 mmol, 1 equiv) in CH₂Cl₂ (37.4 mL, 0.5 M). Trifluoroacetic acid (TFA, 7.2 mL, 93.5 mmol, 5.0 equiv) was slowly added and a color change was observed from orange to dark green. Triethylsilane (78.8 mmol, 4.5 equiv) was added dropwise, and a color change to

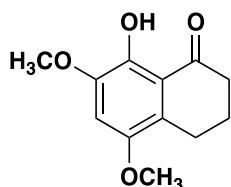
brownish-red was seen. Upon competition, the reaction was quenched with DI H₂O (50 mL) and extracted with CH₂Cl₂ (3 x 70 mL), dried over Na₂SO₄, and concentrated *in vacuo*. The crude residue was purified by flash column chromatography on silica gel (66:34 hexanes:EtOAc) to afford a white flaky solid (3.5 g, 77%): ¹H NMR (400 MHz, CDCl₃) δ 6.68 (s, 1H), 6.51 (s, 1H), 3.88 (s, 3H), 3.83 (s, 3H), 3.79 (s, 3H), 2.62 (t, *J* = 7.3 Hz, 2H), 2.37 (t, *J* = 7.4 Hz, 2H), 1.91 (p, *J* = 7.3 Hz, 2H); AMM *m/z* calcd for C₁₃H₁₉O⁺ (M + H)⁺ 255.1227, found 255.1377.



(143) 5,7,8-trimethoxy-3,4-dihydronaphthalen-1(2H)-one

To a flame dried round bottom flask backfilled with argon was added **141** (2.0 g, 8.0 mmol, 1.0 equiv) and CH₂Cl₂ (20 mL, 0.4 M). The solution was cooled to 0 °C and TFA (1.2 mL, 16.0 mmol, 2.0 equiv) was added. A portion of trifluoroacetic anhydride (TFAA, 2.3 mL, 16.0 mmol, 2.0 equiv) was added over 3 minutes. The solution was allowed to warm to room temperature overnight. The reaction was then made basic with 10% NaOH solution, extracted with CH₂Cl₂ (3 x 50 mL), dried over Na₂SO₄, and concentrated *in vacuo*. The crude residue was purified by flash column chromatography on silica gel (66:34 hexanes:EtOAc) to afford the product **143** (1.2 g, 61%); ¹H NMR (400 MHz, CDCl₃) δ 6.70 (s, 1H), 3.89 (s, 3H), 3.84 (s, 3H), 3.83 (s, 3H), 2.80 (t, *J* = 6.2 Hz, 2H), 2.69 – 2.51 (m, 2H), 2.04 (p, *J* = 6.4 Hz, 2H); ¹³C NMR (101 MHz, CDCl₃) δ 198.0, 152.6, 152.1, 143.1, 127.6, 125.6, 102.1, 61.4, 56.8, 56.1, 40.9, 22.9, 22.5; AMM *m/z* calcd for C₁₃H₁₇O₄⁺ (M + H)⁺ 237.1121, found 237.1119.

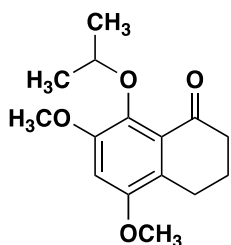
Note: On 0.8 mmol scale, 75% yield.



(144) 8-hydroxy-5,7-dimethoxy-3,4-dihydronaphthalen-1(2H)-one

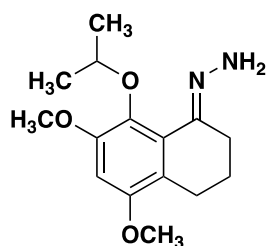
Compound **143** was split over three flame-dried round bottom flasks. The product (972.9 mg, 4.1 mmol, 1 equiv) was added to flame-dried flasks and backfilled with argon and dissolved in CH_2Cl_2 (40 mL, 0.1 M). The solution was cooled to 0 °C and BCl_3 (1 M in CH_2Cl_2 , 4.9 mmol, 1.2 equiv) was added dropwise. The solution was kept at 0 °C until the reaction was complete (2-3 hours) and then quenched with saturated NH_4Cl . All fractions were combined, and the organic layer was extracted with CH_2Cl_2 (3 x 50 mL), washed with H_2O , brine, dried over Na_2SO_4 , and concentrated *in vacuo*. The crude residue was purified by flash column chromatography on silica gel (80:20 hexanes:EtOAc) to afford the product (758 mg, 83%): ^1H NMR (599 MHz, CDCl_3) δ 12.21 (d, $J = 8.7$ Hz, 1H), 6.80 (d, $J = 8.5$ Hz, 1H), 3.92 (d, $J = 8.8$ Hz, 3H), 3.82 (d, $J = 8.8$ Hz, 3H), 2.84 (s, 2H), 2.67 (d, $J = 5.4$ Hz, 2H), 2.16 – 2.01 (m, 2H); ^{13}C NMR (151 MHz, CDCl_3) δ 206.0, 148.2, 147.1, 146.6, 123.6, 117.0, 105.6, 77.4, 77.2, 57.1, 56.8, 39.3, 22.60, 22.59; AMM m/z calcd for $\text{C}_{12}\text{H}_{15}\text{O}_4^+$ ($\text{M} + \text{H}$) $^+$ 223.0965, found 223.0961.

Note: For best yields, each batch was kept around 1.3-1.4 mmol.



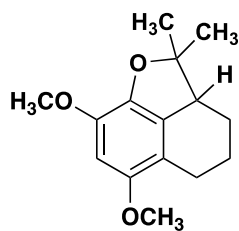
(145) 8-isopropoxy-5,7-dimethoxy-3,4-dihydronaphthalen-1(2H)-one

To a solution of **144** (580 mg, 2.61 mmol, 1 equiv) in CH₃CN (26 mL, 0.1 M) split into two batches in flame-dried 20mL μ W vials, was added Cs₂CO₃ (2.55 g, 7.83 mmol, 3.0 equiv) and isopropyl bromide (1.47 mL, 15.7 mmol, 6.00). The solution was heated to 80 °C overnight, and then cooled, filtered, and concentrated *in vacuo*. The crude residue was purified on silica by flash column chromatography (90:10 to 80:20 hexanes:EtOAc) to afford the product (586 mg, 85%): ¹H NMR (599 MHz, CDCl₃) δ 6.71 (d, *J* = 2.3 Hz, 1H), 4.38 – 4.18 (m, 1H), 3.86 (d, *J* = 2.6 Hz, 3H), 3.84 (d, *J* = 2.5 Hz, 3H), 2.81 (dd, *J* = 8.2, 4.1 Hz, 2H), 2.58 (dd, *J* = 9.1, 4.1 Hz, 2H), 2.12 – 1.95 (m, 2H), 1.29 (d, *J* = 2.5 Hz, 3H), 1.28 (d, *J* = 2.6 Hz, 3H); ¹³C NMR (151 MHz, CDCl₃) δ 198.0, 152.7, 152.3, 141.2, 128.1, 126.0, 102.7, 76.6, 57.1, 56.1, 41.2, 23.2, 22.5, 22.3; AMM *m/z* calcd for C₁₅H₂₁O₄⁺ (M + H)⁺ 265.1434, found 265.1434.



(146) (8-isopropoxy-5,7-dimethoxy-3,4-dihydronaphthalen-1(2H)-ylidene)hydrazine

To a solution of **145** (78 mg, 0.249 mmol, 1.0 equiv) in EtOH (0.83 mL, 0.3 M) was added N₂H₄ (0.063 mL, 1.99 mmol, 8.0 equiv) and acetic acid (0.028 mL, 0.498 mmol, 2.0 equiv). The solution was stirred at room temperature for 2-3 hours. The reaction was diluted with Et₂O (15 mL), washed with DI H₂O (10 mL), and extracted with Et₂O (2 x 15 mL). The combined organic layer was washed with NaCl (aq, sat), dried over Na₂SO₄, and concentrated *in vacuo*. The crude residue was purified on silica by flash column chromatography (80:20 to 60:40 hexanes:EtOAc) to afford the product (75 mg, 93%): ¹H NMR (599 MHz, CDCl₃) δ 6.55 (s, 1H), 6.06 (s, 2H), 4.10 (s, 1H), 3.87 (d, *J* = 7.3 Hz, 3H), 3.81 (d, *J* = 10.7 Hz, 3H), 2.71 – 2.49 (m, 3H), 2.46 (s, 1H), 1.95 (s, 1H), 1.77 (s, 1H), 1.24 – 1.19 (m, 6H); AMM *m/z* calcd for C₁₅H₂₃N₂O₃⁺ (M + H)⁺ 279.1703, found 279.1701.

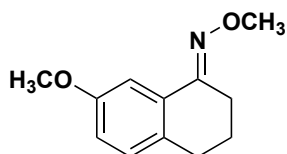


(148) 6,8-dimethoxy-2,2-dimethyl-2a,3,4,5-tetrahydro-2H-naphtho[1,8-*bc*]furan

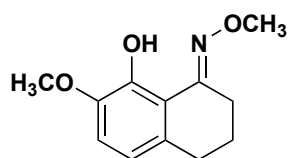
To a solution of **146** (80 mg, 0.244 mmol, 1.0 equiv) in CH₂Cl₂ (15 mL, 0.015 M) was added MnO₂ (169 mg, 1.96 mmol, 8.0 equiv), and the solution was allowed to stir until all the hydrazone had converted to diazo noted by TLC and a pink color (*its very important to make sure all the hydrazone has been oxidized before moving to the next step or else left over hydrazone will react with carbene to form unwanted byproducts*).

The solution was then cooled to -40 °C. The dirhodium catalyst Rh₂(PTAD)₄ (3.80 mg, 0.00244 mmol, 0.01 equiv) was added, and the solution was kept at -40 °C until the reaction was complete. The suspension was then filtered over Celite and concentrated *in vacuo*. The crude residue was purified on silica by flash column chromatography (90:10 hexanes:EtOAc) to afford the product (59.0 mg, 81%, 99:1 e.r.): ¹H NMR (599 MHz, CDCl₃) δ 6.28 (s, 1H), 3.87 (s, 3H), 3.77 (s, 3H), 3.01 (d, *J* = 11.3 Hz, 1H), 2.69 (d, *J* = 17.5 Hz, 1H), 2.39 (s, 1H), 2.13 (s, 1H), 1.97 – 1.84 (m, 1H), 1.63 (s, 3H), 1.60 (s, 1H), 1.30 (d, *J* = 12.4 Hz, 1H), 1.14 (s, 3H); ¹³C NMR (151 MHz, CDCl₃) δ 151.7, 141.8, 138.8, 131.9, 115.7, 97.0, 93.5, 56.9, 56.2, 49.4, 27.5, 23.3, 23.2, 21.8, 21.1; AMM *m/z* calcd for C₁₅H₂₁O₃⁺ (M + H)⁺ 249.1486, found 249.1482.

2.8.2 Right hemisphere: second-generation route



(229) 7-methoxy-3,4-dihydronaphthalen-1(2H)-one O-methyl oxime Following a modified literature precedent,¹⁷⁷ 7-methoxytetralone (20.0 g 113 mmol) and methoxyamine hydrochloride (11.8 g, 170 mmol) were added to a round bottom flask. Pyridine (22.9 mL, 284 mmol) and ethanol (227 mL, 0.5 M) were added, then the reaction was refluxed at 80 °C for 3 hours. After cooling down, the reaction was concentrated and rediluted in CH₂Cl₂, then washed sequentially with 1 M HCl (1 x 50 mL), NaHCO₃(sat) (1 x 50 mL), and brine (1 x 50 mL). The organic layer was dried over Na₂SO₄, filtered, and concentrated *in vacuo*. The crude reaction mixture required no further purification after workup affording oxime **229** as a light yellow solid (21.7 g, 93%): ¹H NMR (400 MHz, CDCl₃) δ 7.50 (d, *J* = 2.7 Hz, 1H), 7.04 (d, *J* = 8.4 Hz, 1H), 6.84 (dd, *J* = 8.4, 2.8 Hz, 1H), 3.99 (s, 3H), 3.83 (s, 3H), 2.73 – 2.63 (m, 4H), 1.87 – 1.76 (m, 2H). ¹H NMR data was consistent with literature values.¹⁷⁷

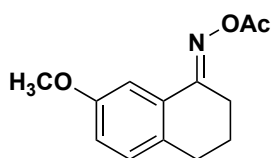


(236) 8-hydroxy-7-methoxy-3,4-dihydronaphthalen-1(2H)-one O-methyl oxime

Following a modified literature procedure,¹⁸⁹ oxime **229** (1.00 g, 4.87 mmol), Pd(OAc)₂ (0.054 g, 0.24 mmol, 5 mol%), triphenylphosphine (0.255 g, 0.974 mmol), and MeCN (16.3 mL, 0.3M) were added to a round bottom flask and stirred at room temperature for 30 minutes. Then K₂S₂O₈ (3.59 g, 5.84 mmol) was added to the reaction, and it was heated at 95 °C for 44 hours. The reaction was cooled down and filtered through a pad of celite.

Note: Specifically, K₂S₂O₈ (the dimer) was used not the related OxoneTM, there is an observed difference in reactivity for this substrate where no reaction is observed with OxoneTM. This has been reported before by the Sanford group.¹⁸⁵

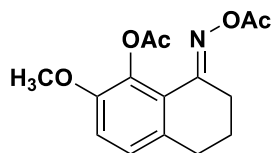
The crude product was solid loaded onto silica and purified by flash column chromatography (80:20 Hexanes:EtOAc) affording the hydroxylated oxime **236** as a yellow solid (Gram scale: 0.381 g, 35%, 500mg scale: 47%) ^1H NMR (400 MHz, CDCl_3) δ 11.62 (s, 1H), 6.81 (d, $J = 8.1$ Hz, 1H), 6.60 (d, $J = 8.2$ Hz, 1H), 3.99 (s, 3H), 3.88 (s, 3H), 2.78 (t, $J = 6.6$ Hz, 2H), 2.72 (t, $J = 5.6$ Hz, 2H), 1.83 (p, $J = 6.5$ Hz, 2H). ^{13}C NMR (101 MHz, CDCl_3) δ 159.68, 148.44, 146.82, 132.57, 118.18, 114.58, 113.28, 62.58, 56.47, 29.64, 24.56, 21.54. AMM (ESI) m/z calcd for $\text{C}_{12}\text{H}_{16}\text{NO}_3^+[\text{M}+\text{H}]^+$ 222.1130, found 222.1130



(257) 7-methoxy-3,4-dihydronaphthalen-1(2H)-one O-acetyl oxime

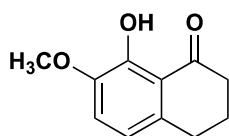
Following a modified literature procedure,¹⁹⁹ 7-methoxytetralone (30.0 g, 170 mmol, 1.0 equiv), hydroxylamine hydrochloride (17.7 g, 225 mmol, 1.5 equiv), EtOH (77 mL, 2.2 M), and pyridine (38 mL, 476 mmol, 2.8 equiv) were added to a round bottom flask. The reaction was heated at 60 °C for 10 hours, then it was cooled down to room temperature. Acetic anhydride (32.1 mL, 340 mmol, 2.0 equiv), DMAP (0.207 g, 1.7 mmol, 0.01 equiv), and pyridine (77 mL) were added. The reaction was stirred at room temperature for 16 hours. The solution was neutralized with NaHCO_3 (sat.) (50 mL), diluted with H_2O (100 mL), and extracted with EtOAc (3 x 70 mL). The organics were combined and washed with brine (2 x 20 mL) and H_2O (2 x 20 mL), dried over Na_2SO_4 , and concentrated *in vacuo*. Often the product is pure after work-up, but if byproducts do remain, it can be purified. The crude product was purified by flash column chromatography (15:85 EtOAc:hexanes) affording *O*-acetyl oxime **257** as a white solid (37.6 g, 95%): ^1H NMR (400 MHz, CDCl_3) δ 7.62 (d, $J = 2.8$ Hz, 1H), 7.09 (d, $J = 8.5$ Hz, 1H), 6.93 (dd, $J = 8.4, 2.8$ Hz, 1H), 3.83 (s, 3H), 2.87 – 2.81 (m, 2H), 2.75 – 2.70 (m, 2H), 2.27 (s, 3H), 1.87 (p, $J = 6.7$ Hz, 2H). ^1H NMR data was consistent with

literature values.²⁴⁰ ¹³C NMR (101 MHz, CDCl₃) δ 169.18, 161.53, 158.10, 133.59, 129.77, 129.67, 118.74, 108.42, 55.54, 28.76, 25.51, 21.57, 19.90. AMM (ESI) *m/z* calcd for C₁₃H₁₆NO₃⁺[M+H]⁺ 234.1125, found 234.1128.



(258) 8-(acetoxylimino)-2-methoxy-5,6,7,8-tetrahydronaphthalen-1-yl acetate

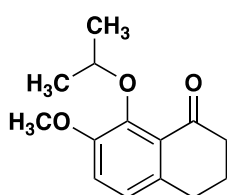
Following a modified literature procedure,^{198,200} **257** (10.0 g, 42.9 mmol, 1.0 equiv), PIDA (21.4 g, 64.3 mmol, 1.5 equiv), Pd(OAc)₂ (0.480 g, 2.14 mmol, 5 mol%), and AcOH/Ac₂O (10:1 v/v, 0.4 M) were added to a flame-dried round bottom flask. The reaction was heated to 70 °C for 24 hours, cooled down to room temperature, and diluted in H₂O. The mixture was extracted with EtOAc (3 x 100 mL), dried over Na₂SO₄, and concentrated *in vacuo*. The crude product was solid-loaded onto celite, and purified by flash column chromatography (0%-50% gradient of EtOAc:hexanes) affording acetoxylated oxime **258** as a yellow-orange solid (10.4 g, 83%): ¹H NMR (300 MHz, CDCl₃) δ 7.04 (d, *J* = 8.4 Hz, 2H), 6.98 (d, *J* = 8.4 Hz, 1H), 3.82 (s, 3H), 2.86 (t, *J* = 6.7 Hz, 2H), 2.71 (t, *J* = 6.1 Hz, 2H), 2.42 (s, 3H), 2.19 (s, 3H), 1.83 (bs, 2H). ¹H NMR data was consistent with literature values.^{191,192}



(227) 7-methoxy-8-hydroxy-3,4-dihydronaphthalen-1(2H)-one

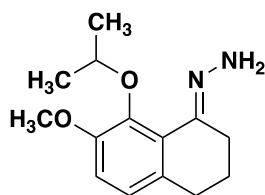
258 (3.52 g, 12.1 mmol, 1.0 equiv) and dioxanes (40.3 mL, 0.3M) were added to a round-bottom. Concentrated HCl (~3 mL) was added to solution, then the reaction was heated at reflux for 3 hours. The reaction was cooled down and slowly quenched with NaHCO₃(sat.) (20 mL). The mixture was diluted in H₂O, extracted with EtOAc (3 x 20 mL), dried over Na₂SO₄ and concentrated *in vacuo*. The crude product was purified by flash column chromatography

(30:70 EtOAc:hexanes) affording phenol **227** as a light yellow solid (2.18 g, 94%): ^1H NMR (400 MHz, CDCl_3) δ 12.71 (s, 1H), 6.99 (d, $J = 8.1$ Hz, 1H), 6.66 (d, $J = 8.2$ Hz, 1H), 3.88 (s, 3H), 2.92 – 2.84 (m, 2H), 2.72 – 2.64 (m, 2H), 2.09 (p, $J = 6.3$ Hz, 2H). ^1H NMR data was consistent with literature values.²⁴¹ ^{13}C NMR (101 MHz, CDCl_3) δ 205.80, 153.04, 146.61, 136.23, 117.76, 117.60, 117.00, 56.34, 39.07, 29.24, 23.27. AMM (ESI) m/z calcd for $\text{C}_{11}\text{H}_{13}\text{O}_3^+[\text{M}+\text{H}]^+$ 193.0864, found 193.0863.



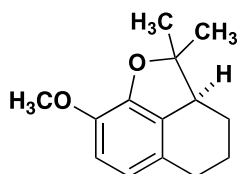
(199) 8-isopropoxy-7-methoxy-3,4-dihydronaphthalen-1(2H)-one

227 (0.733 g, 3.83 mmol, 1.0 equiv) and Cs_2CO_3 (3.73 g, 11.5 mmol, 3.0 equiv) were added to a flame-dried 20 mL microwave vial. The vial was sealed and backfilled with Ar x 3. MeCN (12.7 mL, 0.3M) then *i*Pr-I (0.76 mL, 7.66 mmol, 2.00 equiv) were added to the vial. The solution was heated at 80 °C overnight. The reaction was cooled down to room temperature, Cs_2CO_3 was filtered off, and the filtrate was concentrated *in vacuo*. The crude product was purified by flash column chromatography (20:80 EtOAc:Hexanes), affording isopropylated tetralone **199** as a yellow oil (0.771 g, 86%): ^1H NMR (400 MHz, CDCl_3) δ 7.02 (d, $J = 8.4$ Hz, 1H), 6.91 (d, $J = 8.3$ Hz, 1H), 4.41 (hept, $J = 6.2$ Hz, 1H), 3.82 (s, 3H), 2.87 (t, $J = 6.1$ Hz, 2H), 2.59 (t, $J = 6.6$ Hz, 2H), 2.04 (p, $J = 6.5$ Hz, 2H), 1.31 (s, 3H), 1.30 (s, 3H). ^{13}C NMR (101 MHz, CDCl_3) δ 197.55, 152.75, 148.15, 137.98, 127.77, 123.41, 117.66, 76.84, 56.61, 41.11, 30.31, 23.21, 22.42(2). AMM (ESI) m/z calcd for $\text{C}_{14}\text{H}_{19}\text{O}_3^+[\text{M}+\text{H}]^+$ 257.1147, found 257.1153.



(259) 8-isopropoxy-7-methoxy-3,4-dihydronaphthalen-1(2H)-ylidene hydrazine

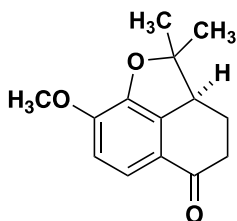
199 (100. mg, 0.427 mmol, 1.0 equiv) in anhydrous EtOH (1.42 mL) was added to a flame-dried round bottom flask backfilled with Ar. Acetic acid (0.049 mL, 0.854 mmol, 2.0 equiv) then hydrazine (0.080 mL, 2.56 mmol, 6.0 equiv) were added. The reaction was stirred at room temperature for 2 hours. The mixture was dumped into H₂O (5 mL), extracted with EtOAc (3 x 5 mL), dried over Na₂SO₄, and concentrated *in vacuo*. The crude reaction mixture required no further purification after workup affording hydrazone **259** as a light yellow oil (105 mg, 99%): ¹H NMR (400 MHz, CDCl₃) δ 6.78 (s, 2H), 5.38 (bs, 2H), 4.27 – 4.17 (m, 1H), 3.82 (s, 3H), 2.59 – 2.52 (m, 3H), 2.46 (t, *J* = 6.7 Hz, 2H), 1.87 – 1.78 (m, 2H), 1.23 (d, *J* = 6.2 Hz, 7H). ¹³C NMR (101 MHz, CDCl₃) δ 153.08, 145.90, 134.62, 128.52, 122.31, 113.27, 75.68, 57.02, 30.50, 25.10, 22.37(2), 22.16.



(192) 8-methoxy-2,2-dimethyl-2a,3,4,5-tetrahydro-2H-naphtho[1,8-*bc*]furan

To a solution of **259** (3.31 g, 13.3 mmol, 1.0 equiv) in CH₂Cl₂ (133 mL, 0.1 M) was added MnO₂ (6.88 g, 80.0 mmol, 6.0 equiv), and the solution was allowed to stir until all the hydrazone had converted to diazo noted by TLC and a pink color, about 3 hours (*its very important to make sure all the hydrazone has been oxidized before moving to the next step or else left over hydrazone will react with carbene to form unwanted byproducts*). The solution was then cooled to 0 °C. The dirhodium catalyst Rh₂(S-PTAD)₄ (208 mg, 0.133 mmol, 0.01

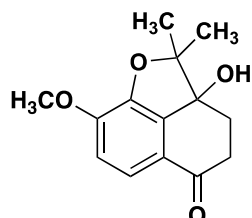
equiv) was added, and the solution was allowed to warm to room temperature until the reaction was complete (complete in 30 mins but can be left to stir overnight without issue). The suspension was then filtered over Celite and concentrated *in vacuo*. The crude residue was purified on silica by flash column chromatography (80:20 hexanes:EtOAc) to afford the product **192** as a clear oil (2.64 g, 91% with 1 mol% catalyst; yield drops to 78% if 0.02 mol% of catalyst used): ^1H NMR (400 MHz, CDCl_3) δ 6.68 (d, $J = 7.3$ Hz, 1H), 6.57 (d, $J = 8.2$ Hz, 1H), 3.84 (s, 3H), 3.05 (dddd, $J = 12.1, 5.7, 2.0, 1.0$ Hz, 1H), 2.74 (ddd, $J = 17.0, 6.6, 1.3$ Hz, 1H), 2.56 (dddt, $J = 17.0, 11.8, 6.7, 1.6$ Hz, 1H), 2.10 (dddd, $J = 13.4, 6.6, 4.2, 2.8, 1.5$ Hz, 1H), 1.91 (dtd, $J = 11.7, 4.4, 3.0$ Hz, 1H), 1.79 – 1.67 (m, 1H), 1.65 (s, 3H), 1.34 (dtd, $J = 13.1, 12.0, 2.8$ Hz, 1H), 1.16 (s, 3H). ^{13}C NMR (101 MHz, CDCl_3) δ 144.97, 142.34, 130.55, 127.34, 119.44, 112.50, 94.03, 56.40, 49.21, 27.63, 25.00, 23.79, 23.56, 21.82.



(193) 8-methoxy-2,2-dimethyl-2,2a,3,4-tetrahydro-5H-naphtho[1,8-*bc*]furan-5-one

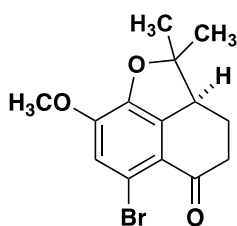
A solution of **192** (1.34 g, 6.14 mmol, 1.0 equiv) in MeCN/ H_2O (5/1 v/v, 0.1M) was cooled to 0 °C. A ground mixture of $\text{KMnO}_4/\text{MnO}_2$ (1:3 w/w, 12.3 g, 2 g per 1 mmol of **192**) was added and the reaction was stirred at 0 °C for 6 hours. The reaction was filtered through a celite and alumina plug and diluted in EtOAc. The filtrate was washed with H_2O (3 x 30 mL) and brine (3 x 50 mL), dried over Na_2SO_4 , and concentrated *in vacuo*. The crude product was purified immediately by flash column chromatography (40:60 EtOAc:hexanes) affording ketone **193** as a white solid (0.331 g, 23%): ^1H NMR (400 MHz, CDCl_3) δ 7.40 (d, $J = 8.5$ Hz, 1H), 6.83 (d, $J = 7.7$ Hz, 1H), 3.94 (s, 3H), 3.42 (dd, $J = 12.5, 4.6$ Hz, 1H), 2.74 (ddd, $J = 17.4, 4.0, 2.5$ Hz,

1H), 2.54 (ddd, $J = 17.4, 13.7, 4.7$ Hz, 1H), 2.14 (ddt, $J = 12.2, 4.7, 2.4$ Hz, 1H), 2.06 – 1.92 (m, 1H), 1.72 (s, 3H), 1.26 (s, 3H). ^{13}C NMR (101 MHz, CDCl_3) δ 196.13, 148.58, 144.07, 139.15, 123.69, 119.28, 112.75, 94.14, 56.31, 48.60, 38.91, 27.90, 25.49, 22.35.



(264) 2a-hydroxy-8-methoxy-2,2-dimethyl-2,2a,3,4-tetrahydro-5H-naphtho[1,8-*bc*]furan-5-one

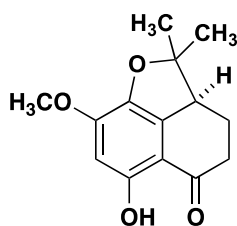
Alcohol 264 was the byproduct of the $\text{KMnO}_4/\text{MnO}_2$ oxidation reaction. It was isolated after the same column of the crude product purified by flash column chromatography 40:60 EtOAc:hexanes affording byproduct **264** as a yellow solid: ^1H NMR (400 MHz, CDCl_3) δ 7.48 (d, $J = 8.4$ Hz, 1H), 6.95 (d, $J = 8.5$ Hz, 1H), 3.98 (s, 3H), 3.14 (ddd, $J = 18.0, 12.6, 5.5$ Hz, 1H), 2.65 (ddd, $J = 17.7, 4.5, 2.1$ Hz, 1H), 2.35 – 2.20 (m, 2H), 1.89 (s, 1H), 1.70 (s, 3H), 1.32 (s, 3H). ^{13}C NMR (76 MHz, CDCl_3) δ 196.16, 149.59, 144.27, 137.42, 123.29, 120.01, 114.14, 96.47, 77.03, 56.42, 35.04, 29.99, 24.30, 20.92.



(260) 6-bromo-8-methoxy-2,2-dimethyl-2,2a,3,4-tetrahydro-5H-naphtho[1,8-*bc*]furan-5-one

193 (0.330 g, 1.42 mmol, 1.0 equiv) and freshly recrystallized NBS (0.278 g, 1.56 mmol, 1.1 equiv) were added to a flame-dried round bottom flask and it was backfilled with Ar x 3. Anhydrous CH_2Cl_2 (4.7 mL, 0.3 M) was added and the reaction was stirred at room temperature

overnight. The reaction was concentrated *in vacuo*, then purified by flash chromatography (40:60 EtOAc:hexanes) to afford the aryl bromide **260** as an orange solid (358 mg, 81%): ¹H NMR (400 MHz, CDCl₃) δ 7.00 (d, *J* = 0.7 Hz, 1H), 3.93 (s, 3H), 3.46 – 3.38 (m, 1H), 2.85 – 2.74 (m, 1H), 2.55 (ddt, *J* = 17.4, 13.8, 5.3 Hz, 1H), 2.09 (dtd, *J* = 12.2, 4.8, 2.4 Hz, 1H), 2.02 – 1.91 (m, 1H), 1.71 (s, 3H), 0.88 (s, 3H).

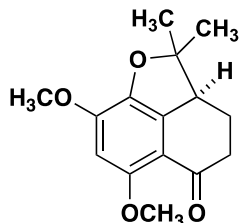


(262) 6-hydroxy-8-methoxy-2,2-dimethyl-2,2a,3,4-tetrahydro-5H-naphtho[1,8-*bc*]furan-5-one

Aryl bromide **260** (91 mg, 0.292 mmol, 1.0 equiv), PdCl₂dppf (2.38 mg, 0.0292 mmol, 10 mol%), B₂pin₂ (297 mg, 1.17 mmol, 4.0 equiv), and KOAc (230 mg, 2.34 mmol, 8.0 equiv) were added to a flame-dried microwave vial and backfilled with Ar x 3. Anhydrous toluene (3.65 mL, 0.08 M) was added, then the reaction was heated to 100 °C for 45 minutes. The reaction was cooled down, diluted in H₂O (5 mL), and extracted with CH₂Cl₂ (3 x 5 mL). The organics were concentrated *in vacuo* and the crude aryl Bpin product was pushed immediately into the next reaction.

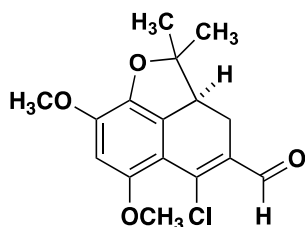
The crude aryl Bpin in MeCN (2.92 mL, 0.1 M) was added to a round bottom flask. H₂O (2.92 mL, 0.1M) was added followed by NaBO₃·4H₂O (462 mg, 2.92 mmol, 10 equiv). The reaction was stirred at room temperature for 2 hours. The mixture was diluted with Na₂S₂O₃(sat.) (5 mL) and H₂O (5 mL), then extracted with EtOAc (3 x 10 mL). The organics were combined, dried over Na₂SO₄, and concentrated *in vacuo*. The crude product was solid loaded on silica and purified by flash chromatography (30:70 EtOAc:hexanes) to afford phenol **262** as a light yellow

solid (47.1 mg, 65% over 2 steps): AMM (ESI) m/z calcd for $C_{15}H_{18}O_4^+[M+H]^+$ 249.1122, found 249.1122.



(150) 6,8-dimethoxy-2,2-dimethyl-2,2a,3,4-tetrahydro-5H-naphtho[1,8-*bc*]furan-5-one

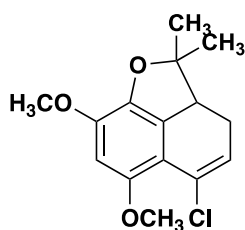
Cs_2CO_3 (200 mg, 0.568 mmol, 3.00 equiv) was added to a flame-dried microwave vial and backfilled with Ar x 3. Phenol **262** (47 mg, 0.189 mmol, 1.0 equiv) in MeCN (1.89 mL, 0.1M) was added, followed by methyl iodide (0.024 mL, 0.378 mmol, 2.0 equiv). The reaction was heated to 50 °C for 2 hours. The reaction was cooled down, filtered, and concentrated *in vacuo*. The crude product was purified by flash chromatography (40:60 EtOAc:hexanes) to afford **150** (47.1 mg, 95%): 1H NMR (600 MHz, $CDCl_3$) δ 6.32 (s, 1H), 3.95 (s, 3H), 3.89 (s, 3H), 3.40 – 3.30(m, 1H), 2.78 – 2.67 (m, 1H), 2.51 (td, $J = 13.6, 6.7$ Hz, 1H), 2.10 – 2.00 (m, 1H), 1.99 – 1.87 (m, 1H), 1.68 (s, 3H), 1.24 (s, 3H); ^{13}C NMR (151 MHz, $CDCl_3$) δ 194.2, 155.5, 148.9, 139.5, 112.4, 96.6, 92.6, 56.6, 56.3, 49.4, 40.0, 27.6, 24.5, 22.1; AMM m/z calcd for $C_{15}H_{19}O_4^+ (M + H)^+$ 263.1278, found 263.1276.



(155) (*S*)-5-chloro-6,8-dimethoxy-2,2-dimethyl-2a,3-dihydro-2H-naphtho[1,8-*bc*]furan-4-carbaldehyde

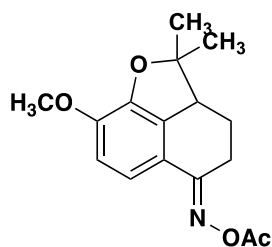
150 (16 mg, 0.061 mmol, 1.0 equiv) in DMF (0.294 mL, 3.05 mmol, 50 equiv) was added to a flame-dried microwave vial under Ar and the solution was heated to 40 °C. $POCl_3$ (0.071 mL,

0.610 mmol, 10 equiv) was added and the reaction was continued to be heated for 30 minutes. The reaction was cooled down to room temperature, quenched with a saturated $\text{K}_2\text{CO}_3(\text{aq})$ solution (1 mL), and stirred at room temperature for 5 minutes. The mixture was extracted with Et_2O (3 x 5 mL), dried over Na_2SO_4 , and concentrate *in vacuo*. The crude product **155** was used without further purification (14.3 mg, 76%): $^1\text{H NMR}$ (300 MHz, CDCl_3) δ 10.06 (s, 1H), 6.77 (dd, $J = 9.9, 0.7$ Hz, 1H), 6.12 (s, 1H), 6.09 (dd, $J = 2.3, 0.7$ Hz, 1H), 5.80 (d, $J = 2.3$ Hz, 1H), 5.55 (d, $J = 9.9$ Hz, 1H), 3.87 (s, 4H), 3.65 (s, 3H), 3.49 (s, 3H), 3.46 – 3.32 (m, 2H), 2.98 (dd, $J = 15.3, 6.9$ Hz, 1H), 2.27 (t, $J = 15.5$ Hz, 1H), 1.49 (s, 6H), 1.46 (s, 4H), 1.33 (s, 4H).



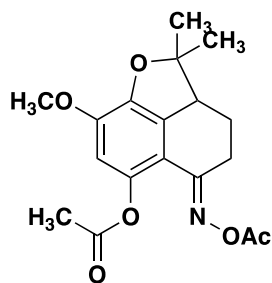
(277) 5-chloro-6,8-dimethoxy-2,2-dimethyl-2a,3-dihydro-2H-naphtho[1,8-*bc*]furan

150 (58 mg, 0.221 mmol, 1.0 equiv) in DMF (0.736 mL, 0.3 M) was added to a flame-dried microwave vial under Ar. POCl_3 (0.027 mL, 0.287 mmol, 1.3 equiv) was added dropwise then the reaction was heated to 40 °C for 1 hour. The reaction was cooled down to room temperature, quenched with a saturated $\text{K}_2\text{CO}_3(\text{aq})$ solution (1 mL), and stirred at room temperature for 5 minutes. The mixture was extracted with EtOAc (3 x 5 mL), dried over Na_2SO_4 , and concentrate *in vacuo*. The crude product was purified by flash chromatography (20:80 EtOAc :hexanes) to afford the vinyl chloride byproduct **277** as a bright yellow oil (45 mg, 66%) that degrades quickly overnight: $^1\text{H NMR}$ (400 MHz, CDCl_3) δ 6.34 (d, $J = 0.9$ Hz, 1H), 5.89 (dd, $J = 7.0, 2.8$ Hz, 1H), 3.88 (s, 3H), 3.81 (s, 3H), 3.37 (dd, $J = 15.0, 8.0$ Hz, 1H), 2.36 – 2.18 (m, 2H), 1.61 (s, 3H), 1.27 (s, 4H).



(267b) 8-methoxy-2,2-dimethyl-2,2a,3,4-tetrahydro-5H-naphtho[1,8-*bc*]furan-5-one *O*-acetyl oxime

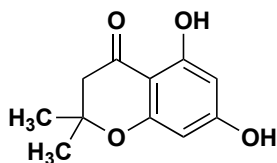
193 (0.086 g, 0.370 mmol, 1.0 equiv), hydroxylamine-HCl (0.103 g, 1.48 mmol, 4.0 equiv), and pyridine (12.3 mL, 0.03 M) were added to a round bottom flask and the reaction was heated to 80 °C overnight. The reaction was cooled down then DMAP (0.023 g, 0.185 mmol, 0.5 equiv) and Ac₂O (3.78 mL, 3.70 mmol, 10.0 equiv) were added and the reaction was stirred at room temperature overnight. The reaction was quenched with NaHCO₃ (aq) (20 mL) and extracted with EtOAc (3 x 20 mL) and dried over Na₂SO₄ and concentrated *in vacuo*. The crude product was purified by flash column chromatography (50:50 EtOAc:hexanes) affording 8-methoxy-2,2-dimethyl-2,2a,3,4-tetrahydro-5H-naphtho[1,8-*bc*]furan-5-one *O*-acetyl oxime (**267b**) as a white solid (0.081 g, 76%): ¹H NMR (300 MHz, CDCl₃) δ 7.51 (d, *J* = 8.5 Hz, 1H), 6.79 (d, *J* = 9.4 Hz, 1H), 3.91 (s, 3H), 3.50 – 3.37 (m, 1H), 3.17 (dd, *J* = 12.6, 4.5 Hz, 1H), 2.47 – 2.32 (m, 1H), 2.26 (s, 3H), 2.02 (td, *J* = 4.8, 2.4 Hz, 1H), 1.69 (s, 4H), 1.67 – 1.53 (m, 1H), 1.22 (s, 4H).



(270) 5-(acetoxyimino)-8-methoxy-2,2-dimethyl-2a,3,4,5-tetrahydro-2H-naphtho[1,8-*bc*]furan-6-yl acetate

267b (0.060 g, 0.207 mmol, 1.0 equiv), Pd(OAc)₂ (0.014 g, 0.062 mmol, 0.3 equiv), PIDA (0.133 g, 0.414 mmol, 2.0 equiv), and 10:1 mix of AcOH/Ac₂O (1.90mL:0.191mL, 0.1M) were added to a microwave vial. The reaction was heated to 80 °C overnight. The reaction was quenched with NaHCO₃ (1 mL), diluted in H₂O (2 mL), and extracted with EtOAc (3 x 2 mL). The combined organics were dried over Na₂SO₄. The crude product was purified by flash column chromatography (50:50 Et₂O:pentanes) affording 5-(acetoxylimino)-8-methoxy-2,2-dimethyl-2a,3,4,5-tetrahydro-2*H*-naphtho[1,8-*bc*]furan-6-yl acetate **270** as a light yellow solid (0.023 g, 32%): ¹H NMR (400 MHz, CDCl₃) δ 6.51 (s, 1H), 3.88 (s, 3H), 3.48 – 3.37 (m, 1H), 3.22 – 3.13 (m, 1H), 2.42 (s, 3H), 2.42 – 2.31 (m, 3H), 2.18 (s, 3H), 1.99 (dtd, *J* = 12.1, 4.9, 2.4 Hz, 1H), 1.67 (s, 3H), 1.63 – 1.57 (m, 1H), 1.24 (s, 3H).

2.8.3 Left hemisphere: phenol functionality

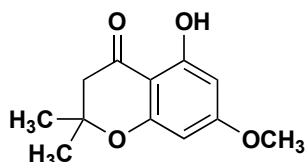


(164) 5,7-dihydroxy-2,2-dimethylchroman-4-one

Adapted from a reported procedure¹¹⁴, phloroglucinol (5.00 g, 39.6 mmol, 1.0 equiv) and 3-methylcrotonic acid (4.75g, 47.5 mmol, 1.2 equiv) were added to a flame dried microwave vial, and then it was backfilled with argon. To the solution was added BF₃-Et₂O (19.6 mL, 158.4 mmol, 4.0 equiv), then the reaction was heated to 80 °C for 10 minutes. The reaction was cooled down to room temperature and left to stir overnight (yellow solution to orange solution). The reaction was poured into an ice water solution adjusted to a pH ~10 using 10% KOH (aq). The aqueous layer was washed with EtOAc (3 x 10 mL), then it was acidified with 10% HCl (aq) to a pH ~1 and stirred for 10 minutes. The solution was filtered, washed with H₂O, and the precipitate was collected affording 5,7-dihydroxy-2,2-dimethylchroman-4-one (**164**) as a white solid (7.80 g, 95%).

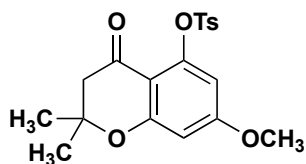
Note: Add anhydrous Et₂O if small scale and more solvent is needed.

¹H NMR (400 MHz, CDCl₃) δ 12.71, 7.26, 7.00, 6.98, 6.67, 6.64, 3.88, 2.89, 2.88, 2.86, 2.70, 2.68, 2.66, 2.14, 2.12, 2.11, 2.10, 2.09, 2.07, 2.07, 2.06, 2.05, 2.05, 0.00.



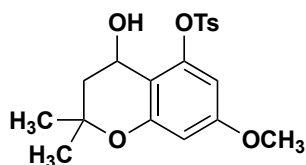
(165) 5-hydroxy-7-methoxy-2,2-dimethylchroman-4-one

Adapted from a reported literature procedure¹¹⁴, add 5,7-dihydroxy-2,2-dimethylchroman-4-one (0.369 g, 1.77 mmol, 1.0 equiv), K₂CO₃ (0.489 g, 3.54 mmol, 2.0 equiv), and acetone (4.0 mL, 0.5M) to flame dried round bottom flask fitted with a reflux condenser. To the solution was added methyl iodide (0.154 mL, 2.48 mmol, 1.4 equiv), then it was heated to reflux (55 °C) for 1 hr. The reaction was cool down to room temperature, filtered, and the filtrate was concentrated *in vacuo*. The crude product was diluted in H₂O and extracted with hexanes (3 x 10 mL). The combined organics were dried over Na₂SO₄, and concentrate *in vacuo* affording 5-hydroxy-7-methoxy-2,2-dimethylchroman-4-one (**165**) as a light orange solid (0.320 mg, 81%): ¹H NMR (400 MHz, CDCl₃) δ 12.00 (s, 1H), 6.01 (d, *J* = 2.3 Hz, 1H), 5.94 (d, *J* = 2.3 Hz, 1H), 3.80 (s, 3H), 2.68 (s, 2H), 1.45 (s, 7H). ¹H NMR data was consistent with literature values^{114,242}



(166) 7-methoxy-2,2-dimethyl-4-oxochroman-5-yl 4-methylbenzenesulfonate

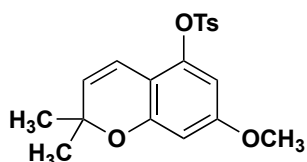
Adapted from a reported literature procedure¹¹⁴, **165** (0.260 g, 1.17 mmol, 1.0 equiv), tosyl chloride (0.223 g, 1.17 mmol, 1.0 equiv), and acetone (4.0 mL, 0.3M) were added to a flame dried round bottom flask under argon. A reflux condenser was added then the reaction was refluxed at 60 °C for 3 hours. The reaction was cooled down, K₂CO₃ was filtered off, and the filtrate was concentrated *in vacuo*. The crude product was purified by flash column chromatography (50:50 EtOAc:hexanes) affording 7-methoxy-2,2-dimethyl-4-oxochroman-5-yl 4-methylbenzenesulfonate (**166**) as a clear oil (0.294 g, 67%): ¹H NMR (599 MHz, cdcl₃) δ 7.89 (dt, *J* = 8.4, 1.9 Hz, 2H), 7.32 (d, *J* = 7.9 Hz, 2H), 6.44 (s, 1H), 6.33 (s, 1H), 3.80 (t, *J* = 1.9 Hz, 4H), 2.54 (s, 3H), 2.43 (s, 4H), 1.36 (t, *J* = 1.9 Hz, 8H). ¹³C NMR (101 MHz, CDCl₃) δ 188.18, 164.72, 162.42, 148.75, 145.23, 132.87, 129.45(2), 128.95(2), 108.31, 104.54, 100.77, 79.45, 55.82, 49.54, 26.34(2), 21.71. IR (thin film) 2976, 1689, 1614, 1433, 1197 cm⁻¹. AMM (ESI) *m/z* calcd for C₁₉H₂₁O₆S⁺[M+H]⁺ 377.1058, found 377.1023.



(166-int) 4-hydroxy-7-methoxy-2,2-dimethylchroman-5-yl 4-methylbenzenesulfonate

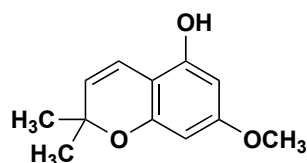
166 (0.260 g, 0.691 mmol, 1.0 equiv) in THF (25 mL, 0.03M) was added to a flame-dried round bottom flask under argon. BH₃·THF (0.889 mL, 0.829 mmol, 1.2 equiv) was added and stirred at 40 °C for 1.5 hrs. The reaction was quenched with H₂O (1 mL), then extracted with Et₂O (3 x 5 mL), dried over Na₂SO₄, and concentrated *in vacuo*. The crude product was purified by flash column chromatography (30:70 EtOAc:hexanes) affording 4-hydroxy-7-methoxy-2,2-dimethylchroman-5-yl 4-methylbenzenesulfonate (**166-int**) as a white solid (0.261 g, 99%): ¹H NMR (300 MHz, CDCl₃) δ 7.87 (d, *J* = 8.4 Hz, 2H), 7.38 (d, *J* = 8.1 Hz, 2H), 6.29 (d, *J* = 2.5 Hz, 1H), 6.18 (d, *J* = 2.4 Hz, 1H), 4.86 – 4.78 (m, 1H), 3.69 (s, 3H), 2.90 (s, 1H), 2.47 (s, 3H), 2.03 (dd, *J* = 14.3, 4.1 Hz, 1H), 1.87 (dd, *J* = 14.4, 5.5 Hz, 1H), 1.45 (s, 3H), 1.32 (s, 3H). ¹³C

NMR (76 MHz, CDCl₃) δ 160.28, 155.45, 149.36, 145.91, 132.66, 130.02(2), 128.53(2), 110.61, 101.65, 100.98, 75.29, 59.43, 55.45, 40.07, 28.69, 26.63, 21.77. IR (thin film) 3203, 1623, 1373, 1178, 1141 cm⁻¹. AMM (ESI) m/z calcd for C₁₉H₂₃O₆S⁺[M+H]⁺ 401.1029, found 401.1035



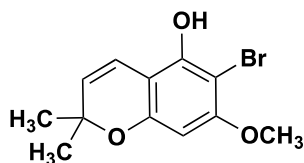
(167) 7-methoxy-2,2-dimethyl-2H-chromen-5-yl 4-methylbenzenesulfonate

166-int (0.261 g, 0.690 mmol, 1.0 equiv) and *p*-TsOH (0.026 g, 10mg/100 mg of **166-int**), and THF (0.3M) were added to a round bottom flask. The reaction was refluxed at 70 °C overnight. Then the reaction was quenched with H₂O (1.0 mL), extracted with Et₂O (3 x 5 mL), dried over Na₂SO₄, and concentrated *in vacuo*. The crude product was purified by flash column chromatography (30:70 EtOAc:hexanes) affording 7-methoxy-2,2-dimethyl-2H-chromen-5-yl 4-methylbenzenesulfonate **167** as a clear oil (0.248 g, 99%): ¹H NMR (300 MHz, DMSO) δ 7.74 (d, J = 8.3 Hz, 2H), 7.45 (d, J = 8.1 Hz, 2H), 6.34 (d, J = 1.7 Hz, 1H), 6.14 (d, J = 2.4 Hz, 1H), 6.10 (d, J = 9.3 Hz, 2H), 5.49 (d, J = 10.0 Hz, 1H), 3.66 (s, 3H), 2.40 (s, 3H), 1.24 (s, 6H). ¹³C NMR (76 MHz, DMSO) δ 159.64, 154.27, 146.00, 145.17, 131.06, 130.21(2), 129.07, 128.38(2), 114.98, 108.20, 101.08, 100.95, 76.57, 55.50, 27.20(2), 21.12. IR (thin film) 2976, 1622, 1374, 1178, 1140 cm⁻¹. AMM (ESI) m/z calcd for C₁₉H₂₁O₅S⁺[M+H]⁺ 361.1109, found 361.1110.



(168) 7-methoxy-2,2-dimethyl-2H-chromen-5-ol

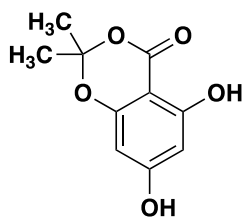
168 (0.042 g, 0.117 mmol, 1.0 equiv), KOH(aq) (1.7 mL, 1 M), and EtOH (1.7 mL, 0.7 M) were added to a microwave vial under argon. The reaction was heated at 80 °C for 1 hour. After cooling the solution to room temperature, the reaction was acidified with 1M NaHSO₄(aq) and extracted with Et₂O (3 x 5 mL). The combined organics were washed with NaHCO₃ (1 x 5 mL) and brine (1 x 5 mL), then dried over MgSO₄ and concentrated *in vacuo*. The crude product was purified by flash column chromatography (30:70 EtOAc:hexanes) affording 7-methoxy-2,2-dimethyl-2*H*-chromen-5-ol **168** as a dark orange solid (0.016 g, 65%): ¹H NMR (300 MHz, CDCl₃) δ 6.53 (d, *J* = 9.2 Hz, 1H), 6.03 (d, *J* = 1.6 Hz, 1H), 5.91 (d, *J* = 2.3 Hz, 1H), 5.46 (d, *J* = 9.9 Hz, 1H), 3.72 (s, 3H), 1.42 (s, 7H). ¹³C NMR (76 MHz, CDCl₃) δ 160.71, 155.01, 152.09, 126.46, 116.15, 103.26, 95.00, 94.80, 76.35, 55.32, 27.76(2). IR (thin film) 3443, 2975, 1617, 1580, 1115 cm⁻¹. AMM (ESI) *m/z* calcd for C₁₂H₁₅O₃⁺[M+H]⁺ 207.1021, found 207.1021.



(274) 6-bromo-7-methoxy-2,2-dimethyl-2*H*-chromen-5-ol

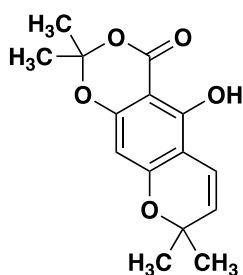
168 (100 mg, 0.485 mmol, 1.00 equiv) and CH₂Cl₂ (4.85 mL, 0.1 M) were added to a flame dried round bottom flask. NBS (86.4 mg, 0.485 mmol, 1.0 equiv) was added and the reaction was stirred at room temperature for 2 hours. The mixture was washed with H₂O (3 x 5 mL), dried over Na₂SO₄, and concentrated *in vacuo*. The crude product was purified by flash chromatography to afford aryl bromide **274** as an orange solid (83%): ¹H NMR (400 MHz, CDCl₃) δ 6.60 (d, *J* = 9.9 Hz, 1H), 6.08 (s, 1H), 5.67 (s, 1H), 5.47 (d, *J* = 9.9 Hz, 1H), 3.83 (s, 3H), 1.42 (s, 6H).

2.8.4 Left hemisphere: ester functionality



(157) 5,7-dihydroxy-2,2-dimethyl-4H-benzo[d][1,3]dioxin-4-one

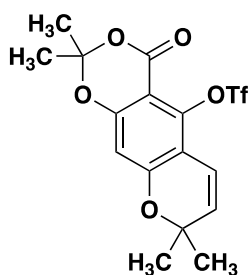
2,4,6-trihydroxybenzoic acid (2.0 g, 10.7 mmol) and acetone (3.94 mL, 53.2 mmol) were added to a round bottom flask. Then TFA (7.10 mL, 1.5 M) and TFAA (2.94 mL, 21.3 mmol) were added sequentially and the reaction was stirred overnight at rt. The mixture was diluted in H₂O, then washed with EtOAc (3 x 20 mL). The organics were combined and washed with H₂O (3 x 10 mL) then dried over Na₂SO₄ and concentrated *in vacuo*. The crude product was purified by flash column chromatography (60:40 Hexanes:EtOAc) affording acetal **157** as a yellow solid (2.04 g, 91%): ¹H NMR (400 MHz, Acetone) δ 6.09 (d, *J* = 1.9 Hz, 1H), 6.02 (d, *J* = 2.0 Hz, 1H), 1.71 (s, 7H). ¹H NMR data was consistent with literature values²⁴³



(158a) 5-hydroxy-2,2,8,8-tetramethyl-4H,8H-[1,3]dioxino[5,4-g]chromen-4-one

To a solution of **157** (1.37 g, 6.5 mmol) in EtOH (22 mL, 0.3 M) was added CaCl₂ (600 mg, 5.4 mmol), Et₃N (3.0 mL, 21.5 mmol), and 3-methylbut-2-enal (1.25 mL, 13.0 mmol). The solution was then heated to 80 °C for 1 hour. The reaction was cooled and acidified with 1M HCl (10 mL). A color change was noticed as the solution changed from dark brown to lighter brown, with a precipitate forming. The organic layer was extracted with EtOAc (3 x 30 mL), washed with DI H₂O (30 mL), dried over Na₂SO₄, and concentrated *in vacuo*. The crude

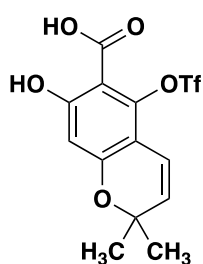
residue was purified by flash column chromatography (80:20 hexanes:EtOAc) to afford the product (1.2 g, 66%): ^1H NMR (400 MHz, CDCl_3) δ 10.64 (s, 1H), 6.60 (d, $J = 10.1$ Hz, 1H), 5.91 (s, 1H), 5.51 (d, $J = 10.1$ Hz, 1H), 1.72 (s, 6H), 1.45 (s, 6H). ^1H NMR data of purified compound was consistent with the reported literature values.¹¹⁰



(160) 2,2,8,8-tetramethyl-4-oxo-4H,8H-[1,3]dioxino[5,4-g]chromen-5-yl

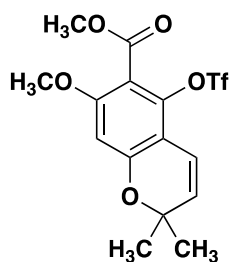
trifluoromethanesulfonate

Following a modified literature procedure,¹¹¹ to a solution of **158a** (1.2 g, 4.2 mmol) in CH_2Cl_2 (42 mL, 0.1 M) was added Et_3N (2.9 mL, 21 mmol) and DMAP (513 mg, 4.2 mmol). The solution was cooled to 0 °C, and trifluoroacetic anhydride (2.1 mL, 12.6 mmol) was added dropwise. The solution was observed to change color from yellow to red. The solution was allowed to warm to room temperature overnight, and then was quenched with Na_2HCO_3 (10 mL). The organic product was extracted with CH_2Cl_2 (3 x 40 mL), washed with NaCl, dried over Na_2SO_4 , and concentrated *in vacuo*. The residue was then purified on flash column chromatography (90:10 to 80:20 hexanes:EtOAc) to afford the product (1.4 g, 79%): ^1H NMR (599 MHz, CDCl_3) δ 6.51 (d, $J = 10.1$ Hz, 1H), 6.39 (s, 1H), 5.79 (d, $J = 10.1$ Hz, 1H), 1.75 (s, 6H), 1.48 (s, 6H).



(161) 7-hydroxy-2,2-dimethyl-5-(((trifluoromethyl)sulfonyl)oxy)-2H-chromene-6-carboxylic acid

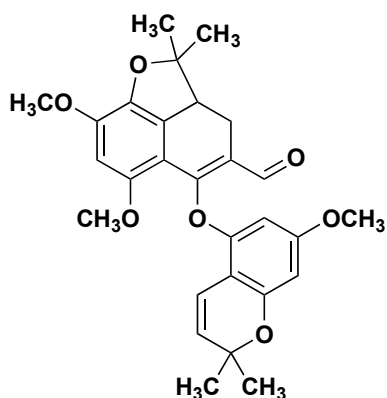
A solution of **161** (261.5 mg, 0.64 mmol) in CH₂Cl₂ (6.4 mL, 0.1 M) was cooled to 0 °C. BCl₃ (1.0 M in CH₂Cl₂, 3.2 mL, 3.2 mmol) was added dropwise. The solution was left stirring overnight, and then cooled to 0 °C before quenching with NH₄Cl (aq, sat.). After drying over Na₂SO₄ and concentrating *in vacuo*, the residue was purified by flash column chromatography (50:50 hexanes:EtOAc) to afford the product (116 mg, 50%): ¹H NMR (400 MHz, CDCl₃) δ 6.47 (d, *J* = 10.2 Hz, 1H), 6.45 (s, 1H), 5.68 (d, *J* = 10.0 Hz, 1H), 3.88 (s, 3H), 3.84 (s, 3H), 1.45 (s, 6H).



(162) methyl 7-methoxy-2,2-dimethyl-5-(((trifluoromethyl)sulfonyl)oxy)-2H-chromene-6-carboxylate

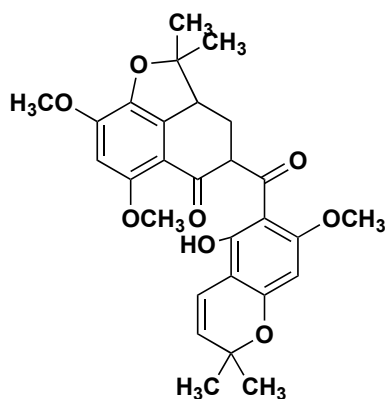
To a solution of **162** (105.6 mg, 0.29 mmol) in reagent grade dry acetone (1.0 mL, 0.3 M) was added K₂CO₃ (160.3 mg, 1.2 mmol) and CH₃I (0.18 mL, 2.9 mmol). The reaction was allowed to stir overnight, and then diluted with DI H₂O (10 mL), and extracted with EtOAc (3 x 10 mL). The organic layer was dried over Na₂SO₄ and concentrated *in vacuo*. The product was carried onto the next reaction without further purification (54.3 mg, 48%): ¹H NMR (400 MHz, CDCl₃) δ 6.47 (d, *J* = 10.2 Hz, 1H), 6.45 (s, 1H), 5.68 (d, *J* = 10.0 Hz, 1H), 3.88 (s, 3H), 3.84 (s, 3H), 1.45 (s, 6H).

2.8.4 Final steps: joining the two hemispheres



(275) 8-((λ^1 -oxidaneyl)- λ^5 -methyl)-6-methoxy-5-((7-methoxy-2,2-dimethyl-2*H*-chromen-5-yl)oxy)-2,2-dimethyl-2a,3-dihydro-2*H*-naphtho[1,8-*bc*]furan-4-carbaldehyde

Left hemisphere **168** (33 mg, 0.162 mmol, 2.5 equiv), Cs₂CO₃ (68.8 mg, 0.194 mmol, 3.0 equiv), and AgNO₃ (11 mg, 0.0648 mmol, 1.0 equiv) were added to a flame-dried microwave vial under Ar. A solution of right hemisphere **155** (20 mg, 0.0648 mmol, 1.0 equiv) in MeCN (~1 mL, 0.1 M) was added, and the sealed vial was heated to 60 °C overnight. The reaction was cooled down to room temperature, filtered, and concentrated *in vacuo*. The crude product was purified by flash chromatography (50:50 EtOAc:hexanes) to afford ether **275** as yellow solid (14.9 mg, 48%): ¹H NMR (300 MHz, CDCl₃) δ 10.06 (s, 1H), 6.77 (dd, *J* = 9.9, 0.7 Hz, 1H), 6.12 (s, 1H), 6.09 (dd, *J* = 2.3, 0.7 Hz, 1H), 5.80 (d, *J* = 2.3 Hz, 1H), 5.55 (d, *J* = 9.9 Hz, 1H), 3.87 (s, 4H), 3.65 (s, 3H), 3.49 (s, 3H), 3.46 – 3.32 (m, 2H), 2.98 (dd, *J* = 15.3, 6.9 Hz, 1H), 2.27 (t, *J* = 15.5 Hz, 1H), 1.49 (s, 6H), 1.46 (s, 4H), 1.33 (s, 4H).



(273) 4-(5-hydroxy-7-methoxy-2,2-dimethyl-2H-chromene-6-carbonyl)-6,8-dimethoxy-2,2-dimethyl-2,2a,3,4-tetrahydro-5H-naphtho[1,8-*bc*]furan-5-one

Add right hemisphere ketone **150** (20 mg, 0.076 mmol, 1.0 equiv) in THF (0.760 mL, 0.1 M) to a flame-dried round bottom flask under Ar. Cool to $-40\text{ }^{\circ}\text{C}$. Add NaH (3.35 mg, 0.084 mmol, 1.1 equiv) and stir for 30 minutes. Add Claisen left hemisphere **162** (36 mg, 0.091 mmol, 1.2 equiv) in THF (0.073 mL, 0.5 M). Stir while allowing to warm to room temperature. No reaction was occurring so 1.0 equiv of NaH was added, then the reaction was heated to $40\text{ }^{\circ}\text{C}$ overnight. The reaction was quenched with NH_4Cl (sat.), diluted in H_2O , and washed with EtOAc (3 x 5 mL). The crude product was purified using flash chromatography (40:60 EtOAc:hexanes) to yield the Claisen product with the triflate cleaved as white solid (3.3 mg, 9%): $^1\text{H NMR}$ (300 MHz, CDCl_3) δ 12.66 (s, 1H), 6.65 (dd, $J = 10.0, 0.6$ Hz, 1H), 6.31 (s, 2H), 5.99 (s, 1H), 5.50 (d, $J = 10.0$ Hz, 1H), 4.01 (s, 3H), 3.95 (d, $J = 0.8$ Hz, 5H), 3.88 (s, 5H), 3.45 – 3.37 (m, 1H), 2.47 (dtd, $J = 13.5, 6.7, 4.3$ Hz, 1H), 2.12 – 2.03 (m, 2H), 1.45 (s, 6H), 1.27 (t, $J = 3.6$ Hz, 4H), 1.22 (s, 6H).

2.9 References

- (1) the International Natural Product Sciences Taskforce; Atanasov, A. G.; Zotchev, S. B.; Dirsch, V. M.; Supuran, C. T. Natural Products in Drug Discovery: Advances and Opportunities. *Nat Rev Drug Discov* **2021**, *20* (3), 200–216. 10.1038/s41573-020-00114-z.

- (2) Lachance, H.; Wetzel, S.; Kumar, K.; Waldmann, H. Charting, Navigating, and Populating Natural Product Chemical Space for Drug Discovery. *J. Med. Chem.* **2012**, *55* (13), 5989–6001. 10.1021/jm300288g.
- (3) Abrams, D. J.; Provencher, P. A.; Sorensen, E. J. Recent Applications of C–H Functionalization in Complex Natural Product Synthesis. *Chem. Soc. Rev.* **2018**, *47* (23), 8925–8967. 10.1039/C8CS00716K.
- (4) Dishman, S. N.; Laconsay, C. J.; Fettinger, J. C.; Tantillo, D. J.; Shaw, J. T. Divergent Stereochemical Outcomes in the Insertion of Donor/Donor Carbenes into the C–H Bonds of Stereogenic Centers. *Chem. Sci.* **2022**, *13* (4), 1030–1036. 10.1039/D1SC04622E.
- (5) Chambers, S. A.; DeSousa, J. M.; Huseman, E. D.; Townsend, S. D. The DARK Side of Total Synthesis: Strategies and Tactics in Psychoactive Drug Production. *ACS Chem. Neurosci.* **2018**, *9* (10), 2307–2330. 10.1021/acchemneuro.7b00528.
- (6) Georgantea, P.; Ioannou, E.; Evain-Bana, E.; Bagrel, D.; Martinet, N.; Vagias, C.; Roussis, V. Sesquiterpenes with Inhibitory Activity against CDC25 Phosphatases from the Soft Coral *Pseudopterogorgia Rigida*. *Tetrahedron* **2016**, *72* (23), 3262–3269. 10.1016/j.tet.2016.04.059.
- (7) Tamaki, M.; Sadhu, S. K.; Ohtsuki, T.; Toume, K.; Koyano, T.; Kowithayakorn, T.; Hayashi, M.; Komiyama, K.; Ishibashi, M. Parviflorene J, a Cytotoxic Sesquiterpene Dimer with a New Rearranged Skeleton from *Curcuma Parviflora*. *ChemInform* **2007**, *38* (39). 10.1002/chin.200739163.
- (8) Yang, J.-H.; Du, X.; He, F.; Zhang, H.-B.; Li, X.-N.; Su, J.; Li, Y.; Pu, J.-X.; Sun, H.-D. Bioactive Abietane and *Ent*-Kaurane Diterpenoids from *Isodon Tenuifolius*. *J. Nat. Prod.* **2013**, *76* (2), 256–264. 10.1021/np300772e.

- (9) Hakim, E. H.; Achmad, S. A.; Juliawaty, L. D.; Makmur, L.; Syah, Y. M.; Aimi, N.; Kitajima, M.; Takayama, H.; Ghisalberti, E. L. Prenylated Flavonoids and Related Compounds of the Indonesian Artocarpus (Moraceae).
- (10) Arbain, D. Inventory, Constituents and Conservation of Biologically Important Sumatran Plants. *Natural Product Communications* **2012**, *7* (6), 1934578X1200700. 10.1177/1934578X1200700627.
- (11) Uvais, M.; Sultanbawa, S.; Surendrakumar, S. Two Pyranodihydrobenzoxanthenes from Artocarpus Nobilis. *Phytochemistry* **1989**, *28* (2), 599–605. 10.1016/0031-9422(89)80059-7.
- (12) Ren, Y.; Kardono, L. B. S.; Riswan, S.; Chai, H.; Farnsworth, N. R.; Soejarto, D. D.; Carcache de Blanco, E. J.; Kinghorn, A. D. Cytotoxic and NF-KB Inhibitory Constituents of *Artocarpus Rigida*. *J. Nat. Prod.* **2010**, *73* (5), 949–955. 10.1021/np1002065.
- (13) Syah, Y. M.; Achmad, S. A.; Aimi, N.; Hakim, E. H.; Juliawaty, L. D.; Takayama, H. Two Prenylated Flavones from the Tree Bark of Artocarpus Lanceifolius. *Z Naturforsch 61b*, 1134–1137.
- (14) Achmad, S. A.; Hakim, E. H.; Juliawaty, L. D.; Makmur, L.; Syah, Y. M.; Mujahidin, D. Organic Chemistry of Natural Products in Indonesia: Opportunity, Achievement and Challenges; Bandung, Indonesia, 2015; p 020002. 10.1063/1.4930622.
- (15) Jagtap, U. B.; Bapat, V. A. Artocarpus: A Review of Its Traditional Uses, Phytochemistry and Pharmacology. *Journal of Ethnopharmacology* **2010**, *129* (2), 142–166. 10.1016/j.jep.2010.03.031.
- (16) Rattanaburi, S.; Sriklung, K.; Watanapokasin, R.; Mahabusarakam, W. New Flavonoids and Xanthone from the Stem Bark of *Artocarpus Rigidus* Blume and Cytotoxicity. *Natural Product Research* **2021**, *35* (21), 4010–4017. 10.1080/14786419.2020.1753734.

- (17) Baiseitova, A.; Lee, G.; Shah, A. B.; Yoon, S.; Kim, J. H.; Lee, Y. H.; Park, K. H. New Dihydrobenzoxanthone Derivatives with Bacterial Neuraminidase Inhibitory Activity Isolated from *Artocarpus Elasticus*. *Bioorganic Chemistry* **2022**, *127*, 105978. 10.1016/j.bioorg.2022.105978.
- (18) Widyawaruyanti, A.; Subehan; Kalauni, S. K.; Awale, S.; Nindatu, M.; Zaini, N. C.; Syafruddin, D.; Asih, P. B. S.; Tezuka, Y.; Kadota, S. New Prenylated Flavones from *Artocarpus Champeden*, and Their Antimalarial Activity in Vitro. *J Nat Med* **2007**, *61* (4), 410–413. 10.1007/s11418-007-0153-8.
- (19) Hano, Y.; Aida, M.; Shiina, M.; Nomura, T.; Kawai, T.; Ohe, H.; Kagei, K. Artonins A and B, Two New Prenylflavones from the Root Bark of *Artocarpus Heterophyllus* Lamk. *Heterocycles* **1989**, *29* (8), 1447–1453. 10.3987/COM-89-5019.
- (20) Hano, Y.; Inami, R.; Nomura, T. Components of the Bark of *Artocarpus Rigida* BL.2.: Structures of Four New Isoprenylated Flavone Derivatives Artonins M, N, O, and P. *Heterocycles* **1993**, *35* (2), 1341–1350.
- (21) Hakim, E. H.; Fahriyati, A.; Kau, M. S.; Achmad, S. A.; Makmur, L.; Ghisalberti, E. L.; Nomura, T. Artoindonesianins A and B, Two New Prenylated Flavones from the Root of *Artocarpus Champeden*. *J. Nat. Prod.* **1999**, *62* (4), 613–615. 10.1021/np980279l.
- (22) Nomura, T.; Hano, Y.; Yamagami, Y.; Kobayashi, M.; Isohata, R. Artonins E and F, Two New Prenylflavones from the Bark of *Artocarpus Communis* Forst. *HETEROCYCLES* **1990**, *31* (5), 877. 10.3987/COM-90-5350.
- (23) Namdaung, U.; Aroonrerk, N.; Suksamrarn, S.; Danwisetkanjana, K.; Saenboonrueng, J.; Arjchomphu, W.; Suksamrarn, A. Bioactive Constituents of the Root Bark of *Artocarpus Rigidus* Subsp. *Rigidus*. *Chem. Pharm. Bull.* **2006**, *54* (10), 1433–1436. 10.1248/cpb.54.1433.

- (24) Ee, G. C. L.; Teo, S. H.; Rahmani, M.; Lim, C. K.; Lim, Y. M.; Go, R. Artomandin, a New Xanthone from *Artocarpus Kemando* (Moraceae). *Natural Product Research* **2011**, 25 (10), 995–1003. 10.1080/14786419.2010.534471.
- (25) Hakim, E. H.; Asnizar; Yurnawilis; Aimi, N.; Kitajima, M.; Takayama, H. Artoindonesianin P, a New Prenylated Flavone with Cytotoxic Activity from *Artocarpus Lanceifolius*. *Fitoterapia* **2002**, 73 (7–8), 668–673. 10.1016/S0367-326X(02)00226-5.
- (26) Hakim, Euis. H.; Juliawaty, L. D.; Syah, Y. M.; Achmad, S. A. Molecular Diversity of *Artocarpus Champeden* (Moraceae): A Species Endemic to Indonesia. *Mol Divers* **2005**, 9 (1–3), 149–158. 10.1007/s11030-005-2710-y.
- (27) Liu, W.; Feng, Y.; Yu, S.; Fan, Z.; Li, X.; Li, J.; Yin, H. The Flavonoid Biosynthesis Network in Plants. *IJMS* **2021**, 22 (23), 12824. 10.3390/ijms222312824.
- (28) Nabavi, S. M.; Šamec, D.; Tomczyk, M.; Milella, L.; Russo, D.; Habtemariam, S.; Suntar, I.; Rastrelli, L.; Daglia, M.; Xiao, J.; Giampieri, F.; Battino, M.; Sobarzo-Sanchez, E.; Nabavi, S. F.; Yousefi, B.; Jeandet, P.; Xu, S.; Shirooie, S. Flavonoid Biosynthetic Pathways in Plants: Versatile Targets for Metabolic Engineering. *Biotechnology Advances* **2020**, 38, 107316. 10.1016/j.biotechadv.2018.11.005.
- (29) Mouradov, A.; Spangenberg, G. Flavonoids: A Metabolic Network Mediating Plants Adaptation to Their Real Estate. *Front. Plant Sci.* **2014**, 5. 10.3389/fpls.2014.00620.
- (30) Remali, J.; Sahidin, I.; Aizat, W. M. Xanthone Biosynthetic Pathway in Plants: A Review. *Front. Plant Sci.* **2022**, 13, 809497. 10.3389/fpls.2022.809497.
- (31) Wei, X.; Matsuda, Y. Unraveling the Fungal Strategy for Tetrahydroxanthone Biosynthesis and Diversification. *Org. Lett.* **2020**, 22 (5), 1919–1923. 10.1021/acs.orglett.0c00285.

- (32) Aida, M.; Yamagami, Y.; Hano, Y.; Nomura, T. Formation of Dihydrobenzoxanthone Skeleton from 3-Isoprenylated 2',4', 5'-Trioxxygenated Flavone. *Heterocycles* **1996**, No. 43, 2561–2565.
- (33) Wang, Y.-H.; Hou, A.-J.; Chen, L.; Chen, D.-F.; Sun, H.-D.; Zhao, Q.-S.; Bastow, K. F.; Nakanish, Y.; Wang, X.-H.; Lee, K.-H. New Isoprenylated Flavones, Artochamins A–E, and Cytotoxic Principles from *Artocarpus c Hama*. *J. Nat. Prod.* **2004**, 67 (5), 757–761. 10.1021/np030467y.
- (34) Sritularak, B.; Tantituvanont, A.; Chanvorachote, P.; Meksawan, K.; Miyamoto, T.; Kohno, Y.; Likhitwitayawuid, K. Flavonoids with Free Radical Scavenging Activity and Nitric Oxide Inhibitory Effect from the Stem Bark of *Artocarpus Gomezianus*. *Journal of Medicinal Plants Research* **2010**, 4 (5), 387–392.
- (35) Cao, S.; Butler, M. S.; Buss, A. D. Flavonoids from *Artocarpus Lanceifolius*. *Natural Product Research* **2003**, 17 (2), 79–81. 10.1080/1478641031000103641.
- (36) Eun-Kyoung, S.; Dongho, L.; Young Geun, S.; Hee-Byung, C.; Navarro, H. A.; Kardono, L. B. S.; Rahman, I.; Cordell, G. A.; Farnsworth, N. R.; Pezzuto, J. M.; Kinghorn, A. D.; Wani, M. C.; Wall, M. E. Bioactive Prenylated Flavonoids from the Stem Bark of *Artocarpus Kemando*. *Arch Pharm Res* **2003**, 26 (2), 124–127. 10.1007/BF02976656.
- (37) Ahmad, M.; Wolberg, A.; Kahwaji, C. I. Electron Transport Chain. In *Biochemistry*; StatPearls Publishing: Treasure Island, FL, 2022.
- (38) Musthapa, I.; Latip, J.; Takayama, H.; Juliawaty, L. D.; Hakim, E. H.; Syah, Y. M. Prenylated Flavones from *Artocarpus Lanceifolius* and Their Cytotoxic Properties against P-388 Cells. *Natural Product Communications* **2009**, 4 (7), 927–930.
- (39) Suhartati, T.; Achmad, S. A.; Aimi, N.; Hakim, E. H.; Kitajima, M.; Takayama, H.; Takeya, K. Artoindonesianin L, a New Prenylated Flavone with Cytotoxic Activity from

- Artocarpus Rotunda. *Fitoterapia* **2001**, 72 (8), 912–918. 10.1016/S0367-326X(01)00343-4.
- (40) Tungsukruthai, S.; Boonchoo, S.; Chanvorachote, P. Cycloartobioxanthone Inhibits Migration and Invasion of Lung Cancer Cells. *Antican Res* **2017**, 6319, 6311–6319. 10.21873/anticanres.12082.
- (41) Arjonen, A.; Kaukonen, R.; Ivaska, J. Filopodia and Adhesion in Cancer Cell Motility. *Cell Adhesion & Migration* **2011**, 5 (5), 421–430. 10.4161/cam.5.5.17723.
- (42) Aguilar, B. J.; Zhou, H.; Lu, Q. Cdc42 Signaling Pathway Inhibition as a Therapeutic Target in Ras-Related Cancers. *CMC* **2017**, 24 (32). 10.2174/0929867324666170602082956.
- (43) Jahid, S.; Ortega, J. A.; Vuong, L. M.; Acquistapace, I. M.; Hachey, S. J.; Flesher, J. L.; La Serra, M. A.; Brindani, N.; La Sala, G.; Manigrasso, J.; Arencibia, J. M.; Bertozzi, S. M.; Summa, M.; Bertorelli, R.; Armirotti, A.; Jin, R.; Liu, Z.; Chen, C.-F.; Edwards, R.; Hughes, C. C. W.; De Vivo, M.; Ganesan, A. K. Structure-Based Design of CDC42 Effector Interaction Inhibitors for the Treatment of Cancer. *Cell Reports* **2022**, 39 (1), 110641. 10.1016/j.celrep.2022.110641.
- (44) Johnson, D. I.; Jacobs, C. W.; Pringle, J. R.; Robinson, L. C.; Carle, G. F.; Olson, M. V. Mapping of TheSaccharomyces Cerevisiae CDC3,CDC25, AndCDC42 Genes to Chromosome XII by Chromosome Blotting and Tetrad Analysis. *Yeast* **1987**, 3 (4), 243–253. 10.1002/yea.320030405.
- (45) PROSITE profiles. Dbl Homology (DH) Domain Profile-PS50010. <https://www.ebi.ac.uk/interpro/entry/profile/PS50010/>.
- (46) Liu, K.; Zheng, M.; Lu, R.; Du, J.; Zhao, Q.; Li, Z.; Li, Y.; Zhang, S. The Role of CDC25C in Cell Cycle Regulation and Clinical Cancer Therapy: A Systematic Review. *Cancer Cell Int* **2020**, 20 (1), 213. 10.1186/s12935-020-01304-w.

- (47) Brenner, A.; Reikvam, H.; Lavecchia, A.; Bruserud, Ø. Therapeutic Targeting the Cell Division Cycle 25 (CDC25) Phosphatases in Human Acute Myeloid Leukemia — The Possibility to Target Several Kinases through Inhibition of the Various CDC25 Isoforms. *Molecules* **2014**, *19* (11), 18414–18447. 10.3390/molecules191118414.
- (48) Jayasinghe, U. L. B.; Samarakoon, T. B.; Kumarihamy, B. M. M.; Hara, N.; Fujimoto, Y. Four New Prenylated Flavonoids and Xanthenes from the Root Bark of *Artocarpus Nobilis*. *Fitoterapia* **2008**, *79* (1), 37–41. 10.1016/j.fitote.2007.07.014.
- (49) Arriffin, N.; Jamil, S.; Basar, N.; Khamis, S.; Abdullah, S. A.; Lathiff, S. M. A. Phytochemical Studies Adn Antioxidant Activities of *Artocarpus Scortechinii* King. *Records of Natural Products* **2017**, No. 3, 299–303.
- (50) Ban, Y. J.; Baiseitova, A.; Nafiah, M. A.; Kim, J. Y.; Park, K. H. Human Neutrophil Elastase Inhibitory Dihydrobenzoxanthenes and Alkylated Flavones from the *Artocarpus Elasticus* Root Barks. *Appl Biol Chem* **2020**, *63* (1), 63. 10.1186/s13765-020-00549-3.
- (51) Gao, Y.; Gao, Y.; Wu, W.; Jiang, H.; Yang, X.; Liu, W.; Li, C.-J. Palladium-Catalyzed Tandem Oxidative Arylation/Olefination of Aromatic Tethered Alkenes/Alkynes. *Chem. Eur. J.* **2017**, *23* (4), 793–797. 10.1002/chem.201605351.
- (52) Ju, B.; Chen, S.; Kong, W. Pd-Catalyzed Enantioselective Double Heck Reaction. *Org. Lett.* **2019**, *21* (23), 9343–9347. 10.1021/acs.orglett.9b03517.
- (53) Yao, T.; He, D. Palladium-Catalyzed Domino Heck/Aryne Carbopalladation/C–H Functionalization: Synthesis of Heterocycle-Fused 9,10-Dihydrophenanthrenes. *Org. Lett.* **2017**, *19* (4), 842–845. 10.1021/acs.orglett.6b03833.
- (54) Li, P.; Li, Q.; Weng, H.; Diao, J.; Yao, H.; Lin, A. Intramolecular Remote C–H Activation via Sequential 1,4-Palladium Migration To Access Fused Polycycles. *Org. Lett.* **2019**, *21* (17), 6765–6769. 10.1021/acs.orglett.9b02392.

- (55) Monte, A. P.; Marona-Lewicka, D.; Lewis, M. M.; Mailman, R. B.; Wainscott, D. B.; Nelson, D. L.; Nichols, D. E. Substituted Naphthofurans as Hallucinogenic Phenethylamine–Ergoline Hybrid Molecules with Unexpected Muscarinic Antagonist Activity. *J. Med. Chem.* **1998**, *41* (12), 2134–2145. 10.1021/jm980076u.
- (56) Chambers, J. J.; Parrish, J. C.; Jensen, N. H.; Kurrasch-Orbaugh, D. M.; Marona-Lewicka, D.; Nichols, D. E. Synthesis and Pharmacological Characterization of a Series of Geometrically Constrained 5-HT_{2A/2C} Receptor Ligands. *J. Med. Chem.* **2003**, *46* (16), 3526–3535. 10.1021/jm030064v.
- (57) Hou, S.; Prichina, A. Y.; Zhang, M.; Dong, G. Asymmetric Total Syntheses of Di- and Sesquiterpenoids by Catalytic C–C Activation of Cyclopentanones. *Angew. Chem. Int. Ed.* **2020**, *59* (20), 7848–7856. 10.1002/anie.201915821.
- (58) Krauss, A.; Taylor, W. Intramolecular Oxidative Coupling of Aromatic Compounds. I. Oxidation of Diphenolic Substrates. *Aust. J. Chem.* **1991**, *44* (9), 1307. 10.1071/CH9911307.
- (59) Taylor, S. K.; May, S. A.; Stansby, E. S. Substituent Effects On Intramolecular Epoxide Cyclizations That Can Competitively Occur at Aromatic or Double Bond Positions ¹. *J. Org. Chem.* **1996**, *61* (6), 2075–2080. 10.1021/jo951945f.
- (60) Rudolph, A.; Rackelmann, N.; Lautens, M. Stereochemical and Mechanistic Investigations of a Palladium-Catalyzed Annulation of Secondary Alkyl Iodides. *Angew. Chem. Int. Ed.* **2007**, *46* (9), 1485–1488. 10.1002/anie.200603888.
- (61) Rudolph, A.; Rackelmann, N.; Turcotte-Savard, M.-O.; Lautens, M. Application of Secondary Alkyl Halides to a Domino Aryl Alkylation Reaction for the Synthesis of Aromatic Heterocycles. *J. Org. Chem.* **2009**, *74* (1), 289–297. 10.1021/jo802180h.

- (62) Catellani, M.; Frignani, F.; Rangoni, A. A Complex Catalytic Cycle Leading to a Regioselective Synthesis of *o,o'*-Disubstituted Vinylarenes. *Angew. Chem. Int. Ed. Engl.* **1997**, *36* (12), 119–122. 10.1002/anie.199701191.
- (63) Zhang, H.; Ma, S.; Xing, Z.; Liu, L.; Fang, B.; Xie, X.; She, X. Rapid Construction of the 6/6/5 Tricyclic Framework via a Tandem Radical Cyclization Reaction and Its Application to the Synthesis of 5-Epi-7-Deoxy-Isoabietenin A. *Org. Chem. Front.* **2017**, *4* (11), 2211–2215. 10.1039/C7QO00550D.
- (64) Misaka, Y.; Mizutani, T.; Sekido, M.; Uyeo, S. The Total Synthesis of (\pm)-Lycoramine. Part II. *J. Chem. Soc. C* **1968**, *0* (0), 2954–2959. 10.1039/J39680002954.
- (65) Horaguchi, T.; Shimizu, T.; Abe, T. Furan Derivatives. II. The Cyclization of 3-(Benzofuran-3-Yl)Propionic Acid Derivatives. *BCSJ* **1976**, *49* (3), 737–740. 10.1246/bcsj.49.737.
- (66) Koo, J. Studies in Polyphosphoric Acid Cyclizations. **1953**, 75.
- (67) Beugelmans, R.; Chastanet, J.; Ginsburg, H.; Quintero-Cortes, L.; Roussi, G. Studies in SRN1 Series. Part 14. Direct Synthesis of Benzo[*c*]Phenanthridines and Benzo[*c*]Phenanthridones via SRN1 Reactions. *J. Org. Chem.* **1985**, *50* (24), 4933–4938. 10.1021/jo00224a057.
- (68) Haefliger, W.; Klöppner, E. Stereospezifische Synthese Einer Neuen Morphin-Teilstruktur. *HCA* **1982**, *65* (6), 1837–1852. 10.1002/hlca.19820650619.
- (69) McKervey, M. A.; Tuladhar, S. M.; Twohig, M. F. Efficient Synthesis of Bicyclo[5.3.0]Decatrienones and of 2-Tetralones via Rhodium(II) Acetate-Catalysed Cyclisation of α -Diazoketones Derived from 3-Arylpropionic Acids. *J. Chem. Soc., Chem. Commun.* **1984**, No. 2, 129–130. 10.1039/C39840000129.

- (70) Shi, Z.; He, C. An Au-Catalyzed Cyclialkylation of Electron-Rich Arenes with Epoxides To Prepare 3-Chromanols. *J. Am. Chem. Soc.* **2004**, *126* (19), 5964–5965. 10.1021/ja031953a.
- (71) Crow, W.; Engkaninan-Low, U.; Pang, Y. Synthetic Applications of Intramolecular Insertion in Arylcarbenes. VII. Aryl-Substituted Benzocycloalkenylienes. *Aust. J. Chem.* **1984**, *37* (9), 1915. 10.1071/CH9841915.
- (72) Sharshira, E. M.; Iwanami, H.; Okamura, M.; Hasegawa, E.; Horaguchi, T. Photocyclization Reactions. Part 4 . Synthesis of Naphtho[1,8- *Bc*]-Furans and Cyclohepta[*Cd*]Benzofurans Using Photocyclization of Ethyl 2-(8-Oxo-5,6,7,8-Tetrahydro-1-Naphthyloxy)Acetates and Ethyl 2-(5-Oxo-6,7,8,9-Tetrahydro-5 *H* -Benzocyclohepten-4-Yloxy)Acetates. *Journal of Heterocyclic Chemistry* **1996**, *33* (1), 137–144. 10.1002/jhet.5570330124.
- (73) Sharshira, E. M. Photocyclization Reactions of Ethyl 2-(8-oxo-5,6,7,8-tetrahydro-1-naphthyloxy)acetate and 8-oxo-5,6,7,8-tetrahydro-1-naphthyloxyacetonitrile in Methanol. *Heterocyclic Communications* **2002**, *8* (1). 10.1515/HC.2002.8.1.83.
- (74) Bissada, S.; Lau, C. K.; Bernstein, M. A.; Dufresne, C. Polycyclic Chromans via Novel Tricyclic-2-Phenyl-4H-1,3,2-Benzodioxaborins. *Tetrahedron Letters* **1994**, *35* (22), 3691–3694. 10.1016/S0040-4039(00)73073-5.
- (75) Horaguchi, T.; Shimizu, T.; Suzuki, T. Furan Derivatives. I. On the Methods of Synthesizing Some Naphtho[1,8- *Bc*]Furans. *BCSJ* **1975**, *48* (4), 1249–1253. 10.1246/bcsj.48.1249.
- (76) Xu, T.; Dong, G. Rhodium-Catalyzed Regioselective Carboacylation of Olefins: A C-C Bond Activation Approach for Accessing Fused-Ring Systems. *Angew. Chem. Int. Ed.* **2012**, *51* (30), 7567–7571. 10.1002/anie.201202771.

- (77) Xu, T.; Ko, H. M.; Savage, N. A.; Dong, G. Highly Enantioselective Rh-Catalyzed Carboacylation of Olefins: Efficient Syntheses of Chiral Poly-Fused Rings. *J. Am. Chem. Soc.* **2012**, *134* (49), 20005–20008. 10.1021/ja309978c.
- (78) Wipf, P.; Jung, J.-K. Formal Total Synthesis of (+)-Diepoxin σ . *J. Org. Chem.* **2000**, *65* (20), 6319–6337. 10.1021/jo000684t.
- (79) Mehl, L.-M.; Maier, M. E. A Radical-Based Synthesis of Lingzhiol. *J. Org. Chem.* **2017**, *82* (18), 9844–9850. 10.1021/acs.joc.7b01416.
- (80) Wang, J.-L.; Li, H.-J.; Wu, Y.-C. Divergent Synthesis of Marine Natural Products Siphonodictyal B, Corallidictyals C/D, and Liphagal Based on the Early Presence of an Aldehyde Group Instead of a Late-Stage Introduction. *J. Org. Chem.* **2018**, *83* (15), 8716–8723. 10.1021/acs.joc.8b00989.
- (81) Liu, X.; Wang, W.; Zhao, Y.; Lai, D.; Zhou, L.; Liu, Z.; Wang, M. Total Synthesis and Structure Revision of Palmarumycin B δ . *J. Nat. Prod.* **2018**, *81* (8), 1803–1809. 10.1021/acs.jnatprod.8b00258.
- (82) Vekariya, R. H.; Aubé, J. Hexafluoro-2-Propanol-Promoted Intermolecular Friedel–Crafts Acylation Reaction. *Org. Lett.* **2016**, *18* (15), 3534–3537. 10.1021/acs.orglett.6b01460.
- (83) Motiwala, H. F.; Vekariya, R. H.; Aubé, J. Intramolecular Friedel–Crafts Acylation Reaction Promoted by 1,1,1,3,3,3-Hexafluoro-2-Propanol. *Org. Lett.* **2015**, *17* (21), 5484–5487. 10.1021/acs.orglett.5b02851.
- (84) Suto, Y.; Sato, M.; Fujimori, K.; Kitabatake, S.; Okayama, M.; Ichikawa, D.; Matsushita, M.; Yamagiwa, N.; Iwasaki, G.; Kiuchi, F.; Hattori, Y. Synthesis and Biological Evaluation of the Natural Product Komaroviquinone and Related Compounds Aiming at a Potential Therapeutic Lead Compound for High-Risk Multiple Myeloma. *Bioorganic & Medicinal Chemistry Letters* **2017**, *27* (19), 4558–4563. 10.1016/j.bmcl.2017.08.054.

- (85) Huang, J.-K.; Yang Lauderdale, T.-L.; Lin, C.-C.; Shia, K.-S. Total Synthesis of Tetarimycin A, (±)-Naphthacemycin A₉, and (±)-Fasamycin A: Structure–Activity Relationship Studies against Drug-Resistant Bacteria. *J. Org. Chem.* **2018**, *83* (12), 6508–6523. 10.1021/acs.joc.8b00802.
- (86) Nishimura, T.; Horikawa, M.; Yamada, K.; Sogabe, A.; Nishii, T.; Kaku, H.; Inai, M.; Tanaka, M.; Takahashi, S.; Tsunoda, T. Xanthouroleuconaphin: A Yellowish Pigment from the Aphid Uroleucon Nigrotuberculatum and Its Total Synthesis. *Tetrahedron* **2013**, *69* (7), 1808–1814. 10.1016/j.tet.2012.12.070.
- (87) Kováčová, S.; Adla, S. K.; Maier, L.; Babiak, M.; Mizushina, Y.; Paruch, K. Synthesis of Carbocyclic Analogs of Dehydroaltenusin: Identification of a Stable Inhibitor of Calf DNA Polymerase α . *Tetrahedron* **2015**, *71* (40), 7575–7582. 10.1016/j.tet.2015.08.005.
- (88) Huang, J.-K.; Yang Lauderdale, T.-L.; Shia, K.-S. Studies on Antibiotics Active against Resistant Bacteria. Total Synthesis of MRSA-Active Tetarimycin A and Its Analogues. *Org. Lett.* **2015**, *17* (17), 4248–4251. 10.1021/acs.orglett.5b02039.
- (89) Salvador, J. A. R.; Sáe Melo, M. L.; Campos Neves, A. S. Copper-Catalysed Allylic Oxidation of Δ^5 -Steroids by t-Butyl Hydroperoxide. *Tetrahedron Letters* **1997**, *38* (1), 119–122. 10.1016/S0040-4039(96)02231-9.
- (90) Li, C.-J.; Xia, F.; Zhang, W.; Wang, K.; Xu, G.; Qin, H.-B. Semisynthesis of Miltirone, 1,2-Dehydromiltirone, Saligerone from Carnosic Acid and Cytotoxicities of Their Derivatives. *Tetrahedron Letters* **2018**, *59* (26), 2607–2609. 10.1016/j.tetlet.2018.05.073.
- (91) Sriram, M.; Hall, J. J.; Grohmann, N. C.; Strecker, T. E.; Wootton, T.; Franken, A.; Trawick, M. L.; Pinney, K. G. Design, Synthesis and Biological Evaluation of Dihydronaphthalene and Benzosuberene Analogs of the Combretastatins as Inhibitors of Tubulin Polymerization in Cancer Chemotherapy. *Bioorganic & Medicinal Chemistry* **2008**, *16* (17), 8161–8171. 10.1016/j.bmc.2008.07.050.

- (92) Liu, G.; Lancefield, C.; Lorion, M.; Slawin, A.; Westwood, N. Synthesis and Oxidative Cleavage of Oxazinocarbazoles: Atropselective Access to Medium-Sized Rings. *Synthesis* **2014**, *46* (20), 2808–2814. 10.1055/s-0034-1378530.
- (93) Cosner, C. C.; Cabrera, P. J.; Byrd, K. M.; Thomas, A. M. A.; Helquist, P. Selective Oxidation of Benzylic and Allylic Alcohols Using $\text{Mn}(\text{OAc})_3$ /Catalytic 2,3-Dichloro-5,6-Dicyano-1,4-Benzoquinone. *Org. Lett.* **2011**, *13* (8), 2071–2073. 10.1021/ol200441g.
- (94) K. C. Nicolaou,*; Baran, P. S.; Zhong, Y.-L. Selective Oxidation at Carbon Adjacent to Aromatic Systems with IBX. *J. Am. Chem. Soc.* **2001**, *123* (13), 3183–3185. 10.1021/ja004218x.
- (95) Yoshimura, A.; Zhdankin, V. V. Advances in Synthetic Applications of Hypervalent Iodine Compounds. *Chem. Rev.* **2016**, *116* (5), 3328–3435. 10.1021/acs.chemrev.5b00547.
- (96) Catino, A. J.; Forslund, R. E.; Doyle, M. P. Dirhodium(II) Caprolactamate: An Exceptional Catalyst for Allylic Oxidation. *J. Am. Chem. Soc.* **2004**, *126* (42), 13622–13623. 10.1021/ja045330o.
- (97) Yusubov, M. S.; Zagulyaeva, A. A.; Zhdankin, V. V. Iodine(V)/Ruthenium(III)-Cocatalyzed Oxidations: A Highly Efficient Tandem Catalytic System for the Oxidation of Alcohols and Hydrocarbons with Oxone. *Chem. Eur. J.* **2009**, *15* (42), 11091–11094. 10.1002/chem.200901953.
- (98) Dijkman, A.; Marino-González, A.; Mairata i Payeras, A.; Arends, I. W. C. E.; Sheldon, R. A. Efficient and Selective Aerobic Oxidation of Alcohols into Aldehydes and Ketones Using Ruthenium/TEMPO as the Catalytic System. *J. Am. Chem. Soc.* **2001**, *123* (28), 6826–6833. 10.1021/ja0103804.
- (99) Yin, L.; Wu, J.; Xiao, J.; Cao, S. Oxidation of Benzylic Methylenes to Ketones with Oxone–KBr in Aqueous Acetonitrile under Transition Metal Free Conditions. *Tetrahedron Letters* **2012**, *53* (33), 4418–4421. 10.1016/j.tetlet.2012.06.036.

- (100) McManus, J. B.; Griffin, J. D.; White, A. R.; Nicewicz, D. A. Homobenzylic Oxygenation Enabled by Dual Organic Photoredox and Cobalt Catalysis. *J. Am. Chem. Soc.* **2020**, *142* (23), 10325–10330. 10.1021/jacs.0c04422.
- (101) Jin, C.; Zhang, L.; Su, W. Direct Benzylic Oxidation with Sodium Hypochlorite Using a New Efficient Catalytic System: TEMPO/Co(OAc)₂. *Synlett* **2011**, *2011* (10), 1435–1438. 10.1055/s-0030-1260760.
- (102) Simplified Preparation of Dimethyldioxirane (DMDO). *Org. Synth.* **2013**, *90*, 350. 10.15227/orgsyn.090.0350.
- (103) Bonvin, Y.; Callens, E.; Larrosa, I.; Henderson, D. A.; Oldham, J.; Burton, A. J.; Barrett, A. G. M. Bismuth-Catalyzed Benzylic Oxidations with *Tert*-Butyl Hydroperoxide. *Org. Lett.* **2005**, *7* (21), 4549–4552. 10.1021/ol051765k.
- (104) Yuan, C.; Eliassen, A. M.; Camelio, A. M.; Siegel, D. Preparation of Phenols by Phthaloyl Peroxide-Mediated Oxidation of Arenes. *Nat Protoc* **2014**, *9* (11), 2624–2629. 10.1038/nprot.2014.175.
- (105) Aubry, S.; Pellet-Rostaing, S.; Lemaire, M. Oxidative Nucleophilic Substitution (SNOx) of the Benzylic Position as a Tunable Synthesis of Tetrahydroisoquinoline Natural Alkaloid Analogues. *Eur. J. Org. Chem.* **2007**, *2007* (31), 5212–5225. 10.1002/ejoc.200700366.
- (106) Zheng, S.-L.; Chen, L. Synthesis of 2 *H*-Chromenes: Recent Advances and Perspectives. *Org. Biomol. Chem.* **2021**, *19* (48), 10530–10548. 10.1039/D1OB01906F.
- (107) Kang, Y.; Mei, Y.; Du, Y.; Jin, Z. Total Synthesis of the Highly Potent Anti-HIV Natural Product Daurichromenic Acid along with Its Two Chromane Derivatives, Rhododaurichromenic Acids A and B. *Org. Lett.* **2003**, *5* (23), 4481–4484. 10.1021/ol030109m.

- (108) Mondal, M.; Puranik, V. G.; Argade, N. P. Facile Synthesis of 1,3,7-Trihydroxyxanthone and Its Regioselective Coupling Reactions with Prenal: Simple and Efficient Access to Osajaxanthone and Nigrolineaxanthone F. *J. Org. Chem.* **2006**, *71* (13), 4992–4995. 10.1021/jo0606655.
- (109) Saimoto, H.; Yoshida, K.; Murakami, T.; Morimoto, M.; Sashiwa, H.; Shigemasa, Y. Effect of Calcium Reagents on Aldol Reactions of Phenolic Enolates with Aldehydes in Alcohol. *J. Org. Chem.* **1996**, *61* (20), 6768–6769. 10.1021/jo961352k.
- (110) Adler, M. J.; Baldwin, S. W. Direct, Regioselective Synthesis of 2,2-Dimethyl-2H-Chromenes. Total Syntheses of Octandrenolone and Precocenes I and II. *Tetrahedron Letters* **2009**, *50* (36), 5075–5079. 10.1016/j.tetlet.2009.06.090.
- (111) Krasley, A. T.; Malachowski, W. P.; Terz, H. M.; Tran Tien, S. Catalytic Enantioselective Birch–Heck Sequence for the Synthesis of Tricyclic Structures with All-Carbon Quaternary Stereocenters. *Org. Lett.* **2018**, *20* (7), 1740–1743. 10.1021/acs.orglett.8b00196.
- (112) Tenneti, S.; Biswas, S.; Cox, G. A.; Mans, D. J.; Lim, H. J.; RajanBabu, T. V. Broadly Applicable Stereoselective Syntheses of Serrulatane, Amphilectane Diterpenes, and Their Diastereoisomeric Congeners Using Asymmetric Hydrovinylation for Absolute Stereochemical Control. *J. Am. Chem. Soc.* **2018**, *140* (31), 9868–9881. 10.1021/jacs.8b03549.
- (113) Tisdale, E. J.; Vong, B. G.; Li, H.; Kim, S. H.; Chowdhury, C.; Theodorakis, E. A. Total Synthesis of Seco-Lateriflorone. *Tetrahedron* **2003**, *59* (35), 6873–6887. 10.1016/S0040-4020(03)00862-7.
- (114) Xie, L.; Takeuchi, Y.; Cosentino, L. M.; McPhail, A. T.; Lee, K.-H. Anti-AIDS Agents. 42. Synthesis and Anti-HIV Activity of Disubstituted (3' R ,4' R)-3',4'-Di- O -(S)-

- Camphanoyl-(+)- *Cis* -Khellactone Analogues. *J. Med. Chem.* **2001**, *44* (5), 664–671.
10.1021/jm000070g.
- (115) Trost, B. M.; Toste, F. D.; Greenman, K. Atom Economy. Palladium-Catalyzed Formation of Coumarins by Addition of Phenols and Alkynoates via a Net C–H Insertion. *J. Am. Chem. Soc.* **2003**, *125* (15), 4518–4526. 10.1021/ja0286573.
- (116) Wolfrom, M. L.; Koos, E. W.; Bhat, H. B. Osage Orange Pigments. XVIII. Synthesis of Osajaxanthone. *J. Org. Chem.* **1967**, *32* (4), 1058–1060. 10.1021/jo01279a043.
- (117) Protection for the Carbonyl Group. In *Greene's Protective Groups in Organic Synthesis*; Wuts, P. G. M., Ed.; John Wiley & Sons, Inc.: Hoboken, New Jersey, 2014; pp 554–685.
10.1002/9781118905074.ch04.
- (118) Carrigan, M. D.; Sarapa, D.; Smith, R. C.; Wieland, L. C.; Mohan, R. S. A Simple and Efficient Chemoselective Method for the Catalytic Deprotection of Acetals and Ketals Using Bismuth Triflate. *J. Org. Chem.* **2002**, *67* (3), 1027–1030. 10.1021/jo016180s.
- (119) Anil, S. M.; Vinayaka, A. C.; Rajeev, N.; Swaroop, T. R.; Mallesha, N.; Rangappa, K. S.; Sadashiva, M. P. Aqueous Chloroplatinic Acid: A Green, Chemoselective and Reusable Catalyst for the Deprotection of Acetals, Ketals, Dioxolanes and Oxathiolanes. *ChemistrySelect* **2018**, *3* (7), 1999–2003. 10.1002/slct.201800032.
- (120) Ohta, R.; Matsumoto, N.; Ueyama, Y.; Kuboki, Y.; Aoyama, H.; Murai, K.; Arisawa, M.; Maegawa, T.; Fujioka, H. Highly Discriminative and Chemoselective Deprotection/Transformations of Acetals with the Combination of Trialkylsilyl Triflate/2,4,6-Collidine. *J. Org. Chem.* **2018**, *83* (12), 6432–6443.
10.1021/acs.joc.8b00675.
- (121) Sun, J.; Dong, Y.; Cao, L.; Wang, X.; Wang, S.; Hu, Y. Highly Efficient Chemoselective Deprotection of *O,O*-Acetals and *O,O*-Ketals Catalyzed by Molecular Iodine in Acetone. *J. Org. Chem.* **2004**, *69* (25), 8932–8934. 10.1021/jo0486239.

- (122) Kaur, G.; Trehan, A.; Trehan, S. Highly Efficient Deprotection of Acetals and Ketals under Neutral and Anhydrous Conditions Using (Trimethylsilyl)Bis(Fluorosulfonyl)Imide. *J. Org. Chem.* **1998**, *63* (7), 2365–2366. 10.1021/jo971756s.
- (123) Kumar, R.; Kumar, D.; Chakraborti, A. Perchloric Acid Adsorbed on Silica Gel (HClO_4 - SiO_2) as an Inexpensive, Extremely Efficient, and Reusable Dual Catalyst System for Acetal/Ketal Formation and Their Deprotection to Aldehydes/Ketones. *Synthesis* **2007**, *2007* (2), 299–303. 10.1055/s-2006-958948.
- (124) Tlili, A.; Xia, N.; Monnier, F.; Taillefer, M. A Very Simple Copper-Catalyzed Synthesis of Phenols Employing Hydroxide Salts. *Angew. Chem. Int. Ed.* **2009**, *48* (46), 8725–8728. 10.1002/anie.200903639.
- (125) Yang, K.; Li, Z.; Wang, Z.; Yao, Z.; Jiang, S. Highly Efficient Synthesis of Phenols by Copper-Catalyzed Hydroxylation of Aryl Iodides, Bromides, and Chlorides. *Org. Lett.* **2011**, *13* (16), 4340–4343. 10.1021/ol2016737.
- (126) Cheung, C. W.; Buchwald, S. L. Palladium-Catalyzed Hydroxylation of Aryl and Heteroaryl Halides Enabled by the Use of a Palladacycle Precatalyst. *J. Org. Chem.* **2014**, *79* (11), 5351–5358. 10.1021/jo500662s.
- (127) Lavery, C. B.; Rotta-Loria, N. L.; McDonald, R.; Stradiotto, M. Pd_2Dba_3 /Bippyphos: A Robust Catalyst System for the Hydroxylation of Aryl Halides with Broad Substrate Scope. *Adv. Synth. Catal.* **2013**, *355* (5), 981–987. 10.1002/adsc.201300088.
- (128) Schulz, T.; Torborg, C.; Schäffner, B.; Huang, J.; Zapf, A.; Kadyrov, R.; Börner, A.; Beller, M. Practical Imidazole-Based Phosphine Ligands for Selective Palladium-Catalyzed Hydroxylation of Aryl Halides. *Angew. Chem. Int. Ed.* **2009**, *48* (5), 918–921. 10.1002/anie.200804898.

- (129) Fier, P. S.; Maloney, K. M. Reagent Design and Ligand Evolution for the Development of a Mild Copper-Catalyzed Hydroxylation Reaction. *Org. Lett.* **2017**, *19* (11), 3033–3036. 10.1021/acs.orglett.7b01403.
- (130) Anderson, K. W.; Ikawa, T.; Tundel, R. E.; Buchwald, S. L. The Selective Reaction of Aryl Halides with KOH: Synthesis of Phenols, Aromatic Ethers, and Benzofurans. *J. Am. Chem. Soc.* **2006**, *128* (33), 10694–10695. 10.1021/ja0639719.
- (131) Paul, R.; Ali, M.; Punniyamurthy, T. Copper-Catalyzed Hydroxylation of Aryl Halides with Tetrabutylammonium Hydroxide: Synthesis of Substituted Phenols and Alkyl Aryl Ethers. *Synthesis* **2010**, *2010* (24), 4268–4272. 10.1055/s-0030-1258965.
- (132) Widlicka, D. W.; Murray, J. C.; Coffman, K. J.; Xiao, C.; Brodney, M. A.; Rainville, J. P.; Samas, B. Two Routes to 4-Fluorobenzisoxazol-3-One in the Synthesis of a 5-HT₄ Partial Agonist. *Org. Process Res. Dev.* **2016**, *20* (2), 233–241. 10.1021/acs.oprd.5b00389.
- (133) Feutrill, G. I.; Mirrington, R. N. Demethylation of Aryl Methyl Ethers with Thioethoxide Ion in Dimethyl Formamide. *Tetrahedron Letters* **1970**, *11* (16), 1327–1328. 10.1016/S0040-4039(01)97960-2.
- (134) Haddad, T.; Gershman, R.; Dilis, R.; Labaree, D.; Hochberg, R. B.; Hanson, R. N. Synthesis and Evaluation of 4-(Substituted Styryl/Alkenyl)-3,5-Bis(4-Hydroxyphenyl)-Isoxazoles as Ligands for the Estrogen Receptor. *Bioorganic & Medicinal Chemistry Letters* **2012**, *22* (18), 5999–6003. 10.1016/j.bmcl.2012.06.097.
- (135) Ahmad, R.; Saa, J. M.; Cava, M. P. Regioselective O-Demethylation in the Aporphine Alkaloid Series. *J. Org. Chem.* **1977**, *42* (7), 1228–1230. 10.1021/jo00427a028.
- (136) Dodge, J. A.; Stocksdales, M. G.; Fahey, K. J.; Jones, C. D. Regioselectivity in the Alkaline Thiolate Deprotection of Aryl Methyl Ethers. *J. Org. Chem.* **1995**, *60* (3), 739–741. 10.1021/jo00108a046.

- (137) O'Brien, C. J.; Nicewicz, D. A. Milled Dry Ice as a C1 Source for the Carboxylation of Aryl Halides. *Synlett* **2021**, 32 (08), 814–816. 10.1055/a-1384-0159.
- (138) Sharique, M.; Tambar, U. K. N-Heterocyclic Carbene Based Catalytic Platform for Hauser–Kraus Annulations. *Chem. Sci.* **2020**, 11 (27), 7239–7243. 10.1039/D0SC03116J.
- (139) Morrison, C. F.; Burnell, D. J. 4-(Trialkylsilyl)Oxybut-2-Ynals as Dienophiles in the Diels–Alder Synthesis of α -(Hydroxymethyl)Benzaldehydes. *Tetrahedron Letters* **2001**, 42 (42), 7367–7369. 10.1016/S0040-4039(01)01541-6.
- (140) Morrison, C. F.; Burnell, D. J. First Rational Synthesis of the Thiothiono Analogue of an Unsymmetrically Substituted Phthalic Anhydride. *Org. Lett.* **2000**, 2 (24), 3891–3892. 10.1021/ol0066375.
- (141) Soriano, M. D. P. C.; Shankaraiah, N.; Santos, L. S. Short Synthesis of Noscapine, Biccuculline, Egenine, Capnoidine, and Corytensine Alkaloids through the Addition of 1-Siloxy-Isobenzofurans to Imines. *Tetrahedron Letters* **2010**, 51 (13), 1770–1773. 10.1016/j.tetlet.2010.01.104.
- (142) Firouzabadi, H.; Iranpoor, N.; Hazarkhani, H. Iodine Catalyzes Efficient and Chemoselective Thioacetalization of Carbonyl Functions, Transthioacetalization of *O*, *O* - and *S*, *O* -Acetals and Acylals. *J. Org. Chem.* **2001**, 66 (22), 7527–7529. 10.1021/jo015798z.
- (143) Ozaki, Y.; Imaizumi, K.; Okamura, K.; Morozumi, M.; Hosoya, A.; Kim, S.-W. Annulation of Ethyl (Bis(Ethylthio)Methyl)Benzoate and Ethyl 2-(1,3)Dithiolan-2-Yl-Benzoate with α,β -Unsaturated Carbonyl Compounds: A New Synthesis of Naphthalene and Anthracene Derivatives. *Chem. Pharm. Bull.* **1996**, 44 (10), 1785–1789. 10.1248/cpb.44.1785.

- (144) Chen, Z.; Hong, A. Y.; Linghu, X. Construction of Polycyclic β -Ketoesters Using a Homoconjugate Addition/Decarboxylative Dieckmann Annulation Strategy. *J. Org. Chem.* **2018**, *83* (11), 6225–6234. 10.1021/acs.joc.8b00754.
- (145) Antien, K.; Viault, G.; Pouységu, L.; Peixoto, P. A.; Quideau, S. Asymmetric Dearomative Spirolactonization of Naphthols Using Λ^3 -Iodanes under Chiral Phase-Transfer Catalysis. *Tetrahedron* **2017**, *73* (26), 3684–3690. 10.1016/j.tet.2017.04.028.
- (146) Couty, S.; Meyer, C.; Cossy, J. A Short Synthesis of Lennoxamine via Ynamides. *Tetrahedron Letters* **2006**, *47* (5), 767–769. 10.1016/j.tetlet.2005.11.093.
- (147) Chang, X.-W.; Han, Q.-C.; Jiao, Z.-G.; Weng, L.-H.; Zhang, D.-W. 1-Aminoxymethylcyclopropanecarboxylic Acid as Building Block of β N–O Turn and Helix: Synthesis and Conformational Analysis in Solution and in the Solid State. *Tetrahedron* **2010**, *66* (51), 9733–9737. 10.1016/j.tet.2010.10.037.
- (148) Prakash, O.; Pundeer, R.; Kaur, H. A New and Facile Iodine(III)-Mediated Approach for the Regioselective Alkoxylation of 2,5-Dihydroxyacetophenone. *Synthesis* **2003**, No. 18, 2768–2770. 10.1055/s-2003-42461.
- (149) Zhang, C.; Sun, P. Palladium-Catalyzed Direct C(Sp²)–H Alkoxylation of 2-Aryloxy pyridines Using 2-Pyridyloxy as the Directing Group. *J. Org. Chem.* **2014**, *79* (17), 8457–8461. 10.1021/jo5014146.
- (150) Aggarwal, Y.; Padmavathi, R.; Singh, P.; Arulananda Babu, S. Pd(II)-Catalyzed, γ -C(Sp²)–H Alkoxylation in α -Methylbenzylamine, Phenylglycinol, 3-Amino-3-Phenylpropanol Toward Enantiopure Aryl Alkyl Ethers. *Asian J Org Chem* **2022**, *11* (9). 10.1002/ajoc.202200327.
- (151) Li, W.; Sun, P. Pd(OAc)₂-Catalyzed Alkoxylation of Arylnitriles via Sp² C–H Bond Activation Using Cyano as the Directing Group. *J. Org. Chem.* **2012**, *77* (18), 8362–8366. 10.1021/jo301384r.

- (152) Hudlicky, T.; Tian, X.; Königsberger, K.; Maurya, R.; Rouden, J.; Fan, B. Toluene Dioxygenase-Mediated *Cis* -Dihydroxylation of Aromatics in Enantioselective Synthesis. Asymmetric Total Syntheses of Pancratistatin and 7-Deoxypancratistatin, Promising Antitumor Agents ¹. *J. Am. Chem. Soc.* **1996**, *118* (44), 10752–10765. 10.1021/ja960596j.
- (153) Behrman, E. J. The Persulfate Oxidation of Phenols and Arylamines (The Elbs and the Boyland-Sims Oxidations). In *Organic Reactions*; John Wiley & Sons, Inc., Ed.; John Wiley & Sons, Inc.: Hoboken, NJ, USA, 1988; pp 421–511. 10.1002/0471264180.or035.02.
- (154) Barontini, M.; Bernini, R.; Crisante, F.; Fabrizi, G. Selective and Efficient Oxidative Modifications of Flavonoids with 2-Iodoxybenzoic Acid (IBX). *Tetrahedron* **2010**, *66* (32), 6047–6053. 10.1016/j.tet.2010.06.014.
- (155) Zhang, Y.-H.; Yu, J.-Q. Pd(II)-Catalyzed Hydroxylation of Arenes with 1 Atm of O₂ or Air. *J. Am. Chem. Soc.* **2009**, *131* (41), 14654–14655. 10.1021/ja907198n.
- (156) Fujimoto, K.; Tokuda, Y.; Maekawa, H.; Matsubara, Y.; Mizuno, T.; Nishiguchi, I. Selective and One-Pot Formation of Phenols by Anodic Oxidation. *Tetrahedron* **1996**, *52* (11), 3889–3896. 10.1016/S0040-4020(96)00056-7.
- (157) Yuan, C.; Liang, Y.; Hernandez, T.; Berriochoa, A.; Houk, K. N.; Siegel, D. Metal-Free Oxidation of Aromatic Carbon–Hydrogen Bonds through a Reverse-Rebound Mechanism. *Nature* **2013**, *499* (7457), 192–196. 10.1038/nature12284.
- (158) Palmisano, G.; Addamo, M.; Augugliaro, V.; Caronna, T.; García-López, E.; Loddo, V.; Palmisano, L. Influence of the Substituent on Selective Photocatalytic Oxidation of Aromatic Compounds in Aqueous TiO₂ Suspensions. *Chem. Commun.* **2006**, No. 9, 1012. 10.1039/b515853b.
- (159) Basu, M.; Sarkar, S.; Pande, S.; Jana, S.; Kumar Sinha, A.; Sarkar, S.; Pradhan, M.; Pal, A.; Pal, T. Hydroxylation of Benzophenone with Ammonium Phosphomolybdate in the

- Solid State via UV Photoactivation. *Chem. Commun.* **2009**, No. 46, 7191. 10.1039/b905718h.
- (160) Long, H.; Chen, T.-S.; Song, J.; Zhu, S.; Xu, H.-C. Electrochemical Aromatic C–H Hydroxylation in Continuous Flow. *Nat Commun* **2022**, *13* (1), 3945. 10.1038/s41467-022-31634-4.
- (161) Mita, S.; Sakamoto, T.; Yamada, S.; Sakaguchi, S.; Ishii, Y. Direct Hydroxylation of Substituted Benzenes to Phenols with Air and CO Using Molybdovanadophosphates as a Key Catalyst. *Tetrahedron Letters* **2005**, *46* (45), 7729–7732. 10.1016/j.tetlet.2005.09.016.
- (162) Li, Z.; Park, H. S.; Qiao, J. X.; Yeung, K.-S.; Yu, J.-Q. Ligand-Enabled C–H Hydroxylation with Aqueous H₂O₂ at Room Temperature. *J. Am. Chem. Soc.* **2022**, *144* (39), 18109–18116. 10.1021/jacs.2c08332.
- (163) Yang, Y.; Lin, Y.; Rao, Y. Ruthenium(II)-Catalyzed Synthesis of Hydroxylated Arenes with Ester as an Effective Directing Group. *Org. Lett.* **2012**, *14* (11), 2874–2877. 10.1021/ol301104n.
- (164) Thirunavukkarasu, V. S.; Hubrich, J.; Ackermann, L. Ruthenium-Catalyzed Oxidative C(Sp²)–H Bond Hydroxylation: Site-Selective C–O Bond Formation on Benzamides. *Org. Lett.* **2012**, *14* (16), 4210–4213. 10.1021/ol3018819.
- (165) Hartwig, J. F. *Organotransition Metal Chemistry: From Bonding to Catalysis*; University Science Books: Mill Valley, 2009.
- (166) α -hydroxylation of a Ketone Using *o*-Iodosylbenzoic acid: α -hydroxyacetophenone via the α -Hydroxy Dimethylacetal. *Org. Synth.* **1986**, *64*, 138. 10.15227/orgsyn.064.0138.
- (167) Baudoux, J.; Cahard, D. Electrophilic Fluorination with N-F Reagents. In *Organic Reactions*; John Wiley & Sons, Inc., Ed.; John Wiley & Sons, Inc.: Hoboken, NJ, USA, 2008; pp 1–326. 10.1002/0471264180.or069.02.

- (168) Wang, Y.; Liu, J. (Jim); Dransfield, P. J.; Zhu, L.; Wang, Z.; Du, X.; Jiao, X.; Su, Y.; Li, A.; Brown, S. P.; Kasparian, A.; Vimolratana, M.; Yu, M.; Pattaropong, V.; Houze, J. B.; Swaminath, G.; Tran, T.; Nguyen, K.; Guo, Q.; Zhang, J.; Zhuang, R.; Li, F.; Miao, L.; Bartberger, M. D.; Correll, T. L.; Chow, D.; Wong, S.; Luo, J.; Lin, D. C.-H.; Medina, J. C. Discovery and Optimization of Potent GPR40 Full Agonists Containing Tricyclic Spirocycles. *ACS Med. Chem. Lett.* **2013**, *4* (6), 551–555. 10.1021/ml300427u.
- (169) Cabrera, E. V.; Sanchez, J. L.; Banerjee, A. K. A Practical Synthesis of 7,8-Dimethoxy-2-Tetralone. *Organic Preparations and Procedures International* **2011**, *43* (4), 364–367. 10.1080/00304948.2011.594008.
- (170) Li, X.-J.; Li, M.; Lu, H.-Y.; Chen, C.-F. A Dinaphtho[8,1,2-Cde:2',1',8'-Uva]Pentacene Derivative and Analogues: Synthesis, Structures, Photophysical and Electrochemical Properties. *Org. Biomol. Chem.* **2015**, *13* (28), 7628–7632. 10.1039/C5OB01008J.
- (171) Uccello Barretta, G.; Mandoli, A.; Balzano, F.; Aiello, F.; De Nicola, B.; Del Grande, A. Monomeric and Dimeric 9- *O* Anthraquinone and Phenanthryl Derivatives of Cinchona Alkaloids as Chiral Solvating Agents for the NMR Enantiodiscrimination of Chiral Hemiesters: NMR Enantiodiscrimination of Chiral Hemiesters. *Chirality* **2015**, *27* (10), 693–699. 10.1002/chir.22488.
- (172) Deichert, J. A.; Mizufune, H.; Patel, J. J.; Hurst, T. E.; Maheta, A.; Kitching, M. O.; Ross, A. C.; Snieckus, V. Expedient Pd-Catalyzed α -Arylation towards Dibenzoxepinones: Pivotal Manske's Ketone for the Formal Synthesis of Cularine Alkaloids: Expedient Pd-Catalyzed α -Arylation towards Dibenzoxepinones: Pivotal Manske's Ketone for the Formal Synthesis of Cularine Alkaloids. *Eur. J. Org. Chem.* **2020**, *2020* (30), 4693–4697. 10.1002/ejoc.202000424.
- (173) Nara, H.; Sato, K.; Naito, T.; Mototani, H.; Oki, H.; Yamamoto, Y.; Kuno, H.; Santou, T.; Kanzaki, N.; Terauchi, J.; Uchikawa, O.; Kori, M. Discovery of Novel, Highly Potent,

- and Selective Quinazoline-2-Carboxamide-Based Matrix Metalloproteinase (MMP)-13 Inhibitors without a Zinc Binding Group Using a Structure-Based Design Approach. *J. Med. Chem.* **2014**, *57* (21), 8886–8902. 10.1021/jm500981k.
- (174) Geng, C.; Du, L.; Liu, F.; Zhu, R.; Liu, C. Theoretical Study on the Mechanism of Selective Fluorination of Aromatic Compounds with Selectfluor. *RSC Adv.* **2015**, *5* (42), 33385–33391. 10.1039/C4RA15202F.
- (175) Fuentes, G.; García, M. F.; Cerecetto, H.; Álvarez, G.; Couto, M.; Romero, A. H. One-Step Synthesis of Favipiravir from Selectfluor® and 3-Hydroxy-2-Pyrazinecarboxamide in an Ionic Liquid. *Org. Biomol. Chem.* **2023**, 10.1039.D3OB00380A. 10.1039/D3OB00380A.
- (176) Wu, Q.; Mao, Y.-J.; Zhou, K.; Wang, S.; Chen, L.; Xu, Z.-Y.; Lou, S.-J.; Xu, D.-Q. Pd-Catalysed Direct C(Sp²)-H Fluorination of Aromatic Ketones: Concise Access to Anacetrapib. *Chem. Commun.* **2021**, *57* (37), 4544–4547. 10.1039/D1CC01047F.
- (177) Ning, Y.; Fukuda, T.; Ikeda, H.; Otani, Y.; Kawahata, M.; Yamaguchi, K.; Ohwada, T. Revisiting Secondary Interactions in Neighboring Group Participation, Exemplified by Reactivity Changes of Iminylium Intermediates. *Org. Biomol. Chem.* **2017**, *15* (6), 1381–1392. 10.1039/C6OB02719A.
- (178) Huang, J.; Chen, Y.; Chan, J.; Ronk, M.; Larsen, R.; Faul, M. An Efficient Copper-Catalyzed Etherification of Aryl Halides. *Synlett* **2011**, *2011* (10), 1419–1422. 10.1055/s-0030-1260761.
- (179) Tikhomirov, A. S.; Ivanov, I. V.; Korolev, A. M.; Shchekotikhin, A. E. β -Hydroxylation of Anthraquinone Derivatives with Benzaldehyde Oxime as a Source of Hydroxyl Group. *Tetrahedron* **2019**, *75* (43), 130623. 10.1016/j.tet.2019.130623.
- (180) Xu, H.-J.; Liang, Y.-F.; Cai, Z.-Y.; Qi, H.-X.; Yang, C.-Y.; Feng, Y.-S. CuI-Nanoparticles-Catalyzed Selective Synthesis of Phenols, Anilines, and Thiophenols from

- Aryl Halides in Aqueous Solution. *J. Org. Chem.* **2011**, *76* (7), 2296–2300. 10.1021/jo102506x.
- (181) Dam, J. H.; Madsen, R. Convergent Synthesis of Pancratistatin from Piperonal and Xylose. *Eur. J. Org. Chem.* **2009**, *2009* (27), 4666–4673. 10.1002/ejoc.200900719.
- (182) Choy, P. Y.; Kwong, F. Y. Palladium-Catalyzed *Ortho* -CH-Bond Oxygenation of Aromatic Ketones. *Org. Lett.* **2013**, *15* (2), 270–273. 10.1021/ol303088z.
- (183) Mo, F.; Trzepakowski, L. J.; Dong, G. Synthesis of *Ortho* -Acylphenols through the Palladium-Catalyzed Ketone-Directed Hydroxylation of Arenes. *Angew. Chem. Int. Ed.* **2012**, *51* (52), 13075–13079. 10.1002/anie.201207479.
- (184) Shah, Sk. S.; Shee, M.; Singh, A. K.; Paul, A.; Singh, N. D. P. Direct Oxygenation of C–H Bonds through Photoredox and Palladium Catalysis. *J. Org. Chem.* **2020**, *85* (5), 3426–3439. 10.1021/acs.joc.9b03197.
- (185) Desai, L. V.; Malik, H. A.; Sanford, M. S. Oxone as an Inexpensive, Safe, and Environmentally Benign Oxidant for C–H Bond Oxygenation. *Org. Lett.* **2006**, *8* (6), 1141–1144. 10.1021/ol0530272.
- (186) Ghaffari, B.; Preshlock, S. M.; Plattner, D. L.; Staples, R. J.; Maligres, P. E.; Krska, S. W.; Maleczka, R. E.; Smith, M. R. Silyl Phosphorus and Nitrogen Donor Chelates for Homogeneous *Ortho* Borylation Catalysis. *J. Am. Chem. Soc.* **2014**, *136* (41), 14345–14348. 10.1021/ja506229s.
- (187) Hoque, M. E.; Hassan, M. M. M.; Chattopadhyay, B. Remarkably Efficient Iridium Catalysts for Directed C(Sp²)–H and C(Sp³)–H Borylation of Diverse Classes of Substrates. *J. Am. Chem. Soc.* **2021**, *143* (13), 5022–5037. 10.1021/jacs.0c13415.
- (188) Shan, G.; Yang, X.; Ma, L.; Rao, Y. Pd-Catalyzed C-H Oxygenation with TFA/TFAA: Expedient Access to Oxygen-Containing Heterocycles and Late-Stage Drug Modification. *Angew. Chem. Int. Ed.* **2012**, *51* (52), 13070–13074. 10.1002/anie.201207458.

- (189) Liang, Y.-F.; Wang, X.; Yuan, Y.; Liang, Y.; Li, X.; Jiao, N. Ligand-Promoted Pd-Catalyzed Oxime Ether Directed C–H Hydroxylation of Arenes. *ACS Catal.* **2015**, *5* (10), 6148–6152. 10.1021/acscatal.5b01700.
- (190) Dick, A. R.; Kampf, J. W.; Sanford, M. S. Unusually Stable Palladium(IV) Complexes: Detailed Mechanistic Investigation of C–O Bond-Forming Reductive Elimination. *J. Am. Chem. Soc.* **2005**, *127* (37), 12790–12791. 10.1021/ja0541940.
- (191) Desai, L. V.; Hull, K. L.; Sanford, M. S. Palladium-Catalyzed Oxygenation of Unactivated Sp³ C–H Bonds. *J. Am. Chem. Soc.* **2004**, *126* (31), 9542–9543. 10.1021/ja046831c.
- (192) Neufeldt, S. R.; Sanford, M. S. *O*-Acetyl Oximes as Transformable Directing Groups for Pd-Catalyzed C–H Bond Functionalization. *Org. Lett.* **2010**, *12* (3), 532–535. 10.1021/ol902720d.
- (193) Dick, A. R.; Hull, K. L.; Sanford, M. S. A Highly Selective Catalytic Method for the Oxidative Functionalization of C–H Bonds. *J. Am. Chem. Soc.* **2004**, *126* (8), 2300–2301. 10.1021/ja031543m.
- (194) Wang, D.-H.; Hao, X.-S.; Wu, D.-F.; Yu, J.-Q. Palladium-Catalyzed Oxidation of *Boc*-Protected *N*-Methylamines with IOAc as the Oxidant: A *Boc*-Directed Sp³ C–H Bond Activation. *Org. Lett.* **2006**, *8* (15), 3387–3390. 10.1021/ol061384m.
- (195) Pan, L.; Wang, L.; Chen, Q.; He, M. Palladium-Catalyzed Oxime Ether Directed Regioselective C-H Alkoxylation of Arenes. *Synthetic Communications* **2016**, *46* (24), 1981–1988. 10.1080/00397911.2016.1242749.
- (196) Shrestha, A.; Lee, M.; Dunn, A. L.; Sanford, M. S. Palladium-Catalyzed C–H Bond Acetoxylation via Electrochemical Oxidation. *Org. Lett.* **2018**, *20* (1), 204–207. 10.1021/acs.orglett.7b03559.

- (197) Chan, C.-W.; Zhou, Z.; Chan, A. S. C.; Yu, W.-Y. Pd-Catalyzed *Ortho* -C–H Acylation/Cross Coupling of Aryl Ketone *O* -Methyl Oximes with Aldehydes Using *Tert* -Butyl Hydroperoxide as Oxidant. *Org. Lett.* **2010**, *12* (17), 3926–3929. 10.1021/ol101618u.
- (198) Haider, M.; Sennari, G.; Eggert, A.; Sarpong, R. Total Synthesis of the *Cephalotaxus* Norditerpenoids (±)-Cephanolides A–D. *J. Am. Chem. Soc.* **2021**, *143* (7), 2710–2715. 10.1021/jacs.1c00293.
- (199) Lusi, R. F.; Sennari, G.; Sarpong, R. Total Synthesis of Nine Longiborneol Sesquiterpenoids Using a Functionalized Camphor Strategy. *Nat. Chem.* **2022**, *14* (4), 450–456. 10.1038/s41557-021-00870-4.
- (200) Lusi, R. F.; Sennari, G.; Sarpong, R. Strategy Evolution in a Skeletal Remodeling and C–H Functionalization-Based Synthesis of the Longiborneol Sesquiterpenoids. *J. Am. Chem. Soc.* **2022**, *144* (37), 17277–17294. 10.1021/jacs.2c08136.
- (201) Dohi, T.; Takenaga, N.; Goto, A.; Fujioka, H.; Kita, Y. Clean and Efficient Benzylic C–H Oxidation in Water Using a Hypervalent Iodine Reagent: Activation of Polymeric Iodosobenzene with KBr in the Presence of Montmorillonite-K10. *J. Org. Chem.* **2008**, *73* (18), 7365–7368. 10.1021/jo8012435.
- (202) Ojha, L.; Kudugunti, S.; Maddukuri, P.; Kommareddy, A.; Gunna, M.; Dokuparthi, P.; Gottam, H.; Botha, K.; Parapati, D.; Vinod, T. Benzylic Carbon Oxidation by an in Situ Formed *O*-Iodoxybenzoic Acid (IBX) Derivative. *Synlett* **2008**, *2009* (01), 117–121. 10.1055/s-0028-1087384.
- (203) Moriyama, K.; Takemura, M.; Togo, H. Direct and Selective Benzylic Oxidation of Alkylarenes via C–H Abstraction Using Alkali Metal Bromides. *Org. Lett.* **2012**, *14* (9), 2414–2417. 10.1021/ol300853z.

- (204) Majetich, G.; Li, Y.; Zou, G. Total Synthesis of (±)-Komaroviquinone. *Heterocycles* **2007**, *73* (1), 217. 10.3987/COM-07-S(U)36.
- (205) Shaabani, A.; Mirzaei, P.; Naderi, S.; Lee, D. G. Green Oxidations. The Use of Potassium Permanganate Supported on Manganese Dioxide. *Tetrahedron* **2004**, *60* (50), 11415–11420. 10.1016/j.tet.2004.09.087.
- (206) Sugimori, M.; Ejima, A.; Ohsuki, S.; Uoto, K.; Mitsui, I.; Matsumoto, K.; Kawato, Y.; Yasuoka, M.; Sato, K. Antitumor Agents. VII. Synthesis and Antitumor Activity of Novel Hexacyclic Camptothecin Analogs. *J. Med. Chem.* **1994**, *37* (19), 3033–3039. 10.1021/jm00045a007.
- (207) Mečiarova, M.; Toma, Š.; Heribanová, A. Ultrasound Assisted Heterogeneous Permanganate Oxidations. *Tetrahedron* **2000**, *56* (43), 8561–8566. 10.1016/S0040-4020(00)00798-5.
- (208) Menger, F. M.; Lee, C. Oxidations with Solid Potassium Permanganate. *J. Org. Chem.* **1979**, *44* (19), 3446–3448. 10.1021/jo01333a051.
- (209) Wolfe, S.; Ingold, C. F. Oxidation of Organic Compounds by Zinc Permanganate. *J. Am. Chem. Soc.* **1983**, *105* (26), 7755–7757. 10.1021/ja00364a054.
- (210) McNeill, E.; Du Bois, J. Ruthenium-Catalyzed Hydroxylation of Unactivated Tertiary C–H Bonds. *J. Am. Chem. Soc.* **2010**, *132* (29), 10202–10204. 10.1021/ja1046999.
- (211) Sur, A.; Jernigan, N. B.; Powers, D. C. Kinetic Probes of the Origin of Activity in MOF-Based C–H Oxidation Catalysis. *ACS Catal.* **2022**, *12* (7), 3858–3867. 10.1021/acscatal.1c05415.
- (212) Niu, K.; Shi, X.; Ding, L.; Liu, Y.; Song, H.; Wang, Q. HCl-Catalyzed Aerobic Oxidation of Alkylarenes to Carbonyls. *ChemSusChem* **2022**, *15* (2). 10.1002/cssc.202102326.
- (213) Leow, W. R.; Ng, W. K. H.; Peng, T.; Liu, X.; Li, B.; Shi, W.; Lum, Y.; Wang, X.; Lang, X.; Li, S.; Mathews, N.; Ager, J. W.; Sum, T. C.; Hirao, H.; Chen, X. Al₂O₃ Surface

- Complexation for Photocatalytic Organic Transformations. *J. Am. Chem. Soc.* **2017**, *139* (1), 269–276. 10.1021/jacs.6b09934.
- (214) Chen, M. S.; White, M. C. A Predictably Selective Aliphatic C–H Oxidation Reaction for Complex Molecule Synthesis. *Science* **2007**, *318* (5851), 783–787. 10.1126/science.1148597.
- (215) Wang, J.; Zhang, C.; Ye, X.-Q.; Du, W.; Zeng, S.; Xu, J.-H.; Yin, H. An Efficient and Practical Aerobic Oxidation of Benzylic Methylens by Recyclable *N*-Hydroxyimide. *RSC Adv.* **2021**, *11* (5), 3003–3011. 10.1039/D0RA10475B.
- (216) Kim, S. S.; Jung, H. C. An Efficient Aerobic Oxidation of Alcohols to Aldehydes and Ketones with TEMPO/Ceric Ammonium Nitrate as Catalysts. *Synthesis* **2003**, No. 14, 2135–2137. 10.1055/s-2003-41065.
- (217) Miller, R. A.; Hoerner, R. S. Iodine as a Chemoselective Reoxidant of TEMPO: Application to the Oxidation of Alcohols to Aldehydes and Ketones. *Org. Lett.* **2003**, *5* (3), 285–287. 10.1021/ol0272444.
- (218) Frank, S. A.; Roush, W. R. Studies on the Synthesis of (–)-Spinosyn A: Application of the Steric Directing Group Strategy to Transannular Diels–Alder Reactions. *J. Org. Chem.* **2002**, *67* (12), 4316–4324. 10.1021/jo025580s.
- (219) Best, W.; Wege, D. Intramolecular Diels–Alder Additions of Benzyne to Furans. Application to the Total Synthesis of Biflorin, and the Mansonone-E, I and F. *Aust. J. Chem.* **1986**, *39* (4), 647. 10.1071/CH9860647.
- (220) Hua, D. H.; Venkataraman, S.; Ostrander, R. A.; Sinai, G. Z.; McCann, P. J.; Coulter, M. J.; Xu, M. R. Asymmetric Synthesis of (+)-Hirsutene. *J. Org. Chem.* **1988**, *53* (3), 507–515. 10.1021/jo00238a007.

- (221) Xu, L.; Wang, C.; Gao, Z.; Zhao, Y.-M. Total Synthesis of (±)-Cephanolides B and C via a Palladium-Catalyzed Cascade Cyclization and Late-Stage Sp³ C–H Bond Oxidation. *J. Am. Chem. Soc.* **2018**, *140* (16), 5653–5658. 10.1021/jacs.8b03015.
- (222) Xiao, Z.; Li, Y.; Gao, S. Total Synthesis and Structural Determination of the Dimeric Tetrahydroxanthone Ascherxanthone A. *Org. Lett.* **2017**, *19* (7), 1834–1837. 10.1021/acs.orglett.7b00592.
- (223) Bernini, R.; Crisante, F.; Gentili, P.; Menta, S.; Morana, F.; Pierini, M. Unexpected Different Chemoselectivity in the Aerobic Oxidation of Methylated Planar Catechin and Bent Epicatechin Derivatives Catalysed by the *Trametes Villosa* Laccase/1-Hydroxybenzotriazole System. *RSC Adv.* **2014**, *4* (16), 8183. 10.1039/c3ra47753c.
- (224) Jadhao, A. R.; Patel, H.; Kodam, K. M.; Gupte, A.; Waghmode, S. B. Selective Oxidation of Benzylic Alcohols by Laccase from White-Rot Mushroom *Tricholoma Giganteum* AGHP: Total Synthesis of Taccabulin A, Taccabulin D and Taccabulin E. *Tetrahedron* **2022**, *128*, 133114. 10.1016/j.tet.2022.133114.
- (225) Tromp, S. A.; Matijošytė, I.; Sheldon, R. A.; Arends, I. W. C. E.; Mul, G.; Kreutzer, M. T.; Moulijn, J. A.; de Vries, S. Mechanism of Laccase-TEMPO-Catalyzed Oxidation of Benzyl Alcohol. *ChemCatChem* **2010**, *2* (7), 827–833. 10.1002/cctc.201000068.
- (226) Dong, J.; Fernández-Fueyo, E.; Hollmann, F.; Paul, C. E.; Pesic, M.; Schmidt, S.; Wang, Y.; Younes, S.; Zhang, W. Biocatalytic Oxidation Reactions: A Chemist's Perspective. *Angew. Chem. Int. Ed.* **2018**, *57* (30), 9238–9261. 10.1002/anie.201800343.
- (227) Capdevielle, P.; Maumy, M. Esters Are Effective Co-Catalysts in Copper-Catalyzed Methanolysis of Aryl Bromides. *Tetrahedron Letters* **1993**, *34* (6), 1007–1010. 10.1016/S0040-4039(00)77477-6.

- (228) Liu, Y.; Park, S. K.; Xiao, Y.; Chae, J. Copper(II)-Catalyzed C–O Coupling of Aryl Bromides with Aliphatic Diols: Synthesis of Ethers, Phenols, and Benzo-Fused Cyclic Ethers. *Org. Biomol. Chem.* **2014**, *12* (26), 4747. 10.1039/c4ob00649f.
- (229) Ishiyama, T.; Murata, M.; Miyaura, N. Palladium(0)-Catalyzed Cross-Coupling Reaction of Alkoxydiboron with Haloarenes: A Direct Procedure for Arylboronic Esters. *J. Org. Chem.* **1995**, *60* (23), 7508–7510. 10.1021/jo00128a024.
- (230) Takagi, J.; Takahashi, K.; Ishiyama, T.; Miyaura, N. Palladium-Catalyzed Cross-Coupling Reaction of Bis(Pinacolato)Diboron with 1-Alkenyl Halides or Triflates: Convenient Synthesis of Unsymmetrical 1,3-Dienes via the Borylation-Coupling Sequence. *J. Am. Chem. Soc.* **2002**, *124* (27), 8001–8006. 10.1021/ja0202255.
- (231) Hayashi, Y.; Yamaguchi, J.; Sumiya, T.; Hibino, K.; Shoji, M. Direct Proline-Catalyzed Asymmetric α -Aminoxylation of Aldehydes and Ketones. *J. Org. Chem.* **2004**, *69* (18), 5966–5973. 10.1021/jo049338s.
- (232) Vidal-Ferran, A.; Moyano, A.; Pericàs, M. A.; Riera, A. Synthesis of a Family of Fine-Tunable New Chiral Ligands for Catalytic Asymmetric Synthesis. Ligand Optimization through the Enantioselective Addition of Diethylzinc to Aldehydes. *J. Org. Chem.* **1997**, *62* (15), 4970–4982. 10.1021/jo9701445.
- (233) Lin, H.-Y.; Haegle, J. A.; Disare, M. T.; Lin, Q.; Aye, Y. A Generalizable Platform for Interrogating Target- and Signal-Specific Consequences of Electrophilic Modifications in Redox-Dependent Cell Signaling. *J. Am. Chem. Soc.* **2015**, *137* (19), 6232–6244. 10.1021/ja5132648.
- (234) Lepore, S. D.; He, Y. Use of Sonication for the Coupling of Sterically Hindered Substrates in the Phenolic Mitsunobu Reaction. *J. Org. Chem.* **2003**, *68* (21), 8261–8263. 10.1021/jo0345751.

- (235) Liu, D.; Sanow, L. P.; Zhang, C. Mitsunobu Reactions of Aliphatic Alcohols and Bulky Phenols. *Tetrahedron Letters* **2014**, *55* (19), 3090–3092. 10.1016/j.tetlet.2014.03.138.
- (236) Schenk, S.; Weston, J.; Anders, E. Density Functional Investigation of the Mitsunobu Reaction. *J. Am. Chem. Soc.* **2005**, *127* (36), 12566–12576. 10.1021/ja052362i.
- (237) Evans, P. A.; Leahy, D. K. Regioselective and Enantiospecific Rhodium-Catalyzed Intermolecular Allylic Etherification with Ortho-Substituted Phenols. *J. Am. Chem. Soc.* **2000**, *122* (20), 5012–5013. 10.1021/ja0003831.
- (238) Takizawa, K.; Sekino, T.; Sato, S.; Yoshino, T.; Kojima, M.; Matsunaga, S. Cobalt-Catalyzed Allylic Alkylation Enabled by Organophotoredox Catalysis. *Angew. Chem. Int. Ed.* **2019**, *58* (27), 9199–9203. 10.1002/anie.201902509.
- (239) Bergstrom, B. D.; Merrill, A. T.; Fettinger, J. C.; Tantillo, D. J.; Shaw, J. T. Divergent Asymmetric Synthesis of Panowamycins, TM-135, and Veramycin F Using C–H Insertion with Donor/Donor Carbenes. *Angew Chem Int Ed* **2022**, *61* (25). 10.1002/anie.202203072.
- (240) Fujita, A.; Tamura, T.; Ikeda, K.; Kashiwagi, D. Oxime Compound, Photosensitive Composition, Color Filter, Method for Production of the Color Filter, and Liquid Crystal Display Element. WO2008/90640, July 31, 2008.
- (241) Carpenter, P. D.; Peesapati, V.; Proctor, G. R. Synthesis of Structural Analogues of 6,7,8,9-Tetrahydro-3-Hydroxy-2-Methoxybenzocyclohepten-5-One. *J. Chem. Soc., Perkin Trans. 1* **1979**, 103. 10.1039/p19790000103.
- (242) Scopton, A.; Kelly, T. R. Synthesis of Azacridone A. *Org. Lett.* **2004**, *6* (21), 3869–3871. 10.1021/ol048382r.
- (243) Huang, W.-L.; Raja, A.; Hong, B.-C.; Lee, G.-H. Organocatalytic Enantioselective Michael–Acetalization–Reduction–Nef Reaction for a One-Pot Entry to the Functionalized Aflatoxin System. Total Synthesis of (–)- Dihydroaflatoxin D₂ and (–)- and (+)- Microminutinin. *Org. Lett.* **2017**, *19* (13), 3494–3497. 10.1021/acs.orglett.7b01473.

A.1 Quantitative structure-selectivity reaction model

A.1.1 Introduction

Lucas Souza in collaboration with the Sigman Lab at The University of Utah wanted to develop a quantitative structure-selectivity reaction model for the Shaw Lab's C–H insertion of donor/donor carbenes methodology. The main objective was to be able to computationally predict the diastereoselectivity and enantioselectivity of a C–H insertion substrate with a catalyst of choice.^{1,2} A predictive computational model would aid current experimental optimization and help drive novel reaction and catalyst design strategies. For instance, running a substrate in the model first would indicate the best catalyst to use for the desired stereoselective outcome.³ Thereby, the wet-bench reaction screening of new C–H insertion donor/donor carbene substrate classes is greatly streamlined. Feasibly, the model could inform new ligand designs to access novel reactivity and stereoselectivity helping to expand the chemical space for donor/donor C–H insertion reactions.⁴

A.1.2 Results and Discussion

A large amount of experimental donor/donor C–H insertion stereoselectivity data was needed to form the training sets that the computational model could be built and tested upon. Lucas Souza enlisted the help of a couple of colleagues in the Shaw Lab to help generate the training set data. I was tasked with synthesizing a cyclohexene (**6**) insertion center and a fused benzodihydrofuran substrate with a tertiary, stereogenic C–H insertion center (**8**) to be used to test the limitations of the generated model. The cyclohexene hydrazone precursor (**6**) was synthesized over 4 steps (Figure A1.1). First, methyl-1-cyclohexene-1-carboxylate (**1**) was reduced to the allylic alcohol (**2**) with diisobutylaluminum hydride (DIBAL-H). Then the alcohol (**2**) was transformed into the

allylic bromide (**3**) with phosphorous tribromide in a near quantitative yield. Alkylation of 2-hydroxybenzophenone (**4**) with allylic bromide (**3**) followed by hydrazine condensation afforded the desired hydrazone precursor (**6**).

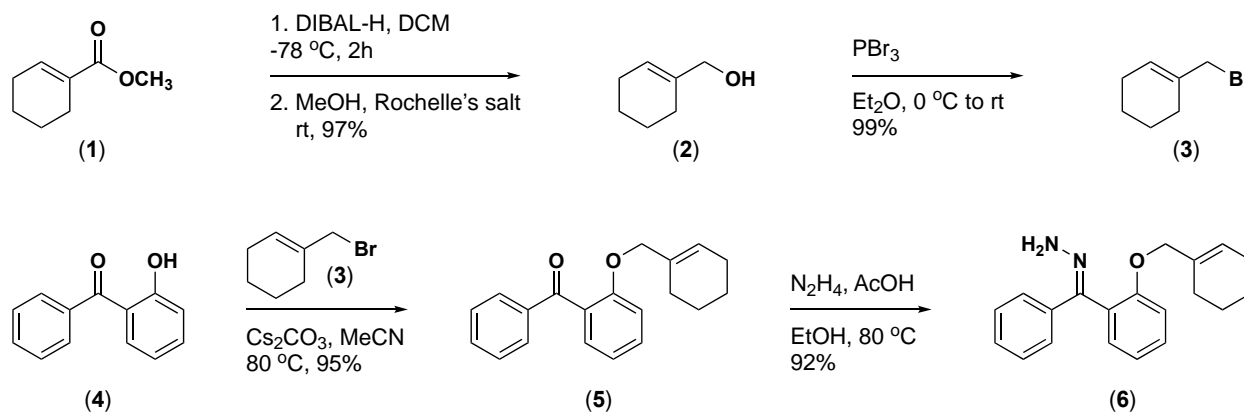


Figure A1.1 Synthesis of cyclohexene hydrazone precursor.

The intramolecular C–H insertion of **6** was highly diastereoselective (Table A1.1). Regardless of the enantiomer of the catalyst used the substrate (**6**) always yielded a single cis diastereomer (**7a**) of the product. Varying the solvent had no effect on the stereoselectivity.

Table A1.1 Allylic C–H insertion site stereoselectivity outcomes.

The reaction scheme shows the intramolecular C–H insertion of **6** to form cis (**7a**) and trans (**7b**) diastereomers. The reaction conditions are: 1. MnO₂, solvent, 2h; 2. catalyst, 0 °C to rt, o/n.

Entry	Catalyst	solvent	dr (7a : 7b)
1	Rh ₂ (PTCC) ₄	CH ₂ Cl ₂	>95:5
2	Rh ₂ (PTCC) ₄	MeCN	>95:5
3	Rh ₂ (ACB) ₄	CH ₂ Cl ₂	>95:5
4	Rh ₂ (ACB) ₄	MeCN	>95:5
5	Rh ₂ (ACP) ₄	CH ₂ Cl ₂	>95:5
6	Rh ₂ (ACP) ₄	MeCN	>95:5
7	Rh ₂ (mes) ₄	CH ₂ Cl ₂	>95:5
8	Rh ₂ (mes) ₄	MeCN	>95:5
9	Rh ₂ (triphenyl) ₄	CH ₂ Cl ₂	>95:5
10	Rh ₂ (triphenyl) ₄	MeCN	>95:5

Conversely, the fused chiral benzodihydrofuran substrate (**8**) showed catalyst control over the diastereomeric ratio (dr) (Table A1.2).⁵ Racemic starting material (**8**) with an achiral catalyst

afforded the cis diastereomer (**9a**) in an 80:20 dr (Table A1.2 entry 1). Switching to the chiral catalyst Rh₂(*R*-PTAD)₄, the cis diastereomer (**9a**) is still the major stereoisomer in an 83:17 dr (Table A1.2 entry 2). The opposite enantiomer of catalyst, Rh₂(*S*-PTAD)₄, preferences the trans diastereomer (**9b**) in 81:19 dr (Table A1.2 entry 3). When a single enantiomer of starting material (**8**) is used, the resulting major diastereomer of the product (**9a/b**) is in high enantioselectivity.

Table A1.2 C–H insertion of a fused bicyclic donor/donor carbene into a stereogenic center.

Entry	Starting Material	Catalyst	Temperature	dr ^a (9a : 9b)	er ^b (major diastereomer)	Yield
1	(<i>R/S</i>)	Rh ₂ (mes) ₄	0 °C to rt	80:20	50:50	75%
2	(<i>R</i>)	Rh ₂ (<i>R</i> -PTAD) ₄	-40 °C	83:17	97:03	78%
3	(<i>R</i>)	Rh ₂ (<i>S</i> -PTAD) ₄	-40 °C	19:81	93:07	62%

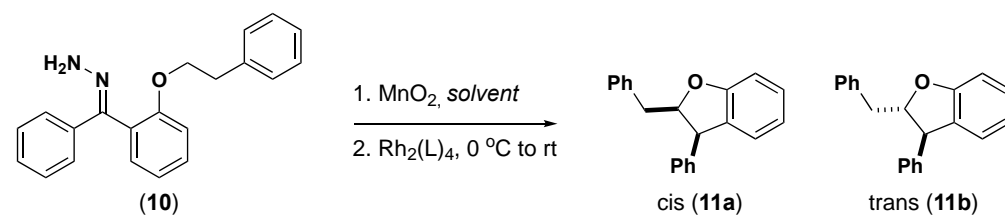
^adr determined by ¹H NMR

^ber determined by CSP-HPLC on OD column

A colleague Ben Bergstrom was gathering data for homobenzylic 1,6-C–H insertion center substrates that could be employed in the synthesis of the drug candidate Cantrixil™ (BDB dissertation A2).⁶ Initial C–H insertion screens with homobenzylic substrates **10** and **12** found that the 1,5-C–H insertion was favored over the 1,6-C–H insertion across a wide variety of dirhodium catalysts. Therefore, the homobenzylic substrates would not be useful in the synthesis of Cantrixil™, but they did provide excellent data to be used as a test substrate of the quantitative structure-selectivity relationship (QSSR) model. Ben initially reported stereoselectivity data where dichloromethane was used as the solvent in the C–H insertion reaction. However, the QSSR model was built using acetonitrile in the solvent model. Therefore, I was tasked with repeating all the C–H insertion catalyst screening data with acetonitrile as the solvent. Since these results in the context

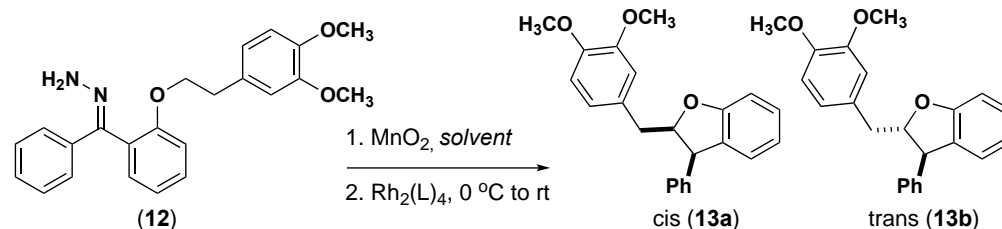
of the QSSR model are still in progress, they will only be reported below with minor commentary (Table A1.3-4). Interestingly, we observed a couple of changes in stereoselectivity from the reaction solvent swap. When $\text{Rh}_2(R\text{-PTAD})_4$ was used with acetonitrile, the diastereomeric ratio increased for both substrates **10** and **12** (Tables A1.3-4 entries 1-2). Conversely, there was an erosion of diastereomeric ratio for substrate **10** in acetonitrile with both $\text{Rh}_2(S\text{-TCPTTL})_4$ and $\text{Rh}_2(S\text{-BTPCP})_4$ (Table A1.3 entries 3-4, 7-8).

Table A1.3 C–H insertion results for homobenzylic insertion substrate **10**.



Entry	Notebook	Catalyst	solvent	dr ^a (11a:11b)
1	BDB	$\text{Rh}_2(R\text{-PTAD})_4$	CH_2Cl_2	66:33
2	SND		MeCN	86:14
3	BDB	$\text{Rh}_2(S\text{-TCPTTL})_4$	CH_2Cl_2	16:84
4	SND		MeCN	59:41
5	BDB	$\text{Rh}_2(S\text{-PTTL})_4$	CH_2Cl_2	57:43
6	SND		MeCN	84:16
7	BDB	$\text{Rh}_2(S\text{-BTPCP})_4$	CH_2Cl_2	93:07
8	SND		MeCN	75:25
9	BDB	$\text{Rh}_2(\text{PTCC})_4$	CH_2Cl_2	55:45
10	SND		MeCN	82:18
11	BDB	$\text{Rh}_2(R\text{-DOSP})_4$	CH_2Cl_2	49:51
12	SND		MeCN	67:33
13	BDB	$\text{Rh}_2(\text{ACyp})_4$	CH_2Cl_2	46:54
14	SND		MeCN	68:32
15	BDB	$\text{Rh}_2(\text{ACB})_4$	CH_2Cl_2	49:51
16	SND		MeCN	64:36
17	BDB	$\text{Rh}_2(\text{OAc})_4$	CH_2Cl_2	58:42
18	SND		MeCN	66:34
19	BDB	$\text{Rh}_2(\text{triphenyl})_4$	CH_2Cl_2	86:14
20	SND		MeCN	93:07

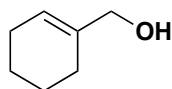
^adr determined by ¹H NMR

Table A1.4 C–H insertion results for homobenzylic insertion substrate **12**.

Entry	Notebook	Catalyst	solvent	dr ^a (13a:13b)
1	BDB	Rh ₂ (<i>R</i> -PTAD)	CH ₂ Cl ₂	71:29
2	SND		MeCN	87:13
3	BDB	Rh ₂ (<i>S</i> -TCPTTL) ₄	CH ₂ Cl ₂	13:87
4	SND		MeCN	21:79
5	BDB	Rh ₂ (<i>S</i> -BTPCP) ₄	CH ₂ Cl ₂	91:09
6	SND		MeCN	97:03
7	BDB	Rh ₂ (PTCC) ₄	CH ₂ Cl ₂	59:41
8	SND		MeCN	76:24
9	BDB	Rh ₂ (<i>R</i> -DOSP) ₄	CH ₂ Cl ₂	50:50
10	SND		MeCN	82:18
11	BDB	Rh ₂ (ACyp) ₄	CH ₂ Cl ₂	56:44
12	SND		MeCN	73:27
13	BDB	Rh ₂ (ACB) ₄	CH ₂ Cl ₂	54:46
14	SND		MeCN	70:30
15	BDB	Rh ₂ (OAc) ₄	CH ₂ Cl ₂	63:37
16	SND		MeCN	63:37
17	BDB	Rh ₂ (triphenyl) ₄	CH ₂ Cl ₂	83:17
18	SND		MeCN	91:09

^adr determined by ¹H NMR

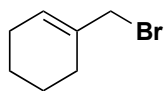
A.1.3 Experimental section



(2) cyclohex-1-en-1-ylmethanol

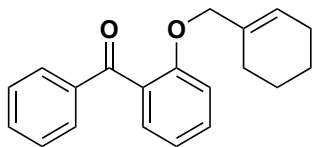
2 was synthesized by following a literature procedure.⁷ Methyl-1-cyclohexene-1-carboxylate (1.0 g, 7.13 mmol, 1.0 equiv) and CH₂Cl₂ (23.8 mL, 0.3 M) were added to a flame-dried round bottom under Ar and cooled to -78 °C. DIBAL-H (1.0 M in THF, 15.7 mL, 15.7 mmol, 2.2 equiv) was added and the reaction was stirred at -78 °C for 2h. Then methanol (14.3 mL, 0.5 M) and Rochelle's salt (aq) (14.3 mL, 0.5 M) were added, and the solution was stirred overnight while allowing the

reaction to warm to room temperature. The reaction was quenched with H₂O, and extracted with CH₂Cl₂ (2 x 10 mL). The organics were combined and concentrated *in vacuo* to yield the desired product **2** (789 mg, 97%) as a clear oil. SND-VI-043. ¹H NMR matched reported data.⁷



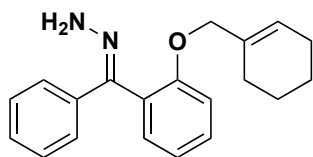
(3) 1-(bromomethyl)cyclohex-1-ene

2 (789 mg, 7.13 mmol, 1.0 equiv) and Et₂O (28.5 mL, 0.25 M) were added to a round bottom and cooled to 0 °C. PBr₃ (0.339 mL, 3.57 mmol, 0.5 equiv) was added to the solution and the reaction was stirred overnight while allowing it to warm to room temperature. The reaction was poured into a solution of K₂CO₃ (aq) then extracted with Et₂O (2 x 10 mL). The organics were combined and washed with brine (1 x 10 mL), dried over Na₂SO₄ and concentrated *in vacuo* to afford the desired product **3** (1.25 g, 99%) as a light yellow oil. SND-VI-047. ¹H NMR matched literature precedent.⁷



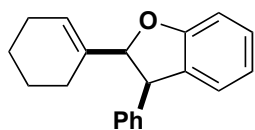
(5) 2-(cyclohex-1-en-1-ylmethoxy)phenyl(phenyl)methanone

2-hydroxybenzophenone (567 mg, 2.86 mmol, 1.0 equiv) in MeCN (9.53 mL, 0.3 M) were added to a flame-dried microwave vial under Ar charged with Cs₂CO₃ (2.79 g, 8.57 mmol, 3.0 equiv). Allylic bromide **3** (1.00 g, 5.71 mmol, 2.0 equiv) was added then the reaction was heated to 80 °C overnight. The reaction was cooled down and Cs₂CO₃ was filtered off. The filtrate was concentrated *in vacuo* to afford ether **5** (790 mg, 95%) as a light-yellow oil. SND-VI-048.



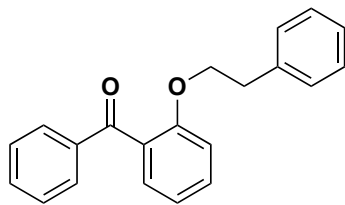
(6) ((2-(cyclohex-1-en-1-ylmethoxy)phenyl)(phenyl)methylene)hydrazine

5 (400 mg, 1.37 mmol, 1.0 equiv) in EtOH (4.57 mL, 0.3 M) was added to a flame-dried microwave vial under Ar. Acetic acid (0.157 mL, 2.74 mmol, 2.00 equiv) then hydrazine (0.344 mL, 10.95 mmol, 8.0 equiv) were added to the solution. The reaction was heated to 80 °C overnight. Once the reaction was cooled down to room temperature, the solution was dumped into H₂O (5 mL) and extracted with EtOAc (3 x 5 mL). The organics were dried over Na₂SO₄ and concentrated *in vacuo* to afford hydrazone **6** (99%) as a yellow oil. SND-VI-050.



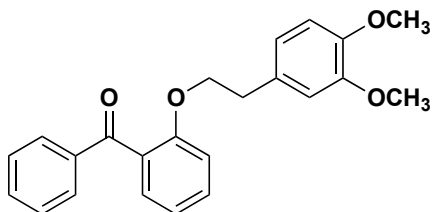
(7) 2-(cyclohex-1-en-1-yl)-3-phenyl-2,3-dihydrobenzofuran

Hydrazone **6** (20 mg, 0.065 mmol, 1.0 equiv) in CH₂Cl₂ (4.33 mL, 0.015 M) was added to a flame-dried scintillation vial. MnO₂ (45 mg, 0.522 mmol, 8.0 equiv) was added and the reaction was stirred at room temperature until all of **6** was fully consumed. Then the reaction was cooled down to 0 °C and Rh₂(*R*-PTAD)₄ (1.0 mg, 0.00065 mmol, 1 mol%) was added and stirred until all the diazo was fully consumed. The reaction was filtered over celite, concentrated *in vacuo*, and purified by flash column chromatography (90:10 hexanes:EtOAc) to afford **7** as a light yellow oil. SND-VI-054-058.



(S1) (2-phenethoxyphenyl)(phenyl)methanone

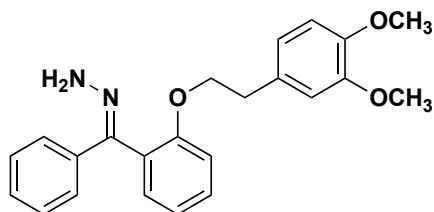
S1 was synthesized by following a modified literature procedure,⁸ by preparing a suspension of NaH (0.337 g, 8 mmol, 4 equiv) in THF (0.25 M). 2-phenylethanol (0.479 mL, 4 mmol, 2 equiv) and 2-fluorobenzophenone (0.400 g, 2 mmol, 1 equiv) were then added and the mixture was heated to 60 °C with stirring overnight. The reaction was then cooled to room temperature, quenched with sat. aq. ammonium chloride (5 mL), washed with brine (10 mL), dried over sodium sulfate, concentrated in vacuo, and purified by flash column chromatography (80:20 hexanes:EtOAc) to afford **S1** (SND-VI-083) as a yellow oil. ¹H NMR (400 MHz, CDCl₃) δ 7.80 (d, *J* = 6.8 Hz, 2H), 7.56 (t, *J* = 7.4 Hz, 1H), 7.46 – 7.37 (m, 4H), 7.18 – 7.12 (m, 3H), 7.03 (t, *J* = 7.4 Hz, 1H), 6.99 – 6.90 (m, 3H), 4.08 (t, *J* = 6.9 Hz, 2H), 2.71 (t, *J* = 6.9 Hz, 2H); ¹³C NMR (100 MHz, CDCl₃) δ 196.9, 156.8, 138.4, 138.1, 132.9, 132.1, 129.8, 129.8, 129.3, 129.0, 128.5, 128.3, 126.5, 120.9, 112.5, 69.5, 35.6; IR (neat) 3061, 3028, 2928, 2873, 1663, 1598, 1450, 1315, 1295, 1240 cm⁻¹; AMM (ESI) *m/z* calcd C₂₁H₁₉O₂⁺ [M+H]⁺ 303.1380, found 303.1382.



(S2) (2-(3,4-dimethoxyphenethoxy)phenyl)(phenyl)methanone

S2 was synthesized by following a modified literature procedure,⁸ by preparing a suspension of NaH (0.337 g, 8 mmol, 4 equiv) in THF (0.25 M). 2-(3,4-dimethoxy)phenylethanol (0.729 g, 2

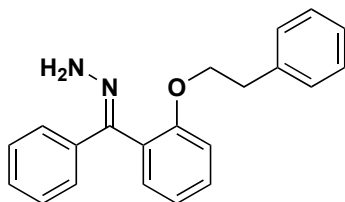
mmol, 2 equiv) and 2-fluorobenzophenone (0.400 g, 2 mmol, 1 equiv) were then added and the mixture was heated to 60 °C with stirring overnight. The reaction was then cooled to room temperature, quenched with sat. aq. ammonium chloride (5 mL), washed with brine (10 mL), dried over sodium sulfate, concentrated in vacuo, and purified by flash column chromatography (80:20 hexanes:EtOAc) to afford **S2** (SND-VI-084) as a yellow oil. ¹H NMR (400 MHz, CDCl₃) δ 7.79 (d, J = 6.9 Hz, 2H), 7.55 (t, J = 7.4 Hz, 1H), 7.45 – 7.36 (m, 4H), 7.03 (t, J = 7.5 Hz, 1H), 6.94 (d, J = 8.4 Hz, 1H), 6.67 (d, J = 8.0 Hz, 1H), 6.58 (d, J = 1.9 Hz, 1H), 6.53 (dd, J = 8.0, 2.1 Hz, 1H), 4.08 (t, J = 6.8 Hz, 2H), 3.82 (s, 3H), 3.78 (s, 3H), 2.68 (t, J = 6.8 Hz, 2H); ¹³C NMR (101 MHz, CDCl₃) δ 196.7, 156.8, 148.8, 147.7, 138.3, 132.9, 132.1, 130.8, 129.8, 129.2, 128.3, 120.9, 120.8, 112.6, 112.4, 111.2, 69.7, 56.0, 55.9, 35.2; IR (neat) 2935, 2834, 1663, 1597, 1259, 1234 cm⁻¹; AMM (ESI) m/z calcd C₂₃H₂₃O₄ + [M+H]⁺ 363.1591, found 363.1595.



(12) ((2-(3,4-dimethoxyphenoxy)phenyl)(phenyl)methylene)hydrazine

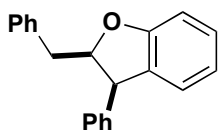
S3 was synthesized by preparing a solution of **S2** (0.120 g, 0.397 mmol, 1 equiv) in EtOH (0.3 M), adding hydrazine (0.100 mL, 3.18 mmol, 8 equiv), glacial acetic acid (0.045 μL, 0.794 mmol, 2 equiv), and heating the mixture to 80 °C overnight in a microwave vial. Cooling the mixture to room temperature, the reaction was diluted with diethyl ether (10 mL), washed with water (5 mL), washed with brine (5 mL), dried over sodium sulfate, concentrated in vacuo, to afford **12** (SND-VI-092) as a yellow oil without further purification. ¹H NMR (400 MHz, CDCl₃) δ 7.46 (dd, J = 7.5, 2.4 Hz, 1H), 7.42 – 7.37 (m, 1H), 7.27 (dd, J = 5.2, 2.2 Hz, 2H), 7.13 (dd, J = 7.5, 1.9 Hz, 1H),

7.01 (d, $J = 8.4$ Hz, 1H), 6.67 – 6.64 (m, 1H), 5.32 (s, 1H), 4.12 (s, 1H), 3.82 (s, 2H), 3.77 (s, 2H), 2.83 (t, $J = 6.6$ Hz, 1H); ^{13}C NMR (101 MHz, CDCl_3) δ 156.1, 148.8, 147.7, 147.4, 138.7, 131.0, 130.6, 130.5, 128.2, 128.0, 126.3, 122.1, 121.7, 121.1, 112.8, 112.6, 111.2, 69.7, 56.0, 55.9, 35.5; IR (neat) 3402, 2932, 1596, 1516, 1488, 1261 cm^{-1} .



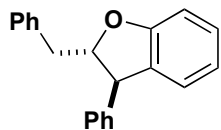
(10) ((2-phenethoxyphenyl)(phenyl)methylene)hydrazine

S1 (0.170 g, 0.469 mmol, 1 equiv) in EtOH (0.3 M) was added to a microwave vial under Ar. Then hydrazine (0.118 mL, 3.75 mmol, 8 equiv) and glacial acetic acid (54 μL , 0.938 mmol, 2 equiv), were added and the reaction was heated to 80 $^\circ\text{C}$ overnight. Cooling the mixture to room temperature, the reaction was diluted with diethyl ether (10 mL), washed with water (5 mL), washed with brine (5 mL), dried over sodium sulfate, concentrated in vacuo, to afford **10** (SND-VI-093) as a yellow oil without further purification. ^1H NMR (400 MHz, CDCl_3) δ 7.50 – 7.44 (m, 2H), 7.42 – 7.36 (m, 1H), 7.32 – 7.25 (m, 3H), 7.19 – 7.13 (m, 3H), 7.13 – 7.07 (m, 3H), 7.05 (d, $J = 7.4$ Hz, 1H), 7.01 (d, $J = 8.3$ Hz, 1H), 5.26 (s, 2H), 4.14 (t, $J = 6.6$ Hz, 2H), 2.89 (t, $J = 6.6$ Hz, 2H); ^{13}C NMR (101 MHz, CDCl_3) δ 155.9, 147.6, 138.6, 138.2, 130.5, 130.4, 129.1, 128.3, 128.1, 127.9, 126.4, 126.2, 122.0, 121.6, 112.6, 69.3, 35.7; IR (neat) 3406, 3027, 2926, 2873, 1597, 1488, 1444, 1240 cm^{-1} .



11a (2R,3R)-2-benzyl-3-phenyl-2,3-dihydrobenzofuran

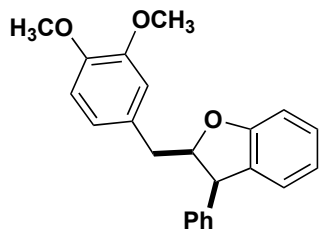
10 (0.010 g, 0.032 mmol, 1 equiv) in DCM (0.015 M) were added to a scintillation vial and manganese dioxide (0.022 g, 0.253 mmol, 8 equiv) was added. This heterogenous mixture was stirred at room temperature for 4 hours before cooling to 0 °C. Rh₂(*R*-PTAD)₄ (0.001 g, 0.00032 mmol, 1 mol%) was then added and the mixture was allowed to stir to room temperature overnight. The reaction was then filtered through celite, concentrated in vacuo, and purified by flash column chromatography (95:5 hexanes:EtOAc) to afford **11a** (84%) as a crystalline white solid. ¹H NMR (400 MHz, CDCl₃) δ 7.29 – 7.22 (m, 5H), 7.21 – 7.15 (m, 2H), 7.11 – 7.04 (m, 3H), 7.04 – 6.99 (m, 2H), 6.91– 6.84 (m, 2H), 5.15 (td, *J* = 9.1, 4.9 Hz, 1H), 4.57 (d, *J* = 8.3 Hz, 1H), 2.71 (dd, *J* = 14.6, 9.1 Hz, 1H), 2.52 (dd, *J* = 14.6, 4.7 Hz, 1H); ¹³C NMR (100 MHz, CDCl₃) δ 159.8, 139.6, 138.4, 131.5, 129.4, 129.2, 128.8, 128.5, 128.4, 127.3, 126.5, 125.8, 121.1, 110.1, 87.6, 51.8, 38.0; IR (neat) 3029, 2922, 1478, 1453, 1231, 728 cm⁻¹



(11b) (2S,3R)-2-benzyl-3-phenyl-2,3-dihydrobenzofuran

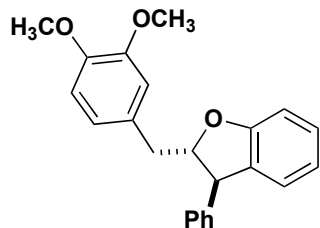
10 (0.010 g, 0.032 mmol, 1 equiv) in DCM (0.015 M) were added to a scintillation vial and manganese dioxide (0.022 g, 0.253mmol, 8 equiv) was added. This heterogenous mixture was stirred at room temperature for 4 hours before cooling to 0 °C. Rh₂(*S*-TCPTTL)₄ (0.001 g, 0.00032 mmol, 1 mol%) was then added and the mixture was allowed to stir to room temperature overnight. The reaction was then filtered through celite, concentrated in vacuo, and purified by flash column chromatography (95:5 hexanes:EtOAc) to afford **11b** (79%) as a a clear oil. ¹H NMR (400 MHz, CDCl₃) δ 7.29 – 7.21 (m, 8H), 7.16 (t, *J* = 7.7 Hz, 1H), 7.03 (d, *J* = 6.6 Hz, 2H), 6.93 (d, *J* = 7.4

Hz, 1H), 6.85 (dd, $J = 10.2, 7.6$ Hz, 2H), 4.84 (td, $J = 7.4, 5.4$ Hz, 1H), 4.32 (d, $J = 7.3$ Hz, 1H), 3.18 (dd, $J = 14.2, 7.5$ Hz, 1H), 3.07 (dd, $J = 14.2, 5.4$ Hz, 1H); ^{13}C NMR (101 MHz, CDCl_3) δ 159.7, 142.7, 137.3, 130.6, 129.7, 128.8, 128.7, 128.6, 128.2, 127.1, 126.8, 125.5, 120.9, 109.9, 92.1, 53.8, 41.0; IR (neat) 3029, 2922, 1478, 1453, 1231, 728 cm^{-1} .



(13a) (2R,3R)-2-(3,4-dimethoxybenzyl)-3-phenyl-2,3-dihydrobenzofuran

12 (0.010 g, 0.027 mmol, 1 equiv) in DCM (0.015 M) were added to a scintillation vial and manganese dioxide (0.019 g, 0.216 mmol, 8 equiv) was added. This heterogenous mixture was stirred at room temperature for 4 hours before cooling to 0 °C. $\text{Rh}_2(\text{R-PTAD})_4$ (0.001 g, 0.00027 mmol, 1 mol%) was then added and the mixture was allowed to stir to room temperature overnight. The reaction was then filtered through celite, concentrated in vacuo, and purified by flash column chromatography (90:10 hexanes:EtOAc) to afford **13a** (78%) as a crystalline white solid. ^1H NMR (300 MHz, CDCl_3) δ 7.30 – 7.23 (m, 3H), 7.18 (t, $J = 7.7$ Hz, 1H), 7.08 – 6.98 (m, 3H), 6.93 – 6.84 (m, 2H), 6.77 (d, $J = 8.3$ Hz, 1H), 6.66 (dd, $J = 8.2, 2.1$ Hz, 1H), 6.55 (d, $J = 2.1$ Hz, 1H), 5.13 (td, $J = 8.7, 5.2$ Hz, 1H), 4.55 (d, $J = 8.3$ Hz, 1H), 3.85 (s, 3H), 3.81 (s, 3H), 2.69 (dd, $J = 14.5, 8.8$ Hz, 1H), 2.49 (dd, $J = 14.5, 5.2$ Hz, 1H).; ^{13}C NMR (76 MHz, CDCl_3) δ 159.7, 148.7, 147.6, 139.6, 131.6, 130.8, 129.4, 128.7, 128.4, 127.2, 125.8, 121.1, 121.0, 112.6, 111.2, 110.0, 87.7, 56.0, 55.8, 51.6, 37.4; IR (neat) 2932, 2834, 1666, 1515, 1479, 1461, 1261, 1231, 1141, 1028 cm^{-1} ; AMM (ESI) m/z calcd $\text{C}_{23}\text{H}_{23}\text{O}_3 + [\text{M}+\text{H}]^+$ 347.1642, found 347.1643.



(13b) (2S,3R)-2-(3,4-dimethoxybenzyl)-3-phenyl-2,3-dihydrobenzofuran

12 (0.010 g, 0.027 mmol, 1 equiv) in DCM (0.015 M) were added to a scintillation vial and manganese dioxide (0.019 g, 0.216 mmol, 8 equiv) was added. This heterogenous mixture was stirred at room temperature for 4 hours before cooling to 0 °C. $\text{Rh}_2(\text{S-TCPTTL})_4$ (0.001 g, 0.00027 mmol, 1 mol%) was then added and the mixture was allowed to stir to room temperature overnight. The reaction was then filtered through celite, concentrated in vacuo, and purified by flash column chromatography (90:10 hexanes:EtOAc) to afford **13b** (68%) as a crystalline white solid. ^1H NMR (300 MHz, CDCl_3) δ 7.31 – 7.24 (m, 3H), 7.19 – 7.13 (m, 1H), 7.08 – 7.03 (m, 2H), 6.93 (dt, $J = 7.4, 1.5$ Hz, 1H), 6.88 – 6.84 (m, 1H), 6.84 – 6.75 (m, 4H), 4.84 (td, $J = 7.3, 5.5$ Hz, 1H), 4.31 (d, $J = 7.4$ Hz, 1H), 3.86 (s, 3H), 3.81 (s, 3H), 3.12 (dd, $J = 14.3, 7.2$ Hz, 1H), 3.03 (dd, $J = 14.3, 5.5$ Hz, 1H); ^{13}C NMR (76 MHz, CDCl_3) δ 159.7, 148.9, 147.9, 142.7, 130.6, 129.8, 128.8, 128.7, 128.3, 127.1, 125.5, 121.8, 120.9, 112.9, 111.3, 109.8, 92.1, 56.0, 55.9, 53.7, 40.4.

A.1.4 References

- (1) Zahrt, A. F.; Athavale, S. V.; Denmark, S. E. Quantitative Structure–Selectivity Relationships in Enantioselective Catalysis: Past, Present, and Future. *Chem. Rev.* **2020**, *120* (3), 1620–1689. 10.1021/acs.chemrev.9b00425.
- (2) Dotson, J. J.; Van Dijk, L.; Timmerman, J. C.; Grosslight, S.; Walroth, R. C.; Gosselin, F.; Püntener, K.; Mack, K. A.; Sigman, M. S. Data-Driven Multi-Objective Optimization Tactics

- for Catalytic Asymmetric Reactions Using Bisphosphine Ligands. *J. Am. Chem. Soc.* **2023**, *145* (1), 110–121. 10.1021/jacs.2c08513.
- (3) Cammarota, R. C.; Liu, W.; Bacsá, J.; Davies, H. M. L.; Sigman, M. S. Mechanistically Guided Workflow for Relating Complex Reactive Site Topologies to Catalyst Performance in C–H Functionalization Reactions. *J. Am. Chem. Soc.* **2022**, *144* (4), 1881–1898. 10.1021/jacs.1c12198.
- (4) Liles, J. P.; Rouget-Virbel, C.; Wahlman, J. L. H.; Rahimoff, R.; Crawford, J. M.; Medlin, A.; O'Connor, V. S.; Li, J.; Roytman, V. A.; Toste, F. D.; Sigman, M. S. Data Science Enables the Development of a New Class of Chiral Phosphoric Acid Catalysts. *Chem* **2023**, S2451929423001122. 10.1016/j.chempr.2023.02.020.
- (5) Dishman, S. N.; Laconsay, C. J.; Fettinger, J. C.; Tantillo, D. J.; Shaw, J. T. Divergent Stereochemical Outcomes in the Insertion of Donor/Donor Carbenes into the C–H Bonds of Stereogenic Centers. *Chem. Sci.* **2022**, *13* (4), 1030–1036. 10.1039/D1SC04622E.
- (6) Bergstrom, B. D. Stereoselective Synthesis of Isochromans and Isochroman-Based Natural Products by C–H Insertions with Donor/Donor Carbenes, University of California, Davis, 2022. <https://escholarship.org/uc/item/4pp8n9mh>.
- (7) Hazelden, I. R.; Carmona, R. C.; Langer, T.; Pringle, P. G.; Bower, J. F. Pyrrolidines and Piperidines by Ligand-Enabled Aza-Heck Cyclizations and Cascades of *N*-(Pentafluorobenzoyloxy)Carbamates. *Angew. Chem. Int. Ed.* **2018**, *57* (18), 5124–5128. 10.1002/anie.201801109.
- (8) Souza, L. W.; Squitieri, R. A.; Dimirjian, C. A.; Hodur, B. M.; Nickerson, L. A.; Penrod, C. N.; Cordova, J.; Fettinger, J. C.; Shaw, J. T. Enantioselective Synthesis of Indolines,

Benzodihydrothiophenes, and Indanes by C–H Insertion of Donor/Donor Carbenes. *Angew. Chem.* **2018**, *130* (46), 15433–15436. 10.1002/ange.201809344.

A.2 Progress towards the total synthesis of *pseudorigols A* and *pseudorigol B*

A.2.1 Introduction

Sesquiterpenes are a vast group of natural products found across a wide variety of plants and insects. They are characterized by containing three isoprene units originating from the 15-carbon farnesyl pyrophosphate (FPP) chain. Many of the sesquiterpene structures are cyclic and possess complex highly saturated scaffolds resulting from enzymatic oxidation or rearrangement reactions.¹ These challenging ring system structures in combination with high biological activity have made sesquiterpenes popular targets for total synthesis efforts.²⁻⁶ Some of these natural product family members have been isolated from marine-derived sources, specifically soft coral species that are prolific producers of these bioactive metabolites.⁷ The Roussis group has become highly interested in isolating the bioactive products from the soft coral *Pseudopterogorgia rigida* found in the Caribbean.^{8,9} In 2016, Georgantea and co-workers isolated pseudorigidol A (**14**) and pseudorigidol B (**15**) from the extract of the Caribbean gorgonian coral.¹⁰ These two natural products contained a 6/6/5 fused tricyclic core that was nearly identical to the tricyclic core we were targeting in the dihydrobenzoxanthone natural product family (see Chapter 2). Pseudorigidol A and B (**14-15**) are diastereomers of each other, and only the relative stereochemistry was assigned in the original isolation paper. Interestingly, the Roussis group reported that both natural products (**14-15**) contained good activity against CDC25 phosphatases, a very popular cancer target in drug discovery.^{11,12} Therefore, we became interested in targeting these two natural products by repurposing synthetic routes already developed to access the left hemisphere of the dihydrobenzoxanthones (see Chapter 2).

Initially, there are two main ways the original Friedel-Crafts route to the left hemisphere (Chapter 2.2.2) could be repurposed to access the desired fused tricyclic core with a methyl group

in the benzylic position (Figure A2.1). Strategy A is to install the benzylic methyl group early in the synthesis (**17**) before tetralone formation. Strategy B is to build the tricyclic core (**19**) first, then undergo late-stage C–C bond formation at the benzylic position to install the methyl group. There are very few reported strategies to make the C_{sp^3} – C_{sp^3} bond. The best precedent originates from the Stahl group, which developed a radical $C(sp^3)$ –H functionalization and cross-coupling reaction in 2021.^{13,14} However, this strategy did not report promising yields for highly electron-donating ring systems such as intermediate **19**. Therefore, we began our initial synthetic efforts with strategy A, where the methyl group could be installed by Grignard addition or Wittig reaction on the benzylic ketone (**21**) followed by reduction to afford the tertiary carbon (**17**).

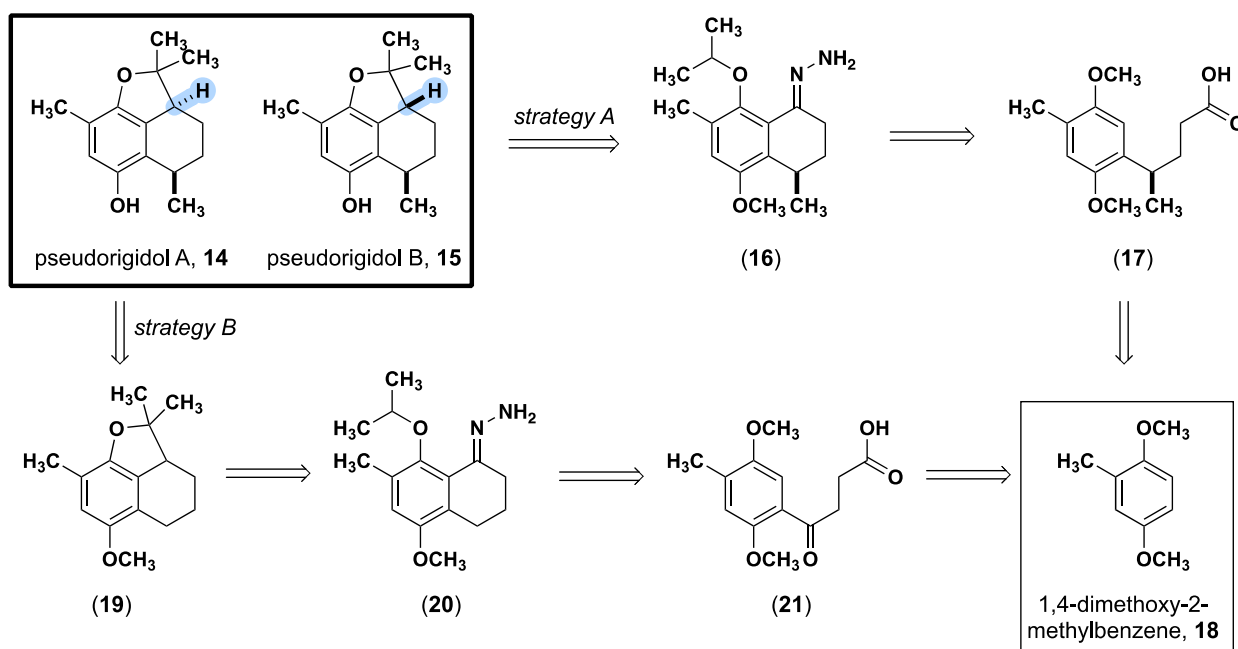


Figure A2.1 Retrosynthetic strategies to access pseudorigidol A and B.

A.2.2 Results and Discussion

This project was going to be handed off to graduate student Linda Ung, therefore the forward synthesis reported below was strictly for exploratory purposes. The goal of the exploratory

chemistry was to make sure the hydrazone precursor with the benzylic methyl group (**16**) could be accessed through strategy A (Figure A2.2), but no further optimization was conducted on each step.

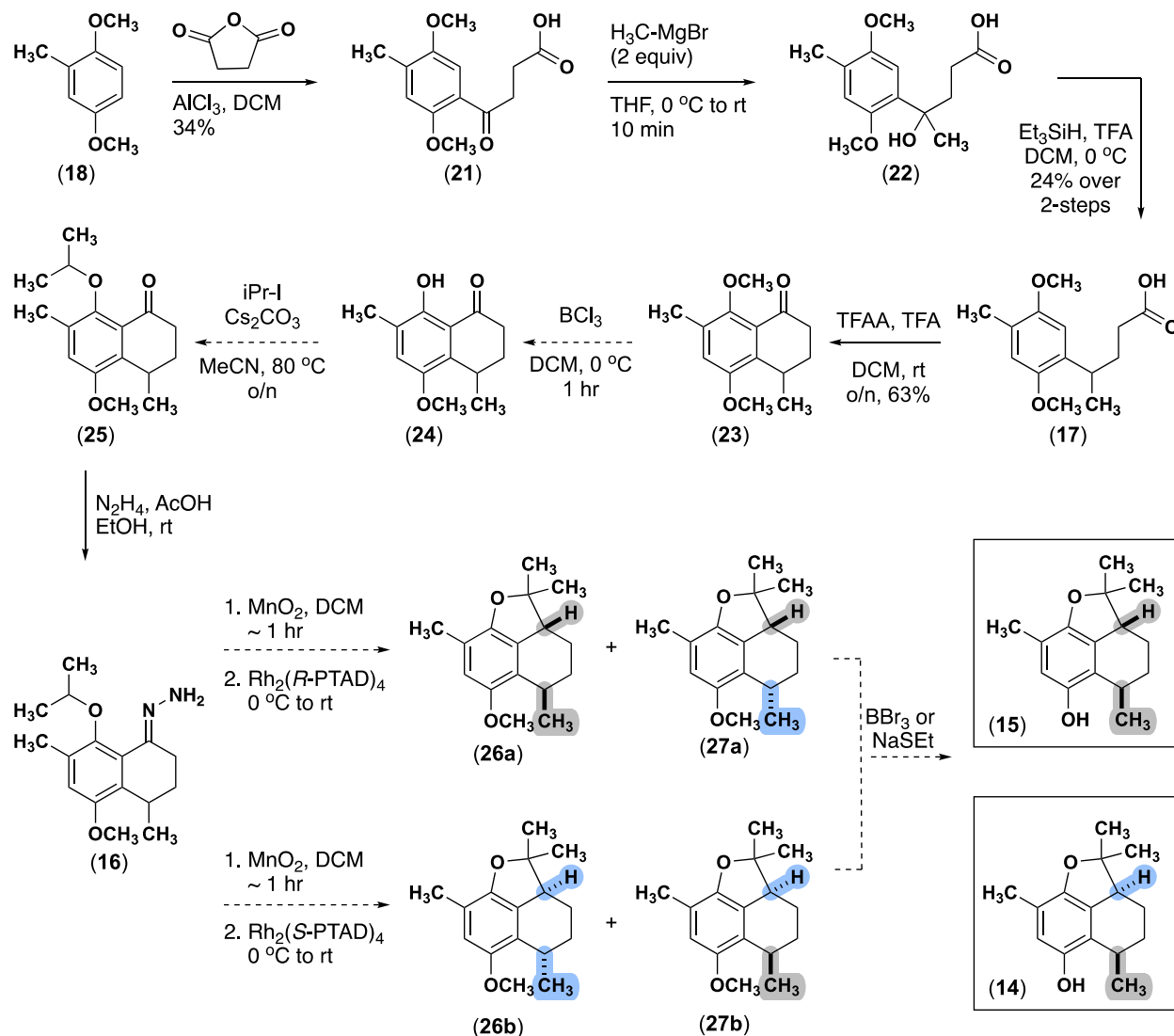


Figure A2.2 Forward synthesis for pseudorigidols.

Starting from 1,4-dimethoxy-2-methylbenzene (**18**), a Friedel-Crafts with succinic anhydride gives the carboxylic acid (**21**) in 34% yield. The addition of methyl Grignard to the benzylic ketone (**21**) affords the tertiary alcohol (**22**), which was telescoped straight into reduction with triethylsilane to afford the benzylic methyl group (**17**) in 24% yield over two steps. A

trifluoroacetic acid and trifluoroacetic anhydride mixture catalyzes the intramolecular EAS reaction to yield the desired tetralone (**23**) in a moderate 56%.

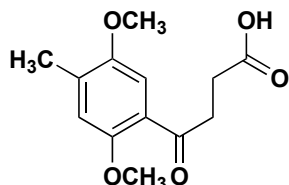
At this point in the synthesis, the project was handed off to Linda Ung. However, the remaining steps consisted of selective ortho deprotection to form the phenol (**24**), followed by alkylation with isopropyl iodide to make the ether (**25**). Hydrazine condensation will form the desired hydrazone precursor (**16**). Since the hydrazone precursor at the benzylic stereocenter is racemic the C–H insertion can make all four possible stereoisomers of the fused tricyclic core (**26-27**). If stereoselectivity trends follow those observed in Chapter 2, then the C–H insertion with $\text{Rh}_2(\text{R-PTAD})_4$ will afford two enantiopure diastereomers. Whereas $\text{Rh}_2(\text{S-PTAD})_4$ will make the opposite enantiomers of each diastereomer. Therefore, each enantiomer of pseudorigidol A (**14**) and pseudorigidol B (**15**) can be selectively accessed to aid in the absolute stereochemical assignment of both natural products as well as biological testing.

A.2.3 Conclusion and Future Work

Current work on this total synthesis has been conducted by Linda Ung. She optimized two key areas of the reported forward synthesis. First, the yield of the Friedel-Crafts reaction with succinic anhydride affording the carboxylic acid (**21**) was unable to be optimized. Switching to a Friedel-Crafts reaction with methyl 4-chloro-4-oxobutanoate yielded the analogous ester in 97% yield. The ester could then be cleaved back to the desired carboxylic acid. Second, Grignard addition and reduction remained low yielding too. Instead, a Wittig reaction on the benzylic ketone was used to make an alkene. Then reduction of the alkene with hydrogen and palladium on carbon afforded the methyl group. This Wittig route has proven to be a more reliable and scalable route to installing the methyl group. Finally, the fused tricyclic core for pseudorigidol A and B has been

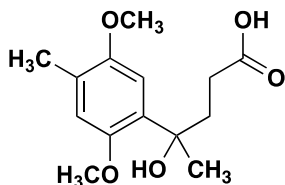
made, and all that remains is methoxy deprotection to afford the final natural products! A route to install the methyl group in an enantiopure fashion is currently under development.¹⁵

A.2.4 Experimentals



(21) 4-(2,5-dimethoxy-4-methylphenyl)-4-oxobutanoic acid

18 (2.99 g, 19.6 mmol, 1.0 equiv), succinic anhydride (3.66 g, 27.5 mmol, 1.4 equiv), and CH₂Cl₂ (65 mL, 0.3M) were added to a flame-dried round bottom. The solution was cooled to 0 °C, then AlCl₃ (2.35 g, 23.5 mmol, 1.2 equiv) was added portionwise over 10 minutes. The reaction was stirred overnight while allowing it to warm to room temperature. Then it was diluted in H₂O (100 mL), acidified to a pH <1 with 1M HCl, and extracted with CH₂Cl₂ (3 x 30 mL). The organics were combined, dried over Na₂SO₄, and concentrated *in vacuo*. The crude reaction was purified by column chromatography (50:50 hexanes:EtOAc) to afford the desired product (1.76 g, 34%) as a yellow solid. SND-VII-032.

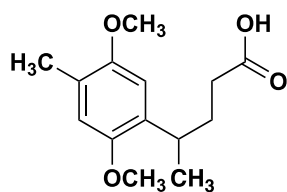


(22) 4-(2,5-dimethoxy-4-methylphenyl)-4-hydroxypentanoic acid

21 (500 mg, 1.98 mmol, 1.0 equiv) in Et₂O (0.1M) was added to a flame-dried round bottom under Ar. The reaction was cooled to 0 °C, then methyl Grignard (1.45 mL, 3M in Et₂O, 2.2 equiv) was

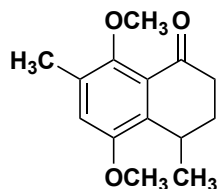
added, and the reaction was stirred until the starting material was fully consumed (~30 minutes). The reaction was quenched with NH₄Cl (sat), extracted with CH₂Cl₂ (3 x 15 mL), dried over Na₂SO₄, and concentrated *in vacuo* to afford the desired alcohol which was telescoped immediately into the next reaction. SND-VII-034.

*Note: methyl lithium can also be used instead of methyl Grignard. This reaction afforded the tertiary alcohol in 42% yield (SND-VII-067).



(17) 4-(2,5-dimethoxy-4-methylphenyl)pentanoic acid

22 (395 mg, 1.47 mmol, 1.0 equiv), Et₃SiH (0.706 mL, 4.42 mmol, 3.0 equiv), TFA (0.338, 4.42 mmol, 3.0 equiv), and DCM (0.1M) were all added to a round bottom. The reaction was stirred overnight at room temperature, then it was quenched with NaHCO₃(sat), extracted with CH₂Cl₂ (3 x 10 mL), and concentrated *in vacuo*. The crude was purified by column chromatography (40:60 hexanes:EtOAc) to afford the desired product (209 mg, 56%) as a yellow solid. SND-VII-070.



(23) 5,8-dimethoxy-4,7-dimethyl-3,4-dihydronaphthalen-1(2H)-one

17 (200 mg, 0.793 mmol, 1.0 equiv), TFA (0.121 mL, 1.59 mmol, 2.0 equiv), TFAA (0.221 mL, 1.59 mmol, 2.0 equiv), and DCM (0.1M) were added to a round bottom and stirred overnight at

room temperature. The reaction was basified with 1M NaOH to a pH >9, then extracted with DCM (3 x 10 mL), and concentrated *in vacuo*. The crude was purified by column chromatography (80:20 hexanes:EtOAc) to afford the desired product (63%) as a light yellow oil. SND-VII-071

A.2.5 References

- (1) Chappell, J.; Coates, R. M. Sesquiterpenes. In *Comprehensive Natural Products II*; Elsevier, 2010; pp 609–641. 10.1016/B978-008045382-8.00005-8.
- (2) Yuan, C.; Zhong, S.; Li, X.; Wang, Y.; Xun, M.-M.; Bai, Y.; Zhu, K. Total Synthesis, Structural Revision and Biological Evaluation of γ -Elemene-Type Sesquiterpenes. *Org. Biomol. Chem.* **2018**, *16* (42), 7843–7850. 10.1039/C8OB02005A.
- (3) Tang, F.; Lan, P.; Bolte, B.; Banwell, M. G.; Ward, J. S.; Willis, A. C. Total Synthesis of (+)-Viridianol, a Marine-Derived Sesquiterpene Embodying the Decahydrocyclobuta[*d*]Indene Framework. *J. Org. Chem.* **2018**, *83* (22), 14049–14056. 10.1021/acs.joc.8b02626.
- (4) Bemis, C. Y.; Ungarean, C. N.; Shved, A. S.; Jamieson, C. S.; Hwang, T.; Lee, K. S.; Houk, K. N.; Sarlah, D. Total Synthesis and Computational Investigations of Sesquiterpene-Tropolones Ameliorate Stereochemical Inconsistencies and Resolve an Ambiguous Biosynthetic Relationship. *J. Am. Chem. Soc.* **2021**, *143* (15), 6006–6017. 10.1021/jacs.1c02150.
- (5) Syntrivanis, L.-D.; Némethová, I.; Schmid, D.; Levi, S.; Prescimone, A.; Bissegger, F.; Major, D. T.; Tiefenbacher, K. Four-Step Access to the Sesquiterpene Natural Product Presilphiperfolan-1 β -Ol and Unnatural Derivatives via Supramolecular Catalysis. *J. Am. Chem. Soc.* **2020**, *142* (12), 5894–5900. 10.1021/jacs.0c01464.

- (6) Broissia, H. D.; Levisalles, J.; Rudler, H. Total Synthesis of the Sesquiterpenes (+)-Daucene, (+)-Carotol, and (-)-Daucol. *J. Chem. Soc., Chem. Commun.* **1972**, No. 15, 855–855. 10.1039/C39720000855.
- (7) Le Bideau, F.; Kousara, M.; Chen, L.; Wei, L.; Dumas, F. Tricyclic Sesquiterpenes from Marine Origin. *Chem. Rev.* **2017**, *117* (9), 6110–6159. 10.1021/acs.chemrev.6b00502.
- (8) Georgantea, P.; Ioannou, E.; Vagias, C.; Roussis, V. Bisabolane and Chamigrane Sesquiterpenes from the Soft Coral Pseudopterogorgia Rigida. *Phytochemistry Letters* **2014**, *8*, 86–91. 10.1016/j.phytol.2014.02.006.
- (9) Georgantea, P.; Ioannou, E.; Vagias, C.; Roussis, V. Perezoperezone and Curcuperezone: Bisabolane Dimers from the Soft Coral Pseudopterogorgia Rigida. *Tetrahedron Letters* **2013**, *54* (50), 6920–6922. 10.1016/j.tetlet.2013.10.041.
- (10) Georgantea, P.; Ioannou, E.; Evain-Bana, E.; Bagrel, D.; Martinet, N.; Vagias, C.; Roussis, V. Sesquiterpenes with Inhibitory Activity against CDC25 Phosphatases from the Soft Coral Pseudopterogorgia Rigida. *Tetrahedron* **2016**, *72* (23), 3262–3269. 10.1016/j.tet.2016.04.059.
- (11) Liu, K.; Zheng, M.; Lu, R.; Du, J.; Zhao, Q.; Li, Z.; Li, Y.; Zhang, S. The Role of CDC25C in Cell Cycle Regulation and Clinical Cancer Therapy: A Systematic Review. *Cancer Cell Int* **2020**, *20* (1), 213. 10.1186/s12935-020-01304-w.
- (12) Mattingly, R. R.; Macara, I. G. Phosphorylation-Dependent Activation of the Ras-GRF/CDC25Mm Exchange Factor by Muscarinic Receptors and G-Protein By Subunits. *Nature* **1996**, *382* (6588), 268–272. 10.1038/382268a0.
- (13) Golden, D. L.; Suh, S.-E.; Stahl, S. S. Radical C(Sp³)–H Functionalization and Cross-Coupling Reactions. *Nat Rev Chem* **2022**, *6* (6), 405–427. 10.1038/s41570-022-00388-4.

- (14) Vasilopoulos, A.; Krska, S. W.; Stahl, S. S. C(Sp³)-H Methylation Enabled by Peroxide Photosensitization and Ni-Mediated Radical Coupling. *Science* **2021**, 372 (6540), 398–403. 10.1126/science.abh2623.
- (15) Hou, S.; Prichina, A. Y.; Zhang, M.; Dong, G. Asymmetric Total Syntheses of Di- and Sesquiterpenoids by Catalytic C–C Activation of Cyclopentanones. *Angew. Chem. Int. Ed.* **2020**, 59 (20), 7848–7856. 10.1002/anie.201915821.